frontiers | Research Topics

Crop abiotic stress: advances in germplasm/gene discovery and utilization

Edited by
Guowei Li, Hui Song, Ran Hovav and Dayong Cui

Published in
Frontiers in Plant Science

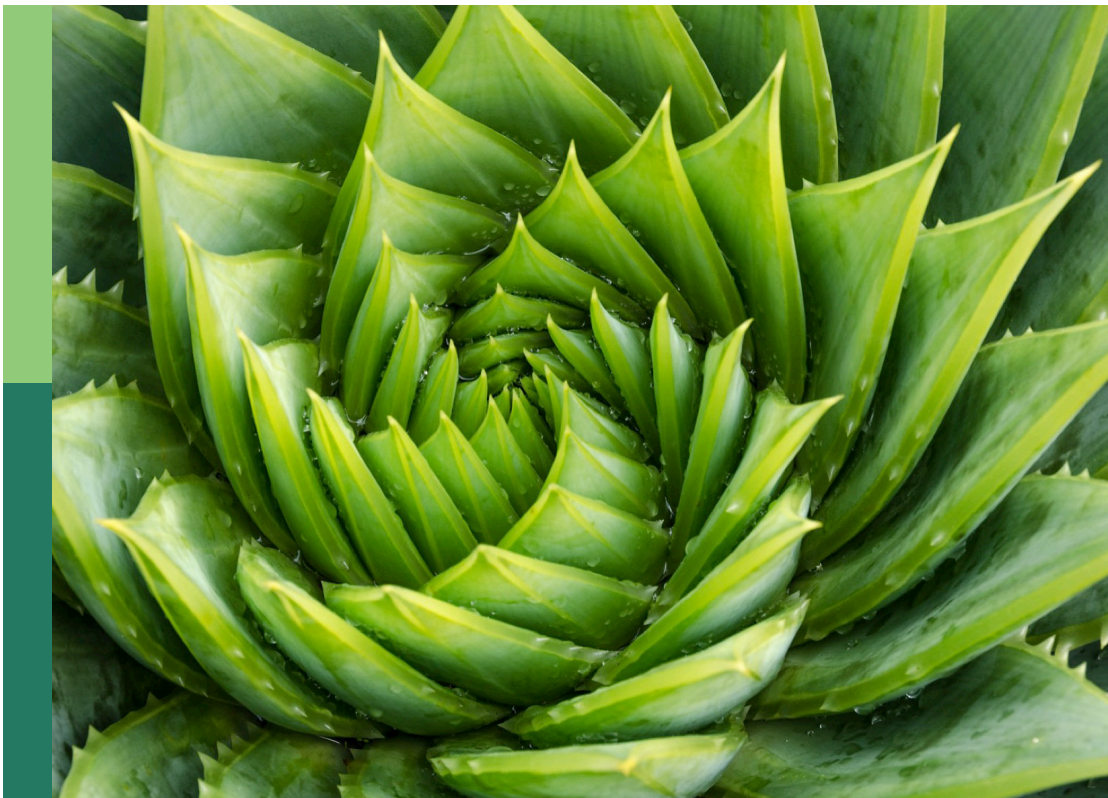

ISSN 1664-8714
ISBN 978-2-8325-5868-3
DOI 10.3389/978-2-8325-5868-3

About Frontiers

Frontiers is more than just an open access publisher of scholarly articles: it is a pioneering approach to the world of academia, radically improving the way scholarly research is managed. The grand vision of Frontiers is a world where all people have an equal opportunity to seek, share and generate knowledge. Frontiers provides immediate and permanent online open access to all its publications, but this alone is not enough to realize our grand goals.

Frontiers journal series

The Frontiers journal series is a multi-tier and interdisciplinary set of open-access, online journals, promising a paradigm shift from the current review, selection and dissemination processes in academic publishing. All Frontiers journals are driven by researchers for researchers; therefore, they constitute a service to the scholarly community. At the same time, the *Frontiers journal series* operates on a revolutionary invention, the tiered publishing system, initially addressing specific communities of scholars, and gradually climbing up to broader public understanding, thus serving the interests of the lay society, too.

Dedication to quality

Each Frontiers article is a landmark of the highest quality, thanks to genuinely collaborative interactions between authors and review editors, who include some of the world's best academicians. Research must be certified by peers before entering a stream of knowledge that may eventually reach the public - and shape society; therefore, Frontiers only applies the most rigorous and unbiased reviews. Frontiers revolutionizes research publishing by freely delivering the most outstanding research, evaluated with no bias from both the academic and social point of view. By applying the most advanced information technologies, Frontiers is catapulting scholarly publishing into a new generation.

What are Frontiers Research Topics?

Frontiers Research Topics are very popular trademarks of the *Frontiers journals series*: they are collections of at least ten articles, all centered on a particular subject. With their unique mix of varied contributions from Original Research to Review Articles, Frontiers Research Topics unify the most influential researchers, the latest key findings and historical advances in a hot research area.

Find out more on how to host your own Frontiers Research Topic or contribute to one as an author by contacting the Frontiers editorial office: frontiersin.org/about/contact

Crop abiotic stress: advances in germplasm/gene discovery and utilization

Topic editors

Guowei Li — Shandong Academy of Agricultural Sciences, China
Hui Song — Qingdao Agricultural University, China
Ran Hovav — Agricultural Research Organization (ARO), Israel
Dayong Cui — Qilu Normal University, China

Citation

Li, G., Song, H., Hovav, R., Cui, D., eds. (2025). *Crop abiotic stress: advances in germplasm/gene discovery and utilization*. Lausanne: Frontiers Media SA.
doi: 10.3389/978-2-8325-5868-3

Table of contents

frontiers | Frontiers in Plant Science

TYPE Editorial
PUBLISHED 12 December 2024
DOI 10.3389/fpls.2024.1524430

OPEN ACCESS

EDITED AND REVIEWED BY
Huihui Li,
Chinese Academy of Agricultural Sciences, China

*CORRESPONDENCE
Guowei Li
ligw_saas@163.com
Hui Song
biosonghui@outlook.com
Dayong Cui
cuidayong@qlnu.edu.cn
Ran Hovav
ranh@volcani.agri.gov.il

RECEIVED 07 November 2024
ACCEPTED 19 November 2024
PUBLISHED 12 December 2024

CITATION
Li G, Song H, Hovav R and Cui D (2024) Editorial: Crop abiotic stress: advances in germplasm/gene discovery and utilization. *Front. Plant Sci.* 15:1524430. doi: 10.3389/fpls.2024.1524430

Editorial: Crop abiotic stress: advances in germplasm/gene discovery and utilization

Guowei Li[1]*, Hui Song[2]*, Ran Hovav[3]* and Dayong Cui[4]*

[1]Institute of Crop Germplasm Resources, Shandong Academy of Agricultural Sciences, Jinan, China, [2]College of Grassland Science, Qingdao Agricultural University, Qingdao, China, [3]Institute of Plant Sciences, Agriculture Research Organization - The Volcani Center, Rishon LeZion, Israel, [4]Shandong Engineering Research Center of Rose Breeding Technology and Germplasm Innovation, School of Life Sciences, Qilu Normal University, Jinan, China

KEYWORDS

editorial, crop, abiotic stress, advance, germplasm

Editorial on the Research Topic
Crop abiotic stress: advances in germplasm/gene discovery and utilization

Global climate variability exerts multiple abiotic stresses on crops, disrupting their growth and development, and resulting in substantial yield losses (Lobell and Gourdji, 2012). This alarming situation highlights the urgent need to explore the mechanisms through which plants mitigate these stressors (Lobell and Gourdji, 2012; Long et al., 2015; Song et al., 2024). Cultivated crops, despite their economic importance, often display limited genetic diversity, whereas their wild relatives, with higher genetic variability, exhibit stronger tolerance to both abiotic and biotic stresses (Fu, 2015; Salgotra and Chauhan, 2023). Thus, collecting, characterizing, and integrating both cultivated and wild germplasm has become a critical component of modern breeding programs. These diverse genetic resources offer significant opportunities for crop improvement but also pose challenges regarding their effective use (Fu, 2015; Liu et al., 2022; Salgotra and Chauhan, 2023). Developing core germplasm collections has therefore become a long-term strategy for optimizing the management and utilization of genetic resources.

The modern crop seed industry is evolving rapidly, but the current utilization of germplasm resources remains inadequate to meet its demands (Yan et al., 2023). A major bottleneck lies in the insufficient characterization of these resources, leading to limited access to high-quality germplasm with broad genetic diversity (Fu, 2015; Salgotra and Chauhan, 2023). Integrating germplasm exploration with investigations into plant responses to abiotic stresses will provide a robust framework for identifying superior materials and facilitating the development of breakthrough crop cultivars.

This Research Topic focuses on recent advances in germplasm and gene discovery related to abiotic stress management in crops, aiming to enhance our understanding of crop responses to abiotic stresses and promote the efficient utilization of genetic resources to support sustainable agricultural practices. Out of 30 submissions, 17 articles were accepted following rigorous peer review, including 16 research papers and 1 review. These studies

cover various abiotic stresses—such as cadmium, calcium, CO_2, cold, drought, heat, salt, selenium, waterlogging, and zinc—affecting crops such as peanut, rice, soybean, tobacco, and wheat. The findings offer valuable insights for exploring stress responses across diverse plant species.

Studies on physiological and biochemical responses

Three articles examine physiological and biochemical responses to abiotic stresses. In soybean, foliar applications of amino acids and zinc not only maintained yield but also enhanced pod and branch numbers while promoting zinc biofortification (Han et al., 2024). Another study explored the unclear relationship between anthocyanin levels and salt stress in peanut, demonstrating that high anthocyanin content activates the antioxidant system, alleviating oxidative stress, and preserving photosynthetic efficiency under salt conditions (Li et al.). In another experiment, calcium-sensitive and calcium-tolerant peanut cultivars were compared under calcium-deficient conditions (Tang et al.). Calcium-sensitive cultivars exhibited a 22.75% reduction in yield, along with increased activities of antioxidant enzymes (SOD, POD, and CAT) and elevated MDA content (Tang et al.). In contrast, calcium-tolerant cultivars maintained stable yield and physiological performance, underscoring calcium's essential role in crop productivity (Tang et al.).

Studies on molecular responses

Several studies focused on molecular responses to abiotic stresses. In rice, sequencing of 541 cultivars followed by genome-wide association studies identified a candidate gene, *OsTMF*, as responsive to salt stress (Liu et al., 2024). Knockout experiments revealed that *OsTMF* promotes germination under salt conditions, demonstrating its potential utility for salt-tolerant breeding (Liu et al., 2024).

In wheat, researchers employed chromosome engineering strategies to introgress chromosome 7el1L from *Thinopyrum* species into wheat chromosome 7AL, producing recombinant lines with enhanced salt tolerance (Tounsi et al.). These lines exhibited notable physiological changes under salt stress, including increased photosynthetic pigment levels, accumulation of compatible solutes, and reduced antioxidant content (such as ascorbate) (Tounsi et al.).

In peanut, bioinformatics analysis identified 16 TPS (Trehalose-6-phosphate synthase) and 17 TPP (Trehalose-6-phosphate phosphatase) genes involved in cold stress responses (Zhong et al.). Notably, *AhTPS9* exhibited differential expression under cold treatment. Overexpression of *AhTPS9* in *Arabidopsis thaliana* improved cold tolerance by stabilizing the photosynthetic system and regulating sugar metabolism, making this gene a promising target for cold-tolerant peanut breeding (Zhong et al.).

In chickpea, Meta-QTL analysis revealed several genes involved in heat stress response, including pollen receptor-like kinase 3, flowering-promoting factor 1, and heat stress transcription factor A-5 (Kumar et al.). These genes influence flowering time, pollen germination, and overall plant development, offering valuable targets for heat-tolerant breeding programs (Kumar et al.).

In *Brassica juncea*, *BjNRAMP1* (Natural Resistance-Associated Macrophage Protein 1) was identified as a key gene involved in cadmium stress tolerance (Li et al.). Expressed in vascular tissues of roots, leaves, and flowers, *BjNRAMP1* facilitates cadmium and manganese accumulation when introduced into yeast and *Arabidopsis*, though its overexpression negatively affects plant growth (Li et al.).

A study in tobacco identified members of the Shaker K^+ channel family, with *NtSKOR1B* up-regulated under salt stress (Yuan et al.). Mutants lacking *ntskor1* exhibited increased biomass and higher K^+ content under salt stress, highlighting its potential role in improving salt tolerance (Yuan et al.). Another study used miRNA sequencing to explore drought stress responses in tobacco (Dai et al.). Thirteen miRNAs were differentially expressed under drought stress, including both known (e.g., nta-miR156b, nta-miR166a) and novel miRNAs (e.g., novel-nta-miR156-5p, novel-nta-miR209-5p) (Dai et al.). These miRNAs targeted genes involved in cell wall expansion, such as *EXT1* and *RWA2*, whose expression decreased under drought but recovered with selenium treatment (Dai et al.). A key regulatory pathway—novel-nta-miR97-5p-LRR-RLK-catechin—was identified, highlighting its importance in drought tolerance (Dai et al.).

In *Medicago sativa* (alfalfa), RNA-seq analysis of plants treated with methyl jasmonate (JA) and salt stress revealed two co-expression modules associated with antioxidant enzyme activity and ion homeostasis. Core genes identified included pyruvate decarboxylase and RNA demethylase, suggesting that JA enhances salt tolerance by modulating antioxidant responses and maintaining ion balance.

Studies in non-crop plants

The Research Topic also includes studies on non-crop plants, offering insights applicable to crop improvement. For example, *Kandelia obovata* exhibits high tolerance to salt and waterlogging (Liu et al.). RNA-seq analysis identified 45 salt-responsive and 16 waterlogging-responsive genes involved in secondary metabolism, highlighting potential targets for enhancing abiotic stress tolerance in crops (Liu et al.).

Author contributions

GL: Writing – original draft, Writing – review & editing. HS: Writing – original draft, Writing – review & editing. DC: Writing – original draft, Writing – review & editing. RH: Writing – original draft, Writing – review & editing.

Funding

The author(s) declare financial support was received for the research, authorship, and/or publication of this article. This research was supported by the Key R&D Program of Shandong Province, China (2022LZGC007, 2024SFGC0402, 2024LZGC031, and 2024LZGC035).

Acknowledgments

The editors express their gratitude to all contributing authors and reviewers for their efforts in making this Research Topic a success.

Conflict of interest

The authors declare that the research was conducted in the absence of any commercial or financial relationships that could be construed as a potential conflict of interest.

Publisher's note

References

Fu, Y. B. (2015). Understanding crop genetic diversity under modern plant breeding. *Theor. Appl. Genet.* 128, 2131–2142. doi: 10.1007/s00122-015-2585-y

Han, S., Sonmez, I., Qureshi, M., Guden, B., Gangurde, S. S., and Yol, E. (2024). The effects of foliar amino acid and Zn applications on agronomic traits and Zn biofortification in soybean (*Glycine max* L.). *Front. Plant. Sci.* 15, 1382397. doi: 10.3389/fpls.2024.1382397

Liu, L., Ma, Y., Zhao, H., Guo, L., Guo, Y., and Liu, C. M. (2024). Genome-wide association studies identified *OsTMF* as a gene regulating rice seed germination under salt stress. *Front. Plant. Sci.* 15, 1384246. doi: 10.3389/fpls.2024.1384246

Liu, Y., Shao, L., Zhou, J., Li, R., Pandey, M. K., Han, Y., et al. (2022). Genomic insights into the genetic signatures of selection and seed trait loci in cultivated peanut. *J. Adv. Res.* 42, 237–248. doi: 10.1016/j.jare.2022.01.016

Lobell, D. B., and Gourdji, S. M. (2012). The influence of climate change on global crop productivity. *Plant Physiol.* 160, 1686–1697. doi: 10.1104/pp.112.208298

Long, S. P., Marshall-Colon, A., and Zhu, X. G. (2015). Meeting the global food demand of the future by engineering crop photosynthesis and yield potential. *Cell* 161, 56–66. doi: 10.1016/j.cell.2015.03.019

Salgotra, R. K., and Chauhan, B. S. (2023). Genetic diversity, conservation, and utilization of plant genetic resources. *Genes* 14, 174. doi: 10.3390/genes14010174

Song, H., Duan, Z., and Zhang, J. (2024). WRKY transcription factors modulate flowering time and resposne to environmental changes. *Plant Physiol. Bioch.* 210, 108630. doi: 10.1016/j.plaphy.2024.108630

Yan, Z., Li, G., and Wan, S. (2023). Oil crops: a potential source of biodiesel. *Engineering* 29, 39–41. doi: 10.1016/j.eng.2023.07.011

frontiers | Frontiers in Plant Science

TYPE Original Research
PUBLISHED 21 August 2023
DOI 10.3389/fpls.2023.1250064

OPEN ACCESS

EDITED BY
Hui Song,
Qingdao Agricultural University, China

REVIEWED BY
Peng Jiao,
Jilin Agricultural University, China
Quanxi Sun,
Chinese Academy of Agricultural Sciences, China

*CORRESPONDENCE
Lin Li
lilindw@hunau.edu.cn
Zinan Luo
luozinan@hunau.edu.cn

†These authors share first authorship

RECEIVED 29 June 2023
ACCEPTED 01 August 2023
PUBLISHED 21 August 2023

CITATION
Tang K, Liu D, Liu N, Zeng N, Wang J, Li L and Luo Z (2023) The physio-biochemical characterization reflected different calcium utilization efficiency between the sensitive and tolerant peanut accessions under calcium deficiency. *Front. Plant Sci.* 14:1250064. doi: 10.3389/fpls.2023.1250064

The physio-biochemical characterization reflected different calcium utilization efficiency between the sensitive and tolerant peanut accessions under calcium deficiency

Kang Tang[1†], Dengwang Liu[1,2,3†], Na Liu[1], Ningbo Zeng[1,2,3], Jianguo Wang[4], Lin Li[1,2,3*] and Zinan Luo[1,2,3*]

[1]College of Agriculture, Hunan Agricultural University, Changsha, Hunan, China, [2]Arid Land Crop Research Institute, Hunan Agricultural University, Changsha, Hunan, China, [3]Hunan Peanut Engineering & Technology Research Center, Changsha, Hunan, China, [4]Shandong Academy of Agricultural Sciences, Jinan, Shandong, China

Peanut yield in southern China is usually limited by calcium deficiency in soil. Most previous studies have found that small-seed varieties showed higher tolerance than large-seed varieties (e.g. Virginia type) under calcium deficiency, however, our preliminary research found that sensitive varieties also existed in small-seed counterparts. Few studies have been conducted to characterize low-calcium tolerance among small-seed germplasms with genetic diversity, and the differences in physiological characteristics between sensitive and tolerant varieties has not been reported yet. Thus, in order to better understand such differences, the current study firstly collected and characterized a diversity germplasm panel consisting of 50 small-seed peanut genotypes *via* a 2-year field trial, followed by the physiological characterization in sensitive (HN032) and tolerant (HN035) peanut genotypes under calcium deficiency. As a result, the adverse effects brought by calcium deficiency on calcium uptake and distribution in HN032 was much larger than HN035. In details, calcium uptake in the aboveground part (leaves and stems) was reduced by 16.17% and 33.66%, while in the underground part (roots and pods), it was reduced by 13.69% and 68.09% under calcium deficiency for HN035 and HN032, respectively; The calcium distribution rate in the pods of HN035 was 2.74 times higher than HN032. The utilization efficiency of calcium in the pods of HN035 was 1.68 and 1.37 times than that of HN032 under calcium deficiency and sufficiency, respectively. In addition, under calcium deficiency conditions, the activities of antioxidant enzymes SOD, POD, and CAT, as well as the MDA content, were significantly increased in the leaves of HN032, peanut yield was significantly reduced by 22.75%. However, there were no significant changes in the activities

of antioxidant enzymes, MDA content, and peanut yield in HN035. Therefore, higher calcium absorption and utilization efficiency may be the key factors maintaining peanut yield in calcium-deficient conditions for tolerant genotypes. This study lays a solid foundation for selecting low-calcium tolerant varieties in future peanut breeding.

KEYWORDS

peanut, calcium deficiency, calcium uptake and distribution, peanut yield, antioxidant enzymes

1 Introduction

Peanut (*Arachis hypogaea* L.) is an important worldwide oilseed and economic crop. Soil acidification is getting intensified especially in the area with plenty rainfall and fertilization misuse, directly leading to calcium deficiency in the soil (Blair et al., 1988; Hue, 2004). The decrease of exchangeable calcium in acidic soil severely inhibits the absorption of calcium in peanut, thus affecting the growth and development of pods and impairing pod yield (Yang et al., 2020).

Calcium can improve the peanut tolerance in response to abiotic stresses. For example, the application of calcium fertilizer can alleviate damage to chloroplasts and cell nucleus caused by high temperature (Yang et al., 2015) and maintain the stability of plasma membrane (Zai et al., 2006) in peanut. Calcium application can also promote peanut growth, dry biomass accumulation, and photosynthetic capacity under cold stress at night (Song et al., 2020; Wu et al., 2020). In contrast, calcium deficiency significantly reduced the fresh biomass accumulation of shoot and root systems, and affected the expression of functional genes related to energy conversion, redox system, intracellular membrane, and cytoskeleton maintenance in peanut young embryos, potentially leading to yield loss and increased number of empty pods (Zhang et al., 2007; Li et al., 2014; Cui et al., 2019). Previous studies have shown that under low calcium conditions, the activities of catalase (CAT) and peroxidase (POD) in peanut leaves are significantly reduced, while the content of malondialdehyde (MDA), a lipid peroxidation product, is increased. This indicates that the active oxygen defense system in peanut plants is damaged, leading to a decrease in the rate of active oxygen elimination, accelerated plant aging, and the accumulation of a large amount of active oxygen. Ultimately, this results in damage to the cell plasma membrane, inhibition of protein synthesis, and adversely affects the healthy growth of peanut plants (Zhang et al., 2004).

Different peanut varieties confer different calcium demands. Large-seed varieties usually require higher calcium supplements than small-seed ones for optimal pod growth and development (Tillman et al., 2010). Gao et al. (2016) found that calcium deficiency in the early seedling stage did not affect the root and shoot growth in YZ9102 (small-to-middle-seed), while a significant reduction has been observed in the both shoot and root biomass in a large-seed variety (LH11). When compared to LH11, YZ9102 has shown a longer root system as well as higher calcium absorption as well as transportation capabilities. Smal et al. (1989a) also found that large-seed variety accumulated more calcium in the pod shell than small-seed one as the soil calcium levels increased. In a sand culture experiment, Zhao and Fang (2017) found that the efficiency of calcium utilization in different peanut varieties decreased under low calcium stress, but the changes in calcium production efficiency and dry matter production efficiency varied among the varieties. Chen (2018) found that the different peanut varieties have varying sensitivities to low calcium conditions mainly due to their different abilities to absorb/accumulate Ca^{2+} in the seeds. Under calcium deficiency, the Ca^{2+} content in the fruit pegs, pods, and seeds of low-calcium sensitive varieties was significantly lower than that under calcium sufficiency, especially in the seeds and pods. However, no significant difference was observed in the seeds of calcium-tolerant varieties.

However, our preliminary studies found that large variation also existed for calcium demands in small-seed peanut varieties. The majority of current researches in peanut abiotic stress mainly focused on salt, cold, drought, and waterlogging resistance (Liu et al., 2015; Liu et al., 2017; Patel et al., 2022; Zeng et al., 2022), with no research conducted to identify and select small-seed varieties conferring low-calcium tolerance. Therefore, the current study aims to explore and select two peanut accessions with different low-calcium tolerance, followed by the physio-biochemical characterization in the two accessions. By comparing the physio-biochemical differences between the two accessions, the current study will lay a solid foundation for future low-calcium tolerance breeding in the peanuts.

2 Materials and methods

2.1 Experimental design

2.1.1 Field screening experiment

A total of 50 small-seed peanut accessions introduced from abroad were used for the 2019-2020 field trials (Table S1), The field trials in 2019-2020 were conducted in Shaoyang (N23.08°, E111.59°) and Yongzhou (N25.37°, E112.18°) in Hunan province with an average annual temperature of 17.4°C and 18.9°C, annual precipitation of 1484.2 mm and 1403 mm, and daylight length of

TABLE 1 Physical and chemical properties of soil in the test site.

Site	pH (H_2O)	OM ($g.kg^{-1}$)	N ($mg.kg^{-1}$)	P ($mg.kg^{-1}$)	K ($mg.kg^{-1}$)	Ca ($mg.kg^{-1}$)
Shaoyang	5.05	7.75	49.00	0.80	61.00	600.00
Yongzhou	5.10	NA	122.00	0.40	74.00	316.00
Miluo	5.15	18.60	96.00	2.90	97.00	750.00

0-20 cm tillage layer. OM stand for organic matter; N stand for hydrolysis of sex of nitrogen; P, available phosphate; K, rapidly available potassium; Ca, exchangeable calcium; NA, Not Available.

1327 h and 1224 h, respectively. The soil types at two sites are typically acidic soil lacking of exchange able calcium with calcium levels lower than 800 $mg.kg^{-1}$ (He, 1994; Wang et al., 2020), as detailed in Table 1. The accessions were sown on May 30, 2019, and June 1, 2020, and harvested on September 31, 2019, and October 1, 2020, respectively. A 2-year field trial was conducted in a randomized complete block design (RCBD) with two calcium treatment levels. The calcium treatment applied base lime (1125 $kg.hm^{-2}$) before sowing, and the calcium deficiency treatment applied no base lime. The experimental plot (2.5 m × 0.8 m) was ridge-planted with two rows (ridge width 0.5 m and furrow width 0.3 m). The row spacing on the same ridge was 30 cm, and the sowing density of intra-row plants was 10 cm. The experimental plot was applied 750 $kg.hm^{-2}$ compound fertilizer (N 15%, phosphorus oxide (P_2O_5) 15%, and potassium oxide (K_2O) 15%) as basal fertilizer. All the experimental treatments were replicated 3 times.

2.1.2 Field trial of two different genotypes for calcium tolerance

The field trial in 2021 was conducted in Yueyang, Hunan, China (N28°55′53.17, E113°09′49.95), with an average annual temperature of 17.0°C, precipitation of 1345 mm, and daylight length of 1650 h. The soil types are typically acidic soil lacking of exchange able calcium with calcium levels lower than 800 $mg.kg^{-1}$ (He, 1994; Wang et al., 2020), as detailed in Table 1. The two selected accessions were sown on May 1, 2021, and harvested on September 1, 2021. The 2021 trial was also set up with two calcium treatments. The calcium treatment applied base lime (750 $kg.hm^{-2}$) before sowing, and the calcium deficiency treatment applied no base lime. A total of 2000 seeds of two selected accessions HN0035 (low-calcium high tolerance, HT) and HN0032 (low-calcium low tolerance, LT) were planted with a plot size of 80 square meters. Each plot was replicated 3 times. The sowing density, fertilization management as well as pest, insect and weed control management were consistent with the field trials in 2019-2020.

2.2 Phenotypic evaluation

2.2.1 Relative chlorophyll content and photosynthetic parameters

A hand-held soil–plant analysis development chlorophyll meter (SPAD–502) (Minolta, Osaka, Japan) was used to determine the relative chlorophyll content (SPAD values). The net photosynthetic rate (Pn), stomatal conductance (Gs), intercellular CO_2 concentration (Ci), and transpiration rate (Tr) were measured using a Li–6400XT portable photosynthesis device (Li–COR, Lincoln, NE, USA). SPAD values and photosynthetic parameters of the third leaves from the main stem were measured between 9:00 and 11:00 AM on a sunny day.

2.2.2 The activities of antioxidant enzymes (SOD, POD, CAT) and MDA contents

The determination of POD, SOD, and CAT activities was carried out using the guaiacol colorimetric method, NBT photoreduction method, and UV absorption method, respectively (Chance, 1955; de Souza et al., 2021). The MDA content was determined using the thiobarbituric acid method (Lin et al., 1984). The specific experimental procedure was carried out according to the study conducted by Li et al. (2023).

2.2.3 Plant architecture and dry biomass accumulation

Seedling emergence was investigated from 10 days after sowing until the maximum number of seedlings was reached and the emergence rate was calculated. At harvest time, the number of plants harvested from the plots was counted to calculate Percentage growing into plants. Six representative plants at the same growing stage were collected from each plot at the flower-pegging, pod-setting, and pod-filling stage, respectively. Three out of six plants were used to measure main stem height (cm), lateral branch length (cm) and the branch number. After measurement, six plants were split into roots, stems, leaves and pods (including pegs) into paper bags and dried at 105°C for 30 min, followed by 80°C for 48 h until complete dehydration. The dry biomass of each organ was then weighted, and the dry matter collected from pod-setting and pod-filling stages were crushed and saved for later elemental determination.

$$\text{Root to crown ratio (R/S)} = \text{root dry weight} / \text{above–ground biomass} \quad (1)$$

$$\text{Vegetative organs/reproductive organs (V/R)} = \text{Dry weight of nutrient organs} / \text{Dry weight of reproductive organs} \quad (2)$$

$$\text{Economic index} = \text{Pod yield} / \text{Total plant dry weight} \quad (3)$$

2.2.4 The determination of yield and its components

The pods from ten representative plants were harvested from each plot at maturity stage, followed by sunlight dehydration for weight determination. The number of full pods, number of unsaturated pods, number of empty pods, number of total pods, dry biomass of pod shells, pod length, pod width, weight of full and unsaturated pods and seeds were recorded. Calculation of yield per plant, hundred pods Weight, hundred seeds Weight, number of kilograms of pods, kernel rate, full pod weight percentage, full seed weight percentage, empty pod rate and plumpness degree of pod.

2.2.5 Calcium content determination

Calcium element was determined by graphite furnace ablation-inductively coupled plasma mass spectrometry. The crushed powder was weighed to 0.5 g plus 5 ml of nitric acid in a digestion tube with a bent-neck funnel overnight. The powder was digested in a graphite furnace the next day until the solution in the tube was nearly clear and transparent. After cooling, the solution was transferred to a 50 ml volumetric flask with fixed volume and mixed, filtered through a microporous membrane in a 10 ml centrifuge tube, and the Ca content was determined in an inductively coupled plasma mass spectrometer (Model: ICPE-9000). The accumulation of calcium element in each organ was measured using the following formats:

$$\text{Calcium uptake (mg per plant)} = \text{Calcium content} * \text{dry matter mass} \quad (4)$$

$$\text{Calcium partitioning rate (\%)} = \text{Calcium uptake in each organ} / \text{calcium uptake of the whole plant} * 100\ \% \quad (5)$$

$$\text{Calcium saponin production efficiency (kg . kg}^{-1}) = \text{pod yield} / \text{total accumulated calcium saponins per plant} \quad (6)$$

2.3 Statistical analysis

2.3.1 Calculation of comprehensive evaluation value (D)

The low-calcium tolerance coefficient (Rx) of 33 phenotypic traits was evaluated for principle component analysis (PCA) following the formula (7); the characteristic value α_{ij} obtained from PCA was used to calculate membership function value X_j following the formula (8); the X_j was then used to calculate membership function value $U(X_j)$ with the formula (9); the comprehensive evaluation D-value was used to evaluate the low-calcium tolerance for each peanut genotype based on the formula (10) and (11).

$$\text{Rx} = \text{phenotypic value under calcium deficiency} / \text{under sufficient calcium} \quad (7)$$

$$X_j = \sum_{i=0}^{n} a_{ij} X_{ij} \quad (8)$$

$$U(X_j) = (X_j - X_{j,\min}) / (X_{j,\max} - X_{j,\min}) \quad (9)$$

α_{ij} stands for the eigenvector that is related to eigenvalue of Rx for each phenotypic trait; X_{ij} is the standardized Rx of each trait; X_j represents the jth comprehensive index; Xx,max and Xx,min represent the maximum and minimum values of the *jth* comprehensive index.

$$W_j = \frac{P_j}{\sum_{j=1}^{n} P_j} \quad (10)$$

$$D = \sum_{j=1}^{n} (U(X_j) x W_j) \quad (11)$$

W_j stands for the weight of the *jth* comprehensive index, and P_j represents the variance contribution rate of the *jth* comprehensive index.

Systematic clustering was conducted according to the above obtained D-value using Euclidean distance square method at the Euclidean distance of 5 (Zhang et al., 2013).

2.3.2 Statistical analysis of two extreme peanut accessions

Data were analyzed using the software IBM SPSS v21.0. The one-way Analysis of Variance (ANOVA) with Duncan's test was used to characterize the differences between different genotypes under two calcium treatments. Differences were considered statistically significant at $p < 0.05$. All the relevant figures were generated by OriginPro 2019.

3 Results

3.1 Selection and evaluation of low-calcium tolerant genotypes from small-seed peanut germplasm panel

A PCA of the low-calcium tolerance coefficients calculated from 33 phenotypic traits revealed that the cumulative contribution of the first 10 principle components (PC) reached 80.088%, explaining most of the phenotypic variation (Table S2). The most weighted traits in the first PC were yield and its components including yield (0.878), number of filled pods per plant (0.759), pod plumpness (0.777), pod shell (0.756), and seed kernel (0.867); Quality traits including oleic acid (0.616), linoleic acid (-0.682), and oleic to linoleic acid ratio (0.681) showed highest weight in the second PC; Seedling growth ability suggested highest weight among the third PC (Table S2). The comprehensive evaluation value (D) showed that HN035 ranked the highest, with has the D value of 0.598, suggesting strongest low-

10.3389/fpls.2023.1250064

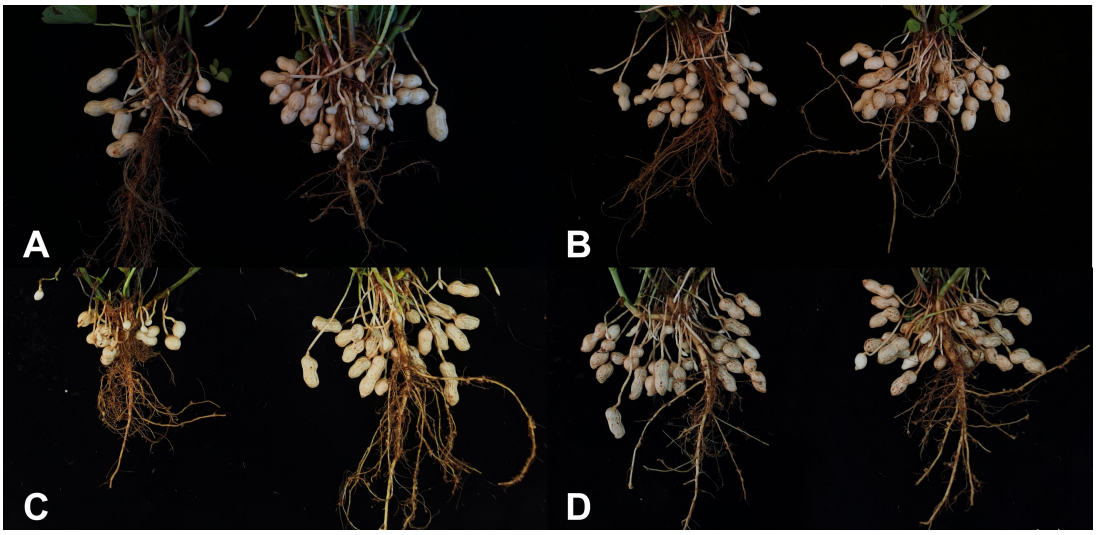

FIGURE 1
The pod morphological differences in two accessions under different calcium treatments. **(A)** the pod morphology in "LT" under different calcium treatments at pod-setting stage; **(B)** the pod morphology in "HT" under different calcium treatments at pod-setting stage; **(C)** the pod morphology in "LT" under different calcium treatments at pod-filling stage; **(D)** the pod morphology in "HT" under different calcium treatments at pod-filling stage.

calcium tolerance, while HN032 performing smallest *D*-value of 0.297 indicated the most weakness in low-calcium tolerance (Figure 1, Table S3). The systematic clustering suggested that the 50 peanut accessions can be classified into four categories ranging from the lowest to highest low-calcium tolerance (Figure 2). Six accessions with highest low-calcium tolerance included HN024, HN028, HN009, HN044, HN025, HN035, while nine accessions including HN002, HN037, HN033, HN020, HN048, HN017, HN004, HN007 and HN032 conferred the lowest low-calcium tolerance (Figure 2). Hence, HN035 (HT) and HN032 (LT) were selected for the subsequent analyses.

3.2 The effects of calcium deficiency on photosynthetic characteristics, antioxidant enzyme activity, plant architecture, biomass accumulation, yield and its components in two different accessions

3.2.1 The effects of calcium deficiency on photosynthetic characteristics in different peanut accessions

Significant differences were observed in two accessions in terms of chlorophyll SPAD value, Pn, Gs, Tr, and Ci during three growing stages (Figure 3). During the full fruit stage, the SPAD value in HN035 did not change significantly, while a significant decrease of 13.70% was observed in HN032 under calcium deficiency (Figure 3A). The Pn of both accessions were adversely affected until the PFS stage, where no significant change was observed in HN035, whereas a significant decrease of 23.63%in HN032 was shown in Figure 3B. The change of Ci in HN035 was not significant during all the three growing stages, but significant increases ranging from 7.70% to 33.30% were observed in HN032 across the three growing periods under calcium deficiency (Figure 3C). The Tr and Gs in HN032 were significantly inhibited under calcium deficiency during all the three periods, but the capability of Tr and Gs in HN035 were recovered during pod-setting stage and full fruit stage, respectively (Figures 3D, E). The tolerance accessions were not affected by low calcium of Tr at pod-setting and Gs at pod-filling stage and the difference was not significant. The change of intercellular carbon dioxide concentration in tolerant accessions was not significant in each period, but the change was great in sensitive accessions, which increased significantly in the three periods, with the increase of 33.30% in full fruit stage under calcium deficiency.

3.2.2 The effects of calcium deficiency on the activities of antioxidant enzymes and MDA content vary among different peanut accessions

The activities of antioxidant enzymes and the levels of MDA content in the leaves of the two accessions increased to varying degrees under calcium deficiency (Figure 4). The activities of SOD and POD in HN032 showed significant increases at three stages under calcium deficiency, while HN035 only showed significant changes during the flower-pegging stage (Figures 4A, B). HN032 showed minor changes in CAT activity during the early stage under low calcium conditions, but significant changes were observed during the pod and ripe fruit stages. HN035 showed no significant changes in CAT activity (Figure 4C). The MDA content of HN032 showed a significant increase of 28.59-45.13%, while HN035 showed no significant change under calcium deficiency (Figure 4D).

3.2.3 The difference in plant architecture of two accessions under calcium deficiency

The main stem height, lateral branch length, shape index and number of branches were measured after harvest. Significant

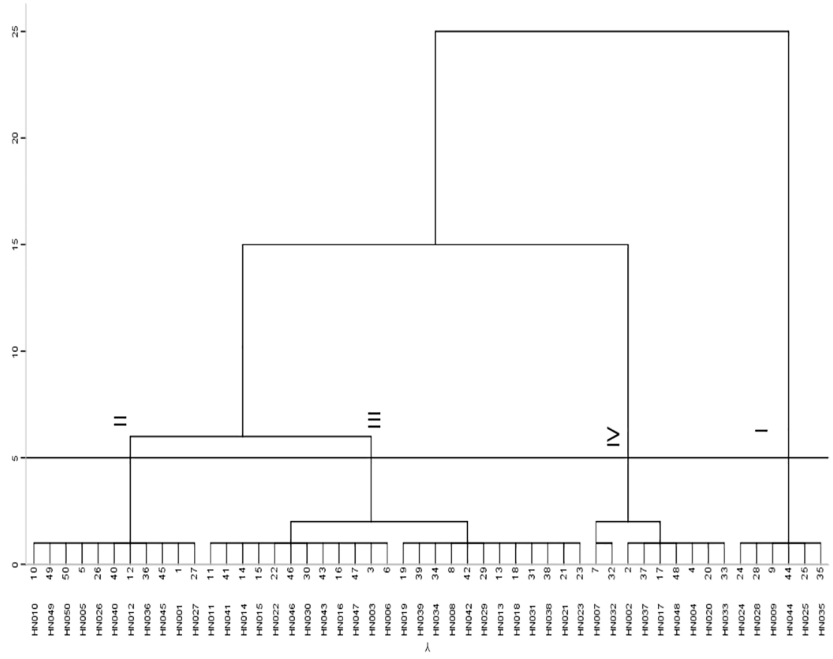

FIGURE 2
Cluster diagram of D values of 50 peanut accessions. I: strong tolerance; II: considerable tolerance; III: intermediate type; IV: calcium sensitivity.

differences were only observed in HN032 with a decrease by 11.75% and 9.60% in main stem height and lateral branch length under calcium deficiency, respectively (Table 2).

3.2.4 The effects of calcium deficiency on dry matter accumulation in different peanut accessions

Even though the dry matter accumulation of vegetative organs significantly changed in both accessions, a significant decrease of 61.28% was only observed in the pods (reproductive organ) of HN032 (Table 3). In addition, the V/R ratio significantly increased 97.36% and economic index significantly dropped with 43.04%, respectively. However, no significant change was observed in pod biomass, V/R and the economic index in HN035 (Table 3).

3.2.5 The effects of calcium deficiency on the yield and composition of different peanut varieties

As for yield and its components, significant changes were observed in all the collected phenotypic traits in HN032 while no significant change in HN035 (Table 4). Especially, the rate of empty pods was largely increased with 182.80% and yield per plant was dropped with 18.37% in HN032 (Table 4).

3.3 The effects of calcium deficiency on calcium uptake, distribution, and utilization efficiency in different peanut accessions.

In general, the calcium in the aboveground and underground organs were mainly accumulated in leaves and pods, respectively (Figure 5). Especially, HN035 accumulated 3.70 and 1.49 times more calcium than HN032 in the pods under calcium deficiency and sufficiency (Figure 4A). The calcium distribution rate of HN035 reached 2.74 and 1.65 times higher than HN032 in the pods under calcium deficiency and sufficiency (Figure 5C). The utilization efficiency of calcium in the pods of HN035 was 1.68 and 1.37 times than that of HN032 under calcium deficiency and sufficiency, respectively (Figure 5D).

4 Discussion

4.1 Germplasm screening identified two accessions with different tolerance under calcium deficiency

Soil calcium deficiency adversely affects peanut yield, and the selection of low-calcium tolerant varieties is one of the most effective way to realize high-yield peanut breeding under calcium deficiency. (Wang et al., 2022) classified 32 peanut accessions into three clusters based on their pod yield and the ratio of unfulfilled pods under calcium deficiency. Among the low-calcium sensitive accessions, two small-seed cultivars were observed, indicating the tolerance variation in small-seed accessions. Likewise, in our previous research, relative yield (the average yield of low-calcium peanut for a certain variety/the average yield of low-calcium peanut for all the participating varieties) and the tolerance coefficient to low-calcium of yield were used for clustering analysis for 105 peanut accessions with various seed size from 15 provinces in China, resulting in five clustered categories: extremely strong (1.90%), strong (0.95%), moderate (18.10%),

10.3389/fpls.2023.1250064

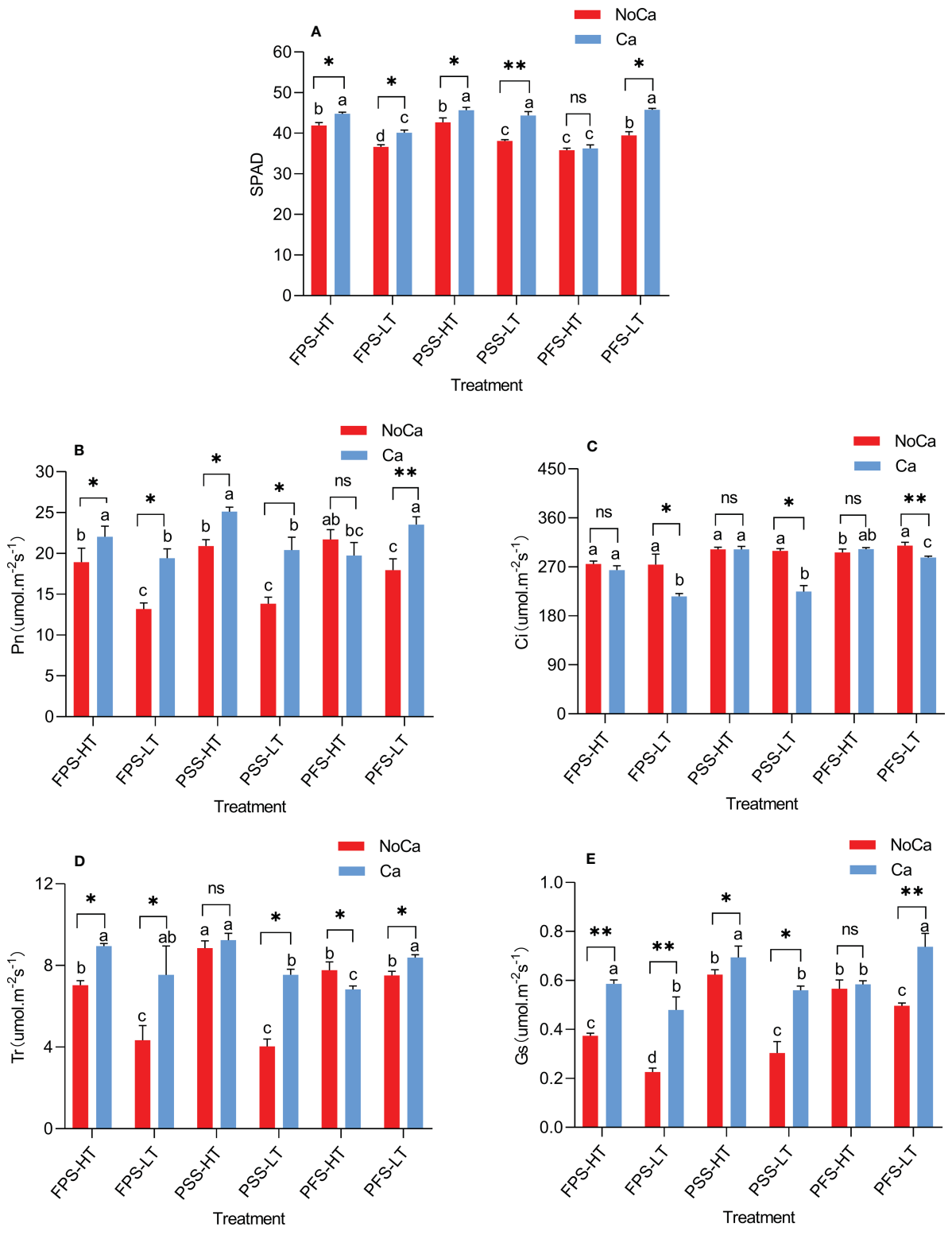

FIGURE 3
SPAD and photosynthetic characteristics at different stages in different peanut accessions under different calcium treatments. **(A)** Chlorophyll SPAD values of two accessions at different stages under different calcium treatments. **(B)** Photosynthetic rates of two accessions at different stages under different calcium treatments. **(C)** Carbon dioxide concentration at saturation of two accessions at different stages under different calcium treatments. **(D)** Transpiration rates of two accessions at different stages under different calcium treatments. **(E)** Stomatal conductance of two accessions at different stages under different calcium treatments. FPS: flower-pegging stage; PSS: pod-setting stage; PFS: pod-filling stage; HT represents low-calcium high tolerance, and LT represents low-calcium low tolerance; NoCa, 0 kg.hm^{-2}; Ca,750 kg.hm^{-2}. "Pn" Net Photosynthetic rate; "Gs" Stomatal conductance; "Tr" transpiration rate; "Ci" intercellular CO_2 concentration. Different lowercase letters represent significant (P<0.05). "*" represents p< 0.05, "**" represents p< 0.01, "ns" non-significant.

10.3389/fpls.2023.1250064

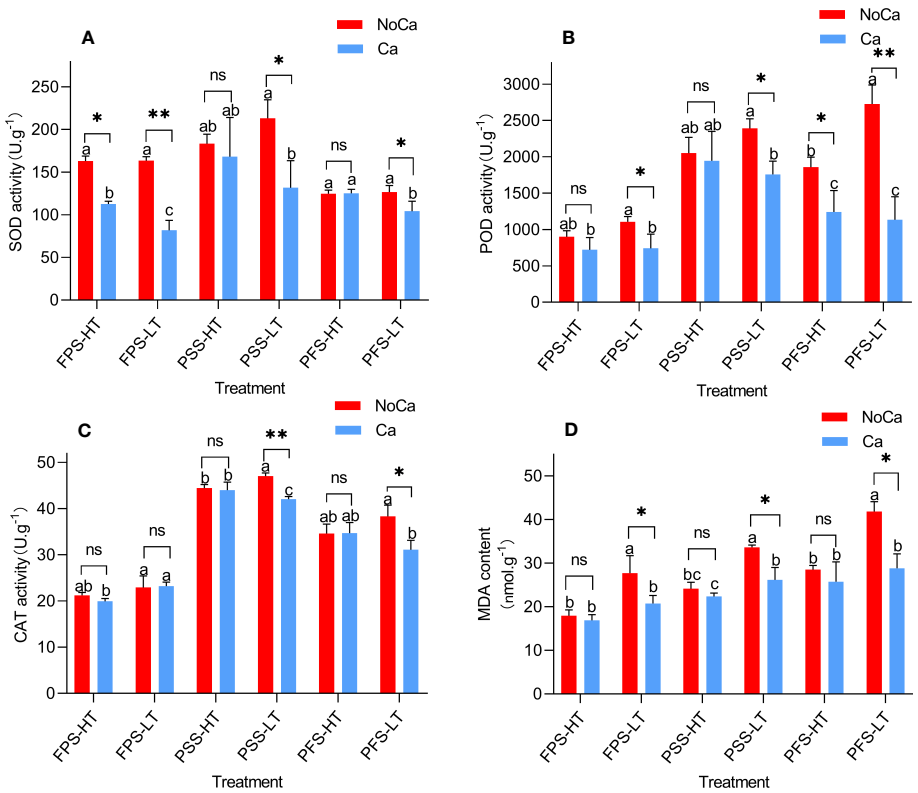

FIGURE 4
Antioxidant enzyme activities SOD, POD, CAT, and MDA contents at different stages in different peanut accessions under different calcium treatments. **(A)** SOD activities of two accessions at different stages under different calcium treatments. **(B)** POD activities of two accessions at different stages under different calcium treatments. **(C)** CAT activities of two accessions at different stages under different calcium treatments. **(D)** MDA contents of two accessions at different stages under different calcium treatments. FPS: flower-pegging stage; PSS: pod-setting stage; PFS: pod-filling stage; HT represents low-calcium high tolerance, and LT represents low-calcium low tolerance; NoCa, 0 kg.hm^{-2}; Ca,750 kg.hm^{-2}.Different lowercase letters represent significant (P<0.05). "*"represents p< 0.05, "**"represents p< 0.01, "ns" non-significant.

sensitive (78.10%, 39 large-seed, 5 medium-seed, and 8 small-seed varieties), and highly sensitive (0.95%, one large-size) under calcium deficiency. We found that the majority of sensitive materials were accounted for by medium and large peanut accessions, but a few small-seed sensitive accessions also exist (Kang et al., 2021). Thus, we further focused on screening tolerant accessions among small-seed peanut germplasm.

The PCA based on a total of 33 indexes of low-calcium tolerance involving plant architecture, chlorophyll content, yield and its components, quality, and calcium content was applied to reflect different weight in various phenotypic traits. The clustering analysis based on *D*-value divided the current germplasm into four categories: strong tolerance (12%),considerable tolerance (22%), intermediate type (48%), and calcium sensitivity (18%), showing that the vast majority of small-seeded accessions were not sensitive to low-calcium stress, but variation in sensitivity still can be observed in accordance with previous studies (Kang et al., 2021; Wang et al., 2022). Among the two extreme categories, HN035 and HN032 were selected for further analysis (Figure 1). The germination rate, the number of full pods per plant, yield per plant, and calcium content of the kernels decreased under calcium deficiency in HN032, while no changes were observed in HN035 (Table S4).

TABLE 2 Plant traits of two types of accessions at maturity period.

Type	Treatment	MSH (cm)	LBL (cm)	NB	SI
HT	NoCa	54.27 ± 0.85b	56.77 ± 2.17b	7.00 ± 0.34a	1.05 ± 0.010a
	Ca	56.03 ± 1.36b	58.53 ± 1.19b	7.55 ± 1.35a	1.04 ± 0.011a
LT	NoCa	56.10 ± 1.67b	58.60 ± 1.08b	7.33 ± 1.15a	1.04 ± 0.01a
	Ca	63.57 ± 2.69a	66.37 ± 0.85a	7.44 ± 0.70a	1.04 ± 0.01a

HT represents low-calcium high tolerance, and LT represents low-calcium low tolerance; NoCa, 0 kg.hm^{-2}; Ca, 750 kg.hm^{-2}. MSH, main stem height; LBL, lateral branch length; NB, Number of branches; SI, Shape Index. Different lowercase letters represent significant (P<0.05).

TABLE 3 Dry matter accumulation of each organ in two accessions under different calcium treatments.

Type	Treatment	Root (g)	Stem (g)	Leaf (g)	Pod (g)	Vegetative organ (g)	R/S	V/R	Economic index
HT	NoCa	0.54 ± 0.04b	12.86 ± 0.74b	13.45 ± 0.47a	12.46 ± 1.44a	26.85 ± 0.87c	0.021ab	2.18 ± 0.28b	0.316 ± 0.03a
	Ca	0.66 ± 0.02a	13.17 ± 0.49b	14.36 ± 0.51a	13.06 ± 2.12a	28.19 ± 0.64b	0.024a	2.20 ± 0.40b	0.316 ± 0.04a
LT	NoCa	0.43 ± 0.04c	11.85 ± 0.73b	11.46 ± 0.79b	3.57 ± 0.44b	23.74 ± 0.1d	0.018bc	6.73 ± 0.88a	0.131 ± 0.01c
	Ca	0.48 ± 0.04bc	15.87 ± 1.26a	14.49 ± 0.58a	9.22 ± 1.58c	30.84 ± 0.79a	0.016c	3.41 ± 0.60b	0.230 ± 0.03b

HT represents low-calcium high tolerance, and LT represents low-calcium low tolerance; NoCa, 0 $kg.hm^{-2}$; Ca, 750 $kg.hm^{-2}$. R/S represents root dry weight/above-ground biomass; V/R represents ratio of vegetative body to reproductive body. Different lowercase letters represent significant ($P<0.05$).

4.2 Low-calcium tolerant accession conferred higher photosynthesis capability than the sensitive one

Photosynthesis is an essential process for plant growth and development. When plants are faced with environmental stress, free calcium ions (Ca^{2+}) are immediately released from calcium repositories and can serve as second messengers to stimulate downstream calcium-dependent metabolic (signaling transduction) pathways. Free Ca^{2+} could also couple with calcium- modulating proteins such as calmodulin (CaM) and calcium-binding proteins (CAS) to mediate stomatal movement, hydrolysis reactions, photosynthetic electron transfer (Kukuczka et al., 2014; Wang et al., 2019; Park and Shin, 2022), photosynthetic carbon assimilation (Kreimer et al., 1988), and photoprotection activities (Maciej et al., 2017). In the current study, HN035 conferred higher SPAD value, photosynthetic rate, stomatal conductance, and transpiration rate in all three periods compared to the sensitive one (HN032), indicating stronger photosynthetic capability in the tolerant accession than the sensitive one under calcium deficiency (Figures 3A, B, D, E). This coincidently matches a previous study related to salt stress in wild soybean, which suggested a higher net photosynthetic rate (Pn) in the salt-tolerant accession than the sensitive one under salt stress (Jiao et al., 2018). It is worth noting that the intercellular CO_2 concentration in HN032 increased significantly in all the three periods under stress, while no significant change was observed in HN035 (Figure 3C). Calcium application could improve photosynthesis capability for both accessions *via* increasing SPAD value, Pn, Tr, Gs and reducing Ci (Figure 3). In accordance with our study, previous studies also found that photosynthesis of the sensitive variety was greatly affected by calcium deficiency and that calcium supplementation can enhance photosynthesis capability (He et al., 2018; Duan et al., 2020; Hu et al., 2022).

4.3 The changes of antioxidant enzymatic activities in the sensitive accession under calcium deficiency were more pronounced than the tolerant one

The antioxidant enzymes play a crucial role in protecting plants from oxidative stress under both abiotic and biotic stresses (Comadira et al., 2015). A significant increase was observed in the activities of SOD, PDD, and CAT in the low-calcium sensitive accesss (Figures 4A-C), which was consistent with the findings of previous studies in peanut and tobacco under nitrogen deficiency stress (Rubio-Wilhelmi et al., 2011; Patel et al., 2020). In contrast, the antioxidant enzymatic activities in tolerant accession remained unchanged, indicating that the degree of oxidative damage to tolerant varieties was mild when compared to sensitive accessions. A study conducted on TG26 also found that SOD and CAT levels remained unchanged under phosphorus or nitrogen deficiency conditions, suggesting that SOD and CAT might be lower than the threshold levels for scavenging excessive production of O_2^- as well as maintaining hydrogen peroxide levels (Panda et al., 2019). The content of MDA can be used to evaluate the extent of oxidative damage caused by abiotic stress in plants. Researchers have studied different salt-tolerant, drought-tolerant, and cold-tolerant peanut varieties and found that the MDA content in sensitive varieties showed greater increases than the tolerant ones. This study indicated that the MDA content increased significantly in the sensitive accession HN032 as the growth period progressed under low calcium stress (Figure 4D). Tolerant accessions, on the other hand, showed no significant changes in MDA content across the

TABLE 4 The differences in yield and its components in two accessions under different calcium treatments.

Type	Treatment	NFP	NEP	YP ($g.plant^{-1}$)	EPR (%)	HPW (g)	HSW (g)	KR (%)	NKP
HT	NoCa	17.31 ± 1.13a	1.23 ± 0.25b	18.69 ± 1.43a	6.02 ± 1.24b	104.73 ± 2.91a	43.67 ± 1.22a	68.14 ± 0.97b	1014.77 ± 41.78c
	Ca	17.17 ± 0.85a	1.10 ± 0.30b	19.44 ± 1.74a	5.49 ± 2.02b	110.15 ± 3.67a	44.99 ± 1.22a	68.96 ± 4.64b	963.62 ± 18.17c
LT	NoCa	13.13 ± 0.64b	2.73 ± 0.12a	9.71 ± 0.28c	15.13 ± 1.01a	66.32 ± 1.43c	35.76 ± 1.04c	70.37 ± 1.02b	1572.26 ± 33.83a
	Ca	16.27 ± 1.21a	1.00 ± 0.20b	12.57 ± 0.26b	5.35 ± 0.67b	74.16 ± 4.16b	38.93 ± 0.53b	78.48 ± 3.07a	1408.64 ± 70.84b

HT represents low-calcium high tolerance, and LT represents low-calcium low tolerance; NoCa, 0 $kg.hm^{-2}$; Ca, 750 $kg.hm^{-2}$. NFP Number of full pods; NEP Number of empty pods; EPR Empty pod rate;YP Yield per plant; HPW Hundred pods Weight; HSW Hundred seeds Weight; KR Kernel rate; NKP Number of kilograms of pods. Different lowercase letters represent significant ($P<0.05$).

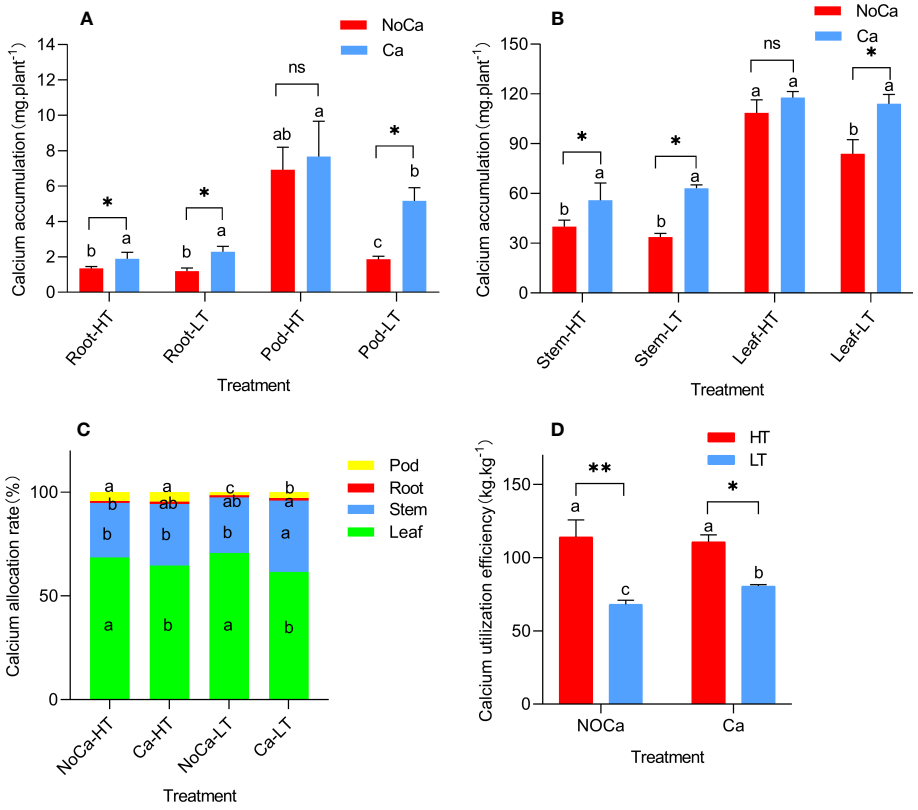

FIGURE 5
Calcium absorption, distribution and utilization efficiency in different accessions. **(A)** Calcium accumulation in underground parts. **(B)** Calcium accumulation in aboveground parts. **(C)** Calcium distribution rate in each organ. **(D)** Calcium utilization efficiency. HT represents low-calcium high tolerance, and LT represents low; NoCa, 0 kg.hm^{-2}; Ca,750 kg.hm^{-2}. Different lowercase letters represent significant (P<0.05). "*"represents p< 0.05, "**"represents p< 0.01, "ns" non-significant. -calcium low tolerance.

three growth stages and accumulated a much lower amount of MDA when compared to the sensitive accession, suggesting that they experienced less oxidation damage to their cell membranes and generated less MDA through lipid peroxidation. These results were consistent with previous studies.

4.4 Low-calcium tolerant accession performed superiority in the agronomic characteristics than the sensitive one

This current study has found significant changes in plant architecture and dry biomass accumulation in the sensitive accession (HN032), while little effects have been observed in HN035 with stronger tolerance under calcium deficiency (Table 3). These findings showed consistency with previous studies under abiotic stress. For example, Liu et al. (2019) found in a hydroponic experiment that large amount of methylesterified pectin was formed under calcium deficiency, coupled with cell wall degradation, inhibition of root elongation and lateral root development, leading to decreased biomass and root growth in peanut. Compared to calcium sufficiency, calcium deficiency led to a significant decrease in dry biomass of nutritional and reproductive organs in HN032, while little change was observed in HN035 (Table 3), indicating that calcium deficiency would lead to growth redundancy in the vegetative development in the sensitive accession (HN032), thus possibly break the balance between vegetative and reproductive growth and impede the normal transportation of photosynthetic products from vegetative or above-ground organs to reproductive organs.

As for yield and its components, the sensitive accession (HN032) showed large reduction under calcium deficiency when compared with HN035 (Table 4), which did not show any significant effects on yield per plant, number of full pods per plant, 100-seed weight, 100-kernel weight, and empty pod ratio. However, significant reductions in yield and the number of full pods per plant were observed in HN032, with a rough two-time increase observed in the empty pod ratio (Table 4). This is consistent with previous researches (Aniefiok et al., 2021; Kadirimangalam et al., 2022; Yang et al., 2022), where tolerant peanut accession have shown stable yields under calcium deficiency due to their higher number of full pods per plant and small number of empty pods per plant.

4.5 Low-calcium tolerant accession conferred higher calcium utilization efficiency (CaUE) than the sensitive one

Peanuts require large amount of calcium for pod fulfillness. However, calcium ions are difficult to be transported from vegetative organs to pods in peanuts (Skelton and Shear, 1971),

thus the calcium needed for pod development must be absorbed from the surrounding soil (Smal et al., 1989a; Zharare et al., 2012). Different peanut varieties showed various demand for calcium nutrition, e.g.Virginia-type (large-seed) peanuts required more calcium (Ca) than Spanish-type (small-seed) peanuts to achieve high yield (Smal et al., 1989b; Zharare et al., 2012). Moreover, different genotypes showed different calcium absorption, transportation, and utilization under calcium deficiency (Romheld and Marschner, 1986). For example, Gao et al. (2016) found that peanut seedlings of YZ9102 have higher calcium absorption and transportation abilities than LH11 under low calcium treatment during the seedling stage.

In agreement, the current study found that calcium accumulation in the leaves and pods of HN035 were higher than HN032 (Figure 5A, 4B) under calcium-deficiency. Even though calcium allocation in leaves were significantly increased in both HN035 and HN032, no significant changes were observed in roots, stems and pods in HN035 (Figure 5C) while a significant decrease was identified in HN032, indicating the difficulty in calcium transportation from vegetative to reproductive organs in the sensitive peanut accession (Behling et al., 1989). In general, the CaUE of HN035 (114.11kg.kg^{-1}, 110.70kg.kg^{-1}) was significantly higher than HN032 (68.06kg.kg^{-1}, 80.53kg.kg^{-1}) under calcium deficiency and sufficiency, but no significant change was observed in HN035 under different calcium treatments, while CaUE in HN032 was significantly impeded under calcium deficiency (Figure 5D), The higher CaUE in HN035 may be due to stronger calcium absorption capability and distribution efficiency. Overally speaking, the differences in low-calcium tolerance were possibly due to different CaUE in two accessions.

Conclusion

This study conducted a two-year field trial to screen 50 small-seed peanut accessions for their low-calcium tolerance and select two accessions with significant differences in low-calcium tolerance. The physio-biochemical studies found that the tolerant peanut accession HN035 showed mild degree of cellular oxidative damage, stronger photosynthetic performance, higher number of full pods per plant, and higher calcium utilization efficiency (CaUE) under calcium deficiency than the sensitive accession HN032. This study will provide a good foundation for subsequent breeding efforts for improving low-calcium-tolerance in peanut accession.

Data availability statement

The original contributions presented in the study are included in the article/Supplementary Material. Further inquiries can be directed to the corresponding authors.

Ethics statement

The author states that the peanuts involved in this study do not involve ethical relations. Experimental research on plants, including the collection of plant material, complies with relevant institutional, national, and international guidelines and legislation. Permissions were obtained to breed the cultivars or collect the sample from the bred cultivars.

Author contributions

LL, DL, and NZ conceived and designed the study. KT carry out the test in the whole process. KT, ZL collected and curated the data. KT and ZL analyzed the data and wrote the manuscript. LL, DL, NZ and JW were responsible for funding acquisition. All authors read, revised and approved the manuscript.

Funding

This work was supported by the Shandong Key R&D Project (ZFJH202310), Chinese Agricultural Research System (CARS-13), Hunan Key R&D Project (No. 2021NK2005) and Hunan Modern Agricultural Research System.

Acknowledgments

We are grateful to the personnel of College of Agriculture at Hunan Agricultural University for providing experimental management. We are also grateful to the editor and reviewers.

Conflict of interest

The authors declare that the research was conducted in the absence of any commercial or financial relationships that could be construed as a potential conflict of interest.

Publisher's note

Supplementary material

The Supplementary Material for this article can be found online at: https://www.frontiersin.org/articles/10.3389/fpls.2023.1250064/full#supplementary-material

References

Aniefiok, E. U., Emmanuel, B. E., Abraham, L. L., and Jessica, E. E. (2021). Performance and dry matter accumulation of groundnut in an ultisol amended with phosphorus and lime. *Pakistan J. Biol. Sci. PJBS.* 24, 847–857. doi: 10.3923/pjbs.2021.847.857

Behling, J. P., Gabelman, W. H., and Gerloff, G. C. (1989). The distribution and utilization of calcium by two tomato (*Lycopersicon esculentumMill.*) lines differing in calcium efficiency when grown under low-Ca stress. *Plant Soil.* 113, 189–196. doi: 10.1007/BF02280180

Blair, G. J., Lithgow, K. B., and Orchard, P. W. (1988). The effects of pH and calcium on the growth of Leucaena leucocephala in an oxisol and ultisol soil. *Plant Soil.* 106, 209–214. doi: 10.1007/BF02371215

Chance, B. (1955). *Methods on enzymology* (New York: Academic Press), 764–765.

Chen, H. (2018). *The cellular and molecular mechanisms of peanut embryo abortion under low calcium in soil* (Fujian Agriculture and Forestry University).

Comadira, G., Rasool, B., Karpinska, B., Morris, J., Verrall, S. R., Hedley, P. E., et al. (2015). Nitrogen deficiency in barley (Hordeum vulgare) seedlings induces molecular and metabolic adjustments that trigger aphid resistance. *J. Exp. Botany.* 66, 3639–3655. doi: 10.1093/jxb/erv276

Cui, L., Guo, F., Zhang, J., Yang, S., Meng, J., Geng, Y., et al. (2019). Synergy of arbuscular mycorrhizal symbiosis and exogenous Ca^{2+} benefits peanut (*Arachis hypogaea* L.) growth through the shared hormone and flavonoid pathway. *Sci. Rep.* 9, 16281. doi: 10.1038/s41598-020-57448-2

de Souza, D. C., Fontaneli, A. C., Peron, A. P., and Froehner, S. (2021). Physiological effects of exposure to copper and chromium in three floating aquatic macrophyte species. *Water Air Soil Pollution.* 232. doi: 10.1007/s11270-020-04960-w

Duan, S., Wu, Y., Zhang, C., Wang, L., Song, S., Ma, C., et al. (2020). Differential regulation of enzyme activities and physio-anatomical aspects of calcium nutrition in grapevine. *Scientia Horticulturae.* 272. doi: 10.1016/j.scienta.2020.109423

Gao, L., Wang, S., Liu, Z., Huang, J., Hilman, Liu, R., et al. (2016). Two cultivars of peanut (*Arachis hypogaea*) seedlings show different tolerance to calcium deficiency. *J. Plant Nutr.* 39, 1016–1025. doi: 10.1080/01904167.2015.1109107

He, D. (1994). Soil fertility and fertilization of cultivated plants in southern China. *Beijing:Science Press*, 1–588.

He, L., Yu, L., Li, B., Du, N., and Guo, S. (2018). The effect of exogenous calcium on cucumber fruit quality, photosynthesis, chlorophyll fluorescence, and fast chlorophyll fluorescence during the fruiting period under hypoxic stress. *BMC Plant Biol.* 18, 180. doi: 10.1186/s12870-018-1393-3

Hu, W., Liu, T., Zhu, C., Wu, Q., Chen, L., Lu, H., et al. (2022). Physiological, Proteomic Analysis, and Calcium-Related Gene Expression Reveal Taxus wallichiana var. mairei Adaptability to Acid Rain Stress Under Various Calcium Levels. *Front. Plant Science.* 13, 845107. doi: 10.3389/FPLS.2022.845107

Hue, N. V. (2004). Responses of coffee seedlings to calcium and zinc amendments to two Hawaiian acid soils. *J. Plant Nutr.* 27, 261–274. doi: 10.1081/PLN-120027653

Jiao, Y., Bai, Z., Xu, J., Zhao, M., Khan, Y., Hu, Y., et al. (2018). Metabolomics and its physiological regulation process reveal the salt-tolerant mechanism in Glycine soja seedling roots. *Plant Physiol. Biochem.* 126, 187–196. doi: 10.1016/j.plaphy.2018.03.002

Kadirimangalam, S. R., Sawargaonkar, G., and Choudhari, P. (2022). Morphological and molecular insights of calcium in peanut pod development. *J. Agric. Food Res.* 9. doi: 10.1016/j.jafr.2022.100320

Kang, T., Zeng, N., Zhang, W., Zhang, H., Wan, S., Liu, D., et al. (2021). Screening of peanut germplasm resources resistant to low calcium in acid red soil area. *Acta Agriculturae Boreali-Sinica.* 36, 62–71. doi: 13.1101.s.20210621.1745.004

Kreimer, G., Melkonian, M., Holtum, J. A., and Latzko, E. (1988). Stromal free calcium concentration and light-mediated activation of chloroplast fructose-1,6-bisphosphatase. *Plant Physiol.* 86, 423–428. doi: 10.1104/pp.86.2.423

Kukuczka, B., Magneschi, L., Petroutsos, D., Steinbeck, J., Bald, T., Powikrowska, M., et al. (2014). Proton gradient regulation5-like1-mediated cyclic electron flow is crucial for acclimation to anoxia and complementary to nonphotochemical quenching in stress adaptation. *Plant Physiol.* 165, 1604–1617. doi: 10.1104/pp.114.240648

Li, L., Dong, M. J., Tang, K., Zhang, H., Zeng, N. B., Yang, H. L., et al. (2023). The effects of calcium fertilization on morphological and physio-biochemical characteristics in peanut seedlings under waterlogging stress. *J. Plant Nutr.* 46, 2865–2881. doi: 10.1080/01904167.2022.2160757

Li, D., Yang, W., Fu, D., Shi, P., Liu, X., Chen, L., et al. (2014). Effects of calcium on biomass and leaf stomata number of two genotypes peanut at seedling stage. *Chin. J. Trop. Agriculture.* 34, 27–30.

Lin, Z., Li, S., Lin, G., Sun, G., and Guo, J. (1984). Superoxide dismutase activity and lipid peroxidation in relation to senescence of rice leaves. *J. Integr. Plant Biol.* 06, 605–615.

Liu, Y., Riaz, M., Lei, Y., Yu, Z., and Jiang, C. (2019). Boron and calcium deficiency disturbing the growth of trifoliate rootstock seedlings (*Poncirus trifoliate* L.) by changing root architecture and cell wall. *Plant Physiol. Biochem.* 144, 345–354. doi: 10.1016/j.plaphy.2019.10.007

Liu, D., Wang, J., Li, L., Tan, H., Ma, J., and Lu, S. (2015). Responses of different peanut cultivars to drought and waterlogging stress and physiological mechanism. *Acta Ecologica Sinica.* 35, 3817–3824.

Liu, S., Wang, W., Li, M., Wan, S., and Sui, N. (2017). Antioxidants and unsaturated fatty acids are involved in salt tolerance in peanut. *Acta Physiologiae Plantarum.* 39. doi: 10.1007/s11738-017-2501-y

Maciej, B., Magdalena, G., Ron, M., and Stanisław, K. (2017). Evidence for the involvement of electrical, calcium and ROS signaling in the systemic regulation of non-photochemical quenching and photosynthesis. *Plant Cell Physiol.* 58, 207–215. doi: 10.1093/pcp/pcw232

Panda, A., Rangani, J., and Parida, A. K. (2019). Cross talk between ROS homeostasis and antioxidative machinery contributes to salt tolerance of the xero-halophyte Haloxylon salicornicum. *Environmental and Experimental Botany*. doi: 10.1016/j.envexpbot.2019.103799

Park, C. J., and Shin, R. (2022). Calcium channels and transporters: Roles in response to biotic and abiotic stresses. *Front. Plant Science.* 13, 964059. doi: 10.3389/fpls.2022.964059

Patel, J., Khandwal, D., Choudhary, B., Ardeshana, D., Kumar, J. R., Tanna, B., et al. (2022). Differential Physio-Biochemical and Metabolic Responses of Peanut (*Arachis hypogaea* L.) under Multiple Abiotic Stress Conditions. *Int. J. Mol. Sci.* 23, 660. doi: 10.3390/IJMS23020660

Patel, M., Rangani, J., Kumari, A., and Parida, A. K. (2020). Mineral nutrient homeostasis, photosynthetic performance, and modulations of antioxidative defense components in two contrasting genotypes of Arachis hypogaea L. (peanut) for mitigation of nitrogen and/or phosphorus starvation. *J. Biotechnol.* 323, 136–158. doi: 10.1016/j.jbiotec.2020.08.008

Romheld, V., and Marschner, H. (1986). Evidence for a specific uptake system for iron phytosiderophores in roots of grasses. *Plant Physiol.* 80, 175–180. doi: 10.1104/pp.80.1.175

Rubio-Wilhelmi, M. M., Sanchez-Rodriguez, E., Rosales, M. A., Begona, B., Rios, J. J., Romero, L., et al. (2011). Effect of cytokinins on oxidative stress in tobacco plants under nitrogen deficiency. *Environ. Exp. Botany.* 72, 167–173. doi: 10.1016/j.envexpbot.2011.03.005

Skelton, B. J., and Shear, G. M. (1971). Calcium translocation in the peanut (*Arachis hypogaea* L.). *Agron. J.* 63, 409–412. doi: 10.2134/agronj1971.00021962006300030018x

Smal, H., Kvien, C. S., Sumner, M. E., and Csinos, A. S. (1989a). Solution calcium concentration and application date effects on pod calcium uptake and distribution in florunner and tifton-8 peanut. *J. Plant Nutr.* 12, 37–52. doi: 10.1080/01904168909363934

Smal, H., Kvien, C. S., Sumner, M. E., and Csinos, A. S. (1989b). Solution calcium concentration and application date effects on pod calcium uptake and distribution in florunner and tifton-8 peanut. *J. Plant Nutr.* 12, 37–52. doi: 10.1080/01904168909363934

Song, Q., Liu, Y., Pang, J., Hong, J. Y. W., Chen, Y., Bai, C., et al. (2020). Supplementary calcium restores peanut (*Arachis hypogaea* L.) growth and photosynthetic capacity under low nocturnal temperature. *Front. Plant Science.* 10, 1637. doi: 10.3389/fpls.2019.01637

Tillman, B. L., Gomillion, M. W., Person, G., and Mackowiak, C. L. (2010). Variation in response to calcium fertilization among four runner-type peanut cultivars. *Agron. J.* 102, 469–474. doi: 10.2134/agronj2009.0306

Wang, J., Tang, Z., Yang, S., Zhang, J., Peng, Z., Meng, J., et al. (2020). Calcium in peanut high-yield cultivation under stress resistance and efficiency cultivation with reduced fertilizer. *Chin. J. Oil Crop Sci.* 42, 951–955. doi: 10.19802/j.issn.1007-9084.2020243

Wang, Q., Yang, S., Wan, S., and Li, X. (2019). The significance of calcium in photosynthesis. *Int. J. Mol. Sci.* 20, 1353. doi: 10.3390/ijms20061353

Wang, X., Zeng, R., Huang, H., Xiao, M., Gao, Y., Wang, Y., et al. (2022). Screening of peanut varieties resistant to Low-Calcium. *J. Peanut science.* 51, 49–58. doi: 10.14001/j.issn.1002-4093.2022.01.007

Wu, D., Liu, Y., Pang, J., Yong, J. W. H., Chen, Y., Bai, C., et al. (2020). Exogenous calcium alleviates nocturnal chilling-induced feedback inhibition of photosynthesis by improving sink demand in peanut (*Arachis hypogaea*). *Front. Plant Science.* 11. doi: 10.3389/fpls.2020.607029

Yang, R., Howe, J. A., Harris, G. H., and Balkcom, K. B. (2022). Reevaluation of calcium source for runner-type peanut (*Arachis hypogaea* L.). *Field Crops Res.* 277. doi: 10.1016/j.fcr.2021.108402

Yang, S., Wang, F., Guo, F., Meng, J., Li, X., and Wan, S. (2015). Calcium contributes to photoprotection and repair of photosystem II in peanut leaves during heat and high irradiance. *J. Integr. Plant Biol.* 57, 486–495. doi: 10.1111/jipb.12249

Yang, S., Wang, J., Tang, Z., Guo, F., Zhang, Y., Zhang, J., et al. (2020). Transcriptome of peanut kernel and shell reveals the mechanism of calcium on peanut pod development. *Sci. Rep.* 10, 15723. doi: 10.1038/s41598-020-72893-9

Zai, X., Wu, G., Qin, P., and Wang, G. (2006). Effects of ca^{2+} on heat tolerance of peanut seedling. *J. Nanjing Forestry University.* 30, 47–50.

Zeng, R., Cao, J., Li, X., Wang, X., Wang, Y., Yao, S., et al. (2022). Waterlogging tolerance and recovery capability screening in peanut: a comparative analysis of waterlogging effects on physiological traits and yield. *PeerJ.* 10, e12741. doi: 10.7717/peerj.12741

Zhang, J., Cai, N., Zhang, X., and Zhuang, W. (2007). Isolation and identification of specific expressed proteins from peanut (*Arachis hypogaea* L.) development/abortion embryo mediated by calcium. *Acta Agronomica Sin.* 33, 814–819.

Zhang, Z., Ci, D., Ding, H., Song, W., Fu, F., Kang, T., et al. (2013). Indices selection and comprehensive evaluation of salinity tolerance for peanut varieties. *Chin. J. Appl. Ecology.* 24, 3487–3494. doi: 10.13287/j.1001-9332.2013.0584

Zhang, H., Shan, S., Cai, L., Guan, D., Li, Y., and Zhuang, W. (2004). Effect of calcium on peanut plant growth and defence system of active oxygen in leaves. *Chin. J. Oil Crop Sci.* 03, 34–37.

Zhao, X., and Fang, Z. (2017). Effects of low ca stress on the characteristics of calcium absorption and distribution of different peanut cultivars. *Acta Agriculturae Boreali-Sinica.* 32, 194–199.

Zharare, G. E., Blamey, F. C., and Asher, C. J. (2012). Effects of pod-zone calcium supply on dry matter distribution at maturity in two groundnut cultivars grown solution culture. *J. Plant Nutr.* 35, 1542–1556. doi: 10.1080/01904167.2012.689913

frontiers | Frontiers in Plant Science

TYPE Original Research
PUBLISHED 28 August 2023
DOI 10.3389/fpls.2023.1268027

OPEN ACCESS

EDITED BY
Hui Song,
Qingdao Agricultural University, China

REVIEWED BY
Xianqin Lu,
Shandong University, China
Yongzhe Ren,
Henan Agricultural University, China

*CORRESPONDENCE
Wei Wang
weiwang@ldu.edu.cn
Jinmin Fu
turfcn@qq.com

RECEIVED 27 July 2023
ACCEPTED 11 August 2023
PUBLISHED 28 August 2023

CITATION
Shao A, Fan S, Xu X, Wang W and Fu J (2023) Identification and evolution analysis of *YUCCA* genes of *Medicago sativa* and *Medicago truncatula* and their expression profiles under abiotic stress. *Front. Plant Sci.* 14:1268027. doi: 10.3389/fpls.2023.1268027

Identification and evolution analysis of *YUCCA* genes of *Medicago sativa* and *Medicago truncatula* and their expression profiles under abiotic stress

An Shao, Shugao Fan, Xiao Xu, Wei Wang* and Jinmin Fu*

Coastal Salinity Tolerant Grass Engineering and Technology Research Center, Ludong University, Yantai, Shandong, China

The YUCCAs (YUC) are functionally identified flavin-containing monooxidases (FMOs) in plants that act as an important rate-limiting enzyme functioning in the auxin synthesis IPA (indole-3-pyruvic acid) pathway. In this study, 12 MsYUCs and 15 MtYUCs containing characteristic conserved motifs were identified in *M. sativa* (*Medicago sativa* L.) and *M. truncatula* (*Medicago truncatula* Gaertn.), respectively. Phylogenetic analysis revealed that YUC proteins underwent an evolutionary divergence. Both tandem and segmental duplication events were presented in *MsYUC* and *MtYUC* genes. Comparative syntenic maps of *M. sativa* with *M. truncatula*, *Arabidopsis* (*Arabidopsis thaliana*), or rice (*Oryza sativa* L.) were constructed to illustrate the evolution relationship of the YUC gene family. A large number of cis-acting elements related to stress response and hormone regulation were revealed in the promoter sequences of *MsYUCs*. Expression analysis showed that *MsYUCs* had a tissue-specific, genotype-differential expression and a differential abiotic stress response pattern based on transcriptome data analysis of *M. sativa* online. In addition, RT-qPCR confirmed that salt stress significantly induced the expression of *MsYUC1/MsYUC10* but significantly inhibited *MsYUC2/MsYUC3* expression and the expression of *MsYUC10/MsYUC11/MsYUC12* was significantly induced by cold treatment. These results could provide valuable information for functional analysis of *YUC* genes via gene engineering of the auxin synthetic IPA pathway in *Medicago*.

KEYWORDS

***Medicago*, YUC, evolution analysis, expression profile, abiotic stress response**

1 Introduction

Auxin is a critical plant hormone, involved in diverse developmental events such as cell division, cell differentiation, and flower development. Indole-3-acetic acid (IAA) is the best-studied naturally occurring active auxin, which are synthesized by two pathways: tryptophan-dependent pathway and tryptophan-independent pathway (Zhao, 2010). For tryptophan-dependent IAA synthesis, there are four proposed branches: (1) indole-3-

pyruvic acid (IPA); (2) tyramine pathway; (3) index-3-acetamide pathway; and (4) index-3-acetoxime pathway (Stepanova et al., 2011). Among the four branches, the IPA branch is the major route of IAA biosynthesis inferred by the pleiotropic abnormal phenotype of *Arabidopsis* mutants (Mashiguchi et al., 2011; Won et al., 2011). In the initial step, IPA is catalyzed by Trp aminotransferase 1 (TAA1) and its related proteins TAR1 and TAR2 with Trp as the precursor. Subsequently, the YUCCA (YUC)-encoded enzyme catalyzes the generation of IAA by IPA (Fraaije et al., 2002; Won et al., 2011). The YUC enzyme is the first functionally identified flavin-containing monooxidase (FMOs) in plants. The conserved domain of FMOs contains two conserved motifs, the flavin purine dinucleotide (FAD) binding site and the reduced coenzyme binding site (NADPH-binding site), which have the same G_XGxxG characteristic structure in their amino acid sequences (Zhao, 2012).

The *YUC* gene was originally identified from *Arabidopsis* mutants with reduced IAA content (Zhao et al., 2001). Genetic and physiological analyses of the loss-of-function mutants of the *YUC* gene have further demonstrated its important role and rate-limiting enzyme function in the auxin synthesis IPA pathway. Overexpression of transgenic *Arabidopsis* lines of the *YUC* gene showed slightly increased auxin levels, accompanied by phenotypic including hypocotyl elongation, cotyledon bias, and enhanced apical dominance (Zhao et al., 2001). Subsequent studies showed that overexpression of the *YUC* gene in plants such as rice, potato, and strawberry could also produce similar phenotypes of auxin overproduction (Kim et al., 2012; Liu et al., 2014). In addition, inactivation of a single *YUC* gene in *Arabidopsis* presented not obvious developmental defects, whereas multiple mutants plants have more severe phenotypes (Cheng et al., 2006), suggesting functional redundancy among *YUC* members. Moreover, gene and protein expression data in *Arabidopsis* indicated that *YUC1*, *2*, *4*, and *6* were mainly expressed in the stems, whereas *YUC 3*, *5*, *7*, *8*, and *9* were mainly functional in the roots (Chen et al., 2014). The *yuc1yuc2yuc4yuc6* quadruple mutants had severe defects in vascular patterning and failed to produce a normal inflorescence but had no root defects, consistent with their stem-localized expression pattern. *YUC3*, *5*, *7*, *8*, and *9* are expressed during root development, and the multiple mutants of the five *YUC* genes developed short and agrotropic roots (Chen et al., 2014). In addition, *YUC* genes expressed in the shoots (*YUC 1*, *2*, *4.1*, and *6*) are localized to the cytoplasm, whereas root *YUC* genes are the ER (endoplasmic reticulum) membrane-binding proteins. In addition, the phenotypes of different sets of individual YUC knockout mutants cannot be complemented by the expression of *YUC* genes expressed in other tissues (Chen et al., 2014; Zhao, 2018). These studies suggested that different sets of *YUC* genes exhibited tissue expression specificity, organ-specific subcellular localization patterns, and differential of gene function for auxin biosynthesis.

Plants often respond to environmental stress by regulating hormonal pathways. Several studies have shown that the auxin biosynthetic pathway is upregulated in response to certain abiotic stresses including regulating the expression of *YUC* genes (Blakeslee et al., 2019). For example, several root-specific *YUC* genes have been reported to mediate aluminum stress-induced inhibition of root growth in *Arabidopsis* (Liu et al., 2016). Heat and low-temperature stress can induce ER sheet formation by inducing a specific *YUC* gene (Pain et al., 2019). In *Arabidopsis*, heat stress led to an indirect increased expression of *YUC8* (Sun et al., 2012), which is similar to the upregulation of *CsYUC8/9* in cucumber. Cold stress also led to the upregulation of CsYUC10b but downregulation of other CsYUC proteins in cucumber (Yan et al., 2016). RNA-seq analysis of *Arabidopsis* under heat and drought stress also revealed a tissue-specific difference in the up- or downregulation of *TAA/YUC* auxin biosynthesis genes, such as the upregulation of *YUC9* expression in leaf tissues after heat stress (Blakeslee et al., 2019). Overexpression of *YUC7* in *Arabidopsis* (Lee et al., 2012), and *YUC6* in potato was able to increase drought tolerance with reduced water loss in transgenic plants by reducing the decomposition of IAA (Kim et al., 2012; Cha et al., 2015). An increased free IAA level and improved drought stress tolerance connected with reduced levels of reactive oxygen species and delayed leaf senescence have been observed for plants such as tomato, maize, rice, and petunia (Ke et al., 2015). In contrast to most results in *Arabidopsis*, increased drought tolerance associated with decreased root IAA levels in rice was found, accompanied by the downregulation of various *YUC* genes (Du et al., 2013; Naser and Shani, 2016). The different expression patterns of *YUC* genes in response to different stresses or in different species suggested a possible functional differentiation of *YUC* genes during stress response.

Medicago sativa L. is a perennial herbaceous legume forages with high yield, nutrient value, and palatability. As a basic component in rations for animals and an important cash crop for biofuel ethanol production, it is widely cultivated (Li et al., 2011). However, the growth and yield of *M. sativa* could be severely inhibited by external stresses such as salt, cold, and drought stress. Recently, large-scale potential genes involved in *M. sativa* responsive to adverse stimuli have been investigated by transcriptional profiling and detected several stress-responsive genes and categories (Postnikova et al., 2013; An et al., 2016; Luo et al., 2019; Ma et al., 2021). Root and leaf transcriptomes under salt stress revealed a hormone interaction involved in salinity adaptation (Lei et al., 2018). Overexpressing IAA within root nodules of *M. sativa* was associated with the improved drought tolerance of plants (Defez et al., 2017). Although *YUCs* have been identified in several species of plants, such as 11 *AtYUCs* in *Arabidopsis* (Mashiguchi et al., 2011), 7 *OsYUCs* in rice (Yamamoto et al., 2007), 22 *TaYUCs* in wheat (Yang et al., 2012), 22 *GmYUCs* in soybean (Wang et al., 2017) and 14 *ZmYUCs* in maize (Li et al., 2015), the IAA biosynthesis-related *YUC* genes in *M. sativa* or its model legume species *M. truncatula* (*Medicago truncatula* Gaertn.) has not yet been identified at the genome-wide level and the tissue-specific and abiotic stress expression patterns have not been analyzed (Li and Brummer, 2012), greatly limiting the improvement of stress adaptability of *M. sativa* by modifying the auxin pathway through genetic engineering.

In this study, a total of 12 *MsYUCs* in *M. sativa* and 15 *MtYUCs* in *M. truncatula* were identified. The gene structure, motif composition, chromosome location, and gene replication events were analyzed, and the evolutionary relationship of other species associated with *M. sativa* was constructed. An overall comparative expression analysis in *M. sativa* was performed to examine the *YUC*

gene expression patterns in different tissues, different varieties, and their responses to cold, drought, and salt stress. These results could provide valuable information for identifying candidate *MsYUCs* involved in different biological processes and various abiotic stress responses in *M. sativa* for further gene functional study and for genetic modification.

2 Materials and methods

2.1 Identification of *Medicago YUC* genes and basic characteristic analysis

Genome sequence and genome annotation information of *M. sativa* variety Zhongmu No. 1 and *M. truncatula* used in this study were downloaded from Ensembl Plants (https://plants.ensembl.org). The amino acid sequences of the *Arabidopsis* YUC family members were downloaded from the TAIR website (https://www.arabidopsis.org/) and used as Query to search the *Medicago* protein sequences by Local BLAST, and the sequences with e-value less than −20 were reserved. The latest version of all schema database files "Pfam-a.hm.gz" from the Pfam database (https://pfam.xfam.org/) were downloaded, and candidate YUC members containing the FMO-like domain (PFam00743) were identified using TBtools' (Chen et al., 2020) simple HMM Search plug-in. Results obtained from BLAST and Pfam search were further merged to remove duplicates. Finally, the Batch CD search function in the NCBI website (https://www.ncbi.nlm.nih.gov/) and the SMART database were used to detect and retain the correct and complete sequences of YUC characteristic conserved motifs (http://smart.embl-heidelberg.de/). The basic features such as molecular weight were determined, and isoelectric point analysis was performed using the ExPASy Proteomic Server (https://web.expasy.org/protparam/).

2.2 Chromosome localization and conserved motif and gene structure analyses

According to the chromosomal location data contained in the downloaded *Medicago* genome annotation information, TBtools was used to map the chromosomal location of YUC members. The YUC members detected in *Medicago* were named according to their position from top to bottom on chromosomes 1–8. The conserved motif of *YUC* genes was identified using online motif detection software (http://meme.nbcr.net/meme/), and the length of the motif was set from 2 to 200 bp to detect a maximum of 12 motifs. Visualization was performed with the TBtools software. For gene structure analysis, TBtools' "gene structure view" function was used to visualize the gene structure (exon and intron number and location) of MsYUC family genes. The "One step build ML tree" plug-in of TBtools was used to get a Newick tree and displayed in the front of the conversed motif and gene structure exhibition.

2.3 Phylogenetic and gene duplication and synteny analysis

A phylogenetic tree was constructed using the YUC amino acid sequences of *Arabidopsis*, rice, *M. truncatula*, and *M. sativa* to analyze the homology relationships. All YUC sequences were aligned to multiple sequences using Clustal W, and the alignment resulted in phylogenetic tree construction using MEGA6.0 software (Larkin et al., 2007; Tamura et al., 2013). The establishment method used the adjacency method (neighbor-joining method) and the *P*-distance model with the bootstrap test for 1,000 times. Replication events of *Medicago YUC* genes and collinear blocks of *YUC* genes within *M. sativa*, *Arabidopsis*, *M. truncatula*, and rice were analyzed using the "One Step MCScanX Wrapper" function of TBtools with the e-value of $1e^{-3}$ and number of blast hits of 10. Tandem and segmental duplicates in the YUC gene family were identified using TBtools by searching the final "tandem" and "gene Linked Region" files after running. Phylogenetic analysis of species was performed using "phyliptree.phy" derived from the "NCBI Taxonomy" function. The Ka (nonsynonymous) and Ks (synonymous) substitution rates of gene duplication pairs were calculated using the "Simple Ka/Ks Calculator" function of TBtools. Ka/Ks <1, = 1, and >1 represent purification selection, neutral selection, and positive selection, respectively (Zhang et al., 2006). The divergence time (million years ago/MYA) was calculated through formula $T = Ks/2\lambda * 10^{-6}$ ($\lambda = 6.5 \times 10^{-9}$).

2.4 Protein structure and subcellular localization prediction

Secondary structure prediction of MsYUCs was performed by Phyre2 (http://www.sbg.bio.ic.ac.uk/servers/phyre2/html/page.cgi?id=index). A tertiary structure model of the MsYUC proteins was predicted by SWISS-MODEL (https://swissmodel.expasy.org//). Global model quality estimation (GMQE) was used to obtain the high score-predicted model. Trans-membrane domain (TMD) prediction was constructed using TMHMM based on the hidden Markov model (https://services.healthtech.dtu.dk/services/TMHMM-2.0/). Using the online website CELLOv.2.5, subcellular localization was predicted (http://cello.life.nctu.edu.tw/) (Yu et al., 2010).

2.5 Analysis of the promoter-based cis-acting elements

Promoter sequences of the *MsYUC* genes (2,000 bp upstream of the ATG) were extracted by the "GTF/Gff3 Sequence Extract" function of TBtools using "genome annotation file" and "genome fasta file." The promoter sequences were submitted to the PlantCARE (http://bioinformatics.psb.ugent.be/webtools/plantcare/html/) website for cis-acting element analysis, and the elements represented by different-colored symbols were visualized using TBtools' "Basic Biosequence viewer" function.

2.6 Analysis of *MsYUC* gene expression patterns in the RNA-seq data

RNA-seq data of different tissue were downloaded from the online LegumeIP V3 website (https://www.zhaolab.org/LegumeIP/gdp). The expression data of different genotypes and under various abiotic stresses were obtained from previous studies (Zhou et al., 2018; Luo et al., 2019). The different expression profiles were exhibited through a heat map constructed by "Amazing Heatmap" function of TBtools.

2.7 RT-qPCR analysis

Eight-week-old seedlings of Zhongmu No. 1 were exposed to untreated control (CK), cold (4°C), and salt (200 mM NaCl) stresses for 6 h. After treatment, RNeasy Kit (Qiagen) was used to extract the total RNA from three biological replicates under control, salt, and cold stresses, respectively. First-strand cDNA of each sample was synthesized using the TaqMan reverse transcription kit (Applied Biosystems). qPCR was conducted on an ABI real-time PCR system with a total volume of 20 µl containing 10 µl of SYBR Green real-time PCR master mix (Toyobo, Japan), 2 µl of cDNA template, 0.2 µM of upstream and downstream primers. The qPCR program was conducted with denaturation at 95°C or 10 min, followed by 40 cycles of amplification (95°C for 30 s, 60°C for 30 s, and 68°C for 1 min) using the ABI real-time PCR system (Applied Biosystems, Foster City, CA). Transcript levels of each sample were determined and normalized to the untreated control sample (CK) as a calibrator with respect to the internal control gene using the $2^{-\Delta\Delta Ct}$ method (Schmittgen and Livak, 2008). Values represent mean ± *SD* of three biological replications. One-way ANOVA test was used, and significant differences from CK and treated plants at $P < 0.05$ are shown by asterisks. All the technical aspects of qPCR experiments fitted the MIQE Guidelines (Bustin et al., 2009). The primers used are listed in Table S1.

2.8 Protein–protein interaction and miRNA target prediction

All MsYUC protein sequences were submitted to the STRING website (http://string-db.org) to build a protein–protein interaction network with their *Arabidopsis* orthologs as a reference. Using *M. truncatula* miRNAs as reference, target miRNAs were predicted through the psRNATarget website (https://www.zhaolab.org/psRNATarget/) with default parameters while selecting target accessibility, as previously described (Dai et al., 2018).

3 Results

3.1 Identification and basic characterization of the MsYUC and MtYUC gene families

Comparative homology analysis was performed using the downloaded *Arabidopsis* YUC protein sequences as Query to search the protein sequences and the genome sequence of *Medicago*, and a total of 12 *MsYUCs* and 15 *MtYUCs* were identified from *M. sativa* and *M. truncatula*, respectively. All members were designated *MsYUC1-MsYUC12* and *MtYUC1-MtYUC15* according to their distribution and location information on the chromosome (Table 1; Figure S1). The *MsYUC* genes showed a significant uneven distribution on eight chromosomes, with the most four *MsYUC* genes on chromosome 1, three *MsYUC* genes on chromosomes 3 and 7, and only one *MsYUC* gene on chromosomes 5 and 6, but no distribution of *MsYUC* genes on chromosomes 2, 4, and 8 (Figure S1A). However, *MtYUC* genes

TABLE 1 Characteristics of the YUC gene family members in *Medicago*.

ID	Name	ORF	Start	End	W/Da	pI	Location
MsG0180001906.01	MsYUC1	423	29138325	29139895	47167.58	9.12	Periplasmic
MsG0180002563.01	MsYUC2	385	40447849	40451427	43510.12	8.67	Cytoplasmic
MsG0180002571.01	MsYUC3	385	40561568	40564952	43526.16	8.78	Cytoplasmic
MsG0180003762.01	MsYUC4	420	67805768	67807662	47025.45	9.01	Cytoplasmic
MsG0380016438.01	MsYUC5	527	83416606	83420598	59400.64	8.98	Periplasmic
MsG0380016439.01	MsYUC6	360	83450071	83452625	40965.77	9.1	Periplasmic
MsG0380017591.01	MsYUC7	425	98226131	98230092	47542.93	8.82	Cytoplasmic
MsG0580025734.01	MsYUC8	511	23344641	23350209	57393.75	8.63	Periplasmic
MsG0680035661.01	MsYUC9	573	110273357	110282037	64111.41	8.78	Cytoplasmic
MsG0780040831.01	MsYUC10	416	83110763	83112388	46856.19	8.62	Cytoplasmic
MsG0780041255.01	MsYUC11	419	88839687	88843914	47701.96	8.7	Cytoplasmic

(Continued)

10.3389/fpls.2023.1268027

TABLE 1 Continued

ID	Name	ORF	Start	End	W/Da	pI	Location
MsG0780041256.01	MsYUC12	383	88846915	88850153	43072.34	8.1	Periplasmic
AES58795	MtYUC1	430	883915	889499	48280.0	8.87	Cytoplasmic
AES58948	MtYUC2	406	2133963	2136290	45687.8	8.91	Periplasmic
KEH41176	MtYUC3	423	17407546	17409111	47142.53	9.12	Periplasmic
KEH42432	MtYUC4	421	29855829	29858303	47130.5	8.95	Cytoplasmic
KEH35392	MtYUC5	398	40705084	40707031	44902.85	8.38	Periplasmic
KEH35393	MtYUC6	391	40711936	40713932	44194.08	8.73	Periplasmic
KEH35394	MtYUC7	398	40720455	40722348	44929.91	8.38	Cytoplasmic
AES73853	MtYUC8	423	50666906	50671263	47154.53	8.81	Cytoplasmic
KEH29783	MtYUC9	399	18624417	18627401	45407.79	8.99	Cytoplasmic
AES96101	MtYUC10	382	14352361	14354443	42872.11	8.7	Cytoplasmic
KEH27129	MtYUC11	408	32789500	32793211	45302.98	9.1	Cytoplasmic
AES81674	MtYUC12	416	39838750	39840931	46783.18	8.72	Cytoplasmic
KEH24362	MtYUC13	383	43925708	43928430	43201.76	8.95	Cytoplasmic
KEH24364	MtYUC14	384	43937223	43940456	43148.61	8.7	Periplasmic
KEH18954	MtYUC15	382	12379792	12381700	42913.26	8.42	Cytoplasmic

were distributed in all chromosomes except for chromosome 2 (Table 1; Figure S1B). Chromosomal localization also showed that all *YUC* genes could be localized to the *Medicago* chromosomal genome. As shown in Table 1, the length of the coding region (ORF) of *MsYUC* genes varied from 360 to 573 amino acids with a molecular weight (MW) from 40.97 to 64.11 kD. The ORF and MW of *MtYUC* genes varied in relatively small ranges, with The ORF from 382 to 430 amino acids and MW from 42.87 to 48.28 kD (Table 1). All YUC proteins were basic proteins with isoelectric points (pI) greater than 8 (ranging from 8.1 to 9.12). Subcellular location prediction showed that both MsYUC and MtYUC proteins had cytoplasmic and periplasmic locations (Table 1).

3.2 Phylogenetic analysis of *Medicago YUC* proteins

To further analyze the kinship of *YUC* genes, YUC protein sequences from *M. sativa* (12 MsYUC), *Arabidopsis* (11 AtYUC), *M. truncatula* (15 MtYUC), and rice (14 OsYUC) were selected, and an evolutionary tree was constructed (Figure 1A). The results showed that 52 YUC proteins in four species can be clustered into two large clusters (clade I and clade II). Clade I can be further subdivided into five small clades, with MsYUC1, 4, 10 and MtYUC3, 4, 12 in clade I-1, MsYUC7, 9 and MtYUC1, 8, 11 in clade I-2. Clade II can be subdivided into four small clades, with MsYUC2, 3, 11, 12 in Clade II-2, MsYUC8, 5 and 6 in clade II-4. MtYUC2 showed a close relationship with AtYUC1 and AtYUC4, which were clustered into clade I-4. MsYUC7/9 and MtYUC1/8/11, belonging to clade I-2, were relatively closely related to AtYUC6. MtYUC10, MtYUC15, and MsYUC8 were closely related to AtYUC10, which belongs to clade II-4 (Figure 1A). A phylogenetic tree of four species was constructed, and the number and distribution of YUC proteins in various subfamilies in four species were counted (Figure 1B). Notably, clade I-3 and cladeII-3 only contained YUC proteins from rice and clade I-4 only contained YUC proteins from the other three species except *M. sativa*. Clade II-2 only contained YUC members from *Medicago* with no homologous gene from *Arabidopsis*. Clade II-4 contained YUC proteins from the other three species except rice. Only two clades, clade I-1 and clade I-2, both contained YUC proteins from the four species (Figure 1C).

3.3 Gene duplication, synteny, and evolution analysis of the YUCs

Tandem and segmental duplication events were analyzed to further investigate the evolutionary pattern of the YUC gene family in *Medicago*. Results revealed that *MsYUC5/MsYUC6* on chromosome 3 and *MsYUC11/MsYUC12* on chromosome 7 were obvious tandem duplication genes (Figure S1A). Only one *MsYUC* gene pair (*MsYUC4/MsYUC10*) could be identified as segmental duplication events (Figure 2A). The MtYUC gene family has an additional tandem repeat gene pair on chromosome 3 (*MtYUC5/6*, *MtYUC6/7*) (Figure S1B; Table S1). Only one *MtYUC* gene pair (*MtYUC1/MtYUC8*) of *M. truncatula* was identified as segmental duplication genes (Figure 2B). Comparative syntenic maps of *M. sativa* with *Arabidopsis*, rice, and *M. truncatula* were constructed to illustrate the evolution relationship of the *YUC* gene family

10.3389/fpls.2023.1268027

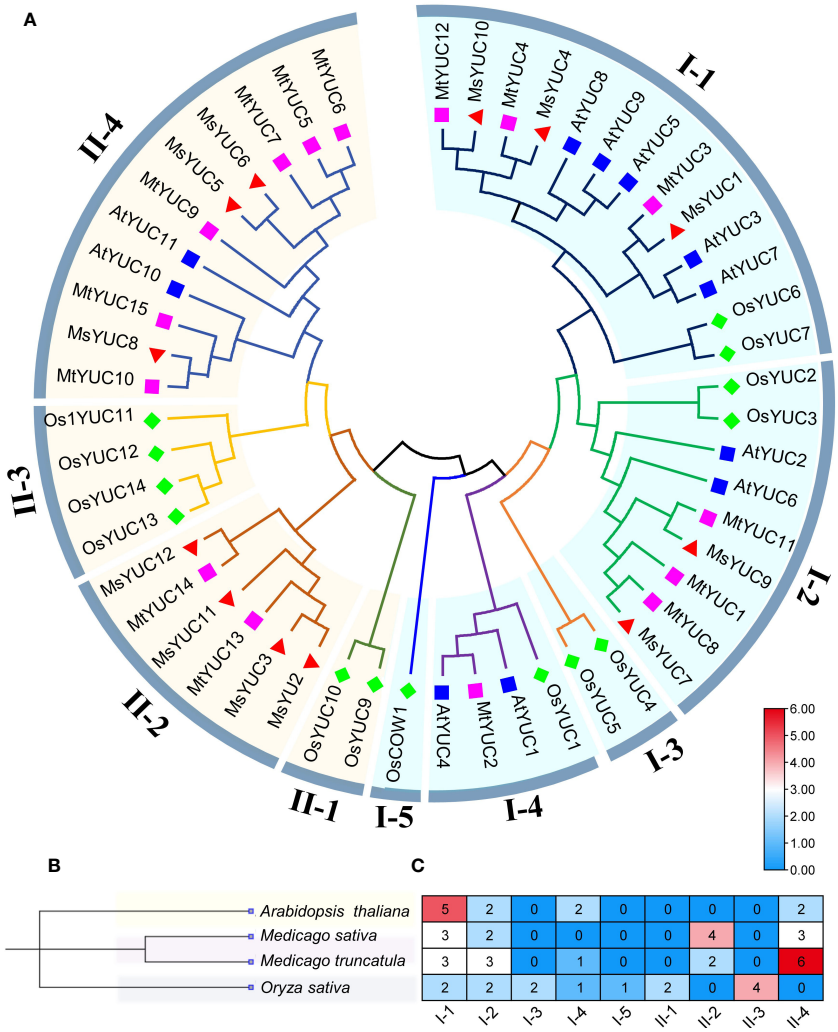

FIGURE 1
The phylogenetic analysis and subfamily clusters of YUC proteins in plants. **(A)** Phylogenetic analysis using YUC proteins in *Medicago* (MsYUC and MtYUC), *Arabidopsis* (AtYUC), and rice (OsYUC). The phylogenetic tree was constructed using the ClustalX program and the neighbor-joining method. **(B)** Evolutionary relationships among four species. Phylogenetic analyses of four species were performed using "phyliptree.phy" from the NCBI Taxonomy function. **(C)** Number of YUC proteins in four species and their distribution in various subfamilies.

(Figure 2C). Notably, 10, 10, and 1 orthologous pairs were found between *M. sativa* and *Arabidopsis*, *M. sativa* and *M. truncatula*, and *M. sativa* and *O. sativa*, respectively (Figure 2C). The collinear blocks in which *MsYUC4, 5, 7, 9, 10* were located is present in *M. truncatula* and *Arabidopsis* except rice. *MsYUC1*-related collinear blocks were found only in *Medicago* but not in *Arabidopsis* or rice (Table S2). Interestingly, one MsYUC family member, *MsYUC9*, had collinear relationships with gene(s) in all species analyzed (Table S2). The Ka/Ks ratio of homologous *MsYUC* gene pairs ranged from 0.19 (*MsYUC4/10*) to 0.49 (*MsYUC5/6*), whereas the Ka/Ks ratio of *MtYUC* homologous ranged from 0.09 (*MtYUC5/6*) to 0.24 (*MtYUC6/7*), indicating that the *YUC* genes of *Medicago* had undergone a great purification selection pressure (Table S3). The evolutionary divergence time (MYA) calculated showed that two homologous gene pairs *MsYUC4/10* (47.83 MYA) and *MtYUC1/8* (57.28 MYA) were derived from the formation period of genus *Medicago*. Three gene pairs of *MsYUC5/6*, *MtYUC5/6*, and *MtYUC6/7* homologous gene pairs were derived around 5 million years ago, and one homologous gene pair (*MsYUC11/12*) was derived around 75.77 MYA (Table S3).

3.4 Motif and gene structure analysis of MsYUC members

Motif analysis showed that 12 MsYUC proteins all contained the conserved FAD-binding motif and NADPH-binding motif (Figure 3A), suggesting a conserved function. Nevertheless, some

10.3389/fpls.2023.1268027

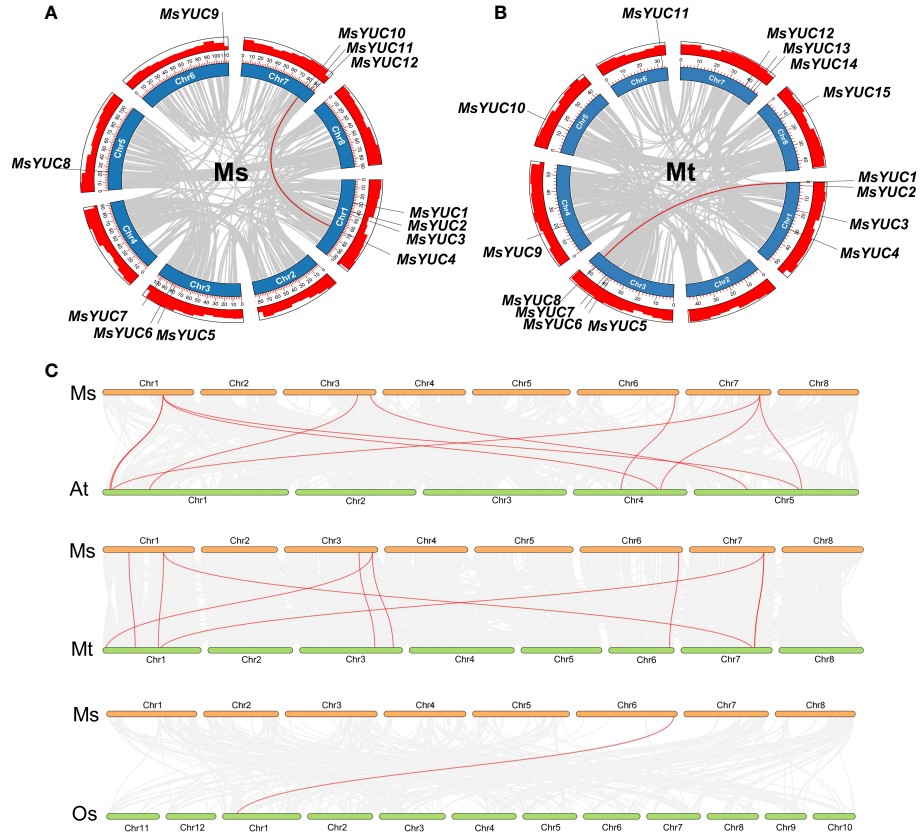

FIGURE 2
Duplication event analysis for the YUC gene family in the *M. sativa* (Ms) and *M. truncatula* (Mt) genome and synteny analysis between *M. sativa* and the other three species. The duplication events in the *M. sativa* genome **(A)** and *M. truncatula* genome **(B)**. Red-colored lines indicate duplication events of MsYUC family members (*MsYUC10/4*) and MtYUC family members (*MsYUC1/8*). **(C)** Collinearity analysis of *M. sativa* (Ms) with *M. truncatula* (Mt) or *Arabidopsis* (At) or rice (Os). Red-colored lines indicate the YUC family members in different species.

differences were observed in the FMO-identifying motif of MsYUC5/6/10 proteins, ATG-containing motif1 of MsYUC2/3/9/11/12 proteins, and ATG-containing motif2 in MsYUC2/3/11/12 proteins, which might contribute to the functional divergences (Figure 3A). In the prediction analysis of the conserved motif of MsYUC proteins, 12 relatively conserved motifs (motifs 1~12) were further identified, including motif1 as the FAD binding site and motif2 as the reduced NADPH binding site (Table S4; Figure 3B). Furthermore, eight conserved motifs (motif1, 2, 4, 5, 6, 8, 9, 10) were present in all MsYUCs examined. Each MsYUC protein contained a minimum of 8 to a maximum of 12 of these motifs. and MsYUC6 protein had the least motif. MsYUC1 and MsYUC4 protein had all 12 conserved motifs and MsYUC7 had 11 conserved motifs except motif12. Seven MsYUC proteins (MsYUC9/12/11/2/3/8/5) contained the same 10 conserved motifs (motif1~10). Only MsYUC10 protein lacked motif8 compared with other members (Figure 3B). Gene structure analysis revealed that the number of exons of *MsYUCs* varied from 3 to 7 whereas *MsYUC9* contained the most numerous introns. Five *MsYUC* genes (*MsYUC2/3/5/8/11*) had five exons. Three *MsYUC* genes (*MsYUC7/12/6*) had four exons, and three *MsYUC* genes (*1/4/10*) had three exons. Seven *MsYUC* genes (*MsYUC12/11/2/3/8/5/6*) containing the same 10 conserved motifs had four exons, whereas three members had only two exons (*MsYUC1/4/10*) (Figure 3C).

3.5 Expression analysis of *MsYUCs* in different tissues and different genotypes

The expression patterns of 12 *MsYUC* genes in different tissues were examined using online transcriptome data. Results indicated a tissue expression specificity of different *MsYUC* genes. For example, *MsYUC10*, *MsYUC12*, and *MsYUC2* had relatively higher expression levels in specific tissues examined, whereas some members (*MsYUC5/6/8*) had very low expression levels and were barely detectable. In addition, *MsYUC2* had a higher expression level in leaves than in other tissues and *MsYUC12* was more highly expressed in both leaves and roots than in other tissues (Figure 4A). In addition, we further analyzed the expression correlation between every two *MsYUC* genes in five tissues. *MsYUC2* showed to be significantly positively correlated with *MsYUC3*, consistent with their close relationship in the phylogenic tree. *MsYUC2* and *MsYUC3* showed to be significantly positively correlated with *MsYUC4* and *MsYUC7*, respectively. *MsYUC3* showed to be significantly positively correlated with *MsYUC4* and *MsYUC7*, respectively. *MsYUC4* and *MsYUC7*, as well as *MsYUC1* and *MsYUC9*, were significantly positively correlated (Figure 4B). There was also a differential expression pattern of *MsYUCs* among different genotypes. For example, *MsYUC10* and

10.3389/fpls.2023.1268027

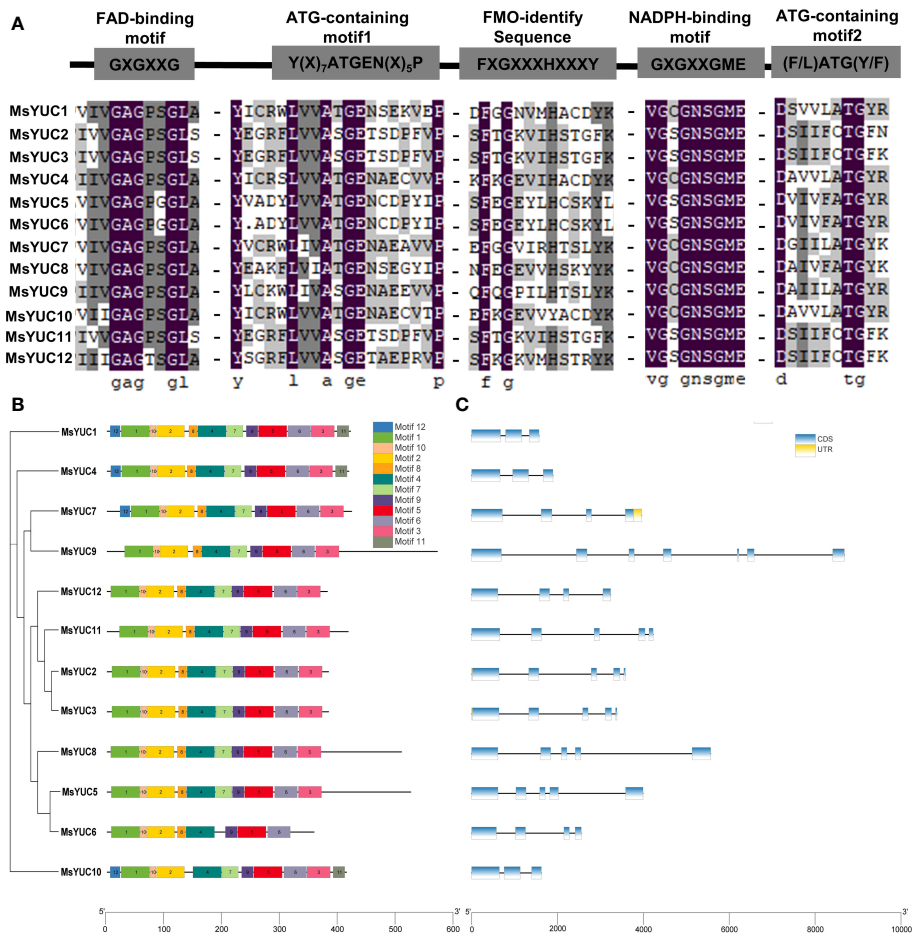

FIGURE 3
Structure and conversed motifs of MsYUC members. **(A)** Alignment of conserved domains in MsYUC proteins. **(B)** Conserved motifs of *MsYUC* genes predicted by MEME. **(C)** Gene structure of *MsYUC* genes. The exons are represented by blue boxes, and black lines are represented by black lines.

MsYUC12 showed a higher expression level in 95-608 compared with other genotypes. *MsYUC11* had a relatively higher expression level in PI251830-K but had the lowest expression detected in 95-608 (Figure 4C).

3.6 Promoter analysis and stress response expression of *MsYUCs*

To predict the possible regulation of *MsYUCs* expression, the cis-acting elements included in the promoter sequence of the *MsYUC* genes were analyzed. Results revealed a variety of stress response elements related to hormone and stress response (Figure 5A). Auxin-responsive elements were found in the promoter region of *MsYUC1*, *4*, *5*, *8*, *12*, and three of their promoters contained AuxRR-core elements. The promoter of *MsYUC8* had the most cis-acting elements (6) involved in the abscisic acid responsiveness (ABRE) (Figure 5B). The *MsYUC7* promoter region contained five CGTCA motifs, which functions in Me-JA responsive. There were also some GA-responsive elements such as GARE-motif, TATC-box, P-Box, and some SA-responsive elements (TCA-element) in the promoters of certain *MsYUCs* (Figure 5A). The promoter of *MsYUC6*, *8*, and *10* contained one cis-acting element involved in low-temperature responsiveness LTR (CCGAAA), respectively. Except for *MsYUC6*, *7*, and *8*, other members all had one or two MYB-binding site (MBS) involved in drought inducibility. Some anaerobic induction, osmotic pressure-responsive, and defense and stress-responsive elements (TC-rich repeats) were also present on certain *MsYUC* promoters (Figure 5A). In addition, all the *MsYUC* promoters had light-response elements. *MsYUC1, 2, 8* had the most light-response elements (6) whereas *MsYUC12* had the least light-response element (1) (Figure 5B). Based on the abiotic transcriptome data analysis, the expressions of *MsYUC1* and *MsYUC10* were significantly increased under salt stress (Figure 5C) and the expressions of *MsYUC10* and *MsYUC12* were induced by cold (Figure 5D). Mannitol treatment significantly induced the expression of *MsYUC10* (Figure 5E). RT-qPCR analysis further confirmed that *MsYUC1* and *MsYUC10* expression could be induced by NaCl (100 mM) and *MsYUC10* and *MsYUC12* could be elevated by cold (4°C) for 3 h treatments (Figures 5F,G). Expression analysis showed that *MsYUC* genes might have a tissue-specific expression and differential abiotic stress response pattern.

10.3389/fpls.2023.1268027

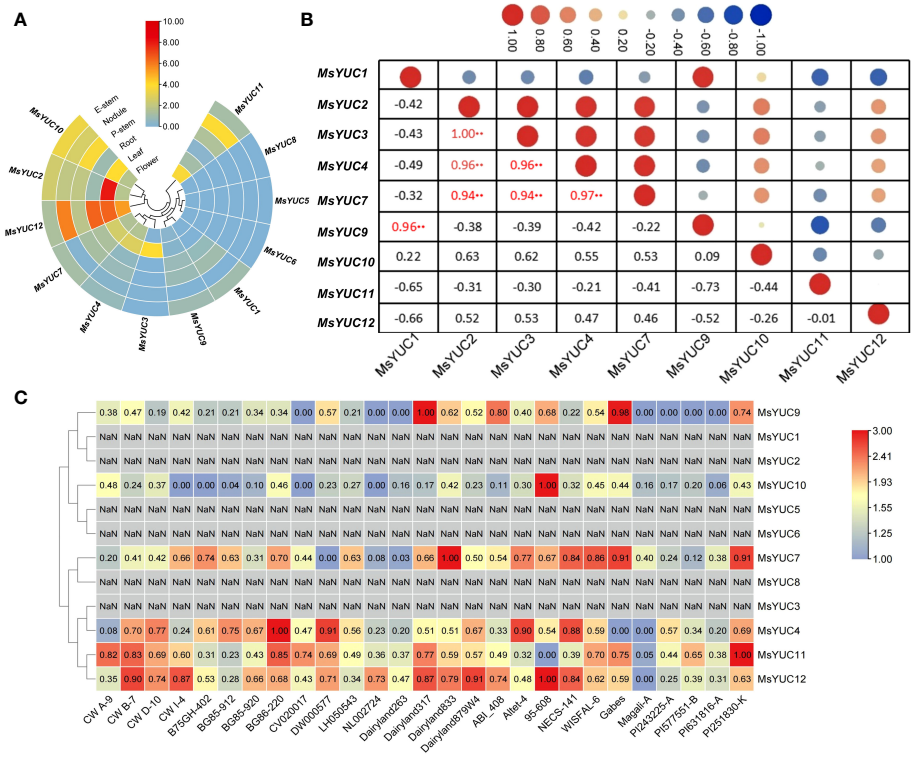

FIGURE 4
Expression pattern of *MsYUC* genes in different tissues and in different genotype. **(A)** Tissue-specific expression analysis of *MsYUC* genes. **(B)** The correlation of gene expression patterns between every two *MsYUC* genes. Red and blue circles represent positive and negative correlations, respectively. **(C)** *MsYUC* expression in different genotypes. The color scale of the heatmap refers to the relative expression level.

3.7 Prediction of the protein interaction network and targeted miRNA of MsYUC members

Protein structure prediction showed that MsYUC proteins shared a unique topology containing several α-helices and β-structures (Figures 6A, S2), indicating structural conservation. The trans-membrane prediction showed that MsYUC4, 9, 10, and 11 proteins possessed one TMD, respectively. The TMD regions of MsYUC9 and 11 proteins were localized in the N-terminal, whereas the TMD regions of MsYUC4 and 10 were localized in the middle of the protein (Figure S3). A predicted protein interaction network indicated that MsYUC proteins had multiple interaction partners (Figure 6B). MsYUC10 protein was predicted to interact with transcription factor NAC089 and NAC-like NTL9, and auxin upregulated F-box protein 1 (AUF1), which is a component of E3 ubiquitin ligase complexes. Both MsYUC9 and MsYUC10 proteins were predicted to interact with phytochrome interacting factor 4 (PIF4). MsYUC9 protein could also interact with TAA1 and amidase 1 (AMI1), which functions in auxin biosynthesis. MsYUC1, 7, 9, 10, 12 were predicted to interact with TAA1, TAR1, and TAR2, which function in the first step of the IPA pathway. We next performed miRNA target site prediction for the *MsYUC* genes. As shown in Figure 6C, *MsYUC2, 3*, and *11* were predicted to be targeted by a similar miRNA5272f. *MsYUC5, 6*, and *8* were predicted to be targeted by a similar miRNA5742. All the coding sequences of *MsYUCs* contained at least three predicted targets for miRNA.

4 Discussion

The YUC gene family proteins involved in auxin biosynthesis are the first identified FMO class family in plants that regulate growth, development, and tolerance in plants (Zhao et al., 2001). In *Medicago*, the YUC number (12 *MsYUCs* and 15 *MtYUCs*) was close to 11 *AtYUC* in *Arabidopsis* and 14 *OsYUC* in rice (Yamamoto et al., 2007; Zhao, 2012). Gene duplication is thought to be the main driver of species evolution and a direct cause of gene family expansion (Lynch and Conery, 2000; Moore and Purugganan, 2003; Maere et al., 2005), and two forms of gene duplication (tandem and segmental) events were identified in *Medicago* YUC gene families. In the MtYUC gene family, there was a gene cluster containing three *MtYUC* members (*MtYUC5/6/7*). Moreover, there was no distribution of *MsYUC* genes on chromosomes 2, 4, and 8 (Table 1, Figure S1A) whereas *MtYUC* genes were distributed in all chromosomes except for chromosome 2 (Table 1; Figure S1B). These reasons may together contribute to the more members of MtYUC than that of MsYUC. Notably, most of the YUC proteins in rice (Monocots) and *Medicago* or *Arabidopsis* (Dicots) could not gather under the same branch, as clade II-4 had no rice YUC protein and clade I-3 and clade II-3 only contained rice YUC

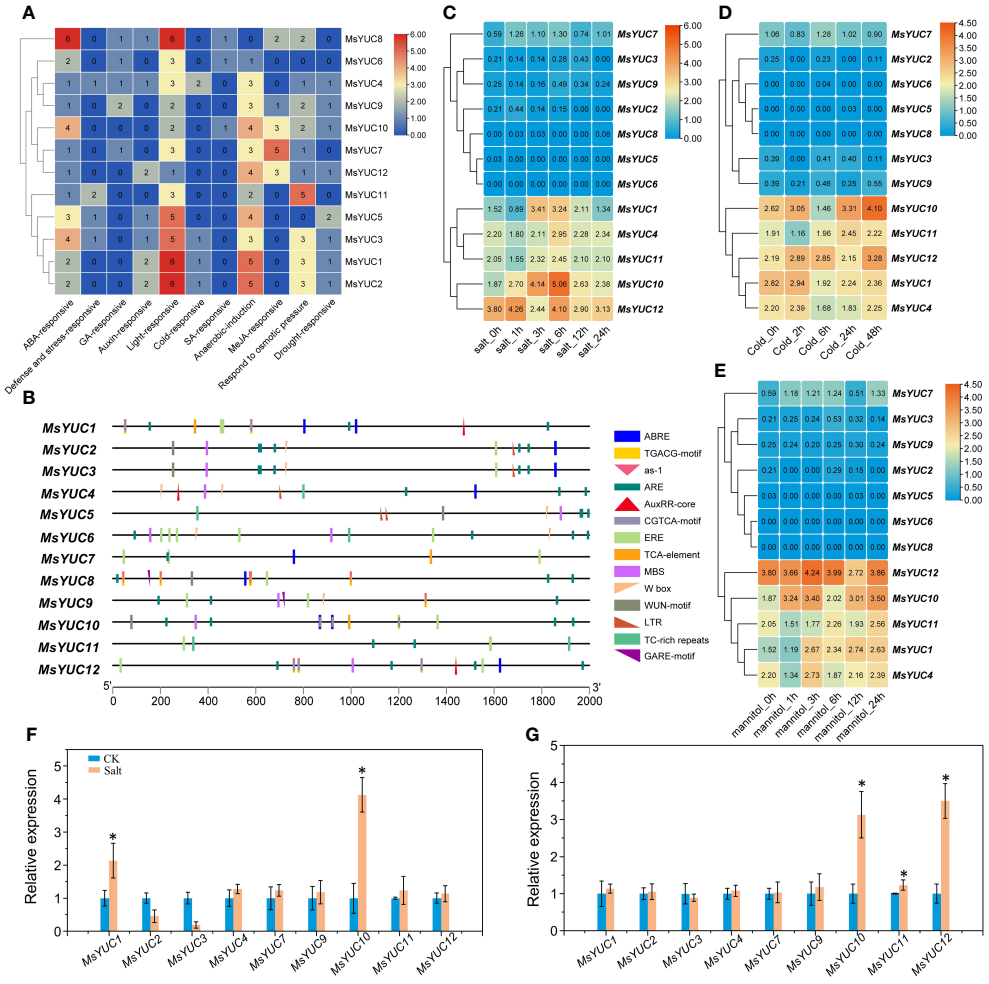

FIGURE 5
Cis elements of *MsYUC* promoter prediction and expression analysis of *MsYUCs* under stress conditions. **(A)** Number of hormone and stress response-related elements of *MsYUCs*. **(B)** Main elements distributed in the promoter region of *MsYUC* genes. Expression of *MsYUC* genes under salt stress **(C)**, mannitol treatment **(D)**, and cold stress **(E)**. The color scale of the heatmap refers to the relative expression level. Relative expression of *MsYUCs* treated by NaCl **(F)** and cold **(G)** determined by RT-qPCR. Three replicates were designed for each sample, and *M. sativa* actin gene expression was used for data normalization. Value represents mean ± *SD* of three replicates. * indicated significant different from untreated control (CK) plants ($p < 0.05$, one-way ANOVA).

proteins, indicating that YUC proteins underwent an evolutionary divergence, as that there are missing or duplication of YUCs during evolution. (Figure 1). In addition, Ka/Ks was used to evaluate their specific positions under positive selection pressure after duplication (Lynch and Conery, 2000; Mayrose et al., 2007). In this study, the Ka/Ks value of each duplication gene pair of YUCs of *Medicago* for all gene pairs was less than 1 (Table S3), which suggested that these genes had evolved under strong purifying selection. Since the divergence time of the Papilionoideae subfamily, which includes the genus *Medicago*, was approximately 34–63.7 millions of years (MYA) (Wang et al., 2023), the evolutionary divergence time of homologous gene pairs *MsYUC4/10* and *MtYUC1/8* was derived from the formation period of Papilionoideae subfamily. Because of the importance of *M. sativa* with high yield, nutrient value, and palatability, the mechanisms regulating its growth are of significant interest (Yamamoto et al., 2007). Functional orthologs of *YUC* genes in model species can provide insight into the functions in *Medicago* (Wei and Gai, 2008). MtYUC2 showed a close relationship with AtYUC1 and AtYUC4 (Figure 2), which have been reported to play vital roles in the formation of floral organs and vascular tissues in *Arabidopsis* (Cheng et al., 2006). However, the *Arabidopsis* AtYUC1 and AtYUC4 had no corresponding homologs in the *M. sativa* genome. Moreover, some YUCs of *M. sativa* had no homologs in *Arabidopsis* or rice, indicating that the gene loss event may have occurred after species divergence (Figure 1; Table S2).

In *Arabidopsis*, the roots and shoots appear to use two separate sets of *YUC* genes for auxin biosynthesis: ER-located YUCs functioning in roots or cytoplasmic-located YUCs functioning in shoots (Kriechbaumer et al., 2015). Phylogenetic tree analysis showed that *AtYUC3, 5, 7, 8*, and *9*, which were reported to function in roots with ER location, clustered in clade I-1 (Kriechbaumer et al., 2015). *MsYUC4* and *MsYUC10*, closely related to *AtYUC5, 8, 9*, also showed a predicted cytoplasmic location (Table 1). In *M. sativa*, *MsYUCs* also showed different expression patterns in different tissues. For example, *MsYUC10*,

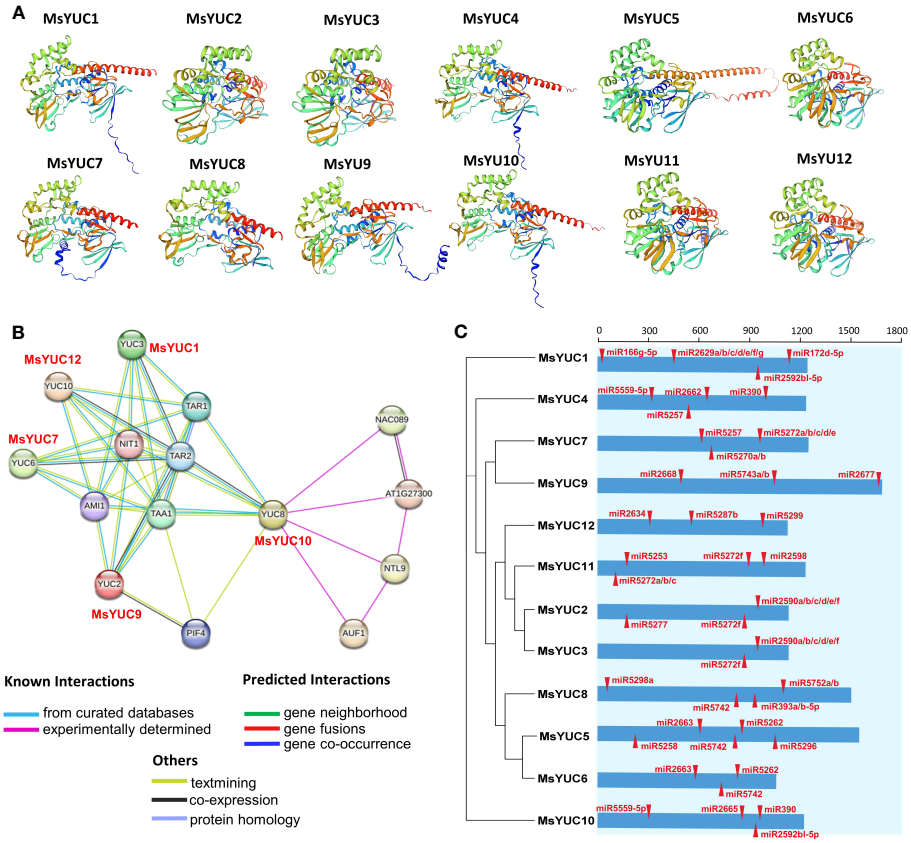

FIGURE 6
Predicted protein interaction network of MsYUC proteins and miRNA target sites in *MsYUC* genes. **(A)** Protein structure prediction of MsYUCs. **(B)** Protein interaction network predicted using MsYUC orthologs from *Arabidopsis*. **(C)** Predicted miRNA targets in the *MsYUC* coding sequence. The red tangles represent the miRNA-targeted *MsYUC* sites.

MsYUC12, and *MsYUC2* had relatively higher expression levels in specific tissues examined and *MsYUC2* had a higher expression level in leaves than in other tissues (Figure 4A). *MsYUC9*, closely related to *AtYUC2*, which was reported to function in shoots, was expressed not only in the shoots but also in roots of *M. sativa*. *MsYUC12*, with no homologous genes in *Arabidopsis*, showed higher expression levels in all tissues and was inferred to have universal roles during plant growth and development (Figure 5A). Therefore, in contrast to *AtYUC* expression, *MsYUC* expression does not seem to be clearly divided into shoot or root independent expression, suggesting a specificity in *M. sativa* compared with *Arabidopsis*.

The IPA-dependent pathway also plays an important role in integrating environmental stress and hormone signaling, and YUCs were reported to be involved in environmental stress response (Blakeslee et al., 2019). Cis-acting elements on the *MsYUCs*' promoter revealed a variety of stress response elements related to hormone such as Auxin-, ABA-, JA-, GA-, and SA-responsive elements in the promoters of certain *MsYUC* genes (Figure 5A). In *Arabidopsis*, ABA can inhibit the transcription of *YUC2/8* via ABI4, thereby inhibiting primary root elongation (Yu et al., 2014). JA has been reported to promote lateral root growth through a direct regulation of *YUC2* by transcription factor ERF109 (Cai et al., 2014). JA also directly activates YUC8/9-dependent auxin biosynthesis to function in mechanical wounding response (Perez-Alonso et al., 2021). In *M. sativa*, six ABRE elements were found in the promoter of *MsYUC8* and five JA response elements were found in the promoter of *MsYUC7*, respectively. In addition, MsYUC7 showed a closer relationship with AtYUC2, implying a similar function in JA response. In *Arabidopsis*, expression levels of *YUC7, 9, 10*, and *11* were upregulated under dehydration conditions (Shi et al., 2014). Activation of *YUC7* enhances drought resistance in *Arabidopsis* (Lee et al., 2012). Overexpressed *YUC6* of *Arabidopsis* in potato and poplar plants or overexpressed *BnaYUC6a* in *Arabidopsis* and oilseed rape showed typical auxin overproduction alternation and conferred high drought resistance (Kim et al., 2012; Ke et al., 2015; Hao et al., 2022). Since *MsYUC11*, which is closely related to *AtYUC6*, had a five-element response to osmotic stress but no drought response elements, suggesting a function differentiation among species (Figure 5A).

YUC expression was also reported to be affected by cold stress. For example, cucumber *CsYUC10b* was upregulated by cold stress whereas other *CsYUCs* were downregulated (Yan et al., 2016). In the hypocotyl, the PIF4-YUC8 regulatory module plays an important role in response to stress signals, including light stress. The accumulation and transcriptional activity of PIF4 are regulated by different proteins, with competition for and interference at the *AtYUC8* promoter by other transcription factors affecting the positive regulation of *AtYUC8*

by PIF4 and consequently affecting biosynthesis of auxin (Ma et al., 2016). In this study, all the *MsYUC* promoters had light-response elements. *MsYUC1, 2*, and *8* promoters had the most light-response elements, whereas the *MsYUC12* promoter had the least light-response element (Figure 5A). MsYUC10 was further predicted to interact with PIF4, indicating a similar function with AtYUC8 in light response (Figure 6B). Transcription factor AGL21 positively regulates *AtYUC5/8* which could be induced by IAA/ABA/JA and a variety of stresses, including salt stress (Yu et al., 2014). MsYUC1 and MsYUC10, which were clustered in the same sub-clade with AtYUC3/5/7/8/9, showed a significantly salt-induced expression (I-1), indicating a salt-response function in *M. sativa* (Figure 5F). The promoter of *MsYUC1, 2*, and *3* contained one cis-acting element (LTR) involved in low-temperature responsiveness, respectively (Figure 5A). Cold stress significantly elevated the expression of *MsYUC10* and *MsYUC12*, indicating an LTR-independent cold stress response function (Figure 6B). Moreover, *MsYUC10* and *MsYUC12* showed a higher expression level in 95-608 compared with other genotypes. Therefore, the stress tolerance of 95-608 should be further compared with other varieties. Studies indicate that miRNA-directed regulation of transcription factors may also play key roles in the precise regulation of IPA-dependent auxin biosynthesis in plants (Luo and Di, 2023). In this study, all *MsYUCs* contained at least three predicted targets for miRNA, suggesting a miRNA-directed regulation of *YUC* in *M. sativa* (Figure 6C).

5 Conclusion

In this study, the YUCs of *M. sativa* and *M. truncatula* were identified on a genome-wide scale. The phylogenetic analysis and comparative syntenic maps of *M. sativa* with other species illustrated their evolution relationship. The tissue and genotype-specific expression and abiotic stress response profiles have also been analyzed to reveal potential functional *YUC* genes. Moreover, RT-qPCR verified that certain *MsYUC* members represented salt or cold stress-affected expression patterns. Results in this study could provide valuable information for functional analysis and for the underlying regulation mechanism study of a specific *MsYUC* gene of *M. sativa*, especially under different tissues and various abiotic stresses through modification of the auxin synthetic IPA pathway in *Medicago*.

Data availability statement

The original contributions presented in the study are included in the article/Supplementary Material. Further inquiries can be directed to the corresponding authors.

Author contributions

AS: Conceptualization, Data curation, Methodology, Writing – original draft. SF: Methodology, Software, Writing – original draft. XX: Validation, Investigation, Writing – review & editing. WW: Funding acquisition, Resources, Writing – review & editing. JF: Project administration, Supervision, Writing – review & editing.

Funding

The author(s) declare financial support was received for the research, authorship, and/or publication of this article. This work was supported by grants from the National Natural Science Foundation of China (No. 32001389) and the Natural Science Foundation of Shandong Province, China (No. ZR2020QC186).

Acknowledgments

We thank the National Natural Science Foundation of China and the Natural Science Foundation of Shandong Province for the financial support.

Conflict of interest

The authors declare that the research was conducted in the absence of any commercial or financial relationships that could be construed as a potential conflict of interest.

Publisher's note

Supplementary material

The Supplementary Material for this article can be found online at: https://www.frontiersin.org/articles/10.3389/fpls.2023.1268027/full#supplementary-material

References

An, Y., Song, L., Liu, Y., Shu, Y., and Guo, C. (2016). *De novo* transcriptional analysis of alfalfa in response to saline-alkaline stress. *Front. Plant Sci.* 7. doi: 10.3389/fpls.2016.00931

Blakeslee, J. J., Tatiana, S. R., and Verena, K. (2019). Auxin biosynthesis: spatial regulation and adaptation to stress. *J. Exp. Bot.* 70, 5041–5049. doi: 10.1093/jxb/erz283

Bustin, S. A., Benes, V., Garson, J. A., Hellemans, J., Huggett, J., Kubista, M., et al. (2009). The MIQE Guidelines: Minimum information for publication of Quantitative Real-Time PCR experiments. *Clin. Chem.* 55, 611–622. doi: 10.1373/clinchem.2008.112797

Cai, X. T., Xu, P., Zhao, P. X., Liu, R., Yu, L. H., and Xiang, C. B. (2014). *Arabidopsis* ERF109 mediates cross-talk between jasmonic acid and auxin biosynthesis during lateral root formation. *Nat. Commun.* 5, 5833. doi: 10.1038/ncomms6833

Cha, J. Y., Kim, W. Y., Kang, S. B., Kim, J. I., Baek, D., Jung, I. J., et al. (2015). A novel thiol-reductase activity of *Arabidopsis* YUC6 confers drought tolerance independently of auxin bio-synthesis. *Nat. Commun.* 6, 8041. doi: 10.1038/ncomms9041

Chen, C., Chen, H., Zhang, Y., Thomas, H. R., Frank, M. H., He, Y., et al. (2020). TBtools: An integrative toolkit developed for interactive analyses of big biological data. *Mol. Plant* 13, 1194–1202. doi: 10.1016/j.molp.2020.06.009

Chen, Q., Dai, X., De-Paoli, H., Cheng, Y., Takebayashi, Y., Kasahara, H., et al. (2014). Auxin overproduction in shoots cannot rescue auxin deficiencies in *Arabidopsis* roots. *Plant Cell Physiol.* 55, 1072–1079. doi: 10.1093/pcp/pcu039

Cheng, Y., Dai, X., and Zhao, Y. (2006). Auxin biosynthesis by the YUCCA flavin monooxygenases controls the formation of floral organs and vascular tissues in *Arabidopsis*. *Genes Dev.* 20, 1790–1799. doi: 10.1101/gad.1415106

Dai, X., Zhuang, Z., and Zhao, P. X. (2018). psRNATarget: A plant small RNA target analysis server. *Nucleic Acids Res.* 46, 49–54. doi: 10.1093/nar/gkr319

Defez, R., Andreozzi, A., Dickinson, M., Charlton, A., Tadini, L., Pesaresi, P., et al. (2017). Improved drought stress response in alfalfa plants modulated by an IAA over-producing rhizobium strain. *Front. Microbiol.* 8. doi: 10.3389/fmicb.2017.02466

Du, H., Wu, N., Chang, Y., Li, X., Xiao, J., and Xiong, L. (2013). Carotenoid deficiency impairs ABA and IAA biosynthesis and deferentially affects drought and cold tolerance in rice. *Plant Mol. Biol.* 83, 475–488. doi: 10.1007/s11103-013-0103-7

Fraaije, M. W., Kamerbeek, N. M., van, Berkel, W. J., and Janssen, D. B. (2002). Identification of a Baeyer-Villiger monooxygenase sequence motif. *FEBS Lett.* 518, 43–47. doi: 10.1016/080394898422544

Hao, M., Wang, W., Liu, J., Wang, H., Zhou, R., Mei, D., et al. (2022). Auxin biosynthesis genes in allotetraploid oilseed rape are essential for plant development and response to drought stress. *Int. J. Mol. Sci.* 23, 15600. doi: 10.3390/ijms232415600

Ke, Q., Baek, D., Park, H. C., Chun, H. J., Oh, D., Lee, M. K., et al. (2015). Transgenic poplar expressing *Arabidopsis YUCCA6* exhibits auxin-overproduction phenotypes and increased tolerance to abiotic stress. *Plant Physiol. Biochem.* 94, 19–27. doi: 10.1016/j.plaphy.2015.05.003

Kim, J. I., Baek, D., Park, H. C., Chun, H. J., Oh, D. H., Lee, M. K., et al. (2012). Overexpression of *Arabidopsis YUCCA6* in potato results in high-auxin developmental phenotypes and enhanced resistance to water deficit. *Mol. Plant* 6, 337–349. doi: 10.1093/mp/sss100

Kriechbaumer, V., Seo, H., Park, W. J., and Hawes, C. (2015). Endoplasmic reticulum localization and activity of maize auxin biosynthetic enzymes. *J. Exp. Bot.* 66, 6009–6020. doi: 10.1093/jxb/erv314

Larkin, M. A., Blackshields, G., Brown, N. P., Chenna, R., McGettigan, P. A., McWilliam, H., et al. (2007). Clustal W and clustal X version 2.0. *Bioinformatics* 23, 2947–2948. doi: 10.1093/bioinformatics/btm404

Lee, M., Jung, J. H., Han, D. Y., Seo, P. J., Park, W. J., and Park, C. M. (2012). Activation of a flavin monooxygenase gene *YUCCA7* enhances drought resistance in. *Arabidopsis. Planta* 235, 923–938. doi: 10.1007/s00425-011-1552-3

Lei, Y., Xu, Y., Hettenhausen, C., Lu, C., Shen, G., Zhang, C., et al. (2018). Comparative analysis of alfalfa (*Medicago sativa* L.) leaf transcriptomes reveals genotype specific salt tolerance mechanisms. *BMC Plant Biol.* 18, 35. doi: 10.1186/s12870-018-1250-4

Li, X. H., and Brummer, E. C. (2012). Applied genetics and genomics in alfalfa breeding. *Agronomy* 2, 40–61. doi: 10.3390/agronomy2010040

Li, X., Wei, Y., Moore, K. J., Michaud, R., Viands, D. R., Hansen, J. L., et al. (2011). Association mapping of biomass yield and stem composition in a tetraploid alfalfa breeding population. *Plant Genome* 4, 24–35. doi: 10.3835/plantgenome2010.09.0022

Li, W., Zhao, X., and Zhang, X. (2015). Genome-wide analysis and expression patterns of the *YUCCA* genes in maize. *J. Genet. Genomics* 42, 707–710. doi: 10.1016/j.jgg.2015.06.010

Liu, G., Gao, S., Tian, H., Wu, W., Robert, H. S., and Ding, Z. (2016). Local transcriptional control of YUCCA regulates auxin promoted root-growth inhibition in response to aluminium stress in *Arabidopsis*. *PloS Genet.* 12, e1006360. doi: 10.1371/journal.pgen.1006360

Liu, H., Xie, W. F., Zhang, L., Ye, Z. W., Gao, Q. H., and Duan, K. (2014). Auxin biosynthesis by the *YUCCA6* flavin monooxygenase gene in woodland strawberry. *J. Integr. Plant Biol.* 56, 350–363. doi: 10.1111/jipb.12150

Luo, P., and Di, D. W. (2023). Precise regulation of the TAA1/TAR-YUCCA auxin biosynthesis pathway in plants. *Int. J. Mol. Sci.* 24, 8514 doi: 10.3390/ijms24108514

Luo, D., Zhou, Q., Wu, Y., Chai, X., Liu, W., Wang, Y., et al. (2019). Full-length transcript sequencing and comparative transcriptomic analysis to evaluate the contribution of osmotic and ionic stress components towards salinity tolerance in the roots of cultivated alfalfa (*Medicago Sativa* L.). *BMC Plant Biolo.* 19, 32. doi: 10.1186/s12870-019-1630-4

Lynch, M., and Conery, J. (2000). The evolutionary fate and consequences of duplicate genes. *Science* 290, 1151–1155. doi: 10.1126/science.290.5494.1151

Ma, D., Li, X., Guo, Y., Chu, J., Fang, S., Yan, C., et al. (2016). Cryptochrome 1 interacts with PIF4 to regulate high temperature-mediated hypocotyl elongation in response to blue light. *Proc. Natl. Acad. Sci. U.S.A.* 113, 224–229. doi: 10.1073/pnas.1511437113

Ma, Q., Xu, X., Wang, W., Zhao, L., Ma, D., and Xie, Y. (2021). Comparative analysis of alfalfa (*Medicago sativa* L.) seedling transcriptomes reveals genotype-specific drought tolerance mechanisms. *Plant Physiol. Biochem.* 166, 203–214. doi: 10.21203/rs.3.rs-75482/v1

Maere, S., De Bodt, S., Raes, J., Casneuf, T., Van Montagu, M., Kuiper, M., et al. (2005). Modeling gene and genome duplications in eukaryotes. *Proc. Natl. Acad. Sci. U.S.A.* 102, 5454–5459. doi: 10.1073/pnas.0501102102

Mashiguchi, K., Tanaka, K., Sakai, T., Sugawara, S., Kawaide, H., Natsume, M., et al. (2011). The main auxin biosynthesis pathway in *Arabidopsis*. *Proc. Natl. Acad. Sci. U.S.A.* 108, 18512–18517. doi: 10.1073/pnas.1108434108

Mayrose, I., Doron-Faigenboim, A., Bacharach, E., and Pupko, T. (2007). Towards realistic codon models: among site variability and dependency of synonymous and nonsynonymous rates. *Bioinformatics* 23, 319–327. doi: 10.1093/bioinformatics/btm176

Moore, R. C., and Purugganan, M. D. (2003). The early stages of duplicate gene evolution. *Proc. Natl. Acad. Sci. U.S.A.* 100, 15682–15687. doi: 10.1073/pnas.2535513100

Naser, V., and Shani, E. (2016). Auxin response under osmotic stress. *Plant Mol. Biol.* 91, 661–672. doi: 10.1007/s11103-016-0476-5

Pain, C., Kriechbaumer, V., Kittelmann, M., Hawes, C., and Fricker, M. (2019). Quantitative analysis of plant ER architecture and dynamics. *Nat. Commun.* 10, 984. doi: 10.1038/s41467-019-08893-9

Perez-Alonso, M. M., Sanchez-Parra, B., Ortiz-Garcia, P., Santamaria, M. E., Diaz, I., and Pollmann, S. (2021). Jasmonic acid-dependent MYC transcription factors bind to a tandem G-box motif in the *YUCCA8* and *YUCCA9* promoters to regulate biotic stress responses. *Int. J. Mol. Sci.* 22, 9768. doi: 10.20944/preprints202107.0142.v1

Postnikova, O. A., Shao, J., and Nemchinov, L. G. (2013). Analysis of the alfalfa root transcriptome in response to salinity stress. *Plant Cell Physiol.* 54, 1041–1055. doi: 10.1093/pcp/pct056

Schmittgen, T. D., and Livak, K. J. (2008). Analyzing real-time PCR data by the comparative C(T) method. *Nat. Protoc.* 3, 1101–1108. doi: 10.1038/nprot.2008.73

Shi, H., Chen, L., Ye, T., Liu, X., Ding, K., and Chan, Z. (2014). Modulation of auxin content in *Arabidopsis* confers improved drought stress resistance. *Plant Physiol. Biochem.* 82, 209–217. doi: 10.1016/j.plaphy.2014.06.008

Stepanova, A. N., Yun, J., Robles, L. M., Novak, O., He, W., Guo, H., et al. (2011). The *Arabidopsis* YUCCA1 flavin monooxygenase functions in the indole-3-pyruvic acid branch of auxin biosynthesis. *Plant Cell* 23, 3961–3973. doi: 10.1105/tpc.111.088047

Sun, J., Qi, L., Li, Y., Chu, J., and Li, C. (2012). PIF4-mediated activation of *YUCCA8* expression integrates temperature into the auxin pathway in regulating *Arabidopsis* hypocotyl growth. *PloS Genet.* 8, e1002594. doi: 10.1371/journal.pgen.1002594

Tamura, K., Stecher, G., Peterson, D., Filipski, A., and Kumar, S. (2013). MEGA6: Molecular evolutionary genetics analysis version 6.0. *Mol. Biol. Evol.* 30, 2725–2729. doi: 10.1093/molbev/mst197

Wang, Y. G., Liu, H. H., Wang, S. P., and Li, H. G. (2017). Genome-wide identification and expression analysis of the *YUCCA* gene family in soybean (*Glycine max* L.). *Plant Growth Regul.* 81, 265–275. doi: 10.1007/s10725-016-0203-x

Wang, Y., Ruan, Q., Zhu, X., Wang, B., Wei, B., and Wei, X. (2023). Identification of Alfalfa SPL gene family and expression analysis under biotic and abiotic stresses. *Sci. Rep.* 13, 84. doi: 10.1038/s41598-022-26911-7

Wei, Z. W., and Gai, J. Y. (2008). Model legume: *Medicago truncatula*. *Acta Prataculturae Sin.* 17, 114–120. doi: 10.1007/s10499-007-9164-4

Won, C., Shen, X., Mashiguchi, K., Zheng, Z., Dai, X., Cheng, Y., et al. (2011). Conversion of tryptophan to indole-3-acetic acid by TRYPTOPHAN AMINOTRANSFERASES OF *ARABIDOPSIS* and YUCCAs in *Arabidopsis*. *Proc. Natl. Acad. Sci. U.S.A.* 108, 18518–18523. doi: 10.1073/pnas.1108436108

Yamamoto, Y., Kamiya, N., Morinaka, Y., Matsuoka, M., and Sazuka, T. (2007). Auxin biosynthesis by the *YUCCA* genes in rice. *Plant Physiol.* 143, 1362–1371. doi: 10.1104/PP.106.091561

Yan, S., Che, G., Ding, L., Chen, Z., and Zhang, X. (2016). Different cucumber *CsYUC* genes regulate response to abiotic stresses and flower development. *Sci. Rep.* 6, 20760. doi: 10.1038/srep20760

Yang, Y., Xu, T., Wang, H., and Feng, D. (2012). Genome-wide identification and expression analysis of the TaYUCCA gene family in wheat. *Mol. Biol. Rep.* 48, 1–11. doi: 10.1007/s11033-021-06197-0

Yu, C. S., Lin, C. J., and Hwang, J. K. (2010). Predicting subcellular localization of proteins for Gramnegative bacteria by support vector machines based on n-peptide compositions. *Protein Sci.* 13, 1402–1406. doi: 10.1110/ps.03479604

Yu, L. H., Miao, Z. Q., Qi, G. F., Wu, J., Cai, X. T., Mao, J. L., et al. (2014). MADS-box transcription factor AGL21 regulates lateral root development and responds to multiple external and physiological signals. *Mol. Plant* 7, 1653–1669. doi: 10.1093/mp/ssu088

Zhang, Z., Li, J., Zhao, X. Q., Wang, J., Wong, K. S., and Yu, J. (2006). KaKs_Calculator: Calculating Ka and Ks through model selection and model averaging. *Genom. Proteom. Bioinf.* 4, 259–263. doi: 10.1016/S1672-0229(07) 60007-2

Zhao, Y. (2010). Auxin biosynthesis and its role in plant development. *Annu. Rev. Plant Biol.* 61, 49–64. doi: 10.1146/annurev-arplant-042809-112308

Zhao, Y. (2012). Auxin biosynthesis: a simple two-step pathway converts tryptophan to indole-3-acetic acid in plants. *Mol. Plant* 5, 334–338. doi: 10.1093/mp/ssr104

Zhao, Y. (2018). Essential roles of local auxin biosynthesis in plant development and in adaptation to environmental changes. *Annu. Rev. Plant Biol.* 69, 417–435. doi: 10.1146/annurev-arplant-042817-040226

Zhao, Y., Christensen, S. K., Fankhauser, C., Cashman, J. R., Cohen, J. D., Weigel, D., et al. (2001). A role for flavin monooxygenase- like enzymes in auxin biosynthesis. *Science* 291, 306–309. doi: 10.1126/science.291.5502.306

Zhou, Q., Luo, D., Chai, X., Wu, Y., Wang, Y., Nan, Z., et al. (2018). Multiple regulatory networks are activated during cold stress in *Medicago sativa* L. *Int. J. Mol. Sci.* 19, 469. doi: 10.3390/ijms19103169

frontiers | Frontiers in Plant Science

TYPE Original Research
PUBLISHED 14 September 2023
DOI 10.3389/fpls.2023.1258498

OPEN ACCESS

EDITED BY
Hui Song,
Qingdao Agricultural University, China

REVIEWED BY
Yan Xie,
Chinese Academy of Sciences (CAS), China
Rui Dong,
Guizhou University, China

*CORRESPONDENCE
ShuGao Fan
fanshugao2006@126.com

†These authors have contributed equally to this work

RECEIVED 14 July 2023
ACCEPTED 28 August 2023
PUBLISHED 14 September 2023

CITATION
Yin YL, Yang TH, Li S, Li X, Wang W and Fan SG (2023) Transcriptomic analysis reveals that methyl jasmonate confers salt tolerance in alfalfa by regulating antioxidant activity and ion homeostasis. *Front. Plant Sci.* 14:1258498. doi: 10.3389/fpls.2023.1258498

Transcriptomic analysis reveals that methyl jasmonate confers salt tolerance in alfalfa by regulating antioxidant activity and ion homeostasis

YanLing Yin[1†], TianHui Yang[1,2†], Shuang Li[1], Xiaoning Li[1], Wei Wang[1] and ShuGao Fan[1*]

[1]School of Resources and Environmental Engineering, Ludong University, Yantai, Shandong, China, [2]Institute of Animal Science, Ningxia Academy of Agriculture and Forestry Sciences, Yinchuan, China

Introduction: Alfalfa, a globally cultivated forage crop, faces significant challenges due to its vulnerability to salt stress. Jasmonates (JAs) play a pivotal role in modulating both plant growth and response to stressors.

Methods: In this study, alfalfa plants were subjected to 150 mM NaCl with or without methyl jasmonate (MeJA). The physiological parameters were detected and a transcriptomic analysis was performed to elucidate the mechanisms underlying MeJA-mediated salt tolerance in alfalfa.

Results: Results showed that exogenous MeJA regulated alfalfa seed germination and primary root growth in a dose-dependent manner, with 5μM MeJA exerting the most efficient in enhancing salt tolerance. MeJA at this concentration elavated the salt tolerance of young alfalfa seedlings by refining plant growth, enhancing antioxidant capacity and ameliorating Na+ overaccumulation. Subsequent transcriptomic analysis identified genes differentially regulated by MeJA+NaCl treatment and NaCl alone. PageMan analysis revealed several significantly enriched categories altered by MeJA+NaCl treatment, compared with NaCl treatment alone, including genes involved in secondary metabolism, glutathione-based redox regulation, cell cycle, transcription factors (TFs), and other signal transductions (such as calcium and ROS). Further weighted gene co-expression network analysis (WGCNA) uncovered that turquoise and yellow gene modules were tightly linked to antioxidant enzymes activity and ion content, respectively. Pyruvate decar-boxylase (PDC) and RNA demethylase (ALKBH10B) were identified as the most central hub genes in these two modules. Also, some TFs-hub genes were identified by WGCNA in these two modules highly positive-related to antioxidant enzymes activity and ion content.

Discussion: MeJA triggered a large-scale transcriptomic remodeling, which might be mediated by transcriptional regulation through TFs or post-transcriptional regulation through demethylation. Our findings contributed new perspectives for understanding the underneath mechanisms by which JA-mediated salt tolerance in alfalfa.

KEYWORDS

MeJA, salt tolerance, antioxidant capacity, ion homeostasis, *Medicago sativa*

Introduction

Soil salinization is progressively becoming a detrimental constraint on plant growth and productivity (Singh, 2021). It is estimated that over 20% of irrigated land is currently influenced by salinity, and this is expected to persistently expand due to warming temperatures, irrigation practices, and soil degradation (Sahab et al., 2021). Among the different types of soil salts, NaCl is the most soluble and common. High levels of Na^+ in the rhizosphere can cause detrimental effects on plants, leading to photosynthetic inhibition, enzyme deactivation, and metabolic alterations (Yang and Guo, 2018). These changes are the results of disruption in plant–water balance (osmotic stress), redox, and ionic homeostasis (Van Zelm et al., 2020). Moreover, to cope with stressful conditions, plants undergo growth and developmental arrest and prioritize defense responses, resulting in physiological and developmental alterations (Lozano-Durán and Zipfel, 2015).

Plants are sessile, rendering them incapable of escaping the environmental salinity. Therefore, they must adopt strategies to confront the adverse consequences of salt stress by modifying their physical attributes and developmental patterns (Heydarian et al., 2018; Nefissi Ouertani et al., 2021). Plant response to salt stress is a temporally and spatially separated two-phase pattern, comprising earlier osmotic stress response and the late ion toxicity response (Munns and Tester, 2008; Yang et al., 2019; Van Zelm et al., 2020). When plants are subjected to salt stress, Ca^{2+} is stimulated as the initial signal molecule (Yang et al., 2019). Elevation in intracellular Ca^{2+} level triggers the expression of genes encoding Ca^{2+} sensors including calmodulin (CaM), CaM-like protein (CML), calcineurin B-like protein (CBL), and calcium-dependent protein kinase (CDPK) (Wang et al., 2018; Yue et al., 2022). Subsequently, genes related to osmoregulation, antioxidants, and ion exclusion/sequestration responded to salt stimuli. Decreased osmotic pressure under salt stress reduces water availability, ultimately inducing osmotic stress (Van Zelm et al., 2020). Plants synthesize osmolytes like proline, soluble sugars, and organic acids, which serve to uphold cellular volume and turgor (Flowers and Yeo, 1995). Genes related to proline biosynthesis, such as *P5CS*, have been documented to be triggered by salt stress. Overexpressed *PvP5CS* in switchgrass led to an enhancement in plant salt tolerance (Silva-Ortega et al., 2008; Guan et al., 2020). Salt stress triggers the expression of genes encoding ion transporters such as salt overly sensitive (SOS), Na^+/H^+ exchanger (NHX), and high-affinity Na^+/K^+-permeable transporter (HKT) (Hauser and Horie, 2010). These transporters are responsible for transferring Na^+ and K^+, thus maintaining ionic balance, as well as reducing the Na^+ accumulation (Saddhe et al., 2021). Reactive oxygen species (ROS) burst happens when the cells suffer from osmotic stress or ion toxicity, causing oxidative damage. ROS, including hydrogen peroxide (H_2O_2), superoxide anion (O^{2-}), and hydroxy radical (OH^-) accumulated in apoplast and organelle rapidly under salt stress, disturbing the balance of cell redox homeostasis (Miller et al., 2010). Subsequently, the antioxidant systems are activated to reduce the production or induce the scavenging of ROS (He et al., 2017). ROS scavenging enzymes, such as superoxide dismutase (SOD), peroxidase (POD), and catalase (CAT), are triggered under salt stress (Singh et al., 2022). Moreover, non-enzymatic antioxidants such as ascorbic acid (ASA), glutathione (GSH), and carotene accumulate under salt stress to quench the ROS (Ahmad et al., 2019). Moreover, MAPK cascades and some second messengers are engaged in mitigating the adverse effects of salt stress (Wei et al., 2022). Many salt stress-responsive transcription factors (TFs; e.g., WRKYs, NACs, and MYBs) are induced by stress to govern the transcription of specific target genes through their interaction with promoter regions (Shah et al., 2021).

Changes in phytohormone levels are downstream signals that significantly contribute to salt stress resistance (Peleg and Blumwald, 2011). The regulation in biosynthesis, metabolism, and signal transduction of phytohormones also leads to the alteration of gene expression levels related to plant salt-adaptive response (Yu et al., 2020). Jasmonates (JAs) including jasmonic acid (JA) and its offshoots such as methyl jasmonate (MeJA) are derivatives of oxidized fatty acids and act as ubiquitous regulators in plant growth and defense (Ali and Baek, 2020). Previous studies have intensively demonstrated the roles of JAs in plant immune responses to pathogens and insects (Du et al., 2017). Moreover, JAs also have attracted attention as protectors against abiotic stress (Ali and Baek, 2020). However, the functions of JAs in salt stress responses remain unclear and even controversial. Many transcriptomic analyses have indeed corroborated the upregulation of genes associated with JA biosynthesis in salt-stressed roots (Jiang and Deyholos, 2006; Geng et al., 2013). Physiology and biochemistry studies documented that the endogenous JA was accumulated under salt stress in tomato (Pedranzani et al., 2013), sweet potato (Zhang et al., 2017), and wheat (Zhu et al., 2022). Exogenous application of JAs significantly mitigated the salt-stressed symptoms in *Triticum aestivum* (Qiu et al., 2014), *Vitis vinifera* (Karimi et al., 2022), and *Nitraria tangutorum* (Gao et al., 2021). Deficiency in A biosynthesis decreased the salt tolerance of maize shoots (Ahmad et al., 2019) and tomato (Abouelsaad and Renault, 2018). Furthermore, overexpression of JA biosynthesis genes of rice in tobacco effectually promoted its salt tolerance (Asfaw et al., 2022). These findings confirmed the beneficial regulatory functions of JA in enhancing plant resilience to salt stress. Furthermore, it has been revealed that JA-improved salt tolerance was involved in the enhancement of antioxidant ability (Gao et al., 2021), rebuilding of ion homeostasis (Ahmad et al., 2019), and striking a balance between plant growth and resistance (Gao et al., 2021). However, mutation of the JA biosynthetic enzyme, ALLENE OXIDE CYCLASE (AOC) in rice, which showed reduced endogenous JA content, enhanced salt tolerance (Hazman et al., 2015). Similarly, overexpression of the master TF of JA signal, MYC2, weakened the salt resilience of *Arabidopsis* by repressing the transcription of *CAT2* (Song et al., 2021). These investigations suggest that JA participates in the salt stress responses in a positive or negative manner for different species. The underlying mechanisms of JA-mediated salt tolerance need further research.

Alfalfa is a worldwide cultivated forage and is famous for its high value in forage quality and ecological protection. Like most crop plants, alfalfa is a glycophyte with neutral salt tolerance (Singer et al., 2018). Alfalfa plants challenged by severe salt stress show decreases in both root and shoot growth, as well as nutritional value (Stritzler et al., 2018). Exploring the regulatory framework linked to salt stress in alfalfa holds significant importance. Here, we hypothesize that the salt

stress responses of alfalfa are mediated by JAs. In this study, we detected the growth and physiological parameters of NaCl-stressed alfalfa with or without MeJA treatment and performed a genome-wide transcriptomic analysis to uncover the differentially expressed genes (DEGs) altered by MeJA and NaCl. Subsequently, we carried out PageMan analysis and weighted gene co-expression network analysis (WGCNA) to reveal the signaling pathways and hub genes regulated by MeJA. The results of this study will illuminate the molecular mechanisms by which JA mediated salt tolerance in alfalfa and provide the potential to offer novel avenues for enhancing the salt tolerance of this crop.

Materials and methods

Plant material and experimental design

Cultivated alfalfa "XinJiangDaYe" used in this research was obtained from the Ningxia Academy of Agriculture and Forestry Sciences. For the germination assay, 100 seeds were germinated in Petri dishes containing 0, 5, 10, 50, and 100 μM of MeJA with or without 150 mM of NaCl. The germination rate and root length were measured on the seventh day of post-treatment. For the young seedling treatments, 3-week-old young seedlings were transplanted into a half-strengthened Hoagland nutrient solution (Hoagland and Arnon, 1950). After adapting growth for 1 week, plants were exposed to 1/2 Hoagland nutrient solution with 5 μM of MeJA and 150 mM of NaCl separately or combined. Physiological parameter detections and transcriptomic analysis were performed after treatment for 24 h. Growth-related characteristics were determined after treatment for 1 week.

Measurement of plant height, root length, and plant biomass

Plant height was measured as the vertical distance from the cotyledonary node to the apical bud using a calibrated ruler. Root length was determined as the length from the tips of the longest root to the cotyledonary node. Fresh weight was measured using a non-destructive method. The entire plants were carefully harvested and separated for the shoot and root parts, with the cotyledon node serving as the demarcation point between these sections. Shoots and roots were washed three to five times using deionized water and dried with absorbent paper. The fresh weight of shoots and roots was then weighed using an electronic balance.

Detection of antioxidant enzyme activity

Crude enzymes were extracted from 0.1-g root samples in ice-cold phosphate buffer saline (PBS; pH 7.8, 50 mM) containing 0.2 mM of EDTA, 2 mM of L-ascorbic acid, and 2% (w/v) polyvinylpolypyrrolidone. The supernatant obtained through centrifugation was used to assess enzyme activity following the method outlined by Xia et al. (2009). SOD activity was measured by the reduction of nitroblue tetrazolium (NBT) by superoxide anions. CAT activity was determined by quantifying the rate of H_2O_2 decomposition. The enzyme activities were quantified by dividing the enzyme activity obtained by the corresponding protein concentration. The protein content in the supernatants was determined using a Bradford Protein Assay Kit (Sigma-Aldrich, Darmstadt, Germany).

Measurement of H_2O_2 and proline contents

H_2O_2 content was measured according to Willekens et al. (1997) with slight modifications. Briefly, a 0.1-g alfalfa root sample was homogenized utilizing 1 M of $HClO_4$. Subsequent to centrifugation at 6,000 *g* for 10 minutes, adjustment of the supernatant pH to the range of 6.0–7.0 was executed through the introduction of 4 M of KOH. Mixing equal volumes of the resulting supernatant with a reaction buffer containing 100 mM of potassium acetate (pH 4.4) and 1 mM of 2,2′-hydra-bis(3-ethylbenzothiazolin-6-sulfonic acid) ensued. The absorption at 412 nm was observed for both instances with the addition of POD enzyme and without it. The disparity in absorbance between these two conditions represented the H_2O_2 content. Precise quantification of H_2O_2 content was achieved by referencing a standard curve based on a gradient of H_2O_2 concentrations.

Proline content was detected based on a previously reported protocol with minor modification (Bates et al., 1973). Fresh root samples (0.1 g) were homogenized in 10 mL of 3% aqueous sulfosalicylic acid, and the homogenate was centrifuged at 10,000 *g* for 10 minutes. The supernatant (2 mL) was mixed with 2 mL of acid ninhydrin and 2 mL of glacial acetic acid, and the mixture was heated in a boiling water bath for 1 h. After cooling, the chromophore was extracted with 4 mL of toluene, and the absorbance of the organic layer was measured at 520 nm using a spectrophotometer. Proline concentration was calculated based on a standard curve generated using known concentrations of proline.

Quantification of Na^+ and K^+

Root and leaf samples were harvested and subjected to a three-times washing using deionized water. The samples were first heated to 105°C for 30 minutes to deactivate the enzymes, followed by a drying process at 75°C for 72 h. Dried samples at 0.1 g were prepared by digestion of plant tissues in a 5:1 mixture of nitric acid and perchloric acid (v/v). The crude extraction was filtered and then diluted to reach a final volume of 50 mL. The Na^+ and K^+ contents were measured using an atomic absorbance spectrophotometer equipped with a flame atomizer (Shimadzu, Kyoto, Japan; A6300).

Detection of chlorophyll *a* fluorescence transient curve

Rapid measurement of leaf chlorophyll fluorescence transient curves was performed using a plus-amplitude modulated fluorometer (PAM2500, Heinz Walz GmbH, Pfullingen, Germany).

After 1-week treatment, the third fully expanded leaves harvested from each treatment were subjected to a 30-minute dark adaptation. Then, a saturating pulse of light (3,500 mmol photons m^{-2} s^{-1}) was applied to the leaves to induce maximum fluorescence (Fm). The resulting chlorophyll fluorescence emission was measured and converted into digital format, with a time resolution ranging from 10 μs to 320 ms.

RNA isolation, cDNA library construction, and Illumina sequencing

Root samples of NaCl, MeJA (J), MeJA combined NaCl (MeJA +NaCl) treatments, and control (CK) were collected after treatment for 24 h. The total RNA was extracted using a Plant total RNA purification kit (GMbiolab Co., Ltd., Taiwan). The RNA purity and quantity were confirmed by Qubit 2.0 fluorometer, and the integrity was detected by 2100 Bioanalyzer (Agilent, Santa Clara, CA, USA).

An input material of 1 μg of RNA per sample was utilized for the preparation of RNA samples. Total mRNA was spliced randomly into short fragments of approximately 300 bp in the NEB Fragmentation Buffer. Random hexamer primers and M-MuLV Reverse Transcriptase (RNase H-) were employed to synthesize the first-strand cDNA using the short fragments as templates. Subsequently, second-strand cDNA was synthesized using DNA Polymerase I and RNase H. NEBNext adaptors with hairpin loop structure were ligated to the double-stranded cDNA fragments. Afterward, the library fragments were purified with the AMPure XP system (Beckman Coulter, Beverly, MA, USA) to obtain 250–300-bp cDNA fragments. The fragments were amplified by PCR and purified through AMPure XP beads to create the final library. The quality of the library was assessed, and the prepared cDNA library was then subjected to high-throughput sequencing on the Illumina sequencing platform by Metware Biotechnology Co., Ltd. (Wuhan, China).

Mapping reads to the reference genome and conducting analysis of expression levels

Quality filtering of raw reads was performed using FASTp. Adapter-containing reads and low-quality reads (Phred quality value < 20, containing poly-N) were removed to generate the clean reads. The subsequent analysis was performed based on clean reads. Then, the clean reads were mapped to the alfalfa XinJiangDaYe genome using HISAT version 2.1.0 with default parameters. The transcription level was estimated by FPKM (Fragments Per Kilobase of transcript per Million fragments mapped).

DEG identification and PageMan analysis

DEGs in the transcriptome data were identified through the utilization of the DESeq2 package (v1.22.1) within the R programming environment. Raw read counts were used as input data for the analysis. DEGs were identified using criteria where the absolute value of $\log_2$ (fold change (FC)) ≥ 1, and the false discovery rate (FDR) < 0.05.

Enrichment analysis of the DEGs was performed using the PageMan software (v3.0.0), which is a commonly used tool for functional analysis of large-scale omics data in plants. The $\log_2$ (FC) of NaCl vs. CK and that of NaCl+MeJA vs. CK were input into PageMan, and the significantly enriched BINs were identified using the Wilcoxon statistical test with default parameters provided by PageMan.

Weighted gene co-correlation network analysis

The construction of co-expression networks and the identification of modules comprising closely correlated genes were carried out using the WGCNA R package. A signed network was constructed using the normalized FPKM of DEGs. The dynamic Tree Cut algorithm was employed to establish modules, ensuring a minimum size of 30 genes for each module. Module eigengenes were calculated, and module–trait associations were tested using Pearson's correlation analysis with physiological trait data. The modules that exhibited the highest correlation coefficient with specific physiological traits at a significance level of $p < 0.05$ were selected to construct the co-expression network. Hub genes within the co-expression network were identified through topological overlap measures and were prioritized using module membership and gene significance.

qRT-PCR analysis

qRT-PCR was employed to validate the RNA-Seq data. Total RNA of 500 ng was reverse-transcribed into cDNA using a first-strand cDNA synthesis kit (Toyobo, Tokyo, Japan; FSQ-201). The expression levels of the eight hub genes were quantified by qRT-PCR using a real-time PCR system (StepOnePlus, Applied Biosystems, Foster City, CA, USA) and a SYBR green master mix (Takara, Mountain View, CA, USA). The relative expression levels of target genes were determined by the $2^{-\Delta\Delta Ct}$ method. The housekeeping gene *MsACTIN* was used as the internal control. Primers for specific genes are presented in Table S1. The experiment comprised three biological replicates for each treatment.

Statistical analysis

Statistical analysis was conducted using SPSS 20 software. A one-way ANOVA was performed to identify any significant differences among groups at a significance level of $p < 0.05$. *Post-hoc* Tukey's test was used to determine the significant differences among groups.

Results

Effects of MeJA on plant growth of NaCl-stressed alfalfa

To investigate the effect of MeJA on seed germination and primary root growth under salt stress, alfalfa seeds were subjected to

different concentrations of MeJA. A higher concentration of MeJA (>10 μM) slightly suppressed seed germination under normal conditions (Figure 1A). NaCl at a concentration of 150 mM depressed the seed germination rate by 30%, whereas 5 μM of MeJA mitigated the adverse impact of NaCl on seed germination (Figure 1A). However, 50 μM of MeJA exacerbated the inhibitory impact of salt stress on seed germination, and 100 μM of MeJA completely abolished the germination of salt-stressed seeds (Figure 1A). The exploration of time-course effects on seed germination under various treatments unveiled a significant acceleration in salt-stressed seeds subjected to 5 μM of MeJA. Impressively, these seeds achieved a 69% germination rate within a mere 4 days, surpassing the germination rate of 65.5% observed for the NaCl treatment over the entire 7-day duration (Figure 1B). Consequently, seeds subjected to the MeJA+NaCl treatment exhibited enhanced primary root development and cotyledon expansion compared to those treated only with NaCl, even though MeJA inhibited root elongation under non-saline conditions (Figures 1C, D). MeJA higher than 20 μM aggravated the negative effect of NaCl on primary root development (Figures 1C, D). Therefore, MeJA at 5 μM was determined as the optimal concentration for improving salt tolerance of alfalfa.

Further exploration was carried out to examine the influence of MeJA on the salt tolerance of young seedlings. As shown in Figure 2A, plants treated with a combination of MeJA and NaCl showed reduced leaf wilting compared to those treated with NaCl alone. Both NaCl treatment and NaCl combined with MeJA treatment decreased the OJIP fluorescence transient curve in leaves compared to the control group. However, the OJIP transient curve under the combined treatment was superior to that under NaCl treatment alone (Figure 2B). In addition, NaCl stress significantly inhibited plant growth, as indicated by the lower plant height and diminished root length in comparison to the control group. Interestingly, MeJA treatment significantly decreased the root length under normal conditions and further decreased when combined with NaCl treatment, compared to NaCl treatment alone (Figure 2C). This suggested that MeJA treatment can exacerbate the adverse impact of NaCl stress on root elongation. However, MeJA application alleviated the inhibition of NaCl stress on plant biomass, as evidenced by the higher fresh biomass of plant shoot and root under MeJA and NaCl combined treatment, as compared to NaCl treatment alone (Figure 2D)

MeJA promoted redox equilibrium and ion homeostasis under salt stress

To further explore the physiological mechanism underlying MeJA-enhanced salt tolerance, the antioxidant potential and ion content of roots under different treatments were measured. NaCl stress triggered a significant elevation in H_2O_2 and proline contents, along with heightened CAT and SOD activities in plant roots, compared to the control. However, plants treated with a combination of MeJA and NaCl exhibited a 25.6% decrease in H_2O_2 accumulation, when compared to those exposed to salt stress alone (Figure 3A). Furthermore, the combined treatment of MeJA

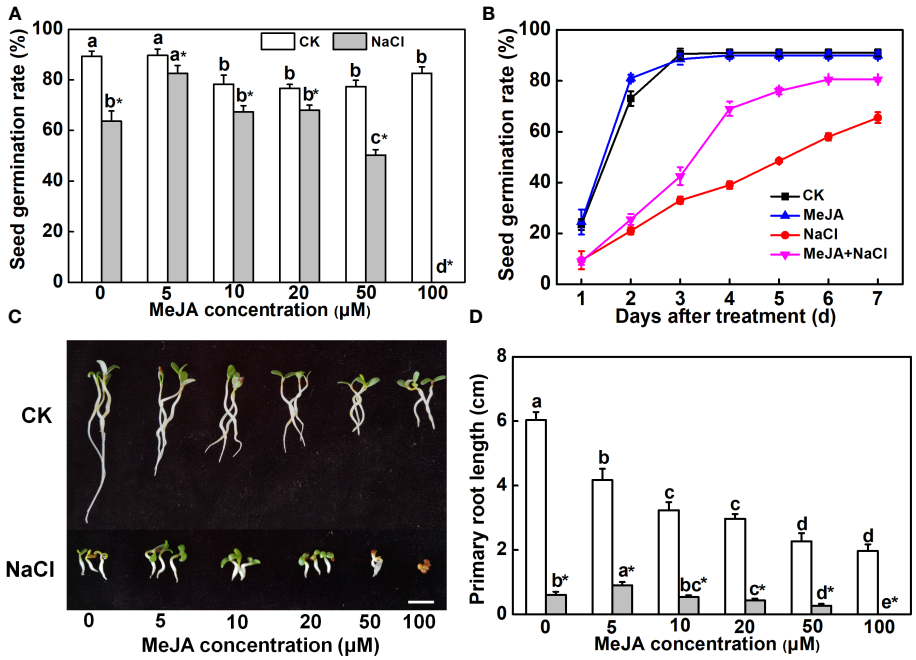

FIGURE 1
Effects of methyl jasmonate (MeJA) application on seed germination and primary root growth. **(A)** Seed germination rate after 7-day treatment. Columns represent average of three biological replicates with standard deviation, and each replicate has 100 seeds. **(B)** Time-course response of seed germination. The concentration of MeJA was 5 μM. **(C)** Primary root phenotypes. Bar = 1 cm. **(D)** Primary root length. Columns with different lowercase letters indicate significant differences among treatments at $p < 0.05$ using Duncan's test. Data represent average of three biological replicates with standard deviation, and each replicate has 10 plants. CK indicates control.

10.3389/fpls.2023.1258498

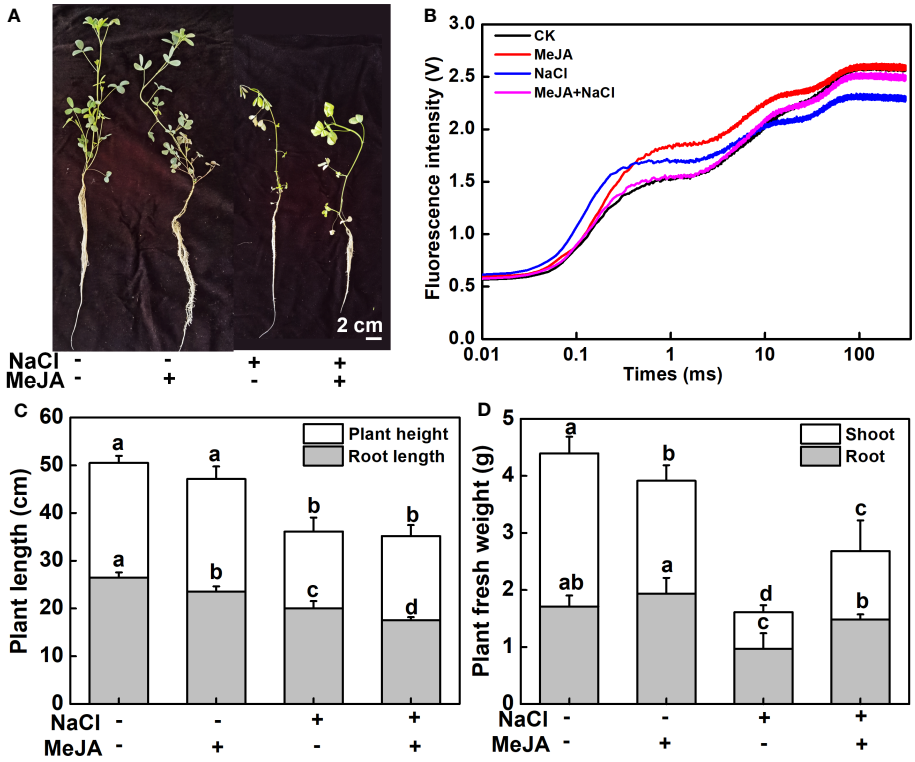

FIGURE 2
Exogenous methyl jasmonate (MeJA) enhances the salt tolerance of young alfalfa seedlings. **(A)** Phenotypes of young seedlings under NaCl treatment with or without exogenous MeJA. Bar = 2 cm. **(B)** Chlorophyll *a* fluorescence transient curves of leaves. CK indicates control. **(C)** Shoot and root length. **(D)** Shoot and root fresh weight. Columns represent average of at least six biological replicates and standard deviation. Columns with different lowercase letters indicate significant differences among treatments at $p < 0.05$ using Duncan's test.

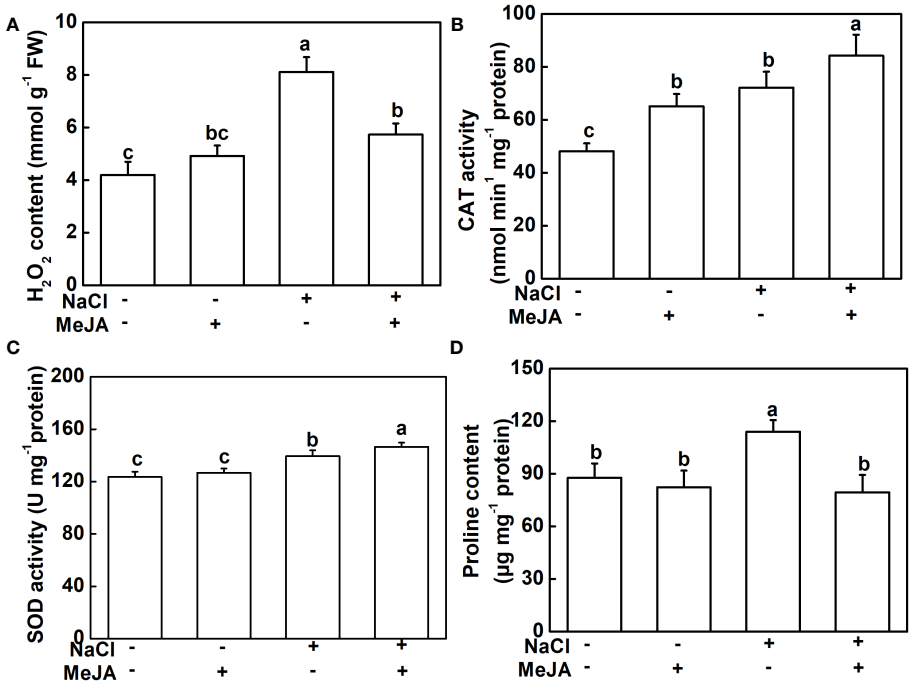

FIGURE 3
Exogenous methyl jasmonate (MeJA) alleviates the oxidative stress caused by NaCl treatment. **(A)** Content of H_2O_2. **(B)** Catalase (CAT) activity. **(C)** Superoxide dismutase (SOD) activity. **(D)** Content of proline. Columns represent average of three biological replicates with standard deviation, and each replicate has 10 plants. Different lowercase letters indicate significant differences among treatments at $p < 0.05$ using Duncan's test.

and NaCl led to 16.7% and 5.1% increases in the activity of the antioxidant enzymes, CAT and SOD, respectively, compared to the NaCl stress group (Figures 3B, C). However, NaCl treatment promoted the production of proline, which could not be further induced by MeJA application, even causing a decrease in proline content compared to NaCl treatment alone (Figure 3D).

The Na^+ and K^+ levels were detected in this study. As expected, NaCl stress caused a remarkable accumulation of Na^+ and a decline of K^+ in both leaves and roots, subsequently leading to higher Na^+/K^+ (Figure 4). MeJA alone did not result in distinguishable changes in Na^+ and K^+ levels, and Na^+/K^+ in leaves and roots (Figure 4). Importantly, MeJA addition effectively mitigated the negative effects of NaCl stress on Na^+ and K^+ homeostasis. Specifically, MeJA+NaCl treatment resulted in a notable reduction of Na^+ accumulation by 26.2% in leaves and 25% in roots. Moreover, K^+ levels exhibited a substantial increase of 30% in both leaves and roots, in stark contrast to the group subjected to salt stress without MeJA intervention (Figure 4). As a result, leaves and roots treated by MeJA+NaCl displayed lower levels of Na^+/K^+, when compared to those treated by NaCl alone (Figures 4C, F).

Identification of genes regulated by MeJA in roots of alfalfa

Furthermore, a genome-wide transcriptomic analysis of alfalfa roots under control (CK), MeJA, NaCl, and MeJA+NaCl was conducted. A total of 7,511 DEGs were identified by pairwise comparisons. Comparisons of NaCl vs. CK, MeJA vs. CK, MeJA +NaCl vs. CK, and MeJA+NaCl vs. NaCl consisted of 2,726, 1,784, 5,874, and 400 upregulated genes, respectively, and 1,456, 1,062, 6,517, and 246 downregulated genes, respectively (Figures 5A–C; Table S2). Importantly, there were 1,551 upregulated genes, and 740 downregulated genes were commonly regulated by both NaCl and MeJA+NaCl, compared to CK (Figures 5A, B). Among these shared genes, 68 exhibited upregulation while 15 displayed downregulation in in MeJA+NaCl vs. NaCl comparison, indicating that these genes were further induced or inhibited by MeJA based on NaCl treatment (Figures 5A, B). Moreover, the MeJA+NaCl vs. NaCl comparison revealed 332 upregulated genes and 230 downregulated genes, which were not detected in the NaCl vs. CK comparison, indicating that these genes were regulated by NaCl and MeJA+NaCl in an opposite direction (Figures 5A, B). A heatmap by clustering all DEGs was constructed to further depict the $\log_2$ (FC) in different comparisons and showed the different regulatory patterns by each treatment (Figure 5D).

Functional categorization of the DEGs

DEGs identified from NaCl vs. CK and MeJA+NaCl vs. CK comparisons were subjected to PageMan analysis to explore significantly over-represented functional pathways. As depicted in Figure 6A, the majority of sub-bins associated with secondary metabolism were down-enriched by both NaCl and MeJA+NaCl treatments, with the latter causing a more pronounced reduction in these sub-bins. Notably, the carotenoid biosynthesis category deviated from this trend, as it was significantly induced by the combined NaCl+MeJA treatment (Figure 6A; Table S3). Some gene categories enriched in phytohormone action were significantly upregulated in MeJA+NaCl vs. CK comparison, including genes involved in auxin transport (auxin efflux carrier component (*PIN*); auxin efflux transporter (*PILS*)) and signaling peptides (genes encoding *SCREW* precursor polypeptides and receptors) (Figure 6B; Table S3). Specifically, among the seven auxin transport genes, five exhibited higher expression levels under MeJA+NaCl treatment compared to their expression levels under NaCl treatment alone (Supplementary Figure S1). For redox homeostasis regulation, NaCl+MeJA treatment up-enriched gene categories related to glutathione-based redox regulation

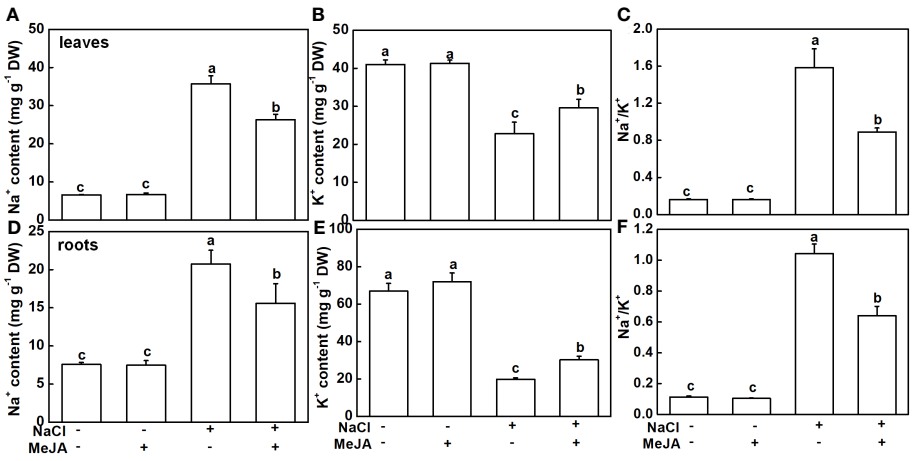

FIGURE 4
Effects of exogenous methyl jasmonate (MeJA) on Na^+ and K^+ contents under NaCl or non-NaCl treatment. **(A)** Content of Na^+ and K^+ **(B)** and Na^+/K^+ **(C)** in leaves. **(D)** Content of Na^+ and K^+ **(E)** and Na^+/K^+ **(F)** in roots. Columns represent average of three biological replicates with standard deviation, and each replicate has 10 plants. Different lowercase letters indicate significant differences among treatments at $p < 0.05$ using Duncan's test.

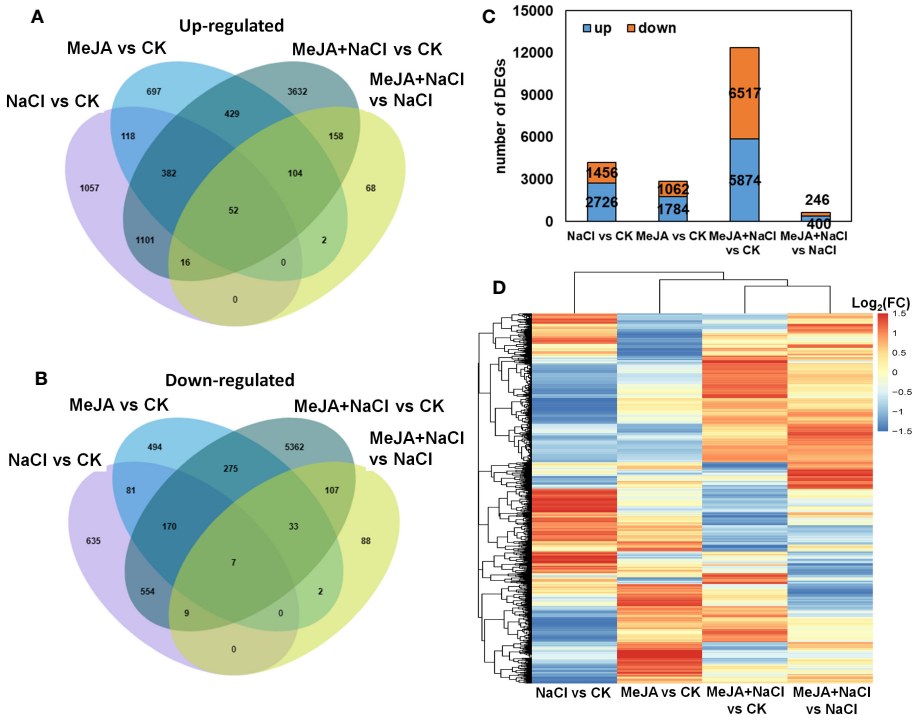

FIGURE 5
Integrated visualization of differentially expressed genes (DEGs) under control (CK), methyl jasmonate (MeJA), NaCl, and MeJA combined with NaCl (MeJA+NaCl). Venn diagrams show the overlap of upregulated **(A)** and downregulated genes **(B)**, indicating the unique and shared DEGs. **(C)** The count of DEGs in different comparisons. **(D)** A heatmap showing the $\log_2$ fold change (FC) of all DEGs across four treatment groups.

(*glutathione S-transferase* (*GST*)) and ROS generation (*NADPH-oxidase*, named *RBOH*) (Figure 6C, Table S3). For the roles of MeJA in the modulation of root elongation under NaCl stress, some cell cycle-associated genes, such as *Cyclins*, were depleted under the NaCl+MeJA condition (Figure 6D, Table S2). Moreover, a series of genes that participated in calcium perception (calcium sensor (*CML*) and *SnRK2-interacting calcium sensor*) were significantly upregulated by both NaCl alone and NaCl+MeJA combination treatment, whereas the latter resulted in a higher induction of these genes (Figure 6E, Table S3). In addition, NaCl+MeJA altered the expression of more external stimulus-responsive genes (such as genes related to toxic compounds and pathogen response) compared to NaCl alone (Figure 6F, Table S3). Furthermore, the regulation of sub-bins involved in RNA biosynthesis, especially TF families, varied between NaCl and MeJA+NaCl treatments. Specifically, certain TFs were exclusively induced by MeJA+NaCl treatment, such as R2R3-MYB, bZIP, ZAT, and WRKY TFs. However, NAC and most AP2/ERF TFs were induced under both NaCl and MeJA+NaCl treatments, with the latter resulting in greater induction of these genes (Figure 6G, Table S3).

Co-expression network of genes related to redox and ion balance

A WGCNA was conducted to investigate the correlation between DEGs and physiological traits associated with salinity response. The analysis identified 11 co-expression modules (Figure 7A, Table S4). The module–trait analysis revealed a strong positive correlation between antioxidant capacity-related parameters (CAT and SOD activities) and transcription levels of genes in the turquoise module, with correlation coefficients ranging from 0.8 to 0.91 (Figure 7B). These results suggest that the genes in the turquoise module might have significant involvement in MeJA-enhanced antioxidant capacity under NaCl stress. Additionally, the eigengenes of the yellow module exhibited a significantly positive correlation with K^+ content and K^+/Na^+, indicating their potential roles in MeJA-mediated ion transportation (Figure 7B).

Further, the turquoise module consisted of a total of 1,675 DEGs, whereas the yellow module contained 696 DEGs (Table S4). The top 30 genes according to the connectivity were characterized as hub genes in these two modules, which represent the integral function of the whole module (Table S4). Notably, most hub genes in the turquoise module were triggered by salt stress and showed the greatest expression level under MeJA+NaCl treatment (Figure 8A). The top 30 hub genes were visualized by Cytoscape software (Figure 7C). The top two hub genes encoding *pyruvate decarboxylase* (*PDC*; *MS.gene000484*) and *pyruvate kinase* (*MS.gene001737*) were identified to be involved in the Glycolysis/Gluconeogenesis process (ko00010) by Kyoto Encyclopedia of Genes and Genomes (KEGG) analysis (Figure 7C, Table S5). Moreover, this module contained four TF hub genes, including the GARP family encoding gene (MS.gene001686), AP2/ERF family encoding gene (MS.gene058814), MYB family encoding gene (MS.gene061226), and Trihelix family encoding gene (MS.gene007615). Among these TF hub genes, AP2/ERF and MYB were interconnected with *PDC*, and *GARP* was interconnected with

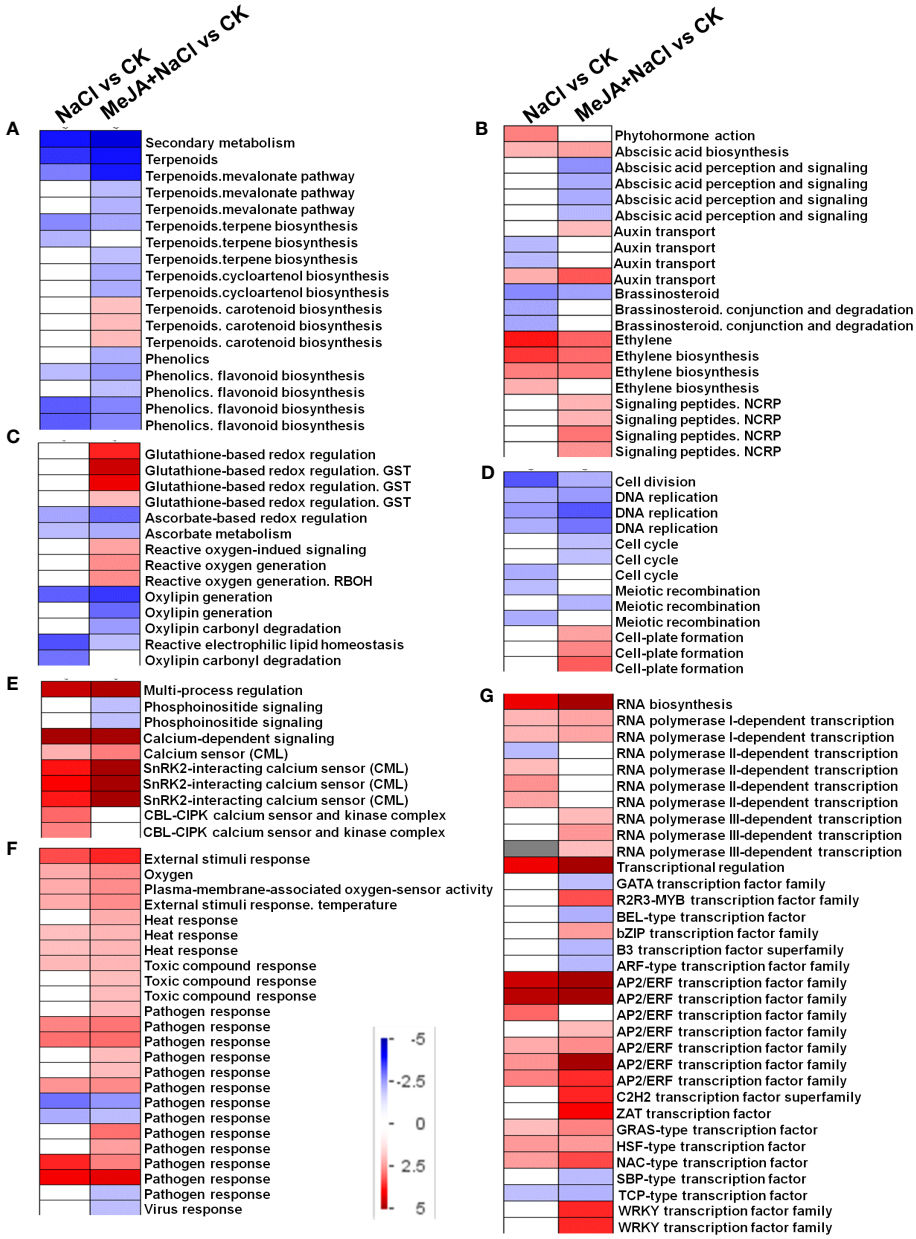

FIGURE 6
PageMan visualization of coordinated gene category changes modulated by NaCl and combined NaCl with methyl jasmonate (MeJA) (MeJA+NaCl). **(A)** Secondary metabolism. **(B)** Phytohormone action. **(C)** Glutathione-based redox regulation. **(D)** Cell division. **(E)** Multi-process regulation. **(F)** External stimulus response. **(G)** RNA biosynthesis. The $\log_2$ fold change (FC) in NaCl vs. CK and MeJA+NaCl vs. NaCl comparisons were subjected to over-representation analysis.

pyruvate kinase. In addition, the most central hub gene in the yellow module was RNA demethylase *ALKBH10B* (*MS.gene005674*), homologous to *At4g02940* in *Arabidopsis* (Figure 7D; Table S5). The subsequent hub gene was ATP-citrate synthase beta chain protein, which was enriched in the tricarboxylic acid (TCA) cycle (ko00020) (Figure 7D; Table S4). A member of the MYB TF family (MS.gene005488) was listed as a hub gene in the yellow module (Figure 7D; Table S5). Most hub genes identified in the yellow module showed higher expression levels under MeJA+NACl treatment, compared to NaCl treatment alone (Figure 8B).

Finally, eight genes were randomly selected from the hub genes of turquoise and yellow modules for relative expressional validation by qRT-PCR (Supplementary Figure S2). The results were similar to the relative expression level (FPKM value) obtained from sequencing data, highlighting the reliability of our transcriptomic data.

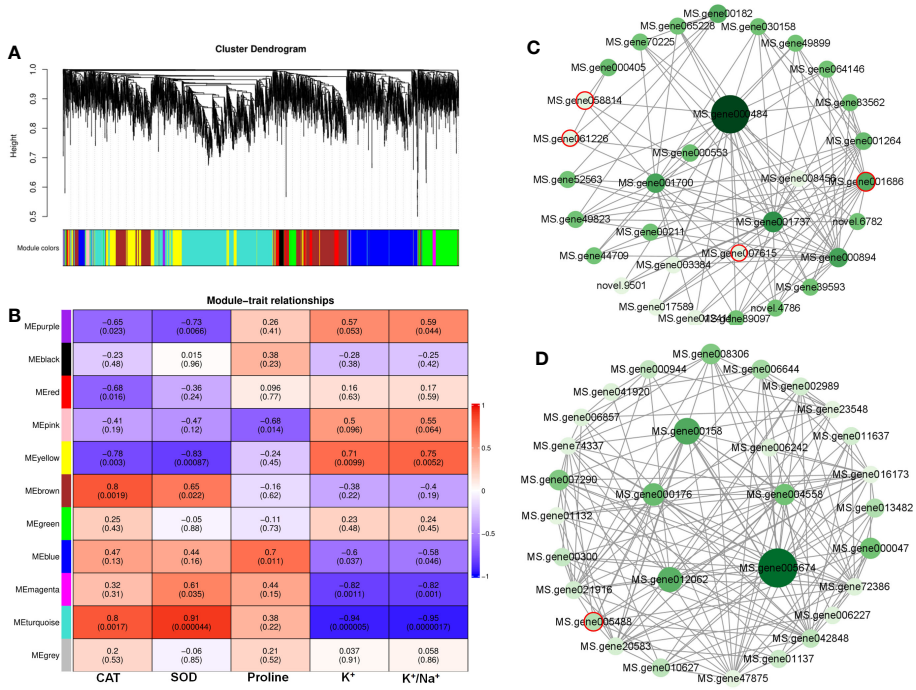

FIGURE 7
Weighted gene co-expression network analysis (WGCNA) reveals correlation between differentially expressed genes (DEGs) and salt stress-related physiological traits regulated by methyl jasmonate (MeJA). **(A)** Dendrogram of DEGs using WGCNA hierarchical clustering. **(B)** The thermogram shows the correlations between the modules and the physiological parameters. **(C)** The co-expression network of DEGs in MEturquoise. **(D)** The co-expression network of DEGs in MEyellow. Circles marked by red-colored edge lines indicate transcription factors.

Discussion

MeJA mediated root growth adaption of alfalfa under salt stress

MeJA exerted a suppressive effect on root elongation under both normal and salt stress conditions. This result aligns with previous studies involving JA-insensitive mutants, such as *jaz* and *coi*, which displayed a diminished response to root inhibition induced by JA (Chen et al., 2011; Geng et al., 2013). Moreover, salt stress-triggered JA signal suppressed cell elongation in the root elongation region of *Arabidopsis* (Valenzuela et al., 2016). *In vitro* experiments also evidenced that the G1 and G2 phases in the cell cycle of tobacco BY-2 cells were disrupted by JA application (Swiatek et al., 2004). Exogenous application of JA repressed root elongation, along with a reduction in root meristem size and expressional level of genes

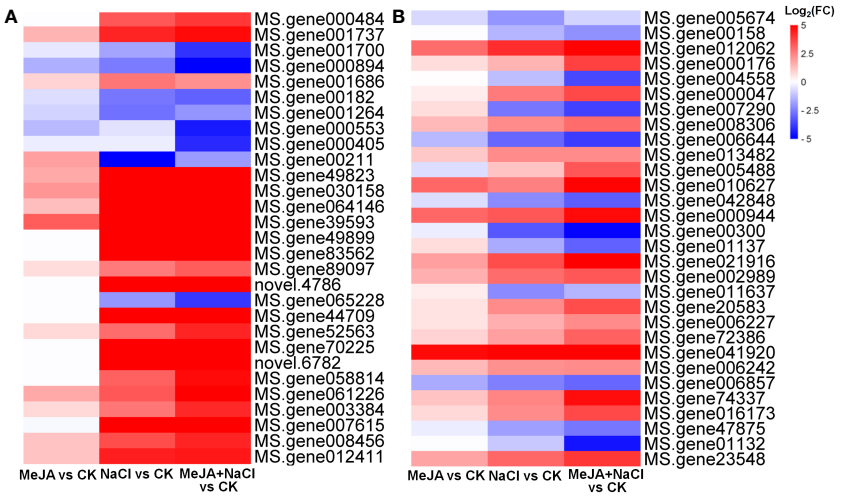

FIGURE 8
Heatmaps showing the $\log_2$ fold change (FC) of genes in turquoise **(A)** and yellow **(B)** modules.

related to cell cycle (Chen et al., 2011). Consistently, MeJA+NaCl treatment caused a more significant downregulation of genes related to the cell cycle, implying that the inhibition of root elongation by JA under salt stress appeared to be influenced, at least partially, by the suppression of genes related to the cell cycle. Although MeJA inhibits root elongation, it leads to an increase in root biomass under salt stress, which might suggest the induction of lateral root formation by MeJA. This hypothesis was supported by that many JA-insensitive mutants exhibited impaired lateral root formation (Raya-González et al., 2012; Cai et al., 2014). JA was reported to directly induce the biosynthesis of auxin through its responsive transcription factor, ERF109, thus promoting lateral root development (Cai et al., 2014). Therefore, the upregulation of auxin transport genes regulated by MeJA under salt stress may contribute to the improvement of root architecture and facilitate better nutrient and water uptake.

Energy supply is decreased in salt-stressed plants because of the consumption of resources for osmotic regulation and inhibition of photosynthesis (Munns and Gilliham, 2015). Photosynthesis, both photosystem and carbon assimilation, is sensitive to salt stress (Kalaji et al., 2011). Chlorophyll *a* fluorescence transient is an effective criterion to estimate the impacts of abiotic stress on photosynthesis, and a decrease in OJIP was paralleled in the total carbon content in leaves (Li et al., 2017). Here, MeJA alleviated the inhibition of chlorophyll fluorescence transient curves caused by NaCl, which might be an important strategy to ensure energy supply. Taking into consideration the observed alterations in plant growth induced by MeJA, we propose that under salt stress conditions, MeJA prioritized the allocation of energy toward lateral root formation rather than overall plant elongation. This form modulation signified an adaptive strategy, wherein resources were strategically channeled to enhance resilience against salt-induced stressors. This hypothesize was supported by the research on *N. tangutorum*, which indicated that the amplification of JA signal by the addition of MeJA enhanced salt tolerance but aggravated salt-inhibited growth, along with the downregulation of growth-promoting genes (Gao et al., 2021).

JA enhanced the salt tolerance of alfalfa by activating antioxidant enzymes and regulating ion transportation

Salt stress is widely acknowledged to induce oxidative stress, which causes severe damage to plants (Miller et al., 2010). JAs have been demonstrated to mitigate the negative impacts of oxidative burst by reducing ROS levels. Exogenous application of JA in wheat effectively promotes the antioxidant enzyme activity during salt stress (Zhu et al., 2022). Conversely, the JA-deficient mutant of tomato exhibited increased sensitivity to salt stress as a result of the depression of activity of antioxidant enzymes (Abouelsaad and Renault, 2018). Our study demonstrated that treatment with MeJA decreased H_2O_2 content and increased the activities of antioxidant enzymes SOD and CAT in roots exposed to salt conditions, together with upregulating specific genes encoding GST, an important enzyme in glutathione-based redox regulation. These findings provide further support for the involvement of JA in promoting plant antioxidant resistance under salinity conditions. In addition, a *PDC* gene was characterized as the hub gene in the module highly positively associated with antioxidant potential in our study. This gene showed the highest expression level under MeJA+NaCl treatment. A proteomic analysis revealed that pyruvate decarboxylase was induced by salt stimuli in rice (Damaris et al., 2016). ROS scavenging under salt stress requires enough energy supply, and alteration of genes related to sugar and starch metabolism may be critical to ensure the energy supply under abnormal conditions. Therefore, MeJA-enhanced antioxidant enzyme activity seems to be closely associated with *PDC*-mediated sugar metabolism.

High salinity results in the toxic accumulation of Na^+ and impairs the uptake of K^+, consequently perturbing ion balance (Yang and Guo, 2018). MeJA facilitated the maintenance of lower Na^+ levels in both the root and shoot of salt-stressed plants by inducing Na^+ efflux in *N. tangutorum* (Gao et al., 2021). As expected, MeJA was observed to decrease the Na^+ content in NaCl-treated shoots and roots. However, K^+ dissipations caused by NaCl in both roots and shoots were mitigated by MeJA application in our study. This finding contrasted with that obtained in salt-stressed *N. tangutorum*, which shows that MeJA improved K^+ content only in shoots and reduced it in roots (Gao et al., 2021). Plants protect themselves from over-accumulation of Na^+ mainly by inhibiting Na^+ absorption by the root, excluding Na^+ from the root, or reducing Na^+ uploading in xylem sap (Zhu et al., 2016). Our results suggested that MeJA-mediated ion balance under salt stress might be dependent on the first two strategies, consequently relieving the inhibition in K^+ uptake. In addition, we identified RNA demethylase gene *ALKBH10B* as one of the hub genes in the module highly related to ion balance. It is well known that the dynamic co-regulation of methylation and demethylation is a major process in regulating RNA transcription, and the demethylation was controlled by demethylase (Shi et al., 2022). *ALKBH* encodes a m6A demethylase, and some members belonging to *ALKBH* demethylase family were documented to be triggered by salt stress, such as *ALKBH9A* in *Arabidopsis* (Růžička et al., 2017). *Populus* plants overexpressed *PagALKBH9B* and *PagALKBH10B* showed enhanced salt resistance compared to the wild type (Zhao et al., 2022). In consequence, MeJA-regulated salt response in alfalfa may be involved in the participation of post-transcriptional regulation. The functions of these hub genes associated with antioxidant ability and ion balance need in-depth research in our further study.

JA triggers other salt-responsive signals

Many second messengers, such as ROS and Ca^{2+}, rapidly respond to salt stress and amplify salt response (Choudhury et al., 2013). The NADPH oxidase/respiratory burst oxidase homolog (*RBOH*s) play vital roles in controlling ROS production and participate in many defense-related signaling transduction (Liu et al., 2020). Transcript abundance of *RBOH* genes was proved to be upregulated by salt stress (Raziq et al., 2022). Grafting cucumber with pumpkin stock enhanced the Na^+ exclusion under salt stress, which was attributed to the induction of NADPH oxidase (Niu et al., 2018). Additionally, changes in cytosolic calcium flux represent early signaling events under salt stress and guarantee the triggering of downstream signal transduction (Kaleem et al., 2018). An increase in calcium level is

sensed by calcium-binding proteins, named calcium sensors, such as CML (Wang et al., 2018). The transcription of *CML*s was elevated by salt stimuli in many species (Sun et al., 2020; Li et al., 2022). Overexpression of an alfalfa *CML*, *MsCML46*, in tobacco enhanced plant salt tolerance by abating oxidative and osmotic stress (Du et al., 2021). These investigations strongly support the correlation between the initiation of ROS and Ca^{2+} and the activation of antioxidant systems and ion transport. Here, genes related to reactive oxygen-induced signaling and *RBOH* were specifically induced by MeJA+NaCl treatment. Also, many CML genes were upregulated by NaCl stress and further induced by MeJA+NaCl. These results suggest that MeJA application enhanced ROS and calcium signals under salt stress, which might contribute to the amplification of downstream salt-responsive signals and prime plants to defend against external salinity stimuli.

Numerous TFs are activated by salt stress to relay stress signals and govern the transcription of salt-responsive target genes by interacting with the *cis*-regulatory elements in promoters (Baillo et al., 2019). Recently, the identification and characterization of stress-responsive TFs have garnered significant interest. Some AP2/ERF TFs are JA-responsive, such as ERF109 in *Arabidopsis* (Cai et al., 2014) and ERF115 in *Salvia miltiorrhiza* (Sun et al., 2019). AP2/ERF TF were identified to act as favorable enhancers of plant salt tolerance, such as in tomato (Li et al., 2018), wheat (Rong et al., 2014), and *Arabidopsis* (Park et al., 2011). NAC TFs are plant-specific and participate in abiotic stress response, and transgenic soybean with overexpressed GmNAC06 exhibited heightened resistance to salt stress when contrasted with the wild type, attributable to their improved antioxidant ability and decreased Na^+/K^+ (Li et al., 2021). In this study, sub-bins associated with AP2/ERF and NAC TFs were upregulated by both NaCl and MeJA+NaCl treatment, with the latter resulting in a higher expression level of these TFs. Additionally, some TFs, such as the R2R3-MYB transcription factor family, WRKY, and ZAT, were not induced by NaCl alone but were remarkably increased by MeJA+NaCl treatment. Also, a MYB TF was identified as a hub gene positively related to ion balance. These results agreed with a transcriptomic analysis of wheat, which showed that R2R3-MYB and WRKY TFs were specifically induced only by MeJA +NaCl (Zhu et al., 2022). In *Arabidopsis*, overexpression of a *Malus domestica* C2H2-type zinc finger transcription factor, MdZAT17, enhanced plant salt resilience by reducing oxidative stress (Wang et al., 2022). Also, increasing evidence has documented that R2R3-MYB and WRKY TFs facilitated the conferral of salt resilience by manipulating the composite regulatory network of salt stress response (Ma et al., 2018; Du et al., 2022). Moreover, WRKY was reported to mediate JA-induced leaf senescence and was transcriptionally regulated by MYC2, the central TF in JA signaling (Wang et al., 2022). Therefore, the greater induction of these TFs responding to MeJA under salt stress could potentially contribute to the augmentation of salt tolerance in alfalfa.

In conclusion, our physiochemical and transcriptomic analyses revealed the roles of MeJA in mediating the salt tolerance of alfalfa. MeJA enhanced salt tolerance by rebuilding plant growth, improving antioxidant capacity, and maintaining ion homeostasis. MeJA addition to salt stress triggered a large-scale transcriptomic remodeling. Many genes related to signal transduction, such as second messengers and master TFs, were altered by MeJA under salt stress. The potential hub genes positively associated with salt-responsive traits are identified through WGCNA, suggesting that these genes might participate in MeJA-regulated salt tolerance. Taken together, we presented detailed evidence to deepen our insight into the molecular mechanisms underlying the role of JA in enhancing plant salt tolerance.

Data availability statement

The original contributions presented in the study are publicly available. This data can be found here: https://www.ncbi.nlm.nih.gov/bioproject/PRJNA907206.

Author contributions

YY: Data curation, Funding acquisition, Investigation, Validation, Writing – original draft, Writing – review & editing. TY: Investigation, Resources, Writing – original draft. SL: Investigation, Validation, Writing – review & editing. WW: Methodology, Software, Writing – review & editing. XL: Investigation, Writing – review & editing. SF: Conceptualization, Supervision, Writing – original draft, Writing – review & editing.

Funding

The authors declare financial support was received for the research, authorship, and/or publication of this article. This work was supported by the Natural Science Foundation of Shandong Province (ZR2020QC039).

Conflict of interest

The authors declare that the research was conducted in the absence of any commercial or financial relationships that could be construed as a potential conflict of interest.

Publisher's note

Supplementary material

The Supplementary Material for this article can be found online at: https://www.frontiersin.org/articles/10.3389/fpls.2023.1258498/full#supplementary-material

References

Abouelsaad, I., and Renault, S. (2018). Enhanced oxidative stress in the jasmonic acid-deficient tomato mutant *def-1* exposed to NaCl stress. *J. Plant Physiol.* 226, 136–144. doi: 10.1016/j.jplph.2018.04.009

Ahmad, R. M., Cheng, C., Sheng, J., Wang, W., Ren, H., Aslam, M., et al. (2019). Interruption of jasmonic acid biosynthesis causes differential responses in the roots and shoots of maize seedlings against salt stress. *Int. J. Mol. Sci.* 20 (24), 6202. doi: 10.3390/ijms20246202

Ali, M. S., and Baek, K. H. (2020). Jasmonic acid signaling pathway in response to abiotic stresses in plants. *Int. J. Mol. Sci.* 21 (2), 621. doi: 10.3390/ijms21020621

Asfaw, K. G., Liu, Q., Eghbalian, R., Purper, S., Akaberi, S., Dhakarey, R., et al. (2022). The jasmonate biosynthesis gene *OsOPR7* can mitigate salinity induced mitochondrial oxidative stress. *Plant Sci.* 316, 111156. doi: 10.1016/j.plantsci.2021.111156

Baillo, E. H., Kimotho, R. N., Zhang, Z., and Xu, P. (2019). Transcription factors associated with abiotic and biotic stress tolerance and their potential for crops improvement. *Genes-Basel* 10 (10), 771. doi: 10.3390/genes10100771

Bates, L., Waldren, R., and Teare, I. (1973). Rapid determination of free proline for water-stress studies. *Plant Soil.* 39, 205–207. doi: 10.1007/BF00018060

Cai, X. T., Xu, P., Zhao, P. X., Liu, R., Yu, L. H., and Xiang, C. B. (2014). Arabidopsis ERF109 mediates cross-talk between jasmonic acid and auxin biosynthesis during lateral root formation. *Nat. Commun.* 5, 5833. doi: 10.1038/ncomms6833

Chen, Q., Sun, J., Zhai, Q., Zhou, W., Qi, L., Xu, L., et al. (2011). The basic helix-loop-helix transcription factor MYC2 directly represses *PLETHORA* expression during jasmonate-mediated modulation of the root stem cell niche in Arabidopsis. *Plant Cell.* 23 (9), 3335–3352. doi: 10.1105/tpc.111.089870

Choudhury, S., Panda, P., Sahoo, L., and Panda, S. K. (2013). Reactive oxygen species signaling in plants under abiotic stress. *Plant Signal. Behav.* 8 (4), e23681. doi: 10.4161/psb.23681

Damaris, R. N., Li, M., Liu, Y., Chen, X., Murage, H., and Yang, P. (2016). A proteomic analysis of salt stress response in seedlings of two African rice cultivars. A proteomic analysis of salt stress response in seedlings of two African rice cultivars. *Biochim. Biophys. Acta* 1864 (11), 1570–1578. doi: 10.1016/j.bbapap.2016.08.011

Du, B., Chen, N., Song, L., Wang, D., Cai, H., Yao, L., et al. (2021). Alfalfa (*Medicago sativa* L.) MsCML46 gene encoding calmodulin-like protein confers tolerance to abiotic stress in tobacco. *Plant Cell Rep.* 40 (10), 1907–1922. doi: 10.1007/s00299-021-02757-7

Du, B., Liu, H., Dong, K., Wang, Y., and Zhang, Y. (2022). Over-expression of an R2R3 MYB gene, MdMYB108L, enhances tolerance to salt stress in transgenic plants. *Int. J. Mol. Sci.* 23 (16), 9428. doi: 10.3390/ijms23169428

Du, M., Zhao, J., Tzeng, D. T. W., Liu, Y., Deng, L., Yang, T., et al. (2017). MYC2 Orchestrates a hierarchical transcriptional cascade that regulates jasmonate-mediated plant immunity in tomato. *Plant Cell.* 29 (8), 1883–1906. doi: 10.1105/tpc.16.00953

Flowers, T., and Yeo, A. (1995). Breeding for salinity resistance in crop plants: where next? *Funct. Plant Biol.* 22 (6), 875–884. doi: 10.1071/PP9950875

Gao, Z., Gao, S., Li, P., Zhang, Y., Ma, B., and Wang, Y. (2021). Exogenous methyl jasmonate promotes salt stress-induced growth inhibition and prioritizes defense response of Nitraria tangutorum Bobr. *Physiol. Plantarum.* 172 (1), 162–175. doi: 10.1111/ppl.13314

Geng, Y., Wu, R., Wee, C. W., Xie, F., Wei, X., Chan, P. M., et al. (2013). A spatio-temporal understanding of growth regulation during the salt stress response in Arabidopsis. *Plant Cell.* 25 (6), 2132–2154. doi: 10.1105/tpc.113.112896

Guan, C., Cui, X., Liu, H. Y., Li, X., Li, M. Q., and Zhang, Y. W. (2020). Proline biosynthesis enzyme genes confer salt tolerance to switchgrass (*Panicum virgatum* L.) in cooperation with polyamines metabolism. *Front. Plant Sci.* 11. doi: 10.3389/fpls.2020.00046

Hauser, F., and Horie, T. (2010). A conserved primary salt tolerance mechanism mediated by HKT transporters: a mechanism for sodium exclusion and maintenance of high K^+/Na^+ ratio in leaves during salinity stress. *Plant Cell Environ.* 33 (4), 552–565. doi: 10.1111/j.1365-3040.2009.02056.x

Hazman, M., Hause, B., Eiche, E., Nick, P., and Riemann, M. (2015). Increased tolerance to salt stress in OPDA-deficient rice ALLENE OXIDE CYCLASE mutants is linked to an increased ROS-scavenging activity. *J. Exp. Bot.* 66 (11), 3339–3352. doi: 10.1093/jxb/erv142

He, L., He, T., Farrar, S., Ji, L., Liu, T., and Ma, X. (2017). Antioxidants maintain cellular redox homeostasis by elimination of reactive oxygen species. *Cell Physiol. Biochem.* 44 (2), 532–553. doi: 10.1159/000485089

Heydarian, Z., Yu, M., Gruber, M., Coutu, C., Robinson, S. J., and Hegedus, D. D. (2018). Changes in gene expression in *Camelina sativa* roots and vegetative tissues in response to salinity stress. *Sci. Rep.* 8 (1), 9804. doi: 10.1038/s41598-018-28204-4

Hoagland, D. R., and Arnon, D. I. (1950). The water culture method for growing plants without soil. *Univ. California. Agric. Exp. Station. Berkeley.* 347, 357–359. doi: 10.1093/femsec/fiw047

Jiang, Y., and Deyholos, M. K. (2006). Comprehensive transcriptional profiling of NaCl-stressed Arabidopsis roots reveals novel classes of responsive genes. *BMC Plant Bio.* 6, 25. doi: 10.1186/1471-2229-6-25

Kalaji, H. M., Bosa, K., Kościelniak, J., and Hossain, Z. (2011). Chlorophyll a fluorescence–A useful tool for the early detection of temperature stress in spring barley (Hordeum vulgare L.). *Omics* 15(12), 925–934. doi: 10.1089/omi.2011.0070

Kaleem, F., Shabir, G., Aslam, K., Rasul, S., Manzoor, H., Shah, S. M., et al. (2018). An overview of the genetics of plant response to salt stress: present status and the way forward. *Appl. Biochem. Biotechnol.* 186 (2), 306–334. doi: 10.1007/s12010-018-2738-y

Karimi, R., Gavili-Kilaneh, K., and Khadivi, A. (2022). Methyl jasmonate promotes salinity adaptation responses in two grapevine (*Vitis vinifera* L.) cultivars differing in salt tolerance. *Food Chem.* 375, 131667. doi: 10.1016/j.foodchem.2021.131667

Li, M., Chen, R., Jiang, Q., Sun, X., Zhang, H., and Hu, Z. (2021). GmNAC06, a NAC domain transcription factor enhances salt stress tolerance in soybean. *Plant Mol. Biol.* 105 (3), 333–345. doi: 10.1007/s11103-020-01091-y

Li, X., Han, S., Wang, G., Liu, X., Amombo, E., Xie, Y., et al. (2017). The fungus aspergillus aculeatus enhances salt-stress tolerance, metabolite accumulation, and improves forage quality in Perennial Ryegrass. *Front. Microbiol.* 8. doi: 10.3389/fmicb.2017.01664

Li, Z., Tian, Y., Xu, J., Fu, X., Gao, J., Wang, B., et al. (2018). A tomato ERF transcription factor, SlERF84, confers enhanced tolerance to drought and salt stress but negatively regulates immunity against *Pseudomonas syringae* pv. tomato DC3000. *Plant Physiol. Bioch.* 132, 683–695. doi: 10.1016/j.plaphy.2018.08.022

Li, Y., Zhang, H., Dong, F., Zou, J., Gao, C., Zhu, Z., et al. (2022). Multiple roles of wheat calmodulin genes during stress treatment and TaCAM2-D as a positive regulator in response to drought and salt tolerance. *Int. J. Biol. Macromol.* 220, 985–997. doi: 10.1016/j.ijbiomac.2022.08.124

Liu, M., Yu, H., Ouyang, B., Shi, C., Demidchik, V., Hao, Z., et al. (2020). NADPH oxidases and the evolution of plant salinity tolerance. *Plant Cell Environ.* 43 (12), 2957–2968. doi: 10.1111/pce.13907

Lozano-Durán, R., and Zipfel, C. (2015). Trade-off between growth and immunity: role of brassinosteroids. *Trends Plant Sci.* 20 (1), 12–19. doi: 10.1016/j.tplants.2014.09.003

Ma, Q., Xia, Z., Cai, Z., Li, L., Cheng, Y., Liu, J., et al. (2018). GmWRKY16 enhances drought and salt tolerance through an ABA-mediated pathway in Arabidopsis thaliana. *Front. Plant Sci.* 9. doi: 10.3389/fpls.2018.01979

Miller, G., Suzuki, N., Ciftci-Yilmaz, S., and Mittler, R. (2010). Reactive oxygen species homeostasis and signalling during drought and salinity stresses. *Plant Cell Environ.* 33 (4), 453–467. doi: 10.1111/j.1365-3040.2009.02041.x

Munns, R., and Gilliham, M. (2015). Salinity tolerance of crops-what is the cost? *New Phytol.* 208 (3), 668–673. doi: 10.1111/nph.13519

Munns, R., and Tester, M. (2008). Mechanisms of salinity tolerance. *Annu. Rev. Plant Biol.* 59, 651–681. doi: 10.1146/annurev.arplant.59.032607.092911

Nefissi Ouertani, R., Arasappan, D., Abid, G., Ben Chikha, M., Jardak, R., Mahmoudi, H., et al. (2021). Transcriptomic analysis of salt-stress-responsive genes in barley roots and leaves. *Int. J. Mol. Sci.* 22 (15), 8155. doi: 10.3390/ijms22158155

Niu, M., Huang, Y., Sun, S., Sun, J., Cao, H., Shabala, S., et al. (2018). Root respiratory burst oxidase homologue-dependent H_2O_2 production confers salt tolerance on a grafted cucumber by controlling Na^+ exclusion and stomatal closure. *J. Exp. Bot.* 69 (14), 3465–3476. doi: 10.1093/jxb/erx386

Park, H. Y., Seok, H. Y., Woo, D. H., Lee, S. Y., Tarte, V. N., Lee, E. H., et al. (2011). AtERF71/HRE2 transcription factor mediates osmotic stress response as well as hypoxia response in Arabidopsis. *Biochem. Bioph. Res. Co.* 414 (1), 135–141. doi: 10.1016/j.bbrc.2011.09.039

Pedranzani, H., Racagni, G., Alemano, S., Miersch, O., Ramírez, I, Peña-Cortés, H., et al. (2013). Salt tolerant tomato plants show increased levels of jasmonic acid. *Plant Growth Regul.* 41, 149–158. doi: 10.1023/A:1027311319940

Peleg, Z., and Blumwald, E. (2011). Hormone balance and abiotic stress tolerance in crop plants. *Curr. Opin. Plant Biol.* 14 (3), 290–295. doi: 10.1016/j.pbi.2011.02.001

Qiu, Z., Guo, J., Zhu, A., Zhang, L., and Zhang, M. (2014). Exogenous jasmonic acid can enhance tolerance of wheat seedlings to salt stress. *Ecotox. Environ. Safe.* 104, 202–208. doi: 10.1016/j.ecoenv.2014.03.014

Raya-González, J., Pelagio-Flores, R., and López-Bucio, J. (2012). The jasmonate receptor COI1 plays a role in jasmonate-induced lateral root formation and lateral root positioning in Arabidopsis thaliana. *J. Plant Physiol.* 169, 1348–1358. doi: 10.1016/j.jplph.2012.05.002

Raziq, A., Wang, Y., Mohi Ud Din, A., Sun, J., Shu, S., and Guo, S. (2022). A comprehensive evaluation of salt tolerance in tomato (Var. *Ailsa Craig*): responses of physiological and transcriptional changes in RBOH's and ABA biosynthesis and signalling genes. *Int. J. Mol. Sci.* 23 (3), 1603. doi: 10.3390/ijms23031603

Rong, W., Qi, L., Wang, A., Ye, X., Du, L., Liang, H., et al. (2014). The ERF transcription factor TaERF3 promotes tolerance to salt and drought stresses in wheat. *Plant Biotechnol. J.* 12 (4), 468–479. doi: 10.1111/pbi.12153

Růžička, K., Zhang, M., Campilho, A., Bodi, Z., Kashif, M., Saleh, M., et al. (2017). Identification of factors required for m(6)A mRNA methylation in Arabidopsis reveals a role for the conserved E3 ubiquitin ligase HAKAI. *New Phytol.* 215 (1), 157–172. doi: 10.1111/nph.14586

Saddhe, A. A., Mishra, A. K., and Kumar, K. (2021). Molecular insights into the role of plant transporters in salt stress response. *Physiol. Plantarum.* 173 (4), 1481–1494. doi: 10.1111/ppl.13453

Sahab, S., Suhani, I., Srivastava, V., Chauhan, P. S., Singh, R. P., and Prasad, V. (2021). Potential risk assessment of soil salinity to agroecosystem sustainability: current status and management strategies. *Sci. Total. Environ.* 764, 144164. doi: 10.1016/j.scitotenv.2020.144164

Shah, W. H., Rasool, A., Saleem, S., Mushtaq, N. U., Tahir, I., Hakeem, K. R., et al. (2021). Understanding the integrated pathways and mechanisms of transporters, protein kinases, and transcription factors in plants under salt stress. *Int. J. Genomics* 2021, 5578727. doi: 10.1155/2021/5578727

Shi, M., Wang, C., Wang, P., Zhang, M., and Liao, W. (2022). Methylation in DNA, histone, and RNA during flowering under stress condition: A review. *Plant Sci.* 324, 111431. doi: 10.1016/j.plantsci.2022.111431

Silva-Ortega, C. O., Ochoa-Alfaro, A. E., Reyes-Agüero, J. A., Aguado-Santacruz, G. A., and Jiménez-Bremont, J. F. (2008). Salt stress increases the expression of *P5CS* gene and induces proline accumulation in cactus pear. *Plant Physiol. Bioch.* 46 (1), 82–92. doi: 10.1016/j.plaphy.2007.10.011

Singer, S. D., Hannoufa, A., and Acharya, S. (2018). Molecular improvement of alfalfa for enhanced productivity and adaptability in a changing environment. *Plant Cell Environ.* 41 (9), 1955–1971. doi: 10.1111/pce.13090

Singh, A. (2021). Soil salinization management for sustainable development: A review. *J. Environ. Manage.* 277, 111383. doi: 10.1016/j.jenvman.2020.111383

Singh, P., Choudhary, K. K., Chaudhary, N., Gupta, S., Sahu, M., Tejaswini, B., et al. (2022). Salt stress resilience in plants mediated through osmolyte accumulation and its crosstalk mechanism with phytohormones. *Front. Plant Sci.* 13. doi: 10.3389/fpls.2022.1006617

Song, R. F., Li, T. T., and Liu, W. C. (2021). Jasmonic acid impairs arabidopsis seedling salt stress tolerance through MYC2-mediated repression of CAT2 expression. *Front. Plant Sci.* 12. doi: 10.3389/fpls.2021.730228

Stritzler, M., Elba, P., Berini, C., Gomez, C., Ayub, N., and Soto, G. (2018). High-quality forage production under salinity by using a salt-tolerant AtNXH1-expressing transgenic alfalfa combined with a natural stress-resistant nitrogen-fixing bacterium. *J. Biotechnol.* 276-277, 42–45. doi: 10.1016/j.jbiotec.2018.04.013

Sun, M., Shi, M., Wang, Y., Huang, Q., Yuan, T., Wang, Q., et al. (2019). The biosynthesis of phenolic acids is positively regulated by the JA-responsive transcription factor ERF115 in *Salvia miltiorrhiza*. *J. Exp. Bot.* 70 (1), 243–254. doi: 10.1093/jxb/ery349

Sun, Q., Yu, S., and Guo, Z. (2020). *Calmodulin-like* (*CML*) gene family in *Medicago truncatula*: genome-wide identification, characterization and expression analysis. *Int. J. Mol. Sci.* 21 (19), 7142. doi: 10.3390/ijms21197142

Swiatek, A., Azmi, A., Stals, H., Inzé, D., and Van Onckelen, H. (2004). Jasmonic acid prevents the accumulation of Cyclin B1;1 and CDK-B in synchronized tobacco BY-2 cells. *FEBS Lett.* 572 (1-3), 118–122. doi: 10.1016/j.febslet.2004.07.018

Valenzuela, C. E., Acevedo-Acevedo, O., Miranda, G. S., Vergara-Barros, P., Holuigue, L., Figueroa, C. R., et al. (2016). Salt stress response triggers activation of the jasmonate signaling pathway leading to inhibition of cell elongation in Arabidopsis primary root. *J. Exp. Bot.* 67 (14), 4209–4220. doi: 10.1093/jxb/erw202

Van Zelm, E., Zhang, Y., and Testerink, C. (2020). Salt tolerance mechanisms of plants. *Annu. Rev. Plant Biol.* 71, 403–433. doi: 10.1146/annurev-arplant-050718-100005

Wang, Z., Gao, M., Li, Y., Zhang, J., Su, H., Cao, M., et al. (2022). The transcription factor SlWRKY37 positively regulates jasmonic acid- and dark-induced leaf senescence in tomato. *J. Exp. Bot.* 73 (18), 6207–6225. doi: 10.1093/jxb/erac258

Wang, X., Hao, L., Zhu, B., and Jiang, Z. (2018). Plant calcium signaling in response to potassium deficiency. *Int. J. Mol. Sci.* 19 (11), 3456. doi: 10.3390/ijms19113456

Wei, L., Feng, L., Liu, Y., and Liao, W. (2022). Mitogen-activated protein kinase is involved in salt stress response in tomato (*Solanum lycopersicum*) seedlings. *Int. J. Mol. Sci.* 23 (14), 7645. doi: 10.3390/ijms23147645

Willekens, H., Chamnongpol, S., Davey, M., Schraudner, M., Langebartels, C., Van Montagu, M., et al. (1997). Catalase is a sink for H_2O_2 and is indispensable for stress defence in C3 plants. *EMBO J.* 16 (16), 4806–4816. doi: 10.1093/emboj/16.16.4806

Xia, X. J., Wang, Y. J., Zhou, Y. H., Tao, Y., Mao, W. H., Shi, K., et al. (2009). Reactive oxygen species are involved in brassinosteroid-induced stress tolerance in Cucumber. *Plant Physiol.* 150 (2), 801–814. doi: 10.1104/pp.109.138230

Yang, Y., and Guo, Y. (2018). Unraveling salt stress signaling in plants. *J. Integr. Plant Biol.* 60 (9), 796–804. doi: 10.1111/jipb.12689

Yang, Z., Wang, C., Xue, Y., Liu, X., Chen, S., Song, C., et al. (2019). Calcium-activated 14-3-3 proteins as a molecular switch in salt stress tolerance. *Nat. Commun.* 10 (1), 1199. doi: 10.1038/s41467-019-09181-2

Yu, Z., Duan, X., Luo, L., Dai, S., Ding, Z., and Xia, G. (2020). How plant hormones mediate salt stress responses. *Trends Plant Sci.* 25 (11), 1117–1130. doi: 10.1016/j.tplants.2020.06.008

Yue, J. Y., Jiao, J. L., Wang, W. W., and Wang, H. Z. (2022). The calcium-dependent protein kinase TaCDPK27 positively regulates salt tolerance in wheat. *Int. J. Mol. Sci.* 23 (13), 7341. doi: 10.3390/ijms23137341

Zhang, H., Zhang, Q., Zhai, H., Li, Y., Wang, X., Liu, Q., et al. (2017). Transcript profile analysis reveals important roles of jasmonic acid signalling pathway in the response of sweet potato to salt stress. *Sci. Rep.* 7, 40819. doi: 10.1038/srep40819

Zhao, Y., Guo, Q., Cao, S., Tian, Y., Han, K., Sun, Y., et al. (2022). Genome-wide identification of the AlkB homologs gene family, PagALKBH9B and PagALKBH10B regulated salt stress response in Populus. *Front. Plant Sci.* 13. doi: 10.3389/fpls.2022.994154

Zhu, M., Liu, Y., Cai, P., Duan, X., Sang, S., and Qiu, Z. (2022). Jasmonic acid pretreatment improves salt tolerance of wheat by regulating hormones biosynthesis and antioxidant capacity. *Front. Plant Sci.* 13. doi: 10.3389/fpls.2022.968477

Zhu, M., Shabala, L., Cuin, T. A., Huang, X., Zhou, M., Munns, R., et al. (2016). Nax loci affect SOS1-like Na^+/H^+ exchanger expression and activity in wheat. *J. Exp. Bot.* 67 (3), 835–844. doi: 10.1093/jxb/erv493

frontiers | Frontiers in Plant Science

TYPE Original Research
PUBLISHED 19 September 2023
DOI 10.3389/fpls.2023.1255682

OPEN ACCESS

EDITED BY
Guowei Li,
Shandong Academy of Agricultural Sciences, China

REVIEWED BY
Parviz Heidari,
Shahrood University of Technology, Iran
Fanrong Zeng,
Yangtze University, China

*CORRESPONDENCE
Yanling Zhang
zhangyanling@ztri.com.cn
Chunlei Yang
ycl193737@163.com

†These authors have contributed equally to this work

RECEIVED 09 July 2023
ACCEPTED 04 September 2023
PUBLISHED 19 September 2023

CITATION
Dai H, Yang J, Teng L, Wang Z, Liang T, Khan WA, Yang R, Qiao B, Zhang Y and Yang C (2023) Mechanistic basis for mitigating drought tolerance by selenium application in tobacco (*Nicotiana tabacum* L.): a multi-omics approach. *Front. Plant Sci.* 14:1255682. doi: 10.3389/fpls.2023.1255682

Mechanistic basis for mitigating drought tolerance by selenium application in tobacco (*Nicotiana tabacum* L.): a multi-omics approach

Huaxin Dai[1†], Jinpeng Yang[2†], Lidong Teng[3], Zhong Wang[4], Taibo Liang[1], Waleed Amjad Khan[5], Ruiwei Yang[2], Baoming Qiao[2], Yanling Zhang[1*] and Chunlei Yang[2*]

[1]Department of Tobacco Agriculture, Zhengzhou Tobacco Research Institute of China National Tobacco Corporation (CNTC), Zhengzhou, China, [2]Department of Research Center on Tobacco Cultivating and Curing, Tobacco Research Institute of Hubei, Wuhan, China, [3]Department of Agronomy, College of Agriculture and Biotechnology, Zhejiang University, Hangzhou, China, [4]China Tobacco Gene Research Center, Zhengzhou Tobacco Research Institute of China National Tobacco Corporation (CNTC), Zhengzhou, China, [5]Tasmanian Institute of Agriculture, University of Tasmania, Hobart, TAS, Australia

The lack of irrigation water in agricultural soils poses a significant constraint on global crop production. In-depth investigation into microRNAs (miRNAs) has been widely used to achieve a comprehensive understanding of plant defense mechanisms. However, there is limited knowledge on the association of miRNAs with drought tolerance in cigar tobacco. In this study, a hydroponic experiment was carried out to identify changes in plant physiological characteristics, miRNA expression and metabolite profile under drought stress, and examine the mitigating effects of selenium (Se) application. The shoot dry weight of drought-stressed plants was approximately half (50.3%) of that in non-stressed (control) conditions. However, plants supplied with Se attained 38.8% greater shoot dry weight as compared to plants with no Se supply under drought stress. Thirteen miRNAs were identified to be associated with drought tolerance. These included 7 known (such as nta-miR156b and nta-miR166a) and 6 novel miRNAs (such as novel-nta-miR156-5p and novel-nta-miR209-5p) with the target genes of *squamosa promoter-binding-like protein 4* (*SPL4*), *serine/threonine protein phosphatase 2A* (*PPP2A*), *cation/calcium exchanger 4-like* (*CCX4*), *extensin-1 -like* (*EXT1*) and *reduced wall acetylation 2* (*RWA2*). Further investigation revealed that the expression levels of *Ext1* and *RWA2* were significantly decreased under drought stress but increased with Se addition. Moreover, key metabolites such as catechin and N-acetylneuraminic acid were identified, which may play a role in the regulation of drought tolerance. The integrated analysis of miRNA sequencing and metabolome highlighted the significance of the novel-nta-miR97-5p- *LRR-RLK*- catechin pathway in regulating drought tolerance. Our findings provide valuable insights into the molecular mechanisms underlying drought tolerance and Se-induced stress alleviation in cigar tobacco.

KEYWORDS

cigar tobacco, drought, selenium, multi-omics, target genes

1 Introduction

In the past few decades, the Earth's climate has been seriously impacted by global warming due to increasing levels of greenhouse gases in the Earth's atmosphere. This has affected normal rainfall patterns, which aggravated drought to extreme levels in many parts of the world, including China. Drought, as a major abiotic constraint on plant growth, has the potential to reduce crop yield by up to 15% (Leng and Hall, 2019). In China, annual losses in agricultural production caused by drought could reach up to 4.2 billion US dollars (USD), equating 0.23% of the national GDP (Su et al., 2018).

Drought stress induces oxidative stress in plants, leading to leaf structure damage and decreased photosynthesis and stomatal activity (Khan et al., 2023). Plants have evolved diverse strategies to cope with the harmful effects of drought, which involve the reprogramming of their transcriptome, proteome and metabolome profiles to enhance stress tolerance. Post-transcriptional regulation by microRNAs (miRNAs) is a crucial regulatory process underlying this reprogramming. The length of miRNAs ranges from 20 to 24 nucleotides in length and these miRNAs are involved in gene silencing in plants (Cuperus et al., 2011), many biological processes, such as plant growth, development, biotic and abiotic stress resistance (Chen, 2005; Cuperus et al., 2011; Teng et al., 2023). Teng et al. (2023) identified 23 differentially expressed miRNAs which were highly associated with Cd tolerance in maize. The target genes of these miRNAs were mainly involved in GSH metabolism, antioxidant enzyme activity and metal transport. Hormones such as abscisic acid and auxin play key roles in regulating drought tolerance in plants. For instance, miR167, which targets auxin response factor, was downregulated by abscisic acid application under drought stress (Liu et al., 2009). Several miRNAs (e.g., miRNA156, miR166, miR167 and miR168) have been demonstrated in certain plant species to regulate the expression of drought-responsive genes, including *SQUAMOSA promoter-binding protein-like* (*SPL*), *cation/Ca2+ exchanger* (*CCX*), *REDUCED WALL ACETYLATION* (*RWA*), *protein phosphatase 2* (*PP2*) *and exostosin glycosyltransferase* (*EXT*) (Gao et al., 2016; Zhang et al., 2018; Feyissa et al., 2019; Liu et al., 2020). Further investigation of drought regulated miRNAs and their target genes would greatly contribute to the understanding of the molecular basis underlying drought-stress tolerance in tobacco.

Tobacco (*Nicotiana tabacum* L.) is an annual or limited perennial herbaceous plant species that belongs to the Solanaceae family. It is a commercial crop extensively cultivated worldwide, including China. In recent years, the global consumption and demands for cigar tobacco have shown steady increase particularly in China and United States (Yan et al., 2021; Wang et al., 2022). Tobacco is primarily cultivated in semi-arid and rain-fed areas, heavily reliant on rainwater to meet the crop water demands. As tobacco is highly susceptible to drought stress, improving tolerance to drought stress in tobacco is of significant economic importance. A comprehensive understanding of drought-responsive transcriptional networks would facilitate the identification of integrated biological pathways involved in mitigating drought stress. Although some key drought responsive miRNAs such as miR160, miR162, miR166, miR168, 390, miR395 and miR398 (Rabara et al., 2015; Yin et al., 2015; Chen et al., 2017) have been identified in tobacco, none of the predicted targets have been further validated through cloning or sequence alignment.

Selenium (Se) is an essential micronutrient in plants and plays a significant role in mitigating the effects of abiotic stress (Cao et al., 2013; Lanza and Dos Reis, 2021). Previous reports have demonstrated the positive effects of Se application on plant drought stress tolerance, including increases in proline and chlorophyll content, accumulation of osmoprotectant and enhancement in antioxidant enzyme activity in plants (Ahmad et al., 2021; Han et al., 2022). Moreover, Se application in plants has been shown to reduce reactive oxygen species (ROS) toxicity under drought stress conditions (Han et al., 2022). Although several studies have reported improved plant performance in tobacco with Se application under drought stress through physiological assessments (Han et al., 2022), the molecular basis underlying this phenomenon remains largely unknown. Therefore, the objectives of this study were: (i) to investigate the negative effect of drought stress on plant growth, (ii) to identify metabolites, miRNAs and prediction of their targeted genes associated with increased drought tolerance, (iii) to demonstrate the effect of Se addition in mitigating plant drought tolerance by inducing the selected miRNAs, target genes and metabolite accumulation in tobacco.

2 Materials and methods

2.1 Plant materials and growth condition

The commercially grown tobacco cultivar 'CX26' is widely used for cigar wrapper production in Hubei Province, China. This cultivar was used in this experiment. Firstly, the seeds were germinated in pots filled with vermiculite and routinely irrigated to maintain adequate moisture levels (Bukhari et al., 2016). Forty-day seedlings were then transplanted to containers containing 12L nutrient solution. The composition of the nutrient solution was set according to Bukhari et al. (2016), which is represented in mg L^{-1}: $(NH_4)_2SO_4$, 48.2; K_2SO_4, 15.9; KNO_3, 18.5; KH_2PO_4, 24.8; $MgSO_4.7H_2O$, 154.88; $Ca(NO_3)_2.4H_2O$, 86.17; $ZnSO_4.7H_2O$, 0.11; Fe-Citrate, 7.0; $CuSO_4.5H_2O$, 0.04; $MnCl_2.4H_2O$, 0.9; H_2MoO_4, 0.01 and H_3BO_3, 2.9 (pH, 5.8). Plants were allowed to grow for 7 days in a glasshouse at the Zhengzhou Tobacco Research Institute before the treatments were added. Three treatments (including control) were used in this study: 20% PEG-6000 (Zhang et al., 2017) was added in the nutrient solution for drought stress (DS), with an additional dose of 3 μM Se (as Na_2SeO_3, Huang et al., 2021) for Se treatment (DSSe). There was no addition of PEG and Se in control plants (CK). The nutrient solutions were renewed weekly and

aerated by using air pumps. Plants were harvested after 6 days of respective treatments and further separated into shoots and roots, by keeping three biological replicates for each treatment. Harvested shoots were immediately stored at -80°C until further use.

2.2 Total RNA extraction, library construction and sequencing of small RNA

RNA was extracted from shoot samples using TRIzol reagent (Invitrogen, Carlsbad, CA, USA) according to the manufacturer's instructions. Nine small RNA libraries were constructed from the collected samples (three samples each per treatment). Total RNA was isolated using small RNA sample pre kit (Illumina, San Diego, California, America) according to the manufacturer's instructions. The adaptors were added to the small RNAs to reverse transcribe them into cDNA followed by amplification. Further, the PCR products were purified, and the libraries were obtained and quality was assessed using Agilent 2100 Bioanalyzer (Agilent, Palo Alto, CA, USA). Lastly, Illumina sequencing of small RNAs was carried out using HiSeq 4000 (Illumina, San Diego, CA, USA).

2.3 Identification of miRNAs

The identification of known and novel miRNAs were performed according to Xu et al. (2013). Briefly, small RNA reads were generated after sequencing and raw data was obtained. The adaptors and low-quality reads were discarded using the ACGT-miR program, and comparisons of clean reads were made using Rfam and GenBank databases. The matched non-coding snRNA, rRNA, tRNA and snoRNA sequences were removed and the remaining clean reads were mapped to the tobacco genome by using Bowtie software v1.1.2 with specific parameter settings according to Langmead et al. (2009). Those sequence reads identical to the known mature miRNAs were selected for subsequent analysis. The unannotated unique miRNAs with fold to stem-loop structure were regarded as novel miRNAs.

2.4 Identification of miRNAs in response to drought and selenium treatments with the prediction of target genes

Transcripts per million (TPM) was used to normalize the frequency of miRNAs according to He et al. (2016). Differentially expressed miRNAs (DEMs) between all treatments were detected using DEGseq. The screening criteria were set as: $\log_2$(DS vs CK) or $\log_2$(DSSe vs DS) > 1 (upregulated) or <−1 (downregulated), and p value ≤0.05. psRNATarget was used to predict target genes of miRNAs (Dai and Zhao, 2011). The prediction of potential target genes for the miRNAs was based on the following criteria: (1) less than four nucleotide mismatches between miRNAs and their target genes; (2) less than three consecutive nucleotide mismatches; and (3) no mismatches at the complementary site between the miRNA sequence and the target mRNA, specifically at positions 10 or 11 of the miRNA sequence, which are considered putative cleavage sites (Kantar et al., 2010).

Total RNA was extracted from stored leaf samples. qRT-PCR was carried out according to Lin et al. (2022). The PCR conditions were comprised of an initial denaturation step at 95°C for 3 min, second denaturation at 94°C for 60 s (40 cycles), annealing at 58°C for 30 s, extension at 72°C for 30 s, and finally extension at 72°C for 5 min. The relative expression level was determined using the ΔΔCT method. The tobacco *NttubA1* was used as a reference gene. The primers of *NtRWA2* and *NtEXT1* were listed in Table S1.

2.5 Metabolomic analysis

The extraction, identification and quantification of leaf metabolites were carried out according to Lin et al. (2022). Briefly, the samples were placed in tubes containing 1 ml extraction solution (methanol: acetonitrile: water, 2: 2: 1). After 40 Hz trituration for 4 min and 5 min sonification, the sample extracts were centrifuged at 12,000 rpm at 4°C for 20 min and supernatants were collected and further analyzed using a liquid chromatography–mass spectrometry (LC-MS) system. The metabolites were separated by a UHPLC system with a UPLC HSS T3 column. Briefly, the chromatographic separation was carried out using Hypersil GOLD aQ Dim column (Thermo Fisher Scientific, USA). The mobile phase consisted of a 0.1% formic acid aqueous solution (A solvent) and acetonitrile containing 0.1% formic acid (B solvent). The elution was conducted using the following gradient: 0-2 minutes, 5% B solvent; 2-22 minutes, 5-95% B solvent; 22-27 minutes, 95% B solvent; 27-27.1 minutes, 95-5% B solvent; 27.1-30 minutes, 5% B solvent. The flow rate was set at 0.3 ml min^{-1}. The temperature of column was set at 40°C, and the volume of injection was 5 µl. The metabolites were detected using a high-resolution tandem mass spectrometer. The data of mass spectrometry was then imported into Compound Discoverer 3.2 (Thermo Fisher Scientific, USA) software. By mapping the BMDB (BGI Metabolome Database, China), mzCloud database, and ChemSpider database, a data matrix that included information such as metabolite peak areas and identification results was obtained. Metabolites with fold change > 1.20 or < 0.83, P value < 0.05, were regarded as differentially accumulated metabolites, which were monitored in DS vs CK and DSSe vs DS treatments.

2.6 Statistical analysis

The illustration of graphs was performed using Origin software (Origin Lab Corporation, Wellesley Hills, Wellesley, MA, USA) and statistical analyses were conducted using Data Processing System

(DPS) statistical software. One-way ANOVA multiple comparisons and Duncan's multiple range test were used to compare the means of all the treatments used in this study. The significance of all tests was determined at a level of $P < 0.05$.

3 Results

3.1 Effects of drought stress and selenium treatment on plant growth

Drought stress markedly inhibited plant growth after 6 days of stress application (Figure 1) with the seedlings exhibiting clear symptoms of leaf chlorosis. The shoot dry weight of DS seedlings was only 50.3% of that of non-stressed (CK) seedlings (Figure 1), albeit no significant difference was found in their root dry weight. The shoot dry weight of DSSe seedlings was 38.8% higher than that of DS seedlings (Figure 1), with no significant differences were recorded in root dry weight.

3.2 Analysis of small RNAs

The differences in plant growth under different treatments led to the identification of drought tolerance-related miRNAs and their target genes. A total of 36,045,627, 36,604,788 and 35,979,733 raw reads were generated from the CK, DS and DSSe treatments, respectively (Table 1) and 35,124,114 (97.44%), 35,779,457 (97.75%) and 35,278,102 (98.05%) reads were remained after filtering and trimming of the CK, DS and DSSe groups, respectively. Of the high-quality sequence reads obtained, 95.38%, 95.36% and 95.37% of the CK, DS and DSSe groups were mapped to the tobacco genome (Table 1). In total, 1,006,917 (2.79%), 994,429 (2.72%) and 1,048,264 (2.91%) miRNA reads were mapped to the reference genome in the CK, DS and DSSe treatments, respectively. Of these, 142, 138 and 135 were conserved miRNAs, whereas 319, 302 and 309 were novel miRNAs identified in control, DS and DSSe treatments, respectively (Table 1).

Regarding the length distribution of miRNAs, the 21-24 nt sequences were found to be dominant with 24 nt sequences being the most abundant length amongst all the treatments (Figure 2). The conserved miRNAs were mainly distributed at 20 nt and 21 nt, whereas the novel miRNAs were mainly distributed at 19 nt, 20 nt and 21 nt (Figure 3).

3.3 Analysis of differentially expressed miRNAs under different treatments

The miRNA expression profiles were greatly influenced by the growth condition with 16 and 27 miRNAs being upregulated and downregulated, respectively, under drought treatment as compared to the control (Figure 4, Tables S1, S2). Among the downregulated miRNAs, 12 were known and 15 were novel. These novel miRNAs included miRNA156, miR166, miR167 and miR168 family miRNAs (Table S1). More than 75% (10) of the upregulated miRNAs were known, with only 3 novel miRNAs (Table S2). Those known miRNAs belonged to 12 miRNA families. Moreover, 28 upregulated and 20 downregulated miRNAs were detected in the DSSe as compared to DS (Tables S3, S4). Amongst 20 downregulated miRNAs identified, 11 were known and 9 were novel (Table S3). The downregulated miRNAs between DSSe and DS consisted of nta-miR156a (25.0-fold), nta-miR399f (24.7-fold) and novel-nta-miR27-5p (22.8-fold). Further, we recorded 12 known and 16 novel upregulated miRNAs in the DSSe as compared to DS and these included miR156b, miR156d, miR166a and miR390a (Table S4).

Interestingly, nine miRNAs were downregulated in DS vs CK but upregulated in DSSe vs DS (Group I, Figures 4, 5). These miRNAs were comprised of six novel (novel-nta-miR156-5p, novel-nta-miR209-5p, novel-nta-miR248-5p, novel-nta-miR345-3p, novel-nta-miR378-3p and novel-nta-miR97-5p) and three known miRNAs (nta-miR156b, nta-miR166a and nta-miR482b-3p). Furthermore, nta-miR156b was found to be downregulated (-24.5-fold) in DS but upregulated (22.8-fold) in DSSe (Table 2). Meanwhile, four miRNAs were upregulated in DS vs CK, while the four miRNAs were downregulated in DSSe vs DS (Group II,

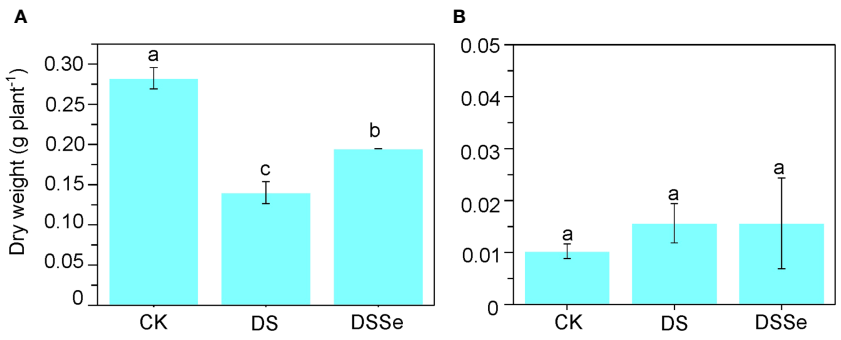

FIGURE 1
Exogenous application of Se drought stress tolerance in tobacco. The dry weight of shoot **(A)** and root **(B)** of CX26 grown under control (CK), drought stress (DS) and drought stress+Se (DSSe) conditions after 40 DAS. Drought stress was applied by adding 20% PEG-6000 into plant nutrient solution, while additional dose of 3 µM Na2SeO3 was supplied to drought + Se treatment. Data are presented as mean ± SD (n = 3). Different letters indicate statistically significant differences. DAS, days after sowing; Se, selenium; PEG, polyethylene glycol.

10.3389/fpls.2023.1255682

TABLE 1 Summary of high-throughput sequencing of small RNAs from tobacco shoots.

	CK[1]	DS	DSSe
Total raw reads	36,045,627	36,604,788	35,979,733
Total clean reads	35,124,114	35,779,457	35,278,102
	(97.44%)	(97.75%)	(98.05%)
Mapped reads	33,500,000	34,120,000	33,643,333
	(95.38%)	(95.36%)	(95.37%)
Total miRNA reads	1,006,917	994,429	1,048,264
	(2.79%)	(2.72%)	(2.91%)
Conserved miRNAs	142	138	135
Novel miRNAs	319	302	309

[1] CK, DS and DSSe correspond to tobacco grown in basic nutrient solution (BNS), BNS with 20% PEG, BNS with 20% PEG + 3 μM Na_2SeO_3, respectively.

Table 3). All those miRNAs were known, including nta-miR156c, nta-miR482c, nta-miR6019b and nta-miR6154a. The miRNAs of Group I and II may play key roles in Se-induced drought alleviation.

3.4 Identification of target genes and function categories of DEMs

We predicted the target genes of the identified miRNAs using psRNATarget. Gene Ontology (GO) analysis showed that these target genes are mainly involved in cellular process, metabolic process, cell, cell part, organelle, binding and catalytic activity (Figure 5A). Kyoto Encyclopedia of Genes and Genomes (KEGG) analysis revealed that these target genes were involved in translation, transcription and carbohydrate metabolism (Figure 5B). Moreover, these target genes were involved in cellular processes, environmental information processes and organismal systems (Figure 5B). We classified the resultant target genes into Groups I and II based on their predicted functions. Group I contained eleven target genes, including transcription factors, metal transporters, protein kinases and detoxification-related proteins (Table 2), with the identification of three transcription-related genes e.g., *transcription factor bHLH30-like*, *squamosa promoter-binding-like protein 4* (*SPL4*) and *homeobox-leucine zipper protein ATHB-15-like*. We also detected two metal transporters (*metal-nicotianamine transporter YSL7* and *cation/calcium exchanger 4-like SlCCX4*) and two protein kinase genes (*serine/threonine-protein kinase RUNKEL* and *LRR receptor-like serine/threonine-protein kinase*). The other four genes included *D-3-phosphoglycerate dehydrogenase 2, protein DETOXIFICATION 49-like, SPX domain-containing membrane protein At4g22990-like* (*SPX*) and *late blight resistance protein homolog R1A-10*. In Group II, the targets of the four miRNAs were *serine/threonine protein phosphatase 2A 55 kDa regulatory subunit B beta isoform-like* (*PP2A*), *TMV resistance protein N-like, extensin-1-like* (*EXT1*) and *Reduced Wall Acetylation 2* (*RWA2*). The putative secondary structures of the six novel miRNAs were also predicted (Figure 6).

To further investigate whether the differentially expressed miRNA target genes were involved in drought tolerance, we selected two target genes (*NtRWA2* and *NtEXT1*) for qRT-PCR analysis. The relative gene expression of *NtRWA2* and *NtEXT1* was significantly decreased in DS vs CK and inceased in DSSe vs DS (Figure 7). These results suggested that *NtRWA2* and *NtEXT1* might play an important function in regulating drought tolerance.

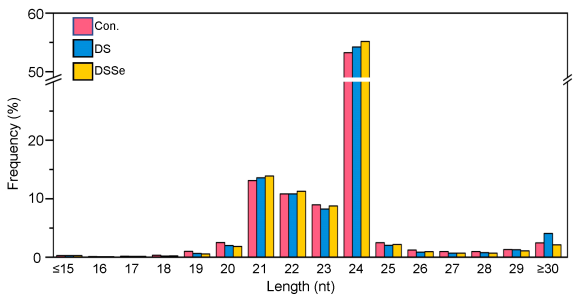

FIGURE 2
Length distribution of small RNAs in shoots of CX26. The X-axis represents the small RNA length (nucleotide) and the Y-axis represents the percentage of small RNA reads. Control (pink), DS (blue) and DSSe (yellow) represent control, drought (20% PEG-6000 treatment) and drought + 3 μM Na_2SeO_3.

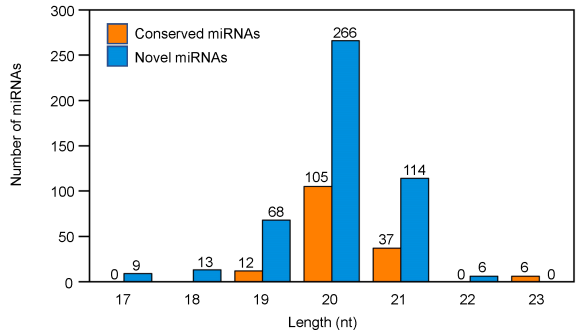

FIGURE 3
Length based distribution of conserved and novel microRNAs (miRNAs) in tobacco shoots.

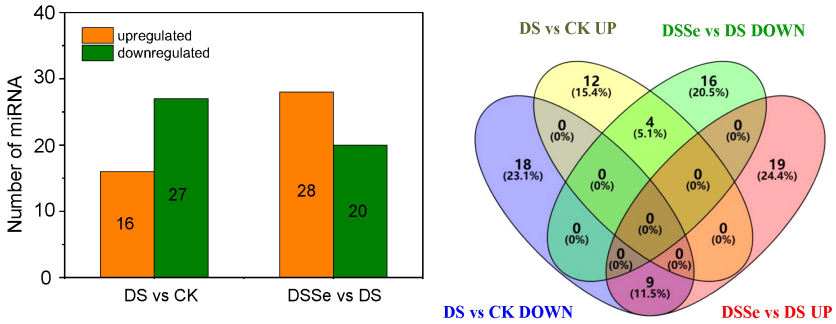

FIGURE 4
Differential expression miRNAs under DS and DSSe treatments. The CK, DS and DSSe represent control, drought and drought+Se.

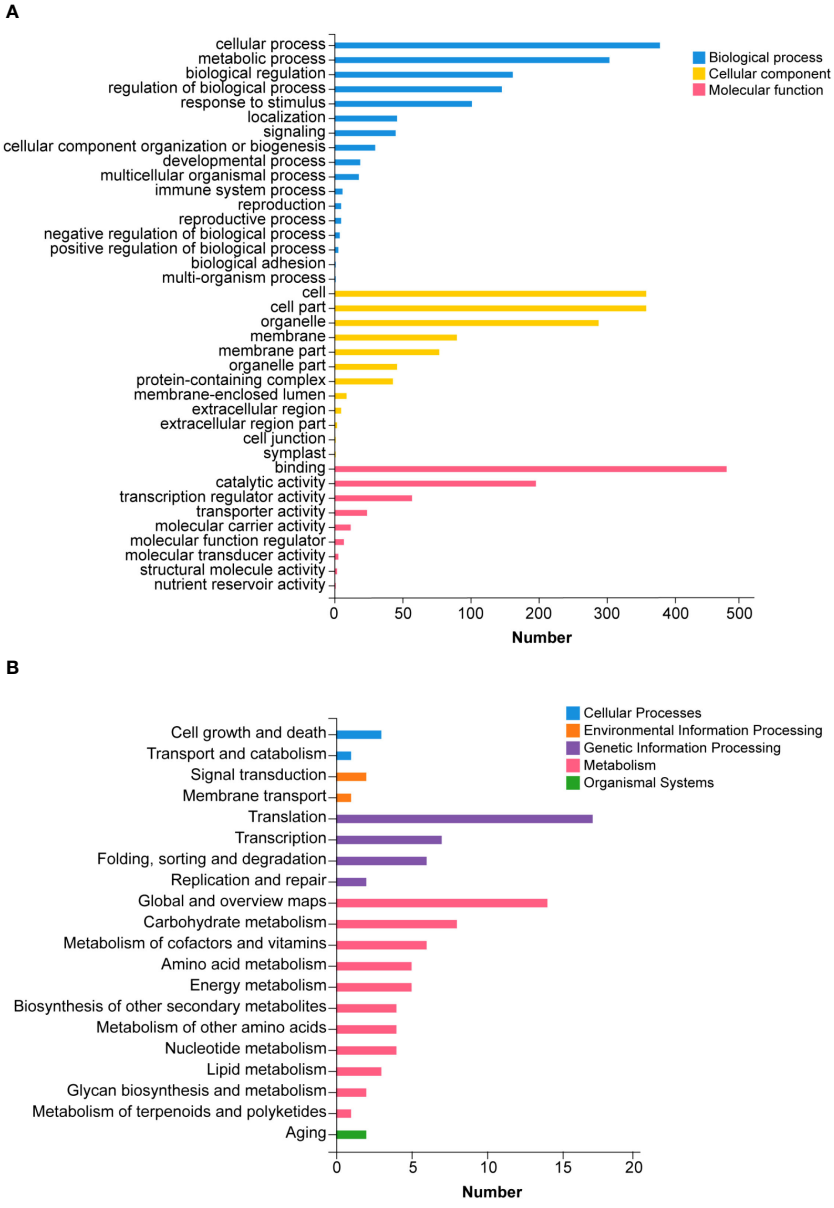

FIGURE 5
Gene Ontology (GO) **(A)** and Kyoto Encyclopedia of Genes and Genomes (KEGG) **(B)** analysis for target genes of differently expressed miRNA under different conditions in tobacco.

TABLE 2 List of miRNAs downregulated under DS treatment (DS vs control) but upregulated under DSSe treatment (DSSe vs D).

Gene ID	log_2 (DS/ CK)	Q value	log_2 (DSSe/ DS)	Q value	Target Gene ID	Annotation
novel-nta-miR156-5p	-2.2	0.001	1.57	3.46E-03	LOC107771768	transcription factor bHLH30-like
					LOC107796775	metal-nicotianamine transporter YSL7
novel-nta-miR209-5p	-1.8	0.043	1.91	1.34E-03	LOC107808871	serine/threonine-protein kinase RUNKEL
					LOC107808555	D-3-phosphoglycerate dehydrogenase 2,
novel-nta-miR248-5p	-7.1	0.003	5.31	7.38E-03	LOC107766225	protein DETOXIFICATION 49-like
novel-nta-miR345-3p	-8.9	0.016	8.86	1.02E-02	LOC107764608	SPX domain-containing membrane protein At4g22990-like
novel-nta-miR378-3p	-1.7	0.036	2.12	4.09E-07	LOC107790606	cation/calcium exchanger 4-like
novel-nta-miR97-5p	-2.7	0.000	1.49	1.69E-02	LOC107761676	LRR receptor-like serine/threonine-protein kinase
nta-miR156b	-24.5	0.000	22.82	3.20E-07	LOC107762327	squamosa promoter-binding-like protein 4
nta-miR166a	-9.2	0.004	9.44	3.32E-03	LOC107760551	homeobox-leucine zipper protein ATHB-15-like
nta-miR482b-3p	-8.8	0.003	9.65	4.71E-05	LOC107760541	putative late blight resistance protein homolog R1A-10

3.5 Analysis of differentially accumulated metabolites under different treatments

This study recorded 130 upregulated and 77 downregulated DAMs after drought treatment (DS vs CK), while there were 64 upregulated and 63 downregulated DAMs after the addition of Se (DSSe vs DS) (Figure S1). Interestingly, eight metabolites including ur-144 n-(2-hydroxypentyl) metabolite and o-[(2e)-hexenedioyl] carnitine were downregulated in DS treatment but were upregulated in DSSe treatment (Table 4). We also identified 14 metabolites were upregulated in DS treatment but downregulated in DSSe treatment, which included 9,10-dibromostearic acid, quinoline-3-carboxamides, lactose, N-acetylneuraminic acid and catechin (Table 5). These DAMs might play key roles in drought tolerance in tobacco.

4 Discussion

This study revealed differences between non-stressed and drought-stressed plants in their biomass production, miRNA expression and metabolite profiling. In addition, these differences were better visualized and understood by adding another treatment of Se, which helped to reduce the yield losses under drought conditions. Our results demonstrated that Se application can be used as a useful strategy to improve drought tolerance in tobacco. Recently, Han et al. (2022) compared the alleviation effects of selenite on drought stress in tobacco and found that different Se species could alleviate drought-induced growth inhibition via elevating photosynthesis, osmotic substance content, antioxidant enzyme activity and stress-responsive genes. However, the regulatory mechanisms of miRNAs conferring drought tolerance in tobacco are largely unknown. Our study has highlighted several important miRNAs that may be involved in regulating drought stress tolerance in tobacco. Based on the identified miRNAs and DAMs, we proposed a tentative model involving drought tolerance (Figure 8).

Establishing a correlation between miRNAs and metabolites could provide a better understanding of Se-induced drought tolerance in tobacco and identify key genes for drought tolerance.

TABLE 3 List of miRNAs upregulated under drought treatment (DS vs CK) but downregulated under DSSe treatment (DSSe vs D).

Gene ID	log_2 (DS/ CK)	Q value	log_2 (DSSe/ DS)	Q value	Target Gene ID	Annotation
nta-miR156c	7.66	0.00	-5.74	2E-02	LOC107770163	serine/threonine protein phosphatase 2A 55 kDa regulatory subunit B beta isoform-like
nta-miR482c	7.89	0.01	-9.78	2E-04	LOC107775023	TMV resistance protein N-like
nta-miR6019b	10.42	0.01	-11.35	4E-02	LOC107778652	extensin-1-like
nta-miR6154a	13.56	0.00	-13.54	3E-04	LOC107800019	protein REDUCED WALL ACETYLATION 2

10.3389/fpls.2023.1255682

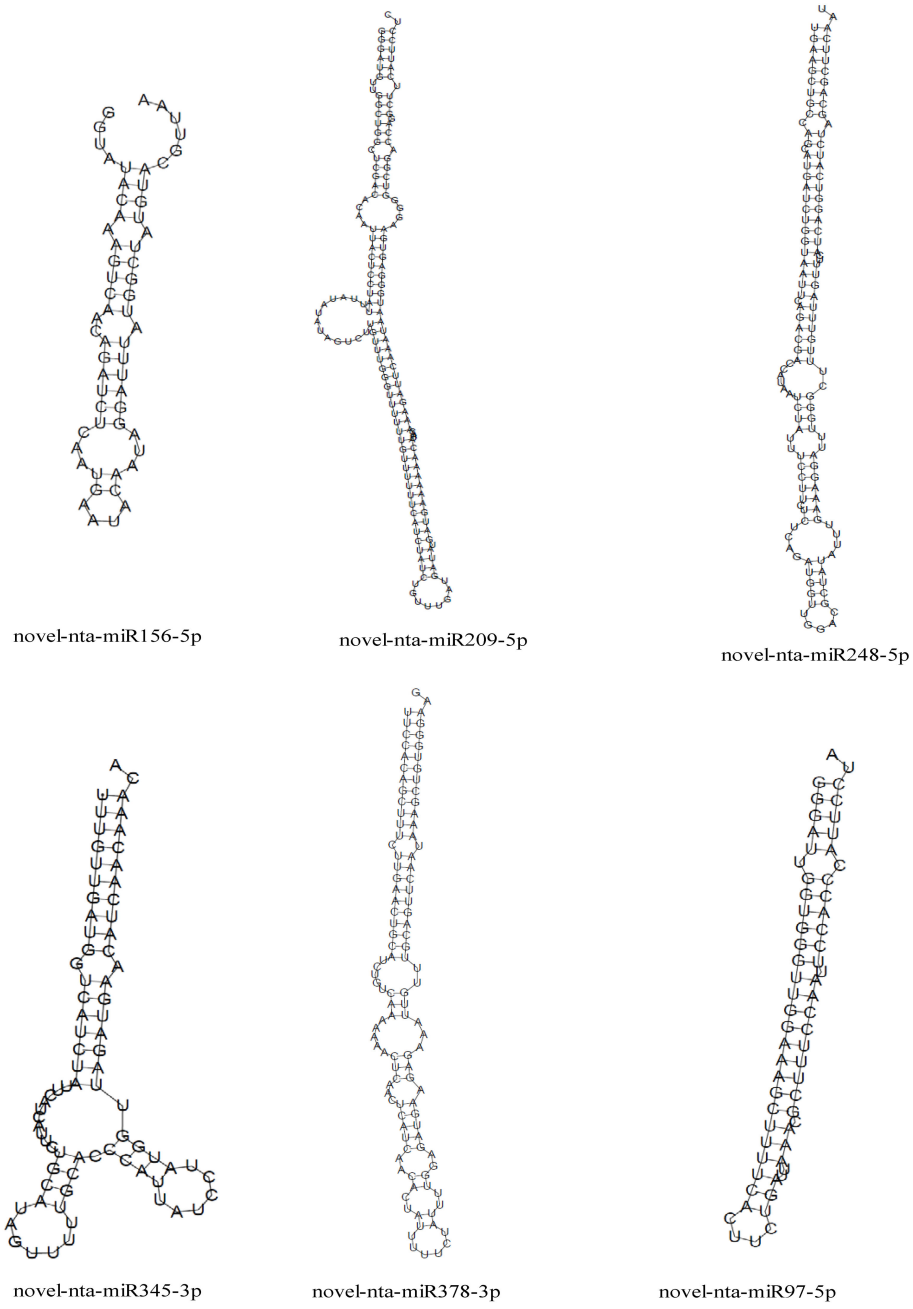

FIGURE 6
Precursor secondary structure prediction of 6 novel miRNAs.

In our study, we identified 2 miRNAs that showed significant positive or negative correlations with 6 metabolites (Table S6, Tables 2-5). The target genes of these miRNAs were *metal-nicotianamine transporter YSL7* (*YSL7*) and *LRR receptor-like serine/threonine-protein kinase* (*LRR-RLK*). Previous studies have reported the involvement of *OsYSL2* in the phloem transport of Fe and Mn in rice (Koike et al., 2004) and *ZmYSL2* for iron distribution and development in maize (Zang et al., 2020). Additionally, *OsYSL9* has been found to play a role in the distribution of Fe in developing rice grains (Senoura et al., 2017). In the present study, the novel-nta-miR156-5p exhibited significantly positive and negative correlation with phenyl hydrogen sulfate and lactose, respectively (Table S6). Similiarly, the novel-nta-miR97-5p exhibited negative correlations with butabarbital, catechin and oglufanide, and its target gene, *LRR-RLK*, has been implicated in regulating abiotic stress tolerance through ABA signaling activation and ROS detoxification (Ye et al., 2017). Catechin, a flavonoid, has been previously reported to enhance flooding tolerance by increasing the capacity of ROS scavenging (Yiu et al., 2011). Henschel et al. (2023) found that foliar

10.3389/fpls.2023.1255682

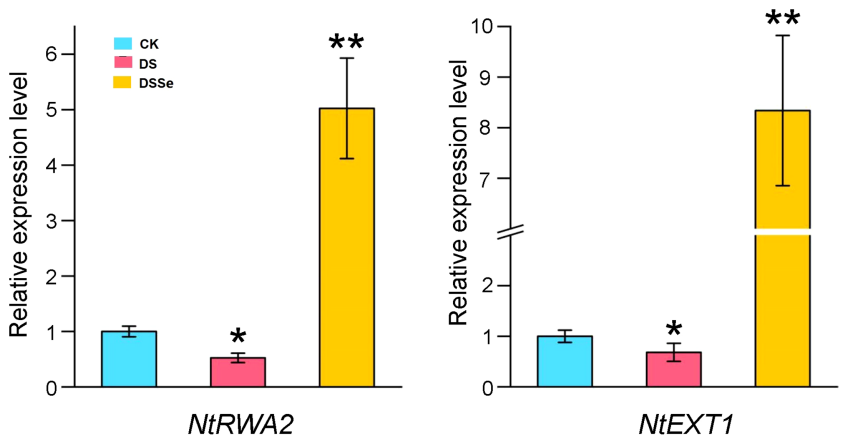

FIGURE 7
Relative expression of *NtRWA2* and *NtEXT1* under DS and DSSe treatments. * and ** represent significant difference at P <0.05 and 0.01, respectively.

application of L-carnitine significantly alleviated drought-induced growth inhibition by elevating membrane integrity and water balance in radish plants. In the present study, the abundance of carnitine was notably decreased under drought stress, but increased after the addition of Se, suggesting a potential positive correlation between carnitine and drought tolerance in tobacco. The accumulation of tea catechins have been found to be improved under drought stress (Lv et al., 2021). The possible mechanism by which catechin responds to drought stress may involve clearing over-accumulated reactive oxidative species (Lv et al., 2021), which is in agreement to the findings of our study. However, the abundance of catechins was found to be decreased after Se addition. This might be due to lower accumulation of ROS in plants under DSSE as compared to DS conditions. These results suggested that the novel-nta-miR97-5p- *LRR-RLK*- catechin pathway might play a central role in drought tolerance, which needs to be further validated in future studies.

Extensin and reduced wall acetylation proteins play numerous functions in plant cell wall (CW) (Manabe et al., 2013). Extensin is the most abundant protein in plant CW and has an important function in plant defense via strengthening the CW (Castilleux et al., 2021). The expression of *extensin-like gene* is significantly induced by drought stress in tolerant wheat genotypes but downregulated in sensitive genotypes under similar circumstances (Keskin, 2019). Manabe et al. (2013) found that the growth of the triple and quadruple *rwa* mutants was severely inhibited through affecting the cell differentiation of secondary CW, thus showing the significance of reduced wall acetylation (RWA) proteins in CW acetylation of plants. In the present study, the expression of *NtRWA2* and *NtEXT1* was significantly decreased in DS treatment but significantly increased in DSSe treatment (Figure 7), which reflects their importance in regulating drought tolerance in tobacco. The results presented in this study needs to be tested by conducting further studies for the better understanding of the drought tolerance mechanism in tobacco.

Several transcription factors regulate gene expression during plant growth and development when grown under stress conditions (Lin et al., 2022). Overexpression of *bHLH55* increases salt tolerance in maize (Yu et al., 2021). On the contrary, the knockout of *OsbHLH24* enhances salt tolerance in rice. Compared with wild type plants, the mutant plants have higher scavenging capacity of reactive oxygen species. Moreover, knock-out of

TABLE 4 List of metabolites downregulated under drought treatment (DS vs CK) but upregulated under DSSe treatment (DSSe vs D).

Metabolites	log_2 (DS/CK)	*P* Value	log_2 (DSSe/DS)	*P* Value
Ur-144 n-(2-hydroxypentyl)	0.49	0.02	1.48	0.03
O-[(2e)-hexenedioyl]carnitine	0.49	0.05	1.78	0.02
N-2-ethylhexyl bicycloheptenedicarboximide	0.33	0.01	3.20	0.01
N-(tetrahydrofuran-2-ylmethyl)quinoline-8-sulfonamide	0.29	0.01	2.31	0.03
1,4:3,6-dianhydro-2-deoxy-5-o-[(4-isopropylphenyl)carbamoyl]-2-[(4-methylbenzoyl)amino]-d-glucitol	0.28	0.02	2.28	0.05
2-[(3s)-1-benzyl-3-pyrrolidinyl]-1-methyl-1h-benzimidazole	0.24	0.04	1.50	0.04
N,N-diethyl-9-oxobicyclononane-3-carboxamide	0.14	0.02	5.86	0.01
phenyl hydrogen sulfate	0.04	0.05	3.15	0.03

phenyl hydrogen sulfate, 2-hydroxy-5-[3-(4-methoxy-1-benzofuran-5-yl)-3-oxopropanoyl]phenyl hydrogen sulfate.

10.3389/fpls.2023.1255682

TABLE 5 List of metabolites upregulated under drought treatment (DS vs CK) but downregulated under DSSe treatment (DSSe vs D).

Metabolites	log_2 (DS/CK)	P Value	log_2 (DSSe/DS)	P Value
9,10-dibromostearic acid	21.64	0.00	0.04	0.00
Quinoline-3-carboxamides	17.39	0.04	0.05	0.02
Lactose	14.34	0.02	0.14	0.05
Oglufanide	6.71	0.01	0.27	0.01
Catechin	3.09	0.02	0.39	0.02
Butabarbital	3.05	0.03	0.26	0.02
Rhusflavanone	2.75	0.01	0.42	0.01
N-acetylneuraminic acid	2.42	0.05	0.19	0.00
Mfcd12912432	2.33	0.01	0.47	0.03
Dl-arginine	1.84	0.02	0.40	0.01
Homosalate	1.49	0.01	0.69	0.02
13,14-dihydro-15-keto-tetranor prostaglandin d2	1.49	0.03	0.70	0.03
(25s)-11alpha,20,26-trihydroxyecdysone	1.37	0.04	0.72	0.03
T-2 triol	1.37	0.04	0.62	0.03

OsbHLH24 also markedly upregulated salt tolerance-related genes, such as *OsSOS1*, *OsHAK7* and *OsHKT1;3* (Alam et al., 2022). In addition, the *SPL* gene family is involved in the activation of the conserved miR156-*SPL* module, which is a key regulator of plant abiotic stress resistance (Wang et al., 2019). Overexpression of *MtHB2* (a homeobox-leucine zipper protein) in transgenic *Arabidopsis* leads to a greater more sensitivity to salt and drought compared with the wild type (Song et al., 2012). In this study, the expressions of novel-nta-miR156-5p, nta-miR156b and nta-miR166a was significantly downregulated in DS treatment but upregulated in DSSe treatment (Table 2). Their targets were *transcription factor bHLH30-like, squamosa promoter-binding-like protein 4* and *homeobox-leucine zipper protein ATHB-15-like*. These results suggested that the transcription factors may negatively regulate drought tolerance and Se addition can inhibit the expression of these genes via regulating miRNA expression.

Drought stress affects the uptake and transport of nutrient element (Lanza and Dos Reis, 2021). The cation/calcium exchanger (CCX) family is involved in the transport of Ca and other cations (Su et al., 2021). Yang et al. (2021) found that apple *MdCCX2* positively regulated salt tolerance by decreasing Na^+ content and elevating the ability of ROS scavenge. SPX proteins play a negative role in regulating phosphorus signaling and are involved in inhibiting the phosphorus starvation response by *PHR* genes (Zhang et al., 2021). In this study, several members of *metal-nicotianamine transporter* (*YSL*), *CCX* and *SPX* family target genes were identified in tobacco (Table 2). Our results suggested that the target genes may elevate drought tolerance via regulating the uptake, transport and distribution of nutrient elements, such as phosphorus. Further research needs to be carried out in future to investigate how miRNA and target genes regulate these processes.

This study identified two protein kinase genes as miRNA targets, *serine/threonine-protein kinase RUNKEL* and *LRR-RLK* (Table 2). Their corresponding miRNAs were novel-nta-miR209-5p and novel-nta-miR97-5p. Previous studies found that serine/threonine-protein kinases were involved in abiotic stress tolerance (Luo et al., 2006). The above differentially expressed miRNAs may negatively regulate drought tolerance by inhibiting the two protein kinases. Meanwhile, we also found four miRNAs that were upregulated in DS and downregulated in DSSe treatment (Table 3). One of their targets was *serine/threonine protein phosphatase 2A (PP2A) 55 kDa regulatory subunit B beta isoform-like*. *PP2A* also positively regulates abiotic stress tolerance in wheat (Liu et al., 2019). These miRNAs and their target modules may positively regulate drought tolerance in tobacco.

This study revealed 22 differentially accumulated metabolites, which might be associated to regulate drought tolerance. We suggest that further research needs to be carried out to investigate the relationship between the identified DAMs and drought tolerance, and how miRNA operates for the activation of metabolite pathways that led to their increased accumulation.

5 Conclusions

Selenium application significantly alleviated drought-induced growth inhibition. The present study identified seven known and six

10.3389/fpls.2023.1255682

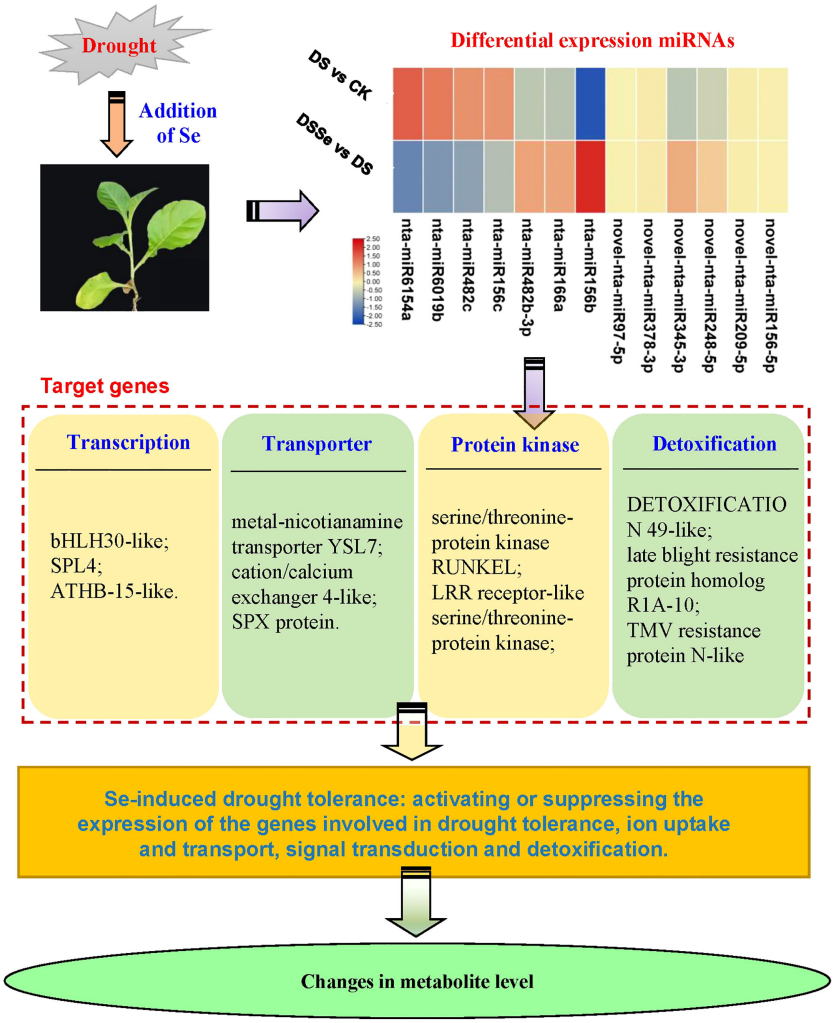

FIGURE 8
A working model of miRNAs and their target genes in tobacco involving in Se-induced increased drought tolerance. ATHB-15-like, homeobox-leucine zipper protein ATHB-15-like; bHLH30-like, transcription factor bHLH30-like; SPX protein, SPX domain-containing membrane protein; SPL4, squamosa promoter-binding-like protein 4.

novel miRNAs in tobacco seedlings associated with Se-induced drought stress alleviation, including nta-miR156c, nta-miR482c, nta-miR6019b and nta-miR6154a. Functional analysis of the identified target genes revealed that these miRNAs belonged to transcription factors, metal transporters, protein kinase, etc. Twenty-two key metabolites were identified to be involved in drought tolerance. The combined analysis of miRNA sequencing and metabolome identified a metabolic pathway associated with regulating drought tolerance. Thus far, this is the first study to investigate the effect of exogenous Se application in regulating plant drought-tolerance in tobacco using a multi-omics strategy. The implications of this research helped to better understand the physiological and molecular basis underlying Se mediated defense mechanisms in tobacco. The identified miRNAs and their targets can be used in future to achieve greater drought tolerance in tobacco.

Data availability statement

The original contributions presented in the study are included in the article/Supplementary Material. Further inquiries can be directed to the corresponding authors.

Author contributions

HD: Conceptualization, Writing – original draft, Writing – review & editing, Data curation. JY: Conceptualization, Methodology, Writing – original draft. LT: Visualization, Writing – original draft. ZW: Data curation, Writing – original draft. TL: Data curation, Formal Analysis, Writing – original draft. WK: Data curation, Writing – review & editing. RY: Formal Analysis, Investigation, Writing – original draft. BQ: Investigation, Writing

– original draft. YZ: Resources, Supervision, Writing – review & editing. CY: Project administration, Resources, Writing – review & editing.

Funding

This work was supported by CNTC Research Program [110202101013(XJ-05)] and the Natural Science Foundation of Henan Province (182300410055).

Conflict of interest

The authors declare that the research was conducted in the absence of any commercial or financial relationships that could be construed as a potential conflict of interest.

Publisher's note

Supplementary material

The Supplementary Material for this article can be found online at: https://www.frontiersin.org/articles/10.3389/fpls.2023.1255682/full#supplementary-material

References

Ahmad, Z., Anjum, S., Skalicky, M., Waraich, E. A., Muhammad, S. T. R., Ayub, M. A., et al. (2021). Selenium alleviates the adverse effect of drought in oilseed crops camelina (*Camelina sativa* L.) and canola (*Brassica napus* L.). *Molecules* 26 (6), 1699. doi: 10.3390/molecules26061699

Alam, M. S., Kong, J., Tao, R., Ahmed, T., Alamin, M., Alotaibi, S. S., et al. (2022). CRISPR/Cas9 mediated knockout of the OsbHLH024 transcription factor improves salt stress resistance in rice (*Oryza sativa* L.). *Plants* 11 (9), 1184. doi: 10.3390/plants11091184

Bukhari, S. A. H., Wang, R., Wang, W., Ahmed, I. M., Zheng, W., and Cao, F. (2016). Genotype-dependent effect of exogenous 24-epibrassinolide on chromium-induced changes in ultrastructure and physicochemical traits in tobacco seedlings. *Environ. Sci. pollut. Res.* 23, 18229–18238. doi: 10.1007/s11356-016-7017-2

Cao, F., Wang, N., Zhang, M., Dai, H., Dawood, M., Zhang, G., et al. (2013). Comparative study of alleviating effects of GSH, Se and Zn under combined contamination of cadmium and chromium in rice (*Oryza sativa*). *Biometals* 26, 297–308. doi: 10.1007/s10534-013-9611-9

Castilleux, R., Plancot, B., Vicré, M., Nguema-Ona, E., and Driouich, A. (2021). Extensin, an underestimated key component of cell wall defence? *Ann. Bot.* 127 (6), 709–713. doi: 10.1093/aob/mcab001

Chen, X. (2005). microRNA biogenesis and function in plants. *FEBS Lett.* 579 (26), 5923–5931. doi: 10.1016/j.febslet.2005.07.071

Chen, Q., Li, M., Zhang, Z., Tie, W., Chen, X., Jin, L., et al. (2017). Integrated mRNA and microRNA analysis identifies genes and small miRNA molecules associated with transcriptional and post-transcriptional-level responses to both drought stress and re-watering treatment in tobacco. *BMC Genomics* 18, 1–16. doi: 10.1186/s12864-016-3372-0

Cuperus, J. T., Fahlgren, N., and Carrington, J. C. (2011). Evolution and functional diversification of *MIRNA* genes. *Plant Cell* 23 (2), 431–442. doi: 10.1105/tpc.110.082784

Dai, X., and Zhao, P. (2011). psRNATarget: a plant small RNA target analysis server. *Nucleic Acids Res.* 39 (suppl_2), W155–W159. doi: 10.1093/nar/gkr319

Feyissa, B. A., Arshad, M., Gruber, M. Y., Kohalmi, S. E., and Hannoufa, A. (2019). The interplay between *miR156/SPL13* and *DFR/WD40–1* regulate drought tolerance in alfalfa. *BMC Plant Biol.* 19 (1), 1–19. doi: 10.1186/s12870-019-2059-5

Gao, F., Wang, N., Li, H., Liu, J., Fu, C., Xiao, Z., et al. (2016). Identification of drought-responsive microRNAs and their targets in *Ammopiptanthus mongolicus* by using high-throughput sequencing. *Sci. Rep.* 6 (1), 34601. doi: 10.1038/srep34601

Han, D., Tu, S., Dai, Z., Huang, W., Jia, W., Xu, Z., et al. (2022). Comparison of selenite and selenate in alleviation of drought stress in *Nicotiana tabacum* L. *Chemosphere* 287, 132136. doi: 10.1016/j.chemosphere.2021.132136

He, X., Zheng, W., Cao, F., and Wu, F. (2016). Identification and comparative analysis of the microRNA transcriptome in roots of two contrasting tobacco genotypes in response to cadmium stress. *Sci. Rep.* 6 (1), 32805. doi: 10.1038/srep32805

Henschel, J. M., Dantas, E. F. O., de Azevedo Soares, V., Dos Santos, S. K., da Silva Gomes, D., Ferreira, L. M., et al. (2023). Drought stress mitigation by foliar application of L-carnitine and its effect on radish morphophysiology. *Physiol. Mol. Biol. Plants* 29, 579–590. doi: 10.1007/s12298-023-01308-6

Huang, H., Li, M., Rizwan, M., Dai, Z., Yuan, Y., Hossain, M. M., et al. (2021). Synergistic effect of silicon and selenium on the alleviation of cadmium toxicity in rice plants. *J. Hazard. Mater.* 401, 123393. doi: 10.1016/j.jhazmat.2020.123393

Kantar, M., Unver, T., and Budak, H. (2010). Regulation of barley miRNAs upon dehydration stress correlated with target gene expression. *Funct. Integr. Genomics* 10, 493–507. doi: 10.1007/s10142-010-0181-4

Keskin, B. C. (2019). Quantitative mRNA expression profiles of germin-like and extensin-like proteins under drought stress in *Triticum aestivum*. *Int. J. Life Sci. Biotechnol.* 2 (2), 95–107. doi: 10.38001/ijlsb.566942

Khan, R., Ma, X., Hussain, Q., Chen, K., Farooq, S., Asim, M., et al. (2023). Transcriptome and anatomical studies reveal alterations in leaf thickness under long-term drought stress in tobacco. *J. Plant Physiol.* 281, 153920. doi: 10.1016/j.jplph.2023.153920

Koike, S., Inoue, H., Mizuno, D., Takahashi, M., Nakanishi, H., Mori, S., et al. (2004). OsYSL2 is a rice metal-nicotianamine transporter that is regulated by iron and expressed in the phloem. *Plant J.* 39 (3), 415–424. doi: 10.1111/j.1365-313X.2004.02146.x

Langmead, B., Trapnell, C., Pop, M., and Salzberg, S. L. (2009). Ultrafast and memory-efficient alignment of short DNA sequences to the human genome. *Genome Biol.* 10, R25. doi: 10.1186/gb-2009-10-3-r25

Lanza, M. G. D. B., and Dos Reis, A. R. (2021). Roles of selenium in mineral plant nutrition: ROS scavenging responses against abiotic stresses. *Plant Physiol. Biochem.* 164, 27–43. doi: 10.1016/j.plaphy.2021.04.026

Leng, G., and Hall, J. (2019). Crop yield sensitivity of global major agricultural countries to droughts and the projected changes in the future. *Sci. Total Environ.* 654, 811–821. doi: 10.1016/j.scitotenv

Lin, K., Zeng, M., Williams, D. V., Hu, W., Shabala, S., Zhou, M., et al. (2022). Integration of transcriptome and metabolome analyses reveals the mechanistic basis for cadmium accumulation in maize. *Iscience* 25 (12), 105484. doi: 10.1016/j.isci.2022.105484

Liu, D., Li, B., Feng, G., Mao, X., Li, A., Chang, X., et al. (2019). TaPP2AbB″;-γ, a wheat regulatory subunit of PP2A enhanced abiotic stress tolerance. *Plant Growth Regul.* 89, 345–355. doi: 10.1007/s10725-019-00540-z

Liu, X., Tan, C., Cheng, X., Zhao, X., Li, T., and Jiang, J. (2020). miR168 targets Argonaute1A mediated miRNAs regulation pathways in response to potassium deficiency stress in tomato. *BMC Plant Biol.* 20 (1), 1–17. doi: 10.1186/s12870-020-02660-5

Liu, Q., Zhang, Y., Wang, C., Luo, Y., Huang, Q., Chen, S., et al. (2009). Expression analysis of phytohormone-regulated microRNAs in rice, implying their regulation roles in plant hormone signaling. *FEBS Lett.* 583, 723–728. doi: 10.1016/j.febslet.2009.01.020

Luo, G. Z., Wang, Y. J., Xie, Z. M., Gai, J. Y., Zhang, J. S., and Chen, S. Y. (2006). The putative Ser/Thr protein kinase gene *GmAAPK* from soybean is regulated by abiotic stress. *J. Integr. Plant Biol.* 48 (3), 327–333. doi: 10.1111/j.1744-7909.2006.00169.x

Lv, Z., Zhang, C., Shao, C., Liu, B., Liu, E., Yuan, D., et al. (2021). Research progress on the response of tea catechins to drought stress. *J. Sci. Food Agric.* 101 (13), 5305–5313. doi: 10.1002/jsfa.11330

Manabe, Y., Verhertbruggen, Y., Gille, S., Harholt, J., Chong, S.-L., Pawar, P. M.-A., et al. (2013). Reduced wall acetylation proteins play vital and distinct roles in cell wall O-acetylation in *Arabidopsis*. *Plant Physiol.* 163 (3), 1107–1117. doi: 10.1104/pp.113.225193

Rabara, R. C., Tripathi, P., Reese, R. N., Rushton, D. L., Alexander, D., Timko, M. P., et al. (2015). Tobacco drought stress responses reveal new targets for Solanaceae crop improvement. *BMC Genomics* 16, 1–23. doi: 10.1186/s12864-015-1575-4

Senoura, T., Sakashita, E., Kobayashi, T., Takahashi, M., Aung, M. S., Masuda, H., et al. (2017). The iron-chelate transporter OsYSL9 plays a role in iron distribution in developing rice grains. *Plant Mol. Biol.* 95, 375–387. doi: 10.1007/s11103-017-0656-y

Song, S., Chen, Y., Zhao, M., and Zhang, W. (2012). A novel Medicago truncatula HD-Zip gene, MtHB2, is involved in abiotic stress responses. *Environ. Exp. Bot.* 80, 1–9. doi: 10.1016/j.envexpbot.2012.02.001

Su, B., Huang, J., Fischer, T., Wang, Y., Kundzewicz, Z. W., Zhai, J., et al. (2018). Drought losses in China might double between the 1.5 C and 2.0 C warming. *Proc. Natl. Acad. Sci. U.S.A.* 115 (42), 10600–10605. doi: 10.1073/pnas.1802129115

Su, W., Zhang, C., Wang, D., Ren, Y., Sun, T., Feng, J., et al. (2021). The CaCA superfamily genes in Saccharum: Comparative analysis and their functional implications in response to biotic and abiotic stress. *BMC Genomics* 22 (1), 1–19. doi: 10.1186/s12864-021-07828-3

Teng, L., Zhang, X., Wang, R., Lin, K., Zeng, M., Chen, H., et al. (2023). miRNA transcriptome reveals key miRNAs and their targets contributing to the difference in Cd tolerance of two contrasting maize genotypes. *Ecotoxicol. Environ. Saf.* 256, 114881. doi: 10.1016/j.ecoenv.2023.114881

Wang, X., Kim, Y., Borowiecki, M., Tynan, M. A., Emery, S., and King, B. A. (2022). Trends in Cigar sales and prices, by product and flavor type—the United States 2016–2020. *Nicotine Tob. Res.* 24 (4), 606–611. doi: 10.1093/ntr/ntab238

Wang, J., Ye, Y., Xu, M., Feng, L., and Xu, L. (2019). Roles of the SPL gene family and miR156 in the salt stress responses of tamarisk (*Tamarix chinensis*). *BMC Plant Biol.* 19, 1–11. doi: 10.1186/s12870-019-1977-6

Xu, F., Liu, Q., Chen, L., Kuang, J., Walk, T., Wang, J., et al. (2013). Genome-wide identification of soybean microRNAs and their targets reveals their organ-specificity and responses to phosphate starvation. *BMC Genomics* 14, 1–30. doi: 10.1186/1471-2164-14-66

Yan, X., Wang, Y., Lei, J., Zhou, J., Pan, Y., Hu, X., et al. (2021). Classification of domestic cigars and its practical application. *Acta Tabacaria Sin.* 27 (5), 100–109. doi: 10.16472/j.Chinatobacco.2021.T0029

Yang, J., Guo, X., Li, W., Chen, P., Cheng, Y., Ma, F., et al. (2021). MdCCX2 of apple functions positively in modulation of salt tolerance. *Environ. Exp. Bot.* 192, 104663. doi: 10.1016/j.envexpbot.2021.104663

Ye, Y., Ding, Y., Jiang, Q., Wang, F., Sun, J., and Zhu, C. (2017). The role of receptor-like protein kinases (RLKs) in abiotic stress response in plants. *Plant Cell Rep.* 36, 235–242. doi: 10.1007/s00299-016-2084-x

Yin, F., Qin, C., Gao, J., Liu, M., Luo, X., Zhang, W., et al. (2015). Genome-wide identification and analysis of drought-responsive genes and microRNAs in tobacco. *Int. J. Mol. Sci.* 16 (3), 5714–5740. doi: 10.3390/ijms16035714

Yiu, J., Tseng, M., and Liu, C. (2011). Exogenous catechin increases antioxidant enzyme activity and promotes flooding tolerance in tomato (*Solanum lycopersicum* L.). *Plant Soil* 344, 213–225. doi: 10.1007/s11104-011-0741-y

Yu, C., Yan, M., Dong, H., Luo, J., Ke, Y., Guo, A., et al. (2021). Maize bHLH55 functions positively in salt tolerance through modulation of AsA biosynthesis by directly regulating GDP-mannose pathway genes. *Plant Sci.* 302, 110676. doi: 10.1016/j.plantsci.2020.110676

Zang, J., Huo, Y., Liu, J., Zhang, H., Liu, J., and Chen, H. (2020). Maize YSL2 is required for iron distribution and development in kernels. *J. Exp. Bot.* 71 (19), 5896–5910. doi: 10.1111/j.1365-313X.2004.02146.x

Zhang, J., Zhang, H., Srivastava, A. K., Pan, Y., Bai, J., Fang, J., et al. (2018). Knockdown of rice microRNA166 confers drought resistance by causing leaf rolling and altering stem xylem development. *Plant Physiol.* 176 (3), 2082–2094. doi: 10.1104/pp.17.01432

Zhang, K., Zhou, Z., Li, J., Wang, J., Yu, L., and Lin, S. (2021). SPX-related genes regulate phosphorus homeostasis in the marine phytoplankton, *Phaeodactylum tricornutum*. *Commun. Biol.* 4 (1), 797. doi: 10.1038/s42003-021-02284-x

Zhang, S., Zhuang, K., Wang, S., Lv, J., Ma, N., and Meng, Q. (2017). A novel tomato SUMO E3 ligase, SlSIZ1, confers drought tolerance in transgenic tobacco. *J. Integr. Plant Biol.* 59, 102–117. doi: 10.1111/jipb.12514

frontiers | Frontiers in Plant Science

TYPE Original Research
PUBLISHED 12 October 2023
DOI 10.3389/fpls.2023.1261518

OPEN ACCESS

EDITED BY
Shaojun Dai,
Shanghai Normal University, China

REVIEWED BY
Jie Zhang,
Foshan University, China
Khurram Bashir,
Lahore University of Management Sciences, Pakistan

*CORRESPONDENCE
Dawei Zhang
zhangdawei@hnust.edu.cn
Mingli Yan
ymljack@126.com

†PRESENT ADDRESS
Ting Li,
Ningyuan First Middle School, Yongzhou, China

‡These authors have contributed equally to this work

RECEIVED 25 July 2023
ACCEPTED 26 September 2023
PUBLISHED 12 October 2023

CITATION
Li T, Li Y, Wang J, Peng J, Liu L, Deng L, Zhang D and Yan M (2023) Expression in *A. thaliana* and cellular localization reveal involvement of *BjNRAMP1* in cadmium uptake.
Front. Plant Sci. 14:1261518.
doi: 10.3389/fpls.2023.1261518

Expression in *A. thaliana* and cellular localization reveal involvement of *BjNRAMP1* in cadmium uptake

Ting Li[1†‡], Yicun Li[1‡], Jiaqi Wang[1], Jiashi Peng[1], Lili Liu[1], Lichao Deng[2], Dawei Zhang[1,2*] and Mingli Yan[2*]

[1]Hunan Key Laboratory of Economic Crops Genetic Improvement and Integrated Utilization, School of Life and Health Science, Hunan University of Science and Technology, Xiangtan, China, [2]Hunan Research Center of Heterosis Utilization in Rapeseed, Crop Research Institute, Hunan Academy of Agricultural Sciences, Changsha, China

Although *Brassica juncea* has demonstrated potential as a hyperaccumulator crop, it was not entirely clear how cadmium (Cd) accumulates in plants. Here, we found that BjNRAMP1 (Natural Resistance-Associated Macrophage Protein 1) plays a crucial role in the accumulation of Cd and manganese (Mn) through its expression in yeast and *Arabidopsis thaliana*. The high concentration of Cd exposure could induce the expression of *BjNRAMP1*. The ectopic expression of *BjNRAMP1* in yeast led to higher accumulation of Cd and Mn compared to the vector control. BjNARAMP1 was localized to the plasma membrane and expressed in the vascular system of roots, leaves, and flowers. The overexpression of *BjNRAMP1* in *A. thaliana* resulted in an increased accumulation of Cd in both roots and shoots, which inhibited the normal growth of transgenic lines. Moreover, Mn uptake in roots was activated by the increase in Cd stress. Together, our results indicated that BjNRAMP1 significantly contributes to the uptake of Mn and Cd in *B. juncea*.

KEYWORDS

***Brassica juncea*, cadmium, cellular localization, manganese, uptake**

1 Introduction

Agricultural soils are under threat of cadmium (Cd) contamination from natural processed and anthropogenic activities, leading to human health risks after chronic dietary exposure (Zhao et al., 2015; Zhao et al., 2022). Among several strategies to prevent the negative effects of Cd, crop breeding or engineering is the key to either increasing the Cd accumulation in nonedible parts for phytoremediation or reducing that in edible parts for safer food (Clemens et al., 2013; Clemens, 2019). Thus, understanding the mechanisms of Cd uptake, translocation, and detoxification provides potential targets for marker-assisted breeding or genetic engineering of crops that accumulated either high or low levels of Cd (Zhao and Wang, 2020).

As a toxic element, Cd was inadvertently taken up into root cells and transported to other plant tissues via membrane transporters for essential or beneficial nutrients. NRAMP5 (Natural Resistance Associated Macrophage Proteins 5) has been identified as a major Cd transporter in rice. The use of RNAi or CRISPR/Cas9 to knock out *OsNramp5* led to a significant reduction in the Cd concentration in the root, shoot, and grain (Sasaki et al., 2012; Tang et al., 2017). OsNRAMP1 was located to the plasma membrane of endodermis and pericycle cells, and it is involved in the Cd uptake and transport within the cells. The higher expression of *OsNRAMP1* in the roots resulted in an increase in Cd accumulation in the shoots. The growth of yeast expressing *OsNRAMP1* was impaired in the presence of Cd compared with yeast transformed with an empty vector (Takahashi et al., 2011). However, the expression of *OsNRAMP1* in *Arabidopsis thaliana* conferred tolerance phenotype with increased Cd accumulation in the root and shoot (Tiwari et al., 2014). *OsNRAMP1* expression could be induced by both Cd treatment and Fe deficiency. The knockout of *OsNRAMP1* resulted in significant decreases in root uptake of Cd and Mn, while the effect was less than in those from knockout of *OsNRAMP5* (Chang et al., 2020).

Brassica juncea is an important vegetable- and oil-use crop worldwide and exhibits the potential to tolerate and accumulate Cd, and it can be considered as a Cd hyperaccumulator plant (Kang et al., 2021; Zeremski et al., 2021). Our previous study suggested that a higher concentration of Cd could induce the expression of *BjNRAMP1*, while its role in Cd transport in *B. juncea* is hitherto unknown (Zhang et al., 2021). Herein, we found that BjNRAMP1 was localized to the plasma membrane and played a vital role in Cd accumulation through its expression in yeast and *A. thaliana*.

2 Materials and methods

2.1 Plant materials and growth condition

The *B. juncea* cultivar "Purple Leaf Mustard" was grown in Cd-contaminated soils as described previously (Zhang et al., 2021).

The *A. thaliana* plants were grown in soil to generate the T3 homozygous transgenic lines. The wild type (Col-0) and T3 lines were cultured in 1/2MS medium containing 0, 10, 30, and 50 μM $CdCl_2$ for 10 days at 22°C under a 16-h light/8-h dark cycle.

2.2 Cloning and sequence analysis of *BjNRAMP1*

Total RNA was extracted and cDNA synthesis was performed using a Thermo Fisher Scientific RevertAid First Strand cDNA Synthesis Kit. Full-length cDNA encoding *BjNRAMP1* was amplified through PCR using gene-specific primers (Table S1). The amplified products of the PCR were cloned into the pMD19-T vector (Takara) and sequenced via the Sanger method. The amino acid sequences of BjNRAMP1 and the other related species were employed to perform multi-sequence alignment using the ClustalW with default parameters in MEGA7. The phylogenetic tree was subsequently constructed using the neighbor-joining approach (no. of bootstrap replications = 1,000) implemented in MEGA7.

2.3 Yeast expression assays

Confirmed *BjNRAMP1* CDS in the pMD19-T vector were digested with restriction enzymes and inserted into the pYES2 expression vector. After sequencing verification, the empty and target vector was transferred into the Cd-sensitive yeast mutant Δ*yap1* and wild-type Y252, according to the yeast transformation and phenotype identification methods provided by Peng et al. (2017). In Δ*yap1*, the vacuolar Cd sequestration was decreased already, resulting in hypersensitivity to Cd relative to wild-type cells (Wemmie et al., 1994). Meanwhile, the plasmids were also extracted and transformed into the zinc-sensitive yeast mutant Δ*zrc1* and its wild-type CM100, and copper-sensitive yeast mutant Δ*cup2* and its wild-type BY4741 using the lithium acetate method as we described before (Zhang et al., 2022).

2.4 Generation of transgenic plants

The *BjNRAMP1* gene fragment was ligated into pEGOEP35S-H, and transformed into *A. thaliana* wild-type Col-0 by the *Agrobacterium tumefaciens* GV3101 dip flowering method. The transformed lines were screened for hygromycin resistance and verified by sequencing. T3 generations of homozygous transgenic lines were used for phenotype identification.

A 1,917-bp promoter sequence located upstream of the *BjNRAMP1* start codon was obtained by PCR amplification. The pBWA(V)BII-GUS vector was cleaved with enzymes *BsaI* and *Eco31I* and the target fragment was ligated to the linear vector using homologous recombination to construct the *proBjNRAMP1:GUS* fusion protein expression vector. The *proBjNRAMP1:GUS* vector was transformed into the *A. thaliana* wild type (Col-0).

2.5 Subcellular localization of BjNRAMP1

To determine the localization of the *BjNRAMP*1 gene in plant cells, the full-length coding sequence without a stop codon of the *BjNRAMP*1 gene was amplified by RT-RCR and transformed into both *A. thaliana* protoplasts and tobacco (*Nicotiana benthamiana*) leaf epidermal cells using a plant expression binary vector pEGOEP35S-H with a GFP fluorescent tag (pEGOEP-H-*35S:BjNRAMP1-GFP*). The preparation of protoplasts and their transformation into *A. thaliana* was performed following the polyethylene glycol method (Peng et al., 2017). Meanwhile, the *Agrobacterium tumefaciens* GV3101 solutions with the pEGOEP-

H- *35S:BjNRAMP1-GFP* vector were injected into the 3-week-old tobacco leaf epidermal cells. After incubation of *A. thaliana* protoplasts at 23℃ in the dark for 20 h and growth of tobacco for 2 days in dark, the GFP fluorescence was examined using a confocal microscope (FV1000; OLYMPUS). The localization marker of the cell plasma membrane is AtPIP2A-RFP.

2.6 qRT-PCR analysis of *BjNRAMP1*

Tissues from *B. juncea* and *A. thaliana* were collected and immediately frozen in liquid nitrogen with three biological replicates. First-strand cDNA was synthesized using a Tsingke Goldenstar RT6 cDNA Synthesis Kit ver.2 (Tsingke, Beijing, China). qRT-PCR was performed using SYBR Premix Ex TaqII on a Bio-Rad CFX 96 Real-Time Detection System as described previously (Zhang et al., 2020a).

2.7 Metal measurement in *A. thaliana* and yeast

For metal measurement in *A. thaliana* lines, the harvested plants were washed with distilled water, followed by drying at 75℃ until completely dehydrated. Plants were ground to fine powder, digested in 70% nitric acid at 100℃ for 2 h, and diluted with ultrapure water for metal determination.

For metal measurement in yeast, yeast cells that were transformed with empty vectors and *BjNRAMP1* were cultured to OD = 0.8 with 20 μM $CdCl_2$ solution, treated, and incubated for 24 h. The cells were collected by centrifugation and washed with sterile water and 2 mmol/L EDTA. After washing well, the cells were dried at 70°C and subsequently nitrated with 70% concentrated nitric acid and diluted. The concentrations of Cd and other elementals in all samples were determined by inductively coupled plasma-mass spectrometry (ICP-MS).

3 Results

3.1 Higher concentration of Cd stress induced the expression of *BjNRAMP1*

Previously, we reported that the *BjNRAMP1* was upregulated when *B. juncea* was exposed to high concentrations of Cd using RNA-Seq (Zhang et al., 2021). Herein, qRT-PCR result confirmed that the expression of *BjNRAMP1* was silenced under either control or 10mg/kg Cd stress, but induced in both leaves and roots when plants were under 30 mg/kg Cd stress, suggesting that *BjNRAMP1* was sensitive to higher concentration of Cd exposure (Figure 1A).

Cloning and sequence analysis indicated that *BjNRAMP1* was 1,566 bp in length, encoding a protein with 521 amino acid residues with 12 predicted transmembrane domains (Figure S1). Multiple alignments indicated that the BjNRAMP1 exhibited high identities to that in *B. rapa* (99%), *B. oleracea* (98.84%), *B. napus* (99%), and *A. thaliana* (85.90%). The phylogenetic analysis showed that *BjNRAMP1* was closely related to its homologous genes in *Brassica*, including *B. rapa*, *B. oleracea*, and *B. napus*, but evolutionarily far away from that in Poaceae, such as *O. sativa*, *Z. mays*, and *H. vulgare* (Figure 1B).

3.2 Ectopic expression of *BjNRAMP1* in yeast promotes Cd and Mn uptake

To investigate the role of *BjNRAMP1* in metal accumulation, the gene was expressed in the yeast heterologous system. Ectopic expression in Cd-sensitive mutant Δ*yap1* showed that the growth of transformed yeasts with *BjNRAMP1* was enhanced as compared with the control with empty vector in the presence of 15 and 30 μM Cd (Figure 2A). The concentration of Cd and Mn of yeasts transformed with *BjNRAMP1* was significantly higher than that in control when yeasts were under 20 μM Cd treatment for 6 and

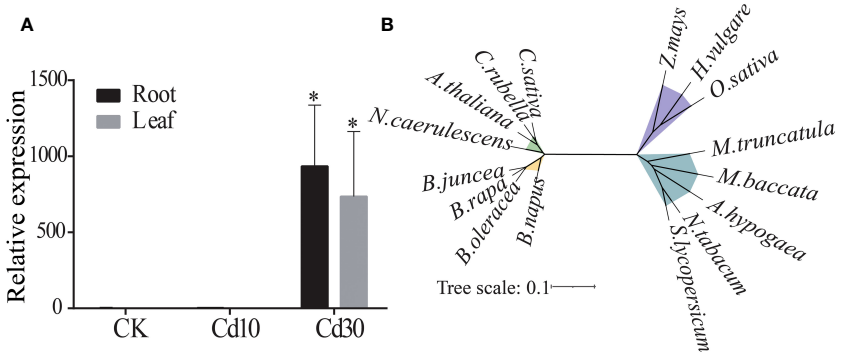

FIGURE 1
Expression and phylogenetic analysis of *BjNRAMP1*. **(A)** Expression of *BjNRAMP1* in root and leaf under different Cd treatments (CK, 0 mg/kg; Cd10, 10 mg/kg; Cd30, 30 mg/kg). The relative expression value under Cd30 was compared with that CK and Cd10 using *t*-test, * represents $p < 0.05$. **(B)** Phylogenetic analysis of the NRAMP1 protein. The sequences could be found in the NCBI database with the accession numbers: *A thaliana* (NP_178198.1), *A hypogaea* (XP_025612907.1), *B napus* (XP_013726991.2), *B oleracea* (XP_013588655.1), *B rapa* (XP_009106714.1), *C sativa* (XP_010472867.1), *C rubella* (XP_006301485.1), *H vulgare* (XP_044960708.1), *M. baccata* (AAU00158.1), *M. truncatula* (KEH35319.1), *N. caerulescens* (JAU89736.1), *N. tabacum* (XP_016485353.1), *O. sativa* (NP_001389971.1), *S. lycopersicum* (NP_001234318.1), and *Z. mays* (XP_008670084.1).

10.3389/fpls.2023.1261518

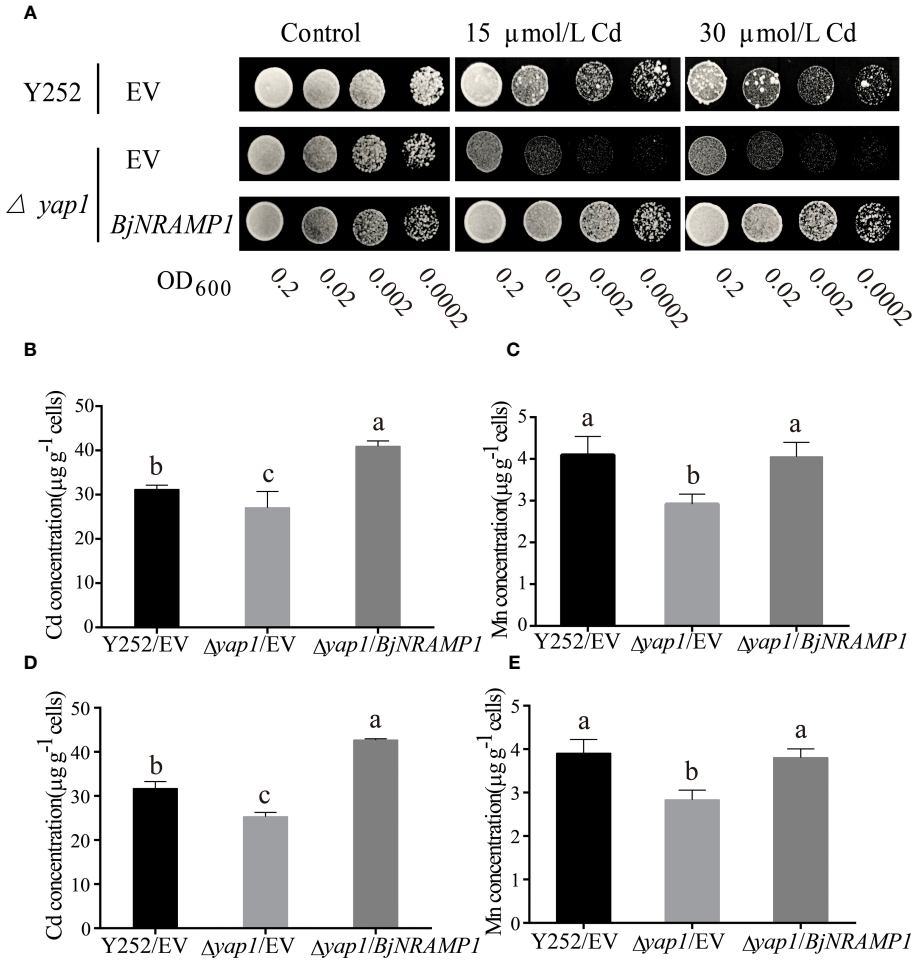

FIGURE 2
Functional characterization of BjNRAMP1 in yeast. **(A)** The Cd transport activity assay of BjNRAMP1 in yeast. Growth of yeast mutant strain *Δyap1* expressing *BjNRAMP1* or empty vector (pYES2) and yeast wild strain Y252 expressing empty vector (pYES2) in a medium containing different concentrations of Cd. Cd **(B)** and Mn **(C)** concentration in yeast with 20 μM $CdCl_2$ treatment for 6 h. Cd **(D)** and Mn **(E)** concentration in yeast with 20 μM $CdCl_2$ treatment for 12 h. Data were analyzed by one-way ANOVA using GraphPad Prism 9.3.1. Different letters indicate significant difference at $p < 0.05$ according to Tukey's multiple comparisons tests.

12 h (Figures 2B–E). After 6 h of Cd treatment, the Cd concentration in yeasts transformed with *BjNRAMP1* (40.93 μg/g) was not only 1.5-fold higher than that in *Δyap1* with empty vector (27.08 μg/g), but also significantly higher than that in wild type (31.18 μg/g). As to Mn, the *BjNRAMP1* transformed yeasts (4.05 μg/g) exhibited a similar level of Mn concentration with wild type (4.09 μg/g), but significantly higher than that in *Δyap1* with the empty vector (3.12 μg/g). Additionally, the results were also observed when yeasts were treated with 20 μM Cd for 12 h, suggesting that BjNRAMP1 could facilitate the uptake of Cd and Mn.

However, no significant increase in the concentration of Zn, Cu, and Fe was measured in *BjNRAMP1* transformed yeasts as compared with the empty vector (Table S2). Meanwhile, no significant phenotypic differences were observed when *BjNRAMP1* is expressed in Zn- and Cu-sensitive mutants (Figure S2), indicating that BjNRAMP1 might be one of the major transporters of Cd and Mn, but not that of Zn and Cu.

3.3 BjNRAMP1 is localized to the plasma membrane in the vascular system

To determine the subcellular localization of BjNRAMP1, the gene was fused with GFP fluorescent tag and under the regulation of the CaMV 35S promoter (*35S:BjNRAMP1-GFP* vector), and then the transiently expressed vector was transformed into both tobacco leaf epidermal cells and *A. thaliana* protoplasts (Figures 3A, B). In the tobacco leaf epidermal cells, the green fluorescence of fusion proteins (BjNRAMP1-GFP) was observed at the plasma membrane and co-localized with the plasma membrane marker AtPIP2A-RFP (Figure 3A). Despite the fact that the fluorescence intensity of BjNRAMP1-GFP in *A. thaliana* was slightly weaker than that in tobacco, the co-localized BjNRAMP1-GFP and plasma membrane marker AtPIP2A-RFP was still found in its protoplasts, confirming that BjNRAMP1 is localized to the plasma membrane (Figure 3B). Histochemical staining of GUS activity driven by the promoter of *BjNRAMP1* (*proBjNRAMP1:GUS*) showed that *BjNRAMP1* was

10.3389/fpls.2023.1261518

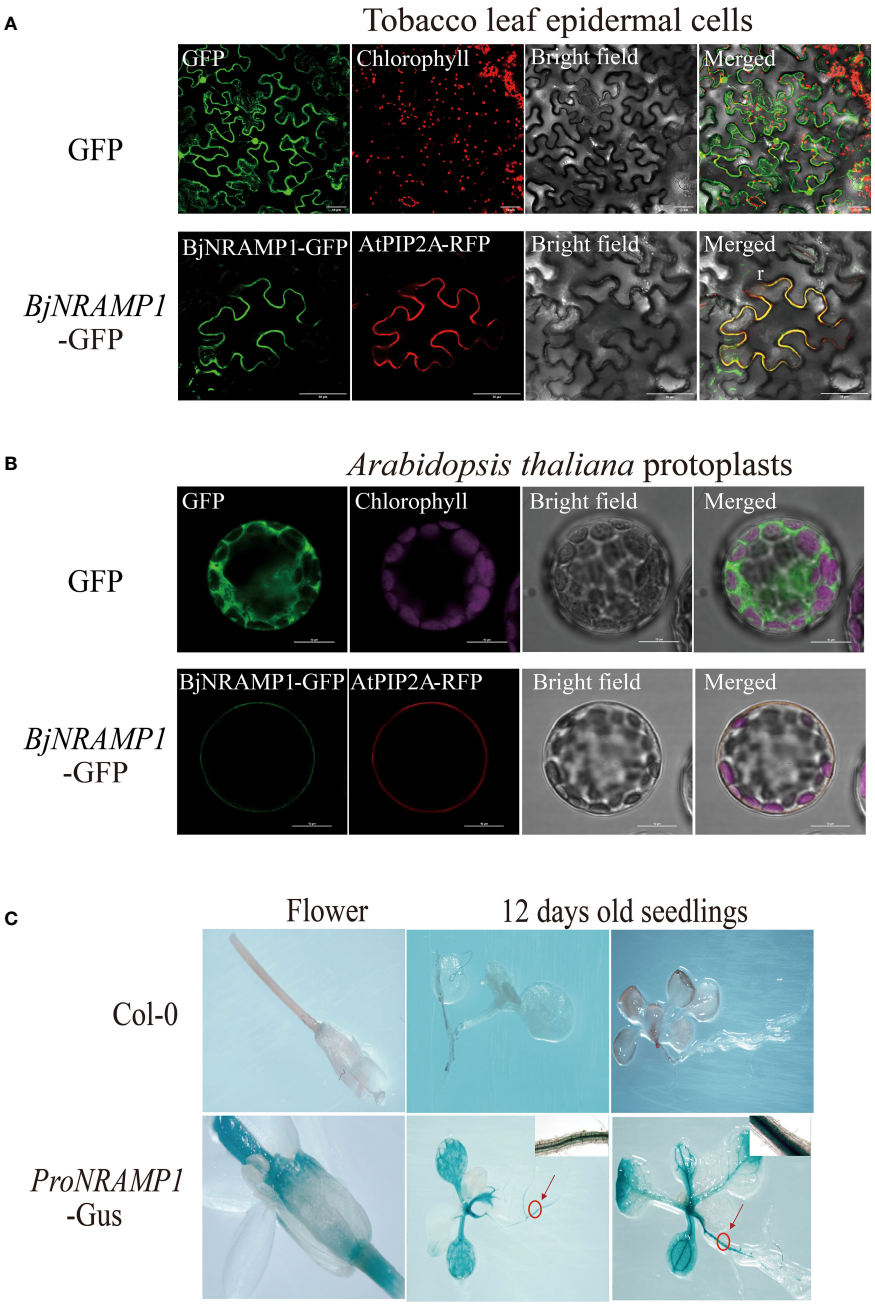

FIGURE 3
Subcellular localization and histochemical staining of BjNRAMP1. **(A)** Subcellular localization of BjNRAMP1 in tobacco epidermal leaf cells. The protein with GFP shows green signals. The plasma membrane marker AtPIP2A-RFP shows red signals. Scale bar, 50 μm. **(B)** Subcellular localization of BjNRAMP1 in *A thaliana* protoplasts. Scale bar, 10 μm. **(C)** Histochemical staining of GUS activity of *proBjNRAMP1-GUS* transgenic plants at the seedling and flowering stage. The image in the upper right is an enlarged view of the root section at the part with a red circle.

mainly expressed in the vascular system of roots and leaves at the seedling stage, as well as stigma at the flowering stage (Figure 3C).

3.4 Overexpression of *BjNRAMP1* increase the Cd accumulation

To further verify the function of *BjNRAMP1*, its coding sequence was driven by the CaMV 35S promoter and transformed into *A. thaliana* Col-0 generating the overexpression lines (Figure 4). After qRT-PCR confirmation, three lines, OE-1 (2.09- to 29.86-fold), OE-3 (9.96- to 59.30-fold), and OE-4 (1.59- to 6.73-fold), which exhibited significantly higher expression than the Col-0, were selected for further analysis (Figure 4B). In the presence of different concentrations (10, 30, and 50 μM) of Cd, the growth of *BjNRAMP1* overexpressing lines was significantly inhibited, displaying smaller seedling size (Figure 4A), lower fresh weight (Figure 4C), and shorter root length (Figure 2D). For example, no

10.3389/fpls.2023.1261518

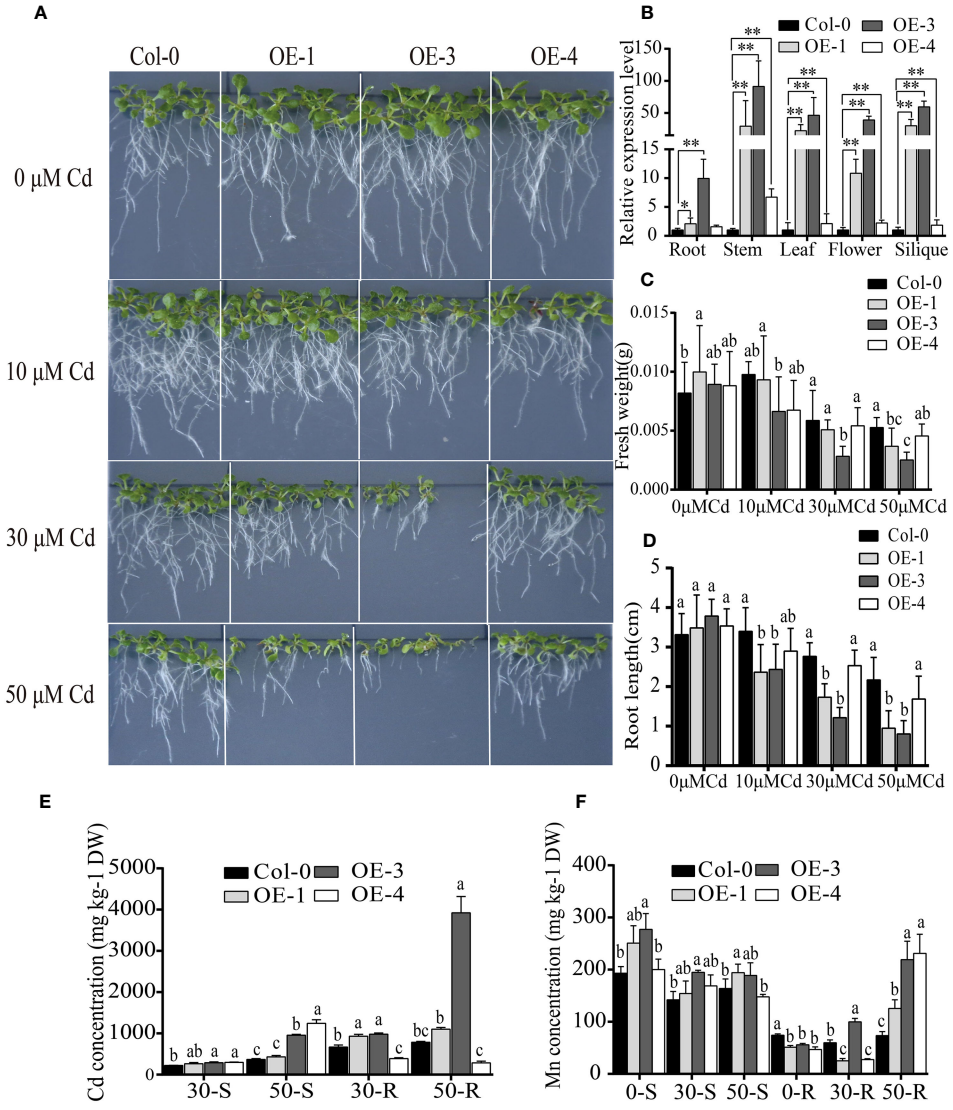

FIGURE 4
Functional analysis of BjNRAMP1 in *A thaliana*. **(A)** Phenotypes of overexpression lines at different concentrations of Cd treatment. **(B)** Relative expression levels of *BjNRAMP1* in overexpressing lines and wild type at different tissues. Col-0 represents Colombian wild-type *A thaliana*, and OE-1, OE-3, and OE-4 represent *BjNRAMP1* overexpression lines. *t*-test was performed between the wild type and each overexpression line. Measurement of root length **(C)** and fresh weight **(D)** in overexpression lines under different Cd concentrations. Determination of Cd **(E)** and Mn **(F)** content in the shoot and root of overexpression lines treated with different Cd concentrations. 0, 30, and 50-S or -R indicate shoots and roots of *A thaliana* under 0, 30, and 50 μM Cd treatment, respectively. DW indicates dry weight. Data were analyzed by one-way ANOVA, followed by comparisons of means of wild type and overexpression lines using Tukey's multiple comparisons test. Different letters indicate significant difference at $p < 0.05$.

significant differences in phenotype ($p > 0.05$) were observed between the non-transformed line Col-0 and the overexpressing line OE-3 when Cd was absent (0 μM). However, the fresh weight and root length of OE-3 were dramatically decreased approximately 29.7% and 32.7% ($p < 0.05$), respectively, as compared with Col-0 under 10 μM Cd treatment. The inhibition effect was increased with the increase in the concentration of Cd, resulting in 50.8% and 54.5% decrease in fresh weight, as well as 52.1% and 71.7% decrease in root length observed under 30 and 50 μM Cd treatment, respectively.

The Cd concentration in the shoots and roots of the overexpression line OE-3 was significantly higher than that of the non-transformed line Col-0 (Figure 4E). Although significantly more Cd was accumulated in the shoots of OE-4, the Cd concentration in the roots was decreased. Together, these results suggested that BjNRAMP1 could increase the Cd accumulation in plants. Meanwhile, the Mn concentration in the roots of overexpression lines was significantly lower under normal growth conditions (Cd0), but significantly higher than that in Col-0 when plants were under 50 μM Cd stress, indicating that high Cd stress could promote the Mn uptake in the roots of overexpression lines (Figure 2G). In accordance with the findings in yeast, no significant increase in concentration of Zn, Cu, and Fe was observed in the *A. thaliana* overexpression lines as compared to the wild type (Table S3).

4 Discussion

Although the role of OsNRAMP1 in rice has been well characterized (Tiwari et al., 2014; Chang et al., 2020), the BjNARAMP1 has not been established unequivocally due to the lack of functional analysis either in yeast or in plant. In the present study, our focus was to elucidate the role of BjNRAMP1 in Cd transport and accumulation using yeast and *A. thaliana* systems. We found that the exposure to higher concentration of Cd could induce the expression of BjNRAMP1, leading to significantly higher transcript levels in both leaves and roots (Figure 1A). Similar results were also observed in rice (Chang et al., 2020) and *M. hupehensis* (Zhang et al., 2020b), suggesting that a similar positive feedback mechanism might have evolved since it would lead to increased Cd uptake. The heterologous expression of *BjNRAMP1* in yeast showed that BjNRAMP1 could promote the uptake of both Cd and Mn (Figure 2), which agrees with the results in rice (Takahashi et al., 2011; Tiwari et al., 2014; Chang et al., 2020). However, when *BjNRAMP1* is overexpressed in Cd-, Zn-, and Cu-sensitive yeast, no significant increase in the concentration of Zn and Cu (Table S2) was observed, and there were no significant differences in phenotype (Figure S2). These results suggest that BjNRAMP1 was capable of uptake of both Cd and Mn, rather than Zn and Cu. A previous study found that the knockout of NRAMP1 had no significant effects on the concentrations of Fe, Zn, or Cu in rice (Chang et al., 2020), which was consistent with our results in yeast and *A. thaliana* (Table S3).

Previous studies have shown that NRAMP1 was a plasma membrane-localized protein that contributed to Cd and Mn uptake in rice (Tiwari et al., 2014; Chang et al., 2020). In *A. thaliana*, it was observed that NRAMP1 has undergone dynamic cycling between the plasma membrane and endosomal compartments, and overexpression of *AtNRAMP1* conferred Cd sensitivity (Castaings et al., 2021; Li et al., 2022). In our study, the results of cellular analysis in both tobacco and *A. thaliana* revealed that BjNRAMP1 was localized to the plasma membrane (Figures 3A, B). GUS staining results indicated that *BjNRAMP1* was mainly expressed in the vascular system of roots and leaves, and stigma of *A. thaliana* (Figure 3C).

Overexpression of *BjNRAMP1* in *A. thaliana* significantly enhanced the accumulation of Cd in roots and shoots, and inhibited the growth of transgenic lines as compared with wild type in the presence of Cd stress (Figure 4). In general, the inhibition effect was increased with the increase in Cd treatment concentration and the expression level of *BjNRAMP1*. It was observed that significantly more Cd accumulated in the shoots but less Cd accumulated in the roots of OE-4 under Cd stress (Figure 4E). *BjNRAMP1* was expressed relatively higher in the stem (6.73-fold) of OE-4 than in the roots (1.5-fold). We assumed that BjNRAMP1 might also be involved in the translocation of Cd from roots to shoots in OE-4, thus reducing the accumulation in roots, conferring better Cd resistance ability than OE-1 and OE-3 (Figures 4C, D). In the study of Tiwari et al. (2014), the expression of *OsNRAMP1* in *A. thaliana* enhanced the Cd accumulation and tolerance, demonstrating the role of OsNRAMP1 in xylem-mediated loading. Therefore, further detailed analyses, such as BjNRAMP1-GFP immunostaining in cross-sections across different tissues and microfocus X-ray fluorescence, are still required to determine its tissue localization and clarify its role in Cd uptake and translocation.

Significantly more Mn accumulated in the roots of overexpression lines than that in wild type when plants were under the higher concentration of Cd stress, suggesting that Mn uptake in roots was activated in addition to the increase in Cd accumulation (Figure 4F). Furthermore, overexpression of *BjNRAMP1* did not change the ratio of Mn translocated from roots to the shoots, indicating that BjNRAMP1 was involved primarily in the uptake of the Mn into the roots, rather than in the root-to-shoot translocation.

5 Conclusion

Together, our results demonstrate that BjNARAMP1 was localized to the plasma membrane, mainly expressed in the vascular system of roots and leaves, and stigma, and involved primarily in the uptake of the Cd and Mn into the roots.

Data availability statement

The raw data supporting the conclusions of this article will be made available by the authors, without undue reservation.

Author contributions

TL: Writing – original draft, Investigation, Visualization. YL: Writing – original draft, Investigation. JW: Writing – original draft, Investigation. JP: Writing – original draft, Investigation, Resources. LL: Writing – original draft, Investigation, Resources. LD: Investigation, Writing – original draft. DZ: Writing – review & editing, Funding acquisition, Project administration, Writing – original draft. MY: Writing – review & editing, Project administration, Supervision.

Funding

The author(s) declare financial support was received for the research, authorship, and/or publication of this article. This work was supported by the National Natural Science Foundation of China (U19A2029 and 32071965), the Science and Technology Innovation Program of Hunan Province (2023JJ40279), and the

Scientific Research Fund of Hunan Provincial Education Department (21B0490).

Acknowledgments

We would like to thank Dr. Dinggang Zhou and Jingfeng Wu for providing the critical reading of this manuscript.

Conflict of interest

The authors declare that the research was conducted in the absence of any commercial or financial relationships that could be construed as a potential conflict of interest.

Publisher's note

Supplementary material

The Supplementary Material for this article can be found online at: https://www.frontiersin.org/articles/10.3389/fpls.2023.1261518/full#supplementary-material

References

Castaings, L., Alcon, C., Kosuth, T., Correia, D., and Curie, C. (2021). Manganese triggers phosphorylation-mediated endocytosis of the Arabidopsis metal transporter NRAMP1. *Plant J.* 106 (5), 1328–1337. doi: 10.1111/tpj.15239

Chang, J., Huang, S., Yamaji, N., Zhang, W., Ma, J., and Zhao, F. (2020). OsNRAMP1 transporter contributes to cadmium and manganese uptake in rice. *Plant Cell Environ.* 43 (10), 2476–2491. doi: 10.1111/pce.13843

Clemens, S. (2019). Safer food through plant science: Reducing toxic element accumulation in crops. *J. Exp. Bot.* 70 (20), 5537–5557. doi: 10.1093/jxb/erz366

Clemens, S., Aarts, M. G. M., Thomine, S., and Verbruggen, N. (2013). Plant science: The key to preventing slow cadmium poisoning. *Trends Plant Sci.* 18 (2), 92–99. doi: 10.1016/j.tplants.2012.08.003

Kang, L., Qian, L., Zheng, M., Chen, L., Chen, H., Yang, L., et al. (2021). Genomic insights into the origin, domestication and diversification of Brassica juncea. *Nat. Genet.* 53 (9), 1392–1402. doi: 10.1038/s41588-021-00922-y

Li, L., Zhu, Z., Liao, Y., Yang, C., Fan, N., Zhang, J., et al. (2022). NRAMP6 and NRAMP1 cooperatively regulate root growth and manganese translocation under manganese deficiency in Arabidopsis. *Plant J.* 110 (6), 1564–1577. doi: 10.1111/tpj.15754

Peng, J., Ding, G., Meng, S., Yi, H., and Gong, J. (2017). Enhanced metal tolerance correlates with heterotypic variation in SpMTL, a metallothionein-like protein from the hyperaccumulator Sedum plumbizincicola. *Plant Cell Environ.* 40 (8), 1368–1378. doi: 10.1111/pce.12929

Sasaki, A., Yamaji, N., Yokosho, K., and Ma, J. F. (2012). Nramp5 is a major transporter responsible for manganese and cadmium uptake in rice. *Plant Cell.* 24 (5), 2155–2167. doi: 10.1105/tpc.112.096925

Takahashi, R., Ishimaru, Y., Senoura, T., Shimo, H., Ishikawa, S., Arao, T., et al. (2011). The OsNRAMP1 iron transporter is involved in Cd accumulation in rice. *J. Exp. Bot.* 62 (14), 4843–4850. doi: 10.1093/jxb/err136

Tang, L., Mao, B., Li, Y., Lv, Q., Zhang, L., Chen, C., et al. (2017). Knockout of OsNramp5 using the CRISPR/Cas9 system produces low Cd-accumulating indica rice without compromising yield. *Sci. Rep.* 7 (1), 14438. doi: 10.1038/s41598-017-14832-9

Tiwari, M., Sharma, D., Dwivedi, S., Singh, M., Tripathi, R. D., and Trivedi, P. K. (2014). Expression in Arabidopsis and cellular localization reveal involvement of rice NRAMP, OsNRAMP1, in arsenic transport and tolerance. *Plant Cell Environ.* 37 (1), 140–152. doi: 10.1111/pce.12138

Wemmie, J., Wu, A., Harshman, K., Parker, C., and Moye-Rowley, W. (1994). Transcriptional activation mediated by the yeast AP-1 protein is required for normal cadmium tolerance. *J. Biol. Chem.* 269 (20), 14690–14697. doi: 10.1016/S0021-9258(17)36680-2

Zeremski, T., Randelović, D., Jakovljević, K., Marjanović Jeromela, A., and Milić, S. (2021). Brassica species in phytoextractions: Real potentials and challenges. *Plants.* 10 (11), 2340. doi: 10.3390/plants

Zhang, D., Du, Y., He, D., Zhou, D., Wu, J., Peng, J., et al. (2021). Use of comparative transcriptomics combined with physiological analyses to identify key factors underlying cadmium accumulation in Brassica juncea L. *Front. Genet.* 12. doi: 10.3389/fgene.2021.655885

Zhang, D., Liu, L., Zhou, D., Liu, X., Liu, Z., and Yan, M. (2020a). Genome-wide identification and expression analysis of anthocyanin biosynthetic genes in Brassica juncea. *J. Integr. Agric.* 19 (5), 1250–1260. doi: 10.1016/S2095-3119(20)63172-0

Zhang, P., Zhang, X., Tang, T., Hu, H., Bai, N., Zhang, D., et al. (2022). Isolation of three metallothionein genes and their roles in mediating cadmium resistance. *Agronomy.* 12, 2971. doi: 10.3390/agronomy12122971

Zhang, W., Yue, S., Song, J., Xun, M., Han, M., and Yang, H. (2020b). MhNRAMP1 from malus hupehensis exacerbates cell death by accelerating Cd uptake in tobacco and apple calli. *Front. Plant Sci.* 11. doi: 10.3389/fpls.2020.00957

Zhao, F., Ma, Y., Zhu, Y., Tang, Z., and McGrath, S. (2015). Soil contamination in China: Current status and mitigation strategies. *Environ. Sci. Technol.* 49 (2), 750–759. doi: 10.1021/es5047099

Zhao, F., Tang, Z., Song, J., Huang, X., and Wang, P. (2022). Toxic metals and metalloids: Uptake, transport, detoxification, phytoremediation, and crop improvement for safer food. *Mol. Plant* 15 (1), 27–44. doi: 10.1016/j.molp.2021.09.016

Zhao, F., and Wang, P. (2020). Arsenic and cadmium accumulation in rice and mitigation strategies. *Plant Soil.* 446, 1–21. doi: 10.1007/s11104-019-04374-6

frontiers | Frontiers in Plant Science

TYPE Original Research
PUBLISHED 20 October 2023
DOI 10.3389/fpls.2023.1274759

OPEN ACCESS

EDITED BY
Hui Song,
Qingdao Agricultural University, China

REVIEWED BY
Hatice Sari,
Akdeniz University, Türkiye
Rafat Sultana,
International Crops Research Institute for the Semi-Arid Tropics (ICRISAT), India
Dayong Cui,
Qilu Normal University, China

*CORRESPONDENCE
Mahendar Thudi
mahendar.thudi@gmail.com

†PRESENT ADDRESS
Pooran M. Gaur,
The UWA Institute of Agriculture,
University of Western Australia,
Perth, WA, Australia

RECEIVED 08 August 2023
ACCEPTED 25 September 2023
PUBLISHED 20 October 2023

CITATION
Kumar R, Sharma VK, Rangari SK, Jha UC, Sahu A, Paul PJ, Gupta S, Gangurde SS, Kudapa H, Mir RR, Gaur PM, Varshney RK, Elango D and Thudi M (2023) High confidence QTLs and key genes identified using Meta-QTL analysis for enhancing heat tolerance in chickpea (*Cicer arietinum* L.). *Front. Plant Sci.* 14:1274759. doi: 10.3389/fpls.2023.1274759

High confidence QTLs and key genes identified using Meta-QTL analysis for enhancing heat tolerance in chickpea (*Cicer arietinum* L.)

Raj Kumar[1,2], Vinay Kumar Sharma[1], Sagar Krushnaji Rangari[1,2], Uday Chand Jha[3], Aakash Sahu[1], Pronob J. Paul[2,4], Shreshth Gupta[1], Sunil S. Gangurde[5], Himabindu Kudapa[2], Reyazul Rouf Mir[6], Pooran M. Gaur[2†], Rajeev K. Varshney[7], Dinakaran Elango[8] and Mahendar Thudi[1,9*]

[1]Department of Agricultural Biotechnology and Molecular Biology, Dr. Rajendra Prasad Central Agricultural University (RPCAU), Pusa, Bihar, India, [2]Research Program-Accelerated Crop Improvement, International Crops Research Institute for the Semi-Arid Tropics (ICRISAT), Patancheru, Telangana, India, [3]Indian Council for Agricultural Research (ICAR)- Indian Institute of Pulses Research (IIPR), Kanpur, Uttar Pradesh, India, [4]Rice Breeding Innovations, International Rice Research Institute (IRRI), South Asia-Hub, Patancheru, Telangana, India, [5]Department of Plant Pathology, University of Georgia, Tifton, GA, United States, [6]Faculty of Agriculture, Sher-e-Kashmir University of Agricultural Sciences and Technology (SKUAST), Sopore, India, [7]Centre for Crop & Food Innovation, WA State Agricultural Biotechnology Centre, Food Futures Institute, Murdoch University, Murdoch, WA, Australia, [8]Department of Agronomy, Iowa State University, Ames, IA, United States, [9]Center for Crop Health, University of Southern Queensland, Toowoomba, QLD, Australia

The rising global temperatures seriously threaten sustainable crop production, particularly the productivity and production of heat-sensitive crops like chickpeas. Multiple QTLs have been identified to enhance the heat stress tolerance in chickpeas, but their successful use in breeding programs remains limited. Towards this direction, we constructed a high-density genetic map spanning 2233.5 cM with 1069 markers. Using 138 QTLs reported earlier, we identified six Meta-QTL regions for heat tolerance whose confidence interval was reduced by 2.7-folds compared to the reported QTLs. Meta-QTLs identified on CaLG01 and CaLG06 harbor QTLs for important traits, including days to 50% flowering, days to maturity, days to flower initiation, days to pod initiation, number of filled pods, visual score, seed yield per plant, biological yield per plant, chlorophyll content, and harvest index. In addition, key genes identified in Meta-QTL regions like *Pollen receptor-like kinase 3 (CaPRK3), Flowering-promoting factor 1 (CaFPF1), Flowering Locus C (CaFLC), Heat stress transcription factor A-5 (CaHsfsA5)*, and *Pollen-specific leucine-rich repeat extensins (CaLRXs)* play an important role in regulating the flowering time, pollen germination, and growth. The consensus genomic regions, and the key genes reported in this study can be used in genomics-assisted breeding for enhancing heat tolerance and developing heat-resilient chickpea cultivars.

KEYWORDS

candidate genes, confidence interval, heat stress, Meta-QTLs, recombinant inbred lines

Introduction

Heat stress is becoming a significant obstacle in achieving sustainable agricultural production in the context of global climate change, putting food security at risk. According to predictions of the Inter-governmental Panel on Climate Change (IPCC), the global average temperature rise of 0.2°C per decade may reach up to 1.5°C between 2030 and 2052 (https://www.bbc.com/news/newsbeat-4894757). The cool season legumes like pea (*Pisum sativum* L.), lentil (*Lens culinaris* Medik.), faba bean (*Vicia faba* L.), and chickpea (*Cicer arietinum* L.) are more affected by the heat stress compared to warm season legumes (Sita et al., 2017). Small holder farmers in the arid and semi-arid regions across the globe cultivate chickpea on the residual soil moisture in over 50 countries (Roorkiwal et al., 2020). According to FAOSTAT (2020), chickpea is the second most important legume crop in the world, after dry beans, with an area under cultivation of 14.5 million hectares and an annual production of 14.7 million tonnes and average seed yield of 1.014 tonnes ha-1. Reproductive stage heat stress adversely affects the production and productivity of chickpea, and average temperatures of 20-28°C are optimal for chickpea production (Devasirvatham et al., 2012). During critical stages of chickpea growth, like flower initiation and pod filling, temperatures over 32°C result in flower drop, pollen sterility, and pod abortion and thus lead to significant yield losses (Kaushal et al., 2013; Gaur et al., 2019; Devi et al., 2022). A brief exposure to chickpea over critical limits especially during the reproductive phase leads to irreversible damage (Kalra et al., 2008; Jha et al., 2021). Furthermore, it has been observed that temperatures ≥35°C under field conditions resulted in yield losses of up to 39% (Devasirvatham et al., 2015). However, the severity of heat stress depends on its intensity, temperature, and the process impacted by the crops.

An in-depth understanding of genetic variability is a pre-requisite for trait improvement. Towards this direction, several efforts were made to understand the genetic variability among the germplasm of chickpea. For instance, a large-scale variation for heat stress tolerance among the chickpea reference set genotypes was reported by Krishnamurthy et al. (2011). Further, in a set of 35 early maturing genotypes assessed for their sensitivity to heat stress, the genotypes ICC 13124, ICC 14284, ICC 14368, and ICC 14653 were reported to be heat stress tolerant and high-yielding (Upadhyaya et al., 2011). Most recently, 39 chickpea genotypes grown in normal-sown and late-sown environments were assessed for their response in relation to influence on seven physiological and four yield and yield-related traits. As a result, it was reported that GNG 1969, GNG 1488, PantG 186, RSG 888, CSJ 315, and GNG 1499 genotypes can be used as donors for enhancing heat tolerance in chickpea cultivars (Devi et al., 2022). Genetic variability was also evaluated among the recombinant inbred line (RIL) populations (Paul et al., 2018a; Kushwah et al., 2021a). A set of 121 genotypes was evaluated at two different locations (India and Ethiopia) and the genetic relationships were assessed at both phenotypic and genotypic levels (Getahun et al., 2021).

Besides assessment of the genetic variability in respect of tolerance to heat stress, some efforts were also made to identify the genomic regions responsible for heat tolerance. QTLs for number of filled pods, total number of seeds per plot, grain yield per plot and % pod setting were reported using RIL population developed from ICC 4567 (heat sensitive) × ICC 15614 (heat tolerant) (Paul et al., 2018b). Using SSR markers, QTLs for primary branch number and chlorophyll content were reported in F_2 population derived from DCP 92-3 × ICCV 92944 (Jha et al., 2019). Additionally, Kushwah et al. (2021b) reported QTLs for heat tolerance using an inter-specific RIL population derived from the cross GPF 2 (heat tolerant) × ILWC 292 (heat sensitive). The related traits associated with QTLs are days to germination, days to flower initiation, days to 50% flowering, days to 100% flowering, plant height, grain yield, and membrane permeability index. Nevertheless, major QTLs for heat tolerance related traits were also reported using RIL population derived from DCP 92-3 (heat sensitive) and ICCV 92944 (heat tolerant). In addition, to QTLs, markers associated with the trait were also reported (Thudi et al., 2014; Varshney et al., 2019). However, only a few QTLs have been validated for their utilization in marker-assisted selection (MAS).

The Meta-QTL approach plays a pivotal role in precisely identifying stable QTLs across multiple studies for highlighting the consistency of location and effect for different QTLs of the same trait. The Meta-QTL analysis approach developed by Goffinet and Gerber (2000) can assist in narrowing down QTL regions with the of stringent selection of precise QTL (Soriano et al., 2021). Ultimately, it determines the "actual" number of QTLs affecting a trait and estimate their "actual" positions in the genome. Meta-QTL analysis has been applied to many cereals (maize, Kaur et al., 2021; rice, Sandhu et al., 2021; wheat, Ma et al., 2022) and legumes (pea, Klein et al., 2020; common bean, Arriagada et al., 2023), but not used for heat tolerance related traits in chickpea till now. In this study, we reported the identification of consensus genomic regions and associated key genes deploying Meta-QTL analyses. Consequently, the identified Meta-QTLs and associated key genes can be used for developing heat stress tolerant chickpea varieties.

Materials and methods

Compilation of reported QTLs for heat tolerance

All the QTLs associated with heat stress tolerance related traits were retrieved from four independent studies reported between 2018 to 2021. The reported QTLs were associated with 28 different heat stress tolerance related traits. The QTLs were re-grouped into four major trait categories (i) morphological (primary branches number, PB; plant height, PH), (ii) phenological (days to flower initiation, DFI; days to maturity, DM; days to 50% flowering, DFF; days to 100% flowering, DHF; and pollen viability, PV) (iii) Physiological (days to germination, DG; chlorophyll content, CHL; nitrogen balance index, NBI; cell membrane stability, CMS; normalized difference vegetation index, NDVI; membrane permeability index, MPI and relative leaf water content, RLWC) and (iv) yield and yield related traits (days to pod initiation, DPI; days to pod formation, DPF; number of filled pods, FPod; 100 seed weight, 100SW; seed yield per plant, SYPP; biological yield per plant, BYPP; harvest index, HI; pod setting percentage, % Podset; total number of seeds per plot, TS; grain

yield, GY; visual score, VS; number of pods per plant, NPP; biomass, BIO and yield, YLD). Among 138 reported QTLs, 59 major (PVE ≥ 10%) and 79 minor QTLs (PVE < 10%) were categorized. We compiled the information on (i) population type and size of the mapping population (ii) QTL ID with closely linked flanking markers (iii) LOD score (iv) phenotypic variation explained (PVE) or R^2 value (v) position of the peak and associated confidence interval (CI). The missing CI values were calculated by using two different equations proposed by Darvasi and Soller (1997) for different mapping populations. The formula used for F_2 and BC population is CI = $530/N \times R^2$ but for RILs CI = $163/N \times R^2$, wherein N denotes size of mapping population and R^2 denotes PVE for each QTL; the numerical value 530 and 163 are the population-specific constants obtained from different simulation. If the peak position was missing in any case, the mean of two flanking markers position was considered as the QTL peak.

Construction of consensus map

Consensus map was constructed by using four genetic maps from different studies to represent all markers associated with QTLs in a single map with the help of R package based LPMerge algorithm (Endelman and Plomion, 2014). LP merge in R constructs consensus maps using the root mean square error (RMSE) value, which is based on the linear programming method. In order to determine the optimal consensus map, the model with the least map size and least RMSE value was chosen and accepted as a final map for performing Meta-QTL analysis. Ultimately, the dense consensus map was constructed based on F_2 and RIL populations using 1771 markers.

QTL projection

The QTLs explaining at least 10% of phenotypic variation for the target trait were projected on the consensus map using BioMercator Version 4.2.3 (Arcade et al., 2004), and associated information for each QTL such as confidence interval (95%), peak position, LOD score and PVE (Sosnowski et al., 2012). In order to project QTLs, only the QTLs having the same flanking markers in the consensus map were used (Soriano et al., 2021).

Meta-QTL analysis

As a result of the projection, Meta-QTL analyses were performed on QTL cluster for each chromosome individually using the two-step algorithm proposed by Veyrieras et al. (2007) in BioMercator Version 4.2.3 (Arcade et al., 2004). In the first step, the best Meta-QTL model was selected out of many models available in the software by using selection criteria as Akaike information criterion (AIC), AIC corrected (AICc), AIC model 3 (AIC3), Bayesian information criterion (BIC), and Average weight of evidence (AWE). In order to select a Meta-QTL model, at least three models must achieve the lowest values of the selection criteria. In the second step, meta-QTLs were generated using best Meta-QTL model, which ensures that the number is generally less than the number of projected QTLs. While performing QTL meta-analysis, it is necessary to have independent QTLs for the same trait from different mapping populations, different locations, and different environmental conditions (Goffinet and Gerber, 2000).

Detecting candidate genes underlying the Meta-QTL region

In order to retrieve the candidate genes in Meta-QTL regions, the physical position of flanking markers was used as an input using the https://cegresources.icrisat.org database with the help of chickpea assembly (Varshney et al., 2013). The function associated with each gene was determined as per Thudi et al. (2021).

Results and discussion

Heat stress is one of the major constraints among abiotic stresses in chickpea. During the flowering stage, elevated temperatures (> 35°C) hamper pollen germination on the stigma and tube growth inside style, preventing it from reaching up to female gametes, and thus it leads to flower drop, pod abortion or abnormal pod setting (Devasirvatham et al., 2012; Devasirvatham et al., 2015; Devasirvatham and Tan, 2018). Efforts were made to identify the heat tolerant germplasm as well as map the genomic regions using both linkage mapping (Paul et al., 2018b; Jha et al., 2019 and Jha et al., 2021; Kushwah et al., 2021b) and linkage disequilibrium mapping (Thudi et al., 2014; Varshney et al., 2019). Nevertheless, the genomic regions reported in different studies were large for use in genomics-assisted breeding programs. To reduce the genomic intervals and identify the consensus genomics regions for heat tolerance, we have used Meta-QTL analysis approach in this study.

QTLs identified for heat stress tolerance

In case of chickpea, to date, a total of four independent studies reported QTLs for heat tolerance related traits. Among these studies, two studies used SNPs based on genotyping by sequencing approach, one study used SNP based on double digest restriction-site associated DNA sequencing approach while the other study used SSR markers. Among three RIL populations, two were intra-specific (ICC 4567 × ICC 15614, DCP 92-3 × ICCV 92944) and another one was inter-specific (GPF 2 × ILWC 292). Using advanced generations of DCP 92-3 × ICCV 92944, QTLs were mapped at F_2 and F_7 stages by Jha and colleagues in 2019 and 2021 respectively. The size of the mapping populations ranged from 184 to 292 lines (Table 1). In total, 138 QTLs were reported earlier for 28 different traits. Further, among 138 QTLs reported earlier, 59 and 79 were major (≥10% phenotypic variation explained, PVE) and minor QTLs (<10% PVE), respectively. The confidence

TABLE 1 Summary of QTLs for heat tolerance related traits reported between 2018-21.

Mapping population	Population type	Population size	Number and type of markers	Traits	QTLs	Reference
ICC 4567 × ICC 15614	RILs (F_{8-9})	292	271 SNPs	6	8	Paul et al., 2018b
DCP 92-3 × ICCV 92944	F_2	206	39 SSRs	2	2	Jha et al., 2019
DCP 92-3 × ICCV 92944	RILs (F_7)	184	788 SNPs	12	77	Jha et al., 2021
GPF 2 × ILWC 292	RILs (F_8)	187	673 SNPs	12	51	Kushwah et al., 2021b

intervals of these QTLs ranged from 2 - 44.29 cM with an average of 9.2 cM (Supplementary Table 1).

QTLs on the consensus map

For projection of all QTLs, a dense consensus map comprising of 1069 markers spanning a total genetic distance of 2233.5 cM was constructed. Nevertheless, individual genetic maps reported 39 (Jha et al., 2019) to 788 markers (Jha et al., 2021). The length of each linkage group varied between 68.1- 497.7 cM, with an average distance of 279.19 cM (Supplementary Table 2). Compared to Kushwah et al. (2021a; 2021b) genetic map (4569.09 cM), a reduction of 2.04 folds genetic distance was observed in the consensus map developed in the present study. Drastic reduction in the genetic distance of consensus map indicated the robustness of consensus map for identification of more precise Meta-QTLs. The number of markers per linkage group ranged from 68 (on CaLG08) to 253 (on CaLG06). The densest map was observed for the linkage group CaLG08 with a marker density of 0.9 marker/cM. Amongst 138 QTLs, 65.21% (90) QTLs could be projected on consensus genetic map we developed. This could be due to lack of common markers for mapping all the QTLs.

Meta-QTLs identified

Of 90 QTLs projected onto the consensus map, 22 were grouped into six Meta-QTL regions, comprising QTLs from at least two different studies (Table 2; Figure 1). The remaining 68 QTLs were either singletons or had a very high confidence interval, and for different traits of same study which could not be considered as Meta-QTL by the Meta-QTL clustering algorithm. The six Meta-QTLs were founded, and distributed on four linkage groups of chickpea (CaLG01, CaLG03, CaLG06, and CaLG07; Figure 2). A maximum of two (on CaLG01 and CaLG06) and a minimum of one (on CaLG03 and CaLG07) Meta-QTLs were identified on linkage groups. The number of QTLs in each Meta-QTL varied from two to six (Table 2). Interestingly, Meta-QTL4 contained six QTLs clustered for four different traits (FPOD, VS, SYPP and BYPP). Similarly, Meta-QTL5 contained five QTLs clustered for three different traits (CHL, BYPP and HI). The average number of QTLs in each Meta-QTL regions was 3.66 QTLs per Meta-QTL. The confidence interval at 95% of each Meta-QTL ranged from 2.97 cM for Meta-QTL4 on CaLG06 to 6.23 cM for Meta-QTL3 on CaLG03. The average confidence interval for the Meta-QTL was 4.49 cM. The Meta-QTLs identified from the QTL clusters were found to have significantly low confidence interval compared to the

TABLE 2 Details of Meta-QTLs identified for heat tolerance related traits in chickpea.

Meta-QTL	Linkage Group	Position			CI (95%)	Flanking markers	No. of QTLs	Traits†
		Absolute	CI start	CI end				
Meta-QTL1	CaLG01	9.46	7.575	11.345	3.77	SCA1_34969214 - SCA1_18234886	2	DM, DFF
Meta-QTL2	CaLG01	152.9	150.885	154.915	4.03	SCA1_19787122 - SCA1_19586410	4	DFI, DM (2), DPI
Meta-QTL3	CaLG03	48.8	45.685	51.915	6.23	TA142 - NCPGR149	2	PB, NDVI
Meta-QTL4	CaLG06	58.31	56.825	59.795	2.97	SCA6_10670773 - SCA6_10672468	6	FPOD, VS, SYPP (2), BYPP (2)
Meta-QTL5	CaLG06	110.96	108.565	113.355	4.79	SCA6_7820481 - SCA6_7929338	5	CHL, HI, BYPP (3)
Meta-QTL6	CaLG07	36.96	31.8	42.12	5.16	SCA7_28235343 - SCA7_36854126	3	HI, RLWC, NBI
Average					4.49		3.66	

†Days to maturity (DM); Days to 50% flowering (DFF); Days to flower initiation (DFI); Days to pod initiation (DPI); Primary branch number (PB); Normalized difference vegetation index (NDVI); Number of filled pods per plot (FPOD); Visual score (VS); Seed yield/plant (SYPP); Biological yield/plant (BYPP); Chlorophyll content (CHL); Harvest index (HI); Relative leaf water content (RLWC); Nitrogen balance index (NBI).

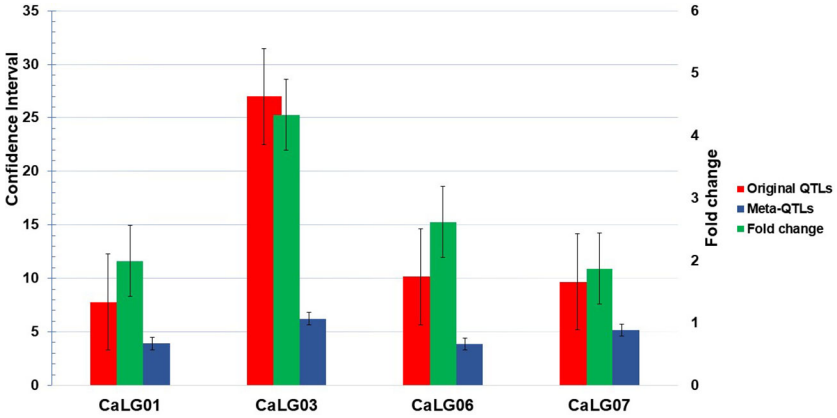

FIGURE 1
Comparison of confidence interval (CI) between original QTL and Meta-QTL; CaLG03 shown maximum reduction in CI (four times against original QTL) but CaLG07 shown minimum reduction in CI.

original projected QTLs. A graphical representation of CI of Meta-QTL and original QTL on each of the chickpea chromosome has been presented in Figure 2. The average CI fold reduction of Meta-QTL compared to original QTLs was computed to be 2.7 folds. These results signify that the Meta-QTLs identified in the present study are highly stable and have reduced confidence interval; thereby enhancing the detection of candidate genes and providing high mapping resolution.

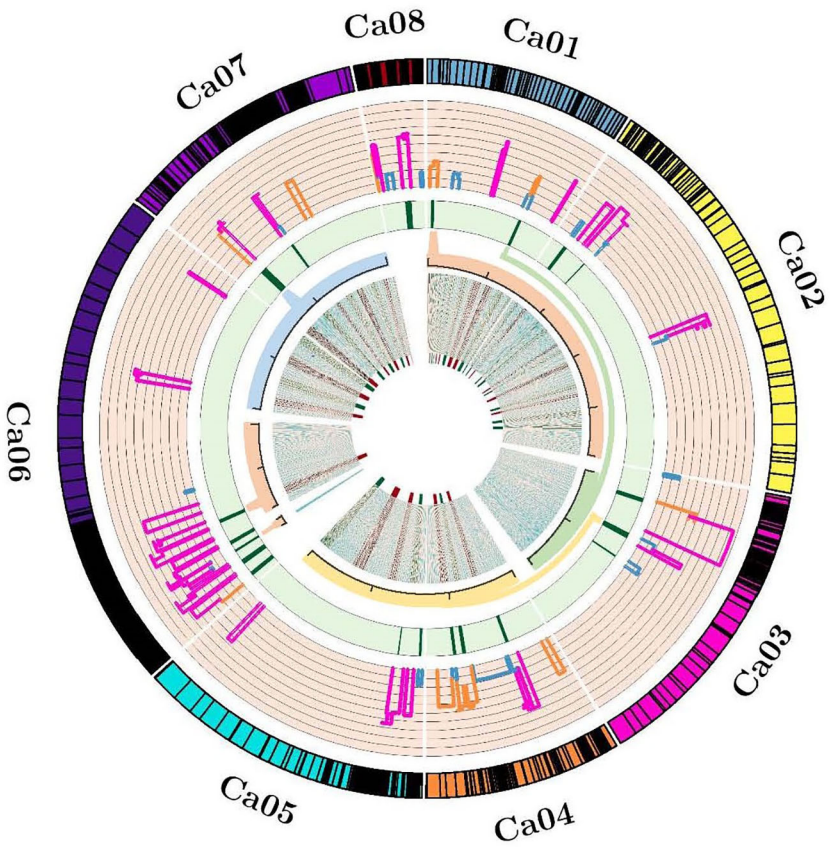

FIGURE 2
Circos indicating the projected QTLs, Meta-QTLs and genes. ***From outside to inside***, Track 1 representing ideogram of linkage groups and black bands are showing marker density; Track 2 representing the histogram of projected QTLs and width of histogram is showing the confidence interval; Track 3 representing heatmap of identified Meta-QTLs and width of heatmap is indicating the reduction in confidence interval of Meta-QTLs; Track 4 representing magnified view of accepted Meta-QTL regions into the redundant physical interval; Track 5 representing the density map of identified candidate genes.

10.3389/fpls.2023.1274759

Key genes in Meta-QTL regions

We identified a total of 1346 genes among 6 Meta-QTL regions (Supplementary Table 3). On annotation, 55 genes belonged to a wide range of gene-families that are directly or indirectly related to abiotic stress tolerance especially heat tolerance (Table 3) and 1291 genes were either putative or uncharacterized. Among 6 Meta-QTL regions, the Meta-QTL6 on CaLG07 harbored maximum number of genes (24 genes) with known functions followed by Meta-QTL1 on CaLG01 (23 genes), Meta-QTL3 on CaLG03 (7 genes) and Meta-QTL4 on CaLG06 harbored single gene with known function (Table 3). A total of 11, six, four and one genes were found to code for ethylene responsive

TABLE 3 Summary of key genes underlying in Meta-QTLs regions with known functions.

Meta-QTL ID	Gene ID	Predicted Function
Meta-QTL1	Ca_14718	Flowering-promoting factor-like protein
	Ca_24217	Pollen-specific leucine-rich repeat extensin-like protein 1
	Ca_24225	Pollen-specific leucine-rich repeat extensin-like protein 1
	Ca_17354	Ethylene response factor
	Ca_22117	Heat shock-like protein, putative
	Ca_19297	Ethylene-responsive transcription factor ERF017-like
	Ca_19296	Ethylene-responsive transcription factor ERF017-like
	Ca_19295	Ethylene-responsive transcription factor erf017-like protein
	Ca_18344	Pollen-specific leucine-rich repeat extensin-like protein 2
	Ca_18341	Heat shock protein
	Ca_18590	Heat shock protein
	Ca_20281	Peroxidase 7-like
	Ca_18530	MADS-box protein FLOWERING LOCUS C-like
	Ca_22571	Zinc finger protein CONSTANS-LIKE 9-like
	Ca_22561	Chaperone dnaj-domain protein, putative
	Ca_22560	Pollen-specific leucine-rich repeat extensin-like protein 1
	Ca_24386	F-box protein
	Ca_19442	Pollen-specific leucine-rich repeat extensin-like protein 1
	Ca_19459	F-box protein SKIP2
	Ca_19466	Putative F-box protein At3g16210
	Ca_25480	Pollen-specific leucine-rich repeat extensin-like protein 1
	Ca_22107	Calcium-transporting atpase 8, plasma membrane-type
	Ca_18324	Dnaj protein ERDJ2A-like
Meta-QTL3	Ca_06050	Receptor protein kinase-like protein
	Ca_06047	Receptor protein kinase-like protein
	Ca_06034	Ethylene-responsive element binding protein 1
	Ca_06032	Ethylene-responsive element binding protein 1
	Ca_06021	Ser/Thr protein kinase
	Ca_06019	Ser/Thr protein kinase
	Ca_05985	Zinc finger protein CONSTANS-like protein
Meta-QTL4	Ca_09583	Putative ETHYLENE INSENSITIVE 3-like 4 protein
Meta-QTL6	Ca_18924	Heat shock protein
	Ca_18948	Ethylene response factor
	Ca_11765	Ethylene-responsive transcription factor CRF1-like
	Ca_10067	Calmodulin-binding family protein
	Ca_10013	Pollen-specific leucine-rich repeat extensin-like protein 3
	Ca_16155	Pollen receptor-like kinase 3
	Ca_16156	F-box protein SKP2A-like
	Ca_16168	COP1-interacting-like protein
	Ca_16170	Dnaj homolog subfamily B member 6-like isoform X3
	Ca_16171	Dnaj homolog subfamily B member 6-like isoform X3
	Ca_16180	Ethylene response factor
	Ca_17621	Calcium-binding protein KIC
	Ca_17627	Myb transcription factor
	Ca_17638	Ethylene-responsive transcription factor ERF023-like
	Ca_17639	ABA-inducible bhlh-type transcription factor
	Ca_17762	Late embryogenesis abundant protein
	Ca_17776	F-box/kelch-repeat plant protein
	Ca_17780	F-box/kelch-repeat protein At3g61590-like
	Ca_17789	F-box/LRR-repeat protein 12
	Ca_17791	F-box protein interaction domain protein
	Ca_13731	Calmodulin-binding receptor-like cytoplasmic kinase
	Ca_18949	Dnaj-class molecular chaperone
	Ca_13761	Calmodulin-binding heat-shock protein
	Ca_13713	Myb transcription factor

transcription factor, leucine rich repeat extension like protein, DnaJ heat shock protein and pollen receptor kinase respectively. Alternatively, some genes encoding proteins like peroxidase and superoxidase dismutase have a role in defying oxidative stress and recovering plants from heat stress damage (Table 3).

In chickpea, completion of the process of pollen germination and growth of the pollen tube is essential for successful fertilization. In Meta-QTL1, five genes namely Ca_24217, Ca_24225, Ca_22560, Ca_19442, and Ca_25480 encode for pollen-specific leucine-rich repeat extensin-like protein 1 and the gene Ca_18344 codes for pollen-specific leucine-rich repeat extensin-like protein 2. While in case of Meta-QTL6 the gene Ca_10013 codes for pollen-specific leucine-rich repeat extensin-like protein 3. Pollen-specific leucine-rich repeat extensin (LRXs), harbor a leucine-rich repeat domain and an extensin domain, are essential for pollen germination and growth in Arabidopsis (Wang et al., 2018). In addition, like the *LePRK2* gene in tomato (*Solanum lycopersicum*), we identified a gene (Ca_16155; referred as *CaPRK2;* Ca stands for *Cicer arietinum*) that encodes pollen receptor kinase, which has been implicated in signaling during pollen germination and tube growth as well as in mediating pollen (tube)-pistil communication. In case of tomato, it was demonstrated that *LePRK2* positively regulates pollen germination and tube growth (Zhang et al., 2008).

We also identified important genes like Flowering-promoting factor 1-like protein 1 (Ca_14718; referred as *CaFPF1*) and MADS-box protein FLOWERING LOCUS C (Ca_18530; referred as *CaFLC*) in Meta-QTL1 genomic region. In addition, we identified a gene Ca_14718 that encodes *FPF1* (*Flowering-promoting factor 1*) reported to be involved in the genetic control of flowering time in plants. For instance, in case of rice, it was demonstrated that the *OsFPFL4* gene was involved in modulating the root and flower development by affecting auxin and ROS homeostasis (Guo et al., 2020). However, MADS-box transcription factors (TFs), *FLOWERING LOCUS C (FLC)* along with *SHORT VEGETATIVE PHASE (SVP)* have been reported to form a complex to repress the expression of genes that initiate flowering in Arabidopsis (Mateos et al., 2015). This indicates that the Meta-QTL1 harbor genes that control both flower initiation as well as repression of the flowering. In general, the genotypes with early flowering feature record higher yield by escaping the reproductive stage heat stress as well as end season drought (Manchikatla et al., 2021). In Meta-QTL1 and 6, we identified genes (Ca_18341, Ca_18590 and Ca_18924), that code for heat shock proteins or heat stress transcription factor A-5 referred as *CaHsfsA5*. Among 20 heat stress transcription factors (*Hsfs*), *Hsfs A4* and *A5* form a group with distinguished gene activity as *A4 Hsfs* are potent activators of heat stress gene expression, whereas *A5 Hsfs* act as specific repressor of *HsfA4* activity (Baniwal et al., 2007). Another gene, referred as *CaERN3* that encodes ethylene-responsive transcription factor *ERN3* was reported to repress the *ERN1/ERN2*-dependent transcription activation in legumes. This Meta-QTL region habors QTLs for NBI and CHL. Reduction of nitrogen balance index and chlorophyll content is the common phenomenon in plants and it was reported in maize during post flowering heat stress (Bheemanahalli et al., 2022).

Conclusions

Meta-QTL analysis for the traits related to heat stress tolerance is an effective approach of unravelling the concise and precise QTLs from many QTLs reported earlier. In the present study, the CI of the identified Meta-QTLs is reduced by 2.7 folds against the original QTL CI. In addition, key genes like *Pollen receptor-like kinase 3* (*CaPRK3), Flowering-promoting factor 1 (CaFPF1), FLOWERING LOCUS C (CaFLC), Heat stress transcription factor A-5* (*CaHsfsA5*), and *Pollen-specific leucine-rich repeat extensin (LRXs)*, identified in the Meta-QTL regions are known to play key role in regulating the flowering, pollen germination and growth etc, which can be further explored in detail. Large-scale germplasm sequence information (Thudi et al., 2016a; Thudi et al., 2016b; Varshney et al., 2019; Varshney et al., 2021; Thudi et al., 2023) and phenotypic data in public domain can be used for haplo-pheno analysis and identify superior haplotypes for use in heat tolerance breeding. The Meta-QTLs with reduced confidence interval as well as key genes reported in the study can be used in chickpea breeding programs for developing heat resilient chickpea varieties.

Data availability statement

The original contributions presented in the study are included in the article/Supplementary Material. Further inquiries can be directed to the corresponding authors.

Author contributions

RK: Data curation, Methodology, Writing – original draft. VKS: Resources, Writing – review & editing. SKR: Formal Analysis, Methodology, Writing – review & editing. UCJ: Resources, Writing – review & editing. AS: Formal Analysis, Writing – review & editing. PJP: Resources, Writing – review & editing. SG: Formal Analysis, Methodology, Writing – review & editing. SSG: Resources, Writing – review & editing. HK: Resources, Writing – review & editing. RRM: Resources, Writing – review & editing. PMG: Resources, Writing – review & editing. RKV: Resources, Writing – review & editing. DE: Writing – review & editing. MT: Conceptualization, Supervision, Writing – review & editing.

Funding

The author(s) declare that no financial support was received for the research, authorship, and/or publication of this article.

Acknowledgments

RK acknowledges the Department of Biotechnology and RPCAU, Pusa for the DBT-JRF and university fellowship to his Ph.D.

Conflict of interest

The authors declare that the research was conducted in the absence of any commercial or financial relationships that could be construed as a potential conflict of interest.

The reviewer RS declared a shared affiliation with the authors PG, HK to the handling editor at the time of review.

The author(s) declared that they were an editorial board member of Frontiers, at the time of submission. This had no impact on the peer review process and the final decision.

Publisher's note

All claims expressed in this article are solely those of the authors and do not necessarily represent those of their affiliated organizations, or those of the publisher, the editors and the reviewers. Any product that may be evaluated in this article, or claim that may be made by its manufacturer, is not guaranteed or endorsed by the publisher.

Supplementary material

The Supplementary Material for this article can be found online at: https://www.frontiersin.org/articles/10.3389/fpls.2023.1274759/full#supplementary-material

SUPPLEMENTARY TABLE 2
Marker order and their position on the consensus genetic map developed using four genetic mapping studies.

References

Arcade, A., Labourdette, A., Falque, M., Mangin, B., Chardon, F., Charcosset, A., et al. (2004). BioMercator: Integrating genetic maps and QTL towards discovery of candidate genes. *Bioinform* 20, 14. doi: 10.1093/bioinformatics/bth230

Arriagada, O., Arévalo, B., Cabeza, R. A., Carrasco, B., and Schwember, A. R. (2023). Meta-QTL analysis for yield components in common bean (*Phaseolus vulgaris* L.). *Plants* 12, 1. doi: 10.3390/plants.2023.12010117

Baniwal, S., Chan, K. Y., Scharf, K. D., and Nover, L. (2007). Role of heat stress transcription factor HsfA5 as specific repressor of HsfA4. *J. Biol. Chem.* 282, 6. doi: 10.1074/jbc.M609545200

Bheemanahalli, R., Vennam, R. R., Ramamoorthy, P., and Reddy, K. R. (2022). Effects of post-flowering heat and drought stresses on physiology, yield, and quality in maize (*Zea mays* L.). *Plant Stress.* 6, 100106. doi: 10.1016/j.stress.2022.100106

Darvasi, A., and Soller, M. (1997). A simple method to calculate resolving power and confidence interval of QTL map location. *Behav. Genet.* 27, 10. doi: 10.1023/A:1025685324830

Devasirvatham, V., Gaur, P. M., Mallikarjuna, N., Tokachichu, R. N., Trethowan, R. M., and Tan, D. K. Y. (2012). Effect of high temperature on the reproductive development of chickpea genotypes under controlled environments. *Funct. Plant Biol.* 39, 12. doi: 10.1071/FP12033

Devasirvatham, V., Gaur, P. M., Raju, T. N., Trethowan, R. M., and Tan, D. K. Y. (2015). Field response of chickpea (*Cicer arietinum* L.) to high temperature. *Field Crops Res.* 172, 10. doi: 10.1016/j.fcr.2014.11.017

Devasirvatham, V., and Tan, D. K. Y. (2018). Impact of high temperature and drought stresses on chickpea production. *Agronomy* 8, 8. doi: 10.3390/agronomy8080145

Devi, P., Jha, U. C., Prakash, V., Kumar, S., Parida, S. K., Paul, P. J., et al. (2022). Response of physiological, reproductive function and yield traits in cultivated chickpea (*Cicer arietinum* L.) under heat stress. *Front. Plant Sci.* 13. doi: 10.3389/fpls.2022.880519

Endelman, J. B., and Plomion, C. (2014). LPmerge: An R package for merging genetic maps by linear programming. *Bioinform* 30, 11. doi: 10.1093/bioinformatics/btu091

FAOSTAT (2020) Food and Agriculture Organization of the United Nations (FAO) statistical databases. www.fao.org.

Gaur, P. M., Samineni, S., Thudi, M., Tripathi, S., Sajja, S. B., Jayalakshmi, V., et al. (2019). Integrated breeding approaches for improving drought and heat adaptation in chickpea (*Cicer arietinum* L.). *Plant Breed.* 138, 4. doi: 10.1111/pbr.12641

Getahun, T., Negash, K., Chang, P. L., Wettberg, E., Carrasquilla-Garcia, N., Gaur, P. M., et al. (2021). Screening of heat-tolerant Ethiopian chickpea accessions: assessment of phenological and agro-morphological traits and genomic relationships. *Agrosyst. Geosci. Environ.* 4, 3. doi: 10.1002/agg2.20211

Goffinet, B., and Gerber, S. (2000). Quantitative trait loci: a meta-analysis. *Genetics* 155, 1. doi: 10.1093/genetics/155.1.463

Guo, Y., Wu, Q., Xie, Z., Yu, B., Zeng, R., Min, Q., et al. (2020). *OsFPFL4* is involved in the root and flower development by affecting auxin levels and ROS accumulation in rice (*Oryza sativa*). *Rice* 13, 1. doi: 10.1186/s12284-019-0364-0

Jha, U. C., Kole, P. C., and Singh, N. P. (2019). QTL mapping for heat stress tolerance in chickpea (*Cicer arietinum* L.). *Legume. Res.* 44, 10. doi: 10.18805/LR-4121

Jha, U. C., Nayyar, H., Palakurthi, R., Jha, R., Valluri, V., Bajaj, P., et al. (2021). Major QTLs and potential candidate genes for heat stress tolerance identified in chickpea (*Cicer arietinum* L.). *Front. Plant Sci.* 12. doi: 10.3389/fpls.2021.655103

Kalra, N., Chakraborty, D., Sharma, A., Rai, H. K., Jolly, M., Chander, S., et al. (2008). Effect of temperature on yield of some winter crops in northwest India. *Curr. Sci.* 94, 82–88.

Kaur, S., Rakshit, S., Choudhary, M., Das, A. K., and Kumar, R. R. (2021). Meta analysis of QTLs associated with popping traits in maize (*Zea mays* L.). *PloS One* 16, 8. doi: 10.1371/journal.pone.0256389

Kaushal, N., Awasthi, R., Gupta, K., Gaur, P., Siddique, K. H. M., and Nayyar, H. (2013). Heat-stress-induced reproductive failures in chickpea (*Cicer arietinum* L.) are associated with impaired sucrose metabolism in leaves and anthers. *Funct. Plant Biol.* 40, 12. doi: 10.1071/FP13082

Klein, A., Houtin, H., Rond-Coissieux, C., Naudet-Huart, M., Touratier, M., Marget, P., et al. (2020). Meta-analysis of QTL reveals the genetic control of yield-related traits and seed protein content in pea. *Sci. Rep.* 10, 1. doi: 10.1038/s41598-020-72548-9

Krishnamurthy, L., Gaur, P. M., Basu, P. S., Chaturvedi, S. K., Tripathi, S., Vadez, V., et al. (2011). Large genetic variation for heat tolerance in the reference collection of chickpea (*Cicer arietinum* L.) germplasm. *Plant Genet. Resour.* 9, 1. doi: 10.1017/S1479262110000407

Kushwah, A., Bhatia, D., Singh, G., Singh, I., Bindra, S., Vij, S., et al. (2021a). Phenotypic evaluation of genetic variability and selection of yield contributing traits in chickpea recombinant inbred line population under high temperature stress. *Physiol. Mol. Biol. Plants* 27, 4. doi: 10.1007/s12298-021-00977-5

Kushwah, A., Bhatia, D., Singh, I., Thudi, M., Singh, G., Bindra, S., et al. (2021b). Identification of stable heat tolerance QTLs using inter-specific recombinant inbred line population derived from GPF 2 and ILWC 292. *PloS One* 16, 8. doi: 10.1371/journal.pone.0254957

Ma, J., Liu, Y., Zhang, P., Chen, T., Tian, T., Wang, P., et al. (2022). Identification of quantitative trait loci (QTL) and Meta-QTL analysis for kernel size related traits in wheat (*Triticum aestivum* L). *BMC Plant Biol.* 22, 1. doi: 10.1186/s12870-022-03989-9

Manchikatla, P., Kalavikatte, D., Mallikarjuna, B. P., Palakurthi, R., Khan, A. W., Jha, U. C., et al. (2021). MutMap approach enables rapid identification of candidate genes and development of markers associated with early flowering and enhanced seed size in chickpea (*Cicer arietinum* L.). *Front. Plant Sci.* 12. doi: 10.3389/fpls.2021.688694

Mateos, J. L., Madrigal, P., and Tsuda, K. (2015). Combinatorial activities of short vegetative phase and flowering locus c define distinct modes of flowering regulation in *Arabidopsis*. *Genome Biol.* 16, 1. doi: 10.1186/s13059-015-0597-1

Paul, P. J., Samineni, S., and Sajja, S. B. (2018a). Capturing genetic variability and selection of traits for heat tolerance in a chickpea recombinant inbred line (RIL) population under field conditions. *Euphytica* 27, 2. doi: 10.1007/s10681-018-2112-8

Paul, P. J., Samineni, S., Thudi, M., Sajja, S. B., Rathore, A., Das, R. R., et al. (2018b). Molecular mapping of QTLs for heat tolerance in chickpea. *Int. J. Mol. Sci.* 19, 8. doi: 10.3390/ijms19082166

Roorkiwal, M., Bharadwaj, C., Barmukh, R., Dixit, G. P., Thudi, M., Gaur, P. M., et al. (2020). Integrating genomics for chickpea improvement: achievements and opportunities. *Theor. Appl. Genet.* 133, 5. doi: 10.1007/s00122-020-03584-2

Sandhu, N., Pruthi, G., Prakash,, Raigar, O., Singh, M. P., Phagna, K., et al. (2021). Meta-QTL analysis in rice and cross-genome talk of the genomic regions controlling

nitrogen use efficiency in cereal crops revealing phylogenetic relationship. *Front. Genet.* 12. doi: 10.3389/fgene.2021.807210

Sita, K., Sehgal, A., HanumanthaRao, B., Nair, R. M., Prasad, P. V., Kumar, S., et al. (2017). Food legumes and rising temperatures: effects, adaptive functional mechanisms specific to reproductive growth stage and strategies to improve heat tolerance. *Front. Plant Sci.* 8. doi: 10.3389/fpls.2017.01658

Soriano, J. M., Colasuonno, P., Marcotuli, I., and Gadaleta, A. (2021). Meta-QTL analysis and identification of candidate genes for quality, abiotic and biotic stress in durum wheat. *Sci. Rep.* 11, 1. doi: 10.1038/s41598-021-91446-2

Sosnowski, O., Charcosset, A., and Joets, J. (2012). BioMercator V3: An upgrade of genetic map compilation and quantitative trait loci meta-analysis algorithms. *Bioinform* 28, 15. doi: 10.1093/bioinformatics/bts313

Thudi, M., Chen, Y., Pang, J., Kalavikatte, D., Bajaj, P., Roorkiwal, M., et al. (2021). Novel genes and genetic loci associated with root morphological traits, phosphorus-acquisition efficiency and phosphorus-use efficiency in chickpea. *Front. Plant Sci.* 12. doi: 10.3389/fpls.2021.636973

Thudi, M., Chitikineni, A., Liu, X., He, W., Roorkiwal, M., Yang, W., et al. (2016a). Recent breeding programs enhanced genetic diversity in both desi and kabuli varieties of chickpea (*Cicer arietinum* L.). *Sci. Rep.* 16, 1. doi: 10.1038/srep38636

Thudi, M., Khan, A. W., Kumar, V., Gaur, P. M., Katta, A. V. S. K., Garg, V., et al. (2016b). Whole genome re-sequencing reveals genome wide variations among parental lines of mapping populations in chickpea (*Cicer arietinum*). *BMC Plant Biol.* 16 (Suppl1), 10. doi: 10.1186/s12870-015-0690-3

Thudi, M., Samineni, S., Li, W., Boer, M. P., Roorkiwal, M., Yang, Z., et al. (2023). Whole genome resequencing and phenotyping of MAGIC population for high resolution mapping of drought tolerance in chickpea. *Plant Genome* 30, e20333. doi: 10.1002/tpg2.20333

Thudi, M., Upadhyaya, H. D., Rathore, A., Gaur, P. M., Krishnamurthy, L., and Roorkiwal, M. (2014). Genetic dissection of drought and heat tolerance in chickpea through genome-wide and candidate gene-based association mapping approaches. *PloS One* 9, 5. doi: 10.1371/journal.pone.0096758

Upadhyaya, H. D., Dronavalli, N., Gowda, C. L. L., and Singh, S. (2011). Identification and evaluation of chickpea germplasm for tolerance to heat stress. *Crop Sci.* 51, 5. doi: 10.2135/cropsci2011.01.0018

Varshney, R. K., Roorkiwal, M., Sun, S., Bajaj, P., Chitikineni, A., Thudi, M., et al. (2021). A chickpea genetic variation map based on the sequencing of 3,366 genomes. *Nature* 599, 622–627. doi: 10.1038/s41586-021-04066-1

Varshney, R. K., Song, C., Saxena, R. K., Azam, S., Yu, S., Sharpe, A. G., et al. (2013). Draft genome sequence of chickpea (*Cicer arietinum*) provides a resource for trait improvement. *Nat. Biotechnol.* 31, 3. doi: 10.1038/nbt.2491

Varshney, R. K., Thudi, M., Roorkiwal, M., He, W., Upadhyaya, H. D., Yang, W., et al. (2019). Resequencing of 429 chickpea accessions from 45 countries provides insights into genome diversity, domestication and agronomic traits. *Nat. Genet.* 51, 5. doi: 10.1038/ng41588-019-0401-3

Veyrieras, J. B., Gofnet, B., and Charcosset, A. (2007). MetaQTL: A package of new computational methods for the meta-analysis of QTL mapping experiments. *BMC Bioinform.* 8, 1. doi: 10.1186/1471-2105-8-49

Wang, X., Wang, K., Yin, G., Liu, X., Liu, M., Cao, N., et al. (2018). Pollen-Expressed Leucine-Rich Repeat Extensins are essential for pollen germination and growth. *Plant Physiol.* 176, 3. doi: 10.1104/pp.17.01241

Zhang, D., Wengier, D., Shuai, B., Gui, C. P., Muschietti, J., McCormick, S., et al. (2008). The pollen receptor kinase LePRK2 mediates growth-promoting signals and positively regulates pollen germination and tube growth. *Plant Physiol.* 148, 3. doi: 10.1104/pp.108.124420

frontiers | Frontiers in Plant Science

TYPE Original Research
PUBLISHED 07 December 2023
DOI 10.3389/fpls.2023.1289507

OPEN ACCESS

EDITED BY
Hui Song,
Qingdao Agricultural University, China

REVIEWED BY
Meng Zhang,
Hunan University, China
Dongna Ma,
Jiangnan University, China

*CORRESPONDENCE
Weiguo Zhang
wgzhang@nwu.edu.cn
Beibei Li
libeibei@nwu.edu.cn

RECEIVED 06 September 2023
ACCEPTED 21 November 2023
PUBLISHED 07 December 2023

CITATION
Yuan G, Zhang N, Zou Y, Hao Y, Pan J, Liu Y, Zhang W and Li B (2023) Genome-wide identification and expression analysis of WRKY gene family members in red clover (*Trifolium pratense* L.). *Front. Plant Sci.* 14:1289507. doi: 10.3389/fpls.2023.1289507

Genome-wide identification and expression analysis of WRKY gene family members in red clover (*Trifolium pratense* L.)

Guoxin Yuan, Nijing Zhang, Yiming Zou, Yaqi Hao, Jiahao Pan, Yongzhao Liu, Weiguo Zhang* and Beibei Li*

Key Laboratory of Resource Biology and Biotechnology in Western China, Ministry of Education, Northwest University, Xi'an, China

Trifolium pratense is an important legume forage grass and a key component of sustainable livestock development. Serving as an essential component, the *WRKY* gene family, a crucial group of regulatory transcription factors in plants, holds significant importance in their response to abiotic stresses. However, there has been no systematic analysis conducted on the *WRKY* gene family in *Trifolium pratense*. This study conducted a comprehensive genomic characterization of the *WRKY* gene family in *Trifolium pratense*, utilizing the latest genomic data, resulting in the identification of 59 *TpWRKY* genes. Based on their structural features, phylogenetic characteristics, and conserved motif composition, the WRKY proteins were classified into three groups, with group II further subdivided into five subgroups (II-a, II-b, II-c, II-d, and II-e). The majority of the TpWRKYs in a group share a similar structure and motif composition. Intra-group syntenic analysis revealed eight pairs of duplicate segments. The expression patterns of 59 *TpWRKY* genes in roots, stems, leaves, and flowers were examined by analyzing RNA-seq data. The expression of 12 *TpWRKY* genes under drought, low-temperature (4°C), methyl jasmonate (MeJA) and abscisic acid (ABA) stresses was analyzed by RT-qPCR. The findings indicated that *TpWRKY46* was highly induced by drought stress, and *TpWRKY26* and *TpWRKY41* were significantly induced by low temperature stress. In addition, *TpWRKY29* and *TpWRKY36* were greatly induced by MeJA stress treatment, and *TpWRKY17* was significantly upregulated by ABA stress treatment. In this research, we identified and comprehensively analyzed the structural features of the *WRKY* gene family in *T.pratense*, along with determined the possible roles of *WRKY* candidate genes in abiotic stress. These discoveries deepen our understandings of how WRKY transcription factors contribute to species evolution and functional divergence, laying a solid molecular foundation for future exploration and study of stress resistance mechanisms in *T.pratense*.

KEYWORDS

***Trifolium pratense*, gene family, WRKY, expression patterns, abiotic stress**

1 Introduction

Plants thrive in dynamic environments characterized by frequent unfavorable conditions that hinder their growth and development. The range of adverse environmental conditions encompasses both biotic stresses, such as pathogen infestation and herbivore predation, and abiotic stresses, including drought, high temperature, cold, UV radiation, as well as elevated levels of salt, and soil contaminants like Pd, and Cd (Zhu, 2016). The geographical distribution of plants in nature, agricultural productivity, and the sustainability of agriculture are profoundly impacted by the primary environmental factors of drought, salinity, and temperature stress. These factors impose limitations and pose threats that directly affect plants. The impact of climate change intensifies the detrimental consequences of these abiotic stresses, contributing to a rise in the occurrence of extreme weather events (Fedoroff et al., 2010). Understanding how plants perceive stress signals and acclimate to hostile environments is a fundamental inquiry in the field of biology. Enhancing plant stress tolerance is of paramount importance for both agricultural productivity and environmental sustainability, as crops with limited resilience tend to require excessive water and fertilizers, placing an immense strain on the environment.

Transcription factors (TFs) have a vital function as essential components of plant signaling pathways, actively in responses to multiple stress responses, while also coordinating internal signals in response to development and various interactions (Joshi et al., 2016). Stress-related genes are predominantly induced at the transcriptional level, and the regulation of specific stress genes' spatiotemporal expression patterns forms a vital component of the plant's stress response. The majority of plant's genomic capacity is dedicated to transcription, with the *Arabidopsis* genome alone containing over 1500 encoded transcription factors (Riechmann et al., 2000). Frequently, these transcription factors are members of expansive gene families, and in certain instances, they exhibit exclusivity to the plant kingdom. When plants perceive biotic and abiotic stress, plants can spontaneously initiate a cascade of response mechanisms, including recoding of stress resistance genes, reconstruction of metabolic pathways and remodeling of cellular tissues. Stress-related TFs, upon receiving stress signals, are activated and function as molecular switches. One of the key components of this network is the interaction of stress-related transcription factors with cis-regulatory elements present in gene promoters. Through this interaction, they exert precise control over the expression of their target genes (Singh et al., 2002). There are many stress-related transcription factors in plants, such as ERF, TCP, NAC, and WRKY. These transcription factors actively contribute to the plant's ability to cope with and respond effectively to both biotic and abiotic stresses. Among the essential and extensive families of transcription factors in plants, WRKY stands out as one of the most significant (Eulgem et al., 2000). Its role is pivotal in numerous metabolic regulatory processes, exerting a profound influence on various aspects of plant physiology and development (Rushton et al., 2010).

The structural domain of the WRKY protein is approximately 60 amino acids in length, with a highly conserved WRKYGQK heptapeptide present prominently at the N-terminus and a zinc finger structure retained at the C-terminus (Ulker and Somssich, 2004). Phylogenetically, the WRKY family is classified into three groups based on the number of conserved WRKY domains and zinc finger structures. The first group contains two conserved WRKY domains, the second group contains one conserved WRKY domain, and both groups I and II possess a C2-H2 type zinc finger structure. On the other hand, the third group comprises a conserved WRKY domain and a C2-HC-type zinc finger structure. The second subfamily further divides into five subgroups (IIa-IIe) based on the sequence characteristics of the DNA-binding structural domains within the WRKY proteins (Eulgem et al., 2000; Riechmann et al., 2000; Rushton et al., 2010). WRKY TFs exhibit selective recognition and binding capability to the W-box (C/T) TGAC(T/C) region in the promoter region of target genes (Ulker and Somssich, 2004; Jiang et al., 2017). This allows them to regulate gene expression at the transcriptional level, acting as either activators or repressors of gene expression depending on the specific regulatory context.

The initial discovery and isolation of the *WRKY* gene (*SPF1*) were first reported in sweet potato (Ishiguro and Nakamura, 1994). The WRKY protein plays a critical role in governing various stress responses associated with defense (Chen et al., 2012), as well as growth and development processes (Gao et al., 2020), phytohormone signaling, and pathogen triggered cellular responses in a variety of plants (Tsuda and Somssich, 2015; Xi et al., 2021). An instance of this is observed in maize, where the WRKY transcription factor *ZmWRKY79* plays a crucial role in enhancing drought tolerance by promoting the biosynthesis of abscisic acid (ABA) (Gulzar et al., 2021). *AtWRKY1* exerts a negative regulatory role in the defense response against *Pst*.DC3000 through the salicylic acid (SA) signaling pathway (Fang et al., 2021). *WRKY71* directly regulates the expression of ETHYLENE INSENSITIVE2 (EIN2) and ORESARA1 (ORE1), genes associated with the ethylene signaling pathway. *WRKY71* could directly activate *ACS2*, thereby stimulating ethylene synthesis and hastening the process of leaf senescence (Yu et al., 2021). In pepper, double W-box in *CaWRKY40* promoter mediates pathogen invasion and heat stress response (Liu et al., 2021). In summary, WRKYs are critical regulators in multiple stress responses, which further illustrates the potential function of WRKYs in enhancing plant stress resistance.

Red clover (*Trifolium pratense* L.) is a perennial herbaceous plant of the genus *Trifolium* in the family Fabaceae. One of the most important forage legumes in temperate agriculture and a key component of sustainable livestock husbandry, its beneficial attributes help reduce the environmental footprint of grassland agriculture (De Vega et al., 2015). Integrating leguminous forages into cropping systems improves soil health and fertility and deleterious effects of biotic and abiotic stresses (Wahdan et al., 2021). To further enhance its role in sustainable agriculture, there is an urgent need to improve our understandings of the genetic basis of genetic improvement such as persistence, disease resistance, and those traits that affect plant yield, quality and nutrition in order to expedite genetic improvement (De Vega et al., 2015).

However, so far, no studies have identified *WRKY* family in the red clover genome. Consequently, conducting a comprehensive investigation into the WRKY proteins of red clover will provide valuable insights into the fundamental molecular mechanisms underlying the development and stress resistance of this plant species. In this study, the *WRKY* family of red clover was comprehensively characterized and 59 *TpWRKYs* were finally identified. In addition, the phylogenetic relationship, chromosome distribution, gene structure, protein motifs, cis-acting elements, collinearity analysis within and between species, and protein interactions of TpWRKY proteins were systematically and comprehensively analyzed. Simultaneously, the expression profiles of *WRKY* gene members across various tissues and in response to abiotic stress and hormone treatments were examined using RNA-seq data or assessed through RT-qPCR assays. In conclusion, a comprehensive study of the *TpWRKYs* gene family and the expression pattern of *TpWRKYs* under abiotic stress lays the foundation for studying the functional properties and expression regulation of *TpWRKY*s in the growth, development, and stress response of red clover.

2 Materials and methods

2.1 Identification of *TpWRKYs* in *Trifolium pratense*

To screen for WRKY genes in *Trifolium pratense*, we obtained genomic data from EnsemblPlants. Download the *Arabidopsis* WRKY protein sequences from the official *Arabidopsis thaliana* website and use BLASTP to search for homologous sequences in the red clover protein database. (TAIR, https://www.arabidopsis.org/). Access the Pfam protein family database to download the Hidden Markov Model (HMM) file for the WRKY structural domain (PF03106) (Mistry et al., 2020), and then HMMER3.0 was used to query the WRKY gene in red clover. Based on the analyses conducted using Pfam, SMART, and CDD, it was determined that all these genes contain the intact WRKY structural domain. Analysis of molecular weight, gene location and isoelectric point of *TpWRKYs* using the seqinr R package. Determination of transmembrane regions using DEEP TMHMM, the latest update of the TMHMM software (DTU/DeepTMHMM – BioLib) (Hallgren et al., 2022).

2.2 Multiple sequence alignment and phylogenetic analysis

For multiple alignment analysis, multiple sequence alignment using MUSCLE (Edgar, 2004) for 151 sequences from 2 species of red clover (59), *Arabidopsis thaliana* (72), and results using msa R package to demonstrate structural features (Bodenhofer et al., 2015). We use IQ-TREE (Nguyen et al., 2015) maximum likelihood (ML) method to construct phylogenetic trees and automatically find the best model with 1000 bootstraps. WRKY proteins from different subfamilies of *Arabidopsis* were used as grouping markers. Evolutionary trees were beautified using the ITOL (Interactive Tree Of Life) online tool (Letunic and Bork, 2021).

2.3 Analysis of chromosomal localization, gene structure, motif, and cis-acting elements of TpWRKYs protein

The genome annotation file was used to obtain the chromosomal location of the *TpWRKY* genes, and this information was then visualized using MapChart (Voorrips, 2002). Using the Gene Structure Display Server (GSDS 2.0) to map the structure of the *TpWRKY* genes (Guo et al., 2007). The conserved motifs of TpWRKY proteins were identified using Multiple Em for Motif Elicitation (MEME,v5.4.1) program with the following parameters: number of repetitions-any, maximum output of 10 motifs, and the optimal motif range was set to 6-200 amino acids (Bailey et al., 2009). To explore the cis-acting elements present in the promoter region of the *TpWRKY* family, we extracted the 2k sequence upstream of each *TpWRKY* gene as the promoter region and submitted it to the PlantCARE database for cis-acting element prediction (Lescot et al., 2002). Ultimately, the analysis and visualization of cis-acting elements were carried out using GSDS and ggplot2 R package.

2.4 Subcellular localization, gene duplication and synteny analysis

Cell-PLoc 2.0 website tools were utilized for predicting subcellular localization (Chou and Shen, 2010). Checking for gene duplication events using the default parameters of the Multiple Collinearity Scan toolkit (MCScanX) (Wang et al., 2012). To explore covariation between red clover and other species, JCVI (Tang et al., 2015) was used to visualize covariation results for red clover with *Arabidopsis* and rice. Circos (Krzywinski et al., 2009) was used to visualise the results of intraspecific covariation in red clover.

2.5 Plant materials, growth conditions and treatments

Growing red clover in the plant greenhouse at Northwest University, the growing conditions are set for 16h light at 25°C and 8h dark at 22°C, with humidity at around 60%. Seedlings of about 60d of healthy growth and uniform size were then selected for subsequent experiments. In the drought treatment, seedlings in Pots were watered with 20% PEG8000. The seedlings were moved to 4°C in an incubator for low temperature stress. The above-ground surface parts of the seedlings were sprayed with 100μM MeJA and ABA for hormone stress treatment, separately. Samples were then taken at 0h (as control), 3h, 6h, 12h, 24h and 48h, respectively, and immediately frozen in liquid nitrogen after sampling at different time points, followed by storage at -80°C for subsequent

experiments. Each treatment was independently replicated three times, and for each replicate, samples were collected from three different plants. In order to study the expression pattern of *TpWRKY* genes under different stress treatments, 12 *TpWRKY* genes were selected for RT-qPCR analysis.

2.6 RNA extraction and synthesis of cDNA

During the process of grinding each plant tissue into a fine powder, liquid nitrogen was continuously added to maintain a low temperature. For sequencing samples, total RNA was extracted from tissues using the MJZol Total RNA Extraction Kit (Majorbio, Shanghai, China). Using the *SteadyPure* Plant RNA Extraction kit (Accurate, Changsha, China), total RNA was extracted from the stress-treated samples. After 1% agarose gel electrophoresis, the integrity of the RNA was checked, and then the RNA quality was determined using a 5300 Bioanalyzer (Agilent). The RNA was quantified using an ND-2000 (NanoDrop Technologies), and high-quality samples were selected for the construction of sequencing libraries. For quantitative cDNA synthesis, reverse transcription was performed with 1μg RNA in a 10 μl system according to the instructions for the Reverse Transcription Kit AG11706 (Accurate, Changsha, China).

2.7 Library preparation, sequencing and RNA-Seq data analysis

At Shanghai Majorbio Bio-pharm Biotechnology Co., Ltd (Shanghai, China), RNA purification, reverse transcription, library construction, and sequencing of the samples were conducted for the sequenced samples. The paired-end RNA-seq sequencing library was finally sequenced (2 x 150 bp read length) using a NovaSeq 6000 sequencer. Quality control and filtering of the raw data from the lower machine using fastp, with clean reads compared to the reference genome by HISAT2 (Chen et al., 2018; Kim et al., 2019). Reads were counted using featureCounts in the subread package (Liao et al., 2013), then normalized by Transcripts Per Kilobase per Million mapped reads (TPM) and finally TPM values were used to assess gene expression levels. Heat map construction of *TpWRKY* gene expression profile with R. We uploaded raw data to NCBI under project number PRJNA1035639.

2.8 RT-qPCR analysis

RT-qPCR was carried out using SYBR Green Pro Taq HS (Accurate, Changsha, China) as the fluorescent dye. The PCR reaction conditions consisted of an initial denaturation step at 95°C for 30 seconds, followed by 40 cycles of denaturation at 95°C for 10 seconds, and annealing/extension at 60°C for 30 seconds. The expression levels of the 15 selected WRKY genes were studied under drought and cold stress as well as MeJA and ABA treatments. Three biological replicates were performed for each sample and there were also three technical replicates for each biological replicate, using a 10-fold dilution of cDNA as template, and primers are listed in the Supplementary Table S1. The relative expression of the *TpWRKY* gene was calculated using the $2^{-\Delta\Delta CT}$ method, using ACTIN as an internal reference gene, and subjected to statistical analysis. Asterisks (*, **, ***, ****) indicate $p < 0.05$, 0.01, 0.001 or 0.0001, respectively, and the differences are statistically significant.

3 Results

3.1 Identification of the WRKY family in *T.pratense*

The WRKY domain model (PF03106) and the protein sequences of *Arabidopsis thaliana* WRKY proteins were utilized as search queries to identify candidate *WRKY* genes in the protein files of red clover. To eliminate redundant sequences and ensure consistent structural features, a filtering process was conducted. The remaining sequences were subjected to identification in SMART, CDD, and Pfam databases. Consequently, this analysis yielded a set of 59 putative *WRKY* genes, which were systematically named as *TpWRKY1* to *TpWRKY59* according to their respective chromosomal positions (Supplementary Table S2). The Supplementary Table S3 contains sequences of *WRKY* genes, including genomic, CDS, and protein sequences. we conducted a comprehensive analysis of each TpWRKY proteins, examining their chromosomal location, protein length, isoelectric point (pI), subcellular localization, and transmembrane structural domain. The length of TpWRKY proteins is between 146 (TpWRKY57) and 1315 (TpWRKY14) amino acids, and the molecular weight is between 16.39 kDa (TpWRKY57) and 146.86 kDa (TpWRKY14). Moreover, the pIs ranged from 4.56 (TpWRKY47) to 10.7 (TpWRKY19). TpWRKYs were predicted to subcellular localized in the nucleus, except that TpWRKY48 was predicted to mitochondria and nucleus, possibly functioning in the mitochondria. All proteins have no transmembrane domain, indicating that they are non-membrane proteins. TpWRKY proteins domain signatures significantly differentiate between varieties of themselves, which suggests their functional diversities in *Trifolium pretense* L.

3.2 Multiple sequence alignment and phylogenetic classification of *TpWRKYs*

To elucidate the distinctive characteristics of the WRKY domain in each TpWRKY proteins, we performed multiple sequence alignment analysis on the approximately 60 amino acids that constitute the WRKY domain. For this analysis, we compared the sequences of 72 AtWRKY proteins and 59 TpWRKY proteins, as depicted in Supplementary Figure S1. As a result, it was observed that complete or nearly complete conserved sequences of WRKYGQK were found in 59 TpWRKY proteins. Interestingly, certain conserved motifs in some of the TpWRKY proteins exhibit specific mutations and evolutionary changes in a few amino acids (Figure S1). For instance, Q mutated to K in the conserved motif of

WRKYGQK in TpWRKY4, TpWRKY25, TpWRKY29, TpWRKY47, Q mutated to R in TpWRKY43, TpWRKY54, TpWRKY55, Q mutated to E in TpWRKY22, and R mutated to I in TpWRKY11. Furthermore, it was observed that the gene sequences of TpWRKY34 and TpWRKY48 lacked zinc finger structures, while some other TpWRKY proteins contained either C2H2 or C2CH zinc finger domains.

To explore the evolutionary relationships among the members of the TpWRKY family, a comparative analysis with 72 AtWRKYs from *Arabidopsis* as a reference was conducted. The phylogenetic tree was constructed using the maximum likelihood method through IQTREE software, incorporating 1000 bootstrap tests to enhance confidence in the results. The tree was based on the sequences of *T. pratense* and *Arabidopsis*, effectively illustrating the genetic relatedness between the two. As a result, all TpWRKY proteins were classified into three distinct groups: Group I, Group II (IIa-IIe) and Group III (Figure 1). The analysis of the phylogenetic tree revealed that Group II had the most abundant representation with a total of 42 WRKY members. Group I and Group III comprised 11 and 6 members, respectively. Among the five subgroups into which Group II was further categorized, subgroups IIc and IIe had the highest number of members, each consisting of 13 members. Subgroups IIb and IId contained six members each, while subgroup IIa had the minimum representation, with only four members. The classification of TpWRKYs has substantiated the diversity in their protein structures and suggests that different members within the subfamilies may possess distinct regulatory functions. This underscores the potential for varied roles played by TpWRKY proteins in coordinating plant responses and adaptations to various environmental cues.

3.3 Chromosomal location of *TpWRKYs* in the *Trifolium pratense* genome

The chromosome location map displayed that the *TpWRKY* genes were evenly distributed on the chromosomes, with 10 genes on chromosomes 1 and 2, 11 genes on chromosome 3, 6 genes on chromosome 4, 2 genes on chromosome 5. Moreover, chromosomes 6 and 7 contained 6 and 13 genes, respectively. But there are fewer genes on chromosome 5, which may be related to the size and structure of chromosome 5. Moreover, by MCScanX collinearity analysis, we found a pair of tandem repeat replicates on each of chromosomes 1, 3, and 7. Remarkably, a significant majority of *TpWRKYs*, which fall under the same subfamily in the phylogenetic tree, exhibit a scattered distribution on the same chromosome or were located on different chromosomes rather than being closely clustered on the same chromosome. Furthermore, some were distributed in close proximity on the same chromosome, but they still do not belong to tandem repeat replication. These indicated that the expansion of *TpWRKY* family

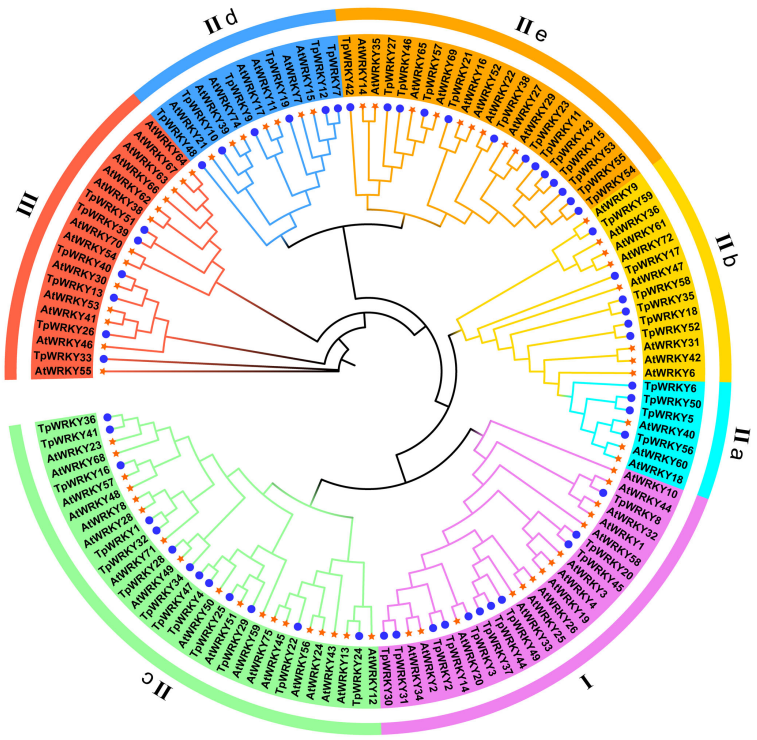

FIGURE 1
Phylogenetic analysis of the full-length structural domains of WRKY proteins in red clover and *Arabidopsis thaliana*. By employing the Maximum Likelihood method, the phylogenetic tree was established using IQ-TREE software, with the application of bootstrap testing for 1000 replicates to assess its robustness. Seven groups/subgroups are indicated by different colors located outside the circle, with blue circles representing *TpWRKYs* and orange stars representing *AtWRKYs*.

is predominantly influenced by mechanisms other than tandem replication events, suggesting a minor contribution of tandem replication events to its expansion.

3.4 Gene structure and conserved motifs of *TpWRKYs*

To gain a comprehensive understanding of the conservation and diversity exhibited by WRKY family, we subjected all TpWRKYs to an analysis of their conserved motifs using the MEME program. Subsequently, we predicted the composition of motifs present within the TpWRKY proteins. As shown in Supplementary Figure S2 and Table S4, a comprehensive selection of 10 distinct motifs was made and labeled as motif 1 to motif 10. These conserved motifs are between 15 and 51 amino acids in length. The quantity of conserved motifs for each TpWRKY proteins was primarily from 1 to 8 (Figure 2B). As expected, the same group or subgroup of TpWRKYs has a highly consistent conserved motif. Motif1, motif2 and motif3 are present in most genes, motif4 is present only in subgroups I, IIb and IIc, motif6 and motif9 are specific to IIa and IIb. Subgroup I contains the specific motif7 and subgroup IIe contains the specific motif5, motif8 and motif10. Notably, TpWRKY24 contains only motif 2, which may be related to the loss of the structural domain. Overall, the closely related TpWRKYs in the phylogenetic tree have similar motif compositions and may perform similar functions. However, the functions of many of these motifs are yet to be clarified.

The diversity of gene structures can provide insights into the evolutionary history of gene families. Therefore, we conducted analyzed the exon/intron distribution and the number of coding exons for each *TpWRKY* gene to further understand the evolutionary history of the WRKY family in *T. pretense*. The coding exons of *TpWRKY* genes varied in number, spanning from 2 to 8. Among the *TpWRKY* genes, the highest proportion (44%) contained 3 coding exons, followed by 5 (20%), 4 (17%), 2 (7%), 6 (8%), and 7 and 8 coding exons each (2%) (Figure 2C). At the same time, the number of coding exons of protein members in the same family converged, thus confirming the phylogenetic plausibility. For example, subgroup IIa TpWRKYs contained 3-4

FIGURE 2
Phylogenetic tree, composition of conserved motifs and gene structures of TpWRKY family members. **(A)** The full-length structural domains of 59 TpWRKY proteins were used to construct an evolutionary tree by maximum likelihood. Different color backgrounds represent different subfamily classifications. **(B)** Conserved motifs of TpWRKY proteins. Different colors and numbers represent different motifs. **(C)** Exon/intron structure analysis of *TpWRKY* genes. Green represents the UTR region, yellow represents the exon region, and black lines represent the intron region.

coding exons, with an intron count of 3. Subgroup IIb TpWRKYs contained 5-6 coding exons and 4-5 introns. Subgroup III TpWRKYs contained 2-3 coding exons and 1-2 introns.

Overall, TpWRKYs that show close relationships in the phylogenetic tree tend to have similar gene structures and conserved motif compositions, suggesting that TpWRKYs within the same taxon may likely have comparable functions.

3.5 Analysis of cis-acting elements in the promoter region of *TpWRKY* genes

In order to gain insights into the role of cis-regulatory elements in *TpWRKYs*, we utilized the PlantCARE software to identify cis-acting elements within the sequences located 2,000 bp upstream of the translation start site (ATG) for each *TpWRKY* genes. A total of 62 different cis-acting elements were identified in 59 *TpWRKY* genes, and we focused our analysis on cis-acting elements related to development-related, phytohormone responsive, stress-responsive, and light-responsive elements (Figure 3 and Supplementary Table S5).

The first category of cis-acting elements related to plant growth and development, including related to meristem expression responsive (CAT-box), differentiation of the palisade mesophyll cells responsive (HD-Zip 1), circadian rhythm control responsive (circadian), endosperm expression responsive (GCN4_motif), metabolism regulation responsive (O2-site), seed-specific regulation responsive (RY-element). Focusing on the regulation of plant growth and development, it is worth noting that *TpWRKY6*, *TpWRKY12*, *TpWRKY23*, *TpWRKY36*, and *TpWRKY50* all exhibit the presence of four distinct plant development-related elements. They may play a key role in various aspects of plant growth and development. The second category of phytohormone-responsive cis-acting elements encompasses various elements, such as abscisic acid responsiveness (ABRE), gibberellin-responsive elements (P-box, TATC-box), MeJA-responsiveness (CGTCA-motif, TGACG-motif), auxin-responsive element (TGA-element) and salicylic acid responsiveness (TCA-element, SARE). Among them, the largest proportion of cis-acting regulatory elements was involved in ABA responsiveness and MeJA responsiveness. Of particular interest, the SARE cis-acting element is exclusively present in the promoter region of *TpWRKY5*, implying a potential involvement of this gene in the salicylic acid (SA) signaling pathway. The third category of adversity stress response cis-acting elements, including anaerobic induction responsiveness (ARE), drought-inducibility responsiveness (MBS), low-temperature responsiveness (LTR), flavonoid biosynthetic responsiveness (MBSI), wound responsiveness (WUN-motif), defense and stress responsiveness

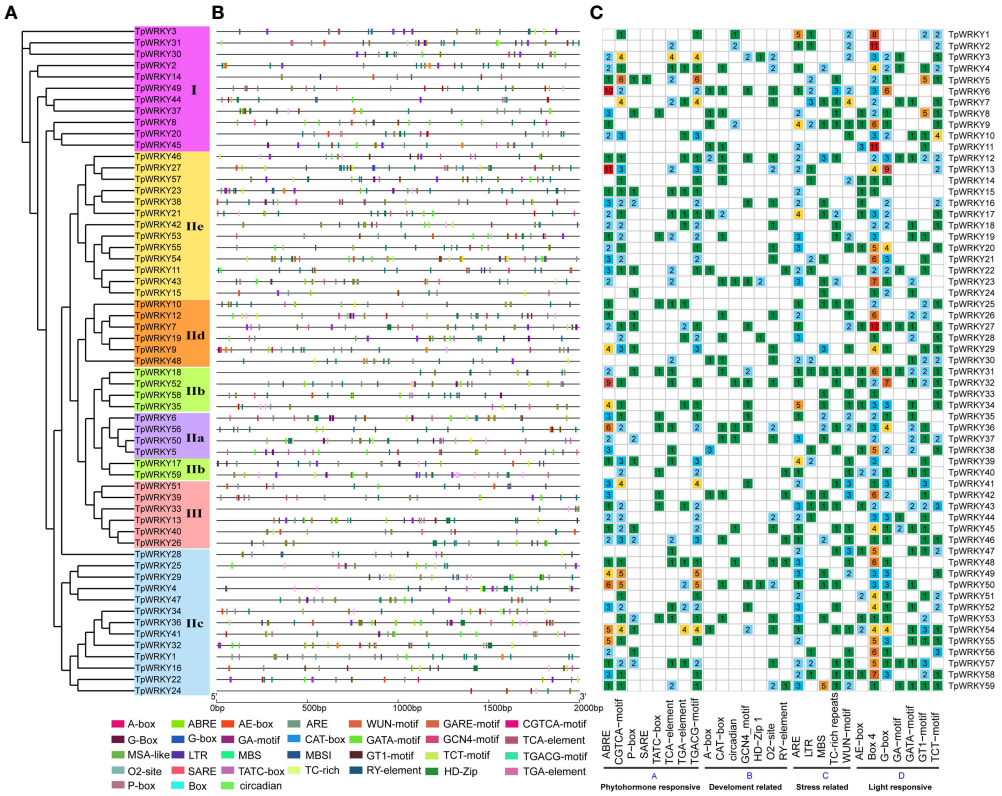

FIGURE 3
Cis-element analysis of the 2kb region upstream of the *TpWRKY* genes. **(A)** The full-length structural domains of 59 TpWRKY proteins were used to construct an evolutionary tree by maximum likelihood. Different color backgrounds represent different subfamily classifications. **(B)** Various types of cis-elements and their respective locations in each *TpWRKY* genes were depicted using distinctively colored blocks. **(C)** The grid displays colors and numbers, representing the count of different cis-acting elements in the initiation regions of *TpWRKY* genes. ggplot2 maps the type, number, and location of cis-acting progenitors of the *TpWRKY* genes.

(TC-rich repeats). Furthermore, 86% of the promoter regions of 51 *TpWRKY* genes were found to contain more than two stress-related cis-acting elements. This implies that *TpWRKYs* may be involved in multiple stress responses. Among the 59 *TpWRKY* genes, most cis-acting elements were found in the fourth category, which encompasses elements related to light response, such as G-box, TCT-motif, GA-motif, and others. Except for *TpWRKY16* and *TpWRKY30*, Box 4 was found in the promoter regions of nearly all *TpWRKYs*.

3.6 Duplication and synteny analysis of *TpWRKY* genes

Conducting a synteny analysis of the *TpWRKY* genes using BLASTP and MCScanX aimed to explore segmental duplication events within the red clover WRKY family. We observed segmental duplication events involving 16 *WRKY* genes and found that genes forming the segmental duplication were from the same subfamily (Figure 4). Meanwhile, tandem duplication events, in which tandem duplication events are defined as chromosomal regions containing two or more genes within a 200 kb distance, are found in the red clover *WRKY* genes (Holub, 2001). To verify whether these gene pairs underwent purifying selection, we computed the non-synonymous substitution rate (Ka) and synonymous substitution rate (Ks). It was noticed that all homozygous *TpWRKY* gene pairs had Ka/Ks ratios below 1, indicating that these gene pairs underwent purifying selection (Supplementary Table S6). The results implied that specific *TpWRKY* genes could have arisen from segmental duplication events, implying that the evolution of *TpWRKY* genes is potentially influenced, at least partially, by both segmental and tandem duplication events.

To further explore the molecular evolutionary relationships between species, we used a dicotyledonous plant (*Aabidopsis*) and a monocotyledonous plant (*Oryza sativa*) to map the covariance of the red clover WRKY family (Figure 5A). Between red clover and *Arabidopsis*, a total of 17 collinear gene pairs were detected, and an additional 3 collinear gene pairs were found between red clover and rice. In addition, we selected soybean and common bean to further investigate the colinearity of *WRKY* genes in legumes. The colinearity analysis showed that red clover had 137 colinear gene pairs with soybean (*Glycine max*) and 70 colinear gene pairs with common bean (*Phaseolus vulgaris*) (Figure 5B). Based on the homology analysis of *TpWRKYs* between red clover and other species, it was indicated that the *TpWRKY* genes exhibited higher homology with legume, potentially attributable to their close genetic relationship. At the same time, they exhibit a higher homology with the dicot model plant *Arabidopsis*, indicating that these genes likely

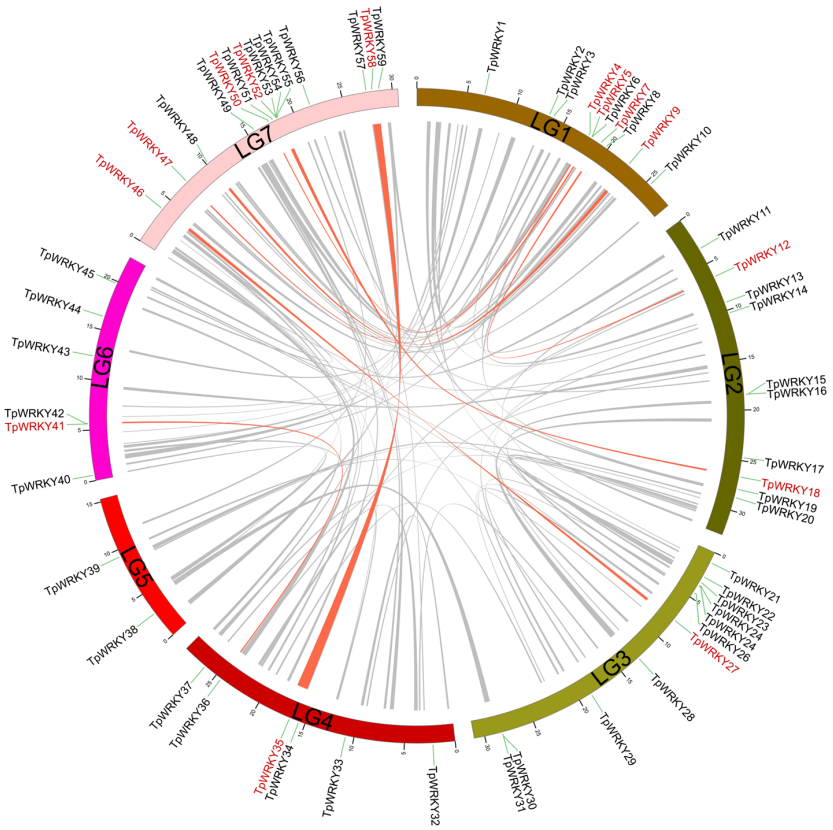

FIGURE 4
Demonstration of interchromosomal relationships in *TpWRKYs*. The gray line indicates all synteny blocks within red clover, and synteny blocks of *WRKY* genes are highlighted with red lines.

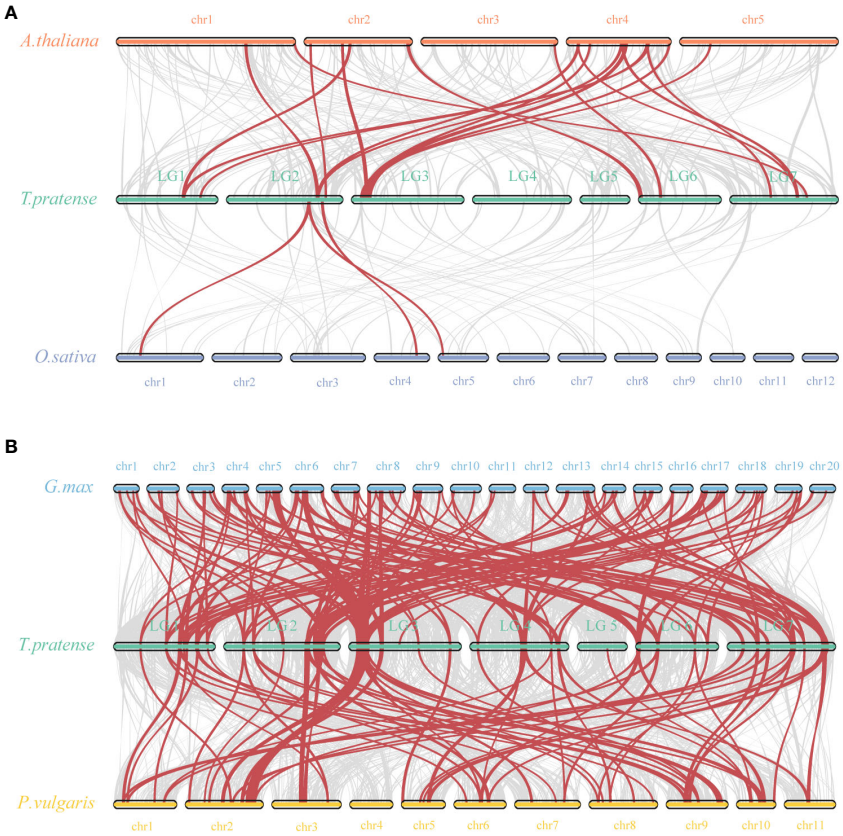

FIGURE 5
Synteny analysis of WRKYs between red clover and other plant species. **(A)** Analysis of synteny between *TpWRKY* genes and *Arabidopsis* and rice. **(B)** Analysis of synteny between TpWRKY genes and soybean and common bean. Interspecies collinear blocks are shown as gray lines, and the synteny *WRKY* gene pairs are marked in red.

emerged after the differentiation of dicots and monocots. Despite chromosomal rearrangements or gene duplications, the synteny analysis of *TpWRKY* genes demonstrated robust collinearity.

3.7 *TpWRKYs* expression profiles in different organs

A standard transcriptome analysis procedure was employed to investigate the transcript abundance of all 59 *TpWRKYs*, utilizing transcriptomic data from four organs of red clover, namely roots, stems, leaves, and flowers (Figure 6 and Supplementary Table S7). Among the 59 *TpWRKY* genes, fifty *TpWRKY* genes were detected in four different organs (TPM > 0),17 genes were constitutively expressed in all samples (TPM > 1). No transcripts of three *TpWRKYs* (*TpWRKY53*, *TpWRKY54* and *TpWRKY55*) were detected in the different developing organs, suggesting that they may be pseudogenes. Conversely, some *TpWRKY* genes showed high expression in specific organs. For instance, 6 genes in flowers, 7 genes in leaves, 13 in roots and 9 genes in stems (TPM > 20). Highly expressed in all organs, *TpWRKY3, 7, 9, 19, 45* may serve an essential role in the overall growth and developmental process of red clover. Analysis of *WRKY* gene expression in different organs showed that *TpWRKY31* was significantly higher in flowers than in roots, stems, and leaves, whereas *TpWRKY9/36/46* had higher expression in roots and relatively lower expression in stems and leaves. Indicating their significance in numerous aspects of plant development, including both the whole plant and specific organs, these results highlighted the vital roles played by these genes.

3.8 Expression patterns of selected *TpWRKY* genes under hormone and abiotic treatments

In order to delve deeper into the potential impact of different stress treatments on the expression of these *TpWRKY* genes, a subset of 12 members from various subfamilies was chosen using RNA-Seq analysis, guided by the examination of known stress-related WRKY proteins and cis-acting elements. Undergoing four distinct stress treatments, red clover seedlings were exposed to drought (20% PEG8000), low temperature (4°C), ABA (100 μM), and MeJA (100 μM). Using RT-qPCR, the expression variations of the selected genes were subsequently analyzed under different stress conditions.

In Figure 7A, the expression of all 12 genes was up-regulated under drought stress. Among them, *TpWRKY46* was highly induced after being subjected to drought stress, and its expression

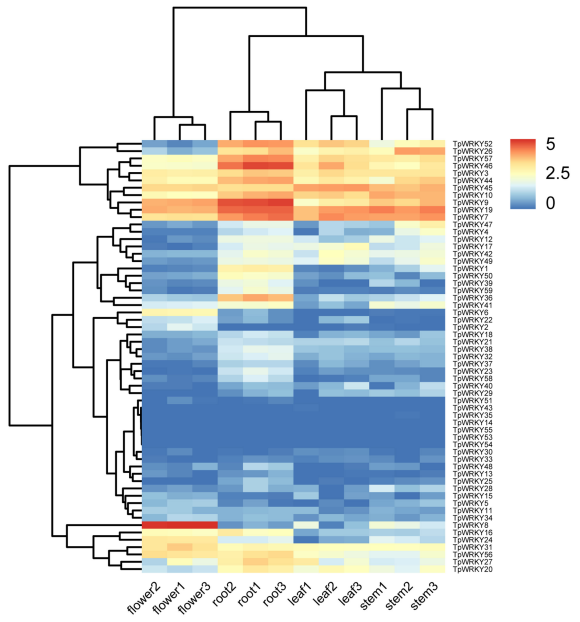

FIGURE 6
Heatmap demonstrating the expression profile of *TpWRKY* genes in four organs. *TpWRKY* gene expression heatmap was plotted using TPM values, and data were normalized relative to the average expression value of each gene in all samples and log2 transformed. Blue and red colors indicate low- and high-expressed genes, respectively.

level peaked at 6 h 139-fold higher than that under normal conditions. It is noteworthy that with the prolongation of stress time all genes had two up-regulated peaks at 6h and 48h of drought stress, except for *TpWRKY46* gene which reached its peak at 6h of drought stress treatment. Most genes were down-regulated under low temperature stress. Among them, *TpWRKY3/10/38/46* were down-regulated at all low temperature stress treatment times, and *TpWRKY46* was most significantly down-regulated at 48h, 0.06-fold of the normal expression level. Interestingly, *TpWRKY7/17/26* were all up-regulated and then down-regulated, and all turned down-regulated at 12 h of low temperature stress treatment, with *TpWRKY26* being 22-fold up-regulated at 6 h of low temperature stress compared to normal levels (Figure 7B).

Under MeJA stress treatment, only *TpWRKY26/38* were down-regulated at all time periods and peaked at 24 h. *TpWRKY29/36/56* were all up-regulated, with *TpWRKY29* peaking 30-fold up-regulated at 48 h of stress treatment and *TpWRKY36* peaking 50-fold up-regulated at 3 h of stress treatment. However, the rest of the genes, except *TpWRKY10* which was down-regulated and then up-regulated, all showed an up-regulated, down-regulated and then up-regulated expression pattern (Figure 7C). Under ABA stress treatment, all were up-regulated except *TpWRKY56* which was up-regulated and then down-regulated. Among them, the expression of *TpWRKY3/10/17/26/46* all peaked at 6 h of ABA stress treatment, and *TpWRKY17* and *TpWRKY46* were highly induced to be expressed at 35 and 29-fold of normal levels. The

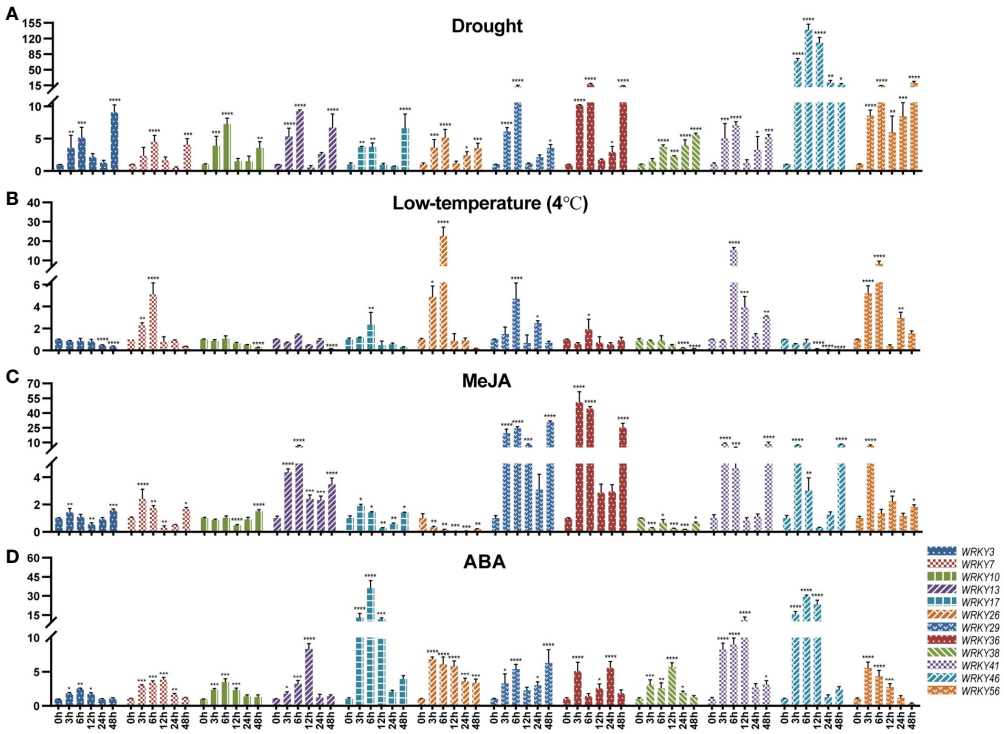

FIGURE 7
qRT-PCR analysis of 12 *TpWRKY* genes under different stress treatments at 0, 3, 6, 12, 24, and 48h. **(A)** Drought. **(B)** low temperature (4°C). **(C)** MeJA. **(D)** ABA. Non-stress level of 0h was used as control. Vertical lines show standard deviation (n = 3). The presence of asterisks denotes a statistically significant difference when compared to the control group. (*p < 0.05, **p < 0.01, ***p < 0.001, ****p < 0.0001).

expression of *TpWRKY7/13/38/41* peaked at 12 h, *TpWRKY13* and *TpWRKY41* were at normal levels of 8 and 10-fold (Figure 7D).

4 Discussion

For the past few years, more and more researchers are focusing on germplasm resources and sustainable development in grass industry (Sato et al., 2005; Yan et al., 2023). Due to its high seedling survival rate, rapid growth, and stress tolerance, red clover (*Trifolium pratense* L.) is a significant forage legume extensively cultivated in various temperate regions (Sato et al., 2005). Plant growth, development and reproduction are usually affected by a variety of biotic and abiotic stresses in natural world (Sharif et al., 2021). Plants have evolved complex regulatory mechanisms involving different TFs, which accommodate unfavorable environmental conditions (Baillo et al., 2019). *WRKY* genes are widely present in plants and play a crucial role in regulating a variety of stress responses (Jiang et al., 2017; Khoso et al., 2022). Currently, the genome-wide analysis of the *WRKY* family has been extensively conducted in numerous sequenced species (Yan et al., 2019; Hu et al., 2021; Kan et al., 2021). WRKY family in red clover has not been identified so far, which has hindered the study of the function of *TpWRKY* genes to some extent. Consequently, our study involved the identification of the WRKY family in red clover, followed by systematic bioinformatic analysis and expression analysis in response to both hormonal and abiotic stresses.

The identification of a total of 59 *TpWRKY* genes was achieved in this study, and they were named as *TpWRKY1* to *TpWRKY59* based on their chromosomal positions. There was no significant correlation between the number of *WRKY* genes and genome size. For example, *Arabidopsis thaliana* genome size 125 Mb (75), *Liriodendron chinense* genome size 1.7 G (44), and *Dendrobium catenatum* genome size 1.11 Gb (62). The quantity of red clover WRKY family members might be linked to its evolutionary process and the way of family expansion, with the quality of genome assembly also serving as a significant factor influencing the gene count. It has been shown that most of the *WRKY* genes are localized in the nucleus (Wang et al., 2018). The physicochemical property analysis revealed notable differences in the MW and pI of TpWRKY proteins, implying that their protein structures may exhibit variations, enabling them to adapt to diverse biotic and abiotic stresses. All WRKY proteins do not have transmembrane structural domains and are localized to the nucleus. These features suggest that *WRKY* genes perform different biological functions under different stresses which may be related to the physicochemical properties and spatial structure of the protein.

WRKY TFs, containing a highly conserved structural domain consisting of approximately 60 amino acids, a highly conserved WRKYGQK structural domain at the N-terminus and a variable zinc finger structure at the C-terminus. (Rushton et al., 2010). It regulates gene expression by binding specifically to the W-box in the promoter region of the target gene. At least one conserved WRKY structural domain is present in the 59 TpWRKY proteins identified in this study. Meanwhile, we found specific mutations and evolution of the highly conserved WRKYGQK core sequence of some TpWRKY proteins. Four mutations were WRKYGKK (*TpWRKY4*, *TpWRKY25*, *TpWRKY29*, *TpWRKY47*), three mutations were WRKYGRK (*TPWRKY43*, *TPWRKY54*, *TpWRKY55*), and one mutation was WRKYGEK (*TpWRKY22*) and WIKYGQK (*TpWRKY11*). In soybean, *GmWRKY6* and *GmWRKY21* have been mutated to the WRKYGKK motif, which results in their inability to bind W-box (Zhou et al., 2008). In tobacco, conserved structural domain of *NtWRKY12* is mutated to WRKYGKK and binds specifically to the WK box (TTTTCCAC) (van Verk et al., 2008). Consequently, our hypothesis suggests that mutations in the WRKYGQK sequence could lead to a substantial reduction or even a complete loss of binding capacity to the W-box. Alternatively, it may result in binding to other motifs, thus participating in novel regulatory mechanisms.

Throughout the evolution history of the plant *WRKY* gene family, group I served as the ancestral group for group II and group III. The further evolution of the *WRKY* gene family led to the formation of group II and group III, involving the retention and deletion of the WRKY structural domain at the N-terminus of group I, as well as modifications in the Zinc finger structural domain at the C-terminus (Wu et al., 2005; Zhang and Wang, 2005). The phylogenetic analysis of WRKY sequences in *Arabidopsis* and rice combined the four branches of clade II into two new clades: IIa + b and IId + e (Rinerson et al., 2015). This may imply that there is a close evolutionary relationship between them, with genes in group IIa being closely related to genes in group IIb, and genes in group IId being closely related to genes in group IIe (Javed and Gao, 2023). These results may shed light on the function of unknown TpWRKYs in red clover based on identified functions of AtWRKYs in *Arabidopsis*. *TpWRKY56* in Group II-a subfamily may have similar functions to *AtWRKY18*, *AtWRKY40*, and *AtWRKY60* and may be involved in plant defense in response to ABA and drought stress (Chen et al., 2010). *AtWRKY32* promotes photomorphogenesis development through the COP1-HY5 signaling pathway. Under dark conditions, COP1 exerts negative regulation over the stability of *WRKY32*. Additionally, *WRKY32* directly interacts with the promoter of HY5, leading to the activation of its transcription and consequently promoting photomorphogenesis (Zhou et al., 2022). This suggests that *TpWRKY8* in *T.pratense* may also be associated with plant photomorphogenesis.

Examining the exon-intron structure of gene families aids in the identification of diverse structural domains and can serve as crucial evidence for discerning the evolutionary relationships of genes (Wang et al., 2011; Gorlova et al., 2014). In this research, a comprehensive analysis of the structural distribution of *WRKY* family members was conducted and discovered that *WRKY* genes within the same subfamily exhibit analogous structural distribution patterns. Three members of each the 11 *TpWRKYs* gene within group I have three, four and five introns, while the other two members have six introns. Members in subgroup IIa all contain three introns, and 83% of *TpWRKYs* have two introns in subgroup III (Figure 2), which is similar to the distribution in *Scutellaria baicalensis* and rice (Xie et al., 2005; Zhang et al., 2022a). The results of the analysis indicate that distribution patterns of exons and

introns were closely related to the subfamily classification. The conserved features of motifs reveal that motif1, 2, 3, 4, and 7 are typical in group I, motif1, 2, 3 are typical in group II, and motif1, 2, 3, and 4 are typical in group III, which is more similar to the motif distribution observed in walnut (Hao et al., 2021). Almost all proteins contained motif1, motif2 and motif3 which is further evidence that all proteins contain conserved WRKY structural domains. Compared to alfalfa, chickpea, and common bean, structural domains 1 and 2 embody the characteristic features of WRKY DNA-binding domains, remaining entirely conserved across all WRKYs, with the exception of a few domains that may be missing (Wang et al., 2016; Waqas et al., 2019). On the other hand, abundant cis-acting elements were found in the upstream 2 kb of the red clover *WRKY* genes, which can be classified into four categories (development-related, phytohormone responsive, stress-responsive and light-responsive elements) and are associated with ABA, JA, SA and multiple biotic/abiotic stresses. These cis-acting elements of *TpWRKYs* gene bind to various stress-related trans-acting factors to regulate the expression and response of red clover stress resistance genes.

Replication modes of genes include whole genome duplication (WGD), tandem duplication, segmental duplication and transposon-mediated transposon duplication, which are the major modes of eukaryotic genome evolution (Panchy et al., 2016). The expansion of the *WRKY* gene family is predominantly driven by tandem and segmental duplication events (Rushton et al., 2010). In sunflower (*Helianthus annuus* L), 21 *HaWRKY* genes were identified as resulting from segmental duplication events on 10 chromosomes, as well as six tandemly duplicated gene pairs found on chromosome 17 (Guo et al., 2019). In pineapple (*Ananas comosus*), seven tandem repeat gene pairs were identified within the *WRKY* gene family, with 17 fragment duplication events in 27 genes (Xie et al., 2018). In maize (*Zea mays*), 52 gene pairs out of 125 *ZmWRKY* genes were identified to be involved in segmental replication events and no tandem replication events were found (Hu et al., 2021). We hypothesize that tandem and fragment replication events promote the expansion of the *TpWRKY* gene family. There are eight pairs of synteny segments within the red clover. Furthermore, we observed that genes with tandem repeat events belong to the same subfamily, such as *TpWRKY5* and *6* belonging to IIa, *TpWRKY30* and *31* belonging to I, and *TpWRKY54* and *55* belonging to IIe. Meanwhile, the synteny map of *TpWRKY* family with monocotyledons (*Oryza sativa*) and dicotyledons (*Arabidopsis thaliana*) was also constructed. These results showed that there were 17 synteny pairs in red clover and *Arabidopsis*, and three pairs of synteny gene pairs with rice. The lower number of synteny gene pairs between red clover and monocotyledons suggested that these gene pairs likely emerged after the divergence of dicotyledons and monocotyledons.

The interconnection between gene expression and gene function is widely acknowledged. Investigating the expression patterns of genes in various tissues is of paramount importance for mining functional genes (Dutta et al., 2018). Research has demonstrated that *WRKY* genes exhibit expression in one or more tissues, and they are crucial for plant growth and development (Feng et al., 2022; Zhang et al., 2022b). The evolutionary relationship between *CsWRKY7* and *AtWRKY7* in *Camellia sinensis* is closely related, and root elongation was higher in *CsWRKY7* than in wild type (Chen et al., 2019). Under stress conditions, seedlings of *WRKY11* and *17* knockout mutants in *Arabidopsis thaliana* exhibited reduced germination rates and impaired root growth compared to the wild type (Ali et al., 2018). We analyzed the transcript levels of red clover *WRKY* genes in roots, stems, leaves, and flowers by RNA-Seq. These genes were expressed at the highest level in the root system (Figure 6), such as *TpWRKY9*, *TpWRKY19*, and *TpWRKY46*, and were more closely related to *AtWRKY7*, *AtWRKY11*, and *AtWRKY17* evolutionarily in *Arabidopsis* (Figure 1). These genes potentially hold significant part in the growth and development of red clover roots and could serve as potential candidates for further functional studies related to the root system.

WRKY proteins play transcriptional regulatory roles in plant adaptations to various stress environments (Wani et al., 2021). In rice, *Arabidopsis* transformed by *OsWRKY45* increased drought resistance by regulating stomatal closure and stress-related genes (Qiu and Yu, 2009). A novel type WRKY TF, *DgWRKY5*, isolated in *Chrysanthemum* was up-regulated under salt, ABA and H_2O_2 (Liang et al., 2017). WRKY TFs play essential roles in plant adaptation to abiotic stresses, and these adaptations are the consequences of the interaction between *WRKY* genes and multiple plant hormones. It has been shown that exogenous administration of different plant hormones can alter the expression of *WRKY* genes under various abiotic stresses such as cold and salt (Gulzar et al., 2021; Huang et al., 2021). WRKY TFs work synergistically or independently in response to diverse stresses. For instance, ABA-induced synergism between two rice *WRKY* genes (*OsWRKY51* and *OsWRKY71*) suppressed gibberellin (GA) signaling in embryos and aleurone cells (Xie et al., 2006). In *Arabidopsis*, *AtWRKY18*, *40*, and *60* are involved in signaling pathways mediated by the phytohormones SA, JA, and ABA (Chen et al., 2010). As previously described, a considerable number of cis-acting elements related to stress and hormone responses were identified in the *WRKY* genes of red clover. Of the 59 *TpWRKY* genes, 46 contained ABRE, 43 contained CGTCA-motif, 45 contained ARE, 24 contained MBS, and 20 contained LTR. This suggests that *TpWRKY* genes play a role in regulating a diverse range of plant hormone and stress response pathways.

During this research endeavor, we examined the expression levels of 15 selected genes under drought, low temperature, MeJA and ABA treatments by using RT-qPCR. The findings indicated that drought stress induced a significant up-regulation of *TpWRKY46* (Figure 7A). *TpWRKY46* contains two drought cis-acting response elements (MBS). Cold stress significantly induced the expression of *TpWRKY26* and *TpWRKY41* (Figure 7B). Interestingly, these two genes do not have cis-acting elements related to low temperature, and we hypothesize that there may be other factors or regulatory pathways besides low-temperature induction that would lead to the high expression of these two genes under low-temperature conditions, as well as the possibility that these two genes may be subjected to subsequent regulation after low-temperature induction, e.g., post-transcriptional regulation, post-translational modification. Among all genes tested,

TpWRKY29 and *TpWRKY36* were the most highly expressed under MeJA stress (Figure 7C), *TpWRKY17* and *TpWRKY46* were the most highly expressed under ABA stress (Figure 7D). *TpWRKY29/36* contained six and four MeJA response elements, respectively, and *TpWRKY17/46* both contained two ABA response elements. This suggests that these cis-acting elements may play a regulatory role under various stresses and provide candidate genes for the selection of stress resistance genes in red clover, which will be further functionally verified in subsequent experiments.

5 Conclusion

In this research, we conducted a comprehensive genome-wide identification of *WRKY* gene family members in red clover, leading to the identification of a total of 59 *TpWRKY* genes. According to the phylogenetic relationships, these genes were categorized into three groups, and within the second group, further subdivision into five subgroups was observed. The physicochemical properties, phylogeny, gene structure, conserved motifs, cis-acting elements, and collinearity of these WRKY proteins were analyzed to establish a foundation for comprehending the evolutionary relationships of the *TpWRKY* gene family. In addition, we explored the expression patterns of *TpWRKY* genes in different tissues by RNA-seq and RT-qPCR, and selected *TpWRKY17*, *TpWRKY26*, *TpWRKY36* and *TpWRKY46* among 12 *TpWRKY* genes, which were highly induced after being subjected to abiotic stresses. This study reveals the basic characteristics of the *TpWRKY* gene family, which lays the foundation for the excavation of resistance genes in red clover and promotes the breeding and propagation of red clover.

Data availability statement

The original contributions presented in the study are included in the article/Supplementary Material. Further inquiries can be directed to the corresponding authors.

Author contributions

GY: Conceptualization, Data curation, Formal analysis, Investigation, Software, Validation, Visualization, Writing – original draft, Writing – review & editing. NZ: Investigation, Software, Validation, Writing – review & editing. YZ: Writing – review & editing, Validation, Visualization. YH: Writing – review & editing, Data curation, Software. JP: Writing – review & editing, Software, Validation. YL: Data curation, Software, Writing – review & editing. WZ: Conceptualization, Funding acquisition, Methodology, Resources, Supervision, Writing – review & editing. BL: Conceptualization, Funding acquisition, Methodology, Resources, Supervision, Writing – review & editing.

Funding

The author(s) declare financial support was received for the research, authorship, and/or publication of this article. This research was funded by the National Natural Science Foundation of China (31872631). Basic Research Project of Shaanxi Academy of Fundamental Science (22JHZ005).

Acknowledgments

We thank Dr.Jianming Zeng(University of Macau), and all the members of his bioinformatics team, biotrainee, for generously sharing their experience and codes. The Use of the biorstudio high performance computing cluster(https://biorstudio.cloud) at Biotrainee and The shanghai HS Biotech Co,Ltd for conducting the research reported in this paper.

Conflict of interest

The authors declare that the research was conducted in the absence of any commercial or financial relationships that could be construed as a potential conflict of interest.

Publisher's note

Supplementary material

The Supplementary Material for this article can be found online at: https://www.frontiersin.org/articles/10.3389/fpls.2023.1289507/full#supplementary-material

References

Ali, M. A., Azeem, F., Nawaz, M. A., Acet, T., Abbas, A., Imran, Q. M., et al. (2018). Transcription factors WRKY11 and WRKY17 are involved in abiotic stress responses in Arabidopsis. *J. Plant Physiol.* 226, 12–21. doi: 10.1016/j.jplph.2018.04.007

Bailey, T. L., Boden, M., Buske, F. A., Frith, M., Grant, C. E., Clementi, L., et al. (2009). MEME SUITE: tools for motif discovery and searching. *Nucleic Acids Res.* 37 (Web Server issue), W202–W208. doi: 10.1093/nar/gkp335

Baillo, E. H., Kimotho, R. N., Zhang, Z., and Xu, P. (2019). Transcription factors associated with abiotic and biotic stress tolerance and their potential for crops improvement. *Genes (Basel)* 10 (10):771. doi: 10.3390/genes10100771

Bodenhofer, U., Bonatesta, E., Horejš-Kainrath, C., and Hochreiter, S. (2015). msa: an R package for multiple sequence alignment. *Bioinformatics* 31 (24), 3997–3999. doi: 10.1093/bioinformatics/btv494

Chen, H., Lai, Z., Shi, J., Xiao, Y., Chen, Z., and Xu, X. (2010). Roles of arabidopsis WRKY18, WRKY40 and WRKY60 transcription factors in plant responses to abscisic acid and abiotic stress. *BMC Plant Biol.* 10, 281. doi: 10.1186/1471-2229-10-281

Chen, L., Song, Y., Li, S., Zhang, L., Zou, C., and Yu, D. (2012). The role of WRKY transcription factors in plant abiotic stresses. *Biochim. Biophys. Acta (BBA) - Gene Regul. Mech.* 1819 (2), 120–128. doi: 10.1016/j.bbagrm.2011.09.002

Chen, S., Zhou, Y., Chen, Y., and Gu, J. (2018). fastp: an ultra-fast all-in-one FASTQ preprocessor. *Bioinformatics* 34 (17), i884–i890. doi: 10.1093/bioinformatics/bty560

Chen, W., Hao, W. J., Xu, Y. X., Zheng, C., Ni, D. J., Yao, M. Z., et al. (2019). Isolation and characterization of csWRKY7, a subgroup IId WRKY transcription factor from camellia sinensis, linked to development in arabidopsis. *Int. J. Mol. Sci.* 20 (11):2815. doi: 10.3390/ijms20112815

Chou, K. C., and Shen, H. B. (2010). Plant-mPLoc: a top-down strategy to augment the power for predicting plant protein subcellular localization. *PloS One* 5 (6), e11335. doi: 10.1371/journal.pone.0011335

De Vega, J. J., Ayling, S., Hegarty, M., Kudrna, D., Goicoechea, J. L., Ergon, A., et al. (2015). Red clover (Trifolium pratense L.) draft genome provides a platform for trait improvement. *Sci. Rep.* 5, 17394. doi: 10.1038/srep17394

Dutta, S., Biswas, P., Chakraborty, S., Mitra, D., Pal, A., and Das, M. (2018). Identification, characterization and gene expression analyses of important flowering genes related to photoperiodic pathway in bamboo. *BMC Genomics* 19 (1), 190. doi: 10.1186/s12864-018-4571-7

Edgar, R. C. (2004). MUSCLE: multiple sequence alignment with high accuracy and high throughput. *Nucleic Acids Res.* 32 (5), 1792–1797. doi: 10.1093/nar/gkh340

Eulgem, T., Rushton, P. J., Robatzek, S., and Somssich, I. E. (2000). The WRKY superfamily of plant transcription factors. *Trends Plant Sci.* 5 (5), 199–206. doi: 10.1016/S1360-1385(00)01600-9

Fang, X., Meng, X., Zhang, J., Xia, M., Cao, S., Tang, X., et al. (2021). AtWRKY1 negatively regulates the response of Arabidopsis thaliana to Pst. DC3000. *Plant Physiol. Biochem.* 166, 799–806. doi: 10.1016/j.plaphy.2021.06.044

Fedoroff, N. V., Battisti, D. S., Beachy, R. N., Cooper, P. J., Fischhoff, D. A., Hodges, C. N., et al. (2010). Radically rethinking agriculture for the 21st century. *Science* 327 (5967), 833–834. doi: 10.1126/science.1186834

Feng, X., Abubakar, A. S., Yu, C., Zhu, A., Chen, J., Chen, K., et al. (2022). Analysis of WRKY resistance gene family in boehmeria nivea (L.) gaudich: crosstalk mechanisms of secondary cell wall thickening and cadmium stress. *Front. Plant Sci.* 13. doi: 10.3389/fpls.2022.812988

Gao, K., Zhou, T., Hua, Y., Guan, C., and Zhang, Z. (2020). Transcription factor WRKY23 is involved in ammonium-induced repression of Arabidopsis primary root growth under ammonium toxicity. *Plant Physiol. Biochem.* 150, 90–98. doi: 10.1016/j.plaphy.2020.02.034

Gorlova, O., Fedorov, A., Logothetis, C., Amos, C., and Gorlov, I. (2014). Genes with a large intronic burden show greater evolutionary conservation on the protein level. *BMC Evol. Biol.* 14 (1), 50. doi: 10.1186/1471-2148-14-50

Gulzar, F., Fu, J., Zhu, C., Yan, J., Li, X., Meraj, T. A., et al. (2021). Maize WRKY transcription factor zmWRKY79 positively regulates drought tolerance through elevating ABA biosynthesis. *Int. J. Mol. Sci.* 22 (18):10080. doi: 10.3390/ijms221810080

Guo, A. Y., Zhu, Q. H., Chen, X., and Luo, J. C. (2007). [GSDS: a gene structure display server]. *Yi Chuan* 29 (8), 1023–1026. doi: 10.1360/yc-007-1023

Guo, H., Zhang, Y., Wang, Z., Lin, L., Cui, M., Long, Y., et al. (2019). Genome-wide identification of WRKY transcription factors in the asteranae. *Plants (Basel)* 8 (10):393. doi: 10.3390/plants8100393

Hallgren, J., Tsirigos, K. D., Pedersen, M. D., Almagro Armenteros, J. J., Marcatili, P., Nielsen, H., et al. (2022). DeepTMHMM predicts alpha and beta transmembrane proteins using deep neural networks. *BioRxiv*, 2022–2004. doi: 10.1101/2022.04.08.487609

Hao, F., Yang, G., Zhou, H., Yao, J., Liu, D., Zhao, P., et al. (2021). Genome-wide identification and transcriptional expression profiles of transcription factor WRKY in common walnut (Juglans regia L.). *Genes (Basel)* 12 (9):1444. doi: 10.3390/genes12091444

Holub, E. B. (2001). The arms race is ancient history in Arabidopsis, the wildflower. *Nat. Rev. Genet.* 2 (7), 516–527. doi: 10.1038/35080508

Hu, W., Ren, Q., Chen, Y., Xu, G., and Qian, Y. (2021). Genome-wide identification and analysis of WRKY gene family in maize provide insights into regulatory network in response to abiotic stresses. *BMC Plant Biol.* 21 (1), 427. doi: 10.1186/s12870-021-03206-z

Huang, S., Hu, L., Zhang, S., Zhang, M., Jiang, W., Wu, T., et al. (2021). Rice osWRKY50 mediates ABA-dependent seed germination and seedling growth, and ABA-independent salt stress tolerance. *Int. J. Mol. Sci.* 22 (16):8625. doi: 10.3390/ijms22168625

Ishiguro, S., and Nakamura, K. (1994). Characterization of a cDNA encoding a novel DNA-binding protein, SPF1, that recognizes SP8 sequences in the 5' upstream regions of genes coding for sporamin and beta-amylase from sweet potato. *Mol. Gen. Genet.* 244 (6), 563–571. doi: 10.1007/bf00282746

Javed, T., and Gao, S. J. (2023). WRKY transcription factors in plant defense. *Trends Genet.* 39 (10), 787–801. doi: 10.1016/j.tig.2023.07.001

Jiang, J., Ma, S., Ye, N., Jiang, M., Cao, J., and Zhang, J. (2017). WRKY transcription factors in plant responses to stresses. *J. Integr. Plant Biol.* 59 (2), 86–101. doi: 10.1111/jipb.12513

Joshi, R., Wani, S. H., Singh, B., Bohra, A., Dar, Z. A., Lone, A. A., et al. (2016). Transcription factors and plants response to drought stress: current understanding and future directions. *Front. Plant Sci.* 7. doi: 10.3389/fpls.2016.01029

Kan, J., Gao, G., He, Q., Gao, Q., Jiang, C., Ahmar, S., et al. (2021). Genome-wide characterization of WRKY transcription factors revealed gene duplication and diversification in populations of wild to domesticated barley. *Int. J. Mol. Sci.* 22 (10):5354. doi: 10.3390/ijms22105354

Khoso, M. A., Hussain, A., Ritonga, F. N., Ali, Q., Channa, M. M., Alshegaihi, R. M., et al. (2022). WRKY transcription factors (TFs): Molecular switches to regulate drought, temperature, and salinity stresses in plants. *Front. Plant Sci.* 13. doi: 10.3389/fpls.2022.1039329

Kim, D., Paggi, J. M., Park, C., Bennett, C., and Salzberg, S. L. (2019). Graph-based genome alignment and genotyping with HISAT2 and HISAT-genotype. *Nat. Biotechnol.* 37 (8), 907–915. doi: 10.1038/s41587-019-0201-4

Krzywinski, M., Schein, J., Birol, I., Connors, J., Gascoyne, R., Horsman, D., et al. (2009). Circos: an information aesthetic for comparative genomics. *Genome Res.* 19 (9), 1639–1645. doi: 10.1101/gr.092759.109

Lescot, M., Déhais, P., Thijs, G., Marchal, K., Moreau, Y., Van de Peer, Y., et al. (2002). PlantCARE, a database of plant cis-acting regulatory elements and a portal to tools for in silico analysis of promoter sequences. *Nucleic Acids Res.* 30 (1), 325–327. doi: 10.1093/nar/30.1.325

Letunic, I., and Bork, P. (2021). Interactive Tree Of Life (iTOL) v5: an online tool for phylogenetic tree display and annotation. *Nucleic Acids Res.* 49 (W1), W293–w296. doi: 10.1093/nar/gkab301

Liang, Q. Y., Wu, Y. H., Wang, K., Bai, Z. Y., Liu, Q. L., Pan, Y. Z., et al. (2017). Chrysanthemum WRKY gene DgWRKY5 enhances tolerance to salt stress in transgenic chrysanthemum. *Sci. Rep.* 7 (1), 4799. doi: 10.1038/s41598-017-05170-x

Liao, Y., Smyth, G. K., and Shi, W. (2013). The Subread aligner: fast, accurate and scalable read mapping by seed-and-vote. *Nucleic Acids Res.* 41 (10), e108. doi: 10.1093/nar/gkt214

Liu, Z.-Q., Shi, L.-P., Yang, S., Qiu, S.-S., Ma, X.-L., Cai, J.-S., et al. (2021). A conserved double-W box in the promoter of CaWRKY40 mediates autoregulation during response to pathogen attack and heat stress in pepper. *Mol. Plant Pathol.* 22 (1), 3–18. doi: 10.1111/mpp.13004

Mistry, J., Chuguransky, S., Williams, L., Qureshi, M., Salazar, G. A., Sonnhammer, E. L. L., et al. (2020). Pfam: The protein families database in 2021. *Nucleic Acids Res.* 49 (D1), D412–D419. doi: 10.1093/nar/gkaa913

Nguyen, L. T., Schmidt, H. A., von Haeseler, A., and Minh, B. Q. (2015). IQ-TREE: a fast and effective stochastic algorithm for estimating maximum-likelihood phylogenies. *Mol. Biol. Evol.* 32 (1), 268–274. doi: 10.1093/molbev/msu300

Panchy, N., Lehti-Shiu, M., and Shiu, S. H. (2016). Evolution of gene duplication in plants. *Plant Physiol.* 171 (4), 2294–2316. doi: 10.1104/pp.16.00523

Qiu, Y., and Yu, D. (2009). Over-expression of the stress-induced OsWRKY45 enhances disease resistance and drought tolerance in Arabidopsis. *Environ. Exp. Bot.* 65 (1), 35–47. doi: 10.1016/j.envexpbot.2008.07.002

Riechmann, J. L., Heard, J., Martin, G., Reuber, L., Jiang, C., Keddie, J., et al. (2000). Arabidopsis transcription factors: genome-wide comparative analysis among eukaryotes. *Science* 290 (5499), 2105–2110. doi: 10.1126/science.290.5499.2105

Rinerson, C. I., Rabara, R. C., Tripathi, P., Shen, Q. J., and Rushton, P. J. (2015). The evolution of WRKY transcription factors. *BMC Plant Biol.* 15, 66. doi: 10.1186/s12870-015-0456-y

Rushton, P. J., Somssich, I. E., Ringler, P., and Shen, Q. J. (2010). WRKY transcription factors. *Trends Plant Sci.* 15 (5), 247–258. doi: 10.1016/j.tplants.2010.02.006

Sato, S., Isobe, S., Asamizu, E., Ohmido, N., Kataoka, R., Nakamura, Y., et al. (2005). Comprehensive structural analysis of the genome of red clover (Trifolium pratense L.). *DNA Res.* 12 (5), 301–364. doi: 10.1093/dnares/dsi018

Sharif, R., Raza, A., Chen, P., Li, Y., El-Ballat, E. M., Rauf, A., et al. (2021). HD-ZIP gene family: potential roles in improving plant growth and regulating stress-responsive mechanisms in plants. *Genes (Basel)* 12 (8):1256. doi: 10.3390/genes12081256

Singh, K. B., Foley, R. C., and Oñate-Sánchez, L. (2002). Transcription factors in plant defense and stress responses. *Curr. Opin. Plant Biol.* 5 (5), 430–436. doi: 10.1016/S1369-5266(02)00289-3

Tang, H., Zhang, X., Miao, C., Zhang, J., Ming, R., Schnable, J. C., et al. (2015). ALLMAPS: robust scaffold ordering based on multiple maps. *Genome Biol.* 16 (1), 3. doi: 10.1186/s13059-014-0573-1

Tsuda, K., and Somssich, I. E. (2015). Transcriptional networks in plant immunity. *New Phytol.* 206 (3), 932–947. doi: 10.1111/nph.13286

Ulker, B., and Somssich, I. E. (2004). WRKY transcription factors: from DNA binding towards biological function. *Curr. Opin. Plant Biol.* 7 (5), 491–498. doi: 10.1016/j.pbi.2004.07.012

van Verk, M. C., Pappaioannou, D., Neeleman, L., Bol, J. F., and Linthorst, H. J. (2008). A Novel WRKY transcription factor is required for induction of PR-1a gene expression by salicylic acid and bacterial elicitors. *Plant Physiol.* 146 (4), 1983–1995. doi: 10.1104/pp.107.112789

Voorrips, R. E. (2002). MapChart: software for the graphical presentation of linkage maps and QTLs. *J. Hered* 93 (1), 77–78. doi: 10.1093/jhered/93.1.77

Wahdan, S. F. M., Tanunchai, B., Wu, Y. T., Sansupa, C., SChadler, M., Dawoud, T. M., et al. (2021). Deciphering Trifolium pratense L. holobiont reveals a microbiome resilient to future climate changes. *Microbiologyopen* 10 (4), e1217. doi: 10.1002/mbo3.1217

Wang, C. T., Ru, J. N., Liu, Y. W., Li, M., Zhao, D., Yang, J. F., et al. (2018). Maize WRKY transcription factor zmWRKY106 confers drought and heat tolerance in transgenic plants. *Int. J. Mol. Sci.* 19 (10):3046. doi: 10.3390/ijms19103046

Wang, Y., Tang, H., Debarry, J. D., Tan, X., Li, J., Wang, X., et al. (2012). MCScanX: a toolkit for detection and evolutionary analysis of gene synteny and collinearity. *Nucleic Acids Res.* 40 (7), e49–e49. doi: 10.1093/nar/gkr1293

Wang, Q., Wang, M., Zhang, X., Hao, B., Kaushik, S. K., and Pan, Y. (2011). WRKY gene family evolution in Arabidopsis thaliana. *Genetica* 139 (8), 973–983. doi: 10.1007/s10709-011-9599-4

Wang, N., Xia, E.-H., and Gao, L.-Z. (2016). Genome-wide analysis of WRKY family of transcription factors in common bean, Phaseolus vulgaris: Chromosomal localization, structure, evolution and expression divergence. *Plant Gene* 5, 22–30. doi: 10.1016/j.plgene.2015.11.003

Wani, S. H., Anand, S., Singh, B., Bohra, A., and Joshi, R. (2021). WRKY transcription factors and plant defense responses: latest discoveries and future prospects. *Plant Cell Rep.* 40 (7), 1071–1085. doi: 10.1007/s00299-021-02691-8

Waqas, M., Azhar, M. T., Rana, I. A., Azeem, F., Ali, M. A., Nawaz, M. A., et al. (2019). Genome-wide identification and expression analyses of WRKY transcription factor family members from chickpea (Cicer arietinum L.) reveal their role in abiotic stress-responses. *Genes Genomics* 41 (4), 467–481. doi: 10.1007/s13258-018-00780-9

Wu, K. L., Guo, Z. J., Wang, H. H., and Li, J. (2005). The WRKY family of transcription factors in rice and Arabidopsis and their origins. *DNA Res.* 12 (1), 9–26. doi: 10.1093/dnares/12.1.9

Xi, X., Hu, Z., Nie, X., Meng, M., Xu, H., and Li, J. (2021). Cross inhibition of MPK10 and WRKY10 participating in the growth of endosperm in arabidopsis thaliana. *Front. Plant Sci.* 12. doi: 10.3389/fpls.2021.640346

Xie, T., Chen, C., Li, C., Liu, J., Liu, C., and He, Y. (2018). Genome-wide investigation of WRKY gene family in pineapple: evolution and expression profiles during development and stress. *BMC Genomics* 19 (1), 490. doi: 10.1186/s12864-018-4880-x

Xie, Z., Zhang, Z. L., Zou, X., Huang, J., Ruas, P., Thompson, D., et al. (2005). Annotations and functional analyses of the rice WRKY gene superfamily reveal positive and negative regulators of abscisic acid signaling in aleurone cells. *Plant Physiol.* 137 (1), 176–189. doi: 10.1104/pp.104.054312

Xie, Z., Zhang, Z. L., Zou, X., Yang, G., Komatsu, S., and Shen, Q. J. (2006). Interactions of two abscisic-acid induced WRKY genes in repressing gibberellin signaling in aleurone cells. *Plant J.* 46 (2), 231–242. doi: 10.1111/j.1365-313X.2006.02694.x

Yan, H., Li, M., Xiong, Y., Wu, J., Teixeira da Silva, J. A., and Ma, G. (2019). Genome-wide characterization, expression profile analysis of WRKY family genes in santalum album and functional identification of their role in abiotic stress. *Int. J. Mol. Sci.* 20 (22):5676. doi: 10.3390/ijms20225676

Yan, H., Sun, M., Zhang, Z., Jin, Y., Zhang, A., Lin, C., et al. (2023). Pangenomic analysis identifies structural variation associated with heat tolerance in pearl millet. *Nat. Genet.* 55 (3), 507–518. doi: 10.1038/s41588-023-01302-4

Yu, Y., Qi, Y., Xu, J., Dai, X., Chen, J., Dong, C. H., et al. (2021). Arabidopsis WRKY71 regulates ethylene-mediated leaf senescence by directly activating EIN2, ORE1 and ACS2 genes. *Plant J.* 107 (6), 1819–1836. doi: 10.1111/tpj.15433

Zhang, Y., and Wang, L. (2005). The WRKY transcription factor superfamily: its origin in eukaryotes and expansion in plants. *BMC Evol. Biol.* 5, 1. doi: 10.1186/1471-2148-5-1

Zhang, C., Wang, W., Wang, D., Hu, S., Zhang, Q., Wang, Z., et al. (2022a). Genome-Wide Identification and Characterization of the WRKY Gene Family in Scutellaria baicalensis Georgi under Diverse Abiotic Stress. *Int. J. Mol. Sci.* 23 (8):4225. doi: 10.3390/ijms23084225

Zhang, T., Xu, Y., Ding, Y., Yu, W., Wang, J., Lai, H., et al. (2022b). Identification and expression analysis of WRKY gene family in response to abiotic stress in dendrobium catenatum. *Front. Genet.* 13. doi: 10.3389/fgene.2022.800019

Zhou, Q. Y., Tian, A. G., Zou, H. F., Xie, Z. M., Lei, G., Huang, J., et al. (2008). Soybean WRKY-type transcription factor genes, GmWRKY13, GmWRKY21, and GmWRKY54, confer differential tolerance to abiotic stresses in transgenic Arabidopsis plants. *Plant Biotechnol. J.* 6 (5), 486–503. doi: 10.1111/j.1467-7652.2008.00336.x

Zhou, H., Zhu, W., Wang, X., Bian, Y., Jiang, Y., Li, J., et al. (2022). A missense mutation in WRKY32 converts its function from a positive regulator to a repressor of photomorphogenesis. *New Phytol.* 235 (1), 111–125. doi: 10.1111/nph.17932

Zhu, J. K. (2016). Abiotic stress signaling and responses in plants. *Cell* 167 (2), 313–324. doi: 10.1016/j.cell.2016.08.029

frontiers | Frontiers in Plant Science

TYPE Original Research
PUBLISHED 19 January 2024
DOI 10.3389/fpls.2023.1343402

OPEN ACCESS

EDITED BY
Guowei Li,
Shandong Academy of Agricultural Sciences, China

REVIEWED BY
Chinedu Charles Nwafor,
University of Nebraska-Lincoln, United States
Yanhao Xu,
Hubei Academy of Agricultural Sciences, China
Muhammad Irfan,
University of Sargodha, Pakistan

*CORRESPONDENCE
Haiqiu Yu
yuhaiqiu@syau.edu.cn

†These authors have contributed equally to this work

RECEIVED 23 November 2023
ACCEPTED 29 December 2023
PUBLISHED 19 January 2024

CITATION
Zhong C, He Z, Liu Y, Li Z, Wang X, Jiang C, Kang S, Liu X, Zhao S, Wang J, Zhang H, Zhao X and Yu H (2024) Genome-wide identification of *TPS* and *TPP* genes in cultivated peanut (*Arachis hypogaea*) and functional characterization of *AhTPS9* in response to cold stress.
Front. Plant Sci. 14:1343402.
doi: 10.3389/fpls.2023.1343402

Genome-wide identification of *TPS* and *TPP* genes in cultivated peanut (*Arachis hypogaea*) and functional characterization of *AhTPS9* in response to cold stress

Chao Zhong[1†], Zehua He[1†], Yu Liu[1], Zhao Li[1], Xiaoguang Wang[1], Chunji Jiang[1], Shuli Kang[1], Xibo Liu[1], Shuli Zhao[1], Jing Wang[1], He Zhang[1], Xinhua Zhao[1] and Haiqiu Yu[1,2*]

[1]College of Agronomy, Shenyang Agricultural University, Shenyang, China, [2]Liaoning Agricultural Vocational and Technical College, Yingkou, China

Introduction: Trehalose is vital for plant metabolism, growth, and stress resilience, relying on *Trehalose-6-phosphate synthase* (*TPS*) and *Trehalose-6-phosphate phosphatase* (*TPP*) genes. Research on these genes in cultivated peanuts (*Arachis hypogaea*) is limited.

Methods: This study employed bioinformatics to identify and analyze *AhTPS* and *AhTPP* genes in cultivated peanuts, with subsequent experimental validation of *AhTPS9's* role in cold tolerance.

Results: In the cultivated peanut genome, a total of 16 *AhTPS* and 17 *AhTPP* genes were identified. *AhTPS* and *AhTPP* genes were observed in phylogenetic analysis, closely related to wild diploid peanuts, respectively. The evolutionary patterns of *AhTPS* and *AhTPP* genes were predominantly characterized by gene segmental duplication events and robust purifying selection. A variety of hormone-responsive and stress-related *cis*-elements were unveiled in our analysis of *cis*-regulatory elements. Distinct expression patterns of *AhTPS* and *AhTPP* genes across different peanut tissues, developmental stages, and treatments were revealed, suggesting potential roles in growth, development, and stress responses. Under low-temperature stress, qPCR results showcased upregulation in *AhTPS* genes (*AhTPS2-5*, *AhTPS9-12*, *AhTPS14*, *AhTPS15*) and *AhTPP* genes (*AhTPP1*, *AhTPP6*, *AhTPP11*, *AhTPP13*). Furthermore, *AhTPS9*, exhibiting the most significant expression difference under cold stress, was obviously induced by cold stress in cultivated peanut, and *AhTPS9*-overexpression improved the cold tolerance of *Arabidopsis* by protect the photosynthetic system of plants, and regulates sugar-related metabolites and genes.

Discussion: This comprehensive study lays the groundwork for understanding the roles of *AhTPS* and *AhTPP* gene families in trehalose regulation within cultivated peanuts and provides valuable insights into the mechanisms related to cold stress tolerance.

KEYWORDS

***TPS* genes, *TPP* genes, peanut (*Arachis hypogaea*), cold stress, trehalose**

1 Introduction

Trehalose, a symmetrical non-reducing disaccharide formed by two glucose molecules through α, α-1,1-glycosidic bonds, exhibits distinctive physicochemical properties setting it apart from analogous sugars (Paul et al., 2008). It holds a pivotal role in maintaining cellular integrity across various organisms, particularly in plant growth and development (O'Hara et al., 2013). Under adverse conditions like high temperatures, freezing, and osmotic stress, cells synthesize trehalose as a defense mechanism, aiding in osmotic regulation, membrane preservation, and signal transduction (Fernandez et al., 2010; Kosar et al., 2019; Hassan et al., 2023). The precursor of trehalose is trehalose 6-phosphate (Tre6P), which has a dual role in plant metabolism and development (Figueroa and Lunn, 2016). It regulates sucrose production in source leaves to balance the demand for sucrose in growing sink organs. Tre6P also functions as a signal of sucrose availability, influencing developmental decisions such as flowering, embryogenesis, and lateral branching, thereby linking sucrose supply to sink organ growth (Paul et al., 2018). For example, Tre6P modulates plant respiration and metabolism by inhibiting SnRK1 activity, which functions as a key regulator of energy and nutrient responses in plants (Emanuelle et al., 2016). Trehalose synthesis, its versatile functions, and its presence in diverse organisms underline its significance in biological systems. This dynamic sugar, balancing energy and protective roles, holds promise for various applications in plant biotechnology and stress management.

Trehalose synthesis mainly involves two indispensable enzymes: trehalose 6-phosphate (Tre6P) synthase (TPS) and Tre6P phosphatase (TPP) (Smeekens, 2015). In plants, the trehalose biosynthesis pathway involves a sequential enzymatic process: Initially, trehalose-6-phosphate synthase (TPS) facilitates the condensation of uridine diphosphate glucose (UDPG) and glucose 6-phosphate (G6P) to yield an intermediary compound trehalose 6-phosphate (Tre6P). Subsequently, this intermediate is subjected to dephosphorylation by trehalose-6-phosphate phosphatase (TPP), resulting in the synthesis of trehalose (Fichtner and Lunn, 2021). TPS and TPP are key enzymes in the trehalose metabolism pathway. *TPS* and *TPP* genes are found in unicellular *chlorophyte algae*, *streptophyte algae*, and across all major groups of terrestrial plants, suggesting their presence from the early stages of the green plant lineage. Initially identified in *Arabidopsis* (*AtTPS1*, *AtTPPA*, and *AtTPPB*), these genes were subsequently recognized as part of extensive gene families after the sequencing of the *Arabidopsis* genome (Kaul et al., 2000). The *Arabidopsis* species possesses a total of 11 *TPS* genes (*AtTPS1–AtTPS11*) and 10 *TPP* genes (*AtTPPA–AtTPPJ*) (Aubourg et al., 2002; Vandesteene et al., 2012). The AtTPS proteins contain TPS and TPP domains, which form two distinct clades in phylogenetic analyses: class I (*AtTPS1–AtTPS4*) and class II (*AtTPS5–AtTPS11*) (Leyman et al., 2001). The *TPS* genes have been extensively studied in the model plant *Arabidopsis*, as well as in other plant species. These genes play a crucial role in serving as a conduit for sucrose signaling, triggering the production of trehalose during stress responses. The research conducted so far has illuminated the significance of *TPS* genes, particularly in terms of their capacity to enhance biotic and abiotic stress tolerance when overexpressed or properly expressed in transgenic plants (Iordachescu and Imai, 2008; Vishal et al., 2019; Fichtner et al., 2020). Furthermore, within plants, a substantial family of compact proteins housing the conserved only TPP domain is prevalent. In contrast, the functional roles of TPPs in the context of trehalose production have unveiled an array of distinct expression patterns across various tissues, underscoring their potential functional diversity (Vandesteene et al., 2012; Van Houtte et al., 2013; Du et al., 2022). It's worth noting, however, that there does exist a degree of overlap in their expression patterns, suggesting a partial redundancy in their functions. Interestingly, through phylogenetic analysis, it has been possible to cluster each *TPP* and its counterparts from different species into distinct groups (Ma et al., 2007; Li et al., 2008). The induction of *TPP* expression comes about through varied hormonal and abiotic stress treatments, and the corresponding *TPPs* have been found to actively participate in plant stress responses. *AtTPPF*, for instance, assumes a proactive role in safeguarding cells against oxidative damage caused by reactive oxygen species during drought stress by augmenting soluble sugar levels (Lin et al., 2019). On the other hand, lines overexpressing *AtTPPD* display heightened salt tolerance due to increased sensitivity to redox shifts in two cysteine residues of *TPPD*. This sensitivity prompts accelerated activity under salt stress, thereby leading to an accumulation of trehalose (Krasensky et al., 2014). The overexpression of *OsTPS1* and *OsTPP1* within rice plants has

been shown to bolster trehalose levels, ultimately enhancing plant survival under low temperature stress (Ge et al., 2008). Moreover, the latter protein, OsTPP1, contributes to the regulation of rice seed germination by engaging in ABA signaling (Wang et al., 2021). Both *TPS* and *TPP* gene families have independently expanded in various plant divisions, contributing to the diversity of stress response functions in plants.

Cultivated peanut (*Arachis hypogaea* L.) is an important oil and economic crop, which is widely planted in the semiarid tropical and subtropical regions (Krishna et al., 2015; Zhuang et al., 2019). Peanut plants are susceptible to various abiotic stresses during their growth, such as temperature, drought, salinity, and metal toxicit (Paul et al., 2001; Shi and Cai, 2009; Puppala et al., 2023). However, among various abiotic stresses, cold stress significantly impairs the growth, production, and quality of many crop plants (Kidokoro et al., 2022; Raza et al., 2023). In recent years, China has experienced an increased frequency of cold damage events, particularly impacting early-sown spring peanuts. These events have a common detrimental effect on various stages of peanut cultivation, including seed germination, growth, development, flowering, and overall yield (Kakani et al., 2002; Chen et al., 2014; Zhang et al., 2019; Xue et al., 2023; Zhang et al., 2023). Identifying key genes that can confer cold stress tolerance is crucial for enhancing crop productivity in regions with low temperatures (Bhat et al., 2022). These genes can be utilized in biotechnological programs to generate improved varieties, which is an urgent requirement in peanut production. Although the *TPS* and *TPP* genes has been identified to participate in growth, development, and response to various stress in multiple plant species, there have been no comprehensive analyses of the *TPS* and *TPP* gene families in peanut, and previous studies have not yet characterized the role of *TPS* and *TPP* genes in responding to environmental stresses. As a tetraploid crop, cultivated peanut contains A and B subgenomes that evolved from two diploid wild peanut varients (*Arachis duranensis* (AA) and *Arachis ipaensis* (BB). The sequencing of the whole genome of cultivated and wild peanut has been completed and uploaded, providing an opportunity for the analysis of the *TPS* and *TPP* gene familes in the context of cold stress in peanut (Bertioli et al., 2016; Bertioli et al., 2019; Chen et al., 2019; Zhuang et al., 2019).

In this study, we identified 16 *TPS* and 17 *TPP* genes in cultivated peanut, and comprehensively analyzed phylogenetic relationships, the chromosomal distributions, gene duplication, motif compositions, gene structures, and *cis*-acting elements of *TPS* and *TPP* genes using bioinformatics methods. Further transcriptome-based tissue-specific expression analysis of *AhTPS* and *AhTPP* genes was conducted, and their expression patterns in response to low temperature were assessed using fluorescence quantitative PCR (qPCR) methods. Among these, key genes were functionally characterized in transgenic *Arabidopsis* to reveal its crucial role in cold tolerance. Our findings lay the groundwork for further investigation into the functions of the *AhTPS* and *AhTPP* families in cultivated peanut. Additionally, this research will facilitate their utilization in the genetic improvement of crops.

2 Materials and methods

2.1 Plant materials and treatment

The cold-stress variety Nonghua5 provided by the Peanut Research Institute, Shenyang Agriculture University, Shenyang, China, was used for cultivation and cold treatment. The peanuts underwent sowing, cultivation, and cold treatment following the protocol outlined in Zhang et al. (2023), with minor adjustments. To ensure sterility, the seeds were surface treated using a 3% sodium hypochlorite solution, rinsed thoroughly with distilled water, and placed in darkness for germination. Germinated seeds were then planted in circular plastic pots filled with a mixture of vermiculite and nutrient soil in a 2:1 ratio. The plants were grown in a climate chamber with a 16-hour light (28°C)/8-hour dark (23°C) cycle, a photosynthetic photon flux density of 400 μmol m^{-2} s^{-1}, and a relative humidity of 70%. To induce cold stress, the temperature in the climate chamber was lowered to 4°C while maintaining other growth conditions. The second leaves were collected at 0, 6, 12, 24, and 48 hours after each treatment, with three biological replicates. The collected leaves were immediately frozen in liquid nitrogen and stored at -80°C.

2.2 Identification of the *TPS* and *TPP* family genes in cultivated peanut and wild peanut

To identify genes encoding TPS and TPP proteins of tetraploid cultivated peanuts (*Arachis hypogaea*) and diploid wild peanuts (*Arachis duranensis* and *Arachis ipaensis*) in Peanut genome database (PeanutBase-BLAST, https://www.peanutbase.org/pb_sequenceserver), the sequences of 11 AtTPS and 10 AtTPP proteins were utilized, with an E-value threshold of < 10^{-5}. The identified *TPS* and *TPP* gene sequences underwent a conserved domain search (http://www.ncbi.nlm.nih.gov/Structure/cdd/wrpsb.cgi), and manually removing peanut protein sequences lacking TPS or TPP domains. SMART (http://smart.embl.de/) and Pfam (http://pfam.xfam.org/) were employed to confirm the conserved domains of TPS and TPP using the remaining protein sequences. The ExPASy database (https://web.expasy.org/protparam/) was utilized to predict the physicochemical properties of *AhTPSs* and *AhTPPs*, including molecular weight, isoelectric point (pI), aliphatic index, and total average hydrophilicity (GRAVY).

2.3 Phylogenetic analysis of *AhTPS* and *AhTPP* genes

The phylogenetic tree was constructed using protein sequences from *TPS* and *TPP* genes in cultivated and wild diploid peanuts (*Arachis hypogae*a, *Arachis duranensis*, and *Arachis ipaensis*), as well as *Arabidopsis*, soybean, rice, and tomato. The protein sequences of TPP and TPS from *Arachis hypogaea*, *Arachis duranensis*, and *Arachis ipaensis* were obtained from the peanut genome database (https://www.peanutbase.org/). Similarly, the

protein sequences of TPP and TPS from *Arabidopsis* and rice were downloaded from NCBI (https://www.ncbi.nlm.nih.gov/), while those from soybean and tomato were obtained from the soybean genome database (https://soybase.org/). Multiple sequence alignments were performed using the MUSCLE method, and the phylogenetic tree was constructed using the neighbor-joining (NJ) method with 1000 bootstrap replications, employing MEGA11 software (Tamura et al., 2021). The resulting tree was visualized using EvolView (https://evolgenius.info//evolview).

2.4 Chromosomal location, gene duplication, and synteny analysis

The chromosomal distribution of *AhTPSs* and *AhTPPs* was determined by MG2C online software. Gene duplication patterns and collinearity relationships of the *AhTPS* and *AhTPP* gene families between tetraploid cultivated and diploid wild peanuts were identified and analyzed using MCScanx of TBtools with default parameters. TBtools was subsequently used to calculate Ka and Ks, with a Ka/Ks to explore the evolutionary dynamics and selection pressure (Chen et al., 2020).

2.5 Analysis of gene structures and motifs

Based on the peanut genome annotation (GFF file), gene exon-intron structures were obtained. TBtools was utilized to construct protein motif and gene structure maps for members of the peanut *TPS* and *TPP* gene families. The MEME program (http://meme-suite.org/tools/meme) was employed to assay the conserved motifs of each protein. The parameters used to identify conserved motifs in the protein sequences were set as follows: a maximum of 20 motifs and other optional default parameters.

2.6 Cis-acting element prediction in the upstream region of *TPPs* and *TPSs*

In order to explore potential *cis*-acting regulatory elements within the promoter regions of *AhTPP* and *AhTPS* genes, the upstream sequence of 2000 bp preceding the coding region was extracted from the peanut genome sequence. Subsequently, this sequence was subjected to *cis*-regulatory element prediction using the PlantCARE database (https://bioinformatics.psb.ugent.be/webtools/plantcare/html/). The predicted *cis*-regulatory elements were categorized based on their regulatory functions, and their distribution within the promoter regions of *AhTPP* and *AhTPS* was visualized as a heatmap.

2.7 Expression profile analysis of *AhTPSs* and *AhTPPs* in different tissues and under different environmental treatments

The transcriptome-based data of different tissues and under different environmental treatments (different hormonal, low temperature and drought treatments) were retrieved from the PeanutBase database (https://www.peanutbase.org/) and Peanut Genome Resource (http://peanutgr.fafu.edu.cn/index.php) (Clevenger et al., 2016; Zhuang et al., 2019). TBtools was used to generate an expression heatmap of the reads per kilobase per million mapped reads (RPKM) data. The transcriptome data were normalized by $\log_2$ (1 +RPKM).

2.8 RNA extraction and quantitative real-time PCR

Total RNA of plant tissues was isolated using the Plant Total RNA Extraction Kit (Tiangen Biotech, Beijing, China) according to the manufacturer's instructions. Then, cDNA was synthesized by PrimeScriptTM RT Kit (TaKaRa, Japan). *AhActin* was used as the reference gene, and the specific primers are designed using Primer-BLAST (https://www.ncbi.nlm.nih.gov/tools/primer-blast/). The gene expression analysis was carried out using the SYBR Premix Ex TaqII kit (TliRNaseH Plus) from TaKaRa, Japan, and fluorescence quantitative reactions were detected using ABI7500 from Applied Biosystems, United States. The relative expression analysis was calculated using the $2^{-\Delta\Delta CT}$ approach.

2.9 Subcelluar localization analysis of AhTPS9 protein

The specific primers (*AhTPS9*-F/R) were utilized to amplify the complete cDNA of *AhTPS9* from tobacco leaves. The coding sequence data for *AhTPS9* from PeanutBase (https://www.peanutbase.org/) were used as a reference. The resulting PCR products were connected to the pBWA (V) HS-GLosgfp vector, generating the pBWA (V) HS- *AhTPS9*-GFP vector which incorporates the green fluorescent protein (GFP) reporter gene. After confirmation through sequencing, the positive clones were transferred into *Agrobacterium tumefaciens* (EHA105) using electrotransformation. Young seedlings (30 days old) were carefully chosen, and injections were performed into the lower epidermis of leaves. Subsequently, these seedlings were cultured under low light conditions for 2 days. Observation and imaging took place using a laser confocal microscope (Nikon C2-ER, Tokyo, Japan), with the corresponding empty vector serving as a control.

2.10 The *AhTPS9* function analysis under cold stress conditions

Gene-specific primers for *AhTPS9* were designed to amplify the cDNA sequence in a cold-tolerance genotype Nonghua5 by Primer Premier 6.0. PCR amplification of the coding sequence of *AhTPS9* was performed using the TransTaq DNA Polymerase High Fidelity Amplification Kit. The PCR reaction program consisted of an initial denaturation at 94°C for 3 minutes, followed by 30 cycles of denaturation at 94°C for 30 seconds, annealing at 58-60°C for 30 seconds, and extension at 72°C for 1 minute. The final extension

was carried out at 72°C for 10 minutes. PCR products were analyzed on a 1% agarose gel, purified using a universal DNA purification recovery kit, and then ligated into the pBWA (V) BS cloning vector. The ligated DNA was transformed into *Escherichia coli Top10* competent cells, positive clones were selected, and their identity was confirmed through sequencing. The recombinant plasmid pBWA (V) BS-*AhTPS9* was transformed into *Agrobacterium tumefaciens* EHA105, which was subsequently introduced into wild-type (WT) *Arabidopsis* using the floral dip method as described by Clough and Bent (1998). Following antibiotic-based screening and PCR verification of the transgenic seedlings, we successfully generated the homozygous transgenic lines in the T_2 generation. Subsequently, homozygous T_3 progeny was examined and selected for further experimental procedures.

The T_3 seeds, previously subjected to a 4°C vernalization treatment on MS medium, were incubated in a growth chamber at 22°C for 14 days. Subsequently, they underwent a 5-day cold treatment at 4°C, followed by phenotypic observations. Columbia wild-type *Arabidopsis* plants (WT) were subjected to the same cold treatment conditions as controls. Leaf samples were collected at 0h (CK) and 24h after the cold treatment to assess changes in the expression levels of low-temperature-responsive genes in both overexpressing plants and wild-type plants. At 72h after the low-temperature treatment, leaf samples were collected to analyze related metabolites and physiological indicators. All samples are stored in liquid nitrogen for further use.

2.11 Physiological indicator and metabolism measurements

To evaluate the physiological indicators in transgenic and wild plants under cold conditions, the contents of proline and MDA, soluble sugar and starch content were measured using the commercial kits according to the manufacturer's instructions (Solarbio, Beijing, China). To determine chlorophyll content, leaves of wild-type and transgenic *Arabidopsis* plants, with and without cold stress treatment, were homogenized in 80% acetone. The homogenized leaves were refrigerated at 4°C for 3 days until they reached near-bleached status. Optical density (OD) values at 645nm and 663nm were then measured, and chlorophyll content was calculated using the formula: (8.02*OD663 + 20.21*OD645) *M/1000/N, where M represents the volume of 80% acetone added, and N is the fresh weight of the aerial plant parts. "The net photosynthetic rate, Fv/Fm, and electrolytic leakage photosynthetic indices were measured using the Li-6400 portable photosynthetic apparatus. Fv/Fm measurements were conducted using the Dual Pam 100, with *Arabidopsis* plants darkened for a minimum of 30 minutes prior to measurement. The electrolytic leakage experiment method was referenced from Bajji et al. (2002). The measurement of sugar metabolism products, including trehalose, Tre6p, and sucrose content, was conducted using high-performance liquid chromatography-mass spectrometry (HPLC-MS), following the method outlined in Lin et al. (2023).

2.12 Statistical analysis

Three replicates were used for all experiments. Statistically significant data were analyzed using one-way analysis of variance (ANOVA) with the least significant difference (LSD) method. The R package ANOVA (https://statsandr.com/blog/anova-in-r/) was employed for this analysis. The calculated values were presented as means ± standard deviation (SD).

3 Result

3.1 Genome-wide identification and characteristics of *AhTPS* and *AhTPP* genes in wild and cultivated peanut

Through BLAST searches and confirmation of conservative domains, a total of 16 *TPS* and 17 *TPP* genes were identified in the cultivated peanut genome (*Arachis hypogaea*). Based on their chromosomal locations, these *TPS* genes were designated as *AhTPS1-16*, while the *TPP* genes were named *AhTPP1-17*. All 16 *TPS* genes contained both *TPS* and *TPP* conserved domains, whereas the 17 *TPP* genes each contained a single typical *TPP* domain (Supplementary Figures 1, 2). Additionally, 19 *TPS* genes and 15 *TPP* genes were identified in the wild diploid peanut genomes *Arachis duranensis* and *Arachis ipaensis*. In the *A. duranensis* genome, 9 *TPS* genes and 7 *TPP* genes were identified and named *AdTPS1 – AdTPS9* and *AdTPP1 – AdTPP7*, respectively. Meanwhile, *A. ipaensis* harbored 10 *TPS* and 8 *TPP* genes designated as *AiTPS1 – AiTPS10* and *AiTPP1 – AiTPP8* (Tables 1, 2).

Physicochemical property analysis revealed that the gene length of *AhTPSs* ranged from 174 to 1022 bp, protein length from 705 to 1022 amino acids, molecular weight from 80.4 kDa to 116.17 kDa. The aliphatic index of *AhTPSs* ranged from 84.03 to 91.58. Isoelectric points of *AhTPS1-AhTPS5*, *AhTPS7-AhTPS12*, and *AhTPS14-AhTPS16* fell within the range of 5.01 to 6.89, indicating an acidic nature due to an abundance of acidic amino acids. In contrast, *AhTPS6* and *AhTPS13* were enriched in basic amino acids. Gene length for *AhTPPs* ranged from 129 to 437 bp, protein length from 245 to 445 amino acids, and molecular weight from 27864.94 Da to 49874.19 Da. The aliphatic index of *AhTPPs* ranged from 74.25 to 92.22. Theoretical isoelectric point analysis indicated that *AhTPP1, AhTPP3, AhTPP9*, *AhTPP10* and *AhTPP13* had isoelectric points between 5.01 and 6.57, suggesting an acidic nature due to acidic amino acids. Conversely, *AhTPP2, AhTPP4-AhTPP8*, *AhTPP11-AhTPP12*, and *AhTPS14-AhTPS17* were rich in basic amino acids. The GRAVY (Grand Average of Hydropathy)

10.3389/fpls.2023.1343402

TABLE 1 Characteristics of *TPS* family members in cultivated peanut (*Arachis hypogaea*).

Gene name	mRNA ID	Genome location	Number of amino acids	Length of gene/bp	Molecular weight/Da	Isoelectric point (pI)	GRAVY	Aliphatic index
AhTPS1	*Arahy.93VR75*	Chr01:87159326-87162241	705	848	80392	6.89	-0.283	85.02
AhTPS2	*Arahy.G88L7W*	Chr01:96802522-96809236	849	916	96026.65	5.81	-0.226	87.68
AhTPS3	*Arahy.RIH8EG*	Chr03:24399601-24405854	1003	973	113229.45	6.22	-0.275	86.12
AhTPS4	*Arahy.IE8W25*	Chr03:133371847-133376625	862	862	97108.04	5.88	-0.189	91.58
AhTPS5	*Arahy.Q3GMD8*	Chr03:136252971-136257365	854	1003	96681.96	5.77	-0.188	91.63
AhTPS6	*Arahy.E48PAY*	Chr07:76447357-76459343	927	1022	104664.21	7.01	-0.383	84.03
AhTPS7	*Arahy.BL0RCS*	Chr09:113085191-113089493	847	853	95865.65	5.6	-0.216	88.58
AhTPS8	*Arahy.A0DAR9*	Chr11:112046409-112051186	848	829	96610.43	5.91	-0.221	86.99
AhTPS9	*Arahy.1XW75L*	Chr11:147434575-147439870	849	849	95996.62	5.81	-0.225	87.68
AhTPS10	*Arahy.FTDL1P*	Chr13:26117125-26123363	973	849	109322.73	5.81	-0.26	84.76
AhTPS11	*Arahy.CM68RF*	Chr13:135800911-135805745	862	860	97165.09	5.79	-0.184	91.8
AhTPS12	*Arahy.FP7P7G*	Chr13:138499685-138504202	853	854	96618.88	5.77	-0.195	91.62
AhTPS13	*Arahy.PK6QLT*	Chr13:145969353-145977152	1022	174	116170.19	8.31	-0.296	89.18
AhTPS14	*Arahy.AKPI0I*	Chr15:26507553-26513085	860	855	96986.1	6.11	-0.175	93
AhTPS15	*Arahy.FZMU71*	Chr15:130260497-130267100	869	862	98141.75	5.73	-0.225	86.94
AhTPS16	*Arahy.9VZ5EJ*	Chr19:156034428-156039218	855	847	96691.62	5.69	-0.196	89.58

values for all 16 TPS and 17 TPP proteins were below 0, indicating their hydrophilic nature.

3.2 Phylogenetic analysis of *AhTPS* and *AhTPP* gene families

To investigate the evolutionary relationships of the *AhTPS* and *AhTPP* gene families, phylogenetic trees were constructed using *TPS* and *TPP* family genes from *Arabidopsis*, soybean, rice, tomato, wild diploid peanut, and cultivated peanut, respectively. Across these species, a total of 87 *TPS* genes and 79 *TPP* genes were used to construct systematic phylogenetic trees. In these species, a total of 87 *TPS* genes and 79 *TPP* genes were employed to build systematic phylogenetic trees. Based on the phylogenetic relationship of rice and *Arabidopsis* (Figure 1A), The *TPS* gene family is categorized into two subfamilies, namely Class I and Class II. Within Class I, there are two subgroups, while Class II is divided into three subgroups. *AtTPS1-4* belong to Class II, while *AtTPS5-11* belong to Class I. The gene counts of *TPS* within different taxa, including cultivated peanut, two wild diploid peanuts (Ad/Ai), rice, soybean, *Arabidopsis*, and tomato, are as follows: Class I-1 (2, 2/2, 1, 5, 1, 2), Class I-2 (0, 0/0, 0, 0, 3, 1), Class II-1 (2, 1/1, 3, 2, 1, 1), Class II-2 (6, 3/4, 2, 7, 3, 2), and Class II-3 (6, 3/3, 5, 6, 3, 5). Except for Class I-2, each group contains at least one gene across the seven species. Comparative analysis suggests a closer genetic relationship between *TPS* genes in the *Arachis* genus and *GmTPS* genes in soybean. Furthermore, *AhTPS6* in Class I-1 clusters alongside *AtTPS1* and *OsTPS1*, implying potential functional similarity among genes within the same group.

The *TPP* gene family is divided into two categories (Figure 1B). Class I *TPP* genes consist of four cultivated peanut genes (*AhTPP5*, *AhTPP7*, *AhTPP9*, and *AhTPP15*), three wild peanut genes (*AdTPP5*, *AiTPP1*, and *AiTPP6*), three soybean genes (*GmTPP6*,

10.3389/fpls.2023.1343402

TABLE 2 Characteristics of *TPP* family members in cultivated peanut (*Arachis hypogaea*).

Gene name	mRNA ID	Genome location	Number of amino acids	Length of gene/bp	Molecular weight/Da	Isoelectric point (pI)	GRAVY	Aliphatic index
AhTPP1	*Arahy.FIK9JS*	Chr03:10868380-10873244	388	388	43213.37	6.57	-0.275	88.92
AhTPP2	*Arahy.P5P8C7*	Chr03:124464638-124467355	355	391	39933.8	9.08	-0.392	80.76
AhTPP3	*Arahy.51Y4LP*	Chr05:14048218-14053780	386	279	43296.31	6.22	-0.381	85.83
AhTPP4	*Arahy.J3QXZL*	Chr07:57504749-57508748	312	388	35412.85	9.31	-0.366	88.4
AhTPP5	*Arahy.0FY2NM*	Chr08:8204445-8216930	373	373	42405.02	9.22	-0.332	85.2
AhTPP6	*Arahy.B1753N*	Chr08:12717424-12719898	309	327	34895.17	9.07	-0.348	87.73
AhTPP7	*Arahy.B2J19D*	Chr08:49036435-49039546	279	245	31689.36	7.79	-0.295	92.22
AhTPP8	*Arahy.SS1VDK*	Chr10:12843901-12849157	391	355	43915.47	9.04	-0.353	81.99
AhTPP9	*Arahy.U769C2*	Chr12:4517116-4529201	334	378	38130.21	5.49	-0.375	86.65
AhTPP10	*Arahy.8AAC5A*	Chr12:27460283-27462833	245	129	27864.94	5.44	-0.203	85.06
AhTPP11	*Arahy.CK7SVG*	Chr13:14488386-14492535	445	437	49874.19	7.59	-0.256	88.49
AhTPP12	*Arahy.FJ2B1F*	Chr13:127868945-127871708	355	374	39946.89	9.22	-0.393	80.76
AhTPP13	*Arahy.5Q8BGE*	Chr15:14981830-14987321	375	386	42051.76	6.03	-0.41	86.27
AhTPP14	*Arahy.DP0G5T*	Chr17:56617699-56620895	313	335	35206.75	9.48	-0.296	83.13
AhTPP15	*Arahy.G2WE73*	Chr17:122383126-122395867	373	334	42431.04	9.33	-0.343	85.2
AhTPP16	*Arahy.KW1U5A*	Chr17:128686117-128688689	327	324	36737.21	9.18	-0.378	85.87
AhTPP17	*Arahy.S15BQI*	Chr20:20822125-20826715	374	313	41950.96	9.12	-0.472	74.25

GmTPP8, and *GmTPP16*), two rice genes (*OsTPP11* and *OsTPP12*), and two tomato genes (*SlTPP1* and *SlTPP5*); the remaining thirteen *TPP* genes belong to Class II. Class II *TPP* genes are divided into two subgroups. *AtTPPA*, *AtTPPG*, and *AtTPPF* belong to Class II-1, while the rest of the *AtTPP* genes belong to Class II-2. Gene counts within groups for cultivated peanut, wild peanut (Ad/Ai), rice, soybean, Arabidopsis, and tomato are as follows: Class I-1 (4, 1/2, 2, 3, 0, and 2), Class II-1 (5, 2/3, 4, 5, 3, and 3), and Class II-2 (8, 4/3, 6, 9, 7, and 3). The phylogenetic relationships between *AhTPPs*, *GmTPPs*, and *AtTPPs* are closer. *AhTPP1*, *AhTPP3*, *AhTPP10*, *AhTPP11*, along with *AtTPPA*, *AtTPPG*, and *AtTPPF*, cluster in Class II-1. *AhTPP6* and *AhTPP16*, along with *AhTPP4*, *AhTPP14*, *AhTPP2*, *AhTPP12*, *AhTPP17*, and *AhTPP8*, cluster in Class II-2. *AtTPPB*, *AtTPPC*, *AtTPPD*, *AtTPPE*, *AtTPPH*, *AtTPPI*, and *AtTPPJ* also cluster in Class II-2. Altogether, *TPS* and *TPP* genes exhibit close relationships within subgenomes of cultivated peanuts and wild diploid peanuts, and share a higher degree of similarity with leguminous crop, soybean.

3.3 Chromosomal location, gene duplication, and synteny analysis of *AhTPS* and *AhTPP* genes

To study the chromosomal locations of *AhTPS* and *AhTPP* genes in the genome of cultivated peanut, the distribution of genes on chromosomes is depicted based on the genome annotation file (GFF) of cultivated peanut (Figure 2). We observed an uneven

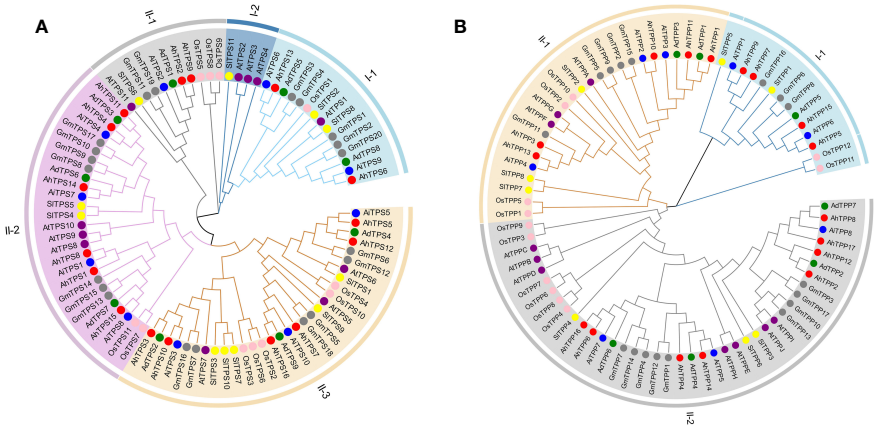

FIGURE 1
Phylogenetic analysis of *TPS* **(A)** and *TPP* **(B)** gene family among cultivated peanut (*Arachis hypogaea*, *Ah*), wild diploid peanut (*Arachis duranensis*, *Ad and Arachis ipaensis*, *Ai*), *Arabidopsis thaliana* (*At*), soybean (*Glycine max*, *Gm*), rice (*Oryza sativa*, *Os*) and tomato (*Solanum lycopersicum*, *Sl*). The phylogenetic tree was constructed using MEGA11 based on the Neighbor-joining method with 1000 bootstrap replicates.

distribution of the *AhTPS* and *AhTPP* genes on the chromosomes of cultivated peanut. The results indicate that peanuts have 20 chromosomes, with 16 *AhTPS* genes distributed across Chrs01, 03, 07, 09, 11, 13, 15, and 19. Seventeen *AhTPP* genes are distributed across chromosomes 03, 05, 07, 08, 10, 12, 13, 15, 17, and 20. Most of these genes are located near the ends of the chromosomes. *TPS* and *TPP* genes were not identified on certain chromosomes, such as Chr02, Chr04, Chr06, Chr14, Chr16, and Chr18. Based on the gene locations on chromosomes, it was found that some *TPS* and *TPP* orthologous genes from the A subgenome (Chr01-10) and the B subgenome (Chr11-20) exhibit consistent positions, such as *AhTPS1* and *AhTPS8*, *AhTPS2* and *AhTPS9*, *AhTPP1* and *AhTPP11*. It suggests their retention during the evolution from wild diploid peanuts to cultivated tetraploid peanut. Conversely, certain genes show distribution differences between the A and B subgenomes. For instance, *TPP* genes on Chr02 have been lost during the evolutionary process, while Chr12 retains *AhTPP9* and *AhTPP10*.

To study evolutionary relationships and reveal the homology relationship of *TPS* and *TPP* genes in different *Arachis* species, two diploid wild peanut, *Arachis duranensis* and *Arachis ipaensis*, were selected for collinear analysis the cultivated peanut *Arachis hypogaea* (Figure 3). According to collinearity analysis, 22 and 21 collinear gene pairs were detected between *AhTPS* genes of *A. duranensis* and *A. hypogaea*, and *A. ipaensis* and *A. hypogaea*, respectively (Figure 3A, Supplementary Table 1). Between *AhTPP* genes of *A. duranensis* and *A. hypogaea*, as well as *A. ipaensis* and *A. hypogaea*, 19 and 14 collinear gene pairs were respectively identified (Figure 3D, Supplementary Table 2). All *TPS* and *TPP* members in cultivated peanuts possess corresponding segments in both wild

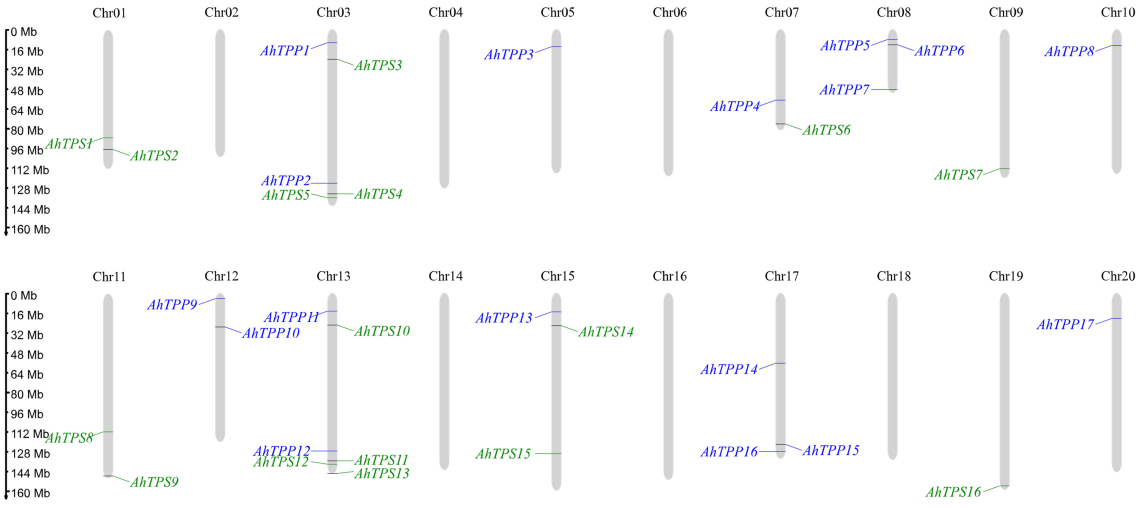

FIGURE 2
Chromosomal location analysis of *AhTPS* and *AhTPP* genes. *AhTPSs* (green) and *AhTPPs* (blue) are marked on chromosomes. The scale bar on the left indicates the length of *A. hypogaea* chromosomes (Mb).

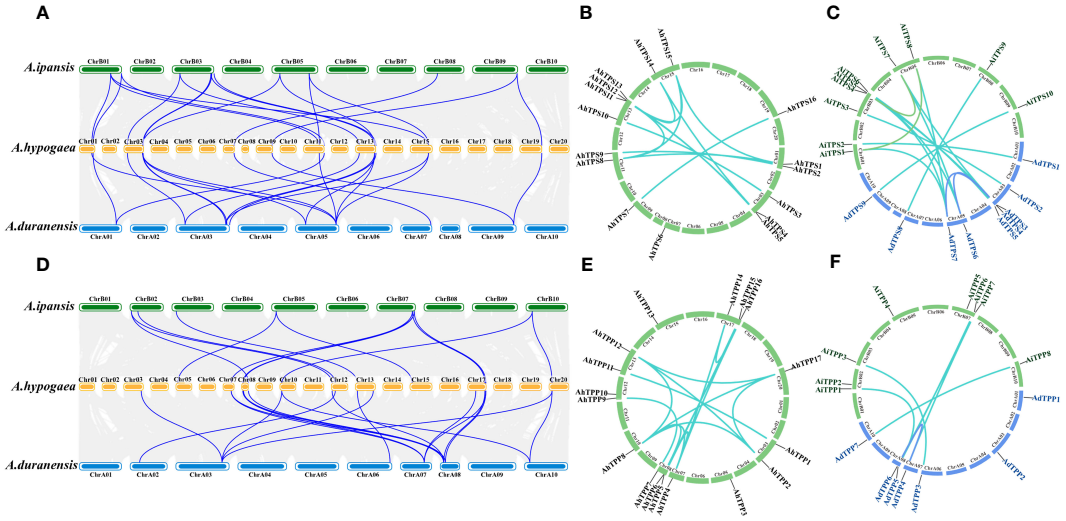

FIGURE 3
Collinearity analysis of the *TPSs* **(A–C)** and *TPPs* **(D–F)** in three *Arachis* species. **(A)** The syntenic relationship of the *AhTPSs* between *A. ipaensis, A. hypogaea* and *A. duranensis* genomes. **(B)** The collinearity relationship of *AhTPSs* within the cultivated peanut (*A. hypogaea*) genome. **(C)** The collinearity relationship of *AhTPSs* between wild diploid peanut *A. ipaensis* and *A. duranensis* genomes. **(D)** The syntenic relationship of the *AhTPPSs* between *A. ipaensis, A. hypogaea* and *A. duranensis* genomes. **(E)** The collinearity relationship of *AhTPPs* within the cultivated peanut (*A. hypogaea*) genome. **(F)** The collinearity relationship of *AhTPPs* between wild diploid peanut *A. ipaensis* and *A. duranensis* genomes.

species, suggesting the genetic conservation of these two family members during the formation of tetraploid peanuts from their wild counterparts. Gene duplication (segmental and tandem duplication) is a major force behind genome evolution. So, *Arachis TPS* and *TPP* gene duplication events were evaluated (Supplementary Tables 3, 4). The *AhTPS* gene family exhibited 12 pairs of segment duplications (Figure 3B), while the *AhTPP* gene family showed 16 pairs of segment duplications (Figure 3E). No tandem duplications were identified in either the *AhTPS* or *AhTPP* gene families. Further collinearity analysis was conducted between the gene families in the diploid wild peanut genomes. Among the *TPS* gene families of the two wild species, 13 pairs of orthologous genes were identified (Figure 3C), and for the *TPP* gene families, 6 pairs of orthologous genes were detected (Figure 3F). Some gene pairs, such as *AdTPS3-AdTPS6*, *AdTPS3-AdTPS7*, and *AiTPS1-AiTPS8* in the *TPS* gene family (Supplementary Table 3), as well as *AdTPP4-AdTPP6* in the *TPP* gene family (Supplementary Table 4), suggested that these segment duplications had already were present during the evolution of wild diploid peanuts. Discrepancies between the collinearity maps of wild diploid and cultivated peanuts may be attributed to the emergence of new segment duplications or transpositions within the *TPS* and *TPP* gene families after the derivation of tetraploid cultivated peanuts from diploid wild peanuts. The ratio of nonsynonymous substitution rate (Ka) to synonymous substitution rate (Ks) provides insights into the evolutionary process and selection pressure. We calculated the Ka/Ks ratio among the *Arachis* species. For both *AhTPS* and *AhTPP* gene members, except for a few genes for which Ka/Ks ratios could not be calculated, most of the calculated Ka/Ks ratios were less than 1, indicating that *AhTPS* and *AhTPP* genes were subject to strong purifying selection pressure during evolution (Supplementary Tables 5, 6).

3.4 Gene structure and motif composition of *AhTPS* and *AhTPP* genes

Gene structure analysis played a crucial role in elucidating the connection between gene family evolution and functional divergence. To unveil the inherent structural attributes of the *AhTPS* and *AhTPP* families, an in-depth investigation of gene structures and conserved motifs was conducted (Figure 4). Based on the phylogenetic analysis (Figure 1; Figures 4A,E), Both *AhTPS* and *AhTPP* members were divided into 2 groups (I and II), respectively, and a total of 20 conserved motifs are identified (Figures 4B,D). In the *AhTPS* gene family, Class I genes possess a greater number of introns (19 and 17) compared to Class II genes (4, 5, or 6), indicating a more complex gene structure (Figure 4C). Genes with close phylogenetic relationships often exhibit higher structural similarity. Among the Class I *AhTPS* genes, *AhTPS3* and *AhTPS10* have 6 introns each, while *AhTPS2* and *AhTPS9* have 4 introns each. Concerning the *AhTPP* gene family, Class I *AhTPP* genes, *AhTPP5* and *AhTPP15*, have the highest number of introns at 14, whereas *AhTPP7* possesses only 7 introns (Figure 4G). In Class I *AhTPP* genes, *AhTPP11* has 14 introns, *AhTPP8* and *AhTPP17* have 11 introns, *AhTPP2* and *AhTPP12* contain 12 introns, *AhTPP6* and *AhTPP16* have 10 introns, and *AhTPP8* and *AhTPP17* possess 11 introns. Subsequently, we employed the online tool MEME to identify conserved motifs within AhTPS and AhTPP proteins. All AhTPS proteins contain motifs 1, 2, 3, 4, 5, 7, and 15. Except for AhTPS1, all AhTPS proteins contain motifs 6 and 13, and motifs 18 are present in all AhTPS proteins except AhTPS13. Most AhTPS proteins encompass motifs 8, 9, 10, 11, 12, 16, 17, 19, and 20. The fewest motifs (11) are found in AhTPS13. Generally, AhTPP proteins exhibit fewer motifs compared to AhTPS proteins, with AhTPP11 having the lowest count of motifs (13) (Figures 4F,

10.3389/fpls.2023.1343402

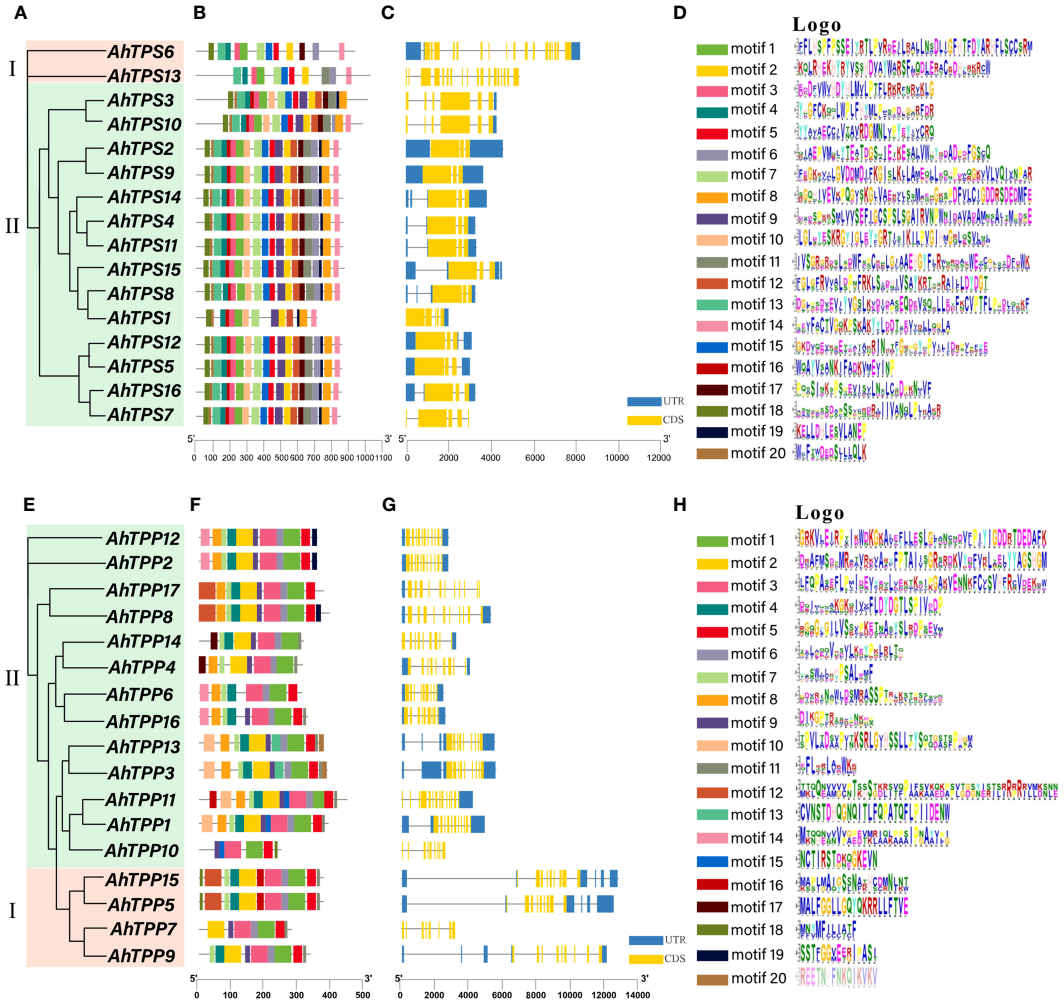

FIGURE 4
The phylogenetic trees, motifs, and gene intron/exon structures of 16 *AhTPS* genes and 17 *AhTPP* genes in cultivated peanut. **(A, E)** Phylogenetic tree based on AhTPS and AhTPP protein sequences using Neigbour-joining Tree method. **(B, F)** The motif compositions of AhTPS and AhTPP proteins. specific motifs were indicated using different colors. **(C, G)** The exon and intron distribution of *AhTPS* and *AhTPP* genes. Exons and intron regions are represented by yellow rectangles and grey lines, respectively. **(D, H)** Sequence logos of 20 motifs in cultivated AhTPS and AhTPP proteins, respectively.

H). All AhTPP proteins share motif 1, while motifs 13 and 20 are exclusively present in AhTPP3 and AhTPP13, motif 17 only in AhTPP4 and AhTPP14, and motif 18 only in AhTPP5 and AhTPP10. Identified conserved domains are listed according to their conservation levels within the *AhTPS* (Figure 4D) and *AhTPP* (Figure 4H) gene families. The results reveal that the most conserved motifs in *AhTPS* are generally located at the N-terminal, whereas the conserved motifs in the *AhTPP* family are predominantly situated at the C-terminal. This could be attributed to the positioning of TPS domains at the N-terminal and TPP domains at the C-terminal.

3.5 *Cis*-element analysis in the upstream region of *AhTPS* and *AhTPP* genes

Cis-elements are necessary for gene expression and are widely involved in the regulation of plant growth and development and stress response. To further investigate the potential regulatory mechanisms of the *AhTPS* and *AhTPP* genes under stress conditions, we predicted and summarized the *cis*-regulatory elements within the first 2000 bp segments upstream of *AhTPSs* and *AhTPPs*, respectively (Supplementary Tables 7, 8). Cluster analysis of *cis*-regulatory elements in promoter regions reveals that orthologous genes from A and B subgenomes of cultivated peanut exhibit similar *cis*-element distributions, both in *AhTPS* and *AhTPP* genes (Figure 5). In the *AhTPS* genes, a total of 61 *cis*-regulatory elements were identified, including hormone-responsive elements such as abscisic acid (ABA), auxin (IAA), gibberellin (GA), salicylic acid (SA), and methyl jasmonate (MeJA) response elements, as well as stress-related elements like light response, anaerobic response, low temperature, wound, and MYB elements. Almost all *AhTPS* genes contain a significant number of light-responsive elements. However, considerable variation exists among different genes with respect to other hormones and stress responses. For instance, *AhTPS2*, *AhTPS5*, *AhTPS9*, and *AhTPS12* contain

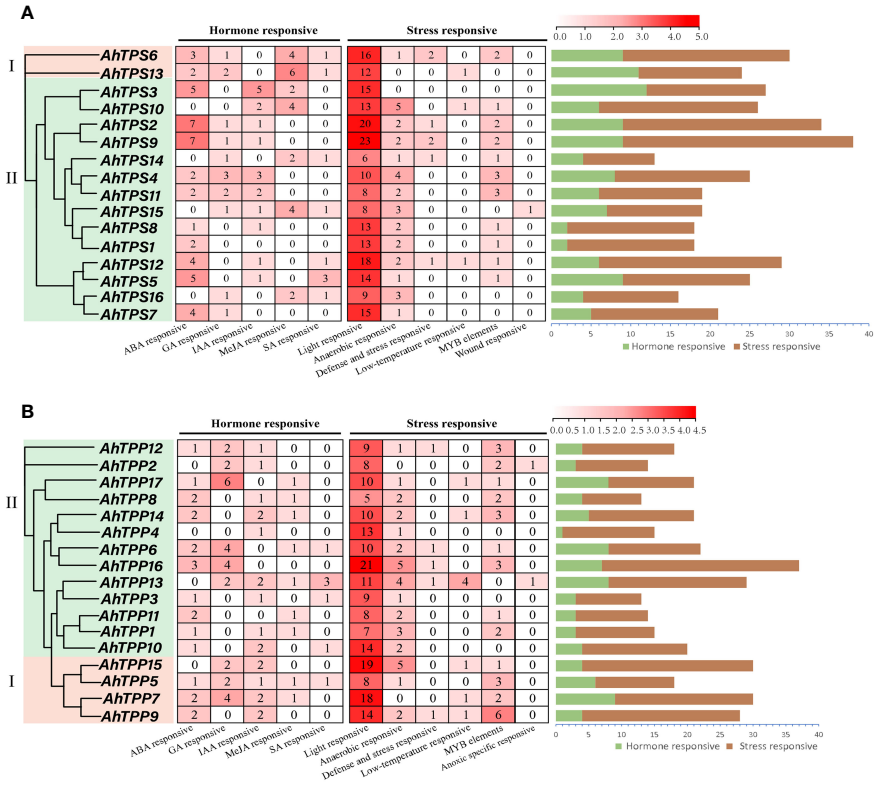

FIGURE 5
Cis-regulatory elements in the promoters of *AhTPS* **(A)** and *AhTPP* **(B)** genes in peanut. Various *cis*-regulatory elements are displayed in different colored boxes.

numerous ABA-responsive elements, while *AhTPS6* and *AhTPS13* have a higher abundance of MeJA-responsive elements. In *AhTPP* genes, a total of 54 *cis*-regulatory elements were identified, including elements responsive to hormones such as ABA, MeJA, GA, IAA, SA, and stress-related elements like light, anaerobic conditions, and low temperature. Similarly, the most abundant category of *cis*-elements in *AhTPP* genes is related to light response. These findings indicate that both *AhTPS* and *AhTPP* genes are involved in distinct hormone regulatory pathways and responses to environmental stresses in cultivated peanut.

3.6 Expression analysis of *AhTPS* and *AhTPPs* in various tissues and under different environmental treatments

The specific expression patterns of genes can indicate their potential roles in growth and development. We utilized publicly available RNA-seq data related to peanut growth and development from the peanut genome database to investigate the expression profiles of 16 *AhTPS* and 17 *AhTPP* genes across various tissues (Clevenger et al., 2016; Zhuang et al., 2019). Furthermore, we conducted a detailed analysis of the expression pattern changes of *AhTPSs* and *AhTPPs* in leaves under different hormonal, low temperature, and drought treatments using a publicly available transcriptome dataset (Figure 6). The results suggested that there were differences in the expression levels of the *AhTPS* genes in many tissue types across multiple developmental stages.

In both sets of transcriptomic data, the expression levels of *AhTPS1*, *AhTPS8*, and *AhTPS13* are consistently low across various tissues and treatments, indicating a potential loss of gene function during evolution. Conversely, other *AhTPS* genes exhibit differential expression across different developmental stages and tissues. Certain genes, such as *AhTPS9* and *AhTPS14* (Figures 6A, B), maintain consistently high expression levels across nearly all developmental stages and tissues. Some genes, like *AhTPS5* and *AhTPS12*, are predominantly expressed in seed coats and early embryos, while *AhTPS2*, *AhTPS9*, and *AhTPS14* show significantly higher expression levels in roots and root nodules compared to other *AhTPS* genes. Moreover, the expression levels of almost all *AhTPS* genes decline during late embryonic development stages (Embryo-III and Embryo-IV) (Figure 6B). These findings suggest diverse functional roles of different *TPS* genes in various tissues and developmental stages. Under drought and low-temperature treatments, *AhTPS* genes exhibit a notable increase in expression, particularly *AhTPS2*, *AhTPS9*, and *AhTPS14*, suggesting their potential importance in peanut's response to adverse conditions. Regarding hormone treatments, the expression levels of *AhTPS6*, *AhTPS7*, and *AhTPS16* significantly increase in response to salicylic acid and paclobutrazol treatment, while other *AhTPS* genes do not show significant expression level changes in response to hormone treatments.

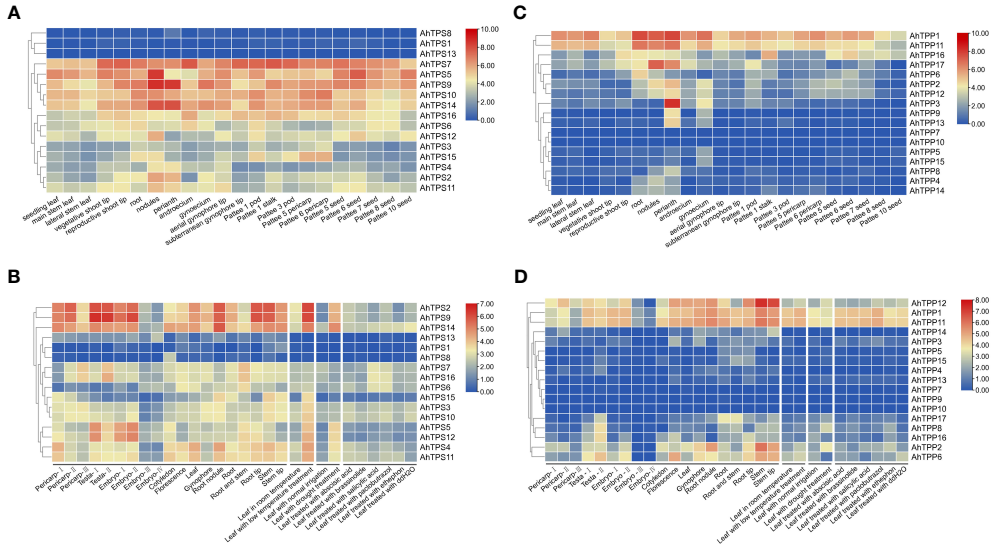

FIGURE 6
Heat map of *AhTPS* and *AhTPP* genes in different tissues, and under hormones and abiotic stresses. The color scale represents Log_2 expression values (1+RPKM). **(A)** Expression profiles of *AhTPSs* in 22 different tissues (Clevenger et al., 2016). **(B)** Transcriptome expression of *AhTPSs* under different tissue, hormones and stress conditions (Zhuang et al., 2019). **(C)** Expression profiles of *AhTPPs* in 22 different tissues (Clevenger et al., 2016). **(D)** Transcriptome expression of *AhTPPs* under different tissues, hormones and stress conditions (Zhuang et al., 2019).

As for *AhTPP* genes, closely related homologs *AhTPP1* and *AhTPP11* share similar expression patterns and significantly higher expression levels across various tissues compared to other *AhTPP* genes (Figures 6C, D). On the other hand, *AhTPP7*, *AhTPP9*, *AhTPP10*, and *AhTPP13* consistently exhibit low expression levels across both transcriptomic datasets. *AhTPP* gene expression also varies in different developmental stages and tissues. For instance, *AhTPP3* show higher expression levels in floral organs (Figure 6C), while *AhTPP12* and *AhTPP17* display elevated expression levels in root tissues. Despite some changes in expression levels in response to stress and hormone treatments, *AhTPP* genes do not exhibit the same magnitude of expression differences as observed in *AhTPS* genes (Figure 6D).

3.7 Real-time expression of *AhTPSs* and *AhTPPs* under cold treatment

To further explore the expression patterns of the *AhTPS* and *AhTPP* genes under low-temperature conditions, we employed qPCR to assess the changes in expression levels of these genes at different time points in the leaves (Figure 7). Primers used for this experiment are included in Supplementary Table 9. Consistent with the expression patterns from transcriptomic data, no expression levels were detected for *AhTPS1*, *AhTPS8*, and *AhTPS13* within the *AhTPS* gene family, as well as *AhTPP4*, *AhTPP7*, *AhTPP9*, and *AhTPP10* within the *AhTPP* gene family at any time point under low-temperature treatment (Figure 7A). However, the remaining genes were all detectable. Within the *AhTPS* gene family, *AhTPS2-5*, *AhTPS9-12*, *AhTPS14*, and *AhTPS15* exhibited varying degrees of upregulation in their expression levels under low-temperature treatment. Except for *AhTPS3*, which reached its highest expression level at 48 hours post-treatment, the other *AhTPS* genes reached their expression peaks at 12 or 24 hours, indicating a relatively similar expression pattern for these genes under low-temperature treatment. On the other hand, *AhTPS6*, *AhTPS7*, and *AhTPS16* showed insignificant differences in expression levels under low-temperature treatment, suggesting that these genes might not respond to cold induction. Compared to the *AhTPS* genes, most of the *AhTPP* genes did not exhibit substantial differences in expression levels under low-temperature treatment. *AhTPP1*, *AhTPP6*, *AhTPP11*, and *AhTPP13* showed elevated expression levels under low-temperature treatment, with the highest expression level observed at 48 hours post-treatment (Figure 7B). Among these, the most significant alteration in expression levels under low-temperature treatment was observed for *AhTPP6*. However, the expression levels of other genes did not display significant changes.

3.8 Subcellular localization of *AhTPS9*

In order to further elucidate the protein function and expression patterns of the *AhTPS* gene in peanut, and in conjunction with findings derived from transcriptomic analysis and qPCR validation, the *AhTPS9*, displaying the most pronounced differential expression under low-temperature conditions, was specifically chosen for subcellular localization analysis. The subcellular distribution of the *AhTPS9* protein was investigated using the *Agrobacterium*-mediated transient expression technique, with green fluorescent protein (GFP) tagging, in the epidermal cells of tobacco leaves. Microscopic imaging of fluorescence revealed that, in leaves transformed with the control vector, GFP exhibited a uniform distribution across the epidermal cells (Figure 8). Furthermore, subsequent to the transient expression of AhTPS9-GFP fusion

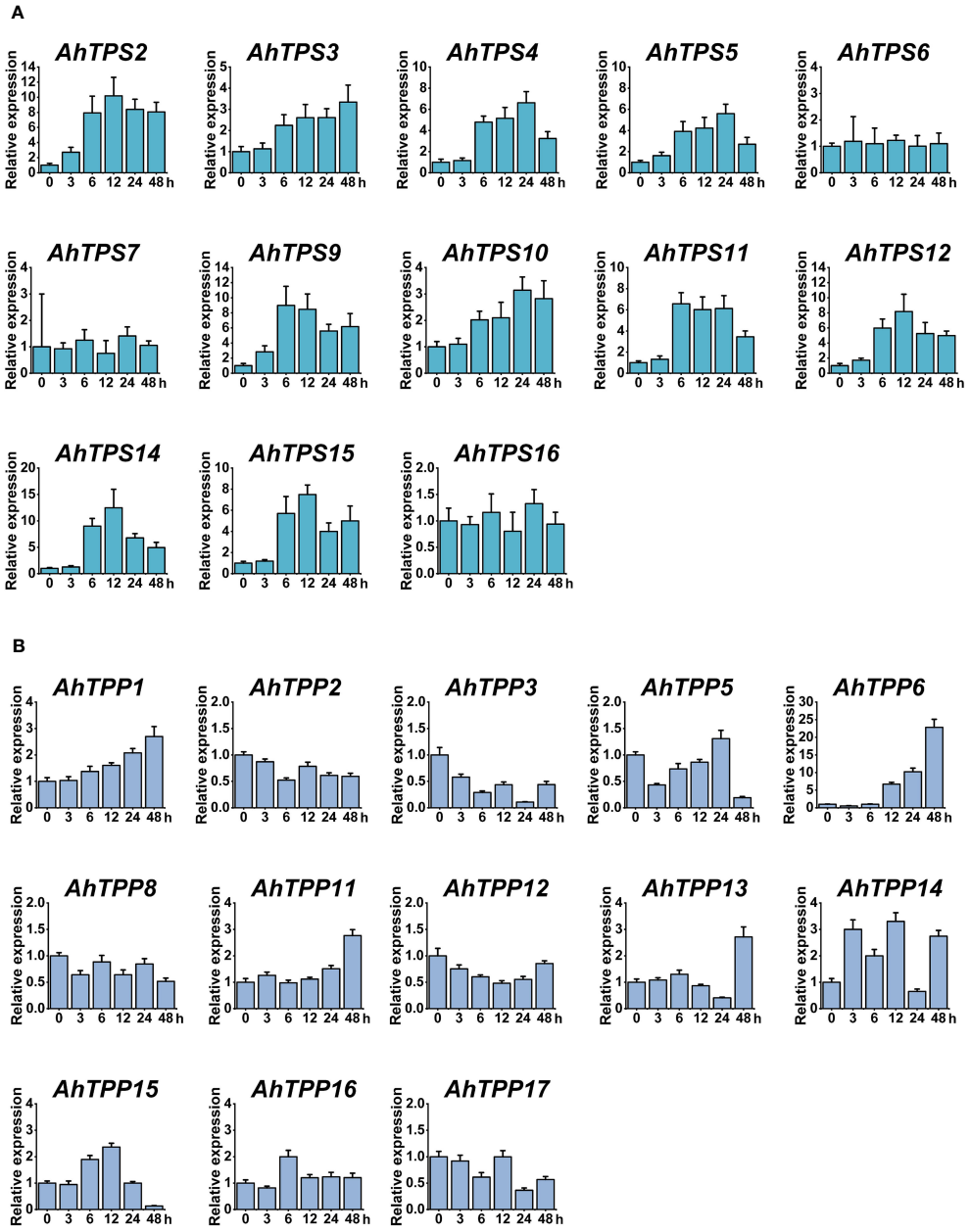

FIGURE 7
Expression patterns of *AhTPS* **(A)** and *AhTPP* **(B)** genes in leaf tissues under low-temperature stress. Data represents the mean ± standard deviation of three biological replicates each with three technical replicates. Relative transcript levels of the selected genes were calculated using the $2^{-\Delta\Delta Ct}$ method, with *Actin* gene in cultivated peanut as the internal reference.

proteins in tobacco epidermal cells, the GFP signals were observed within both the cytoplasm and the nucleus. These results collectively indicate the dual localization of AhTPS9 within both the nucleus and cytoplasm of tobacco leaves.

3.9 Overexpression of *AhTPS9* confers cold stress in transgenic *Arabidopsis*

We conducted an analysis of *AhTPS9* function under cold stress conditions in transgenic *Arabidopsis* plants. Two transgenic *Arabidopsis* lines, *AhTPS9-OE2* and *AhTPS9-OE6*, overexpressing *AhTPS9*, were generated through the construction of *AhTPS9* overexpression vectors and genetic transformation of *Arabidopsis*. Since *AhTPS9* is induced by low-temperature stress, both wild-type (WT) and various *AhTPS9* overexpression (OE) seedlings were subjected to cold treatment. No observable phenotypic differences under normal conditions (22°C). However, under cold treatment, wild-type *Arabidopsis* plants exhibited a cold-sensitive phenotype compared to the two *AhTPS9* overexpression lines (Figure 9). Physiological indicators indicated lower levels of proline and MDA in the *AhTPS9* overexpression lines under low-temperature

10.3389/fpls.2023.1343402

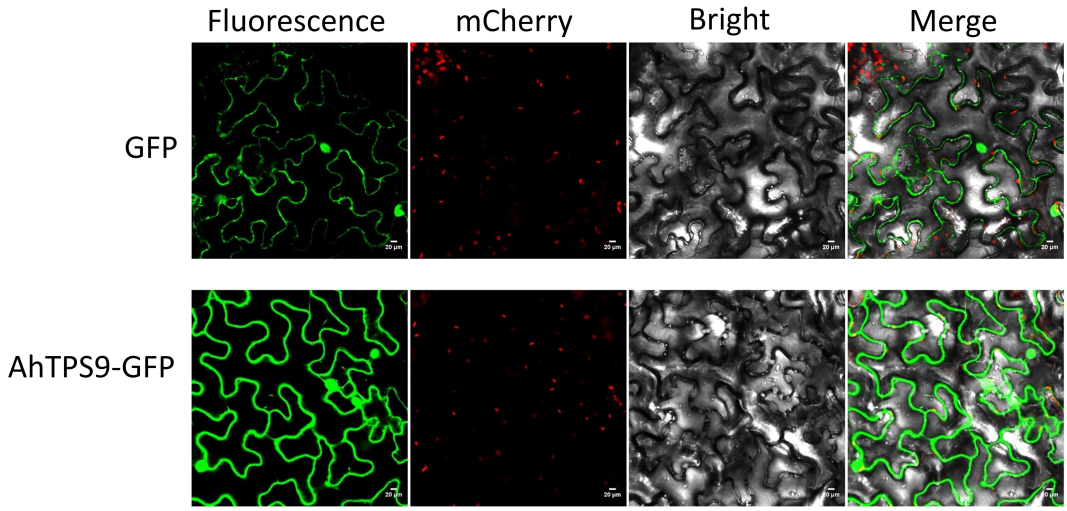

FIGURE 8
The subcellular localization of *AhTPS9* in *Nicotiana benthamiana* leaf epidermal cells is depicted utilizing a confocal fluorescence microscope. Scale bars represent 20 μm.

treatment, suggesting that *AhTPS9* can mitigate cold-induced damage in plants.

The measurement of key indicators related to the photosynthetic system revealed that, under normal temperature conditions, there were no significant differences between wild-type *Arabidopsis* (WT) and the overexpressing plants (*AhTPS9-OE2* and *AhTPS9-OE6*) in terms of Chlorophyll content, Fv/Fm (maximum quantum yield of photosystem II), Pn (photosynthesis rate), and Electrolytic Leakage. However, under low-temperature treatment, the wild-type plants exhibited a significant reduction in Chlorophyll content, Pn, and Fv/Fm, while showing an increase in electrolytic leakage compared to *AhTPS9* overexpressing plants (*AhTPS9-OE2* and *AhTPS9-OE6*). This indicates that the overexpression of *AhTPS9* has the ability to alleviate the damage caused by low temperatures to the photosynthetic system in *Arabidopsis thaliana*. Further analysis of sugar metabolites and gene expression levels in the trehalose biosynthesis pathway revealed that, under low-temperature conditions, *AhTPS9* expression was significantly higher in the overexpression lines than in the wild type. Additionally, downstream *AtTPPI* gene expression levels were also

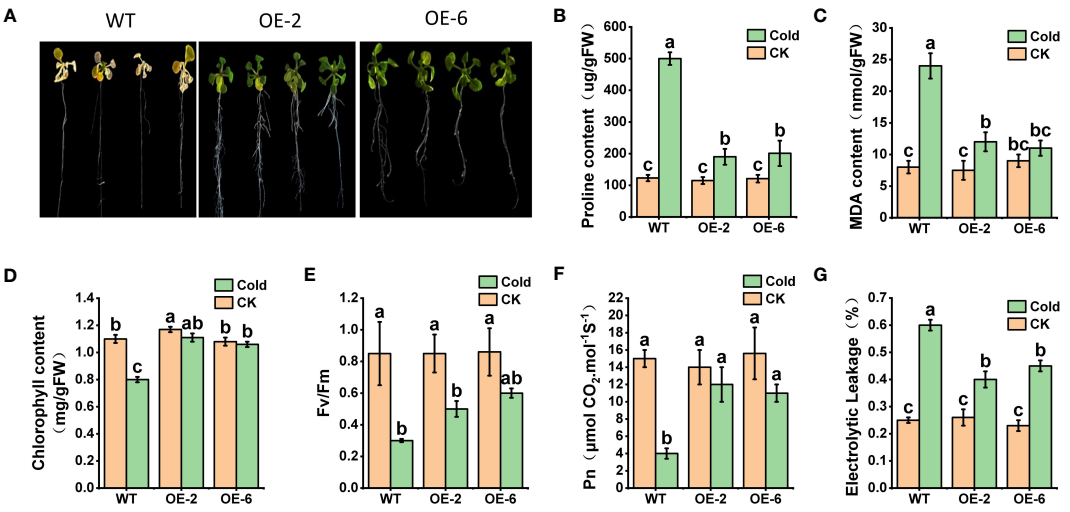

FIGURE 9
Phenotypes of *Arabidopsis* overexpressing *AhTPS9*, OE2 and OE6, along with the wild-type (WT) control, following a 72-hour cold treatment. Arabidopsis plants were grown on MS medium for 14 days and subsequently exposed to a cold environment at 4°C for 72 hours **(A)**. The endogenous levels of stress-responsive parameters, including Proline **(B)** and MDA **(C)**, were measured. Additionally, photosynthesis-related parameters under cold conditions were assessed, including chlorophyll content **(D)**, Fv/Fm **(E)**, net photosynthetic rate (Pn) **(F)**, and electrical leakage **(G)**. The data presented are expressed as the means ± standard errors (SEs) derived from three independent biological replicates. Statistically significant distinctions among the lines are denoted by different lowercase letters (a–c) based on Duncan's test (p-value < 0.05).

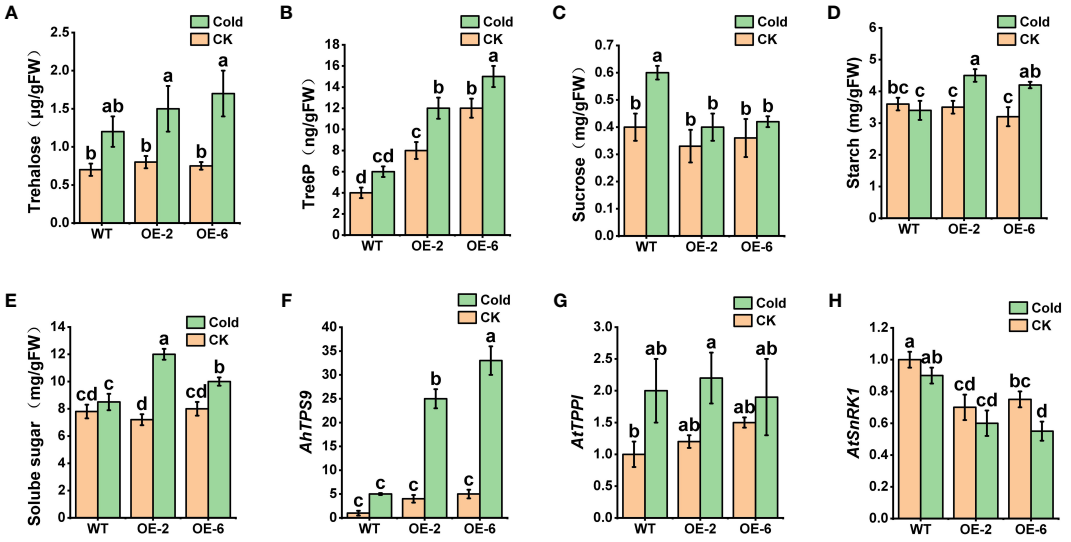

FIGURE 10
Changes in sugar metabolism and related genes in *AhTPS9* overexpressing transgenic plants, including **(A)** Trehalose content, **(B)** Tre6P content, **(C)** sucrose content, **(D)** starch content, **(E)** soluble sugar content, as well as the relative expression levels of *AhTPS9*, *AtTPPI*, and *AtSnRK1* (**F**–**H**). The data are presented as means ± standard errors (SEs) derived from three independent biological replicates. Statistically significant differences among the lines are indicated by different lowercase letters (a–c) based on Duncan's test (p-value < 0.05).

elevated in the *AhTPS9-OE2* and *AhTPS9-OE6* compared to the wild type (Figure 10). Moreover, the overexpression lines exhibited higher levels of Tre6p and trehalose but lower levels of sucrose compared to the wild type. In contrast, the overexpressing plants of *AhTPS9* exhibited significantly higher levels of soluble sugars and starch content compared to the wild-type plants. The expression levels of key genes related to sucrose and Tre6P, such as *AtSnRK1*, were also examined. It was observed that, under normal temperature conditions, the expression of *AtSnRK1* was higher in the WT plants than in *AhTPS9* overexpressing plants. However, under cold stress conditions, the expression levels of *AtSnRK1* significantly decreased. These findings suggest that *AhTPS9* may regulate sugar metabolism pathways to alleviate the damage caused by low-temperature stress. Overall, our study demonstrates that *AhTPS9* plays a crucial role in enhancing plant tolerance to cold stress, potentially by modulating sugar metabolism pathways.

4 Discussion

In response to low-temperature stress, plants rely on molecular mechanisms, with the trehalose biosynthesis pathway and its associated genes playing a crucial role. In plants, trehalose plays a role in regulating the response of plants to various environmental stresses (Paul et al., 2008). Recent research has suggested that the low levels of trehalose in plants may be involved in regulating their response to environmental stress in conjunction with its precursor, Tre6P (Dijken et al., 2004; Schluepmann et al., 2004; O'Hara et al., 2013). This implies that trehalose within plants may serve as an important signaling molecule in mediating the perception and regulation of both biotic and abiotic stresses. Therefore, investigating the trehalose signaling pathway in plants will contribute to the refinement of the plant sugar signaling network and uncovering the mechanisms by which sugars participate in regulating plant growth and development. Key genes in this context include *TPS* and *TPP* genes (Eastmond and Graham, 2003). These gene families regulate the synthesis and metabolism of trehalose, serving as vital components in the plant's response to low temperatures (Kandror et al., 2002; Iordachescu and Imai, 2008). Numerous studies have been conducted on various plant species, such as *Arabidopsis*, rice, and common bean, revealing the expression and functions of *TPS* and *TPP* genes in cold stress responses (Fernandez et al., 2010; Liu et al., 2019; Lin et al., 2023; Liu et al., 2023). They contribute to the maintenance of membrane stability, protein protection, and ultimately enhance the plant's cold resistance (Elbein et al., 2003). Therefore, in this study, we identified the *TPS* and *TPP* genes involved in the synthesis pathway of trehalose in peanuts and explored their roles in the response to low temperatures.

In this study, a total of 16 *AhTPS* and 17 *AhTPP* genes were identified in the cultivated peanut genome, while in the genome of wild diploid peanut *A. duranensis*, there were 9 *AdTPS* genes and 7 *AdTPP* genes, and in the genome of *A. ipaensis*, there were 10 *AiTPS* genes and 8 *AiTPP* genes (Figure 1, Table 1). Most of the *TPS* and *TPP* gene family members in wild diploid peanuts showed orthologous relationships with genes in the A and B subgenomes of cultivated peanuts, with differences in their numbers possibly arising from new duplication events between the two subgenomes of cultivated peanuts. Although cultivated peanuts have a larger number of *AhTPS* and *AhTPP* genes compared to other species such

as *Arabidopsis*, rice, soybean, tomato, watermelon and cucumber (Vogel et al., 2001; Zang et al., 2011; Dan et al., 2021; Yuan et al., 2021; Lin et al., 2023), this may be attributed to the fact that cultivated peanuts, being tetraploids derived from two wild diploid peanuts, *A. duranensis* and *A. ipaensis*, have larger genomes (Bertioli et al., 2016; Bertioli et al., 2019; Zhuang et al., 2019). The *AhTPS* and *AhTPP* genes have been classified into two main groups based on other crops such as *Arabidopsis*, rice, and soybean (Figure 6). The *AhTPS* and *AhTPP* gene sequences are relatively conserved, with *TPS* or *TPP* orthologous genes within the *Arachis* species clustering together. However, the similarity between non-orthologous genes within the *Arachis* species is lower than the relationship between the *Arachis* species and the leguminous crop soybean. This implies that *AhTPS* genes and *AhTPP* genes exhibit a higher degree of conservation across species, while the similarity among family members is lower than that between species. Different *AhTPS* and *AhTPP* genes may undergo functional differentiation, and various *AhTPS* and *AhTPP* members may share similar functions with soybean. Gene duplication plays a crucial role in evolutionary processes, including chromosomal rearrangements, the diversification of gene functions, and the enlargement of gene families (Cannon et al., 2004; Huang and Rieseberg, 2020; Mérot et al., 2020). Hence, the duplication events of *AhTPS* and *AhTPP* gene members during the evolutionary process were identified, and the results indicate that both gene families, *AhTPS* and *AhTPP*, exhibit similarities in their evolutionary history. This is manifested by the absence of tandem duplications in both gene families, with evolution primarily relying on segment duplications, both in wild diploid peanuts and cultivated tetraploid peanuts (Figure 3). Therefore, the combination of phylogenetic and collinearity analysis results demonstrates that the *AhTPS* and *AhTPP* genes maintain a relatively conserved orthologous relationship among species, and the evolutionary process within the peanut species predominantly involves segment duplication.

The analysis of promoter *cis*-acting elements and gene expression patterns reveals that members of the *AhTPS* and *AhTPP* gene families play crucial roles in the growth, development, hormonal regulation, and stress responses of cultivated peanuts (Figures 5–7). The regulation pathways of trehalose in plant growth, development, and stress responses are intricate. Trehalose plays a vital role in safeguarding bioactive compounds and cellular components, such as proteins, nucleic acids, and biological membranes, from harsh environmental conditions like high salinity, drought, extreme temperatures, freezing, and oxidative stress (Nunes et al., 2013; O'Hara et al., 2013). Its most crucial role lies in modulating the synthesis and metabolism of carbohydrates in response to various biological processes and stressors (Oszvald et al., 2018; Hassan et al., 2023). In this study, both the *AhTPS* and *AhTPP* gene families were found to contain a significant number of light-responsive elements (Figure 5), suggesting their potential importance in photosynthesis and energy-related pathways. Combining data from various transcriptome databases and qPCR validation (Bertioli et al., 2019; Zhuang et al., 2019), some of these genes exhibited expression throughout the entire growth process of peanuts and participated in different stress and hormone regulatory mechanisms. Notably, the *AhTPS* family members, *AhTPS2*, *AhTPS9*, and *AhTPS14*, as well as the *AhTPP* family members, *AhTPP1* and *AhTPP11*, were identified to be involved in such processes. Additionally, *AhTPS2* and *AhTPS9*, along with *AhTPP1* and *AhTPP11*, represented two pairs of orthologous genes originating from the A and B subgenomes, as depicted in Figure 2. These orthologous genes have been retained during the evolutionary process of wild diploid peanut species (Figure 1), indicating their potential significance within the *Arachis* genus.

To our knowledge, the manipulation of the *Arachis hypogaea AhTPS* genes in plants has not previously been reported. Combining bioinformatics and gene expression analysis, we observed that the expression levels of *AhTPS2* and *AhTPS9* were significantly higher than others (Figure 6, Figure 7). These genes exhibited similar gene structures and regulatory elements and showed similar expression levels in different tissues, hormonal treatments, and stress conditions. This suggests that they may have similar functions in the cultivated peanut genome, potentially indicating functional redundancy. To further explore the role of *AhTPS* genes under cold stress, *AhTPS9* was selected for heterologous transformation into *Arabidopsis* plants to validate its function. Regulation of *TPS* genes has been shown to enhance abiotic stress tolerance in plants (Pilon-Smits et al., 1998; Garg et al., 2002; Chary et al., 2008; Fernandez et al., 2010; Li et al., 2011; Wang et al., 2016).For instance, constitutive expression of yeast *ScTPS1* in potatoes improved drought tolerance but led to pleiotropic growth abnormalities, such as dwarfism, chlorotic leaves, and aberrant root development (Yeo et al., 2000). Transgenic tomato expressing ScTPS1 exhibited improved drought and salt tolerance but also showed other phenotypic changes (Cortina and Culiáñez-Macià, 2005). In tobacco, *ScTPS1* expression increased drought tolerance without growth aberrations (Karim et al., 2007). Similarly, overexpression of *OsTPS1* in rice improved tolerance to cold, salinity, and drought without visible phenotypic changes (Li et al., 2011). Overexpression of *Triticum aestivum TaTPS11* in *Arabidopsis* enhanced cold tolerance without adverse phenotypes, suggesting its potential value in wheat cold-tolerance breeding (Liu et al., 2019). In this study, in *Arabidopsis* plants overexpressing *AhTPS9*, compared to wild-type plants, no significant phenotypic changes were observed during germination and growth processes. However, under cold stress, the AhTPS9-overexpressing plants exhibited improved tolerance, showing reduced levels of proline and MDA, and without significant wilting. This suggests that *AhTPS9*, similar to *OsTPS1* and *TaTPS11*, can alleviate stress without affecting key phenotypic changes. *AhTPS9* can mitigate the damage to the photosynthetic system caused by low temperatures, including chlorophyll content, Pn, and Fv/Fm, which were significantly higher in the overexpressing plants compared to the wild type. *TPS* genes and their product, Tre6P, have been reported to enhance photosynthesis under stress

conditions (Paul et al., 2001). In maize, Tre6P has been shown to regulate photosynthesis and assimilate distribution in reproductive tissues (Oszvald et al., 2018). In tomatoes, co-expression of *TPS* and *TPP* enhances photosynthesis under drought and salt stress without affecting plant growth (Lyu et al., 2013). *AhTPS9* contains abundant photosynthesis-related elements (Figure 5) and is regulated by multiple hormones (Figure 6). Therefore, the specific regulatory mechanism of *AhTPS9* in protecting photosynthesis under low-temperature conditions requires further research.

Sugar metabolism plays a crucial role in plant responses to low-temperature stress (Nägele and Heyer, 2013; Kovi et al., 2016; Hassan et al., 2023). As a soluble sugar, trehalose is present at extremely low levels, making it unable to provide the necessary osmotic stress protection independently. However, the intermediate product Tre6P plays a critical role in sucrose regulation. Tre6P acts as both a signal for sucrose levels and a negative feedback regulatory factor, contributing to the maintenance of sucrose levels within an appropriate range (Figueroa and Lunn, 2016). Tre6P can interact with *Sucrose Non-Fermenting 1-Related Kinase 1* (*SnRK1*) to regulate sucrose levels antagonistically (Baena-Gonzalez and Lunn, 2020). In this study, we also examined key genes related to trehalose metabolism and their metabolic products in transgenic Arabidopsis and its wild type. The results showed that AhTPS9-overexpressing plants exhibited significantly higher levels under low-temperature conditions, leading to the accumulation of Tre6P and a decrease in sucrose levels, which is consistent with the model of Tre6P-SnRK1 regulation of sucrose levels proposed by previous studies (Baena-Gonzalez and Lunn, 2020). *AtTPP1* can enhance *Arabidopsis* cold tolerance by accumulating soluble sugars and jasmonic acid. In this study, the expression level of this gene increased under low-temperature treatment, but it was not affected by *AhTPS9*. However, it resulted in higher levels of trehalose, suggesting that the upregulation of this gene's expression may be regulated by CBF genes (Lin et al., 2023). Overexpression of *AtTPS11* in *Arabidopsis* under low-temperature conditions significantly increased starch content (Singh et al., 2011). As an orthologous gene (Figure 1), *AhTPS9* similarly increased starch content in overexpressing plants under low-temperature conditions. However, soluble sugar accumulation in overexpressing plants was significantly higher than in the wild type under low-temperature conditions. Therefore, there are complex interactions between sugar metabolism-related genes in the trehalose pathway and cold tolerance, which require further detailed investigation.

5 Conclusion

Collectively, the current study identified 16 *AhTPS* and 17 *AhTPP* genes in the peanut genome through bioinformatics analysis. Phylogenetic analysis revealed two distinct subgroups closely related to wild diploid peanuts. Evolutionary patterns suggested gene segmental duplication events and robust purifying selection. Based on expression pattern analysis, *AhTPS9* exhibits the most significant differential expression under cold stress. Functional validation revealed that *Arabidopsis* plants overexpressing *AhTPS9* demonstrate enhanced cold tolerance by improving the photosynthetic system and regulating related products and genes involved in sugar metabolism.

Data availability statement

The original contributions presented in the study are included in the article/Supplementary Material. Further inquiries can be directed to the corresponding author.

Author contributions

CZ: Conceptualization, Data curation, Formal analysis, Funding acquisition, Investigation, Methodology, Writing – original draft, Writing – review & editing. ZH: Conceptualization, Data curation, Formal analysis, Investigation, Methodology, Writing – original draft, Writing – review & editing. YL: Data curation, Formal analysis, Investigation, Writing – review & editing. ZL: Data curation, Formal analysis, Investigation, Writing – review & editing. XW: Data curation, Formal analysis, Project administration, Supervision, Validation, Visualization, Writing – review & editing. CJ: Data curation, Formal analysis, Project administration, Supervision, Validation, Visualization, Writing – review & editing. SK: Data curation, Formal analysis, Project administration, Supervision, Validation, Visualization, Writing – review & editing. XL: Data curation, Formal analysis, Project administration, Supervision, Validation, Visualization, Writing – review & editing. SZ: Data curation, Formal analysis, Project administration, Supervision, Validation, Visualization, Writing – review & editing. JW: Data curation, Formal analysis, Project administration, Supervision, Validation, Visualization, Writing – review & editing. HZ: Data curation, Formal analysis, Project administration, Supervision, Validation, Visualization, Writing – review & editing. XZ: Data curation, Formal analysis, Project administration, Supervision, Validation, Visualization, Writing – review & editing. HY: Funding acquisition, Resources, Supervision, Validation, Visualization, Writing – review & editing.

Funding

The author(s) declare financial support was received for the research, authorship, and/or publication of this article. This study was supported by the earmarked fund for CARS-13, Liaoning Provincial Natural Science Foundation (2023-MS-214), Liaoning Revitalization Talents Program (XLYC1902002), and Science and Technology Program of Shenyang (No. 21–110-3–17), (No. 23-410-2-08).

Conflict of interest

The authors declare that the research was conducted in the absence of any commercial or financial relationships that could be construed as a potential conflict of interest.

Publisher's note

All claims expressed in this article are solely those of the authors and do not necessarily represent those of their affiliated organizations, or those of the publisher, the editors and the reviewers. Any product that may be evaluated in this article, or claim that may be made by its manufacturer, is not guaranteed or endorsed by the publisher.

Supplementary material

The Supplementary Material for this article can be found online at: https://www.frontiersin.org/articles/10.3389/fpls.2023.1343402/full#supplementary-material

References

Aubourg, S., Lecharny, A., and Bohlmann, J. (2002). Genomic analysis of the terpenoid synthase (*AtTPS*) gene family of *Arabidopsis thaliana*. *Mol. Genet. Genomics* 267, 730–745. doi: 10.1007/s00438-002-0709-y

Baena-Gonzalez, E., and Lunn, J. E. (2020). SnRK1 and trehalose 6-phosphate–two ancient pathways converge to regulate plant metabolism and growth. *Curr. Opin. Plant Biol.* 55, 52–59. doi: 10.1016/j.pbi.2020.01.010

Bajji, M., Kinet, J.-M., and Lutts, S. (2002). The use of the electrolyte leakage method for assessing cell membrane stability as a water stress tolerance test in durum wheat. *Plant Growth Regul.* 36, 61–70. doi: 10.1023/A:1014732714549

Bertioli, D. J., Cannon, S. B., Froenicke, L., Huang, G., Farmer, A. D., Cannon, E. K., et al. (2016). The genome sequences of *Arachis duranensis* and *Arachis ipaensis*, the diploid ancestors of cultivated peanut. *Nat. Genet.* 48 (4), 438–446. doi: 10.1038/ng.3517

Bertioli, D. J., Jenkins, J., Clevenger, J., Dudchenko, O., Gao, D., Seijo, G., et al. (2019). The genome sequence of segmental allotetraploid peanut Arachis hypogaea. *Nat. Genet.* 51 (5), 877–884. doi: 10.1038/s41588-019-0405-z

Bhat, K. A., Mahajan, R., Pakhtoon, M. M., Urwat, U., Bashir, Z., Shah, A. A., et al. (2022). Low temperature stress tolerance: An insight into the omics approaches for legume crops. *Front. Plant Sci.* 13. doi: 10.3389/fpls.2022.888710

Cannon, S. B., Mitra, A., Baumgarten, A., Young, N. D., and May, G. (2004). The roles of segmental and tandem gene duplication in the evolution of large gene families in *Arabidopsis thaliana*. *BMC Plant Biol.* 4 (1), 1–21. doi: 10.1186/1471-2229-4-10

Chary, S. N., Hicks, G. R., Choi, Y. G., Carter, D., and Raikhel, N. V. (2008). Trehalose-6-phosphate synthase/phosphatase regulates cell shape and plant architecture in *Arabidopsis*. *Plant Physiol.* 146 (1), 97–107. doi: 10.1104/pp.107.107441

Chen, C., Chen, H., Zhang, Y., Thomas, H. R., Frank, M. H., He, Y., et al. (2020). TBtools: an integrative toolkit developed for interactive analyses of big biological data. *Mol. Plant* 13 (8), 1194–1202. doi: 10.1016/j.molp.2020.06.009

Chen, N., Yang, Q., Hu, D., Pan, L., Chi, X., Chen, M., et al. (2014). Gene expression profiling and identification of resistance genes to low temperature in leaves of peanut (*Arachis hypogaea* L.). *Sci. Hortic.* 169, 214–225. doi: 10.1016/j.scienta.2014.01.043

Chen, X., Lu, Q., Liu, H., Zhang, J., Hong, Y., Lan, H., et al. (2019). Sequencing of cultivated peanut, *Arachis hypogaea*, yields insights into genome evolution and oil improvement. *Mol. Plant* 12 (7), 920–934. doi: 10.1016/j.molp.2019.03.005

Clevenger, J., Chu, Y., Scheffler, B., and Ozias-Akins, P. (2016). A developmental transcriptome map for allotetraploid *Arachis hypogaea*. *Front. Plant Sci.* 7. doi: 10.3389/fpls.2016.01446

Clough, S. J., and Bent, A. F. (1998). Floral dip: a simplified method for Agrobacterium-mediated transformation of Arabidopsis thaliana. *The plant journal,* 16 (6), 753–743. doi: 10.1046/j.1365-313x.1998.00343.x

Cortina, C., and Culiáñez-Macià, F. A. (2005). Tomato abiotic stress enhanced tolerance by trehalose biosynthesis. *Plant Sci.* 169 (1), 75–82. doi: 10.1016/j.plantsci.2005.02.026

Dan, Y., Niu, Y., Wang, C., Yan, M., and Liao, W. (2021). Genome-wide identification and expression analysis of the trehalose-6-phosphate synthase (*TPS*) gene family in cucumber (Cucumis sativus L.). *PeerJ* 9, e11398. doi: 10.7717/peerj.11398

Dijken, A., Schluepmann, H., and Smeekens, S. C. (2004). *Arabidopsis* trehalose-6-phosphate synthase 1 is essential for normal vegetative growth and transition to flowering. *Plant Physiol.* 135 (2), 969–977. doi: 10.1104/pp.104.039743

Du, L., Li, S., Ding, L., Cheng, X., Kang, Z., and Mao, H. (2022). Genome-wide analysis of trehalose-6-phosphate phosphatases (*TPP*) gene family in wheat indicates their roles in plant development and stress response. *BMC Plant Biol.* 22 (1), 120. doi: 10.1186/s12870-022-03504-0

Eastmond, P. J., and Graham, I. A. (2003). Trehalose metabolism: a regulatory role for trehalose-6-phosphate? *Curr. Opin. Plant Biol.* 6 (3), 231–235. doi: 10.1016/S1369-5266(03)00037-2

Elbein, A. D., Pan, Y., Pastuszak, I., and Carroll, D. (2003). New insights on trehalose: a multifunctional molecule. *Glycobiology* 13 (4), 17R–27R. doi: 10.1093/glycob/cwg047

Emanuelle, S., Doblin, M. S., Stapleton, D. I., Bacic, A., and Gooley, P. R. (2016). Molecular insights into the enigmatic metabolic regulator, SnRK1. *Trends Plant Sci.* 21 (4), 341–353. doi: 10.1016/j.tplants.2015.11.001

Fernandez, O., Béthencourt, L., Quero, A., Sangwan, R. S., and Clément, C. (2010). Trehalose and plant stress responses: friend or foe? *Trends Plant Sci.* 15 (7), 409–417. doi: 10.1016/j.tplants.2010.04.004

Fichtner, F., and Lunn, J. E. (2021). The role of trehalose 6-phosphate (Tre6P) in plant metabolism and development. *Annu. Rev. Plant Biol.* 72, 737–760. doi: 10.1146/annurev-arplant-050718-095929

Fichtner, F., Olas, J. J., Feil, R., Watanabe, M., Krause, U., Hoefgen, R., et al. (2020). Functional features of TREHALOSE-6-PHOSPHATE SYNTHASE1, an essential enzyme in *Arabidopsis*. *Plant Cell* 32 (6), 1949–1972. doi: 10.1105/tpc.19.00837

Figueroa, C. M., and Lunn, J. E. (2016). A tale of two sugars: trehalose 6-phosphate and sucrose. *Plant Physiol.* 172 (1), 7–27. doi: 10.1104/pp.16.00417

Garg, A. K., Kim, J.-K., Owens, T. G., Ranwala, A. P., Choi, Y. D., Kochian, L. V., et al. (2002). Trehalose accumulation in rice plants confers high tolerance levels to different abiotic stresses. *Proc. Natl. Acad. Sci.* 99 (25), 15898–15903. doi: 10.1073/pnas.252637799

Ge, L. F., Chao, D. Y., Shi, M., Zhu, M. Z., Gao, J.-P., and Lin, H. X. (2008). Overexpression of the trehalose-6-phosphate phosphatase gene *OsTPP1* confers stress tolerance in rice and results in the activation of stress responsive genes. *Planta* 228, 191–201. doi: 10.1007/s00425-008-0729-x

Hassan, M. U., Nawaz, M., Shah, A. N., Raza, A., Barbanti, L., Skalicky, M., et al. (2023). Trehalose: a key player in plant growth regulation and tolerance to abiotic stresses. *J. Plant Growth Regul.* 42 (8), 4935–4957. doi: 10.1007/s00344-022-10851-7

Huang, K., and Rieseberg, L. H. (2020). Frequency, origins, and evolutionary role of chromosomal inversions in plants. *Front. Plant Sci.* 11. doi: 10.3389/fpls.2020.00296

Iordachescu, M., and Imai, R. (2008). Trehalose biosynthesis in response to abiotic stresses. *J. Integr. Plant Biol.* 50 (10), 1223–1229. doi: 10.1111/j.1744-7909.2008.00736.x

Kakani, V., Prasad, P., Craufurd, P., and Wheeler, T. (2002). Response of in *vitro* pollen germination and pollen tube growth of groundnut (*Arachis hypogaea* L.) genotypes to temperature. *Plant. Cell Environ.* 25 (12), 1651–1661. doi: 10.1046/j.1365-3040.2002.00943.x

Kandror, O., DeLeon, A., and Goldberg, A. L. (2002). Trehalose synthesis is induced upon exposure of Escherichia coli to cold and is essential for viability at low temperatures. *Proc. Natl. Acad. Sci.* 99 (15), 9727–9732. doi: 10.1073/pnas.142314099

Karim, S., Aronsson, H., Ericson, H., Pirhonen, M., Leyman, B., Welin, B., et al. (2007). Improved drought tolerance without undesired side effects in transgenic plants producing trehalose. *Plant Mol. Biol.* 64, 371–386. doi: 10.1007/s11103-007-9159-6

Kaul, S., Koo, H. L., Jenkins, J., Rizzo, M., and Rooney, T. (2000). Analysis of the genome sequence of the flowering plant *Arabidopsis thaliana*. *nature* 408 (6814), 796–815. doi: 10.1038/35048692

Kidokoro, S., Shinozaki, K., and Yamaguchi-Shinozaki, K. (2022). Transcriptional regulatory network of plant cold-stress responses. *Trends Plant Sci* 27, 922-935. doi: 10.1016/j.tplants.2022.01.008

Kosar, F., Akram, N. A., Sadiq, M., Al-Qurainy, F., and Ashraf, M. (2019). Trehalose: a key organic osmolyte effectively involved in plant abiotic stress tolerance. *J. Plant Growth Regul.* 38, 606–618. doi: 10.1007/s00344-018-9876-x

Kovi, M. R., Ergon, Å., and Rognli, O. A. (2016). Freezing tolerance revisited—effects of variable temperatures on gene regulation in temperate grasses and legumes. *Curr. Opin. Plant Biol.* 33, 140–146. doi: 10.1016/j.pbi.2016.07.006

Krasensky, J., Broyart, C., Rabanal, F. A., and Jonak, C. (2014). The redox-sensitive chloroplast trehalose-6-phosphate phosphatase AtTPPD regulates salt stress tolerance. *Antioxid. Redox Signaling* 21 (9), 1289–1304. doi: 10.1089/ars.2013.5693

Krishna, G., Singh, B. K., Kim, E. K., Morya, V. K., and Ramteke, P. W. (2015). Progress in genetic engineering of peanut (*Arachis hypogaea* L.)—A review. *Plant Biotechnol. J.* 13 (2), 147–162. doi: 10.1111/pbi.12339

Leyman, B., Van Dijck, P., and Thevelein, J. M. (2001). An unexpected plethora of trehalose biosynthesis genes in *Arabidopsis thaliana*. *Trends Plant Sci.* 6 (11), 510–513. doi: 10.1016/S1360-1385(01)02125-2

Li, P., Ma, S., and Bohnert, H. J. (2008). Coexpression characteristics of trehalose-6-phosphate phosphatase subfamily genes reveal different functions in a network context. *Physiol. Plant.* 133 (3), 544–556. doi: 10.1111/j.1399-3054.2008.01101.x

Li, H. W., Zang, B. S., Deng, X. W., and Wang, X. P. (2011). Overexpression of the trehalose-6-phosphate synthase gene *OsTPS1* enhances abiotic stress tolerance in rice. *Planta* 234, 1007–1018. doi: 10.1007/s00425-011-1458-0

Lin, Q., Wang, J., Gong, J., Zhang, Z., Wang, S., Sun, J., et al. (2023). The Arabidopsis thaliana trehalose-6-phosphate phosphatase gene *AtTPPI* improve chilling tolerance through accumulating soluble sugar and JA. *Environ. Exp. Bot.* 205, 105117. doi: 10.1016/j.envexpbot.2022.105117

Lin, Q., Yang, J., Wang, Q., Zhu, H., Chen, Z., Dao, Y., et al. (2019). Overexpression of the trehalose-6-phosphate phosphatase family gene *AtTPPF* improves the drought tolerance of Arabidopsis thaliana. *BMC Plant Biol.* 19 (1), 1–15. doi: 10.1186/s12870-019-1986-5

Liu, X., Fu, L., Qin, P., Sun, Y., Liu, J., and Wang, X. (2019). Overexpression of the wheat trehalose 6-phosphate synthase 11 gene enhances cold tolerance in *Arabidopsis thaliana*. *Gene* 710, 210–217. doi: 10.1016/j.gene.2019.06.006

Liu, W., Zhang, H.-H., Long, Z.-X., Chi, X.-N., and Wang, Y.-P. (2023). Identification, evolutionary relationship analysis of the trehalose-6-phosphate synthase (*TPS)* gene family in common bean (*Phaseolus vulgaris)* and their expression in response to cold stress. *J. Plant Growth Regul.* 1-18. doi: 10.1007/s00344-023-11087-9

Lyu, J. I., Min, S. R., Lee, J. H., Lim, Y. H., Kim, J.-K., Bae, C.-H., et al. (2013). Overexpression of a trehalose-6-phosphate synthase/phosphatase fusion gene enhances tolerance and photosynthesis during drought and salt stress without growth aberrations in tomato. *Plant Cell. Tissue Organ Cult. (PCTOC).* 112, 257–262. doi: 10.1007/s11240-012-0225-7

Ma, S., Gong, Q., and Bohnert, H. J. (2007). An Arabidopsis gene network based on the graphical Gaussian model. *Genome Res.* 17 (11), 1614–1625. doi: 10.1101/gr.6911207

Mérot, C., Oomen, R. A., Tigano, A., and Wellenreuther, M. (2020). A roadmap for understanding the evolutionary significance of structural genomic variation. *Trends Ecol. Evol.* 35 (7), 561–572. doi: 10.1016/j.tree.2020.03.002

Nägele, T., and Heyer, A. G. (2013). Approximating subcellular organisation of carbohydrate metabolism during cold acclimation in different natural accessions of *Arabidopsis thaliana*. *New Phytol.* 198 (3), 777–787. doi: 10.1111/nph.12201

Nunes, C., Schluepmann, H., Delatte, T. L., Wingler, A., Silva, A. B., Fevereiro, P. S., et al. (2013). Regulation of growth by the trehalose pathway: relationship to temperature and sucrose. *Plant Signaling Behav.* 8 (12), e26626. doi: 10.4161/psb.26626

O'Hara, L. E., Paul, M. J., and Wingler, A. (2013). How do sugars regulate plant growth and development? New insight into the role of trehalose-6-phosphate. *Mol. Plant* 6 (2), 261–274. doi: 10.1093/mp/sss120

Oszvald, M., Primavesi, L. F., Griffiths, C. A., Cohn, J., Basu, S. S., Nuccio, M. L., et al. (2018). Trehalose 6-phosphate regulates photosynthesis and assimilate partitioning in reproductive tissue. *Plant Physiol.* 176 (4), 2623–2638. doi: 10.1104/pp.17.01673

Paul, M. J., Gonzalez-Uriarte, A., Griffiths, C. A., and Hassani-Pak, K. (2018). The role of trehalose 6-phosphate in crop yield and resilience. *Plant Physiol.* 177 (1), 12–23. doi: 10.1104/pp.17.01634

Paul, M., Pellny, T., and Goddijn, O. (2001). Enhancing photosynthesis with sugar signals. *Trends Plant Sci.* 6 (5), 197–200. doi: 10.1016/S1360-1385(01)01920-3

Paul, M. J., Primavesi, L. F., Jhurreea, D., and Zhang, Y. (2008). Trehalose metabolism and signaling. *Annu. Rev. Plant Biol.* 59, 417–441. doi: 10.1146/annurev.arplant.59.032607.092945

Pilon-Smits, E. A., Terry, N., Sears, T., Kim, H., Zayed, A., Hwang, S., et al. (1998). Trehalose-producing transgenic tobacco plants show improved growth performance under drought stress. *J. Plant Physiol.* 152 (4-5), 525–532. doi: 10.1016/S0176-1617(98)80273-3

Puppala, N., Nayak, S. N., Sanz-Saez, A., Chen, C., Devi, M. J., Nivedita, N., et al. (2023). Sustaining yield and nutritional quality of peanuts in harsh environments: Physiological and molecular basis of drought and heat stress tolerance. *Front. Genet.* 14. doi: 10.3389/fgene.2023.1121462

Raza, A., Charagh, S., Najafi-Kakavand, S., Abbas, S., Shoaib, Y., Anwar, S., et al. (2023). Role of phytohormones in regulating cold stress tolerance: physiological and molecular approaches for developing cold-smart crop plants. *Plant Stress* 100152. doi: 10.1016/j.stress.2023.100152

Schluepmann, H., Van Dijken, A., Aghdasi, M., Wobbes, B., Paul, M., and Smeekens, S. (2004). Trehalose mediated growth inhibition of *Arabidopsis* seedlings is due to trehalose-6-phosphate accumulation. *Plant Physiol.* 135 (2), 879–890. doi: 10.1104/pp.104.039503

Shi, G., and Cai, Q. (2009). Leaf plasticity in peanut (*Arachis hypogaea* L.) in response to heavy metal stress. *Environ. Exp. Bot.* 67 (1), 112–117. doi: 10.1016/j.envexpbot.2009.02.009

Singh, V., Louis, J., Ayre, B. G., Reese, J. C., and Shah, J. (2011). TREHALOSE PHOSPHATE SYNTHASE11-dependent trehalose metabolism promotes *Arabidopsis thaliana* defense against the phloem-feeding insect *Myzus persicae*. *Plant J.* 67 (1), 94–104. doi: 10.1111/j.1365-313X.2011.04583.x

Smeekens, S. (2015). From leaf to kernel: trehalose-6-phosphate signaling moves carbon in the field. *Plant Physiol.* 169 (2), 912–913. doi: 10.1104/pp.15.01177

Tamura, K., Stecher, G., and Kumar, S. (2021). MEGA11: molecular evolutionary genetics analysis version 11. *Mol. Biol. Evol.* 38 (7), 3022–3027. doi: 10.1093/molbev/msab120

Vandesteene, L., López-Galvis, L., Vanneste, K., Feil, R., Maere, S., Lammens, W., et al. (2012). Expansive evolution of the trehalose-6-phosphate phosphatase gene family in. *Arabidopsis. Plant Physiol.* 160 (2), 884–896. doi: 10.1104/pp.112.201400

Van Houtte, H., López-Galvis, L., Vandesteene, L., Beeckman, T., and Van Dijck, P. (2013). Redundant and non-redundant roles of the trehalose-6-phosphate phosphatases in leaf growth, root hair specification and energy-responses in *Arabidopsis*. *Plant Signaling Behav.* 8 (3), e23209. doi: 10.4161/psb.23209

Vishal, B., Krishnamurthy, P., Ramamoorthy, R., and Kumar, P. P. (2019). Os TPS 8 controls yield-related traits and confers salt stress tolerance in rice by enhancing suberin deposition. *New Phytol.* 221 (3), 1369–1386. doi: 10.1111/nph.15464

Vogel, G., Fiehn, O., Jean-Richard-dit-Bressel, L., Boller, T., Wiemken, A., Aeschbacher, R. A., et al. (2001). Trehalose metabolism in *Arabidopsis*: occurrence of trehalose and molecular cloning and characterization of trehalose-6-phosphate synthase homologues. *J. Exp. Bot.* 52 (362), 1817–1826. doi: 10.1093/jexbot/52.362.1817

Wang, G., Li, X., Ye, N., Huang, M., Feng, L., Li, H., et al. (2021). *OsTPP1* regulates seed germination through the crosstalk with abscisic acid in rice. *New Phytol.* 230 (5), 1925–1939. doi: 10.1111/nph.17300

Wang, C. L., Zhang, S. C., Qi, S. D., Zheng, C. C., and Wu, C. A. (2016). Delayed germination of *Arabidopsis* seeds under chilling stress by overexpressing an abiotic stress inducible. *GhTPS11. Gene* 575 (2), 206–212. doi: 10.1016/j.gene.2015.08.056

Xue, Y., Wu, F., Chen, R., Wang, X., Inkabanga, A. T., Huang, L., et al. (2023). Genome-wide analysis of fatty acid desaturase genes in chia (*Salvia hispanica*) reveals their crucial roles in cold response and seed oil formation. *Plant Physiol. Biochem.* 199, 107737. doi: 10.1016/j.plaphy.2023.107737

Yeo, E. T., Kwon, H. B., Han, S. E., Lee, J. T., Ryu, J. C., and Byu, M. (2000). Genetic engineering of drought resistant potato plants by introduction of the trehalose-6-phosphate synthase (*TPS1*) gene from *Saccharomyces cerevisiae*. *Molecules. Cells* 10 (3), 263–268. doi: 10.1007/s11240-004-8124-1

Yuan, G., Liu, J., An, G., Li, W., Si, W., Sun, D., et al. (2021). Genome-wide identification and characterization of the trehalose-6-phosphate synthetase (*TPS*) gene family in watermelon (*Citrullus lanatus*) and their transcriptional responses to salt stress. *Int. J. Mol. Sci.* 23 (1), 276. doi: 10.3390/ijms23010276

Zang, B., Li, H., Li, W., Deng, X. W., and Wang, X. (2011). Analysis of trehalose-6-phosphate synthase (*TPS*) gene family suggests the formation of TPS complexes in rice. *Plant Mol. Biol.* 76, 507–522. doi: 10.1007/s11103-011-9781-1

Zhang, H., Dong, J., Zhao, X., Zhang, Y., Ren, J., Xing, L., et al. (2019). Research progress in membrane lipid metabolism and molecular mechanism in peanut cold tolerance. *Front. Plant Sci.* 10. doi: 10.3389/fpls.2019.00838

Zhang, H., Yu, Y., Wang, S., Yang, J., Ai, X., Zhang, N., et al. (2023). Genome-wide characterization of phospholipase D family genes in allotetraploid peanut and its diploid progenitors revealed their crucial roles in growth and abiotic stress responses. *Front. Plant Sci.* 14. doi: 10.3389/fpls.2023.1102200

Zhuang, W., Chen, H., Yang, M., Wang, J., Pandey, M. K., Zhang, C., et al. (2019). The genome of cultivated peanut provides insight into legume karyotypes, polyploid evolution and crop domestication. *Nat. Genet.* 51 (5), 865–876. doi: 10.1038/s41588-019-0402-2

frontiers | Frontiers in Plant Science

TYPE Original Research
PUBLISHED 07 February 2024
DOI 10.3389/fpls.2024.1354249

OPEN ACCESS

EDITED BY
Hui Song,
Qingdao Agricultural University, China

REVIEWED BY
Zhaokui Du,
Taizhou University, China
Xinwei Xu,
Wuhan University, China

*CORRESPONDENCE
Qiuxia Chen
yzscqx@163.com
Jinwang Wang
wangjw@zaas.ac.cn

RECEIVED 12 December 2023
ACCEPTED 15 January 2024
PUBLISHED 07 February 2024

CITATION
Liu H, An X, Liu X, Yang S, Liu Y, Wei X, Li X, Chen Q and Wang J (2024) Molecular mechanism of salinity and waterlogging tolerance in mangrove *Kandelia obovata*. *Front. Plant Sci.* 15:1354249. doi: 10.3389/fpls.2024.1354249

Molecular mechanism of salinity and waterlogging tolerance in mangrove *Kandelia obovata*

Huizi Liu[1], Xia An[2], Xing Liu[1], Sheng Yang[1], Yu Liu[1], Xin Wei[1], Xiaowen Li[1], Qiuxia Chen[1*] and Jinwang Wang[1*]

[1]Zhejiang Institute of Subtropical Crops, Zhejiang Academy of Agricultural Sciences, Wenzhou, China, [2]Zhejiang Xiaoshan Institute of Cotton and Bast Fiber Crops, Zhejiang Institute of Landscape Plants and Flowers, Zhejiang Academy of Agricultural Sciences, Hangzhou, China

Mangrove forests are colloquially referred to as “Earth’s kidneys” and serve many important ecological and commercial functions. Salinity and waterlogging stress are the most important abiotic stressors restricting the growth and development of mangroves. *Kandelia obovata (K. obovata)* is the greatest latitudinally-distributed salt mangrove species in China.Here, morphology and transcriptomics were used to study the response of *K. obovata* to salt and waterlogging stress. In addition, weighted gene co-expression network analysis of the combined gene expression and phenotypic datasets was used to identify core salinity- and waterlogging-responsive modules. In this study, we observed that both high salinity and waterlogging significantly inhibited growth and development in *K. obovata.* Notably, growth was negatively correlated with salt concentration and positively correlated with waterlogging duration, and high salinity was significantly more inhibitive than waterlogging. A total of 7, 591 salt-responsive and 228 waterlogging-responsive differentially expressed genes were identified by RNA sequencing. Long-term salt stress was highly correlated with the measured physiological parameters while long-term waterlogging was poorly correlated with these traits. At the same time, 45 salinity-responsive and 16 waterlogging-responsive core genes were identified. All 61 core genes were mainly involved in metabolic and biosynthesis of secondary metabolites pathways. This study provides valuable insight into the molecular mechanisms of salinity and waterlogging tolerance in *K. obovata,* as well as a useful genetic resource for the improvement of mangrove stress tolerance using molecular breeding techniques.

KEYWORDS

***Kandelia obovata*, salt stress, waterlogging stress, transcriptomic analysis, weighted gene co-expression network**

Introduction

Mangroves are unique bionetworks of halophytic trees, shrubs, and other woody plants, which develop in tidal zones along tropical and subtropical coastlines (Parida and Jha, 2010; Bai et al., 2021). Mangroves thrive in inhospitable environments and serve unique ecological functions such as purifying water, protecting coastlines, and providing breeding habitats, and they are considered to be one of the most important blue carbon ecosystems (Costanza et al., 1997; Duke et al., 2007; Parida and Jha, 2010; Donato et al., 2011; Alongi, 2014; Lee et al., 2014; Lovelock and Duarte, 2019). Mangrove dispersal is affected by temperature and ocean currents at the global and regional scales, and salinity and flooding duration at the estuarine and intertidal scales (Srikanth et al., 2016). Salinity and flooding are the primary abiotic stressors restricting the growth and development of mangroves. However, our understanding of how mangrove plants respond to harsh environmental conditions at the molecular level is incomplete.

Flooding is often an accompaniment to natural disasters, and the resulting waterlogging of the soil creates a low-oxygen environment that affects plant growth and development (Loreti et al., 2016; Klumb et al., 2017). Mangrove plants have evolved several adaptations to flooding stress, including the development of various types of air roots such as pillar roots, geniculate roots, surface roots, plate roots, and respiratory roots (McKee, 1993; Alongi, 2009; Srikanth et al., 2016). During the formation of air roots, the parenchyma cells gradually disintegrate as the air cavity is enlarged, and the degree of aerated tissue development is positively correlated with the ability to withstand flooding (Curran et al., 1996; Allaway et al., 2001; Chen et al., 2004; Srikanth et al., 2016). Additionally, mangroves and other plants exhibit an array of physiological and molecular responses to flooding stress. In the mangrove *Sonneratia apetala*, long-term waterlogging results in increased root porosity, cell wall lignification, and outer cortex iron plaque content (Cheng et al., 2015). In soybean seedlings, waterlogging decreases protein biosynthesis and lignin deposition in root and hypocotyl cell walls (Komatsu et al., 2010). In poplar, flooding downregulates the expression of 4CL, C4H, CCoAOMT, COMT, F5H, and PAL (Kreuzwieser et al., 2009). In addition, several families of transcription factors (TFs) play important roles in the flooding stress response, including NAC, MYB, and WRKY (Li et al., 2017; Dhungana et al., 2021; Yao, 2021). In rice, overexpression of *OsMYB2* reduces flooding-induced reactive oxygen species (ROS) accumulation, while overexpression of *OsDREB6*, *OsEREBP1*, *OsSNORKEL1*, and *OsSNORKEL2* promotes adaptation to waterlogging (Hattori et al., 2009; Yang et al., 2012; Ke et al., 2014; Jisha et al., 2015).

Salt stress negatively affects all aspects of plant growth and development, as well as the productivity of agroforestry operations and the quality of their products (Safdar et al., 2019; Vishal et al., 2019; Yaldiz and Camlica, 2021). Salt stress can depress growth rates and even lead to the cessation of growth altogether, as seen in rice (Hussain et al., 2017). While well known for providing mechanical support and transporting nutrients and water, roots also rapidly sense and respond to abiotic stressors such as high salinity, waterlogging, and drought (Overvoorde et al., 2010; Petricka et al., 2012; Czyzewicz et al., 2015; Jourquin et al., 2020). Notably, low concentrations of salt promote root growth in the mangroves *Bruguiera sexangula* var. *rhynchopetala* and *Kandelia obovata*, while high concentrations inhibit root growth (Shiau et al., 2017). In addition, salt stress can result in increased cork formation and root vacuole volume in mangroves (Werner and Stelzer, 1990; Parida and Jha, 2010). Woody plants have evolved an array of physiological and molecular mechanisms to adjust their growth and development under adverse conditions. One such mechanism involves the activation of salinity-responsive TFs, such as MYB, bZIP, and GRF (Kim et al., 2004; Ye et al., 2013; Jiang et al., 2018; Nguyen and Cheong, 2018; Wang et al., 2021; Li et al., 2023). Other salinity-responsive TFs have been reported in *Oryza sativa*, *Nicotiana tabacum*, *Solanum lycopersicum*, *Malus domestica*, *Manihot esculenta*, *Eucalyptus camaldulensis*, and *Betula platyphylla* (Liu et al., 2012; Wang et al., 2012; Zhu et al., 2018; Chen et al., 2019; Tran et al., 2019; Zou et al., 2008; Liu et al., 2024).

K. obovata is the most latitudinally distributed salt-excreting mangrove plant species in the Northern Hemisphere and has been widely used in coastal wetland ecological restoration (Zhao et al., 2021). Previous studies primarily focused on the changes in morphological structure, accumulation and migration of mineral ions, physiological characteristics, and gene level of *K. obovata* under a single stress factor (Krauss et al., 2008; Liu et al., 2023). In this study, we evaluated the structural and morphological characteristics of *K. obovata* roots under multiple stress factors, including high salinity and waterlogging stress. In addition, we performed RNA sequencing (RNA-seq) and weighted gene co-expression network analysis (WGCNA) to correlate the phenotypic data with gene expression patterns. We extracted gene modules directly related to salt and waterlogging stress and then constructed co-expression networks to discover core TFs and hub genes. We preliminarily identified the regulatory pathway where the core genes are located. This is the first study to identify the key gene network responsive to high salinity and flooding in *K. obovata*. The results presented here will provide a theoretical basis for future studies of the molecular mechanisms underlying the plant abiotic stress response.

Materials and methods

Plant materials and stress treatment

All experiments were performed using *K. obovata* hypocotyls collected from the germplasm resource garden located along the Aojiang River (China). All hypocotyl samples were free of pests and diseases, well-developed, and of similar age. The hypocotyls were planted at a depth of 10 cm in a simulation trough filled with silt from the Aojiang River to a depth of 30 cm and cultivated at 21°C–25°C. Experimental plants were subjected to high salinity and waterlogging stress for 6 months prior to analysis. Experimental *K. obovata* plants were subjected to up to 6 months of stress treatment, including high salinity (NaCl; 10‰, 20‰, and 30‰), waterlogging (WL; 3 h, 6 h, and 9 h of flooding), and high salinity–waterlogging (NaCl + WL). Details of the stress tests are shown in Supplementary Table 1. Control plants were not subjected to any stressors. Following treatment, the survival rate was calculated.

Morphological analysis

After 6 months of stress treatment, the plants were carefully harvested to avoid root damage and washed. Leaf and root growth was evaluated using a LA2400 scanner and analyzed using WinRHIZO (Regent Instruments, Québec, QC, Canada). Stem length was measured using a meter stick and averaged. Electronic weighing scales were used to measure the fresh weights of whole plants, roots, stems, leaves, and hypocotyls. To measure the dry weight, whole plants, roots, stems, leaves, and hypocotyls were separately dried to a constant weight in a 60°C forced-air oven.

RNA extraction and sequencing

Using the RNA extracted from root tissues, RNA-seq was performed to identify genes responsive to high salinity and waterlogging. The total RNA was extracted using a Qiagen RNeasy Mini Kit (Qiagen, Hilden, Germany) following Lin et al. (2013; 2014). RNA-seq libraries were constructed using a NEBNext Ultra II RNA library preparation kit. Libraries were constructed for the control (no stress), NaCl (10‰, 20‰, and 30‰), and WL (3 h, 6 h, and 9 h of flooding) treatments, with three biological replicates per sample. A total of 16 libraries were sequenced using an Illumina HiSeq4000 platform, obtaining paired-end reads with an average length of 150 bp. After removing library index sequences, the clean reads were mapped to the *K. obovata* genome (GWHACBH00000000.1; Genome Warehouse; https://ngdc.cncb.ac.cn/gwh/jbrowse/index) using Bowtie2 (Langmead and Salzberg, 2012). The raw counts were quantified and normalized following an established analysis pipeline (Lin et al., 2013). Differentially expressed genes (DEGs) were identified using DEseq2 (Love et al., 2014), with a false discovery rate (FDR) < 0.05. The raw sequencing data were deposited in the National Center for Biotechnology Information (NCBI) database under accession numbers PRJNA1051648 (waterlogging) and PRJNA1051781 (high salinity).

Weighted gene co-expression network analysis

WGCNA was carried out according to an established protocol (Langfelder and Horvath, 2008). Briefly, WGCNA is a method to analyze the gene expression patterns of multiple samples. According to the concept of scale-free network distribution, the correlation coefficients of the expression matrix are weighted so that highly coevolutionary genes can be allocated to the same gene cluster within the whole network. Then, whole genes can be allocated to multiple modules.

Statistical analysis

Student's *t*-tests were carried out using SPSS software (v.19.0) to determine statistically significant differences between treatments (*$p < 0.05$; **$p < 0.01$).

Results

High salinity and waterlogging reduce growth in *K. obovata*

Exposure to high salinity, waterlogging, and high salinity–waterlogging significantly impacted the root and leaf characteristics of *K. obovata* (Figure 1). Compared to control plants, all stress-exposed plants exhibited stunted growth and reduced root length, and the mean projected areas of individual roots and leaves were negatively correlated with salt concentration (Figure 1). Notably, growth inhibition gradually weakened with increased waterlogging duration (Figures 1B–D). In addition, the magnitude of the negative effects varied with different combinations of salt concentration and waterlogging duration. For example, the most optimal combination was 10‰ NaCl + 6-h waterlogging, while the least optimal was 30‰ NaCl + 9-h waterlogging (Figures 1B–D). Exposure to high salinity–waterlogging tended to result in significantly worse growth outcomes than exposure to high salinity or waterlogging separately (Figure 1). For example, exposure to high salinity and high salinity–waterlogging decreased root length by 17.2%–79.8% and 28.7%–81.6%, respectively, while exposure to waterlogging alone reduced root length by only 17.2%–39.7% (Figure 1B). Similar trends were observed in both surface area and volume (Supplementary Figure 1). These results suggest that exposure to high salinity has a more significant impact on the growth of *K. obovata* than exposure to waterlogging.

High salinity and waterlogging reduce biomass production in *K. obovata*

The accumulation of biomass in *K. obovata* plants exposed to high salinity and waterlogging was further evaluated. Overall, stress exposure significantly inhibited biomass production (Figure 2). Notably, the degree of biomass reduction was positively correlated with salt concentration and negatively correlated with flooding time (Figure 2). Biomass production was particularly inhibited in the combined high salinity–waterlogging treatment and also inhibited by high salinity under all waterlogging durations (Figure 2). Compared with control plants, exposure to high salinity, waterlogging, and high salinity–waterlogging reduced the fresh weight of *K. obovata* plants by 21.9%–65.4%, 5.9%–52.9%, and 22.3%–64.9%, respectively (Figure 2A). The same trend was observed for dry weight (Figure 2B). Consistent with the phenotypic results, the optimal combination was found to be 10‰ NaCl + 6-h waterlogging (Figure 2). Biomass inhibition was observed in all tested tissues before greenhouse trees were harvested for analysis (Supplementary Figure 2). In general, exposure to high salinity resulted in a greater reduction in plant biomass than exposure to waterlogging.

10.3389/fpls.2024.1354249

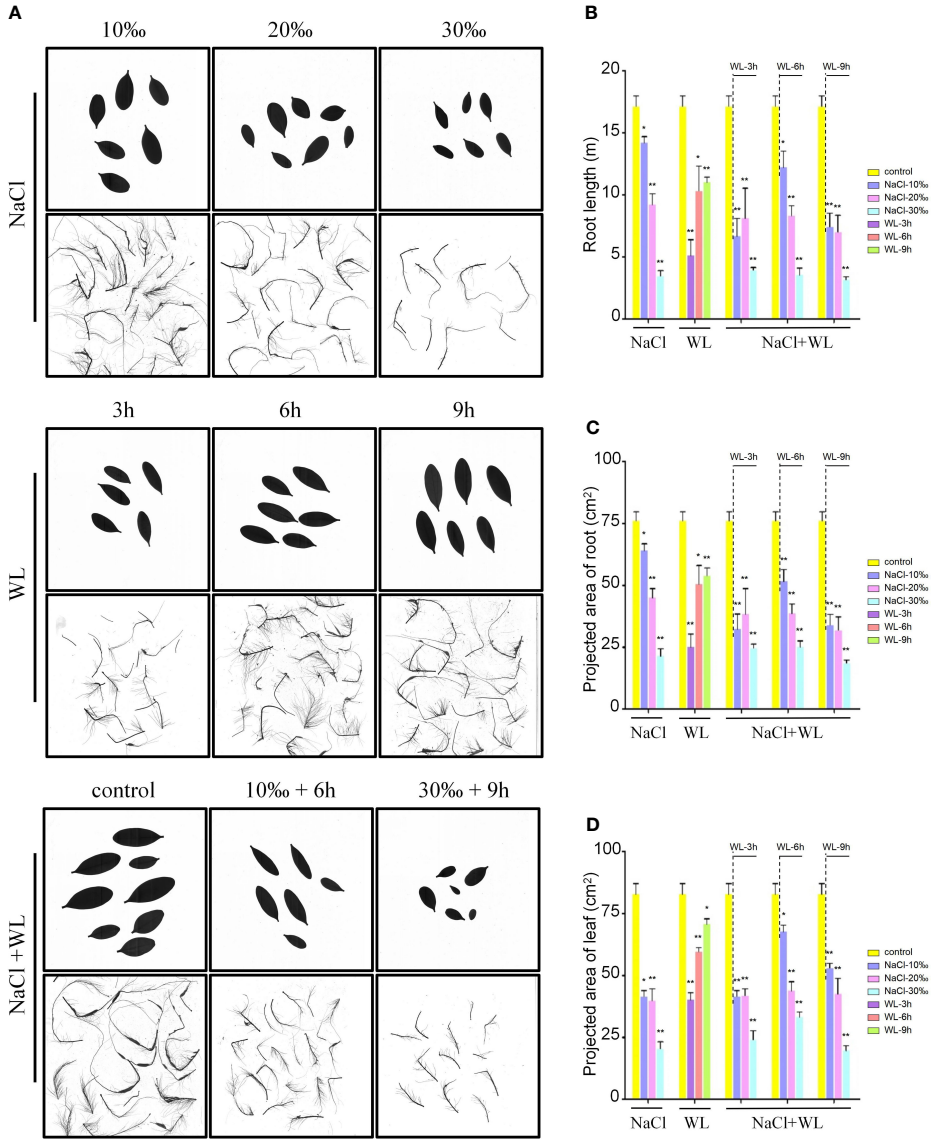

FIGURE 1
The effects of exposure to high salinity and waterlogging on the growth characteristics of *Kandelia obovata*. Growth performance was analyzed using 6-month-old soil-grown plants. **(A)** Photographs of representative roots and leaves. Bars = 10 cm. **(B–D)** Mean root length (m) **(B)** and mean projected area (cm^2) of individual roots **(C)** and leaves **(D)**. Error bars represent SEs of three independent experiments. *$p < 0.05$, **$p < 0.01$ (Student's *t*-test).

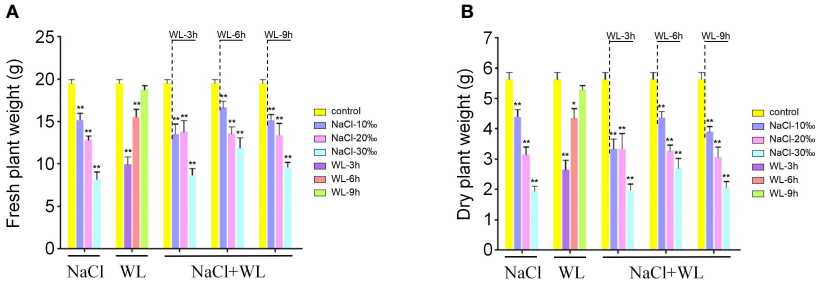

FIGURE 2
The effects of exposure to high salinity and waterlogging on biomass production in *Kandelia obovata*. **(A, B)** Mean fresh weight (g) **(A)** and mean dry weight (g) **(B)**. Error bars represent SEs of three biological replicates. *$p < 0.05$, **$p < 0.01$ (Student's *t*-test).

RNA sequencing results

After 6 months of treatment, RNA-seq was conducted on control plants (no stress) and experimental plants exposed to NaCl (10‰, 20‰, and 30‰) and WL (3 h, 6 h, and 9 h of flooding) to identify key salinity- and waterlogging-responsive genes. Eight RNA-seq libraries (three biological replicates per library) were sequenced for each stress treatment. In total, between 41.23 and 49.81 million clean reads representing between 6,107,823,135 and 7,320,824,121 bp were obtained (Supplementary Table 1). The N content of 6,397–11,917 single-ended sequencing reads was 2%–3% of the reading length (Supplementary Table 2). The base error rate was 2.95%–3.15%, the Q20 was 95.40%, the Q30 was 88.79%, and the guanine–cytosine (GC) content was between 44.77% and 45.31% (Supplementary Figure 3 and Supplementary Table 2). Pearson's correlation coefficients were calculated using R and indicated that the three replicates for each treatment exhibited high reproducibility (Supplementary Figure 4). Overall, these results suggest that the RNA-seq data were suitable for further analysis.

Salinity- and waterlogging-responsive genes in *K. obovata*

In total, we identified 7,591 DEGs across all high-salinity treatments (p-value < 0.05; Figure 3A; Supplementary Table 3). Notably, the number of DEGs increased with increasing salt concentration, with 1,297 DEGs (1,139 upregulated and 158 downregulated) identified under 10‰ NaCl, 2,129 DEGs (1,630 upregulated and 499 downregulated) identified under 20‰ NaCl, and 4,165 DEGs (2,240 upregulated and 1,925 downregulated) identified under 30‰ NaCl (Figures 3A, B; Supplementary Table 3). Of the 7,591 total identified DEGs, 400 were common to all high-salinity treatments, including genes encoding TFs (Figure 3A).

In addition, 228 DEGs were induced in response to waterlogging (p-value <0.05; Figure 3C; Supplementary Table 3). Among these, 87 DEGs (36 upregulated and 51 downregulated) were identified after 3-h waterlogging, 80 DEGs (33 upregulated and 47 downregulated) were identified after 6-h waterlogging, and 61 DEGs (39 upregulated and 22 downregulated) were identified after 9-h waterlogging (Figure 3D; Supplementary Table 3). Only 18 common DEGs were identified among waterlogging treatments (Figure 3C). In accordance with the phenotypic results, exposure to high salinity had a more significant impact on gene expression in *K. obovata* than exposure to waterlogging.

Principal component analysis

Inter-group differences and intra-group sample duplication were evaluated by principal component analysis (PCA). Overall, genes tended to cluster according to salt concentration, indicating that gene expression was specific to different levels of salinity stress (Figure 4A). In addition, the different waterlogging treatments could be separated, albeit with somewhat less specificity (Figure 4B). The results of the RNA-seq correlation analysis were similar: different salt concentrations showed good separation, with greater differences in concentration resulting in more pronounced separation (Supplementary Figure 4A). However, Pearson's correlation coefficients were not significantly different between different waterlogging durations (Supplementary Figure 4B). Once again, it appears that high salinity has a greater impact on growth than waterlogging in *K. obovata*.

Weighted gene co-expression network analysis of salinity-responsive gene modules

We performed a WGCNA of all DEGs to explore the effect of different salt stress concentrations. Overall, the genes were grouped into six co-expression modules according to their pairwise correlation evaluation (Figures 5A, B), and each set of highly correlated genes corresponds to a branch on the tree (Figure 5A). We observed high topological overlap between genes within the same module. A cluster visualization analysis of salinity-responsive mRNA expression indicated that genes within each module are independent of each other, highlighting the high degree of independence between modules and the relative independence of gene expression within each module (Figure 5B). The turquoise module contained the greatest number of eigengenes (2331). With the exception of the gray modules (which contained genes that did not fit into any one module), the red module contained the fewest eigengenes (257) (Supplementary Figure 5A). To identify the co-expression modules highly correlated with salinity tolerance, we performed a correlation with the 17 measured phenotypic traits. The blue and yellow modules were significantly associated with all phenotypic characteristics, with correlation coefficients ranging from 0.65 to 0.95 (Figure 5C). These results suggest that the eigengenes within these two modules are likely involved in salinity tolerance in *K. obovata*.

Weighted gene co-expression network analysis of waterlogging-responsive gene modules

We performed a WGCNA of all DEGs to explore the effect of different waterlogging durations. Overall, we grouped the genes into five co-expression modules according to their pairwise correlation evaluation (Figures 6A, B). Cluster visualization analysis showed high levels of interdependence between modules and the relative independence of gene expression within each module (Figure 6B). The turquoise module contained the greatest number of eigengenes (96), and the green module contained the fewest (7) (Supplementary Figure 5B). We performed a correlation with the 17 measured phenotypic traits and found that the turquoise module was highly correlated with trait 7 (root volume) and trait 15 (dry root weight) (Figure 6C). These results suggest that the eigengenes within this module are likely involved in waterlogging tolerance in *K. obovata*.

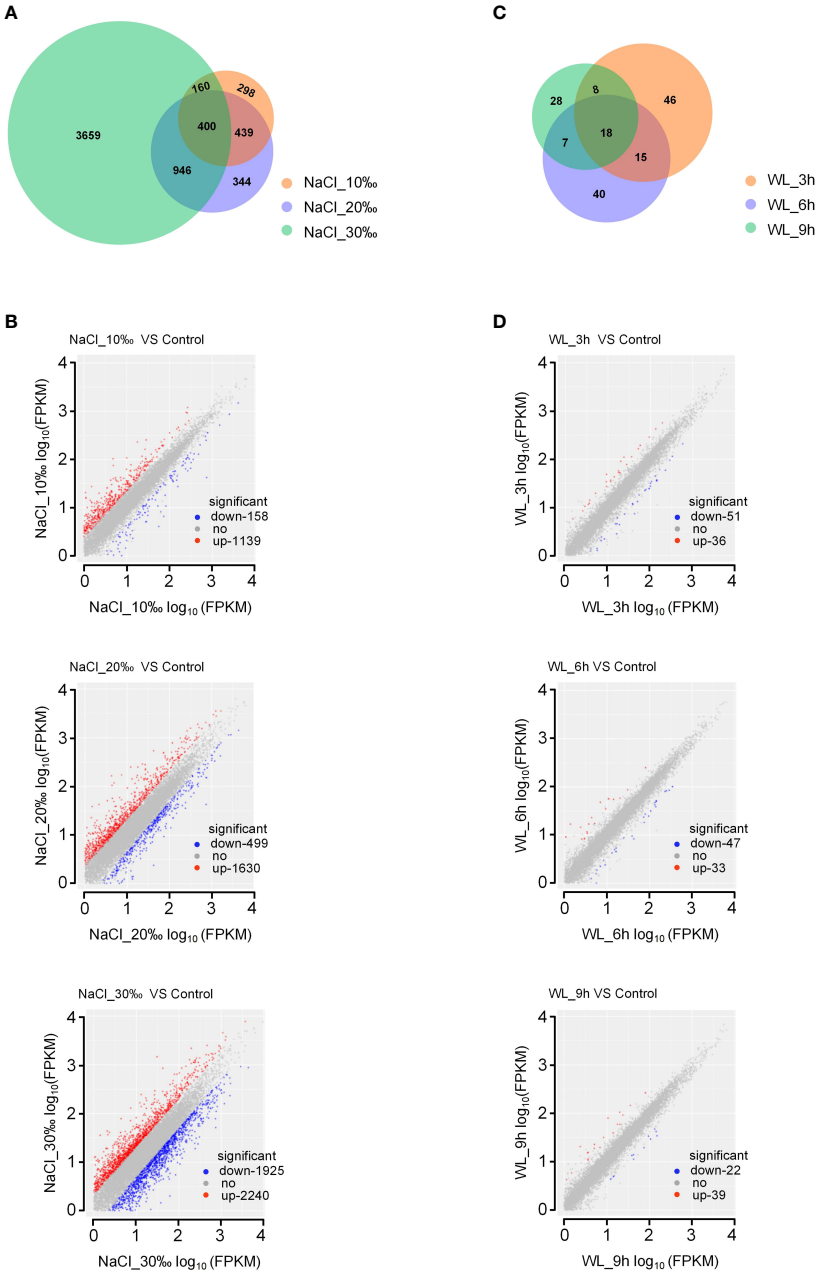

FIGURE 3
Differentially expressed genes in *Kandelia obovata* exposed to high salinity and waterlogging. **(A, C)** Venn diagrams of salinity-responsive **(A)** and waterlogging-responsive **(C)** differentially expressed genes. **(B, D)** Scatter plots of salinity-responsive **(B)** and waterlogging-responsive **(D)** differentially expressed genes.

Functional prediction of salinity- and waterlogging-responsive modules

The key modules identified in the WGCNA were subjected to Gene Ontology (GO) functional enrichment analysis. Figures 7A, B summarize the GO enrichment analysis results for the salinity-responsive MEblue and MEyellow modules. The MEblue module was the most significantly enriched in the response to abiotic stimulus (GO:0009628), organic acid biosynthetic process (GO:0016053), and carboxylic acid biosynthetic process (GO:0046394) biological processes (BPs); the membrane part (GO:0044425), intrinsic component of membrane (GO:0031224), and integral component of membrane (GO:0016021) cellular components (CCs); and the protein binding (GO:0005515), nucleic acid binding transcription factor activity (GO:0001071), and transcription factor activity, sequence-specific DNA binding (GO:0003700) molecular functions (MFs) (Figure 7A). The MEyellow module was the most significantly enriched in the single-organism process (GO:0044699), single-organism cellular process (GO:0044763), and carbohydrate metabolic process (GO:0005975) BPs; the intrinsic component of membrane (GO:0031224), integral component of membrane (GO:0016021),

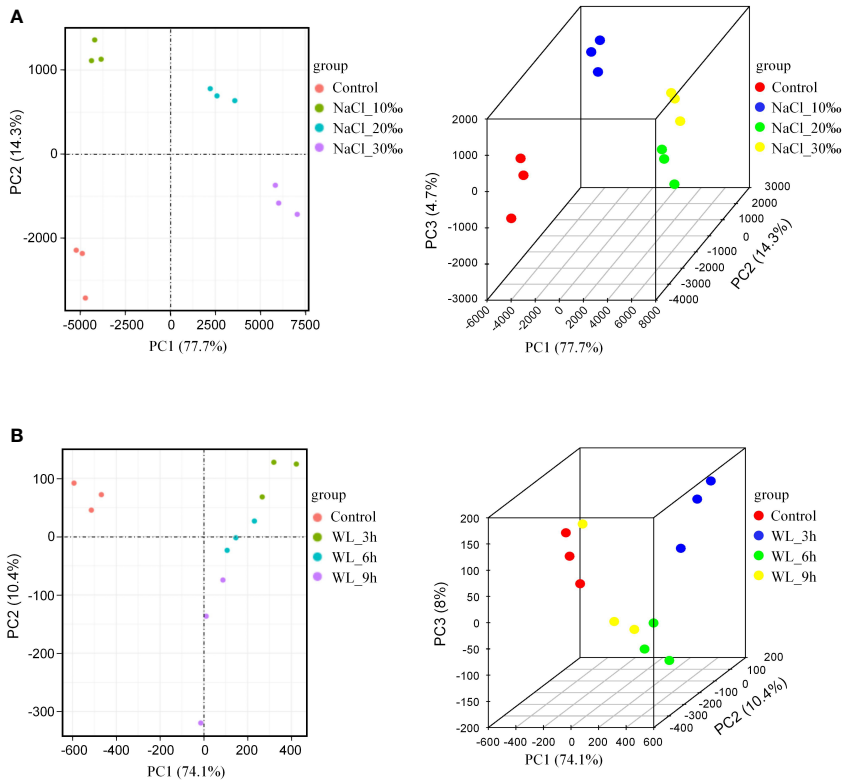

FIGURE 4
Principal component analysis (PCA). **(A)** PCA of salt stress treatment shown in 2D (left) and 3D (right). **(B)** PCA of waterlogging stress treatment shown in 2D (left) and 3D (right). PC1 is the most influential factor affecting variation, PC2 is the second, and PC3 is the third.

and cell periphery (GO:0071944) CCs; and the catalytic activity (GO:0003824), oxidoreductase activity (GO:0016491), and transporter activity (GO:0005215) MFs (Figure 7B). Overall, eigengenes in both modules were related to plant abiotic stress response, indicating that these genes likely play a role in salinity tolerance in *K. obovata*.

Figure 7C summarizes the GO enrichment analysis results for the waterlogging-responsive MEturquoise module. The MEturquoise module was the most significantly enriched in the lipid metabolic process (GO:0006629), cellular lipid metabolic process (GO:0044255), and defense response (GO:0006952) BPs; the membrane (GO:0016020), membrane part (GO:0044425), and intrinsic component of membrane (GO:0031224) CCs; and the catalytic activity (GO:0003824), metal ion binding (GO:0046872), and cation binding (GO:0043169) MFs. Overall, eigengenes in the turquoise module were related to plant abiotic stress response, indicating that these genes likely play a role in waterlogging tolerance in *K. obovata*.

We further carried out Kyoto Encyclopedia of Genes and Genomes (KEGG) pathway analysis in order to determine the pathways in which the genes in these three modules were involved. Notably, the genes within each of the modules were found to be related to metabolic processes (Figure 8). Genes within the salinity-responsive MEblue module were related to metabolic pathways, biosynthesis of secondary metabolites, and phenylpropanoid biosynthesis (Figure 8A). Genes within the salinity-responsive MEyellow module were related to metabolic pathways, the biosynthesis of secondary metabolites, and plant hormone signal transduction (Figure 8B). Finally, genes within the waterlogging-responsive MEturquoise module were related to metabolic pathways, secondary metabolite biosynthesis, and galactose, starch, and sucrose metabolism (Figure 8C).

Screening of core salinity- and waterlogging-responsive genes

To identify key genes within the co-expression network, we used Cytoscape to visualize the gene network map (Shannon et al., 2003). The co-expression network in the salinity-responsive MEblue module contained 24 TFs and 251 structural genes (Figure 9A, Supplementary Table 4). Among these, 35 key genes were found to be related to salt stress, including three TFs: geneMaker00002309, geneMaker00007290, and geneMaker00012453 (Figure 9A, Supplementary Table 4). The salinity-responsive MEyellow module co-expression network contained 17 TFs and 160 functional genes (Figure 9B, Supplementary Table 4). Ten genes were found to act as the core of the interaction network, including the TF geneMaker00006547 (Figure 9B, Supplementary Table 4). The 45 core genes in the MEblue and MEyellow modules related to salt stress were mainly involved in metabolic pathways and the biosynthesis of secondary

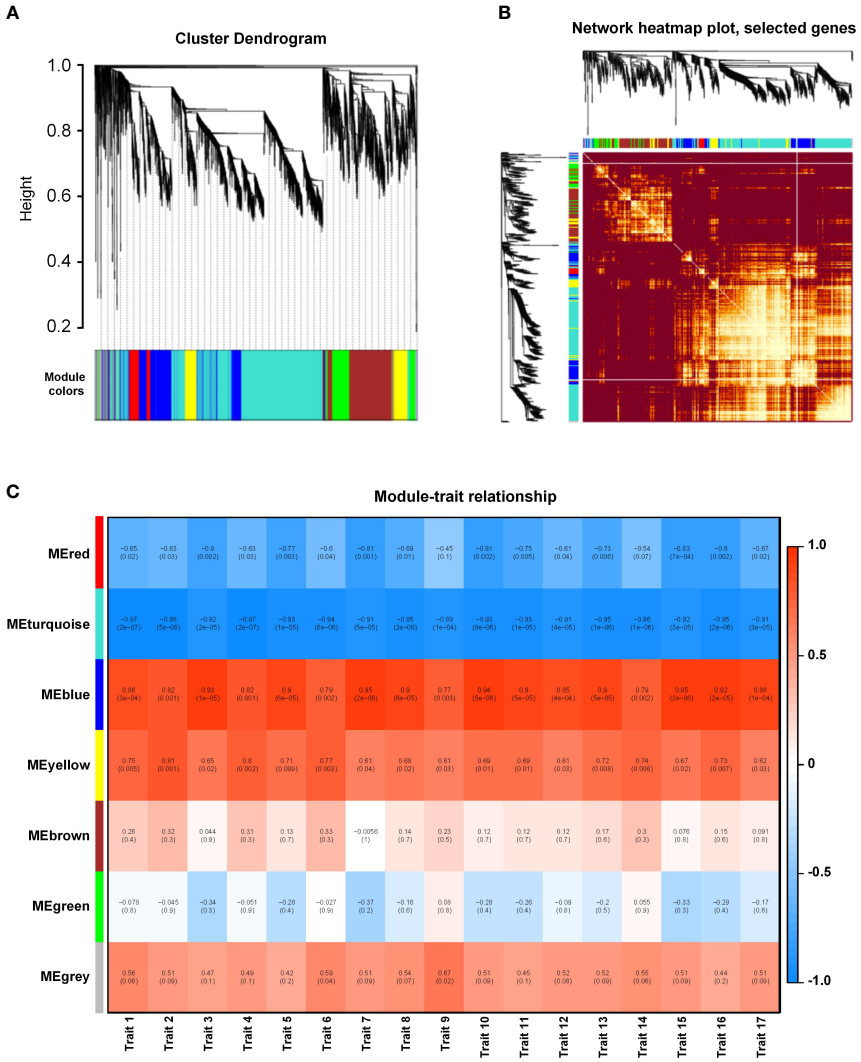

FIGURE 5
Weighted gene co-expression network analysis (WGCNA) of salinity-responsive gene modules in *Kandelia obovata*. **(A)** Clustering dendrogram with dissimilarity based on topological overlap, together with assigned module colors. **(B)** Heatmap showing Pearson's correlation among the eigengenes in co-expression gene modules. **(C)** Correlation between modules and traits. Traits 1–17 respectively represent root length, projected root area, projected leaf area, root surface area, leaf surface area, root volume, leaf volume, fresh plant weight, fresh root weight, fresh stem weight, fresh leaf weight, fresh hypocotyl weight, dry plant weight, dry root weight, dry stem weight, dry leaf weight, and dry hypocotyl weight.

metabolites (Supplementary Table 5). The TFs within these two modules belonged to 12 and 13 families (Figure 9B, Supplementary Table 4), highlighting the sensitivity of *K. obovata* to salt stress. The homologous *Arabidopsis thaliana* genes encoding these TFs were identified as BBX21 (also known as salt tolerance homolog2 (STH2)), WRKY23, and MYBD. Research indicates that these TFs regulate shoot branching, phytohormone biosynthesis, photomorphogenesis, and abiotic stress response (Ding et al., 2013; Guo and Qin, 2016; Crocco et al., 2018; Xu et al., 2018). Finally, the co-expression network in the waterlogging-responsive MEturquoise module contained 16 genes, which were involved in metabolic pathways and the biosynthesis of secondary metabolite pathway (Supplementary Table 5). The only identified TF was geneMaker00001122, which was at the core of the interaction network (Supplementary Figure 7, Supplementary Table 4).

Discussion

Usually, the mangrove growth zone is located on the tidal flat above the average sea level. Salinity and waterlogging time are both the main limiting factors for the growth of mangrove plants. The results of literature studies on the impact of waterlogging on the growth of *K. obovata* young individuals are inconsistent. In a salinity environment of 10‰, the optimal waterlogging time for *K. obovata* was 8–12 h per day (Liao et al., 2009). Additionally, it had been found that in a 15‰ salinity environment, the optimal waterlogging time was 4–8 h per day for *K. obovata* (Chen et al., 2005). The reasons for these differences may be due to the different simulated salinities and experimental durations in these studies. The former experiment lasted for 3 months, while the latter lasted for 5 months. Overall, longer waterlogging time inhibited the plant

10.3389/fpls.2024.1354249

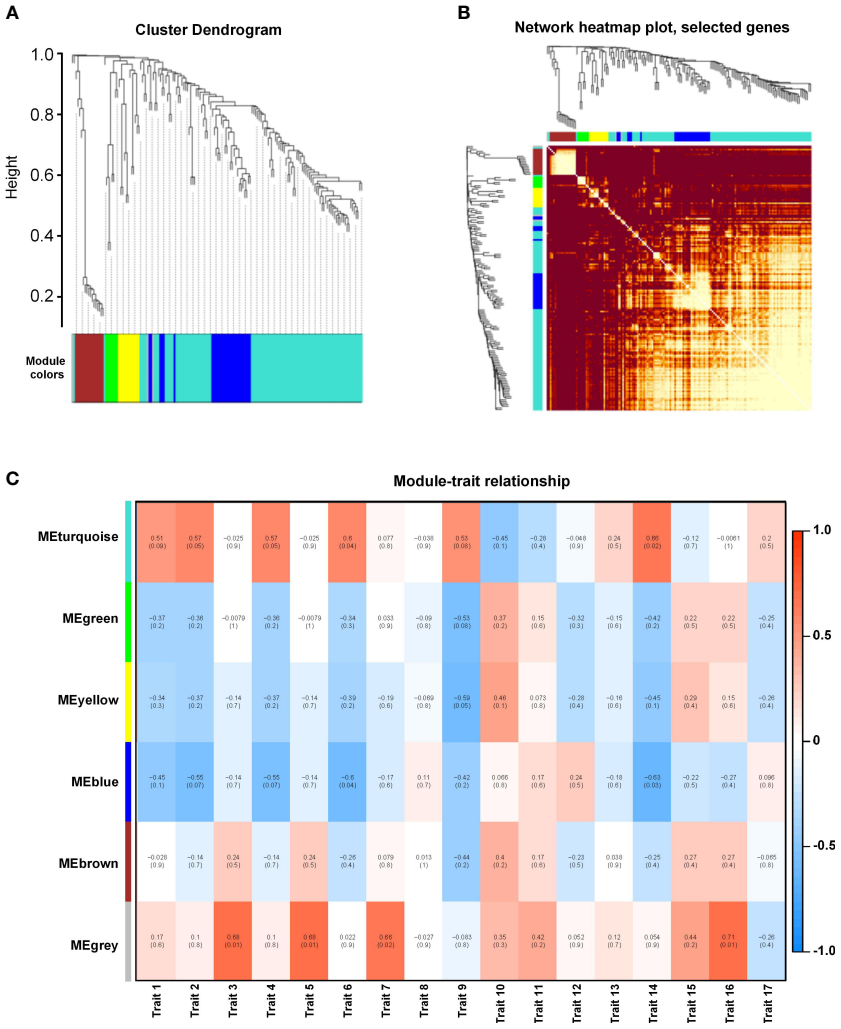

FIGURE 6
Weighted gene co-expression network analysis (WGCNA) of waterlogging-responsive gene modules in *Kandelia obovata*. **(A)** Clustering dendrogram with dissimilarity based on topological overlap, together with the assigned module colors. **(B)** Heatmap showing Pearson's correlation among the eigengenes in co-expression gene modules. **(C)** Correlation between modules and traits. Traits 1–17 respectively represent root length, projected root area, projected leaf area, root surface area, leaf surface area, root volume, leaf volume, fresh plant weight, fresh root weight, fresh stem weight, fresh leaf weight, fresh hypocotyl weight, dry plant weight, dry root weight, dry stem weight, dry leaf weight, and dry hypocotyl weight.

growth of *K. obovata*. In this study, it was found that a longer waterlogging duration led to a decrease in the length, surface area, and volume of roots in *K. obovata*, as well as a decrease in biomass accumulation. Field observation showed that the *K. obovata* plants grew well in an 8‰–25‰ salinity environment (Li, 2000). The growth of *K. obovata* seedlings was inhibited when the salinity was higher than 25‰ in the controlled condition (Liao, 2010). The biomass accumulation of *K. obovata* was lower in the higher-salinity environment in this study. There are reports of differences between the salt tolerance ranges observed in field observations and controlled experiments on mangrove plants. This may be due to the periodic changes in environmental salinity. The periodicity of tides and the supply of freshwater in the field were different from the stability of salinity under controlled conditions. In addition, compared to waterlogging, salinity had a more significant impact on the growth of young *K. obovata* plants, and there was no significant interaction between the two factors, which was consistent with the results of literature studies (Liao, 2010).

Here, we not only measured and examined the root morphological parameters and biomass accumulation under salt and waterlogging stress but also performed RNA-seq and WGCNA to correlate the phenotypic data with gene expression patterns, and we discovered core TFs and hub genes. Overall, waterlogging was found to inhibit the growth of *K. obovata*, which was negatively correlated with waterlogging duration. However, the reason for the low correlation between phenotypic characteristics and transcriptomic results under waterlogging stress remains unclear. The reason may have to do with the fact that our waterlogging stress treatment was not dynamic or perhaps may be related to certain innate adaptive traits of the plants themselves. When stressful environmental conditions remain stable, plants may express stress-related genes early but adapt as the duration increases. On the contrary, we found that certain early responders were restored

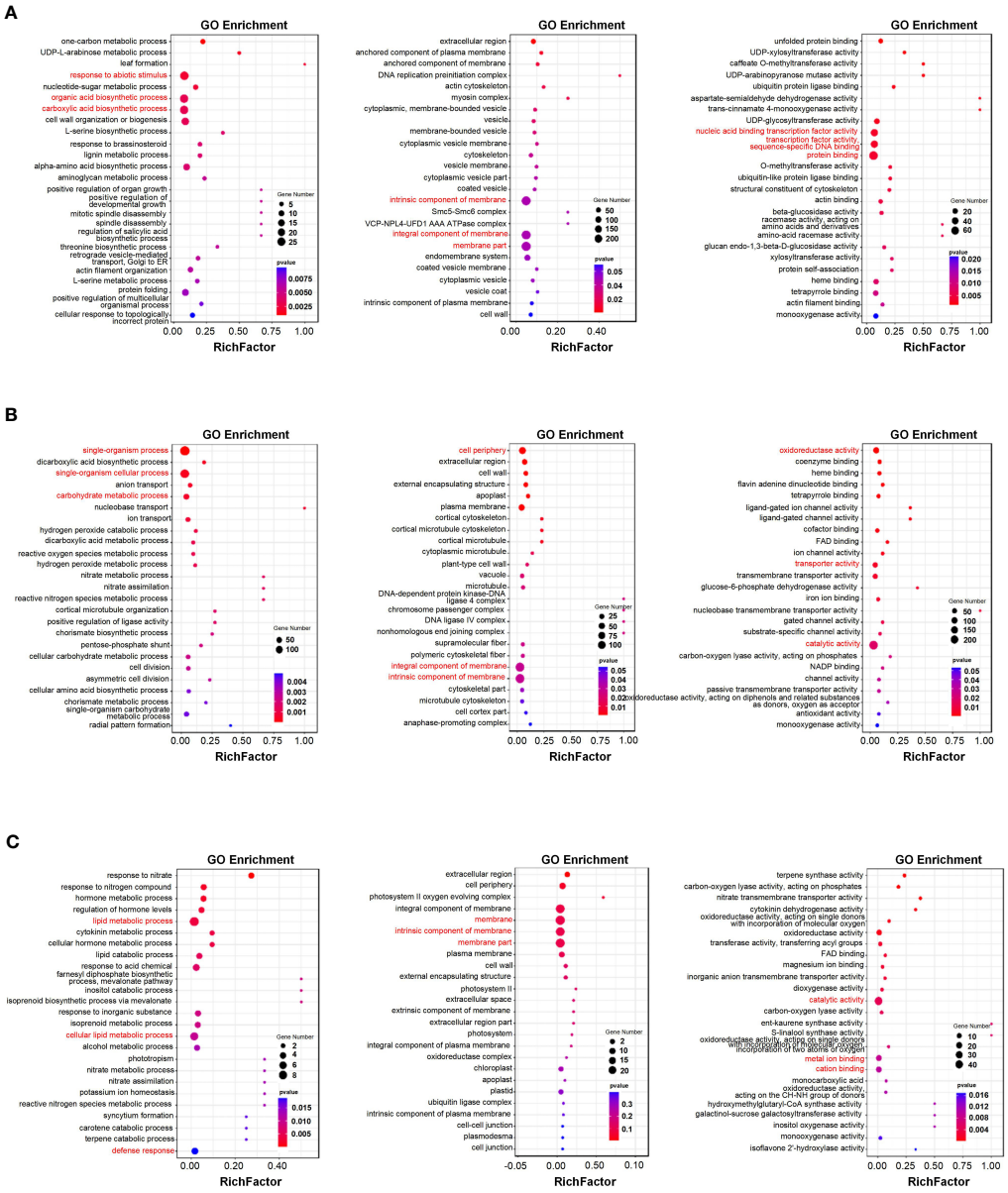

FIGURE 7
Functional enrichment analyses of key salinity- and waterlogging-responsive modules. **(A, B)** Gene Ontology (GO) enrichment analysis of genes in the salinity-responsive MEblue **(A)** and MEyellow **(B)** modules. **(C)** GO enrichment analysis of genes in the waterlogging-responsive MEturquoise module. Each figure depicts biological pathways (left), cell components (middle), and molecular functions (right). The node size reflects the gene count, and the node color reflects the *p*-value [$-\log10^{(p\text{-value})}$].

in later periods. Therefore, we suggest that adaptive traits are the more likely explanation, as the observed phenotypic changes did not significantly alter differential gene expression.

Mangroves respond to high salinity and waterlogging through a complex array of molecular mechanisms. WGCNA can provide valuable insights into convoluted genomic networks by mining data to predict gene clusters linked to certain conditions. We performed WGCNA to search for potential biomarkers of salinity and waterlogging stress in *K. obovata*. Specifically, we performed RNA-seq on *K. obovata* exposed to high salinity and waterlogging and correlated the gene expression levels with phenotypic traits to identify core salinity- and waterlogging-responsive modules (Figures 5, 6). Genes within the salinity-responsive MEblue module were highly correlated with traits 3, 5, 7, 10, 11, 13, 15, and 16 (correlation coefficient ≥ 0.9; Figure 5), indicating that these genes were activated or repressed in response to high salinity. In contrast, only traits 6 and 14 were correlated with genes within the waterlogging-responsive MEturquoise module, albeit insignificantly (Figure 6), indicating that these genes may be weakly related to flooding stress. According to GO enrichment and KEGG pathway

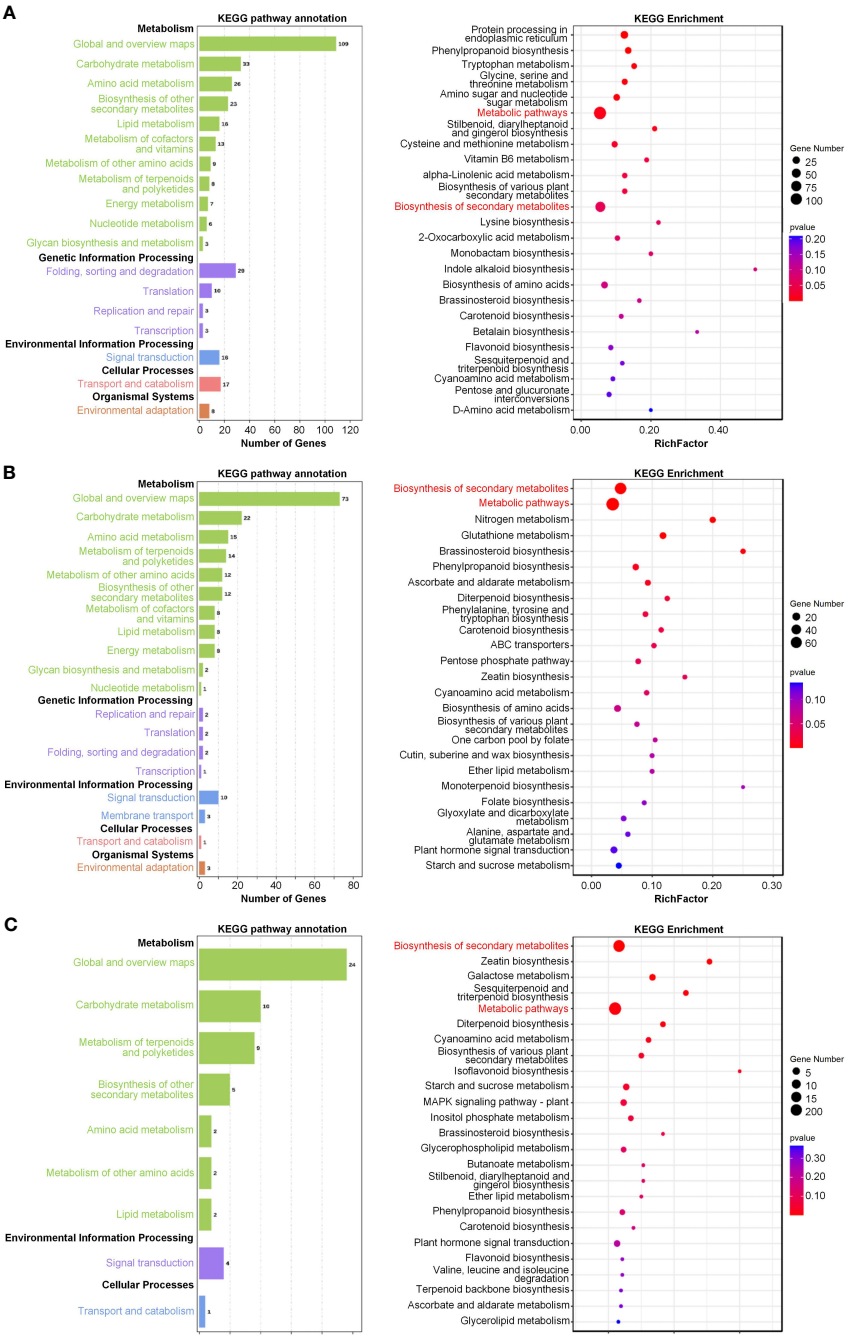

FIGURE 8
Pathway enrichment analyses of key salinity- and waterlogging-responsive modules. **(A, B)** Kyoto Encyclopedia of Genes and Genomes (KEGG) analysis of genes in the salinity-responsive MEblue **(A)** and MEyellow **(B)** modules. **(C)** KEGG analysis of genes in the waterlogging-responsive MEturquoise module. The node size reflects the gene count, and the node color reflects the *p*-value [$-\log10^{(p\text{-value})}$].

analysis, we found that genes in these key modules were enriched in biological processes related to salinity and waterlogging tolerance, such as response to abiotic stimulus, the organic acid biosynthetic process, the carboxylic acid biosynthetic process, the lignin metabolic process, defense response, the biosynthesis of secondary metabolites, metabolic pathways, phenylpropanoid biosynthesis, and plant hormone signal transduction. Therefore, it appears that genes within the key modules identified by WGCNA may be crucial for salinity and waterlogging tolerance in *K. obovata*.

Secondary metabolites are essential to plant life activities, play a significant part in how plants adapt to their surroundings, and are frequently connected to plants' indirect defense (Kutchan, 2001; Richter et al., 2015; Alseekh and Fernie, 2018). For instance, UV-B irradiation can raise the amount of flavonoid–secondary

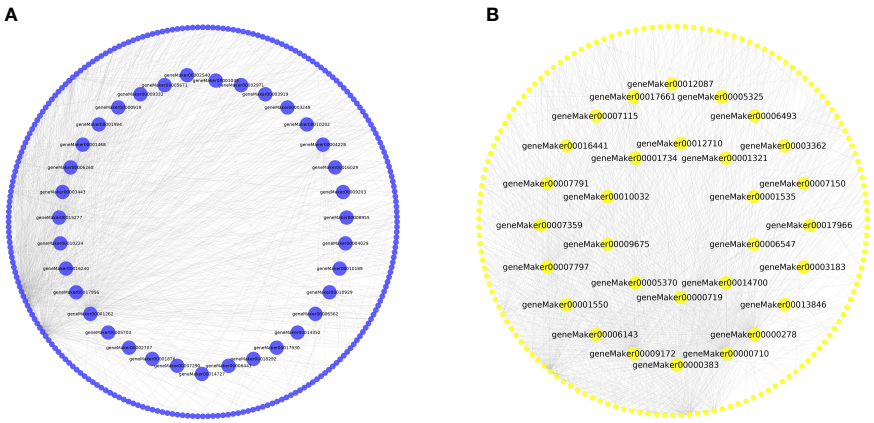

FIGURE 9
Gene interaction network of hub genes. **(A)** MEblue module. **(B)** MEyellow module.

metabolites in the fruticose lichen *Cladonia arbuscula* (Buffoni Hall et al., 2002), *Arabidopsis* (Li et al., 1993), and *Camellia sinensis* (Zagoskina et al., 2005). Secondary metabolites as multifunctional compounds were involved in many stress reactions such as salt and heavy metals (Kumar et al., 2012; Lushchak and Mosiichuk, 2012; Yusuf et al., 2012; Wang et al., 2016; Li et al., 2019; Jayaraman et al., 2021). In this study, we identified many salt- and waterlogging-related core genes involved in the biosynthesis of secondary metabolites in *K. obovata*. These results indicate that the secondary metabolic pathway plays an important role in response to salt and waterlogging stress, and it may be involved in the expression of related genes in each stress response process.

Phenylpropanoid is one of the secondary metabolites in plants and contributes to plant development and plant–environment interplay (Dong and Lin, 2021). Lignin is the main branch of the phenylpropyl metabolic pathway. Recent studies revealed that transcriptional upregulation of lignin biosynthesis genes such as C4H, C3H, CAD, F5H, HCT, 4CL, COMT, CCR, and CCoAOMT results in the deposition of lignin, thickening of the secondary cell wall, and enhanced salt and osmotic resistance (Dong and Lin, 2021; Liu et al., 2022). As shown in Figure 8, the salt- and waterlogging-response genes were enriched into the phenylpropanoid metabolism pathway, suggesting that phenylpropanoids might play vital roles in *K. obovata* coping with natural harsh conditions. Thus, further research is needed to investigate the contribution of phenylpropanoid metabolism to the high salinity and waterlogging resistance of *K. obovata*.

When plants are stimulated by the environment, the signaling pathway of plant hormones is activated, thus playing an important role in the response to various biological and abiotic stresses. Under salt stress, the expression of ethylene (ET) signaling pathway-related genes was upregulated by the MAPK3 pathway to enhance plant tolerance to salt stress (Shu et al., 2022). The increase in jasmonic acid (JA) synthesis can enhance the salt tolerance of *S. lycopersicum*, *O. sativa*, and *Zea mays* L. (Capiati et al., 2006; Wan and Xin, 2022). Moreover, JA can also participate in the resistance of plants to high temperature, low temperature, drought, and heavy metal stress (MaChado et al., 2015; Ghorbel et al., 2021; Zeng et al., 2022). In addition, abscisic acid (ABA), salicylic acid (SA), gibberellin (GA), indole-3-acetic acid (IAA), and brassinolide (BR) are also widely involved in abiotic stress response in plants (Ali and Baek, 2020). Our research results also found that the salt- and waterlogging-related genes were distributed in hormone signaling pathways, so the response of plant hormones to stressed environments can be used as the direction of subsequent research.

Conclusion

In this study, we evaluated the effects of high salinity and waterlogging on the growth response and gene expression of the mangrove *K. obovata*. We combined growth indices, microscopic observation, RNA-seq, PCA, and WGCNA to elucidate the molecular mechanisms underlying salinity and waterlogging stress tolerance in this important mangrove species. We found that both growth and biomass accumulation were significantly inhibited by high salinity and waterlogging, although the effects were much more dramatic in response to high salinity. Notably, growth was negatively correlated with salt concentration and positively correlated with waterlogging duration. High-throughput RNA-seq successfully identified 7,591 salinity-responsive genes and 228 waterlogging-responsive genes. WGCNA on gene expression and phenotypic characteristics identified 45 highly correlated core genes related to salt stress and 16 poorly correlated genes related to waterlogging stress. All the core genes are mainly involved in metabolic pathways and the biosynthesis of secondary metabolites. We preliminarily defined the enrichment pathway of the salinity- and waterlogging-response genes in *K. obovata*. We speculate that the low correlation resulted from adaptation to long-term waterlogging stress, which leads to the recovery of gene expression over time. In summary, our study preliminarily analyzed the molecular mechanism of salinity and waterlogging stress tolerance in *K. obovata*. These results will be useful for improving the stress resistance of mangrove forest trees using molecular breeding techniques.

Data availability statement

The data presented in the study are deposited in the National Center for Biotechnology Information Sequence Read Archive repository, accession number PRJNA1051648, and PRJNA1051781.

Author contributions

HL: Data curation, Writing – original draft. XA: Conceptualization, Data curation, Formal analysis, Writing – review & editing. XL: Data curation, Formal analysis, Writing – review & editing. SY: Conceptualization, Formal analysis, Writing – review & editing. YL: Investigation, Methodology, Writing – review & editing. XW: Methodology, Resources, Writing – review & editing. XWL: Methodology, Software, Writing – review & editing. QC: Conceptualization, Formal analysis, Funding acquisition, Writing – review & editing. JW: Conceptualization, Data curation, Formal analysis, Funding acquisition, Resources, Writing – review & editing.

Funding

The author(s) declare financial support was received for the research, authorship, and/or publication of this article. This work was supported by the National Natural Science Foundation Program (no. 31972864) and the Key R&D Program of Zhejiang Province, China (2023C02003).

Acknowledgments

The authors thank the editor and reviewers for their comments. They also thank the Zhejiang Academy of Agricultural Sciences and the Wenzhou Key Laboratory of Resource Plant Innovation and Utilization for their support of this study.

Conflict of interest

The authors declare that the research was conducted in the absence of any commercial or financial relationships that could be construed as a potential conflict of interest.

Publisher's note

Supplementary material

The Supplementary Material for this article can be found online at: https://www.frontiersin.org/articles/10.3389/fpls.2024.1354249/full#supplementary-material

References

Ali, M. S., and Baek, K. H. (2020). Jasmonic acid signaling pathway in re-sponse to abiotic stresses in plants. *Int. J. Mol. Sci.* 21, 621. doi: 10.3390/ijms21020621

Allaway, W. G., Curran, M., Hollington, L. M., Ricketts, M. C., and Skelton, N. J. (2001). Gas space and oxygen exchange in roots of Avicennia marina (Forssk.) Vierh. var. australasica (Walp.) Moldenke ex N.C. Duke, the Grey Mangrove. *Wetl. Ecol. Manage.* 9, 221–228. doi: 10.1023/A:1011160823998

Alongi, D. M. (2009). *The energetics of mangrove forests* (New York: Springer). doi: 10.1007/978-1-4020-4271-3

Alongi, D. M. (2014). Carbon cycling and storage in mangrove forests. *Ann. Rev. Mar. Sci.* 6, 195–219. doi: 10.1146/annurev-marine-010213-135020

Alseekh, S., and Fernie, A. R. (2018). Metabolomics 20 years on: what have we learned and what hurdles remain? *Plant J.* 94, 933–942. doi: 10.1111/tpj.13950

Bai, J. K., Meng, Y., Gou, R. K., Lu, J., Dai, Z., Diao, X., et al. (2021). Mangrove diversity enhances plant biomass production and carbon storage in Hainan island, China. *Funct. Ecol.* 35, 774–786. doi: 10.1111/1365-2435.13753

Buffoni Hall, R. S., Bornman, J. F., and Björn, L. O. (2002). UV-induced changes in pigment content and light penetration in the fruticose lichen Cladonia arbuscular. *J. Photoch. Photobio. B.* 66, 13–20. doi: 10.1016/s1011-1344(01)00270-6

Capiati, D. A., País, S. M., and Téllez-Iñón, M. T. (2006). Wounding increases salt tolerance in tomato plants: evidence on the participation of calmodulin-like activities in cross-tolerance signaling. *J. Exp. Bot.* 57, 2391–2400. doi: 10.1093/jxb/erj212

Chen, K. Q., Song, M. R., Guo, Y. N., Li, L. F., Xue, H., Dai, H. Y., et al. (2019). MdMYB46 could enhance salt and osmotic stress tolerance in apple by directlyactivating stress-responsive signals. *Plant Biotechnol. J.* 17, 2341–2355. doi: 10.1111/pbi.13151

Chen, L. Z., Wang, W. Q., and Lin, P. (2004). Influence of waterlogging time on the growth of Kandelia candel seedlings. *Acta Oceanol. Sin.* 23, 149–115. doi: 10.1029/2003JC001866

Chen, L., Wang, W., and Lin, P. (2005). Influence of waterlogging time on the growth of *Kandelia candel* seedlings. *Acta Oceano Sin.* 27, 41–47. doi: 10.3321/j.issn:0253-4193.2005.02.018

Cheng, H., Wang, Y. S., Fei, J., Jiang, Z. Y., and Ye, Z. H. (2015). Differences in root aeration, iron plaque formation and waterlogging tolerance in six mangroves along a continues tidal gradient. *Ecotoxicology* 24, 1659–1667. doi: 10.1007/s10646-015-1474-0

Costanza, R., d'Arge, R., De Groot, R., Farber, S., Grasso, M., Hannon, B., et al. (1997). The value of the world's ecosystem services and natural capital. *Nat. (Lond.)* 387, 253–260. doi: 10.1016/S0921-8009(98)00020-2

Crocco, C. D., Gomez-Ocampo, G., Mantese, A., Ploschuk, E. L., and Botto, J. F. (2018). Heterologous expression of AtBBX21 enhances the rate of photosynthesis and alleviates photoinhibition in solanumtuberosum. *Plant Physiol.* 177, 369–380. doi: 10.1104/pp.17.01417

Curran, M., James, P., and Allaway, W. G. (1996). The measurement of gas spaces in the roots of aquatic plants-Archimedes revistited. *Aquat. Botany.* 54, 255–261. doi: 10.1016/0304-3770(96)01049-2

Czyzewicz, N., Shi., C. L., Vu, L. D., Cotte, B. V. D., Hodgman, C., Butenko, M. A., et al. (2015). Modulation of Arabidopsis and monocot root architecture by CLAVATA3/EMBRYO SURROUNDING REGION 26 peptide. *J. Exp. Bot.* 66, 5229–5243. doi: 10.1093/jxb/erv360

Dhungana, S. K., Kim, H. S., Kang, B. K., Seo, J. H., Kim, H. T., Oh, J. H., et al. (2021). Analysis of differentially expressed genes in soybean leaf tissue of tolerant and susceptible cultivars under flooding stress revealed by RNA sequencing. *J. Crop Sci. Biotechnol.* 24, 83–91. doi: 10.1007/s12892-020-00061-6

Ding, Y., Liu, N., Virlouvet, L., Riethoven, J. J., Fromm, M., and Avramova, Z. (2013). Four distinct types of dehydration stress memory genes in *Arabidopsis thaliana*. *BMC Plant Biol.* 30, 13:229. doi: 10.1186/1471-2229-13-229

Donato, D. C., Kauffman, J. B., Murdiyarso, D., Kurnianto, S., Stidham, M., and Kanninen, M. (2011). Mangroves among the most carbon-rich forests in the tropics. *Nat. Geosci.* 4, 293–297. doi: 10.1038/NGEO1123

Dong, N. Q., and Lin, H. X. (2021). Contribution of phenylpropanoid metabolism to plant development and plant–environment interactions. *J. Integr. Plant Biol.* 63 (1), 180–209. doi: 10.1111/jipb.13054

Duke, N. C., Meynecke, J. O., Dittmann, S., Ellison, A. M., Anger, K., Berger, U., et al. (2007). A world without mangroves? *Science* 317, 41–42. doi: 10.1126/science.317.5834.41b

Ghorbel, M., Brini, F., Sharma, A., and Landi, M. (2021). Role of jasmonic acid in plants: the molecular point of view. *Plant Cell Rep.* 40, 1471–1494. doi: 10.1007/s00299-021-02687-4

Guo, D. S., and Qin, G. J. (2016). EXB1/WRKY71 transcription factor regulates both shoot branching and responses to abiotic stresses. *Plant Signal Behav.* 11, e1150404. doi: 10.1080/15592324.2016.1150404

Hattori, Y., Nagai, K., Furukawa, S., Song, X. J., Kawano, R., Sakakibara, H., et al. (2009). The ethylene response factors SNORKEL1 and SNORKEL2 allow rice to adapt to deep water. *Nature* 460, 1026–1030. doi: 10.1038/nature08258

Hussain, S., Zhang, J., Zhong, C., Zhu, L. F., Cao, X. C., Yu, S. M., et al. (2017). Effects of salt stress on rice growth, development characteristics, and the regulating ways: a review. *J. Integr. Agr.* 16, 2357–2374. doi: 10.1016/S2095-3119(16)61608-8

Jayaraman, K., Raman K, V., Sevanthi, A. M., Sivakumar, S. R., Gayatri, Viswanathan, C., et al. (2021). Stress inducible expression of chalcone isomerase2 gene improves accumulation of flavonoids and imparts enhanced abiotic stress tolerance to rice. *Environ. Exp. Bot.* 190, 104582. doi: 10.1016/j.envexpbot.2021.104582

Jiang, X. Q., Li, S., Ding, A., Zhang, Z., Hao, Q., Wang, K., et al. (2018). The novel rose MYB transcription factor RhMYB96 enhances salt tolerance intransgenic *Arabidopsis*. *Plant Mol. Biol. Rep.* 36, 406–417. doi: 10.1007/s11105-018-1094-y

Jisha, V., Dampanaboina, L., Vadassery, J., Mithöfer, A., Kappara, S., and Ramanan, R. (2015). Overexpression of an AP2/ERF type transcription factor OsEREBP1 confers biotic and abiotic stress tolerance in rice. *PloS One* 10, e0127831. doi: 10.1371/journal.pone.0127831

Jourquin, J., Fukaki, H., and Beeckman, T. (2020). Peptide-receptor signal-ing controls lateral root development. *Plant Physiol.* 182, 1645–1656. doi: 10.1104/pp.19.01317

Ke, Y. G., Yang, Z. J., Yu, S. W., Li, T. F., Wu, J. H., Gao, H., et al. (2014). Characterization of Os DREB6 responsive to osmotic and cold stresses in rice. *J. Plant Biol.* 57, 150–161. doi: 10.1007/s12374-013-0480-0

Kim, S., Kang, J. Y., Cho, D. I., Park, J. H., and Kim, S. Y. (2004). ABF2, an ABRE-binding bZIP factor, is an essential componentof glucose signaling and its overexpression affects multiplestress tolerance. *Plant J.* 40, 75–87. doi: 10.1111/j.1365-313X.2004.02192.x

Klumb, E. K., Arge, L. W. P., Do Amaral, M. N., Rickes, L. N., Benitez, L. C., Braga, E. J. B., et al. (2017). Transcriptome profiling of Prunus persica plants under flooding. *Tree* 31, 1127–1135. doi: 10.1007/s00468-017-1532-8

Komatsu, S., Kobayashi, Y., Nishizawa, K., Nanjo, Y., and Furukawa, K. (2010). Comparative proteomics analysis of differentially expressed proteins in soybean cell wall during flooding stress. *Amino Acids* 39, 1435–1449. doi: 10.1007/s00726-010-0608-1

Krauss, K. W., Lovelock, C. E., McKee, K. L., Lopez-Hoffman, L., Ewe, S. M. L., and Sousa, W. P. (2008). Environmental drivers in mangrove establishment and early development: A review. *Aquat. Bot.* 89, 105–127. doi: 10.1016/j.aquabot.2007.12.014

Kreuzwieser, J., Hauberg, J., Howell, K. A., Carroll, A., Rennenberg, H., Millar, A. H., et al. (2009). Differential response of gray poplar leaves and roots underpins stress adaptation during hypoxia. *Plant Physiol.* 149, 461–473. doi: 10.1104/pp.108.125989

Kumar, A., Prasad, M., and Sytar, O. (2012). Lead toxicity, defense strategies and associated indicative biomarkers in Talinum triangulare grown hydroponically. *Chemosphere* 89, 1056–1065. doi: 10.1016/j.chemosphere.2012.05.070

Kutchan, T. M. (2001). Ecological arsenal and developmental dispatcher. The paradigm of secondary metabolism. *Plant Physiol.* 125, 58–60. doi: 10.1104/pp.125.1.58

Langfelder, P., and Horvath, S. (2008). WGCNA: an R package for weighted correlation network analysis. *BMC Bioinf.* 29, 9:559. doi: 10.1186/1471-2105-9-559

Langmead, B., and Salzberg, S. L. (2012). Fast gapped-read alignment with Bowtie 2. *Nat. Methods* 9, 357–359. doi: 10.1038/nmeth.1923

Lee, S. Y., Primavera, J. H., Dahdouh-Guebas, F., McKee, K., Bosire, J. O., Cannicci, S., et al. (2014). Ecological role and services of tropical mangrove ecosystems: a reassessment. *Global Ecol. Biogeogr.* 23, 726–743. doi: 10.1111/geb.12155

Li, Q. (2000). Analyzing influences of the ecological factor on the growth of *Kandelia* on a coastal shoal. *J. Fujian Forestry Sci. Tech.* 27, 31–34. doi: 10.13428/j.cnki.fjlk.2000.04.008

Li, B. Z., Fan, R. N., Guo, S. Y., Wang, P. T., Zhu, X. H., Fan, Y. T., et al. (2019). The Arabidopsis MYB transcription factor, MYB111 modulates salt responses by regulating flavonoid biosynthesis. *Environ. Exp. Bot.* 166, 103807. doi: 10.1016/j.envexpbot.2019.103807

Li, Q. P., Fu, H. Q., Xiang, Y., Xing, W., Guo, H. W., Guo, Y., et al. (2023). The SOS2-CTR1 module coordinates plant growth and salt tolerance in Arabidopsis. *J. Exp. Bot.* 18, erad368. doi: 10.1093/jxb/erad368

Li, D. H., Liu, P., Yu, J. Y., Wang, L. H., Dossa, K., Zhang, Y. X., et al. (2017). Genome-wide analysis of WRKY gene family in the sesame genome and identification of the WRKY genes involved in responses to abiotic stresses. *BMC Plant Biol.* 17, 152. doi: 10.1186/s12870-017-1099-y

Li, J., Ou-Lee, T. M., Raba, R., Amundson, G., and Last, R. L. (1993). Flavonoid mutants are hypersensitive to UV-B irradiation. *Plant Cell.* 5, 171–179. doi: 10.1105/tpc.5.2.171

Liao, B. (2010). *The adaptability of seedlings of three mangrove species to tide-flooding and water salinity* (Chinese Academy of Forestry: Beijing).

Liao, B., Qiu, F., Tam, N. F., Zeng, W., and Xu, D. (2009). Study on adaptability of mangrove Kandelia candel seedlings to simulated tidal inundation. *J. China Agric. Univ.* 30, 49–54. doi: 10.3969/j.issn.1001-411X.2009.03.012

Lin, Y. C., Li, W., Chen, H., Li, Q. Z., Sun, Y. H., Shi, R., et al. (2014). A simple improved -throughput xylem protoplast system for studying wood formation. *Nat. Protoc.* 9, 2194–2205. doi: 10.1038/nprot.2014.147

Lin, Y. C., Li, W., Sun, Y. H., Kumari, S., Wei, H., Li, Q., et al. (2013). SND1 transcription factor-directed quantitative functional hierarchical genetic regulatory network in wood formation in *Populus trichocarpa*. *Plant Cell.* 25, 4324–4341. doi: 10.1105/tpc.113.117697

Liu, H., Gao, J., Sun, J., Li, S., Zhang, B., Wang, Z., et al. (2022). Dimer ization of PtrMYB074 and PtrWRKY19 mediates transcriptional activation of *PtrbHLH186* for secondary xylem development in *Populus trichocarpa*. *New Phytol.* 234, 918–933. doi: 10.1111/nph.18028

Liu, J., Hua, W., Yang, H. L., Zhan, G. M., Li, R. J., Deng, L. B., et al. (2012). The BnGRF2 gene (GRF2-like gene from Brassica napus) enhances seed oilproduction through regulating cell number and plant photosynthesis. *J. Exp. Bot.* 63, 3727–3740. doi: 10.1093/jxb/ers066

Liu, S., Yang, S., Liu, H., Hu, Q., Liu, X., Wang, J., et al. (2023). Physiological and transcriptomic analysis of the mangrove species *Kandelia obovata* in response to flooding stress. *Mar. pollut. Bull.* 196, 115598. doi: 10.1016/j.marpolbul.2023.115598

Liu, Z., Zhang, T., Xu, R., Liu, B., Han, Y., Dong, W., et al. (2024). BpGRP1 acts downstream of BpmiR396c/BpGRF3 to confer salt tolerance in Betula platyphylla. *Plant Biotechnol. J.* 22, 131–147. doi: 10.1111/pbi.14173

Loreti, E., van Veen, H., and Perata, P. (2016). Plant responses to flooding stress. *Curr. Opin. Plant Biol.* 33, 64–71. doi: 10.1016/j.pbi.2016.06.005

Love, M. I., Huber, W., and Anders, S. (2014). Moderated estimation of fold change and dispersion for RNA-seq data with DESeq2. *Genome Biol.* 15, 550.

Lovelock, C. E., and Duarte, C. M. (2019). Dimensions of blue carbon and emerging perspectives. *Biol. Lett.* 15, 20180781. doi: 10.1098/rsbl.2018.0781

Lushchak, V., and Mosiichuk, N. (2012). Tocopherol biosynthesis: chemistry, regulation and effects of environmental factors. *Acta Physiol. Plant* 34, 1607–1628. doi: 10.1007/s11738-012-0988-9

MaChado, R. A. R., Arce, C. C. M., Ferrieri, A. P., Baldwin, I. T., and Erb, M. (2015). Jasmonate-dependent depletion of solublesugars compromises plant resistance to Manducaserta. *New Phytol.* 207, 91–105. doi: 10.1111/nph.13337

McKee, K. L. (1993). Soil physicochemical patterns and mangrove species distribution reciprocal effects? *J. Ecol.* 81, 477–487. doi: 10.2307/2261526

Nguyen, N. H., and Cheong, J. J. (2018). H2A.Z-containing nucleosomes are evicted to activate AtMYB44 transcription in response to salt stress. *Biochem. Biophys. Res. Commun.* 499, 1039–1043. doi: 10.1016/j.bbrc.2018.04.048

Overvoorde, P., Fukaki, H., and Beeckman, T. (2010). Auxin control of root development. *CSH Perspect. Biol.* 2, a001537. doi: 10.1101/cshperspect.a001537

Parida, A. K., and Jha, B. (2010). Salt tolerance mechanisms in mangroves: A review. *Trees-Struct* 24, 199–217. doi: 10.1007/s00468-010-0417-x

Petricka, J. J., Winter, C. M., and Benfey, P. N. (2012). Control of Arabidopsis root development. *Annu. Rev. Plant Biol.* 63, 563–590. doi: 10.1146/annurev-arplant-042811-105501

Richter, A., Seidl-Adams, I., Kollner, T. G., Schaff, C., Tumlinson, J. H., and Degenhardt, J. (2015). A small, differentially regulated family of farnesyl diphosphate synthases in maize (Zea mays) provides farnesyl diphosphate for the biosynthesis of herbivore-induced sesquiterpenes. *Planta* 241, 1351–1361. doi: 10.1007/s00425-015-2254-z

Safdar, H., Amin, A., Shafiq, Y., Ali, A., Yasin, R., Shoukat, A., et al. (2019). A review: Impact of salinity on plant growth. *Nat. Sci.* 1, 34–40. doi: 10.7537/marsnsj170119.06

Shannon, P., Markiel, A., Ozier, O., Baliga, N. S., Wang, J. T., Ramage, D., et al. (2003). Cytoscape: a software environment for integrated models of biomolecular interaction networks. *Genome Res.* 13, 2498–2504. doi: 10.1101/gr.1239303

Shiau, Y. J., Lee, S. C., Chen, T. H., Tian, G., and Chiu, C. Y. (2017). Water salinity effects on growth and nitrogen assimilation rate of mangrove (*Kandelia candel*) seedlings. *Aquat. Bot.* 137, 50–55. doi: 10.1016/J.AQUABOT.2016.11.008

Shu, P., Li, Y. J., Li, Z. Y., Sheng, J., and Shen, L. (2022). SlMAPK3 enhances tolerance to salt stress in tomato plants by scavenging ROS accumulation and up-regulating the expression of ethylene signaling related genes. *Environ. Exp. Bot.* 193, 104698. doi: 10.1016/j.envexpbot.2021.104698

Srikanth, S., Lum, S. K. Y., and Chen, Z. (2016). Mangrove root: adaptations and ecological importance. *Trees* 30, 451–465. doi: 10.1007/s00468-015-1233-0

Tran, N. H. T., Oguchi, T., Akatsuka, N., Matsunaga, E., Kawaoka, A., Yamada, A., et al. (2019). Development and evaluation of novel salt-tolerant eucalyptus trees bymolecular breeding using an RNA-Binding-Protein gene derived from common ice plant (Mesembryanthemumcrystallinum L.). *Plant Biotechnol. J.* 17, 801–811. doi: 10.1111/pbi.13016

Vishal, B., Krishnamurthy, P., Ramamoorthy, R., and Kumar, P. P. (2019). OsTPS8 controls yield-related traits and confers salt stress tolerance in rice by enhancing suberin deposition. *New Phytol.* 221, 1369–1386. doi: 10.1111/nph.15464

Wan, S. W., and Xin, X. F. (2022). Regulation and integration of plant jasmonate signaling: a comparative view of monocot and dicot. *J. Genet. Genomics* 49, 704–714. doi: 10.1016/j.jgg.2022.04.002

Wang, F. B., Hui, Z., Chen, D. H., Li, Z. J., Peng, R. H., and Yao, Q. H. (2016). A grape bHLH transcription factor gene, VvbHLH1, increases the accumulation of flavonoids and enhances salt and drought tolerance in transgenic *Arabidopsis thaliana*. *PCTOC* 125, 387–398. doi: 10.1007/s11240-016-0953-1

Wang, L., Qiu, T. Q., Yue, J. R., Guo, N. N., He, Y. J., Han, X. P., et al. (2021). Arabidopsis ADF1 is regulated by MYB73 and is involved in response to salt stress affecting actin filament organization. *Plant Cell Physiol.* 62, 1387–1395. doi: 10.1093/pcp/pcab081

Wang, C., Zhang, D. W., Wang, Y. C., Zheng, L., and Yang, Z. P. (2012). A glycine-rich RNA-binding protein can mediate physiological responses intransgenic plants under salt stress. *Mol. Biol. Rep.* 39, 1047–1053. doi: 10.1007/s11033-011-0830-2

Werner, A., and Stelzer, R. (1990). Physiological responses of the mangrove Rhizophora mangle grown in the absence and presence of NaCl. *Plant Cell Environ.* 13, 243–255. doi: 10.1111/J.1365-3040.1990.TB01309.X

Xu, D., Jiang, Y., Li, J., Holm, M., and Deng, X. W. (2018). The B-box domain protein BBX21 promotes photomorphogenesis. *Plant Physiol.* 176, 2365–2375. doi: 10.1104/pp.17.01305

Yaldiz, G., and Camlica, M. (2021). Impact of various environmental stress factors on productivity, quality, and secondary metabolites of fenugreek (*Trigonella foenum-graecum L.*). *Fenugreek* 13, 301–326. doi: 10.1007/978-981-16-1197-1_14

Yang, A., Dai, X., and Zhang, W. H. (2012). A R2R3-type MYB gene, OsMYB2, is involved in salt, cold, and dehydration tolerance in rice. *J. Exp. Bot.* 63, 2541–2556. doi: 10.1093/jxb/err431

Yao, Q. (2021). Crucial waterlogging-responsive genes and pathways revealed by comparative physiology and transcriptome in tropical and temperate maize (*Zea mays L.*) inbred lines. *J. Plant Biol.* 64, 313–325. doi: 10.1007/s12374-021-09298-2

Ye, J. M., Zhang, W. H., and Guo, Y. (2013). Arabidopsis SOS3 plays an important role in salt tolerance by mediating calcium-dependent microfilament reorganization. *Plant Cell Rep.* 32, 139–148. doi: 10.1007/s00299-012-1348-3

Yusuf, M., Fariduddin, Q., Varshney, P., and Ahmad, A. (2012). Salicylic acid minimizes nickel and/or salinity-induced toxicity in Indian mustard (*Brassica juncea*) through an improved antioxidant system. *Environ. Sci. pollut. Res. Int.* 19, 8–18. doi: 10.1007/s11356-011-0531-3

Zagoskina, N. V., Alyavina, A. K., Gladyshko, T.O., Lapshin, P. V., Egorova, E. A., Bukhov, N. G., et al (2005). Ultraviolet rays promote development of photosystem II photochemical activity and accumulation of phenolic compounds in the tea callus culture(Camellia sinensis). *Russ J Plant Physl.* 52, 731–739. doi: 10.1007/s11183-005-0109-3

Zeng, X., Jiang, J., Wang, F., Liu, W., Zhang, S., Du, J., et al (2002). Rice OsClo5, a caleosin protein, negatively regulates cold tolerance through the jasmonate signalling pathway. *Plant Biol.* 24, 52–61. doi: 10.1111/plb.13350

Zhao, Y. Z., Zhong, Y. F., Ye, C. T., Liang, P. P., Pan, X. B., Zhang, Y. Y., et al. (2021). Multi-omics analyses on *Kandelia obovata* reveal its response to transplanting and genetic differentiation among populations. *BMC Plant Biol.* 21, 341. doi: 10.1186/s12870-021-03123-1

Zhu, M. G., Meng, X. Q., Cai, J., Li, G., Dong, T. T., and Li, Z. Y. (2018). Basic leucine zipper transcription factor SlbZIP1 mediates salt and drought stresstolerance in tomato. *BMC Plant Biol.* 18, 83. doi: 10.1186/s12870-018-1299-0

Zou, M. J., Guan, Y. C., Ren, H. B., Zhang, F., and Chen, F. (2008). A bZIP transcription factor, OsAB15, is involved in rice fertility and stress tolerance. *Plant Mol. Biol.* 66, 675–683. doi: 10.1007/s11103-008-9298-4

frontiers | Frontiers in Plant Science

TYPE Review
PUBLISHED 08 February 2024
DOI 10.3389/fpls.2024.1353436

OPEN ACCESS

EDITED BY
Hui Song,
Qingdao Agricultural University, China

REVIEWED BY
Chao Ma,
Shanghai Jiao Tong University, China
Xia An,
Zhejiang Institute of Garden Plants and Flowers, China

*CORRESPONDENCE
Xiujie Li
lixiujie-2007@163.com

RECEIVED 10 December 2023
ACCEPTED 17 January 2024
PUBLISHED 08 February 2024

CITATION
Han Y and Li X (2024) Current progress in research focused on salt tolerance in *Vitis vinifera* L.. *Front. Plant Sci.* 15:1353436. doi: 10.3389/fpls.2024.1353436

Current progress in research focused on salt tolerance in *Vitis vinifera* L.

Yan Han and Xiujie Li*

Shandong Academy of Grape, Ji'nan, Shandong, China

Soil salinization represents an increasingly serious threat to agronomic productivity throughout the world, as rising ion concentrations can interfere with the growth and development of plants, ultimately reducing crop yields and quality. A combination of factors is driving this progressive soil salinization, including natural causes, global climate change, and irrigation practices that are increasing the global saline-alkali land footprint. Salt stress damages plants both by imposing osmotic stress that reduces water availability while also inducing direct sodium- and chlorine-mediated toxicity that harms plant cells. *Vitis vinifera* L. exhibits relatively high levels of resistance to soil salinization. However, as with other crops, grapevine growth, development, fruit yields, and fruit quality can all be adversely affected by salt stress. Many salt-tolerant grape germplasm resources have been screened in recent years, leading to the identification of many genes associated to salt stress and the characterization of the mechanistic basis for grapevine salt tolerance. These results have also been leveraged to improve grape yields through the growth of more tolerant cultivars and other appropriate cultivation measures. The present review was formulated to provide an overview of recent achievements in the field of research focused on grapevine salt tolerance from the perspectives of germplasm resource identification, the mining of functional genes, the cultivation of salt-tolerant grape varieties, and the selection of appropriate cultivation measures. Together, we hope that this systematic review will offer insight into promising approaches to enhancing grape salt tolerance in the future.

KEYWORDS

gene mining, germplasm resources, grape, salt tolerance, variety

Introduction

23% of the cultivated arable lands are saline over 100 countries in all continents. 20% (45 million ha) irrigated lands are human-induced salt-affected soils (secondary salinization) in the world (Zaman et al., 2018). For instance, 2.6×10^7 hectares (ha) of the total land area are salt affected mainly in the north part and tidal coastal regions and 6.7 million ha lands of the irrigated areas are affected by secondary salinization in China. It is thought that productivity

enhancement of salt-affected lands in irrigated areas is one important method to provide more food, fruit, feed, and fiber to the expanding population worldwide (Qadir et al., 2014).

Vitis L. is among the most highly valued genera in the Vitaceae family, as the fruits it produces are rich in polyphenols and resveratrol that reportedly exhibit anti-aging activity. In addition to being consumed as fresh fruits, these grapes are also processed to produce raisins, juice, sauces, vinegar, and wine, all of which are important to the global fruit trade. Grapevines are plant species with a relatively high level of salt tolerance. Despite this advantageous trait, progressive soil salinization can still adversely impact the growth, fruit yield, and fruit quality (i.e. flavor, sugar content etc.), and further negatively affecting wine quality. The most effective approaches to improving grape production in lightly salinized soil and enhancing the growth and fruit quality of grapevines cultivated in the presence of soil salinization have thus been a focus of intensive research interest in recent years. This review was compiled in an effort to gain insight into the most effective means of improving the salt tolerance of grape plants, offering a theoretical reference for efforts to better explore the mechanistic basis for such salt tolerance, cultivate salt-tolerant grape varieties, and improve overall grape growth in saline soil (Figure 1).

Studies of salt-tolerant grape germplasm resources

Germplasm resources serve as the basic materials for the breeding of novel cultivars while also enabling biotechnological research and germplasm innovation. Certain varieties of wild grapes exhibit high levels of adaptability and resistance to a variety of stressors, and thus represent valuable resources that can be used to broaden the gene pool as a means of expanding the genetic repertoire of cultivated grape varieties (Aradhya et al., 2003; Wan et al., 2008). Prior studies have established grapes as being moderately sensitive to salt stress (Maas and Hoffman, 1977). Salt-treated leaves generally exhibit higher chloride levels than sodium levels during various stages of growth, with this difference being elevated by an order of magnitude in leaves exhibiting stress symptoms. The ability of grape plants to minimize chloride accumulation has thus been used as a criterion when attempting to screen for salt-tolerant germplasm resources (Fort et al., 2013). The chloride exclusion abilities of *V. acerifolia*, *V. arizonica*, *V. berlandieri*, *V. doaniana*, and *V. girdiana* accessions gathered from the southwestern United States have been categorized and compared to the benchmark chloride excluder *V. rupestris* 'St. George' (Heinitz et al., 2014). Longii 9018/9035, NM:03-17, and GRN1 with lower chloride accumulation in leaves were identified as chloride excluders from among 16 grape rootstocks treated with 75 mM NaCl for three weeks, highlighting a clear relationship between the degree of fine root production and chloride accumulation (Bent, 2017). Approximately 60 wild *Vitis* species have been identified in four main eco-geographic regions of China, but their relative levels of salt tolerance remain to be assessed (Wan et al., 2008). Currently, the Ramsey and Dogridge rootstocks of the *V. champinii* species, as well as the Fall grape, 140 Ruggeri, and 1103 Paulsen progenies of the *V. berlandieri* × *V. rupestris* cross have been established as salt-tolerant germplasms such that they are commonly used as rootstocks when seeking to breed novel salt-tolerant cultivars (Zhou-Tsang et al., 2021).

Given the long history of grape cultivation throughout the globe together with the diverse range of complex hybrids and rootstocks

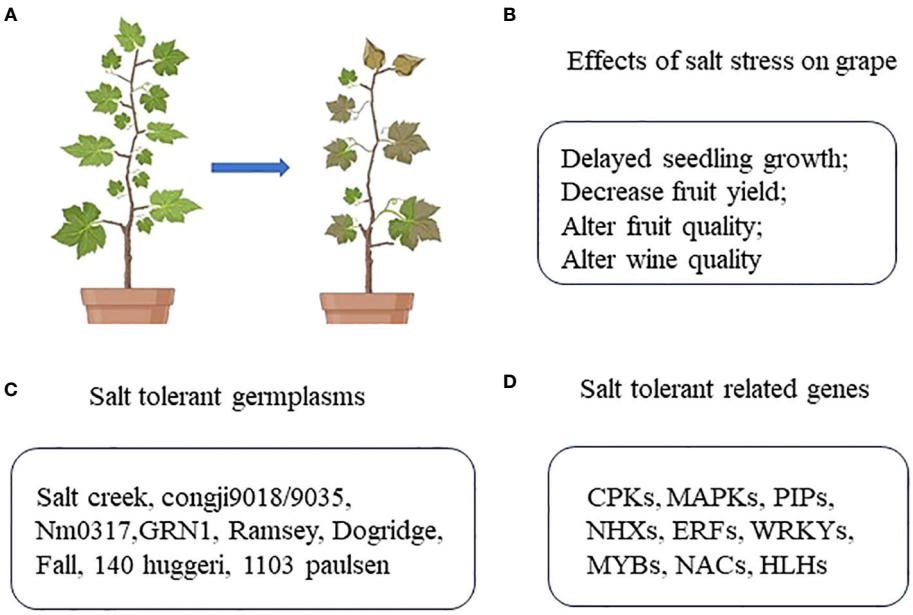

FIGURE 1
The effect of salt stress to grape. **(A)** The photo of a salt germplasm after watered with 100 mM NaCl for 4 weeks in pots. **(B)** The efffects of salt stress on grape. **(C)** The screened salt tolerant germplasms. **(D)** Identified salt tolerant related gen.

generated through vegetative propagation, anywhere from 6,000 to 10,000 grape cultivars are thought to exist, providing ample opportunities for germplasm resource collection (Laucou et al., 2011). While researchers have tirelessly worked to study the relative ability of different grape varieties to tolerate saline conditions, these efforts have not been comprehensive or systematic. As no unified standards for identifying salt-tolerant cultivars have been established and cultivation conditions may vary across studies, comparing the results of these different analyses is often not possible. There is thus a clear need to establish a precise high-throughput platform for analyzing grapevine germplasm salt tolerance, as such a system would enable to more effective identification of the raw materials needed to breed cultivars and rootstock varieties better equipped to tolerate soil salinization period.

Identification of salt tolerance-related grape genes

Exposure to salt stress subjected plants to simultaneous ionic and osmotic stress, with relevant grapevine research conducted to date having largely focused on osmotic responses, ion accumulation, and the physiological characteristics of tolerant tissues. Under high levels of salt stress, osmotic changes occur rapidly with a half-time to the inhibition of Arabidopsis seedling root conductivity of just 45 min in response to 100 mM NaCl (Boursiac et al., 2005). Ion accumulation and osmoprotectant production can alter the ability of plant cells to balance water retention, and the aquaporin family of water channel proteins have been identified as particularly important regulators of plant salt stress responses (Li et al., 2014a). Further, plants would induce salt stress signaling pathway to decrease the adverse effects of excess Na^+ and other ions. For instance, Ca^{2+}, phytohormone (abscisic acid, ethylene, salicylic acid etc.), reactive oxygen species and related cascade signal transduction reactions will be activated to adapt the salinity environment (Zhao et al., 2021).

Grapevines exhibiting high levels of soluble sugar and proline accumulation reportedly exhibit less severe growth inhibition and higher leaf chlorophyll and carotenoid concentrations (Fozouni et al., 2012). A range of other genes have also been shown to be induced in cultivars exposed to salt stress including glycine betaine-associated genes and genes encoding proteins that are abundant during the late phases of embryogenesis including *VvDNHN1* and *VvLEA-D29L* (İbrahime et al., 2019; Haider et al., 2019). Multiple aquaporins have also been reported to play a role in osmotic regulation and salt tolerance in grapevines at the cellular and whole-plant levels (Galmés et al., 2007; Vandeleur et al., 2009). However, the fine regulation mechanisms of the aquaporins are still unclear and the expression pattern of some genes is ecotype-dependent. For instance, *VvPIP2;2* expression has been shown to be induced in salt-sensitive Shirazi plants, yet its expression is inhibited in salt-tolerant Gharashani plants (Mohammadkhani et al., 2012).

While some grape varieties are better able than others to exclude salt ions, the ion concentrations in these plants will inevitably be higher when cultivated in saline soil as compared to non-saline soil. Accordingly, these plants must engage a series of processes at the molecular level to adapt to or mitigate this ionic stress. Protein kinases and transcription factors have been shown to be particularly important proteins that can integrate inputs from multiple ion homeostasis- and stress signaling-related pathways in *Vitis*. *VaCPK21* was reportedly significantly up-regulated in wild grape (*Vitis amurensis* Rupr.) plants exposed to salt stress, with improved salt tolerance following the overexpression of this gene in grape callus samples (Dubrovina et al., 2016). Ji et al. found that *VvMAPK9* can serve as a positive regulator of Arabidopsis and grape callus adaptability through its ability to regulate antioxidant system activity. The highest levels of *VvMAPK9* expression were observed in root and leaf tissues, with pronounced induction in grapes in response to abscisic acid (ABA) or abiotic stressors such as high temperatures, salt, or drought conditions. Arabidopsis seedlings overexpressing *VvMAPK9* exhibited enhanced salt tolerance, and the germination rates of transgenic lines were higher, with these plants exhibiting superior growth and longer roots under salt stress conditions as compared to wild-type plants. The expression of antioxidant enzyme (SOD and POD)s and ion transporter-related proteins (NHXP, HKT1, HKT2) was also significantly elevated in these *VvMAPK9*-overexpressing grape callus samples under salt stress conditions (Ji et al., 2022).

Transcription factors are expressed in all eukaryotic species and are essential regulators of signaling activity in plants exposed to abiotic stress conditions, promoting the upregulation of stress resistance-related genes such that they are an important focus of research exploring stress tolerance in plants. A transcriptomic analysis of grapes exposed to salt stress identified 52 transcription factors including WRKYs, EREBs, MYBs, NACs, and bHLHs among the 343 differentially expressed genes (Upadhyay et al., 2018). The C-repeat (CRT)/dehydration-responsive element (DRE) protein family is comprised of key regulators of plant abiotic stress tolerance, and the CRT/DRE binding factor *VaCBF4* can be induced in *V. amurensis* in response to cold, drought, ABA, saline conditions, and other abiotic stressors, improving the ability of Arabidopsis seedlings to tolerate cold, drought, and salt stress when overexpressed (Li et al., 2013). VvWRKY30 is a transcription factor that is primarily expressed in leaves and shoot tips and that can be induced in response to salt stress, H_2S, and H_2O_2, enhancing the ability of plant seedlings to tolerant saline conditions through the enhanced elimination of reactive oxygen species and osmotic membrane accumulation. When *VvWRKY30* is overexpressed, seedlings reportedly exhibit improved antioxidant activity and corresponding reductions in reactive oxygen species, together with increases in soluble sugar and proline content and the concomitant upregulation of genes associated with antioxidant biosynthesis, sugar metabolism, and proline biosynthesis under salt stress conditions (Zhu et al., 2019). The *VviERF073* transcription factor is a member of the APETALA2/ethylene response factor (*AP2/ERF*) family firstly identified as a salt stress-inducible gene in a salt stress EST library, although subsequent reports of its functional role in grape plants exposed to salt stress conditions have been lacking (Shinde et al., 2017). The helix-loop-helix transcription factor *VvbHLH1* can significantly enhance flavonoid accumulation within Arabidopsis seedlings when

overexpressed in a codon-optimized isoform, with further research suggesting that it can also shape drought and salt tolerance in Arabidopsis plants through the augmentation of ABA signal transduction and flavonoid accumulation (Wang et al., 2016). *VpSBP16* encodes a SQUAMOSA promoter binding protein (SBP) box transcription factor that was cloned from the Chinese wild grape 'Baihe 35-1' variety that was found to regulate SOS and ROS signaling cascades to improve salt and drought stress tolerance during seed germination. Consistently, transgenic Arabidopsis seedlings in which *VpSBP16* was overexpressed exhibited increased root length and seed germination rates as compared to wild-type plants exposed to osmotic stress (Hou et al., 2018).

Under salt stress conditions, Na^+/H^+ antiporter (NHX) proteins can facilitate the ATP-dependent transport and sequestration of Na^+, thereby effectively mitigating ionic stress in plants. The *AtNHX1* gene reportedly conferred 'Thompson seedless' grape plants with a level of salt tolerance similar to that observed for other salt-tolerant cultivars ('Pedro Gimenez' and 'Criolla Chica'). 'Thompson seedless' seedlings overexpressing the Arabidopsis-derived *AtNHX1* gene exhibited growth that was better than that of wild-type seedlings when treated for 7 weeks with 150 mM NaCl including significant improvements in stem length, leaf area, and dry weight (Venier et al., 2018). When overexpressed in potato seedlings, grape-derived *VvNHX1* was similarly able to improve salt tolerance. These transgenic seedlings also reportedly exhibited higher levels of soluble sugar, Mg^{2+}, and K^+, together with enhanced antioxidant enzyme activity and reductions in Na^+ accumulation and oxidative stress (Li et al., 2014b; Charfeddine et al., 2019).

Cultivation practices that can improve the salt tolerance of grape plants

The application of optimized cultivation and management practices has the potential to improve the ability of grape plants to tolerate salt stress. Appropriately managing soil and water can help decrease the adverse effects of saline conditions on grape plants. Low ABA concentrations, for example, can render cells better able to adapt to saline conditions while reducing transpiration and the passive absorption of salt ions, supporting a link between ABA accumulation and the expression of functional genes including *VvNHX1* and *VvOSM1* (Saleh et al., 2020). Vineyard management technologies can help alleviate salinization by prolonging irrigation time to leach Na^+ and Cl^- accumulated in the root zone, or by artificial ditches to induce rainfall inflow to leach salt in the soil below a depth of 1.5 m in the ground. The partial root drying (PRD) technique was designed to optimize the efficiency of water use for viticulture by reducing irrigation while improving fruit quality (Dry et al., 2000). Degaris et al. explored the effects of moderately saline water on Shiraz and Grenache vines grown in pots using the PRD irrigation technique, which reduces the amount of water used by 50% relative to control conditions (Degaris et al., 2016). Their results suggested that PRD-irrigated vines exhibited higher levels of Cl^-, Na^+, K^+, and Ca^{2+} ions, but that Cl^- can be partitioned away from leaves on a total content basis relative to controls. These results demonstrate that combining PRD irrigation techniques and saline water can alter ion levels and allocation within grapevines, underscoring the need to monitor field water during the growing season to promote long-term vine health and improved fruit composition.

ABA can reportedly induce phytochemical and morphological changes that can enhance the ability of grape plants to tolerate salt stress. Grape rootstocks with superior tolerance characteristics have been found to accumulate higher levels of ABA when exposed to salt stress (Upreti and Murti, 2010). Relative to untreated seedlings, seedlings subjected to exogenous ABA treatment exhibited increases in plant height, leaf area, leaf number, and shoot dry matter together with increases in leaf flavonoid, proline, soluble sugar, and phenol levels and enhanced activity of antioxidant enzymes including catalase, guaiacol peroxidase, and ascorbic acid peroxidase (Stevens et al., 2011). Acetic acid and oxalic acid irrigation can also promote significant increases in the root activity and leaf chlorophyll content of treated 'Fuke' cuttings exposed to salt stress while reducing root malondialdehyde levels and leaf H_2O_2 concentrations (Guo et al., 2018).

Discussion

Soil salinization represents an increasingly severe threat to agronomic productivity throughout the globe, endangering the reliable production of foods necessary for human survival. Most popular grape varieties cultivated at present are of European provenance, but many of these exhibit relatively low poor tolerance for soil salinity. Further efforts to leverage stress-resistant wild grape germplasm resources thus have the potential to provide key genes and rootstocks needed to breed salt-tolerant grape varieties. *V. riparia*, *V. champini*, *V. berlandier*, and *V. shuttleworthii* are salt-resistant North American grape varieties that represent promising rootstock materials for the further breeding of salt-tolerant varieties. Further efforts to understand the physiological and ecological characteristics and mechanisms governing rootstock salt tolerance will offer a scientific basis for the more effective breeding and cultivation of grape varieties that can tolerate rising levels of soil salinity.

Recent studies of grape salt tolerance have largely centered around efforts to evaluate germplasm resources, characterize physiological salt tolerance mechanisms, and related topics, providing a foundation for the breeding of salt-tolerant grapes. However, insufficient work focused on the isolation, cloning, and regulated expression of salt tolerance-related grape genes has been performed to date. There is thus an urgent need to develop biotechnology-based approaches to enhancing the adaptability of grape plants to salinized soil. The ongoing development of proteomics and functional genomics platforms, together with the application of novel technologies such as expressed sequence tags, cDNA microarrays, transposon tags, and T-DNA tags provide new opportunities for the more straightforward isolation and characterization of salt tolerance-associated genes in the future.

Based on the findings reported in this review, we believe that research evaluating salt-tolerant grape germplasm resources is still in its early stages with a clear lack of systematic research efforts. It is

therefore crucial that a salt-tolerant germplasm resource database be established to provide robust data that can support breeding efforts. Wild grape resources are widely distributed and represent a rich source of novel genetic elements that warrant a higher degree of attention. These ongoing efforts to identify key salt tolerance-related genes and to more fully outline the functional relationship between salt stress and signaling activity in wild grapes may provide a foundation for the targeted breeding of salt-tolerant grapes through the appropriate application of genomics and proteomics techniques.

To date, studies focused on identifying salt-tolerant grape germplasm resources have largely been restricted to laboratory settings, since NaCl irrigation is generally used to simulate soil salinization as a means of testing seedling or seed responses to a range of salt concentrations. These artificial conditions, however, differ from true soil salinity. Tests of salt tolerance-related gene functions have also primarily been conducted in Arabidopsis model plants, limiting efforts to comprehensively survey and validate salt tolerance in grape germplasm resources. As such, while these prior findings provide a valuable foundation for further research efforts, they must be interpreted with caution owing to these limitations, underscoring the need for additional systematic physiological research efforts to better expand the current understanding of salt tolerance in grape cultivars.

Author contributions

YH: Conceptualization, Project administration, Writing – original draft, Writing – review & editing. XL: Conceptualization, Funding acquisition, Investigation, Supervision, Writing – original draft, Writing – review & editing.

Funding

The author(s) declare financial support was received for the research, authorship, and/or publication of this article. Key R&D Plan of Shandong Province (2022TZXD0011); Shandong Province Agricultural Major Technology Collaborative Promotion Project (SDNYXTTG-2023-18) and the Innovation program of SAAS (CXGC2023A47).

Conflict of interest

The authors declare that the research was conducted in the absence of any commercial or financial relationships that could be construed as a potential conflict of interest.

Publisher's note

References

Aradhya, M. K., Dangl, G. S., Prins, B. H., Boursiquot, J.-M., Walker, M. A., Meredith, C. P., et al. (2003). Genetic structure and differentiation in cultivated grape, Vitis vinifera L. *Genet. Res.* 81, 179–192. doi: 10.1017/S0016672303006177

Bent, C. M. (2017). *Root Architecture Traits of Grapevine Rootstocks are Related to Salt Tolerance* (California, USA: University of California, Davis).

Boursiac, Y., Chen, S., Luu, D.-T., Sorieul, M., Van Den Dries, N., Maurel, C., et al. (2005). Early effects of salinity on water transport in Arabidopsis roots. Molecular and cellular features of aquaporin expression. *Plant Physiol.* 139, 790–805. doi: 10.1104/pp.105.065029

Charfeddine, S., Charfeddine, M., Hanana, M., and Gargouri-Bouzid, R. (2019). Ectopic expression of a grape vine vacuolar NHX antiporter enhances transgenic potato plant tolerance to salinity. *J. Plant Biochem. Biotech.* 28, 50–62. doi: 10.1007/s13562-018-0462-x

Degaris, K., Walker, R. R., Loveys, B., and Tyerman, S. (2016). Comparative effects of deficit and partial root-zone drying irrigation techniques using moderately saline water on ion partitioning in Shiraz and Grenache grapevines. *Aus. J. Grape Wine Res.* 22, 296–306. doi: 10.1111/ajgw.12220

Dry, P., Loveys, B., and Düring, H. (2000). Partial drying of the rootzone of grape. I. Transient changes in shoot growth and gas exchange. *Vitis* 39, 3–7.

Dubrovina, A. S., Kiselev, K. V., Khristenko, V. S., and Aleynova, O. A. (2016). VaCPK21, a calcium-dependent protein kinase gene of wild grapevine Vitis amurensis Rupr., is involved in grape response to salt stress. *Plant Cell Tiss. Org.* 124, 137–150. doi: 10.1007/s11240-015-0882-4

Fort, K. P., Lowe, K. M., Thomas, W. A., and Walker, M. A. (2013). Cultural conditions and propagule type influence relative chloride exclusion in grapevine rootstocks. *Am. J. Enol. Vitic.* 64, 241–250. doi: 10.5344/ajev.2013.12073

Fozouni, M., Abbaspour, N., and Baneh, H. D. (2012). Leaf water potential, photosynthetic pigments and compatible solutes alterations in four grape cultivars under salinity. *Vitis* 51, 147–152.

Galmés, J., Pou, A., Alsina, M. M., Tomas, M., Medrano, H., Flexas, J., et al. (2007). Aquaporin expression in response to different water stress intensities and recovery in Richter-110 (Vitis sp.): relationship with ecophysiological status. *Planta* 226, 671–681. doi: 10.1007/s00425-007-0515-1

Guo, S.-H., Niu, Y.-J., Zhai, H., Han, N., and Du, Y.-P. (2018). Effects of alkaline stress on organic acid metabolism in roots of grape hybrid rootstocks. *Sci. Hortic.* 227, 255–260. doi: 10.1016/j.scienta.2017.09.051

Haider, M. S., Jogaiah, S., Pervaiz, T., Yanxue, Z., Khan, N., and Fang, J. (2019). Physiological and transcriptional variations inducing complex adaptive mechanisms in grapevine by salt stress. *Environ. Exp. Bot.* 162, 455–467. doi: 10.1016/j.envexpbot.2019.03.022

Heinitz, C., Fort, K., and Walker, M. A. (2014). "Developing drought and salt resistant grape rootstocks," in *XI International Conference on Grapevine Breeding and Genetics 1082*, Beijing, China, 305–312.

Hou, H., Jia, H., Yan, Q., and Wang, X. (2018). Overexpression of a SBP-box gene (VpSBP16) from Chinese wild Vitis species in Arabidopsis improves salinity and drought stress tolerance. *Int. J. Mol. Sci.* 19, 940. doi: 10.3390/ijms19040940

İbrahime, M., Kibar, U., Kazan, K., Yüksel Özmen, C., Mutaf, F., Demirel, A. S., et al. (2019). Genome-wide identification of the LEA protein gene family in grapevine (Vitis vinifera L.). *Tree Genet. Genomes* 15, 1–14.

Ji, X., Sui, C., Yu, Y., Liu, X., Li, B., and Sun, Q. (2022). Grape VvMAPK9 positively regulates salt tolerance in Arabidopsis and grape callus through regulating the antioxidative system. *Plant Cell Tiss. Org.* 148, 609–622. doi: 10.1007/s11240-021-02218-9

Laucou, V., Lacombe, T., Dechesne, F., Siret, R., Bruno, J.-P., Dessup, M., et al. (2011). High throughput analysis of grape genetic diversity as a tool for germplasm collection management. *Theor. Appl. Genet.* 122, 1233–1245. doi: 10.1007/s00122-010-1527-y

Li, J., Jia, H., Wang, J., Cao, Q., and Wen, Z. (2014b). Hydrogen sulfide is involved in maintaining ion homeostasis *via* regulating plasma membrane Na^+/H^+ antiporter

system in the hydrogen peroxide-dependent manner in salt-stress Arabidopsis thaliana root. *Protoplasma* 251, 899–912. doi: 10.1007/s00709-013-0592-x

Li, G., Santoni, V., and Maurel, C. (2014a). Plant aquaporins: roles in plant physiology. *BBA Gen. Subj.* 1840, 1574–1582. doi: 10.1016/j.bbagen.2013.11.004

Li, J., Wang, N., Xin, H., and Li, S. (2013). Overexpression of VaCBF4, a transcription factor from Vitis amurensis, improves cold tolerance accompanying increased resistance to drought and salinity in Arabidopsis. *Plant Mol. Biol. Rep.* 31, 1518–1528. doi: 10.1007/s11105-013-0627-7

Maas, E. V., and Hoffman, G. J. (1977). Crop salt tolerance-current assessment. *J. Irrig. Drain. Division* 103, 115–134. doi: 10.1061/JRCEA4.0001137

Mohammadkhani, N., Heidari, R., Abbaspour, N., and Rahmani, F. (2012). Growth responses and aquaporin expression in grape genotypes under salinity. *Iran J. Plant Physiol.* 2, 497–507.

Qadir, M., Quillérou, E., Nangia, V., Murtaza, G., Singh, M., Thomas, R. J., et al. (2014). Economics of salt-induced land degradation and restoration. *Nat. Resour. Forum* 38 (4), 282–295. doi: 10.1111/1477-8947.12054

Saleh, B., Alshehadah, E., and Slaman, H. (2020). Abscisic acid (ABA) and salicylic acid (SA) content in relation to transcriptional patterns in Grapevine (*Vitis vinifera* L.) under salt stress. *J. Plant Biochem. Physiol.* 8, 245.

Shinde, M., Upadhyay, A., Iquebal, M., and Upadhyay, A. (2017). Identification, characterization and expression analysis of ERF transcription factor VviERF073 and standardization of stable reference genes under salt stress in grape. *Vistis* 55, 165–171.

Stevens, R. M., Harvey, G., Norton, S., and Frahn, W. (2011). Over-canopy saline sprinkler irrigation of grapevines during different growth stages. *Agric. Water Manage.* 101, 62–70. doi: 10.1016/j.agwat.2011.09.003

Upadhyay, A., Gaonkar, T., Upadhyay, A. K., Jogaiah, S., Shinde, M. P., Kadoo, N. Y., et al. (2018). Global transcriptome analysis of grapevine (*Vitis vinifera* L.) leaves under salt stress reveals differential response at early and late stages of stress in table grape cv. Thompson Seedless. *Plant Physiol. Biochem.* 129, 168–179. doi: 10.1016/j.plaphy.2018.05.032

Upreti, K., and Murti, G. (2010). Response of grape rootstocks to salinity: changes in root growth, polyamines and abscisic acid. *Biol. Plant* 54, 730–734. doi: 10.1007/s10535-010-0130-z

Vandeleur, R. K., Mayo, G., Shelden, M. C., Gilliham, M., Kaiser, B. N., and Tyerman, S. D. (2009). The role of plasma membrane intrinsic protein aquaporins in water transport through roots: diurnal and drought stress responses reveal different strategies between isohydric and anisohydric cultivars of grapevine. *Plant Physiol.* 149, 445–460. doi: 10.1104/pp.108.128645

Venier, M., Agüero, C., Bermejillo, A., Filippini, M., Hanana, M., et al. (2018). Analysis of salinity tolerance of Vitis vinifera'Thompson Seedless' transformed with AtNHX1. *Vitis* 57, 143–150.

Wan, Y., Schwaninger, H., Li, D., Simon, C., Wang, Y., and He, P. (2008). The eco-geographic distribution of wild grape germplasm in China. *Vitis* 47, 77.

Wang, F., Zhu, H., Chen, D., Li, Z., Peng, R., and Yao, Q. (2016). A grape bHLH transcription factor gene, *VvbHLH1*, increases the accumulation of flavonoids and enhances salt and drought tolerance in transgenic Arabidopsis thaliana. *Plant Cell Tiss. Org.* 125, 387–398. doi: 10.1007/s11240-016-0953-1

Zaman, M., Shahid, S. A., Heng, L., Shahid, S. A., Zaman, M., and Heng, L. (2018). "Soil salinity: Historical perspectives and a world overview of the problem," in *Guideline for Salinity Assessment, Mitigation and Adaptation Using Nuclear and Related Techniques*. (Cham: Springer Nature), 43–53.

Zhao, S., Zhang, Q., Liu, M., Zhou, H., Ma, C., and Wang, P. (2021). Regulation of plant responses to salt stress. *Int. J. Mol. Sci.* 22 (9), 4609. doi: 10.3390/ijms22094609

Zhou-Tsang, A., Wu, Y., Henderson, S., Walker, A., Borneman, A., Walker, R. R., et al. (2021). Grapevine salt tolerance. *Aust. J. Grape Wine R.* 27, 149–168. doi: 10.1111/ajgw.12487

Zhu, D., Hou, L., Xiao, P., Guo, Y., Deyholos, M. K., and Liu, X. (2019). VvWRKY30, a grape WRKY transcription factor, plays a positive regulatory role under salinity stress. *Plant Sci.* 280, 132–142. doi: 10.1016/j.plantsci.2018.03.018

frontiers | Frontiers in Plant Science

TYPE Original Research
PUBLISHED 11 March 2024
DOI 10.3389/fpls.2024.1368260

OPEN ACCESS

EDITED BY
Hui Song,
Qingdao Agricultural University, China

REVIEWED BY
Qi Wang,
Shandong Peanut Research Institute, China
Rajib Roychowdhury,
Volcani Center, Israel

*CORRESPONDENCE
Chuanzhi Zhao
chuanzhiz@126.com

RECEIVED 10 January 2024
ACCEPTED 26 February 2024
PUBLISHED 11 March 2024

CITATION
Li G, Guo X, Sun Y, Gangurde SS, Zhang K, Weng F, Wang G, Zhang H, Li A, Wang X and Zhao C (2024) Physiological and biochemical mechanisms underlying the role of anthocyanin in acquired tolerance to salt stress in peanut (*Arachis hypogaea* L.). *Front. Plant Sci.* 15:1368260. doi: 10.3389/fpls.2024.1368260

Physiological and biochemical mechanisms underlying the role of anthocyanin in acquired tolerance to salt stress in peanut (*Arachis hypogaea* L.)

Guanghui Li[1], Xin Guo[1], Yanbin Sun[1], Sunil S. Gangurde[2], Kun Zhang[3], Fubin Weng[1,4], Guanghao Wang[1], Huan Zhang[1,4], Aiqin Li[1], Xingjun Wang[1] and Chuanzhi Zhao[1]*

[1]Shandong International Joint Laboratory of Agricultural Germplasm Resources Innovation, Institute of Crop Germplasm Resources (Institute of Biotechnology), Shandong Academy of Agricultural Sciences, Jinan, China, [2]Center of Excellence in Genomics & Systems Biology (CEGSB), International Crops Research Institute for the Semi-Arid Tropics (ICRISAT), Hyderabad, India, [3]College of Agronomy, Shandong Agricultural University, Taian, China, [4]College of Life Sciences, Shandong Normal University, Jinan, China

Anthocyanin is an important pigment that prevents oxidative stress and mediates adaptation of plants to salt stress. Peanuts with dark red and black testa are rich in anthocyanin. However, correlation between salt tolerance and anthocyanin content in black and dark red testa peanuts is unknown. In this study, three peanut cultivars namely YZ9102 (pink testa), JHR1 (red testa) and JHB1 (black testa) were subjected to sodium chloride (NaCl) stress. The plant growth, ion uptake, anthocyanin accumulation, oxidation resistance and photosynthetic traits were comparatively analyzed. We observed that the plant height, leaf area and biomass under salt stress was highly inhibited in pink color testa (YZ9102) as compare to black color testa (JHB1). JHB1, a black testa colored peanut was identified as the most salt-tolerance cultivar, followed by red (JHR1) and pink(YZ9102). During salt stress, JHB1 exhibited significantly higher levels of anthocyanin and flavonoid accumulation compared to JHR1 and YZ9102, along with increased relative activities of antioxidant protection and photosynthetic efficiency. However, the K^+/Na^+ and Ca^{2+}/Na^+ were consistently decreased among three cultivars under salt stress, suggesting that the salt tolerance of black testa peanut may not be related to ion absorption. Therefore, we predicted that salt tolerance of JHB1 may be attributed to the accumulation of the anthocyanin and flavonoids, which activated antioxidant protection against the oxidative damage to maintain the higher photosynthetic efficiency and plant growth. These findings will be useful for improving salt tolerance of peanuts.

KEYWORDS

peanut, testa color, salt stress, anthocyanin, oxidation resistance, photosynthesis

1 Introduction

Peanut (*Arachis hypogaea* L.) is widely cultivated in more than 100 countries, with the annual yield of 43.98 million tons, representing one of the most important oil and cash crops specially in Africa and Asia (Zhao et al., 2020). Peanut seeds containing 44% to 56% oil, are the fourth largest source of edible oil globally. In addition, peanuts are rich in protein (22%-30%), carbohydrates (10%-20%), as well as vitamins, essential fatty acids, and necessary minerals for human nutrition (Mondal et al., 2020). China has the greatest peanut production in the world, and is second, after India in the plant area (4.45 million hectares). China is expected to account for more than 40% of the world's peanut oil (Zhao et al., 2012). Over the past few decades, the most planting and processing of peanut cultivars are with pink or red testa. The variation of peanut testa color is mainly due to the difference in anthocyanin content, a highly diverse group of secondary metabolism product that contribute to plants color. Recently, the peanut planting and consumption pattern with market demands has been changed. Peanuts with purple and black testa color have attracted increasing attention of consumers in the market, due to their higher anthocyanin and microelements contents important for human health (Bonku and Yu, 2020).

Soil salinization is a major threat for agriculture worldwide, limits crop yield and restricts use of arable and uncultivated land. It has been estimated that more than 8% of the world's land is affected by salinity, and it is continuously increasing (Ait-El-Mokhtar et al., 2020). Soil salinity causes a more than 20% reduction of agricultural yields (Porcel et al., 2012). Salinity can cause osmotic stress, ion imbalance and oxidative damage to plants normal physiological processes, and the plants have evolved sophisticated mechanisms to cope with salinity stress (Abogadallah, 2010).

Peanut was considered to be moderately salt-tolerant crop by the Food and Agriculture Organization (FAO). However, peanut production suffers great challenge by salt-stress because of the widely distributed saline-alkaline land in major peanut regions in China, India and United States of America (Luo et al., 2021). Salinity significantly inhibits peanut germination, relative growth rate and dry mass production (Meena et al., 2016), induced photo-inhibition because of damaging the photosynthetic apparatus (Qin et al., 2011), and restrained Ca, K and other mineral elements uptake, and eventually reduced yield and quality (Zhang et al., 2020). Significant genetic diversity is available for salinity tolerance among peanut germplasms (Zou et al., 2020).

In the past few years, a series of agronomic measures were widely adopted to enhance salt-tolerance of peanut, including selecting salt-tolerant cultivars (Meena et al., 2016; Zhang et al., 2020), mulching film and potassium application (Chakraborty et al., 2016; Meena et al., 2022), inoculating salt-tolerant rhizobacteria and arbuscular mycorrhizal fungi (El-Akhal et al., 2012; Sharma et al., 2016; Qin et al., 2021), and exogenous growth regulator (Tian et al., 2019; Li W. J. et al., 2022). In addition, the identification and utilization of salt tolerant genes have been used to improve the salinity tolerance of peanut cultivars (Banavath et al., 2018; Zhu et al., 2021). However, the production and economical outcome of peanut in saline-alkali soil was still limited. Therefore, improvement of salt tolerance is necessary to minimize the resulting yield loss due to salt stress.

Secondary metabolites play a key role in the adaptation of plants to the changing environment and in overcoming stress conditions. Anthocyanin, a secondary metabolite in plants, serves as an important antioxidant, increases the antioxidant activity and enhances the ability of abiotic stress tolerance (Xu and Rothstein, 2018). The salt-tolerant cultivars showed higher anthocyanin content and total antioxidant activity than the salt-sensitive cultivars under salt stress, exhibited more physiological activities (Daiponmak et al., 2010). Accumulation of higher levels of anthocyanin is considered as one of the selection criteria for salt tolerance (Eryılmaz, 2006). The cultivars with deep red or black color (more intense anthocyanin) in apple (Wang et al., 2015), rice (Chunthaburee et al., 2016), spinach (Kitayama et al., 2019) and *Brassica napus* (Kim et al., 2017) suffered less physiology and cellular damages and lower growth inhibition under salt stress as compared to the ones with less anthocyanin content, showed a stronger salt tolerance.

Most of the previous studies on salt stress or enhancing salt-tolerance in peanut mainly used common cultivars with pink testa color. There is significant difference in anthocyanin content among peanut cultivars with different testa colors. However, there are no reports on the salt tolerance and regulatory mechanism of peanut cultivars with black and red testa colors. Therefore, a pot experiment was conducted in greenhouse to screen the salt tolerance among three peanut cultivars with different testa colors. The data recorded on anthocyanin and flavonoid contents, ion uptake, antioxidant activity and photosynthetic traits of three peanut cultivars in response to salinity stress. This work provided a foundation for screening salt resistant peanut cultivars and peanut high-yield cultivation in saline-alkali soil, and laid a basis for further revealing the salt-tolerant mechanism of colored peanut.

2 Materials and methods

2.1 Plant materials and treatments

Three peanut cultivars, YZ9102 (pink testa), JHR1 (red testa) and JHB1 (black testa), were used in this study (Figure 1A). YZ9102, bred by Henan Academy of Agriculture Sciences, was offspring of "BS1016" (♀) × "A. *coacoense*" (♂). JHR1 and JHB1, bred by our group, were offspring of "YZ9102" (♀) × "ZH12" (♂), and "FH1" (♀) × "ZH9" (♂), respectively.

The pot experiment was conducted in a growth chamber in controlled conditions. Matured seeds no pests or diseases and with uniform size and weight were selected, and surface sterilized by soaking in 75% ethyl alcohol with slightly shaking for 5 min and rinsed using sterilized deionized water for 3 times. Three seeds were sown in each square plastic pot (10.5 cm top diameter, 11 cm height) filled with sterilized clean river sand 0.95 kg, and two

10.3389/fpls.2024.1368260

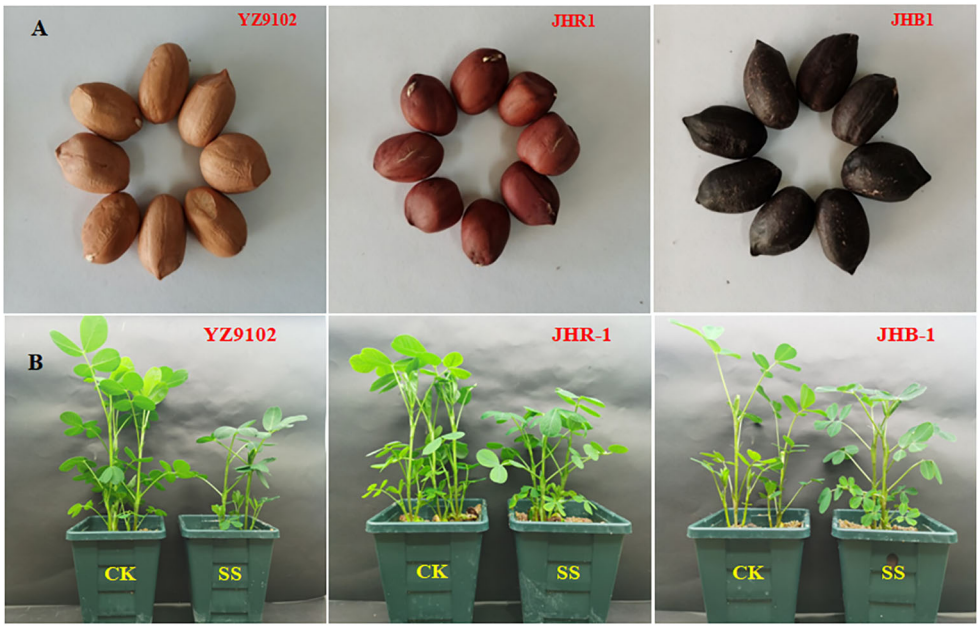

FIGURE 1
The seeds of three peanut cultivars **(A)** and the phenotype of three peanut cultivars under CK and SS **(B)**. CK, meaning plants were watered by Hoagland solution without NaCl, and SS, meaning plants were watered by Hoagland solution with 150 mM NaCl.

uniform seedlings were kept in each pot after germination. The climatic chamber was controlled at 25°C, alternation of light and dark period at 16 h/8 h. Seven days after germination, the plants of each cultivar were divided into two groups. Our preliminary experiment showed that the salt tolerance had the most significant difference in ten peanut cultivars under 150 mM NaCl stress. So, one group was designated as control (CK) irrigated by the Hoagland solution, the other group was challenged with salt stress treatment (SS) irrigated by the Hoagland solution and salt concentration of 150 mM NaCl. Each treatment consisting of twenty pots was watered daily uniformly with 100 mL Hoagland solution with or without NaCl per pot to maintain the treatment level.

After 1, 5 and 10 days of salt stress, leaf materials were sampled and immediately transferred into liquid nitrogen and stored at -80° C to estimate enzymatic activity. The flavonoid and anthocyanin contents were determined with the leaf samples at 5 and 10 days of salt stress. Leaf gas exchange and chlorophyll fluorescence parameters were measured on the second top leaf on the main stem after 5 and 10 days of salt stress. K^+, Na^+, and Ca^{2+} contents in leaf and stem were determined after 10 days of salt stress. Furthermore, the plants were harvested at 10 d after salt stress for biomass and phenotypic analysis.

2.2 Determination of dry weight and leaf area

Five representative plants were selected from each treatment after 10 d of salt stress, and separated into roots, stems and leaves. In each treatment, fifty random leaflets were punched into wafers with 1.2 cm diameter avoiding the main vein. All plant samples were oven dried at 105°C for 30 min followed at 80 °C until reaching a constant dry weight. The total dry weight (DW), the total wafers area (S1), wafers dry weight (M1) and other leaves dry weight (M2) were recorded. The leaf area (S) was calculated using the following formula: S= S1× (M1+M2)/M1.

2.3 Determination of Na^+, K^+ and Ca^{2+} ions

Dried leaf and stem samples were milled to powder, weighed, and then digested by nitric acid in a bottle tube at 320°C for 5 h. Na^+, K^+ and Ca^{2+} ion concentration was measured by atomic adsorption spectrometer with a flame photometer (ZL5100, PerkinElmer Inc., USA). Each treatment was repeated with three biological replicates and three technical replicates.

2.4 Determination of total flavonoids

Total flavonoids content was measured by the colorimetric method (Jia et al., 1999). 0.3 g fresh leaf was cutinto pieces and extracted in a 60°C water bath for 1 hour in a test tube with 70% ethanol (10 mL), and then filtered through two layers of filter paper. The 5 mL filtrate was added into 0.5 mL of 5% $NaNO_2$ and 6 min later 0.5 mL of 10% $Al(NO_3)_3$. After 6 min, 4 mL of 4% NaOH was added to the mixture. The solution was mixed well, and after 15 min, the absorbance was recorded at 510 nm in spectrophotometer (U-3000, HITACHI, Japan).

2.5 Determination of anthocyanin

The anthocyanin content was measured using the protocol reported by Zhang et al. (2022). Frozen leaf (approximately 50 mg) was ground in a 5 mL centrifuge tube using liquid nitrogen. Then, homogenized sample was extracted at 4°C by adding 700 µL acidic methanol (the volume ratio of methanol to HCl is 99:1). After overnight incubation, the homogenates were centrifuged at 4°C at 12,000×*g* for 10 min. About 600 µL supernatant was collected and mixed with 1 mL trichloromethane and 400 µl distilled water, centrifuged at 4°C at 12,000×*g* for 10 min. The absorbance of the supernatant was recorded at 530 and 657 nm using spectrophotometer (U-3000, HITACHI, Japan).

2.6 Antioxidant enzymes activity and MDA content

Leaf samples (0.5 g) were homogenized using a pre-cooled mortar in 50 mM potassium phosphate buffer (pH7.8) at 0~4°C. The homogenate was filtered through two layers of filter paper and centrifuged at 10,000×*g* for 20 min at 4°C. The supernatant was used for enzyme activity analysis.

Superoxide dismutase (SOD) activity was measured by the method of Giannopolitis and Ries (1977). The reaction mixture consisted of 50 mM phosphate buffer (pH 7.8), 13 mM methionine, 75 mM nitrotetrazolium blue chloride (NBT), 0.1 mM ethylene diamine tetraacetic acid (EDTA) and 2 mM riboflavin. Reactions with 50 µL enzyme extract and 3 mL reaction mixture were carried out in a light incubator under a light intensity of 4000 Lux for 30 min. One unit of SOD was defined as the amount of enzyme which causes 50% inhibition of the NBT reduction. The reduction of NBT was measured by an ultraviolet spectrophotometer at 560 nm.

Peroxidase (POD) activity was determined based on guaiacol colorimetric method. Reaction mixture contained 50 mL 100 mM potassium phosphate (pH 6.0), 30 µL 0.3 mM guaiacol, and 20 µL 30% H_2O_2. The 20 µL enzyme solution and 3 mL reaction mixture were added into the colorimetric cup to start the reaction. Absorbance was recorded at 470 nm at every 30 s intervals for a total of 5 readings. The activity of the POD enzyme was expressed by the change of value of absorbance per minute (Nickel and Cunningham, 1969).

Catalase (CAT) activity was measured according to Aebi (1984). 50 µL enzyme solution was added into 3 mL reaction system (2.4 mL of 100 mM potassium phosphate (pH 7.0), 0.6 mL of 100 mM H_2O_2). Absorbance was recorded at 240 nm at every 30 s intervals for a total of 5 readings. The activity of the CAT enzyme was expressed by the reduction of absorbance per minute.

Malondialdehyde (MDA) was assayed by the thiobarbituric acid reaction method (Hodges et al., 1999). Frozen sample of 0.5 g was homogenized in 0.1% (w/v) trichloroacetic acid (TCA) solution. The homogenate was centrifuged at 12,000×*g* for 10 min. 1 mL supernatant was added to 2 mL of 20% TCA containing 0.6% thiobarbituric acid (TBA) in a clean glass tube. The mixture was heated in a water bath at 90°C for 30 min, cooled on ice immediately, and centrifuged at 4000×*g* for 10 min. The absorbance was recorded at 600, 532 and 450 nm.

2.7 Determination of gas exchange

After 5 and 10 days of salt stress, leaf photosynthesis was determined on the second top leaf on the main stem of five plants in each treatment. Leaf photosynthesis rate (P_n), transpiration rate (T_r) and stomatal conductance (G_s) were measured with a portable photosynthesis system (Li-6400; LI-COR Inc., Lincoln, NE, USA) at 9:00-11:30 AM. The chamber was equipped with a red/blue LED light source setting PAR at 1200 µmol m^{-2} s^{-1} and ambient atmospheric CO_2 levels at 385µmol mol^{-1}. The water use efficiency of leaves (WUE) was calculated by using formula P_n/T_r.

2.8 Measurement of leaf chlorophyll fluorescence

Chlorophyll fluorescence parameters were measured with a portable pulse modulated fluorometer (FMS-2, Hansatech, England) on the same leaf whose gas exchange was measured. Tested leaves were kept in the dark for 30 min before measurement. The minimum (F_0), maximum fluorescence (F_m), steady state fluorescence (F_s), minimum fluorescence (F_0') and maximum fluorescencein the irradiation-adapted state (F_m') were determined. Quantum yield of PS II (*ΦPSII*), maximal photochemical efficiency (F_v/F_m) photochemical quenching coefficient (*qP*), electron transport rate (*ETR*), and non-photochemical quenching coefficient (*qNP*) were calculated as described by Rasouli et al. (2023).

2.9 Statistical analysis

All parameters were measured in at least three replications and expressed as means± standard deviation. The average of each trait was calculated with Microsoft Excel 2010, plotted by Sigmaplot10.0. Duncan's multiple range test was used to determine the significant difference between treatments ($P<0.05$) by SPSS Statistics 23. The relative values were calculated via the trait values under salt stress compared with those of CK.

3 Results

3.1 Plant growth and biomass accumulation

All of the tested peanut cultivars were observed to certain growth inhibition when subject to salt stress (Table 1 and Figure 1B). The plant stem height, leaf areas, fresh weight of all cultivars were significantly decreased as compared to CK under salt stress, those relative values were 0.60, 0.48 and 0.72 in YZ9102, 0.59, 0.52 and 0.79 in JHR1, and 0.69, 0.67 and 0.92 in JHB1, respectively.

TABLE 1 The phenotype and individual biomass accumulation of three peanut cultivars after 10 days under salt stress.

Cultivars	Treatment	Plant height (cm)	Leaf area (cm^2)	Fresh weight (g)	Dry weight (g)
YZ9102	CK	11.80 ± 0.57a	92.70 ± 5.84a	7.50 ± 0.38a	0.78 ± 0.04a
	SS	7.04 ± 0.60b	44.19 ± 5.27b	5.38 ± 0.49b	0.71 ± 0.07a
JHR1	CK	10.96 ± 0.71a	76.71 ± 9.64a	5.26 ± 0.19a	0.57 ± 0.02a
	SS	6.44 ± 0.59b	39.91 ± 5.64b	4.15 ± 0.21b	0.53 ± 0.05a
JHB1	CK	10.80 ± 0.81a	77.08 ± 7.66a	5.54 ± 0.23a	0.79 ± 0.02a
	SS	7.50 ± 0.69b	51.54 ± 3.68b	5.12 ± 0.11a	0.75 ± 0.04a

Data are means ± SD of three biological replicates. Different lowercase letters indicate significantly different between CK and SS at $p<0.05$. CK, meaning plants were watered by Hoagland solution without NaCl, and SS, meaning plants were watered by Hoagland solution with 150 mM NaCl.

The relative total dry weight values of YZ9102, JHR1 and JHB1 were 0.91, 0.93 and 0.95 under salt stress as compared to CK, reflecting the different salt tolerance of three cultivars.

3.2 Content of Na^+, K^+ and Ca^{2+}

Salt stress significantly enhanced the content of Na^+ in leaf and stem as compared to CK in all three cultivars (Figure 2A). The Na^+content in JHB1 showed the minimum increase of 83.10% and 84.44% in leaf and stem, and the maximum increase of 114.50% in leaf in JHR1, 103.71% in stem in YZ9102. With or without salt stress, the K^+ content of JHB1 was the most, following by JHR1.To compare with CK, all cultivars exhibited a slightly increased K^+ content in the leaf, however, a significantly decreased K^+ in the stem under salt stress (Figure 2B). The content of K^+ was slightly declined (23.65%) in stem of JHR1, and approximately 30% reduction in the other two cultivars under salt stress. With or without salt stress, JHR1 and JHB1 showed similar content of Ca^{2+}, and significantly higher than YZ9102. Salt stress significantly increased Ca^{2+}content of Ca^{2+} in the leaf tissue of three cultivars, and inappreciably restrained the content in stem as compared to CK (Figure 2C). The maximum increase (22.01%) of Ca^{2+} content in leaf was found in JHR1, followed by JHB1 and YZ9102.

The values of K^+/Na^+ were approximately consistent among all three cultivars, whereas, dramatically decrease under salt stress, as compared to CK (Figure 2D). K^+/Na^+ in leaf were decreased by 46.44%, 53.58% and 42.61% in YZ9102, JHR1 and JHB1, respectively. While, in stem the K^+/Na^+ were reduced by 65.44%, 65.39% and 62.74% among YZ9102, JHR1 and JHB1 cultivars respectively under salt stress. The values of Ca^{2+}/Na^+ showed the similar variation trend with K^+/Na^+ among the three cultivars under salt stress, whereas those experienced a smaller reduction under salt stress than that of K^+/Na^+ (Figure 2E).

3.3 Content of flavonoid and anthocyanin

The flavonoid content of YZ9102, JHR1 and JHB1 increased by 11.45%, 21.18% and 22.80% after 5 days of salt stress as compare to CK, further at 10 days of salt stress it was increased by 17.26%, 35.13% and 25.43% (Figure 3A). The higher level of flavonoid content was observed in JHB1, followed by JHR1 and YZ9102 in both control and salt stress. Salt stress significantly increased anthocyanin content in all three cultivars as compared to CK (Figure 3B). Maximum increase in anthocyanin content was recorded in JHR1, increasing 103.17% and 117.99% in contrast to CK after 5 and 10 days of salt stress, respectively. In cultivar YZ9102, the trend of increased anthocyanin content was much more apparent at 10 day of salt stress (74.39%) than that at 5 days (32.51%). Whereas, it was stable in cultivar JHB1 increased by 42.37% and 43.46% at 5 and 10 days of salt stress. With or without salt stress, the content of anthocyanin in JHB1 was significantly higher than those in JHR1 and YZ9102.

3.4 Antioxidant enzyme activity

We observed significant differences among the responses of antioxidant enzyme activities of SOD, POD and CAT in three cultivars to salt stress (Figure 4). In comparison with CK, the SOD activity of YZ9102 was significantly decreased by 30.80% after 1 day of salt stress, but it was a slightly increased at 5 and 10 days of salt stress. There was a relatively constant increase in SOD activity of JHR1 during 10 days of salt stress. Significant increase in SOD activity in JHB1 was observed under salt stress, and it showed maximum increase (49.43%) at 10 day of salt stress. The increase of SOD activity in JHB1 was higher than that in JHR1 and YZ9102.

POD activity was significantly decreased in YZ9102 under salt stress as compared to CK. The maximum decrease (34.01%) was recorded at 10 days of salt stress. POD activity of cultivar JHR1 was decreased by 13.77% at 1 day of salt stress, however, increased by 27.72% and 23.38% at 5 and 10 days of salt stress. POD activity of JHB1 was significantly increased under salt stress, and the maximum increase (94.80%) was observed at 5 days of salt stress. JHB1 showed higher levels of POD activity than the other cultivars.

The response pattern of CAT activity of YZ9102 under salt stress was similar with that of its POD activity. The CAT activity of JHR1 significantly increased by 32.96% and 25.11% after 1 and 5 days of salt stress as compared to CK, however it was decreased by 16.92% at 10 days of salt stress. Though the CAT activity of JHB1 was slightly increased under salt stress, there was no significant difference between salt stress and CK.

MDA content was significantly increased in all three cultivars under salt stress (Figure 4). The MDA content of YZ9102 was recorded higher as compared to other two cultivars, and it showed a

10.3389/fpls.2024.1368260

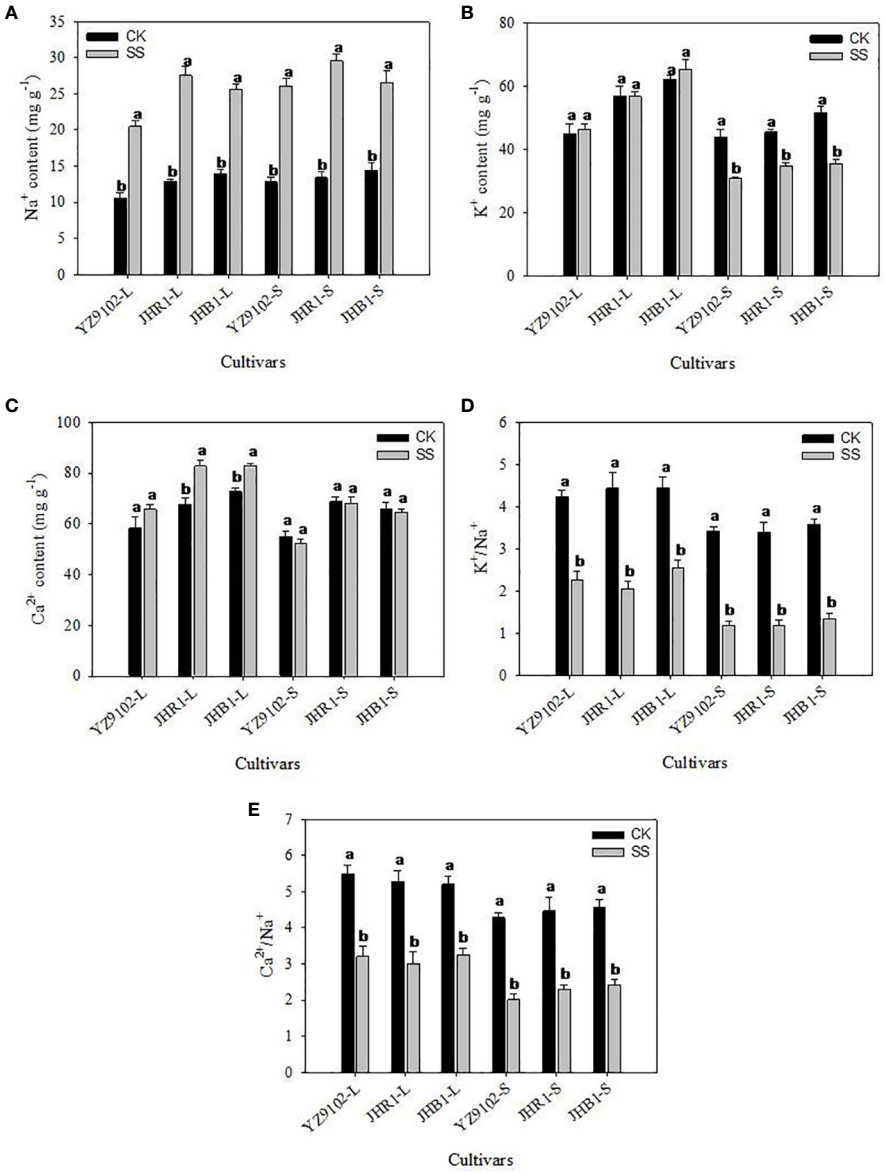

FIGURE 2
The Na^+ **(A)**, K^+ **(B)**, Ca^{2+} **(C)**, K^+/Na^+ **(D)** and Ca^{2+}/Na^+ **(E)** of three peanut cultivars in leaves and stems under salt stress for 10 days. L and S represented leaf and stem, respectively. Different lowercase letters in the bar graph indicate significantly different between CK and SS at $p<0.05$. CK, meaning plants were watered by Hoagland solution without NaCl, and SS, meaning plants were watered by Hoagland solution with 150 mM NaCl.

rapid increase from 37.00% to 72.05% from 1 to 10 days as compared to CK under salt stress. The MDA content of JHR1 and JHB1 exhibited a slight increase at 1 day of salt stress, however it was increased by 51.56% and 39.17% at 10 days of salt stress as compared to CK, respectively. JHB1 showed the minimum MDA content in the presence or absence of salt stress.

3.5 Photosynthetic parameters

Photosynthetic rate (P_n) was significantly decreased in all three cultivars at the first 5 days of salt exposure, and this reduction was more pronounced at 10 days, as compared to CK (Figure 5A). The P_n of YZ9102 was found to a maximum reduction among three cultivars, decreased by 57.61% and 88.89% at 5 and 10 days under salt stress. The decrease of P_n in JHR1 reached to 33.13% and 73.76% after 5 and 10 days of salt stress, which was slightly higher than that in JHB1.

The stomatal conductance (G_s) significantly decreased with the salt stress time (Figure 5B). The G_s in YZ9102 was highly decreased, followed by JHR1 and JHB1. In comparison with CK, the G_s significantly decreased by 73.95%, 44.35% and 36.71% in YZ9102, JHR1 and JHB1 at 5 days of salt stress, further it decreased by 85.95%, 67.78% and 63.95% at 10 days of salt stress, respectively.

The response patterns of transpiration rate (T_r) in all three cultivars under salt stress was similar with that of their photosynthetic rate (P_n) (Figure 5C). The maximum decrease in T_r was recorded in YZ9102 in all three cultivars, reaching 53.28%

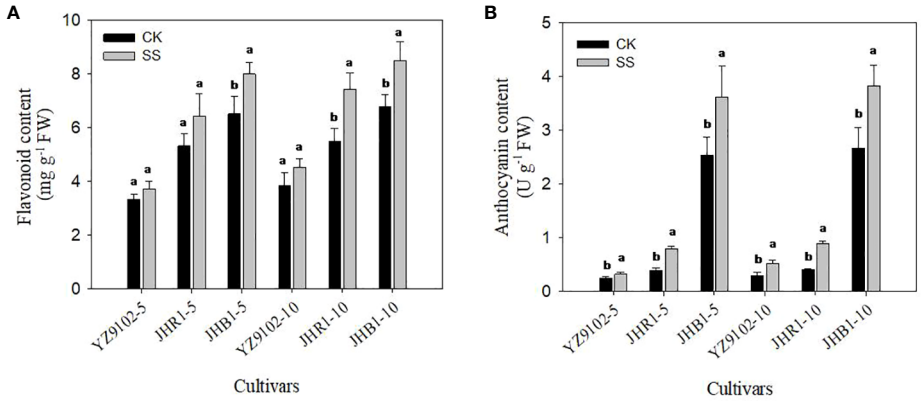

FIGURE 3
The contents of flavonoid **(A)** and anthocyanin **(B)** in leaves under salt stress for 5 and 10 days. Different lowercase letters in the bar graph indicate significantly different between CK and SS at $p<0.05$. CK, meaning plants were watered by Hoagland solution without NaCl, and SS, meaning plants were watered by Hoagland solution with 150 mM NaCl. The 5 and 10 in abscissa represented 5 and 10 days after salt stress, respectively.

and 86.81% at 5 and 10 days of salt stress. The minimum decrease of T_r was recorded in JHR1 (40.04%) and JHB1 (74.20%), after 5 and 10 days of salt stress, respectively.

The variation of water use efficiency (*WUE*) in response to salt stress was observed in three cultivars (Figure 5D). The *WUE* of YZ9102 showed a slight decrease (9.08%) at 5 days under salt stress, and significantly decreased by 15.58% after 10 days as compared to CK. An increased trend in *WUE* was observed in JHR1 and JHB1 during 10 days of salt stress, which showed a stable increase in JHR1 at 11.5% approximately. The maximum increase (24.71%) of *WUE* was recorded at 5 days of salt stress in JHB1.

3.6 Chlorophyll fluorescence parameters

Salt stress significantly decreased photochemical efficiency (F_v/F_m), quantum yield of PS II (*ΦPSII*), electron transport rate (*ETR*) and photochemical quenching coefficient (*qP*) in all three cultivars (Table 2). The $F_v/F_m$was not significantly affected in all three cultivars at 5 days of salt stress, however it was significantly decreased after 10 days of salt stress as compared to CK. No significant difference was recorded for F_v/F_m between JHR1 and JHB1. However, $F_v/F_m$was highly decreased in the cultivar YZ9102. Similar trends were observed in *ΦPSII*, *ETR* and *qP* during 10 days under salt stress. The maximum decreases in *ΦPSII*, *ETR* and *qP* were observed in YZ9102, followed by JHR1 and JHB1 at the 10 days under salt stress as compared to CK.

The non-photochemical quenching coefficient (*qNP*) was significantly increased after salt exposure for 5 days as compared to CK, but that showed an inferior increase in three cultivars at 10 days under salt stress (Table 2). The *qNP* in YZ9102 increased by 40.03% and 31.88% after 5 and 10 days for salt stress, that exhibited the maximum increase in three cultivars. The *qNP* in JHB1 increased by 17.09% and 10.12% after 5 and 10 days for salt stress, as compared to CK. JHR1 showed the minimum increase in *qNP*.

4 Discussion

Peanut is moderately sensitive or comparatively sensitive (Meena et al., 2016) to soil saline stress conditions. Previous reports suggested that there is huge genetic diversity in the salt tolerance among peanut germplasms (Pal and Pal, 2022). The agronomic traits such as survival under salt stress, plant height, relative growth rate reflected the salt tolerance of peanut (Yasmine et al., 2019). The salt tolerance coefficient that was calculated as biomass accumulation ratio under salt stress to unstressed control in each genotype was considered as selection criteria for salt tolerance in peanut (Pal and Pal, 2022). In the present study, the maximum inhibition of growth and biomass under salt stress was recorded in YZ9102, followed by JHR1 and JHB1. Our results suggested that JHB1 is a relatively salt-tolerant cultivar compared to YZ9102. Higher levels of anthocyanin in cultivars showed stronger salt tolerance, as compare to the cultivars with low anthocyanin content which has been observed in rice (Chunthaburee et al., 2016) and *Brassica napus* (Kim et al., 2017).

The homeostasis of intracellular K^+, Ca^{2+} and Na^+ concentrations under salt stress is essential for maintaining membrane potential, and for the activities of many enzymes and an appropriate osmotic regulation (Zhu, 2003). Ion imbalances induced oxidative stress in response to imbalances in ROS, and resulted in nutrient deficiency and ion toxicity. In the current study, Na^+ accumulation was significantly increased in leaves and stems under salt stress. However, a slight or significant increase in the content of K^+ and Ca^{2+} under salt stress was observed in leaves of three peanut cultivars. This might suggest that peanut can improve relatively stable K^+ and Ca^{2+} accumulation in leaves by adjusting the transport capacity of mineral ions to alleviate the adverse effect of Na^+ excessive accumulation (Li Q. et al., 2022). In our study, the K^+/Na^+ and Ca^{2+}/Na^+ were significantly decreased in all three cultivars under salt stress, and decreased more severely in stems than that in leaves. Similar results have been observed in wheat (Rahnama et al., 2011) and rice (Nemati et al., 2011). This might

10.3389/fpls.2024.1368260

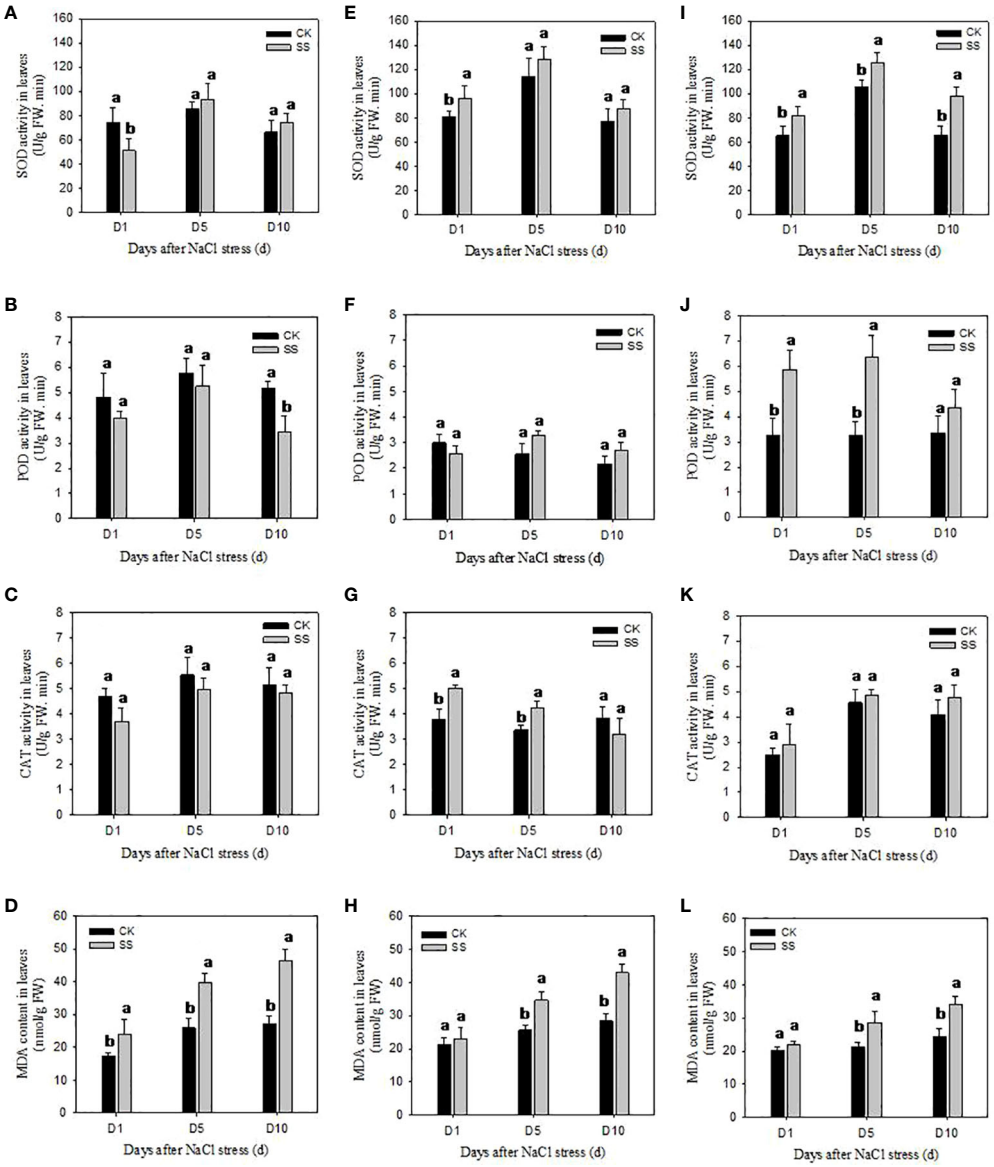

FIGURE 4
The antioxidant enzyme activities and MDA content in leaves of YZ9102 **(A–D)**, JHR1 **(E–H)** and JHB1 **(I–L)** under salt stress. D1, D5, D10 represent salt stress for 1, 5 and 10 days. Different lowercase letters in the bar graph indicate significantly different between CK and SS at $p<0.05$. CK, meaning plants were watered by Hoagland solution without NaCl, and SS, meaning plants were watered by Hoagland solution with 150 mM NaCl.

suggest that the selective ion transport and partitioning may be contributing to the adaptation to salt stress of plants (Ran et al., 2021). In this study, the descend range of K^+/Na^+ and Ca^{2+}/Na^+ were similar in leaves or stems among the three cultivars. Our results are inconsistent with the previous reports suggesting that the ion ratio was related to salt tolerance under salt stress (Guo et al., 2022). These results indicated that the salt tolerance of black peanut may not be related to ion absorption.

Flavonoid is an important plant secondary metabolite, is proved to be major component of plant antioxidant defense system against abiotic stresses through preventing generation of ROS or scavenging already generated ROS (Hernández et al., 2009). In the present study, salt stress significantly increased the contents of flavonoid and anthocyanin in all three cultivars. Similar results have been reported in *Brassica napus* (Kim et al., 2017) and pea (Farooq et al., 2021), which found that the contents of total flavonoid and phenolic compounds showed a significant increase to improve resistance in response to salt stress. In this study, JHR1 and JHB1 showed the higher increase of anthocyanin and flavonoid than YZ9102 under salt stress. These findings are consistent with wheat (Liu et al., 2012), suggesting that the salt-tolerant cultivars had higher increase of anthocyanin content than salt-sensitive under salt stress. With or without salt stress, the anthocyanin and flavonoid contents of JHB1 were higher than those of JHR1 and YZ9102, suggesting that the salt-tolerant cultivars had higher anthocyanin content than the salt-sensitive cultivars to possess

10.3389/fpls.2024.1368260

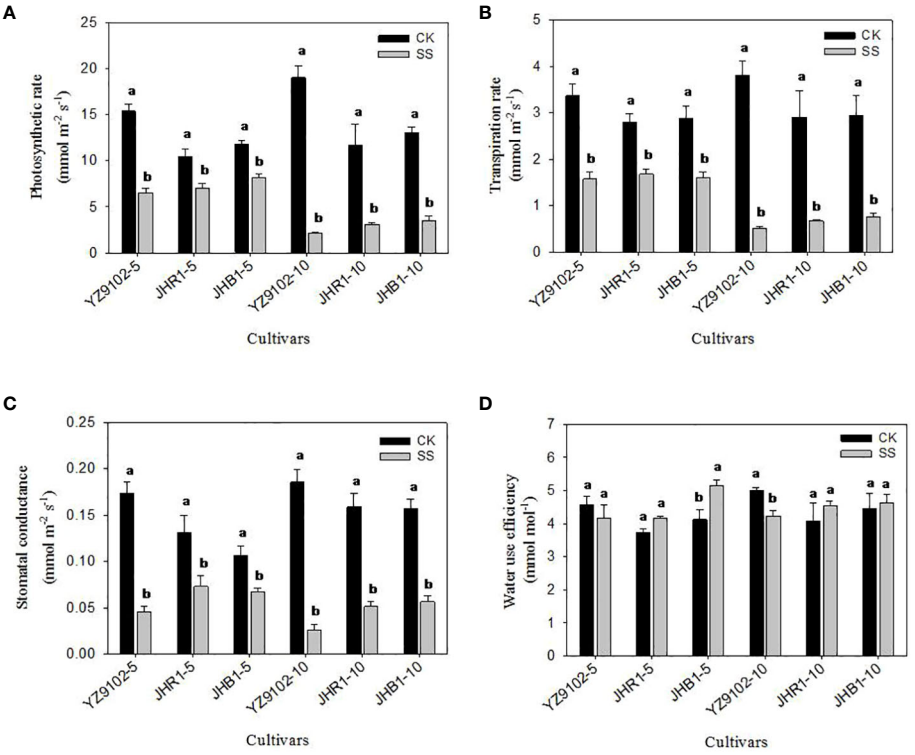

FIGURE 5
The photosynthetic rate **(A)**, transpiration rate **(B)**, stomatal conductance **(C)** and water use efficiency **(D)** of peanut leaves under salt stress for 5 and 10 days. Different lowercase letters in the bar graph indicate significantly different between CK and SS at $p<0.05$. CK, meaning plants were watered by Hoagland solution without NaCl, and SS, meaning plants were watered by Hoagland solution with 150 mM NaCl. The 5 and 10 in abscissa represented 5 and 10 days after salt stress, respectively.

more physiological activities (Daiponmak et al., 2010). Majority of the research community has confirmed these results. Over expression the genes related to the flavonoid and anthocyanin biosynthesis in transgenic plants increased the flavonoid and anthocyanin accumulation, enhanced the oxidation resistance and salt tolerance (Li et al., 2016; Wang et al., 2016).The anthocyanin free (Kang et al., 2014) and flavonoid deficiency (Sugimoto et al., 2021) mutants failed to produce anthocyanin and flavonoid in all tissues because of inactivation of flavonoid biosynthetic enzymes, and increased production of reactive oxygen species (ROS).

TABLE 2 The chlorophyll fluorescence parameters of three peanut cultivars after 5 and 10 days under salt stress.

Days (d)	Cultivars	Treatment	*Fv/Fm*	*ΦPSII*	*ETR*	*qP*	*qNP*
5	YZ9102	CK	0.89 ± 0.02a	0.28 ± 0.02a	2.51 ± 0.21a	0.32 ± 0.01a	0.90 ± 0.10b
		SS	0.87 ± 0.02b	0.23 ± 0.02b	2.06 ± 0.17b	0.26 ± 0.02b	1.27 ± 0.13a
	JHR1	CK	0.89 ± 0.01a	0.27 ± 0.03a	2.50 ± 0.30a	0.29 ± 0.04a	0.95 ± 0.03a
		SS	0.88 ± 0.01a	0.25 ± 0.02a	2.34 ± 0.20a	0.27 ± 0.03a	1.00 ± 0.04a
	JHB1	CK	0.88 ± 0.01a	0.33 ± 0.03a	2.83 ± 0.31a	0.35 ± 0.03a	0.95 ± 0.09b
		SS	0.87 ± 0.02a	0.31 ± 0.03a	2.62 ± 0.24a	0.33 ± 0.03a	1.11 ± 0.13a
10	YZ9102	CK	0.93 ± 0.03a	0.33 ± 0.02a	2.69 ± 0.20a	0.37 ± 0.02a	0.87 ± 0.04b
		SS	0.86 ± 0.01b	0.24 ± 0.02b	1.91 ± 0.19b	0.27 ± 0.03b	1.15 ± 0.13a
	JHR1	CK	0.91 ± 0.01a	0.32 ± 0.03a	2.83 ± 0.25a	0.35 ± 0.04a	0.82 ± 0.03a
		SS	0.88 ± 0.0 b	0.25 ± 0.02b	2.23 ± 0.20b	0.29 ± 0.02b	0.84 ± 0.05a
	JHB1	CK	0.91 ± 0.01a	0.35 ± 0.03a	2.84 ± 0.20a	0.39 ± 0.03a	0.92 ± 0.05a
		SS	0.88 ± 0.02b	0.29 ± 0.02b	2.31 ± 0.12b	0.32 ± 0.03b	1.02 ± 0.08a

Data are means ± SD of five biological replicates. Different lowercase letters in the same column indicate significantly different between CK and SS at p<0.05. CK, meaning plants were watered by Hoagland solution without NaCl, and SS, meaning plants were watered by Hoagland solution with 150 mM NaCl.

High concentration of salt stress caused rapid increase of ROS, which could perturb cellular redox homeostasis, results in oxidative stress and induce a series of cell damage. The ROS scavenging system of plants could be activated to alleviate such oxidative damages for enhancing salt tolerance (Choudhury et al., 2013). The antioxidative enzymes including SOD, POD and CAT could cooperatively scavenge the ROS and maintain the ROS below toxic range (Kaya et al., 2020). In this study, the antioxidative enzyme activities of SOD, POD and CAT were activated by salt stress in JHR1 and JHB1, however, those were restrained in YZ9102. Different responses of enzyme activities to salt stress may be responsible for the different sensitivities among the cultivars under salt stress (Guo et al., 2022). The activation of enzyme activities was more obvious in JHB1 than JHR1. Similar with our findings, cultivars e.g. maize (Hichem et al., 2009) and apple (Wang et al., 2015) with more intense anthocyanin showed higher increase of total antioxidant activity than less ones under salt stress, and exhibited more redox stabilization and better behavior of salt-challenge. Exogenous anthocyanin treatments suggested that anthocyanin not only acted as free radical scavengers but promoted activation of antioxidant enzymes and other non-enzymatic antioxidants, and improved the physiological state of plants (Paul et al., 2017; Maleva et al., 2018), which indirectly confirmed our results. In the current study, the activation effect of three antioxidant enzyme activities in JHB1 gradually increased from 1 to 10 d after salt stress, however those in JHR1 were found to decrease or inactivate at late stage compared with the early salt stress. It may be attributed to that there were differences with resistance to salt stress duration and intensity among cultivars (Wang et al., 2019; El-Badri et al., 2021). In our study, MDA content showed a maximum and minimum increase in YZ9102 and JHB1 under salt stress, respectively. Similar results in maize (Hichem et al., 2009) also suggested that genotypes with high anthocyanin content were able to maintain lower MDA content and significant higher dry matter production than yellow ones upon salt stress. The MDA content in YZ9102 showed a rapid increase, however, it was slowly increased in JHB1 under salt stress. The result was consistent with the trend of enzyme activities of three cultivars. Our results indicated that activating antioxidant enzymes via anthocyanin under salt stress could effectively alleviate cell damage caused by oxidative stress (Daiponmak et al., 2010).

Photosynthesis reduction under salt stress is mainly due to stomatal closure and CO_2 diffusion hindered via a reduction in guard cell turgor, and partially to photosystem II (PSII) photo inhibition. The net photosynthetic rate decreased with increasing intensity of salt stress, and showed greater reduction in the salt-sensitive cultivar than that in tolerant (Dionisio-Sese and Tobita, 2000). Similar results were obtained in this study. The photosynthetic traits (P_n, G_s, and T_r) significantly decreased at 5 days under salt stress, and further decreased at 10 days of salt stress. Maximum reductions of photosynthetic traits were recorded in cultivar YZ9102, followed by JHR1 and JHB1. It may be attributed to that the tolerant cultivars had more responsive stomata that tended to close faster when exposure to salt stress at the first few hours, followed by partial recovery after a temporary acclimation. However, the recovery ability of stomata in sensitive cultivars was deficiency coping with salt stress (Foad and Ismail, 2007). Similar results in water spinach also suggested that P_n, G_s, and T_r in green cultivar were more sensitive to salt stress than that in red cultivar, and showed a severe decline under the same salt stress (Kitayama et al., 2019). Exogenous antioxidant alleviated photosynthesis inhibition in rapeseed (Ma et al., 2017) and soybean (Alharbi et al., 2021) under salt stress by activating antioxidant systems, mitigated the salt stress damage, which explained that the photosynthetic capacity in more intense in anthocyanin rich cultivars were less affected by salt stress. The water use efficiency (WUE), estimated as the ratio of P_n to T_r, showed a gradually downward in tomato when exposure to 0.3%~0.9% salt stress (Yang et al., 2019). However, WUE exhibited a significant increase in tartary buckwheat under 100 mM NaCl stress, and a little change in common buckwheat (Matsuura et al., 2005). The response of WUE to salt stress represented the salt tolerance of different species or cultivars. In this study, the WUE was found to a downward in YZ9102 during salt stress duration, and showed an increase trend in JHR1 and JHB1after10 days of salt stress. It may be mainly attributed to the diverse maintenance of P_n and G_s under salt stress.

Chlorophyll fluorescence, providing insights into the response of photosynthesis to environmental stresses, is a rapid and non-destructive tool used to screen cultivars for salt tolerance (Zribi et al., 2009). In the present study, the chlorophyll fluorescence including F_v/F_m, *ΦPSII*, *ETR* and *qP* showed a slight reduction in three cultivars at 5 days after salt stress, and significantly decreased at 10 days. Similar result was found in sorghum (Netondo et al., 2004). It may be responsible for the PSII photo inhibition turn into the main limitation of photosynthesis reduction at late stage of salt stress (Dionisio-Sese and Tobita, 2000). The maximum decrease in chlorophyll fluorescence was observed in YZ9102, followed by JHR1 and JHB1 under salt stress. Similar result in brassicas suggested that salt-tolerant cultivars exhibited better PSII quantum efficiency and utilization of photochemical energy than salt-sensitive cultivars under salt stress (Ahmed et al., 2023). Water spinach cultivars with higher anthocyanin content also showed lesser inhibition in PSII quantum efficiency than those with lower anthocyanin content (Kitayama et al., 2019). In this study, the *qNP* in YZ9102 showed the maximum increase under salt stress, followed by JHB1 and JHR1. Our results are consistent with rice (Foad and Ismail, 2007), suggesting that PSII reaction center could alleviate excitation pressure via diverting light energy into heat to maintain an adequate balance between absorption and utilization of light (Krause and Weis, 1991). Salt stress inhibited electron transport involving PSII, and increased the *qNP* in Arabidopsis, however, did not affected the photochemical efficiency in *Thellungiella* (Stepien and Johnson, 2009), suggesting that the photosystem of salt-tolerant crops showed greater stability.

5 Conclusions

In conclusion, a prominent difference in response to salt stress among the three tested cultivars of different testa color was observed in this study. The strength of salt tolerance was higher in black color testa genotype (JHB1) followed by red (JHR1) and pink (YZ9102) on the basis of the relative growth value. JHB1 showed maximum accumulation of flavonoid and anthocyanin than JHR1 and YZ9102

with or without salt stress. In salt treated, the ion imbalances, expressed as the ratio of K^+/Na^+ and Ca^{2+}/Na^+, were shown to be similar among the three cultivars. The relative activation of antioxidant enzyme activities and membrane stability in JHB1 were more outstanding than the other two cultivars when subjected to salt stress. The most tolerant to salt stress in JHB1 was mainly attributed to the accumulation of the anthocyanin and flavonoid activating antioxidant protection against the oxidative damage to maintain the higher photosynthetic efficiency and plant growth under salt stress. It is necessary to study the underlying molecular mechanisms of salt tolerance in black peanut or exogenous anthocyanin regulated salt tolerance.

Data availability statement

The original contributions presented in the study are included in the article/supplementary material. Further inquiries can be directed to the corresponding author.

Author contributions

GL: Conceptualization, Formal analysis, Investigation, Methodology, Supervision, Writing – original draft, Writing – review & editing. XG: Data curation, Investigation, Writing – original draft. YS: Data curation, Investigation, Writing – original draft. SG: Writing – review & editing. KZ: Data curation, Methodology, Software, Writing – original draft. FW: Data curation, Investigation, Writing – original draft. GW: Data curation, Methodology, Software, Writing – original draft. HZ: Data curation, Investigation, Writing – original draft. AL: Data curation, Formal Analysis, Writing – original draft. XW: Funding acquisition, Project administration, Supervision, Writing – review & editing. CZ: Funding acquisition, Project administration, Supervision, Writing – review & editing.

Funding

The author(s) declare that financial support was received for the research, authorship, and/or publication of this article. This research was funded by Key Research and Development Project of Shandong Province (2022LZGC007, 2022LZGC022), National Natural Science Foundation of China (32072090), Agricultural scientific and technological innovation project of Shandong Academy of Agricultural Sciences, New 20 Policies for Universities in Jinan (202333047), Taishan Scholar Project of Shandong Province.

Acknowledgments

The authors thank Prof. Bo Feng for providing the portable photosynthesis system. The laboratory staff provided help in auxiliary work.

Conflict of interest

The authors declare that the research was conducted in the absence of any commercial or financial relationships that could be construed as a potential conflict of interest.

Publisher's note

References

Abogadallah, G. M. (2010). Insights into the significance of antioxidative defense under salt stress. *Plant Signa. Behav.* 5, 369–374. doi: 10.4161/psb.5.4.10873

Aebi, H. (1984). Catalase in *vitro*. *Metho Enzym.* 105, 121–126. doi: 10.1016/S0076-6879(84)05016-3

Ahmed, M. Z., Fatima, S., Nawaz, M. A., Abideen, Z., Nielsen, B. L., and Ahmad, N. (2023). Salt-induced modulation of ion transport and PSII photoprotection determine the salinity tolerance of amphidiploid brassicas. *Plants* 12, 2590. doi: 10.3390/PLANTS12142590

Ait-El-Mokhtar, M., Baslam, M., Ben-Laouane, R., Anli, M., Boutasknit, A., Mitsui, T., et al. (2020). Alleviation of detrimental effects of salt stress on date palm (*Phoenix dactylifera* L.) by the application of arbuscular mycorrhizal fungi and/or compost. *Front. Sustain. Food Syst.* 4. doi: 10.3389/FSUFS.2020.00131

Alharbi, B. M., Elhakem, A. H., Alnusairi, G. S. H., Soliman, M. H., Hakeem, K. R., Hasan, M. M., et al. (2021). Exogenous application of melatonin alleviates salt stress-induceddecline in growth and photosynthesis in *Glycine max* (L.) seedlings by improving mineral uptake, antioxidant and glyoxalase system. *Plant Soil Environ.* 67, 208–220. doi: 10.17221/659/2020-PSE

Banavath, J. N., Chakradhar, T., Pandit, V., Konduru, S., Guduru, K. K., Akila, C. S., et al. (2018). Stress inducible overexpression of *AtHDG11*leads to improved drought and salt stress tolerance in peanut (*Arachis hypogaea* L.). *Front. Chem.* 6. doi: 10.3389/fchem.2018.00034

Bonku, R., and Yu, J. M. (2020). Health aspects of peanuts as an outcome of its chemical composition. *Food Sci. Hum. Wellness.* 9, 21–30. doi: 10.1016/j.fshw.2019.12.005

Chakraborty, K., Bhaduri, D., Meena, H. N., and Kalariya, K. (2016). External potassium (K^+) application improves salinity tolerance by promoting Na^+-exclusion, K^+-accumulation and osmotic adjustment in contrasting peanut cultivars. *Plant Physiol. Biochem.* 103, 143–153. doi: 10.1016/j.plaphy.2016.02.039

Choudhury, S., Panda, P., Sahoo, L., and Panda, S. K. (2013). Reactive oxygen species signaling in plants under abiotic stress. *Plant Signal. Behav.* 8, 23681. doi: 10.4161/psb.23681

Chunthaburee, S., Sakuanrungsirikul, S., Wongwarat, T., Sanitchon, J., Pattanagul, W., and Theerakulpisut, P. (2016). Changes in anthocyanin content and expression of anthocyanin synthesis genes in seedlings of black glutinous rice in response to salt stress. *Asian J. Plant Sci.* 15, 56–65. doi: 10.3923/ajps.2016.56.65

Daiponmak, W., Theerakulpisut, P., Thanonkao, P., Vanavichit, A., and Pratheph, P. (2010). Changes of anthocyanin cyanidin-3-glucoside content and antioxidant activity in Thai rice varieties under salinity stress. *Sci. Asia.* 36, 286–291. doi: 10.2306/scienceasia1513-1874.2010.36.286

Dionisio-Sese, M. L., and Tobita, S. (2000). Effects of salinity on sodium content and photosynthetic responses of rice seedlings differing in salt tolerance. *J. Plant Physiol.* 157, 54–58. doi: 10.1016/S0176-1617(00)80135-2

El-Akhal, M. R., Rincón, A., Coba de la Peña, T., Lucas, M. M., El Mourabit, N., Barrijal, S., et al. (2012). Effects of salt stress and rhizobial inoculation on growth and nitrogen fixation of three peanut cultivars. *Plant Biol.* 15, 415–421. doi: 10.1111/j.1438-8677.2012.00634.x

El-Badri, A. M., Batool, M., Mohamed, I. A. A., Wang, Z. K., Khatab, A., Sherif, A., et al. (2021). Antioxidative and metabolic contribution to salinity stress responses in two rapeseed cultivars during the early seedling stage. *Antioxidants* 10, 1227. doi: 10.3390/antiox10081227

Eryılmaz, F. (2006). The relationships between salt stress and anthocyanin content in higher plants. *Biotechnol* 20, 47–52. doi: 10.1080/13102818.2006.10817303

Farooq, M., Ahmad, R., Shahzad, M., Sajjad, Y., Hassan, A., Shah, M. M., et al. (2021). Differential variations in total flavonoid content and antioxidant enzymes activities in pea under different salt and drought stresses. *Sci. Hortic.* 287, 110258. doi: 10.1016/j.scienta.2021.110258

Foad, M., and Ismail, A. M. (2007). Responses of photosynthesis, chlorophyll fluorescence and ROS-scavenging systems to salt stress during seedling and reproductive stages in rice. *Ann. Bot.* 99, 1161–1173. doi: 10.1093/aob/mcm052

Giannopolitis, C. N., and Ries, S. K. (1977). Superoxide Dismutases: I. Occurrence in higher plants. *Plant Physiol.* 59, 309–314. doi: 10.1104/pp.59.2.309

Guo, X., Ahmad, N., Zhao, S. Z., Zhao, C. Z., Zhong, W., Wang, X. J., et al. (2022). Effect of salt stress on growth and physiological properties of asparagus seedlings. *Plants* 11, 2836. doi: 10.3390/plants11212836

Hernández, I., Alegre, L., Van Breusegem, F., and Munné-Bosch, S. (2009). How relevant are flavonoids as antioxidants in plants? *Trends Plant Sci.* 14, 125–132. doi: 10.1016/j.tplants.2008.12.003

Hichem, H., Mounir, D., and Naceur, E. A. (2009). Differential responses of two maize (*Zea mays* L.) varieties to salt stress: Changes on polyphenols composition of foliage and oxidative damages. *Ind. Crop Prod.* 30, 144–151. doi: 10.1016/j.indcrop.2009.03.003

Hodges, D. M., DeLong, J. M., Forney, C. F., and Prange, R. K. (1999). Improving the thiobarbituric acid-reactive-substances assay for estimating lipid peroxidation in plant tissues containing anthocyanin and other interfering compounds. *Planta* 207, 604–611. doi: 10.1007/s004250050524

Jia, Z. S., Tang, M. C., and Wu, J. M. (1999). The determination of flavonoid contents in mulberry and their scavenging effects on superoxide radicals. *Food Chem.* 64, 555–559. doi: 10.1016/S0308-8146(98)00102-2

Kang, J. H., McRoberts, J., Shi, F., Moreno, J. E., Jones, A. D., and Howe, G. A. (2014). The flavonoid biosynthetic enzyme chalcone isomerase modulates terpenoid production in glandular trichomes of tomato. *Plant Physiol.* 164, 1161–1174. doi: 10.1104/pp.113.233395

Kaya, C., Higgs, D., Ashraf, M., AlYemeni, M. N., and Ahmad, P. (2020). Integrative roles of nitric oxide and hydrogen sulfide in melatonin-induced tolerance of pepper (*Capsicum annuum* L.) plants to iron deficiency and salt stress alone or in combination. *Physio Planta.* 168, 256–277. doi: 10.1111/ppl.12976

Kim, J., Lee, W. J., Vu, T. T., Jeong, C. Y., Hong, S. W., and Lee, H. (2017). High accumulation of anthocyanins via the ectopic expression of AtDFR confers significant salt stress tolerance in *Brassica napus* L. *Plant Cell Rep.* 36, 1215–1224. doi: 10.1007/s00299-017-2147-7

Kitayama, M., Tisarum, R., Theerawitaya, C., Samphumphung, T., Takagaki, M., and Kirdmanee, C. (2019). Regulation on anthocyanins, α-tocopherol and calcium in two water spinach (*Ipomoea aquatica*) cultivars by NaCl salt elicitor. *Sci. Hortic.* 249, 390–400. doi: 10.1016/j.scienta.2019.02.021

Krause, G. H., and Weis, E. (1991). Chlorophyll fluorescence and photosynthesis: the basics. *Ann. Rev. Plant Physiol. Plant Mol. Biol.* 42, 313–349. doi: 10.1146/annurev.pp.42.060191.001525

Li, P., Li, Y. J., Zhang, F. J., Zhang, G. Z., Jiang, X. Y., Yu, H. M., et al. (2016). The Arabidopsis UDP-glycosyltransferases UGT79B2 and UGT79B3, contribute to cold, salt and drought stress tolerance via modulating anthocyanin accumulation. *Plant J.* 89, 85–103. doi: 10.1111/tpj.13324

Li, Q., Qin, Y. Z., Hu, X. X., Jin, L. P., Li, G. C., Gong, Z. P., et al. (2022). Physiology and gene expression analysis of potato (*Solanum tuberosum* L.) in salt stress. *Plants* 11, 1565. doi: 10.3390/plants11121565

Li, W. J., Sun, J., Zhang, X. Q., Ahmad, N., Hou, L., Zhao, C. Z., et al. (2022). The mechanisms underlying salt resistance mediated by exogenous application of 24-epibrassinolide in Peanut. *Int. J. Mol. Sci.* 23, 6376. doi: 10.3390/ijms23126376

Liu, C., Li, S., Wang, M. C., and Xia, G. M. (2012). A transcriptomic analysis reveals the nature of salinity tolerance of a wheat introgression line. *Plant Mol. Biol.* 78, 159–169. doi: 10.1007/s11103-011-9854-1

Luo, L., Wan, Q., Zhang, K., Zhang, X. R., Guo, R. J., Wang, C., et al. (2021). AhABI4s negatively regulate salt-stress response in peanut. *Front. Plant Sci.* 12. doi: 10.3389/fpls.2021.741641

Ma, N., Hu, C., Wan, L., Hu, Q., Xiong, J. L., and Zhang, C. L. (2017). Strigolactones improve plant growth, photosynthesis, and alleviate oxidative stress under salinity in rapeseed (*Brassica napus* L.) by regulating gene expression. *Front. Plant Sci.* 8. doi: 10.3389/fpls.2017.01671

Maleva, M., Garmash, E., Chukina, N., Malec, P., Waloszek, A., and Strzałka, K. (2018). Effect of the exogenous anthocyanin extract on key metabolic pathways and antioxidant status of Brazilian elodea (*Egeria densa* (Planch.) Casp.) exposed to cadmium and manganese. *Ecotoxi. Environ.Safety.* 160, 197–206. doi: 10.1016/j.ecoenv.2018.05.031

Matsuura, H., Inanaga, S., and Murata, K. (2005). Differences in the vegetative growth between common and tartary buckwheat in saline hydroponic culture. *Plant Prod. Sci.* 8, 533–538. doi: 10.1626/pps.8.533

Meena, H. N., Ajay, B. C., Rajanna, G. A., Yadav, R. S., Jain, N. K., and Meena, M. S. (2022). Polythene mulch and potassium application enhances peanut productivity and biochemical traits under sustained salinity stress condition. *Agric. Water Manage.* 273, 107903. doi: 10.1016/j.agwat.2022.107903

Meena, H. N., Meena, M., and Yadav, R. S. (2016). Comparative performance of seed types on yield potential of peanut (*Arachis hypogaea* L.) under saline irrigation. *Field Crops Res.* 196, 305–310. doi: 10.1016/j.fcr.2016.06.006

Mondal, M., Skalicky, M., Garai, S., Hossain, A., Sarkar, S., Banerjee, H., et al. (2020). Supplementing nitrogen in combination with rhizobium inoculation and soil mulch in peanut (*Arachis hypogaea* L.) production system: Part I. effects on productivity, soil moisture, and nutrient dynamics. *Agronomy* 10, 1582. doi: 10.3390/agronomy10101582

Nemati, I., Moradi, F., Gholizadeh, S., Esmaeili, M. A., and Bihamta, M. R. (2011). The effect of salinity stress on ions and soluble sugars distribution in leaves, leaf sheaths and roots of rice (*Oryza sativa* L.) seedlings. *Plant Soil Environ.* 57, 26–33. doi: 10.17221/71/2010-PSE

Netondo, G. W., Onyango, J. C., and Beck, E. (2004). Sorghum and salinity: II. Gas exchange and chlorophyll fluorescence of sorghum under salt stress. *Crop Sci.* 44, 806–811. doi: 10.2135/cropsci2004.8060

Nickel, K. S., and Cunningham, B. (1969). Improved peroxidase assay method using leuco 2,3′,6-trichloroindophenol and application to comparative measurements of peroxidatic catalysis. *Anal. Biochem.* 27, 292–299. doi: 10.1016/0003-2697(69)90035-9

Pal, A., and Pal, A. K. (2022). Differential responses on chlorophyll content, osmolyte accumulation and membrane damage parameters under salinity stress on tolerant and susceptible genotypes of groundnut. *Legume Res.* 45, 1506–1516. doi: 10.18805/LR-4284

Paul, S., Roychoudhury, A., Banerjee, A., Chaudhuri, N., and Ghosh, P. (2017). Seed pre-treatment with spermidine alleviates oxidative damages to different extent in the salt (NaCl)-stressed seedlings of three indica rice cultivars with contrasting level of salt tolerance. *Plant Gene.* 11, 112–123. doi: 10.1016/j.plgene.2017.04.002

Porcel, R., Aroca, R., and Ruiz-Lozano, J. M. (2012). Salinity stress alleviation using arbuscular mycorrhizal fungi. A review. *Agron. Sustain. Dev.* 32, 181–200. doi: 10.1007/s13593-011-0029-x.hal-00930499

Qin, L. Q., Li, L., Bi, C., Zhang, Y. L., Wan, S. B., Meng, J. J., et al. (2011). Damaging mechanisms of chilling and salt stress to *Arachis hypogaea* L. leaves. *Photosynthetica* 49, 37–42. doi: 10.1007/s11099-011-0005-3

Qin, W. J., Yan, H. Y., Zou, B. Y., Guo, R. Z., Ci, D. W., Tang, Z. H., et al. (2021). Arbuscular mycorrhizal fungi alleviate salinity stress in peanut: Evidence from pot-grown and field experiments. *Food Energy Secur.* 10, e314. doi: 10.1002/fes3.314

Rahnama, A., Poustini, K., Tavakkol-Afshari, R., Ahmadi, A., and Alizadeh, H. (2011). Growth properties and ion distribution in different tissues of bread wheat genotypes (*Triticum aestivum* L.) differing in salt tolerance. *J. Agr. Crop Sci.* 197, 21–30. doi: 10.1111/jac.2010.197.issue-1

Ran, X., Wang, X., Gao, X. K., Liang, H. Y., Liu, B. X., and Huang, X. X. (2021). Effects of salt stress on the photosynthetic physiology and mineral ion absorption and distribution in white willow (*Salix alba* L.). *PloS One* 16, e0260086. doi: 10.1371/journal.pone.0260086

Rasouli, F., Amini, T., Skrovankova, S., Asadi, M., Hassanpouraghdam, M. B., Ercisli, S., et al. (2023). Influence of drought stress and mycorrhizal (*Funneliformis mosseae*) symbiosis on growth parameters, chlorophyll fluorescence, antioxidant activity, and essential oil composition of summer savory (*Satureja hortensis* L.) plants. *Front. Plant Sci.* 14. doi: 10.3389/fpls.2023.1151467

Sharma, S., Sharma, S., Kulkarni, J., and Jha, B. (2016). Halotolerant rhizobacteria promote growth and enhance salinity tolerance in peanut. *Front. Microbiol.* 7, 1600. doi: 10.3389/fmicb.2016.01600

Stepien, P., and Johnson, G. N. (2009). Contrasting responses of photosynthesis to salt stress in the glycophyte Arabidopsis and the halophyte thellungiella: Role of the plastid terminal oxidase as an alternative electron sink. *Plant Physiol.* 149, 1154–1165. doi: 10.1104/pp.108.132407

Sugimoto, K., Zager, J. J., Aubin, B. S., Lange, B. M., and Howe, G. A. (2021). Flavonoid deficiency disrupts redox homeostasis and terpenoid biosynthesis in glandular trichomes of tomato. *Plant Physiol.* 188, 1450–1468. doi: 10.1093/plphys/kiab488

Tian, S. F., Guo, R. Z., Zou, X. X., Zhang, X. J., Yu, X. N., Zhan, Y., et al. (2019). Priming with the green leaf volatile (Z)-3-Hexeny-1-yl Acetate enhances salinity stress tolerance in peanut (*Arachis hypogaea* L.) seedlings. *Front. Plant Sci.* 10. doi: 10.3389/fpls.2019.00785

Wang, F. B., Kong, W. L., Wong, G., Fu, L. F., Peng, R. H., Li, Z. J., et al. (2016). *AtMYB12* regulates flavonoids accumulation and abiotic stress tolerance in transgenic *Arabidopsis thaliana*. *Mol. Genet. Genomics* 291, 1545–1559. doi: 10.1007/s00438-016-1203-2

Wang, J. Z., Jin, C., Wang, Y. P., and Chen, B. Q. (2019). Effects of salt stress on antioxidant system activity and peroxidation damage in root tip cells of strawberry. *Afr. J. Biotec.* 18, 702–706. doi: 10.5897/AJB2019.16840

Wang, X. Q., Li, C. Y., Liang, D., Zou, Y. J., Li, P. M., and Ma, F. W. (2015). Phenolic compounds and antioxidant activity in red-fleshed apples. *J. Funct. Foods.* 18, 1086–1094. doi: 10.1016/j.jff.2014.06.013

Xu, Z. H., and Rothstein, S. J. (2018). ROS-induced anthocyanin production provides feedback protection by scavenging ROS and maintaining photosynthetic capacity in *Arabidopsis*. *Plant Signal. Behav.* 13, 1364–1377. doi: 10.1080/15592324.2018.1451708

Yang, H., Shukla, M. K., Mao, X. M., Kang, S. Z., and Du, T. S. (2019). Interactive regimes of reduced irrigation and salt stress depressed tomato water use efficiency at leaf and plant scales by affecting leaf physiology and stem sap flow. *Front. Plant Sci.* 10. doi: 10.3389/fpls.2019.00160

Yasmine, F., Rahman, M. A., Hasan, M. M., Alam, M. A., Haque, M. S., Ismail, M. R., et al. (2019). Morphophysiological and yield attributes of groundnut varieties under different salinity stress conditions. *Legume Res.* 42, 684–687. doi: 10.18805/LR-398

Zhang, G. C., Dai, L. X., Ding, H., Ci, D. W., Ning, T. Y., Yang, J. S., et al. (2020). Response and adaptation to the accumulation and distribution of photosynthetic product in peanut under salt stress. *J. Integra. Agric.* 19, 690–699. doi: 10.1016/S2095-3119(19)62608-0

Zhang, K., Yuan, M., Xia, H., He, L. Q., Ma, J., Wang, M. X., et al. (2022). BSA-seq and genetic mapping reveals AhRt2 as a candidate gene responsible for red testa of peanut. *Theor. Appl. Genet.* 135, 1529–1540. doi: 10.1007/s00122-022-04051-w

Zhao, X. Y., Chen, J., and Du, F. L. (2012). Potential use of peanut by-products in food processing: a review. *J. Food Sci. Technol.* 49, 521–529. doi: 10.1007/s13197-011-0449-2

Zhao, Y. H., Ma, J. J., Li, M., Deng, L., Li, G. H., Xia, H., et al. (2020). Whole-genome resequencing-based QTL-seq identified *AhTc1* gene encoding a R2R3-MYB transcription factor controlling peanut purple testa colour. *Plant Biotechnol. J.* 18, 96–105. doi: 10.1111/pbi.13175

Zhu, J. K. (2003). Regulation of ion homeostasis under salt stress. *Curr. Opin. Plant Biol.* 6, 441–445. doi: 10.1016/S1369-5266(03)00085-2

Zhu, H., Jiang, Y. A., Guo, Y., Huang, J. B., Zhou, M. H., and Tang, Y. Y. (2021). A novel salt inducible WRKY transcription factor gene, *AhWRKY75*, confers salt tolerance in transgenic peanut. *Plant Physiol. Biochem.* 160, 175–183. doi: 10.1016/j.plaphy.2021.01.014

Zou, K. Y., Kang, D., Kim, K. S., and Jun, T. H. (2020). Screening of salinity tolerance and genome-wide association study in 249 peanut accessions (*Arachis hypogaea* L.). *Plant Breed. Biotech.* 8, 434–438. doi: 10.9787/PBB.2020.8.4.434

Zribi, L., Fatma, G., Fatma, R., Salwa, R., Hassan, N., and Néjib, R. M. (2009). Application of chlorophyll fluorescence for the diagnosis of salt stress in tomato "*Solanum lycopersicum* (variety Rio Grande)". *Sci. Hortic.* 120, 367–372. doi: 10.1016/j.scienta.2008.11.025

frontiers | Frontiers in Plant Science

TYPE Original Research
PUBLISHED 25 March 2024
DOI 10.3389/fpls.2024.1333286

OPEN ACCESS

EDITED BY
Hui Song,
Qingdao Agricultural University, China

REVIEWED BY
Md Mahfuzur Rob,
Sylhet International University, Bangladesh
Atikaimu Maimaiti,
Xinjiang Agricultural University, China
Muhammad Uzair,
The University of Tennessee, Knoxville, United States

*CORRESPONDENCE
Irfan Ali Sabir
irfanalisabir@sjtu.edu.cn
Muhammad Shafiq
shafiq.iags@pu.edu.pk
Muhammad Aamir Manzoor
aamirmanzoor1@hotmail.com

RECEIVED 05 November 2023
ACCEPTED 08 February 2024
PUBLISHED 25 March 2024

CITATION
Ali M, Shafiq M, Haider MZ, Sami A, Alam P, Albalawi T, Kamran Z, Sadiq S, Hussain M, Shahid MA, Jeridi M, Ashraf GA, Manzoor MA and Sabir IA (2024) Genome-wide analysis of *NPR1*-like genes in citrus species and expression analysis in response to citrus canker (*Xanthomonas axonopodis* pv. *citri*). *Front. Plant Sci.* 15:1333286. doi: 10.3389/fpls.2024.1333286

Genome-wide analysis of *NPR1*-like genes in citrus species and expression analysis in response to citrus canker (*Xanthomonas axonopodis* pv. *citri*)

Mobeen Ali[1], Muhammad Shafiq[1]*, Muhammad Zeshan Haider[2], Adnan Sami[2], Pravej Alam[3], Thamir Albalawi[3], Zuha Kamran[1], Saleh Sadiq[1], Mujahid Hussain[4], Muhammad Adnan Shahid[4], Mouna Jeridi[5], Ghulam Abbas Ashraf[6], Muhammad Aamir Manzoor[7]* and Irfan Ali Sabir[8]*

[1]Department of Horticulture, Faculty of Agricultural Sciences, University of the Punjab, Lahore, Pakistan, [2]Department of Plant Breeding & Genetics, Faculty of Agriculture Sciences, University of the Punjab, Lahore, Pakistan, [3]Department of Biology, College of Science and Humanities in Al-Kharj, Prince Sattam Bin Abdulaziz University, Al-Kharj, Saudi Arabia, [4]Horticultural Science Department University of Florida-Institute of Food and Agricultural Sciences (IFAS) North Florida Research and Education Center, Gainesville FL, United States, [5]Biology Department, College of Science, King Khalid University, Abha, Saudi Arabia, [6]College of Environment, Hohai University, Nanjing, China, [7]School of Agriculture and Biology, Shanghai Jiao Tong University, Shanghai, China, [8]College of Horticulture, South China Agricultural University, Guangzhou, China

Citrus fruits, revered for their nutritional value, face significant threats from diseases like citrus canker, particularly impacting global citrus cultivation, notably in Pakistan. This study delves into the critical role of *NPR1*-like genes, the true receptors for salicylic acid (SA), in the defense mechanisms of citrus against *Xanthomonas axonopodis* pv. *citri* (Xcc). By conducting a comprehensive genome-wide analysis and phylogenetic study, the evolutionary dynamics of *Citrus limon* genes across diverse citrus cultivars are elucidated. Structural predictions unveil conserved domains, such as the BTB domain and ankyrin repeat domains, crucial for the defense mechanism. Motif analysis reveals essential conserved patterns, while cis-regulatory elements indicate their involvement in transcription, growth, response to phytohormones, and stress. The predominantly cytoplasmic and nuclear localization of *NPR1*-like genes underscores their pivotal role in conferring resistance to various citrus species. Analysis of the Ks/Ka ratio indicates a purifying selection of *NPR1*-like genes, emphasizing their importance in different species. Synteny and chromosomal mapping provide insights into duplication events and orthologous links among citrus species. Notably, Xac infection stimulates the expression of *NPR1*-like genes, revealing their responsiveness to pathogenic challenges. Interestingly, qRT-PCR profiling post-Xac infection reveals cultivar-specific alterations in expression within susceptible and resistant citrus varieties. Beyond genetic factors, physiological parameters like peroxidase, total soluble protein, and secondary metabolites respond to SA-dependent PR genes, influencing plant characteristics. Examining the impact of defense genes (NPR1) and plant

characteristics on disease resistance in citrus, this study marks the inaugural investigation into the correlation between NPR1-associated genes and various plant traits in both susceptible and resistant citrus varieties to citrus bacterial canker.

KEYWORDS

citrus, expression profile of *NPR1*, phylogenetic analysis, salicylic acid, biotic stress

1 Introduction

Globally, citrus fruits stand out as the predominant category of commercially cultivated fruit within the Rutaceae family, offering a wealth of nutritional benefits and playing a crucial role in the world economy (Russo et al., 2021). Unfortunately, the citrus plant faces a significant threat from various diseases such as greening, citrus decline, and gummosis (Malik et al., 2021). Among these is Citrus Canker Disease (CCKD), caused by *Xanthomonas axonopodis* pv. *citri* (Xcc), which poses a major risk to citrus crop yield and quality worldwide, with particular severity in Pakistan (Malamud et al., 2011; Sami et al., 2023a; Sami et al., 2023b). The Sargodha region's citrus orchards contribute over 90% to Pakistan's national citrus production. Yield losses in Pakistan due to citrus canker can range from 10% to 50%, depending on infection severity and environmental conditions (Sabir et al., 2010; Almas et al., 2023). However, their potential is hampered by the onslaught of canker, evidenced by symptoms like discoloration, abrasions, and water-soaked lesions on fruit, stems, or leaves (Shahbaz et al., 2023). Several commercially important citrus varieties, including grapefruit, sweet oranges [*C. sinensis C. sinensis* (L.) Osbeck], lemons [*C.limon* (L.) Burm. F.], and key lime (*Citrus aurantifolia* Swingle), are susceptible to bacterial canker (Graham et al., 2004) impacting both the quantity and quality of fresh and processed fruit. This, in turn, leads to substantial economic losses for citrus growers (Spreen et al., 2003). The economic repercussions extend beyond the orchards, as limited fruit trade among states or internationally from canker-affected regions takes a severe toll on the overall economy (Duan et al., 2009; Khan et al., 2023).

Several alternative strategies for disease management have been devised with the aim of establishing enduring solutions for disease control in the long term. These methods encompass plant defense mechanisms specifically crafted to counteract various stressors, encompassing attacks from pathogens (Kushalappa et al., 2016; Manzoor et al., 2023). Resistance genes are considered one of the major factors in defense mechanisms against pathogenic attacks. Resistance (R) genes often trigger downstream signaling responses during plant disease resistance (Malamud et al., 2011; Khan et al., 2023). An immune response, SAR (Shahbaz et al., 2022), promotes the exploration of the resistant gene family to an infectious pathogen. SAR is considered a prime factor for activating numerous pathogenesis-related (PR) genes, such as *NPR1* gene with its paralogues (*NPR3* and *NPR4*) (Fu and Dong, 2013). Exogenous application of some chemicals, like benzol 1,2,3-thiadiazole-7-carbothermic acid, 2,6-dichloroisonicotinic acid, salicylic acid, and S-methyl ester on plants are considered to be responsible for the stimulation of the SAR system (Durango et al., 2013). Additionally, it is noted that during specific hypersensitive responses, the signal transduction pathway(s) connecting HR to SAR involves the endogenous production of SA (Cao et al., 1997).

Based on structural motifs, transmembrane areas, interleukin-1 receptor domain, leucine rich repeat (LRR) domain, coiled coil (Spoel et al., 2003) domains, and nucleotide-binding sites (NBSs), resistant proteins are grouped into numerous superfamilies. The two most prevalent R genes (NBS-LRR) found in plants (Meyers et al., 2003) are further divided into sub-groups based on N-terminal CC or TIR domain (Li et al., 2018). *NPR1* genes and their homologues were revealed to regulate the resistance of disease in the citrus family against various pathogens (Peng et al., 2021). NONEXPRESSOR OF PATHOGENESIS-RELATED GENES 1 (*NPR1*, along with their NPR3 and NPR4 as paralogues) serves as authentic SA receptors, actively participating in both local and systemic immunity by regulating SA-mediated processes (Birkenbihl et al., 2017; Sami et al., 2023c).

The investigation of the resistant gene family across various citrus species is vital in light of the aforementioned findings (Ahmad et al., 2023; Hussain et al., 2023). Thus, this resistant gene family was recognized and analyzed thoroughly in different species of citrus (*Citrus sinensis*, *Citrus reticulata*, *Citrus fortunella*, *Citrus maxima*, *Citrus medica*, *Citrus ichangenesis*, *Atlanta buxifolia*, and *Poncirus trifoliata*) that ranged from susceptible to highly resistant against canker. Phylogenic classification, characterization on molecular basis conserved motifs, residues of amino acids, distribution on chromosomes, and composition of protein domains were investigated. Furthermore, the stress-related expression pattern of citrus-resistant genes in different regions was also analyzed using citrus species sequencing of RNA (RNA-seq) datasets (Haider et al., 2023b). The findings underscore the need for substantial support to facilitate applied research and in-depth exploration of resistant genes in citrus species and related plant families. This exploration holds promise for influencing the creation of disease-resistant citrus varieties using various breeding

methods such as double haploid technology, hybridization, tissue culture, and backcrossing.

2 Materials and methods

2.1 Sequence data sources retrieval

Data pertaining to the amino acid sequences of *C. sinensis*, *C. reticulata*, *C. fortunella*, *C. limon*, *C. maxima*, *C. ichangenesis*, *C. maxima*, *P. trifoliata*, *C. clementina*, *A. buxifolia*, and *C. medica* were obtained from Citrus Genome database (https://www.citrusgenomedb.org). To confirm the presence of *NPR1*-like domains, retrieved amino acid sequences were subjected to searches at the SMART (http://smart.embl-heidelberg.de/) (Letunic et al., 2006; Haider et al., 2023a) and NCBI CDD (Conserved Domain Database) (https://www.ncbi.nlm.nih.gov/Structure/cdd/cdd.shtml) (Marchler-Bauer et al., 2013) with the default parameters.

2.2 Data retrieval of *NPR1*-like genes

The NPR reference sequences from *A. thaliana* were employed to identify homologous genes in the protein database of 11 citrus species via the https://www.citrusgenomedb.org/blast platform, with an E-value threshold of $< 1.2 \times 10^{-14}$. Subsequently, genomic, protein, CDS, and promoter sequences for all NPR genes were retrieved. In-depth analysis included the thorough examination of protein sequences to pinpoint representative sequences within duplicated genes. This process involved the utilization of TBtools and the verification of the existence of distinctive NPR domains, encompassing ANK repeats and N-terminal BTB/POZ domains. Additionally, motif analysis was conducted on these protein sequences using the motif finder tool (https://www.genome.jp/tools-bin/search_motif_lib) (Arabbeigi et al., 2018). The identified motifs were then compared against the canonical pattern found in "*AtNPR1*"-like proteins.

2.3 Gene characterization and structure analysis of *NPR1*-like genes

Multiple sequence alignments of *CsNPRs*, *CrNPRs*, *CfNPRs*, *CcNPRs*, *ClNPRs*, *CmdNPRs*, *CmNPRs*, *AbNPRs*, *PtNPRs*, and *CiNPRs* were generated using the MUSCLE Method in the Mega-X program and were visualized (Xu et al., 2020). Gene Structure Display Server (GSDS, http://gsds.cbi.pku.edu.cn/) (Guo et al., 2007) exhibited the exon–intron structures of *NPR1*-like genes in different citrus species. Moreover, NCBI-Conserved Domain Database (CDD) was used for the identification of the conservative domain compositions of 63 distinct *CsNPRs*, *CrNPRs*, *CfNPRs*, *ClNPRs*, *CcNPRs*, *CmdNPRs*, *CmNPRs*, *AbNPRs*, *PtNPRs*, and *CiNPRs* and the results of which were visualized by the TBtools software (https://www.genome.jp/tools/motif/) (Nakasu et al., 2019). The MEME Suite, accessible at https://meme-suite.org/meme/tools/meme, was utilized to identify protein motifs encoded by these genes. Additionally, an online tool was employed to pinpoint the locations of these motifs within the peptide sequences (Haider et al., 2023b).

2.4 Phylogeny analysis

Furthermore, the protein sequences of *A. thaliana* were retrieved from the GenBank (Sayers et al., 2022) database (https://www.ncbi.nlm.nih.gov/genbank/) to find out the phylogenetic integration among these *NPR1*-like proteins and CsNPRs, CrNPRs, CfNPRs, CcNPRs, ClNPRs, CmdNPRs, CmNPRs, AbNPRs, PtNPRs, and CiNPRs-like proteins. The full-length sequences of *Arabidopsis* proteins and the protein sequences of *NPR1*-like genes in 10 different citrus species were aligned using the Clustal W method (Nakasu et al., 2019). As a result, an unrooted phylogenetic tree was generated using the maximum-likelihood (ML) algorithm, employing MEGA-X software, with the specified parameters including the bootstrap method (1,000 replicates), the Jones–Taylor–Thornton model, and the inclusion of all sites (Shafiq et al., 2024).

2.5 Nonsynonymous (Ka) and synonymous (Ks) substitution rates calculation

The Ks and Ka values of genes from *CsNPRs*, *CrNPRs*, *CfNPRs*, *CcNPRs*, *ClNPRs*, *CmdNPRs*, *CmNPRs*, *AbNPRs*, *PtNPRs*, and *CiNPRs* were also determined. To achieve this, duplicate gene pairs resembling *NPR1*-like genes, originating from various duplication mechanisms, were employed to calculate substitution rates for Ka and Ks. TBtools were utilized to compute Ka and Ks values for these duplicated gene pairs and their respective Ka/Ks ratios using the simple Ka/Ks calculator feature. The Ka/Ks ratio was assessed to elucidate the molecular evolutionary rates of each gene pair. Generally, a Ka/Ks value <1 suggests purifying selection in evolution, Ka/Ks equals to 1 indicates neutral selection, while Ka/Ks >1 signifies positive selection (Haider et al., 2023b). Furthermore, the calculation of the divergence time for these gene pairs was conducted using the formula t = Ks/2r, with r (1.5×10^{-8}) serving as the representative value for neutral substitution rates (Campos et al., 2023).

2.6 Subcellular localization analysis

Subcellular localization of identified genes expressed was performed by using the WoLF PSORT program (https://wolfpsort.hgc.jp/) (Horton et al., 2006). Similarly, other factors regarding *CsNPRs*, *CrNPRs*, *CfNPRs*, *CcNPRs*, *ClNPRs*, *CmdNPRs*, *CmNPRs*, *AbNPRs*, *PtNPRs*, and *CiNPRs* genes and their respective coded proteins like molecular weight (Mw), isoelectric point (pI) value, amino acid (AA) length, length of mRNA, and chromosome number of all *CNPR* genes were gathered from the online tools like ExPASy-Protparam Tool (https://web.expasy.org/protparam/) (da

Silva et al., 2020) and Citrus genome database (https://www.citrusgenomedb.org/).

2.7 Chromosomal mapping of NPR genes

The chromosomal Id, start and end position of *NPR1* genes of *CsNPRs*, *CrNPRs*, *CfNPRs*, *CcNPRs*, *ClNPRs*, *CmdNPRs*, *CmNPRs*, *CbNPRs*, *PtNPRs*, and *CiNPRs* were retrieved using "Citrus Genome Database" (https://www.citrusgenomedb.org), and the length of chromosomes was found using "FASTA stats" tool (https://bio.tools/gfastats). Three files, "Chromosome ID and length," "Chromosome ID, start position/end position," and "gene pairs", derived from the Ks/Ka analysis, were driven to the "Gene Location Visualize Advance" window of TBtools, and the graph of chromosomal mapping was retrieved (Islam et al., 2023).

2.8 Cis-regulatory element and synteny data retrieval

PlantCARE database (http://bioinformatics.pAb.ugent.be/webtools/plantcare/htmL/) (Haider et al., 2023b) was used to identify Cis-regulatory elements. The promoter sequences of *NPR1*-like genes were extracted from genome sequences of 10 citrus species by TBtools software. Chromosome IDs and coordinates were sourced from the Citrus Genome Database, then Advanced Circos in TBtools was used to create the synteny graph.

2.9 Citrus NPR gene expression in diverse tissues and organs

The study of ESTs (expressed sequence tags) to find resistance genes in citrus species and characterize their expression levels across multiple citrus plant tissues and organs, leveraging the online NCBI Gene Expression Omnibus (GEO) database (Grechkin et al., 2017). The Blast P search was performed using a default parameter with an e-value of 1e−04. Various genes exhibited expression in distinct segments of the citrus plant, encompassing the flower, root, fruit, leaf, stem, and more, in response to diverse forms of biotic stress and various influencing factors. Heat maps were used to analyze the expression patterns of specific resistance genes across different tissues and organs in different citrus species.

2.10 Plant material

The four citrus cultivars *C. sinensis* (sweet orange), *C. reticulata* (mandarin), *C. limon* (lemon), and *C. fortunella* (kumquat) were inoculated with citrus bacterial culture (*Xanthomonas axonopodis* pv. *citri*) and chosen for gene expression. The experiment was conducted in a greenhouse (day/night temperature, 25°C; light/dark periods, 16/8) using the method of completely randomized design (CRD) and three replicates of each treatment.

2.11 RNA extraction and qRT-PCR analysis

mRNA was extracted using the triazole method (Fujino et al., 2016), and first-strand cDNA was synthesized using AB script II cDNA first-strand synthesis kit. SYBR Green (Wiz pure) was used to perform qRT-PCR. Standard curves were created to estimate the proportion of citrus *NPR1*-like genes, and housekeeping gene quantity in samples was determined using real-time PCR (Illumina) and software (https://biomolecularsystems.com/mic-qpcr/software/). To analyze the dynamics of expression, we conducted three biological and three technical replicates. Significance differences were assessed using Student's t-tests ($p < 0.05$).

2.12 Statistical analysis

The data were subjected to statistical analysis using a two-way factorial completely randomized design (CRD). Analysis of variance (ANOVA) was utilized to assess variances, and means were differentiated using the least significant difference (LSD) method, with a significance level set at $p < 0.05$. The entire statistical analysis was carried out using the Statistix 8.1 software suite.

3 Results

3.1 Identification, description, and evolutionary analysis of *NPR1* homologues in citrus varieties

Approximately 63 non-redundant *NPR1*-like genes were retrieved from the genome of *C. sinensis*, *C. reticulata*, *C. fortunella*, *C. limon*, *C. maxima*, *C. ichangenesis*, *C. maxima*, *P. trifoliata*, *C. climentina*, *A. buxifolia*, and *C. medica*. Utilizing bioinformatics tools like BLAST search, 63 *NPR1*-like genes were discovered in the genome and named as *CsNPRs*, *CrNPRs*, *CfNPRs*, *ClNPRs*, *CcNPRs*, *CmdNPRs*, *CmNPRs*, *AbNPRs*, *PtNPRs*, and *CiNPRs*. Using NCBI CDD Domain analysis, all the proteins that lack N-terminal BTB/POZ domain or ANK repeats in the middle region were excluded. As a result, different species have different number of *NPR1*-like genes, like nine in *C. sinensis*; seven in *C. reticulata*; two in *C. fortunella*; six in *C. limon*, *A. thaliana*, and *C. medica*; 10 in *C. climentina* and *C. ichangensis*; seven in *C. maxima* and *P. trifoliata*; and three in *A. boxifolia* (Figure 1).

The mRNA lengths of these CsNPRs, CrNPRs, CfNPRs, CcNPRs, CmdNPRs, CmNPRs, AbNPRs, PtNPRs, and CiNPRs genes have nucleotides that range from 1,119 to 69,428, while the amino acid lengths of their respective proteins vary between 372 and 1,379 amino acids. Additionally, the overall pI values vary from 4.91 to 8.74, and the molecular weight of described genes CsNPRs, CrNPRs, ClNPRs, CfNPRs, CcNPRs, CmdNPRs, CmNPRs, AbNPRs, PtNPRs, and CiNPRs proteins vary from 118,053.42 to 46,773.06 (Table 1).

The evolutionary tree from the protein sequences of *NPR1*-like was constructed among the various species of citrus (*C. sinensis*, *C. reticulata*, *C. fortunella*, *C. maxima*, *C. medica*, *C. ichangenesis*, *C.*

10.3389/fpls.2024.1333286

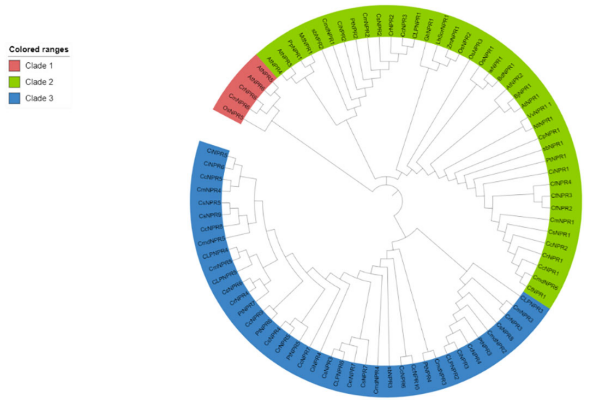

FIGURE 1
Polygenetic tree of NPR1 like proteins in *CsNPRs, CrNPRs, CfNPRs, CcNPRs, CmdNPRs, CmNPRs, sbNPRs, PtNPRs* and *CiNPRs* and its homologous in, A. thaliana (At).

limon), and *A. buxifolia* and *P. trifoliata*, and references the *A. thaliana* species as a model (Cao et al., 1997; Spoel et al., 2003; Peng et al., 2021). A 1,000 bootstrap tree was constructed using the UPGMA model in MegaX software. The phylogeny analysis demonstrated the presence of NPR-like proteins categorized into three distinct classes or clades, matching patterns found in other species. Clade I include 41 NPR-related proteins, and clade II comprised 16 NPR-related proteins. Proteins from the same clade appear to be structurally and functionally related (Sami et al., 2024).

3.2 Gene duplication analysis

To estimate the approximate gene divergence time, the TBtools program was utilized, and it furnished values for Ks, Ka, and Ka/Ks ratios as specified. The value of synonymous substitutions per synonymous site was denoted by Ks, while the value of non-synonymous substitutions per non-synonymous site was quantified by Ka. The balance between synonymous and non-synonymous mutations can be seen in the Ka/Ks ratio. The evolutionary investigation revealed six gene pairs associated with gene duplication within the NPR family. The first pair included *ClNPR4*/*CmNPR5*, the second pair *CsNPR4*/*CrNPR5*, the third pair *CrNPR3*/*CsNPR8*, the fourth pair *CmNPR6*/*CrNPR6*, the fifth pair *AtNPR6*/*AtNPR5*, and the sixth pair *AbNPR1*/*AtNPR2* (Table 2).

A measure that evaluates the selection pressure affecting amino acid substitutions was the Ka/Ks ratio. When the Ka/Ks ratio declines below 1, it denotes an evolutionary process of purifying selection

TABLE 1 Physiochemical properties of NPR1 gene family in different citrus species.

	Gene	Accession Number	A. A length	mRNA length	M. W	pI
C. reticulata	CrNPR1	MSYJ077460_1	585	4206	65789.71	6.31
	CrNPR2	MSYJ131960_1	587	3267	65938.7	5.7
	CrNPR3	MSYJ281930_1	592	9064	65764.77	5.9
	CrNPR4	MSYJ281950_1	565	69428	63352.37	5.8
	CrNPR5	MSYJ281960_1	800	20268	89049.19	7.45
	CrNPR6	MSYJ281940_1	416	2238	47346.89	8.74
	CrNPR7	MSYJ287170_1	448	2671	49421.35	6.28
C. sinensis	CsNPR1	Cs4g14600_1	585	2219	65789.71	6.31
	CsNPR2	Cs2g10790_1	532	2263	65884.67	5.77
	CsNPR3	Cs7g18670_1	576	1732	64992.27	5.64
	CsNPR4	Cs7g18690.1	1045	3203	118053.42	7.44
	CsNPR5	Cs7g18600_1	488	2360	54861.44	6.35
	CsNPR6	Cs7g18670_1	576	1732	64992.27	5.64
	CsNPR7	Cs7g18690_1	1045	3203	118053.42	7.44
	CsNPR8	Cs7g18620_1	1379	4506	155423.04	5.83
	CsNPR9	Cs7g18630_1	577	2056	64773.85	5.65
	CsNPR10	Cs7g18680_1	590	2188	66226.62	5.48
	CsNPR12	orange1_1t02156.1	416	1251	46773.06	6.98
C. fortunella	CfNPR1	sjg283810_1	451	4547	50546.84	5.91
	CfNPR2	sjg245720_1	441	4842	48518.38	6.22

(Continued)

10.3389/fpls.2024.1333286

TABLE 1 Continued

	Gene	Accession Number	A. A length	mRNA length	M. W	pI
C. limon	CLNPR1	CL2G008891011.t1_pri	615	1848	69287.44	5.72
	CLNPR2	CL7G026056011.t1_pri	640	1923	71573.98	6.6
	CLNPR3	CL7G026057011.t1_pri	583	1785	65056.09	5.98
	CLNPR4	CL7G026062011.t1_pri	989	2970	110582.54	8.32
	CLNPR5	CL7G026072011.t1_pri	566	1731	63864.33	5.46
	CLNPR6	CL7G026061011.t1_pri	550	1668	61634.47	6.02
C. clementina	CcNPR1	clementine0.9_006073m	574	2040	64590.19	6.31
	CcNPR2	clementine0.9_005813m	585	2073	65789.71	6.31
	CcNPR3	clementine0.9_007280m	527	1802	59573.35	5.49
	CcNPR4	clementine0.9_005587m	595	2503	66349.57	6.08
	CcNPR5	clementine0.9_005201m	616	1867	68892.48	5.27
	CcNPR6	clementine0.9_034478m	553	1662	61768.05	5.02
	CcNPR7	clementine0.9_035825m	416	1248	46699.2	5.25
	CcNPR8	clementine0.9_005876m	582	1749	65152.2	5.67
	CcNPR9	clementine0.9_007701m	514	1545	57551.7	5.7
	CcNPR10	clementine0.9_011886m	405	1387	45454.63	4.91
C. maxima	CmNPR1	Cg4g008720.1	517	1722	58000.45	5.97
	CmNPR2	Cg2g038060.1	587	2547	65885.66	5.7
	CmNPR3	Cg7g012270.2.1	600	2595	66636.75	6.15
	CmNPR4	Cg7g012290.1	794	2385	89459.31	6.02
	CmNPR5	Cg7g012280.1	593	1782	66655.55	5.55
	CmNPR6	Cg9g017270.1	506	1704	55418.89	6.15
	CmNPR7	Cg7g012320.1	398	1197	43695.7	6.1
C. ichangensis	CiNPR1	Ci293640.2	434	3617	48430.58	5.9
	CiNPR2	Ci150300.1	587	2567	66020.83	5.83
	CiNPR3	Ci132570.2	595	2600	66397.57	6.08
	CiNPR4	Ci132560.1	484	1455	54036.56	5.34
	CiNPR5	Ci132530.1	477	1434	52840.71	5.05
	CiNPR6	Ci296910.1	580	1743	64783.49	5.5
P. trifoliate	PtNPR1	Ptrif.0001s0987.3.v1.3.1	435	4266	48742.99	5.85
	PtNPR2	Ptrif.0002s2330.2.v1.3.1	587	4440	65916.64	5.91
	PtNPR3	Ptrif.0004s1251.1.v1.3.1	594	4436	66333.51	6.08
	PtNPR4	Ptrif.0004s1256.1.v1.3.1	467	2810	52059.48	5.47
	PtNPR5	Ptrif.0004s1259.1.v1.3.1	407	1875	45680.06	5.59
	PtNPR6	Ptrif.0004s1254.1.v1.3.1	594	4854	66690.75	5.3
	PtNPR7	Ptrif.0004s1252.2.v1.3.1	252	1922	28077.37	5.28
S. buxifolia,	SbNPR1	sb23887.4	434	4017	48442.57	5.91
	SbNPR2	sb12905.3	447	2834	50436.9	5.66
	SbNPR3	sb24964.1	445	1337	49597.08	6.26

(Continued)

TABLE 1 Continued

	Gene	Accession Number	A. A length	mRNA length	M. W	pI
C. medica	CmdNPR1	Cm196830.1	587	2836	65986.78	5.7
	CmdNPR2	Cm144560.1	957	3067	106809.87	5.68
	CmdNPR3	Cm144640.1	372	1119	41541.5	5.67
	CmdNPR4	Cm144610.1	433	1302	48576.58	5.2
	CmdNPR5	Cm144680.1	585	1758	65371.25	5.19
	CmdNPR6	Cm127070.1	398	1197	45000.1	6.09

AA, amino acid sequence length; MW, molecular weight; pI, isoelectric point

(Parmley and Hurst, 2007). If this ratio was exceeding value 1, it may indicate the probability of positive selection (Biswas and Akey, 2006). The findings showed that the Ka/Ks ratios varied significantly across NPR groups. The Ka/Ks ratios for *ClNPR4/CmNPR5*, *CsNPR4/CrNPR5*, *CmNPR6/CrNPR6*, *AtNPR6/AtNPR5*, and *AbNPR1/AtNPR2* indicate purifying selection, with values below 1, while the Ka/Ks ratio for *CrNPR3/CsNPR8* suggests positive selection, as it exceeds 1, indicating environmental influence (Sami et al., 2023d).

3.3 Genes structure and sequence analysis

To gain deeper insights into the functions of *CsNPRs*, *CrNPRs*, *CfNPRs*, *CcNPRs*, *ClNPRs*, *CmdNPRs*, *CmNPRs*, *AbNPRs*, *PtNPRs*, and *CiNPRs* genes, structural features and sequence composition analysis was conducted using online tools GSDS and NCBI-CDD. Intron/exon profiles of NPR genes were generated using GSDS 2.0 (Figure 2). Notably, the majority of NPRs, including *CsNPR6*, *CcNPR9*, *CmdNPR5*, *CcNPR8*, *CcNPR5*, *CsNPR5*, *CsNPR9*, *CiNPR5*, *CiNPR6*, *CiNPR7*, *CiNPR4*, *CsNPR3*, *CsNPR7*, *CmdNPR4*, *AbNPR3*, *CcNPR6*, *CcNPR10*, *CmdNPR3*, *CsNPR8*, *CmdNPR2*, *CcNPR4*, *CiNPR3*, *AbNPR2*, *CiNPR2*, *CmdNPR1*, *CsNPR2*, *CcNPR3*, *AbNPR1*, *CiNPR1*, *CsNPR1*, *CiNPR2*, and *CmdNPR6*, exhibited lack of introns. In contrast, the four *Arabidopsis* sequences, *AtNPR1*, *AtNPR2*, *AtNPR3*, and *AtNPR4*, contained two introns, while *AtNPR5* and *AtNPR6* had only one intron each. *ClNPR4* had seven introns; *CmNPR4* had six introns; *CmNPR5*, *CrNPR4*, and *ClNPR3* had four introns; and *ClNPR5*, *PtNPR6*, *CmNPR7*, *CmNPR3*, *PtNPR3*, *ClNPR3*, *AtNPR3*, *AtNPR4*, *PtNPR2*, *CmNPR2*, and *CrNPR1* had three introns. *CrNPR6*, *CmNPR1*, and *CrNPR3* had two introns, while *PtNPR5*, *CmdNPR5*, *PtNPR4*, and *CmNPR6* possessed a single intron only. The number of introns per gene ranged from 0 to 7. Interestingly, no results were obtained for *CcNPR1*, *CfNPR1*, *CfNPR2*, and *CcNPR6*. These findings highlight significant variations in the number of introns–exons among *CsNPRs*, *CrNPRs*, *CfNPRs*, *ClNPRs*, *CcNPRs*, *CmdNPRs*, *CmNPRs*, *AbNPRs*, *PtNPRs*, *CiNPRs*, and *A. thaliana* genes.

3.4 Motif analysis

Conserved domain analysis was employed to filter out sequences exclusively featuring the BTB domain. Following that, motif analysis, along with conserved domain analysis, was carried out using TBtools. The analysis revealed that several genes, including *ClNPR4*, *CmNPR5*, *ClNPR5*, *CsNPR6*, *CcNPR9*, *PtNPR6*, *CcNPR8*, *CcNPR5*, *CmNPR2*, *CsNPR2*, *CrNPR2*, *CLNPR1*, *AtNPR1*, *AtNPR2*, *AbNPR1*, *PtNPR1*, *CfNPR2*, and *CrNPR4* possessed motifs in the order of 8, 7, 2, 9, 5, 6, 1, 4, 3, and 10. However, *PtNPR5* shows all these motifs except motif 5, while *CrNPR5* featured all of them except for motifs 8 and 10, and *CsNPR4* included motifs 7, 2, 9, 5, 6, 1, 4, 3, and 10, in addition to others. *CsNPR5* and *CsNPR9* displayed motifs 8, 9, 7, 2, 5, 6, 1, 4, 3, and 10, followed by motifs 9, 5, 6, 7, 4, 3, and 10. Some sequences had minor variations, such as *ClNPR6* lacking motifs 2 and 3; *CcNPR6* lacking motif 5; *CmdNPR3* and *CmdNPR2* featuring motifs 7, 2, 9, 5, 6, 1, and 4 in addition; and *CrNPR5* missing motifs 8 and 10, along with motifs 6, 1, 4, 3, and 10. *CsNPR7* possessed an additional motif 10; *CmdNPR6* lacked motifs 8, 7, 2, 1, and 6; *CsNPR8* lacked motifs 4,

TABLE 2 The expression ka/ks represents the ratio of mutations involving synonymous substitutions (ks) to mutations involving non-synonymous substitutions (ka).

Seq-1	Seq-2	ka	Ks	Ka-ks	T(MYA)	Protein homology
CLPNPR4	CmNPR5	0.0685414	0.090403078	0.758175584	30134359.2	23.5
CsNPR4	CrNPR5	0.0795171	0.11444433	0.694810345	38148110.08	92.3
CrNPR3	CsNPR8	1.8985625	1.740752009	1.090656475	580250669.7	98.5
CmNPR6	CrNPR6	9.80E-04	0.015658189	0.062571218	5219396.255	17.6
AtNPR6	AtNPR5	0.0782242	1.098978008	0.071179016	366326002.7	82.9
sbNPR1	AtNPR2	0.3066207	1.641364596	0.186808411	547121531.9	54.6

The gene duplication over selection and evolutionary pressure to paralogous pairings of NPR genes were calculated based on ks and ka values.

10.3389/fpls.2024.1333286

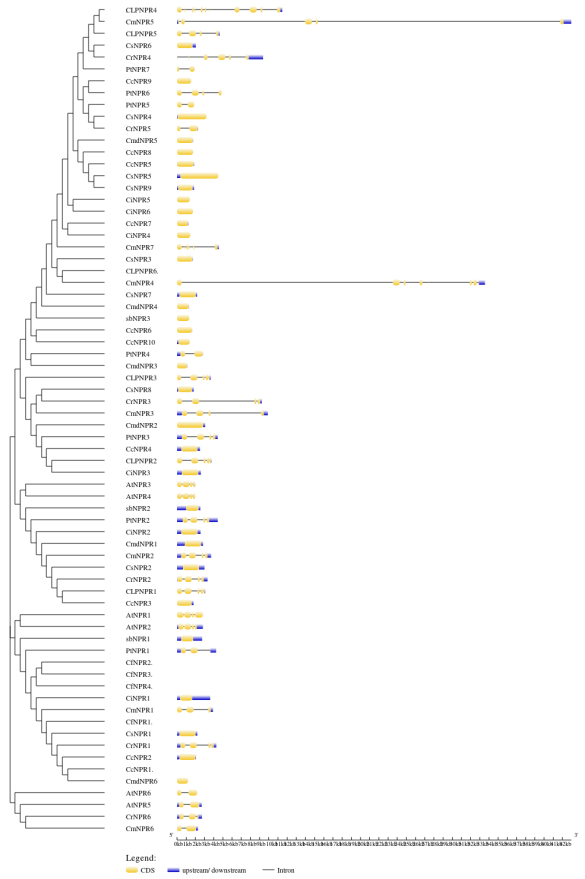

FIGURE 2
Phylogenetic relationship and gene structure of NPR1 genes from *CsNPRs, CrNPRs, CfNPRs, CcNPRs, CmdNPRs, CmNPRs, sbNPRs, PtNPRs* and *CiNPRs*. The phylogenetic tree was constructed using full length sequences of *CsNPRs, CrNPRs, CfNPRs, CcNPRs, CmdNPRs, CmNPRs, sbNPRs, PtNPRs* and *CiNPRs*-like genes. Yellow boxes indicate exons; and black lines indicate introns.

1, 3, and 10; *ClNPR2* had an additional motif 3; *CmNPR4* had motifs 8, 9, 1, 4, 3, and 10 in addition; *CmdNPR3* lacked motifs 5, 6, and 10; *AtNPR3* and *AtNPR4* were lacking motif 3; and *CcNPR3* lacked motif 1. *PtNPR7* exhibited motifs 7, 2, 9, 5, 6, and 1, while *CiNPR5* lacked motif 6, as did *CiNPR6* and *CcNPR7*. *CmNPR7* only possessed motifs 8, 7, 2, 9, 4, and 10. *CiNPR1*, *CmNPR1*, *CfNPR1*, *CsNPR1*, *CrNPR1*, *CcNPR2*, and *CcNPR1* did not have motif 6, whereas *AtNPr5*, *AtNPR6*, *CrNPR6*, and *CmNPR6* had an additional motif 6 (Figure 3).

3.5 Subcellular localization of NPR-like gene

The subcellular localization analysis indicated that cytoplasm was the predominant location for *CsNPR1*, *CrNPR1*, *CcNPR2*, *PtNPR7*, *CiNPR1*, and *PtNPR1*. Chloroplasts and plastids showed lower quantities of *CsNPR9*, *CsNPR7*, *CLNPR5*, *CcNPR7*, *CcNPR10*, *PtNPR4*, *CcNPR5*, *CsNPR3*, *CLNPR5*, *CmNPR4*, *CfNPR2*, *CmNPR1*, *CcNPR1*, *PtNPR2*, *AbNPR1*, *CfNPR1*, *CmdNPR6*, *CmNPR7*, *CsNPR5*, *CsNPR9*, *CcNPR6*, *PtNPR6*, *CiNPR4*, *CmdNPR3*, and *CmdNPR4*. Chloroplasts had lower levels of *ClNPR1*. Cyto-nucleus contained reduced amounts of *ClNPR1*, *CiNPR3*, *CcNPR4*, *PtNPR3*, *CrNPR3*, *CcNPR3*, and *CmdNPR2*. Peroxisomes contained minimal quantities of *CiNPR2*, *CmdNPR1*, *CsNPR2*, *CrNPR2*, and *CcNPR3*. The nucleus was the primary site for *ClNPR3*, *ClNPR1*, *CiNPR3*, *CcNPR4*, *PtNPR3*, *CrNPR3*, and *CmNPR3*, with *CmNPR6*, *CrNPR5*, and *PtNPR7*, absent from the nucleus. Other proteins were present in lower amounts in the nucleus. ER exhibited limited concentrations of *CcNPR7*, *CcNPR10*, *PtNPR4*, *CsNPR4*, *CmNPR6*, *CrNPR6*, *CsNPR6*, *CmdNPR5*, and *CcNPR8*. Vacuoles contained *CcNPR6*, *CmNPR4*, *CLNPR6*, *CcNPR5*, *CLNPR5*, *CsNPR7*, *CCNPR9*, *CrNPR6*, *CmNPR6*, *CsNPR4*, *CLNPR2*, and *AbNPR3* in small quantities. Mitochondria housed the highest quantity of *CmNPR5*, while *CcNPR7*, *CcNPR10*, *PtNPR4*, *CrNPR4*, *PtNPR5*, *CrNPR6*, and *CmNPR6* were present in smaller amounts. R-vacuoles contained small numbers of *CmdNPR6*, *CfNPR1*, *PtNPR1*, *CiNPR1*, and *CmdNPR1*. Golgi apparatus had *ClNPR2*, CL*NPR1*, and *PtNPR4* in small quantities. ER plastids contained *CcNPR10* and *CcNPR7* in lower numbers, and cyto-ER contained only *CmdNPr6* in moderate quantities (Figure 4).

3.6 Chromosomal mapping of NPR genes

Comparative chromosomal mapping of several citrus species, including *C. sinensis*, *C. clementina*, *C. medica*, *C. maxima*, *C. ichangenesis*, *C. limon*, *C. fortunella*, *A. buxifolia*, and *P. trifoliata*, about *A. thaliana*, revealed the presence of five pairs of orthologous genes among these citrus species. Specifically, Scaffold 86 of *C. reticulata* contained *CrNPR6*, which had an ortholog, *CsNPR4*, on chromosome 7 of *C. sinensis*. Additionally, *CrNPR3* on Scaffold 86 of *C. reticulata* exhibited orthology with *CsNPR7* on chromosome 7 of *C. sinensis*, while *CrNPR5* on Scaffold 86 of *C. reticulata* shared orthology with *CmNPR6* on chromosome 9 of *C. maxima*. Furthermore, *AbNPR1* on Scaffold 15601 of *A. buxifolia* was found to be orthologous to *AtNPR2* on chromosome 4 of *A. thaliana*, and *AtNPR5* on Chromosome 2 of *A. thaliana* displayed orthologous relationships with *AtNPR6* on chromosome 3 of *A. thaliana* (Figure 5).

3.7 Cis-regulatory elements in *NPR1*-like genes

Numerous cis-regulatory elements were identified within the 55 promoter regions of *CsNPRs*, *CrNPRs*, *CfNPRs*, *CcNPRs*, *ClNPRs*, *CmdNPRs*, *CmNPRs*, *AbNPRs*, *PtNPRs*, and *CiNPRs*, including widely observed CAAT and TATA boxes. Additionally, phytohormone-responsive elements such as ABRE, TGACG-motif, TCA-element, P-box, GARE-motif, TATC-box, TGA-box, and AuxRR-core were detected across various genes and are involved in the response to auxin, GA, SA, abscisic acid, etc., prominently in *CsNPRs*, *CrNPRs*, *CcNPRs*, *CfNPRs*, *CiNPRs*, *CmdNPRs*, *CmNPRs*, *PtNPRs*, *AbNPRs*, and *AtNPRs*. Light-responsive elements such as Box 4, CAG-motif, G-Box, GT1-motif, ACE, AT1-motif, TCT-motif, I-box, TCCC-motif, chs-CMA2a, AE-box, ATCT-motif, GATA-motif,

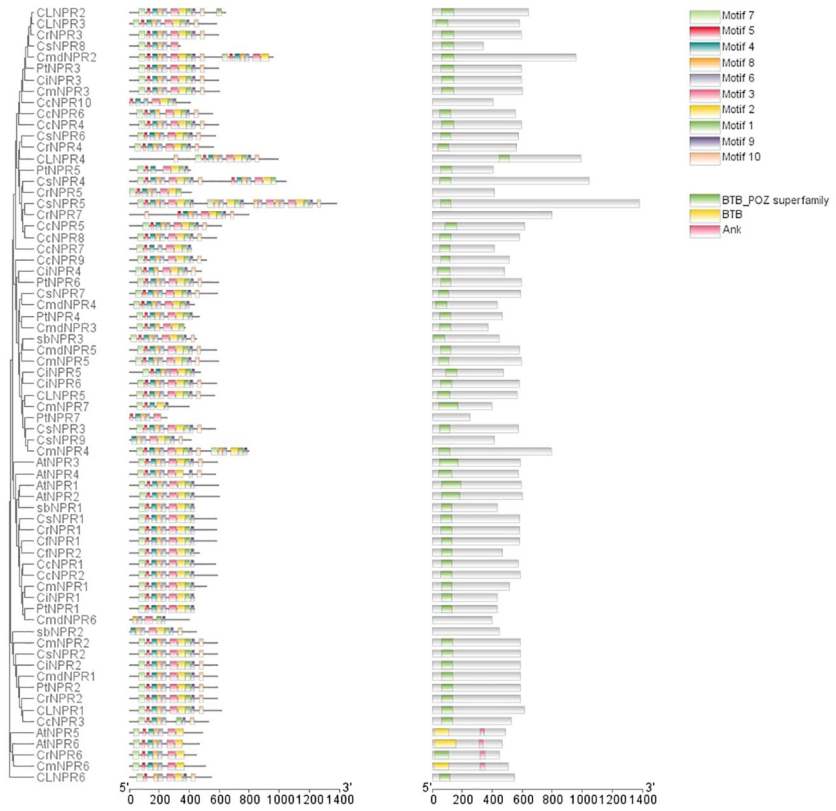

FIGURE 3
The domain arrangements of putative *NPR1*-like genes in *C. sinensis, C. reticulata, C. fortunella, C. limon, C. medica, C. maxima, C. clementina, C. ichangensis, P. trifoliate, A. buxifolia*, and *A. thaliana* connected with the phylogenetic tree.

Gap-box, LAMP-element, GA-motif, Pc-CMA2c, and Sp1 were notably present in various genes. Furthermore, specific cis-regulatory elements like LRR, ACII, and ref2f-1 were discovered in selected genes, implicated in regulating circadian rhythm, zein metabolism, anaerobic induction, and drought stress among other processes (Figure 6).

3.8 Syntenic relationship of NPR gene of different plants

To determine the collinearity relationships among orthologous genes of *C. sinensis*, *C. fortunella*, *C. reticulata*, *C. medica*, *C. maxima*, *C. limon*, *A. buxifolia*, *P. trifoliata*, *C. ichangenesis*, and *C. climentina*, a synteny analysis was conducted. Notably, scaffolds 1, 2, and 4 of *P. trifoliata* did not exhibit orthologous gene counterparts. In *A. buxifolia*, *AbNPR1* genes located on scaffold 10 shared orthologs with chromosome 4 of *A. thaliana*, which also houses *AtNPR4* and *AtNPR3*. Similarly, in *A. thaliana*, the gene *AtNPR5* found on chromosome 2 exhibited orthologs on chromosome 3, including AtNPR6. Moreover, genes located on scaffold 86 of *C. reticulata*—specifically, *CrNPR3*, *CrNPR4*, *CrNPR5*, and *CrNPR6* showed orthology with *CmNPR6* on chromosome 9 of *C. maxima* and with genes *CsNPR3* through *CsNPR9* on chromosome 7 of *C. sinensis* (Figure 7).

3.9 Expression analysis of NPR genes in citrus

CmNPR1 and *CmNPR5* were derived from previously generated *in silico* data that focused on *NPR1* expression during the flavonoid biosynthesis process in both red and white cultivars *of C. maxima.* The results did not indicate any substantial upregulation or downregulation of *CmNPR1* or *CmNPR5*, implying that *NPR1* might not have a significant influence on flavonoid biosynthesis (Zhao et al., 2020) within *C. maxima*.

3.9.1 Sweet orange fruit expression data across developmental stages

The role of *CsNPR1* in the developmental phases of *C. sinensis* was scrutinized, revealing its active involvement across various stages. Notably, the expression of *CsNPR1* remained consistent across all four treatments, suggesting a stable pattern without significant fluctuations in up- or downregulation. This constancy in expression implies that *CsNPR1* maintains a steady involvement throughout the developmental processes, indicating a potential regulatory role that remains relatively unaltered across the conditions tested. The observed consistency in expression underscores the significance of *CsNPR1* in the intricate orchestration of developmental events within *C. sinensis*.

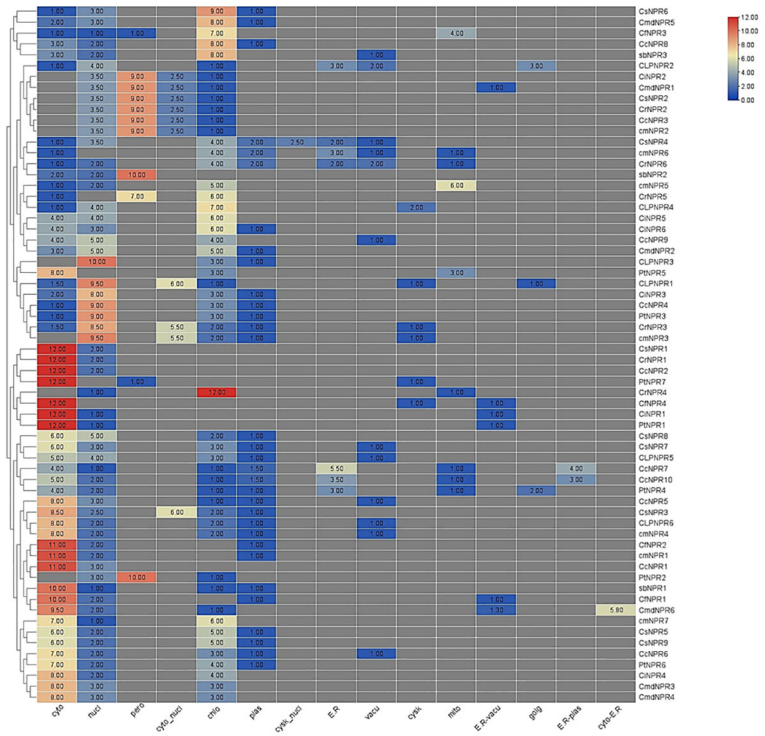

FIGURE 4
An abundance of putative *NPR1*-like genes in various species of citrus, connected to a phylogeny tree, enables a better understanding of gene function and analogy. Cytoplasm exhibited the highest abundance of *CsNPR1, CrNPR1, CcNPR2, PtNPR7, CiNPR1*, and *PtNPR1*, while various organelles had distinct but lower quantities of these proteins, indicating diverse subcellular distributions.

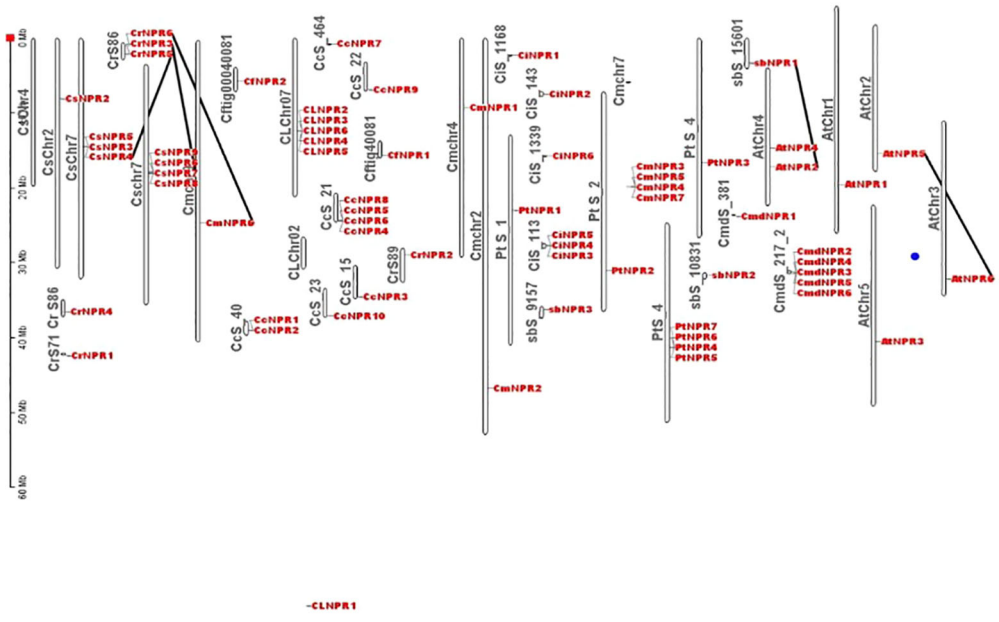

FIGURE 5
Different citrus species chromosomes location and duplication occurrences to *NPR1*-like genes revealed 5 orthologous pairs, e.g., *CrNPR6* in *C. reticulata* aligns with *CsNPR4* in *C. sinensis*. Additionally, *AbNPR1* in A. buxifolia corresponds to *AtNPR2* in *A. thaliana*, while *AtNPR5* aligns with AtNPR6 within *A. thaliana*.

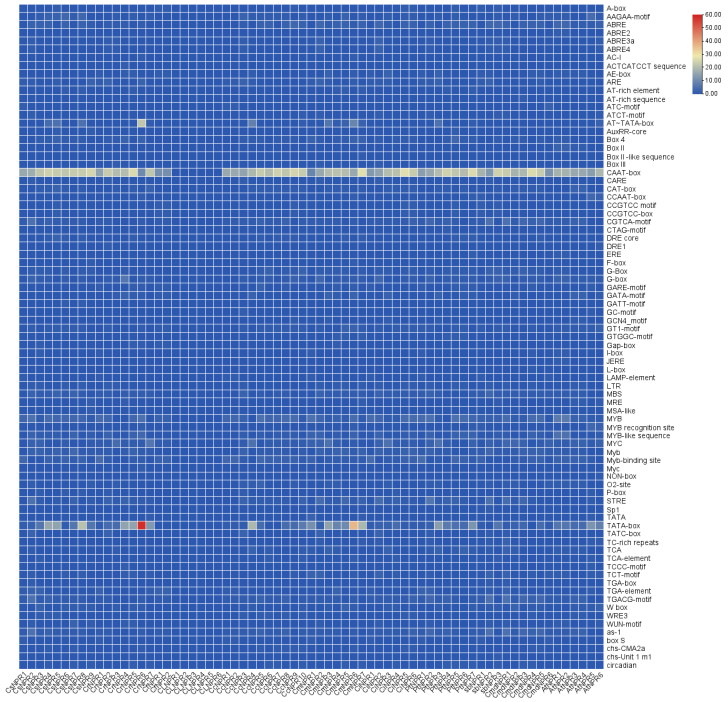

FIGURE 6
Illustration of cis elements of NPR1 in different citrus spiecies.

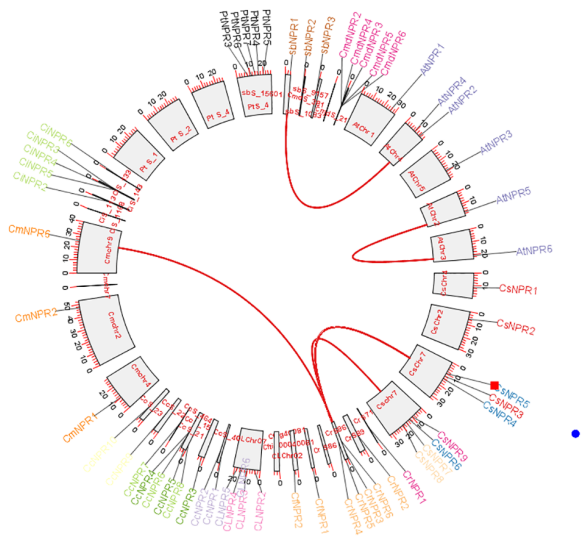

FIGURE 7
A Circos plot depicting the *NPR1*-like gene family in citrus species. The red connections indicate instances of gene duplications occurring both within and between various species. Synteny analysis revealed collinearity relationships among orthologs from various citrus species and identified specific gene matches, such as *AbNPR1* in *A. buxifolia*, *AtNPR5* in *A. thaliana*, and *CrNPR3*, *CrNPR4*, *CrNPR5*, *CrNPR6* in *C. reticulata* with their respective orthologs in related species.

3.9.2 RNA-seq and targeted metabolomics reveal *C. sinensis* leaf responses to prolonged low pH exposure

In the face of diverse low pH conditions ranging from 2 to 6, tested at intervals of 1 h, 2 h, 3 h, 4 h, and 10 h, *CsNPR1* displayed a remarkable resilience. Importantly, throughout these varying acidic stress conditions, there was no discernible alteration in the expression of *CsNPR1*. This steadfastness in expression levels strongly suggests that *CsNPR1* remains unaffected by acidic stress within the tested pH range and exposure durations. The consistent expression of *CsNPR1* despite the challenging acidic conditions underscores its robust nature and resilience to environmental stressors, highlighting its potential role as a key player in mitigating the impact of low pH stress on the biological processes it governs *NPR1* (Zhang et al., 2022).

3.9.3 Analyzing cuticle regulation in Newhall navel oranges during fruit development and ripening

CsNPR1 expression was identified in the regulation of cuticle formation during two distinct developmental stages, a finding consistent across two separate replicates. Importantly, there were no significant fluctuations observed in the expression levels of *CsNPR1* during these stages. This stability in expression implies that *CsNPR1* consistently plays a role in the control of cuticle formation at these specific developmental points. The lack of

notable changes in *CsNPR1* expression levels underscores its reliability as a regulator in the intricate processes involved in cuticle development, emphasizing its potential importance in maintaining the integrity and protective function of the cuticle across these specific developmental milestones.

3.9.4 The expression levels of CNPRs genes in different citrus species in response to citrus canker using qRT-PCR

The quantitative analysis using qRT-PCR revealed the presence of *NPR1* genes expression in *C. sinensis* following inoculation with *Xanthomonas axonopodis* pv. *citri*. Out of the nine *CsNPR1* genes, statistical analysis showed that three genes (*CsNPR1*, *CsNPR4*, and *CsNPR5*) did not exhibit significant differences (Figure 8). Conversely, the remaining six genes (*CsNPR2*, *CsNPR3*, *CsNPR6*, *CsNPR7*, *CsNPR8*, and *CsNPR9*) displayed statistically significant responses. Notably, all samples that were treated with infected citrus bacterial canker exhibited higher relative expression of the *NPR1* gene compared to the control group. Among them, *CsNPR7*- and *CsNPR9*-treated samples demonstrated the highest gene expression levels. However, it is important to note that control samples displayed higher expression levels than the other control samples.

The results obtained from qRT-PCR analysis indicated the expression of *NPR1* genes across all treatments in *C. reticulata*. Notably, all *NPR1* genes in *C. reticulata* displayed statistically significant expression, except for *CrNPR1*, which exhibited varying results. Among these genes, *CrNPR3*, *CrNPR4*, and *CrNPR6* demonstrated the highest levels of expression in the treated samples compared to the control group, while *CrNPR2* and *CrNPR5* exhibited higher expression levels in the control samples than in other genes (Figure 9).

In the case of *C. fortunella*, the real-time qPCR findings showed significant expression of *NPR1* genes, particularly *CfNPR1* and *CfNPR2*. Interestingly, *CfNPR2* displayed increased expression in the control samples compared to the treated (infected with citrus bacterial canker) samples (Figure 10).

Similarly, *NPR1* genes were found to be expressed in all treated samples of *C. limon* compared to the control. Among these, *ClNPR1*, *ClNPR3*, and *ClNPR6* yielded statistically non-significant results, while *ClNPR2*, *ClNPR4*, and *ClNPR5* exhibited statistically significant responses. Notably, *ClNPR2* and *ClNPR4* upregulated the expression of the *NPR1* gene in the treated samples, whereas

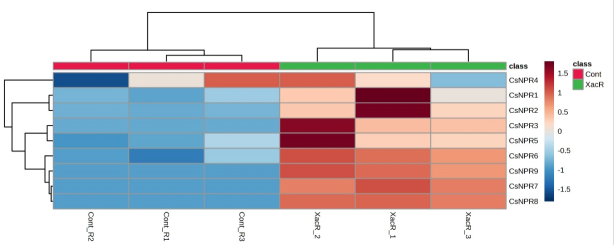

FIGURE 8
Relative expression of *NPR1* genes in *C. sinensis* infected and healthy plants.

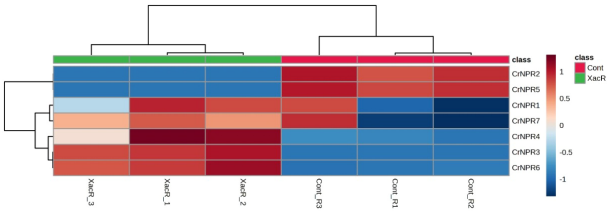

FIGURE 9
Relative expression of *NPR1* genes in *C. reticulata* infected and healthy plants.

ClNPR5 showed higher expression in the control samples compared to the treated ones (Figure 11).

4 Discussion

This study marks the inaugural genome-wide exploration of *NPR1*-like gene families and their corresponding expression patterns in reaction *to Xanthomonas axonopodis* pv. *citri* infection within four distinct citrus species (Cao et al., 1997; Spoel et al., 2003; Li et al., 2018; Peng et al., 2021).

NPR1 (Non-expressor of pathogenesis related genes 1) serves as the authentic receptor for salicylic acid, playing a crucial role in plant immunity (Cao et al., 1997; Spoel et al., 2003; Li et al., 2018; Peng et al., 2021). *NPR1* plays a pivotal role in the signaling pathway of salicylic acid and systemic acquired resistance (SAR) in plants. Additionally, other members of the *NPR1* gene family are associated with various reactions to both biotic and abiotic stresses (Cao et al., 1997; Peng et al., 2021). The basic significance of studies on *NPR1* is due to its extensive role in plant defense (Cao et al., 1997; Peng et al., 2021). It is generally postulated that salicylic acid-based defense shields plants against host- or semi-host-dependent pathogens, while jasmonic acid-based defense protects against necrotrophic pathogens (Wally et al., 2009). This study represents the first comprehensive examination of the *NPR1*-like gene family in various citrus species, identifying a total of 63 *NPR1*-like genes across 10 citrus species (Irfan et al., 2023).

The phylogenetic tree illustrates three distinct clades of *NPR* genes, with members within the same clade grouping together based on their presumed similar functions. Gene structure predictions using intron–exon displays and motif analysis revealed that most *NPR1* sequences lacked introns, although some had between 1 and 7. In motif analysis, it was observed that motifs 8, 2, 7, 9, 5, 1, 4, 3,

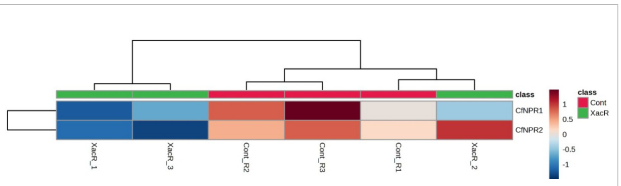

FIGURE 10
Relative expression of *NPR1* genes in *C. fortunella* infected and healthy plants.

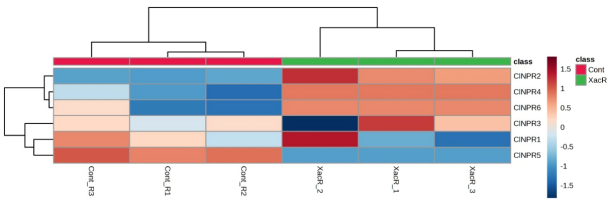

FIGURE 11
Relative expression of *NPR1* genes in *C. limon*-infected and healthy plants.

and 10 were commonly found in the majority of sequences. Nevertheless, variations, including the presence or absence of specific motifs, were evident, even among sequences within the same clade. These variations suggest that the *NPR1* gene has undergone structural mutations, including insertions and deletions, over time. The orthologous relationships inferred from gene mapping and syntenic analysis support the notion of a shared evolutionary history among NPR sequences. For *NPR1* to upregulate plant resistance genes, it must localize in the nucleus (Kinkema et al., 2000). Changes in redox potentials influence its nuclear-cytoplasmic localization (Bassene et al., 2011). Typically, *NPR1* exists as a cytoplasmic oligomer under normal conditions. However, upon detecting pathogen infection and salicylic acid accumulation, which alters cellular redox potential, *NPR1* translocates to the nucleus as an active monomer, where it interacts with bZIP transcription factors from the TGA family (Després et al., 2000). The results of subcellular localization confirm that *NPR1* is primarily located in both the cytoplasm and the nucleus, thereby substantiating its involvement in conferring resistance among various citrus species (Spoel et al., 2003; Wally et al., 2009; Després et al., 2000).

Examining selective pressure unveils the benefits of particular amino acid sequence modifications within proteins, offering insights into functional residues and alterations in protein function. The analysis of synteny and chromosomal mapping of *NPR1*-like genes reveals evidence of tandem and segmental duplications, along with the identification of orthologous relationships among different citrus species. This information provides valuable insights into gene duplications, rearrangements, and the evolutionary history of these species. *C. sinensis* and *C. reticulata* share a common ancestor, supported by the presence of various orthologs on chromosome 7 of *C. sinensis* and scaffold 86 of *C. reticulata*. A duplication event occurred in scaffold 86 of *C. reticulata* and chromosome 9 of *C. maxima*, *A. buxifolia*, and *A. thaliana* diverged from a common ancestor, sharing an ortholog.

Analyzing gene expression patterns of *NPR1*-like genes using existing data reveals variations in their expression levels under different stresses (biotic and abiotic).The expression of *CsNPR1* exhibits a remarkable consistency and stability across diverse conditions, reflecting its pivotal role in *C.sinensis* development and stress response. In developmental phases, *CsNPR1* maintains a steady presence, suggesting its regulatory involvement throughout these processes. Its resilience to varying low pH conditions, tested over different time intervals, underscores its robust nature in withstanding acidic stress. Notably, *CsNPR1* expression remains unaffected, implying a key role in mitigating the impact of low pH stress on biological processes. Furthermore, in the regulation of cuticle formation, *CsNPR1* demonstrates reliability with no significant fluctuations in expression levels across distinct developmental stages. Collectively, these findings emphasize the versatility and importance of *CsNPR1*, positioning it as a central player in orchestrating developmental events, responding to environmental stressors, and regulating key processes like cuticle formation in *C. sinensis*. A joint transcriptome analysis was conducted to indicate changes in gene expression of *CmNPR1* and *CmNPR5* during flavonoid biosynthesis, although the differences were not significant (Chen et al., 2022). When *C. sinensis* is subjected to acidic stress for a long time, the expression of *CsNPR1* modulates in the leaves, although this variation is minimal. Similar variations in *CsNPR1* expression were detected during cuticle development in Newhall navel orange fruits (Liu et al., 2022). In *C. sinensis*, all *NPR1*-like genes exhibited upregulated expression in response to Xac infection compared to the control. *CsNPR3*, *CsNPR7*, *CsNPR8*, and *CsNPR9* lacked significant expression in the control group. Except for *CrNPR2* and *CrNPR5*, which exhibited no significant expression in Xac-infected samples, all *NPR1*-like genes in *C. reticulata* showed higher expression. Conversely, *NPR1*-like genes in *C. fortunella* exhibited downregulated expression in response to Xac treatment compared to control samples, while in *C. limon*, *NPR1*-like genes were downregulated except for *ClNPR4* and *ClNPR6*.

Citrus bacterial canker (*Xanthomonas axonopodis* pv. *citri*) stress was studied in terms of *NPR1*-like genes and their associated expression. Citrus species were picked based on their reported resistance to citrus bacterial canker. Two resilient species, *C. sinensis* and *C. limon*, and two vulnerable species, *C. sinensis* and *C. limon*, were picked for a complete comparative study. *C. sinensis* and *C. limon* are vulnerable to citrus bacterial canker, although *C. reticulata* and *C. fortunella* are resistant (Licciardello et al., 2022). The first identified and characterized citrus bacterial canker through cultural, biochemical, and molecular analysis, confirming the presence of *Xanthomonas axonopodis* pv. *citri*, a Gram-negative bacterium (Chaudhari et al., 2022). PCR results using *Xanthomonas axonopodis* pv. *citri*-specific primers XACF (5′-CGTCGCAATACGATTGGAAC-3′) and reverse primer XACR (5′–CGGAGGCATTGTCGAAGGAA-3′) yielded a 581-bp product.

Previous investigations into *NPR1*-like gene families in model organism *A. thaliana* had already established the importance of these families of genes in enhancing tolerance to both biotic and abiotic stress factors (Cao et al., 1997; Després et al., 2000; Kinkema et al., 2000; Spoel et al., 2003; Wally et al., 2009; Peng et al., 2021). This current study unveils alterations in the expression analysis of *NPR1*-like genes in response to an attack by Xac bacteria, with varying responses observed across different citrus species. Notably, in *C. limon* and *C. sinensis*, there was an upregulation in the expression of *NPR1*-like genes. Conversely, in *C. fortunella*, a lower expression of *NPR1*-like genes was observed under Xac attack, rendering it more resistant to the pathogen. *C. reticulata* exhibited varying *NPR1*-like gene expression, indicating a moderate level of resistance to Xac attack. These findings were further

corroborated by physiological and biochemical analyses in *C. limon*, which showed decreased levels of chlorophyll a and b, alongside an increase in flavonoid and carotenoid compounds, known for their roles in defense mechanisms against biotic stress. However, the production of secondary metabolites like phenols and soluble proteins was suppressed. Additionally, the activity of vital enzymes, such as catalase and peroxidase, was found to decrease, subsequently impeding the plant's growth and development. This groundbreaking research addresses a critical gap by conducting the inaugural analysis of the correlation between *NPR1*-associated genes and diverse physiological plant parameters in both citrus cultivars susceptible and resistant to citrus bacterial canker. The findings offer potential implications for the development of disease-resistant citrus varieties through employing multiple breeding techniques, including double haploid technology, hybridization, tissue culture, and backcrossing.

5 Conclusion

In conclusion, the comprehensive genome-wide analysis of *NPR1*-like gene families across diverse citrus species provides compelling evidence of their pivotal role in citrus plants resistance mechanisms against biotic stress factors. This exploration not only enhances our understanding of the evolutionary relationships within these gene families but also offers promising avenues for addressing challenges in citrus production and elevating fruit quality. Our hypothesis proposes the targeted modification of the *NPR1* gene through CRISPR Cas9 technology, with the potential to yield a resilient *C. limon* variant resistant to Xac infection. Moreover, a thorough investigation into the roles played by SA and *NPR1* during biotic stress emerges as a promising direction for future research. By integrating modern natural breeding techniques—such as double haploids, hybridization, tissue culture, and backcrossing—we aim to fortify susceptibility-prone varieties, bolstering their resilience against both biotic and abiotic stresses. In this way, our holistic approach not only advances citrus resilience but also contributes to a broader understanding of plant resistance mechanisms, marking a significant step forward in the pursuit of sustainable and robust citrus cultivation.

Data availability statement

The datasets presented in this study can be found in online repositories. The names of the repository/repositories and accession number(s) can be found in the article/supplementary material.

Author contributions

MA: Conceptualization, Methodology, Writing – original draft. MS: Conceptualization, Data curation, Writing – review & editing. MZH: Conceptualization, Data curation, Visualization, Writing – review & editing. AS: Formal analysis, Investigation, Methodology, Writing – review & editing. PA: Project administration, Validation, Writing – review & editing. TA: Funding acquisition, Supervision, Validation, Writing – review & editing. ZK: Conceptualization, Formal analysis, Resources, Writing – review & editing. SS: Conceptualization, Data curation, Software, Writing – review & editing. MH: Investigation, Methodology, Writing – review & editing. MAS: Funding acquisition, Supervision, Visualization, Writing – review & editing. MJ: Funding acquisition, Visualization, Writing – review & editing. GA: Formal analysis, Funding acquisition, Investigation, Visualization, Writing – review & editing. MM: Data curation, Investigation, Methodology, Writing – review & editing. IS: Funding acquisition, Validation, Writing – review & editing.

Funding

The author(s) declare financial support was received for the research, authorship, and/or publication of this article. The authors extend their appreciation to the Deanship of Scientific Research at King Khalid University, Saudi Arabia for funding this work through Large Groups Project under Grant Number (RGP.2/176/44).

Acknowledgments

The authors extend their appreciation to the Deanship of Scientific Research at King Khalid University, Saudi Arabia for funding this work through Large Groups Project under Grant Number (RGP.2/176/44). The authors express their gratitude to Khalid Ali Khan, for his unwavering support and encouragement throughout the study.

Conflict of interest

The authors declare that the research was conducted in the absence of any commercial or financial relationships that could be construed as a potential conflict of interest.

Publisher's note

References

Ahmad, B., Mahmood, A., Sami, A., and Haider, M. Z. (2023). Impact of climate change on fruits and crops production in south punjab: farmer's perspective. *Biol. Agric. Sci. Res. J.* 2023, 22. doi: 10.54112/basrj.v2023i1.22

Almas, M. H., Sami, A., Shafiq, M., Bhatti, M. H. T., Haider, M. Z., Hashmi, M., et al. (2023). Sale price comparison of saggian flower market: a case study. *Bull. Biol. Allied Sci. Res.* 2023, 39. doi: 10.54112/bbasr.v2023i1.39

Arabbeigi, M., Arzani, A., Majidi, M. M., Sayed-Tabatabaei, B. E., and Saha, P. (2018). Expression pattern of salt tolerance-related genes in Aegilops cylindrica. *Physiol. Mol. Biol. Plants* 24, 61–73. doi: 10.1007/s12298-017-0483-2

Bassene, J.-B., Froelicher, Y., Navarro, L., Ollitrault, P., and Ancillo, G. (2011). Influence of mitochondria on gene expression in a citrus cybrid. *Plant Cell Rep.* 30, 1077–1085. doi: 10.1007/s00299-011-1014-1

Birkenbihl, R. P., Liu, S., and Somssich, I. E. (2017). Transcriptional events defining plant immune responses. *Curr. Opin. Plant Biol.* 38, 1–9. doi: 10.1016/j.pbi.2017.04.004

Biswas, S., and Akey, J. M. (2006). Genomic insights into positive selection. *Trends Genet.* 22, 437–446. doi: 10.1016/j.tig.2006.06.005

Campos, P. E., Pruvost, O., Boyer, K., Chiroleu, F., Cao, T. T., Gaudeul, M., et al. (2023). Herbarium specimen sequencing allows precise dating of Xanthomonas citri pv. citri diversification history. *Nat. Commun.* 14, 4306. doi: 10.1038/s41467-023-39950-z

Cao, H., Glazebrook, J., Clarke, J. D., Volko, S., and Dong, X. (1997). The Arabidopsis NPR1 gene that controls systemic acquired resistance encodes a novel protein containing ankyrin repeats. *Cell* 88, 57–63. doi: 10.1016/S0092-8674(00)81858-9

Chaudhari, K., Kolase, S., Shete, M., Chandanshive, A., and Patil, M. (2022). Cultural and bio-chemical characterization of bacterial canker disease caused by Xanthomonas axonopodis pv. *Citri Acid lime*. doi: 10.22271/tpi

Chen, J., Shi, Y., Zhong, Y., Sun, Z., Niu, J., Wang, Y., et al. (2022). Transcriptome Analysis and HPLC Profiling of Flavonoid Biosynthesis in Citrus aurantium L. during Its Key Developmental Stages. *Biology* 11, 1078. doi: 10.3390/biology11071078

da Silva, E. S., Huber, S., Alcantara-Neves, N. M., Asam, C., Silveira, E. F., de Andrade Belitardo, E. M. M., et al. (2020). N-terminal peptide deletion influences immunological and structural features of Blo t 5. *Allergy* 75, 1503–1507. doi: 10.1111/all.14176

Després, C., DeLong, C., Glaze, S., Liu, E., and Fobert, P. R. (2000). The Arabidopsis NPR1/NIM1 protein enhances the DNA binding activity of a subgroup of the TGA family of bZIP transcription factors. *Plant Cell* 12, 279–290. doi: 10.1105/tpc.12.2.279

Duan, Y., Zhou, L., Hall, D. G., Li, W., Doddapaneni, H., Lin, H., et al. (2009). Complete genome sequence of citrus huanglongbing bacterium,'Candidatus Liberibacter asiaticus' obtained through metagenomics. *Mol. Plant-Microbe Interact.* 22, 1011–1020. doi: 10.1094/MPMI-22-8-1011

Durango, D., Pulgarin, N., Echeverri, F., Escobar, G., and Quiñones, W. (2013). Effect of salicylic acid and structurally related compounds in the accumulation of phytoalexins in cotyledons of common bean (Phaseolus vulgaris L.) cultivars. *Molecules* 18, 10609–10628. doi: 10.3390/molecules180910609

Fu, Z. Q., and Dong, X. (2013). Systemic acquired resistance: turning local infection into global defense. *Annu. Rev. Plant Biol.* 64, 839–863. doi: 10.1146/annurev-arplant-042811-105606

Fujino, T., Suzuki, T., Okada, K., Kogashi, K., Yasumoto, K.-I., Sogawa, K., et al. (2016). Chimeric RNA oligonucleotides incorporating triazole-linked trinucleotides: synthesis and function as mRNA in cell-free translation reactions. *J. Organic Chem.* 81, 8967–8976. doi: 10.1021/acs.joc.6b01618

Graham, J. H., Gottwald, T. R., Cubero, J., and Achor, D. S. (2004). Xanthomonas axonopodis pv. citri: factors affecting successful eradication of citrus canker. *Mol. Plant Pathol.* 5, 1–15. doi: 10.1046/j.1364-3703.2004.00197.x

Grechkin, M., Poon, H., and Howe, B. (2017). Wide-Open: Accelerating public data release by automating detection of overdue datasets. *PLOS Biol.* 15. doi: 10.1371/journal.pbio.2002477

Guo, A.-Y., Zhu, Q.-H., Chen, X., and Luo, J.-C. (2007). GSDS: a gene structure display server. *Yi chuan= Hereditas* 29, 1023–1026. doi: 10.1360/yc-007-1023

Haider, M. Z., Sami, A., Mazhar, H., Akram, J., Nisa, B. U., Umar, M., et al. (2023a). Exploring morphological traits variation in gomphrena globosa: a multivariate analysis. *Biol. Agric. Sci. Res. J.* 2023, 21. doi: 10.54112/basrj.v2023i1.21

Haider, M. Z., Sami, A., Shafiq, M., Anwar, W., Ali, S., Ali, Q., et al. (2023b). Genome-wide identification and in-silico expression analysis of carotenoid cleavage oxygenases gene family in Oryza sativa (rice) in response to abiotic stress. *Front. Plant Sci.* 14. doi: 10.3389/fpls.2023.1269995

Horton, P., Park, K.-J., Obayashi, T., and Nakai, K. (2006). "Protein subcellular localization prediction with WoLF PSORT," in *Proceedings of the Proceedings of the 4th Asia-Pacific bioinformatics conference*. 3:39–48.

Hussain, Z., Muzamil, M., Saeed, M. R., Naheed, K., Kareem, M., Munir, A., et al. (2023). Trait correlations and implications for yield potential in cotton: a comprehensive study. *Biol. Agric. Sci. Res. J.* 2023, 24. doi: 10.54112/basrj.v2023i1.24

Irfan, U., Haider, M., Shafiq, M., Sami, A., and Ali, Q. (2023). Genome editing for early and late flowering in plants. *Bull. Biol. Allied Sci. Res.* 2023, 45–45. doi: 10.54112/bbasr.v2023i1.45

Islam, M. A. U., Nupur, J. A., Shafiq, M., Ali, Q., Sami, A., and Shahid, M. A. (2023). In silico and computational analysis of zinc finger motif-associated homeodomain (ZF-HD) family genes in chilli (Capsicum annuum L). *BMC Genomics* 24, 603. doi: 10.1186/s12864-023-09682-x

Khan, F., Shafiq, M., Haider, M. Z., Sami, A., Arshad, A., and Anees, M. M. (2023). Impact of various concentrations of nacl on morphological attributes of different citrus rootstocks under field conditions. *Bull. Biol. Allied Sci. Res.* 2023, 50. doi: 10.54112/bbasr.v2023i1.50

Kinkema, M., Fan, W., and Dong, X. (2000). Nuclear localization of NPR1 is required for activation of PR gene expression. *Plant Cell* 12, 2339–2350. doi: 10.1105/tpc.12.12.2339

Kushalappa, A. C., Yogendra, K. N., and Karre, S. (2016). Plant innate immune response: qualitative and quantitative resistance. *Crit. Rev. Plant Sci.* 35, 38–55. doi: 10.1080/07352689.2016.1148980

Letunic, I., Copley, R. R., Pils, B., Pinkert, S., Schultz, J., and Bork, P. (2006). SMART 5: domains in the context of genomes and networks. *Nucleic Acids Res.* doi: 10.1093/nar/gkj079

Li, M., Chen, H., Chen, J., Chang, M., Palmer, I. A., Gassmann, W., et al. (2018). TCP transcription factors interact with NPR1 and contribute redundantly to systemic acquired resistance. *Front. Plant Sci.* 9, 1153. doi: 10.3389/fpls.2018.01153

Licciardello, G., Caruso, P., Bella, P., Boyer, C., Smith, M. W., Pruvost, O., et al. (2022). Pathotyping citrus ornamental relatives with Xanthomonas citri pv. citri and X. citri pv. aurantifolii refines our understanding of their susceptibility to these pathogens. *Microorganisms* 10, 986.

Liu, D., Guo, W., Guo, X., Yang, L., Hu, W., Kuang, L., et al. (2022). Ectopic overexpression of CsECR from navel orange increases cuticular wax accumulation in tomato and enhances its tolerance to drought stress. *Front. Plant Sci.* 13, 924552. doi: 10.3389/fpls.2022.924552

Malamud, F., Torres, P. S., Roeschlin, R., Rigano, L. A., Enrique, R., Bonomi, H. R., et al. (2011). The Xanthomonas axonopodis pv. citri flagellum is required for mature biofilm and canker development. *Microbiology* 157, 819–829. doi: 10.1099/mic.0.044255-0

Malik, A. U., Hasan, M. U., Khalid, S., Mazhar, M. S., Shafique, M., Khalid, M. N. K., et al. (2021). Biotic and abiotic factors causing rind blemishes in citrus and management strategies to improve the cosmetic quality of fruits. *Int. J. Agric. Biol.* 25, 298–318. doi: 10.17957/IJAB

Manzoor, M., Hamza, A., Javaid, A., Anees, M., Tariq, M. R., Firdosi, M. F. H., et al. (2023). Bioefficacy of Some Botanical Extracts against Brinjal Fruit and Shoot Borer [Leucinodes orbonalis (Guenee); Lepidoptera, Pyrallidae. *Plant Prot.* 7, 263–272. doi: 10.33804/pp.007.02.4728

Marchler-Bauer, A., Zheng, C., Chitsaz, F., Derbyshire, M. K., Geer, L. Y., Geer, R. C., et al. (2013). CDD: conserved domains and protein three-dimensional structure. *Nucleic Acids Res.* 41, D348–D352. doi: 10.1093/nar/gks1243

Meyers, B. C., Kozik, A., Griego, A., Kuang, H., and Michelmore, R. W. (2003). Genome-wide analysis of NBS-LRR–encoding genes in Arabidopsis. *Plant Cell* 15, 809–834. doi: 10.1105/tpc.009308

Nakasu, E. Y., Hedil, M., Nagata, T., Michereff-Filho, M., Lucena, V. S., and Inoue-Nagata, A. K. (2019). Complete genome sequence and phylogenetic analysis of a novel dicistrovirus associated with the whitefly Bemisia tabaci. *Virus Res.* 260, 49–52. doi: 10.1016/j.virusres.2018.11.008

Parmley, J. L., and Hurst, L. D. (2007). How common are intragene windows with KA> KS owing to purifying selection on synonymous mutations? *J. Mol. Evol.* 64, 646–655. doi: 10.1007/s00239-006-0207-7

Peng, A., Zou, X., He, Y., Chen, S., Liu, X., Zhang, J., et al. (2021). Overexpressing a NPR1-like gene from Citrus paradisi enhanced Huanglongbing resistance in C. sinensis. *Plant Cell Rep.* 40, 529–541. doi: 10.1007/s00299-020-02648-3

Russo, C., Maugeri, A., Lombardo, G. E., Musumeci, L., Barreca, D., Rapisarda, A., et al. (2021). The second life of Citrus fruit waste: A valuable source of bioactive compounds. *Molecules* 26, 5991. doi: 10.3390/molecules26195991

Sabir, H. M., Khan, M. B., and Hussain, Z. (2010). Marketing margin of mandarin: A case study of Sargodha region, Pakistan. *Pakistan J. Soc. Sci.* 30, 275–291.

Sami, A., Haider, M. Z., Imran, M., Abbas, A., and Javed, M. M. (2023a). Synergizing food safety, quality and genetic improvement: the intersection of food microbiology and processing. *Bull. Biol. Allied Sci. Res.* 2023, 44. doi: 10.54112/bbasr.v2023i1.44

Sami, A., Haider, M. Z., Iqbal, M., Bhatti, M. H. T., Ahmad, S., and Khalid, M. N. (2023b). Deterrence effect of colored diversion sheets on the population density of melon fruit flies bactrocera cucurbitae (coquillett) and yield parameters of bitter gourd (momordica charantia l.). *Biol. Agric. Sci. Res. J.* 2023, 17. doi: 10.54112/basrj.v2023i1.17

Sami, A., Haider, M. Z., Meeran, M. W., Ali, M. H., Abbas, A., Ali, Q., et al. (2023c). Exploring morphological traits variation in chenopodium murale: a comprehensive multivariate analysis. *Bull. Biol. Allied Sci. Res.* 2023, 43. doi: 10.54112/bbasr.v2023i1.43

Sami, A., Haider, M. Z., and Shafiq, M. (2024). "Microbial nanoenzymes: Features and applications," in *Fungal secondary metabolites* (Elsevier), 353–367. doi: 10.1016/B978-0-323-95241-5.00015-0

Sami, A., Haider, M. Z., Shafiq, M., Sadiq, S., and Ahmad, F. (2023d). Genome-wide identification and in-silico expression analysis of CCO gene family in sunflower (Helianthus annnus). *Plant Mol. Biol.* doi: 10.21203/rs.3.rs-3344879/v1

Sayers, E. W., Cavanaugh, M., Clark, K., Pruitt, K. D., Schoch, C. L., Sherry, S. T., et al. (2022). GenBank. *Nucleic Acids Res.* 50, D161–D164. doi: 10.1093/nar/gkab1135

Shafiq, M., Manzoor, M., Bilal, M., Manzoor, T., Anees, M. M., Rizwan, M., et al. (2024). Genome-wide analysis of plant specific YABBY transcription factor gene family in watermelon (Citrullus lanatus) and arabidopsis. *J. Appl. Res. Plant Sci.* 5, 63–78.

Shahbaz, E., Ali, M., Shafiq, M., Atiq, M., Hussain, M., Balal, R. M., et al. (2022). Citrus canker pathogen, its mechanism of infection, eradication, and impacts. *Plants* 12, 123. doi: 10.3390/plants12010123

Shahbaz, E., Ali, M., Shafiq, M., Atiq, M., Hussain, M., Balal, R. M., et al. (2023). Citrus canker pathogen, its mechanism of infection, eradication, and impacts. *Plants* 12, 123.

Spoel, S. H., Koornneef, A., Claessens, S. M., Korzelius, J. P., Van Pelt, J. A., Mueller, M. J., et al. (2003). NPR1 modulates cross-talk between salicylate-and jasmonate-dependent defense pathways through a novel function in the cytosol. *Plant Cell* 15, 760–770. doi: 10.1105/tpc.009159

Spreen, T. H., Zansler, M. L., and Muraro, R. P. (2003). "The costs and value loss associated with Florida citrus groves exposed to citrus canker," in *Proceedings of the Proceedings of the Florida State horticultural society*, vol. pp. , 289–294.

Wally, O., Jayaraj, J., and Punja, Z. K. (2009). Broad-spectrum disease resistance to necrotrophic and biotrophic pathogens in transgenic carrots (Daucus carota L.) expressing an Arabidopsis NPR1 gene. *Planta* 231, 131–141. doi: 10.1007/s00425-009-1031-2

Xu, S., Yao, S., Huang, R., Tan, Y., and Huang, D. (2020). Transcriptome-wide analysis of the AP2/ERF transcription factor gene family involved in the regulation of gypenoside biosynthesis in Gynostemma pentaphyllum. *Plant Physiol. Biochem.* 154, 238–247. doi: 10.1016/j.plaphy.2020.05.040

Zhang, J., Chen, X.-F., Huang, W.-T., Chen, H.-H., Lai, N.-W., Yang, L.-T., et al. (2022). Mechanisms for increased pH-mediated amelioration of copper toxicity in Citrus sinensis leaves using physiology, transcriptomics and metabolomics. *Environ. Exp. Bot.* 196, 104812. doi: 10.1016/j.envexpbot.2022.104812

Zhao, C., Wang, F., Lian, Y., Xiao, H., and Zheng, J. (2020). Biosynthesis of citrus flavonoids and their health effects. *Crit. Rev. Food Sci. Nutr.* 60, 566–583. doi: 10.1080/10408398.2018.1544885

frontiers | Frontiers in Plant Science

TYPE Original Research
PUBLISHED 27 March 2024
DOI 10.3389/fpls.2024.1384246

OPEN ACCESS

EDITED BY
Dayong Cui,
Qilu Normal University, China

REVIEWED BY
Babatope Samuel Ajayo,
Sichuan Agricultural University, China
Chuanzhi Zhao,
Shandong Academy of Agricultural Sciences, China

*CORRESPONDENCE
Chun-Ming Liu
cmliu@ibcas.ac.cn

RECEIVED 09 February 2024
ACCEPTED 15 March 2024
PUBLISHED 27 March 2024

CITATION
Liu L, Ma Y, Zhao H, Guo L, Guo Y and Liu C-M (2024) Genome-wide association studies identified *OsTMF* as a gene regulating rice seed germination under salt stress. *Front. Plant Sci.* 15:1384246. doi: 10.3389/fpls.2024.1384246

Genome-wide association studies identified *OsTMF* as a gene regulating rice seed germination under salt stress

Lifeng Liu[1,2], Yanling Ma[1], Heng Zhao[1], Lin Guo[1], Yan Guo[2] and Chun-Ming Liu[1,3,4,5]*

[1]Institute of Crop Sciences, Chinese Academy of Agricultural Sciences, Beijing, China, [2]State Key Laboratory of Plant Environmental Resilience, College of Biological Sciences, China Agricultural University, Beijing, China, [3]Key Laboratory of Plant Molecular Physiology, Institute of Botany, Chinese Academy of Sciences, Beijing, China, [4]College of Life Sciences, University of Chinese Academy of Sciences, Beijing, China, [5]School of Advanced Agricultural Sciences, Peking University, Beijing, China

Introduction: Salt tolerance during seed germination is an important trait for direct seeding and low-cost rice production. Nevertheless, it is still not clear how seed germination under salt stress is regulated genetically.

Methods: In this study, genome-wide association studies (GWAS) were performed to decipher the genetic basis of seed germination under salt stress using 541 rice varieties collected worldwide.

Results and discussion: Three quantitative trait loci (QTLs) were identified including *qGRG3-1* on chromosome 3, *qGRG3-2* on chromosome 5, and *qGRG4* on chromosome 4. Assessment of candidate genes in these loci for their responses to salt stress identified a TATA modulatory factor (*OsTMF*) in *qGRG3-2*. The expression of *OsTMF* was up-regulated in both roots and shoots after exposure to salt stress, and *OsTMF* knockout mutants exhibited delayed seed germination under salt stress. Haplotype analysis showed that rice varieties carrying *OsTMF-Hap2* displayed elevated salt tolerance during seed germination. These results provide important knowledge and resources to improve rice seed germination under salt stress in the future.

KEYWORDS

rice, seed germination, salt stress, GWAS, *OsTMF*

1 Introduction

Salinity is a major abiotic stress threatening global food production. High salt concentrations in soil cause osmotic stress, ionic toxicity and nutrient deficiency, and hamper plant growth and crop productivity (Hu et al., 2012; Yang and Guo, 2018). For rice production, about 30% agricultural land in the world suffers from high salinity,

representing nearly ten thousand hectares in China alone (Takehisa et al., 2004; He and Luo, 2021).

Efforts have been made in the past decades to decipher the mechanisms underlying salt sensitivity in rice through genetic studies. These studies allowed us to identify multiple quantitative trait loci (QTLs) for salt tolerance, although only few genes have been cloned and functionally characterized. *Shoot K^+ Concentration 1* (*SKC1*) was identified from a F_2 population generated by crossing the salt-tolerant (ST) *indica* variety 'Nona Bokra' with the salt-sensitive (SS) *japonica* variety 'Koshihikari'. *SKC1* encodes a high-affinity K^+ transporter that maintains K^+/Na^+ equilibrium under salt stress (Lin et al., 2004; Ren et al., 2005). A zinc-finger transcription factor, Drought and Salt Tolerance (DST), regulates salt and drought responses by modulating reactive oxygen species (ROS) homeostasis and stomatal movements (Huang et al., 2009). *Hitomebore Salt Tolerant 1* (*HST1*) was identified as a negative regulator of salt tolerance, and the introduction of a non-functional *hst1* allele to a cultivated variety through backcrosses resulted in improved salt tolerance (Takagi et al., 2015).

With the tremendous progresses made in whole-genome sequencing, genome-wide association studies (GWAS) become a powerful tool to elucidate molecular machinery underlying traits regulated by multiple genes, such as salt tolerance (Wang et al., 2005). In *Arabidopsis*, GWAS was employed to identify genetic components regulating root architecture under salt stress, yielding *Cytochrome P450 family 79 subfamily B2* (*CYP79B2*) as a positive regulator, and *High-Affinity K^+ Transporter 1* (*HKT1*) as a negative regulator (Julkowska et al., 2017). Zhang et al. (2019) identified *ZmHAK4* that encodes a Na^+ transporter as a Na^+ level regulator in maize. In wheat, a QTL in a 1.5 Mb genomic region on chromosome 7B was identified, in which three putative K^+ transporters (*TaHKT8-B*, *TaHKT9-B* and *TaHKT10-B*) were located. Lines overexpressing *TaHKT9-B* and varieties carrying the In-1077 haplotype of *TaHKT9-B* displayed higher salt sensitivity due to lower K^+ accumulation in shoots (Du et al., 2024). Recently, two genes were identified *via* GWAS, a transcription factor OsWRKY53 that regulates water contents in shoots, and a mitogen-activated protein kinase kinase 10.2 (OsMKK10.2) that is implicated in seedling survival under salt stress (Yu et al., 2023).

Seed germination is a critical developmental stage for plants to start a new phase of life. Under salt stress, seed germination in most crop species is compromised, manifested primarily by lower germination rates and longer germination time (Shi et al., 2017; Hasseb et al., 2022; Yang et al., 2023). Increased osmotic pressures induced by salt stress may affect water absorption, starch mobilization and catabolism of storage products during seed germination (Xu et al., 2017; Yan et al., 2022; Xiong et al., 2024). Enzymatic and antioxidant activities, hormone levels and ion homeostasis are also affected by salt stress, which may consequently impact both seed germination and seedling establishment (Munns and Tester, 2008; Yang and Guo, 2018; He et al., 2019).

In recent years, direct seeding is increasingly used in many rice-growing areas because of lower labor input, which demands uniform seed germination and high seedling vigor, especially under stress conditions (Farooq et al., 2011). A QTL for seed germination and seedling establishment under salt stress, *Seedling Establishment 3* (*qSE3*), was identified using substitution lines generated by introgressions of chromosomal segments from a *japonica* variety 'Jiucaiqing' (with low seedling establishment under salt stress) into an *indica* variety 'IR26' (with high seedling establishment under salt stress). High-resolution mapping revealed that *High-Affinity K^+ Transporter 21* (*OsHAK21*) is likely to be the candidate gene in *qSE3*, which confers higher salt tolerance by decreasing ROS levels in abscisic acid (ABA)-dependent manner (He et al., 2019). Beyond this, very little is known about the genetic machinery underlying rice seed germination under salt stress.

The aim of this study is to characterize the genetic basis of rice seed germination under salt stress conditions, with the long-term goal to improve seed germination for direct seeding in saline land. We conducted GWAS to dissect the process using a panel of 541 rice varieties collected from different regions of the world. Three QTLs, *qGRG3-1* on chromosome 3, *qGRG3-2* on chromosome 5 and *qGRG4* on chromosome 4, were detected under treatments of two concentrations of NaCl. *OsTMF* was showed to be the candidate gene in *qGRG3-2* as its expression was highly responsive to salt stress, and *ostmf* mutants exhibited delayed seed germination under salt stress.

2 Materials and methods

2.1 Plant materials

A total of 541 accessions of rice (*Oryza sativa* L.) from major rice-growing areas worldwide, consisting of 328 *indica*, 162 *japonica*, 18 *admix*, 17 *aus*, and 16 *basmati* varieties (Supplementary Table S1), were obtained from the China Rice Data Center and the 3,010 Rice Genomes Project (Wang et al., 2018). All varieties were planted, and seeds were harvested in Lingshui, Hainan Province, China. A single nucleotide polymorphism (SNP) dataset was downloaded from the Rice SNP-Seek database (https://snpseek.irri.org/) (Mansueto et al., 2016). Non-sequenced varieties were sequenced on an Illumina HiSeq 2000 Sequencing Platform (Illumina Inc., San Diego, CA, USA), with an average sequencing depth of approximately 10×.

2.2 Evaluations of seed germination under salt stress

Fully mature seeds were harvested in field right after the grains turned to yellow, and dried in a 37°C oven for 7 days to break dormancy. Fifty rice varieties (Supplementary Table S2) were randomly chosen for germination test to determine the optimal salt stress conditions using 0.3%, 0.4%, 0.5%, 0.6%, 0.7%, 0.8%, 0.9% and 1.0% NaCl (w/v) dissolved in deionized water. Accordingly, the concentrations of 0.3% and 0.5% were subsequently used for GWAS. For each variety, 90 seeds were divided into three replicates and placed onto two layers of filter paper soaked with either 8 mL of deionized water, or 0.3% or 0.5% NaCl solutions, in 6-cm petri dishes without seal. All solutions were refreshed every

two days. These dishes were cultured in an incubator at 28°C under a 12 h light/12 h dark photoperiod for 7 days. Germinated seeds, with the criterion of root lengths longer than the seed length, and shoot lengths longer than half of the seed length (Shi et al., 2017), were counted to calculate their germination rates on the 3rd day (GR3), germination rates on the 4th day (GR4), and germination indexes in 7 days (GI), with the calculation formula of GR3 = accumulated number of germinated seeds on the 3rd day/the total number of seeds used × 100%; GR4 = accumulated number of germinated seeds on the 4th day/the total number of seeds used × 100%; GI = $\sum(G_t/T_t)$, where G_t is the number of germinated seeds on day t and T_t is the time in days corresponding to G_t (Shi et al., 2017). To obtain germination rate grades on the 3rd (GRG3) and the 4th day (GRG4), and germination index grades (GIG), the ratios of GR3, GR4 or GI for salt treatment to those in the control condition were calculated, and then assigned to germination grades from 1 to 11 (Supplementary Table S3). For seed germination in saline soil, pots with the size of 7 cm × 7 cm × 10 cm were filled with soil, and immersed in either deionized water or 0.5% NaCl solution for 24 hours to ensure saturation. Thirty seeds were sown into each pot and covered with a thin layer of soil. Subsequently, these pots were placed in an incubator at 28°C under 12 h light/12 h dark, watered with either deionized water or 0.5% NaCl solution in every two days. The germinated rates and shoot lengths were measured on the 10th day after sowing.

2.3 GWAS and haplotype analyses

The general linear model (GLM) with the first three principal components matrix calculated from genotypes was employed using Tassel 5.2.54 software (Bradbury et al., 2007) to perform GWAS for seed germination under salt stress. Across the whole panel of varieties, 302,900 high-quality SNPs were used for GWAS after removing SNPs with missing rates of more than 20% and minor allele frequencies of less than 5% (Ju et al., 2022; Mei et al., 2022). To identify significant SNPs, the Bonferroni correction method was used to calculate suggestive significance thresholds of associations, resulting in a p value of 1.65×10^{-7} (0.05/N, with N = number of SNPs) (Shi et al., 2017). The qqman package in R3.4.1 software was used to generate Manhattan plots (Turner, 2014). Functional annotations for genes within genomic regions of interest were obtained in reference to the Nipponbare genome IRGSP 1.0 (Kawahara et al., 2013). Haplotype analyses were performed using SNPs in the coding sequences, with each haplotype possessing at least twenty rice varieties (Mei et al., 2022).

2.4 qRT-PCR analyses

Candidate genes were investigated by quantitative real-time PCR (qRT-PCR) using RNA extracted from shoots and roots of 7-day-old Zhonghua11 (a *japonica* rice variety, ZH11) seedlings grown under 0.3% or 0.5% NaCl, or control (deionized water) conditions. To examine expression levels of candidate genes in varieties with different germination grades, shoots from 7-day-old seedlings of ST (L_363, L_417 and L_505, with GRG3 and GRG4 ≤ 2) and SS varieties (L_065, L_274 and L_352, with GRG3 and GRG4 ≥9) grown under 0.5% NaCl or control conditions were collected and analyzed by qRT-PCR. To examine expression patterns of *OsTMF* in time-course salt stress treatments, germinated seeds under 0.5% NaCl or control conditions for 1, 2, or 3 days, and seedlings grown in Hoagland solution treated with or without 0.5% NaCl for 1, 3, or 7 days, were sampled. Total RNA was extracted using TRIzol™ reagent (Thermo Fisher, USA), cDNA was synthesized using the PrimeScript™ RT reagent kit (Takara, Japan), and qRT-PCR was conducted using TB Green® Premix Ex Taq™ II (Takara, Japan) on LightCycler® 96 (Roche Life Science, Switzerland). Primers for qRT-PCR were designed using Primer3 (https://primer3.ut.ee) based on coding sequences of genes (Supplementary Table S4). *OsActin1* was used as an internal control for normalization, and the $2^{-\triangle\triangle CT}$ method was used to calculate relative expression levels.

2.5 Generations of knockout mutants using CRISPR/Cas9

Clustered regularly interspaced short palindromic repeat (CRISPR)/CRISPR-associated nuclease 9 (CRISPR/Cas9) constructs were made according to Cheng et al. (2021), using the guide sequences for candidate genes designed by the web tool CRISPR-GE (http://cbi.hzau.edu.cn/cgi-bin/CRISPR) (Xie et al., 2017; Supplementary Table S5), and transformed into ZH11 *via Agrobacterium*-mediated transformation (Nishimura et al., 2007). Sanger sequencing (Sangon Biotech, Beijing) was performed to identify homozygous mutants. PCR products amplified with *HPT*-F (5′-TGCCGTCAACCAAGCTCTGA-3′) and *HPT*-R (5′-GCTTCGATGTAGGAGGGCGT-3′) primers were used to select transgene-free lines.

2.6 Statistical analysis

Correlation analyses and significant differences were assessed between pairs of evaluated traits using SAS software (Shi et al., 2017). Differences between varieties, subpopulations, treatments, or haplotypes were examined using a one-way ANOVA method based on a significance level of 0.01. Figures were generated using GraphPad Prism 8.0 software (https://www.graphpad.com).

3 Results

3.1 Phenotypic variations of rice varieties for seed germination under salt stress

To define optimal conditions for assessing rice seed germination under salt stress, seeds of 50 varieties randomly selected from 541 varieties collected from different regions of the world (Supplementary Table S2) were germinated in either deionized water (control) or different concentrations of NaCl

solutions (see Materials and Methods). Well-germinated seeds, according to the criterion reported (Shi et al., 2017) were counted every day over a 7-day period. GRG3, GRG4 and GIG were calculated, with germination grade 1 for the highest, and grade 11 for the lowest salt tolerances (see Materials and Methods). Results showed that, under 0.3% and 0.5% NaCl treatments, all three traits were consistently distributed (Supplementary Figure S1), therefore, these two treatments were used for subsequently experiments.

To examine variations in seed germinations under salt stress in 541 rice varieties, seeds of these varieties were placed on plates with water, 0.3% or 0.5% NaCl, and germinations were counted daily over a 7-day period. Variations of seed germinations under salt stress were observed in different varieties (Supplementary Table S1). As showed for two representative varieties, L_541 with lower salt tolerance, and L_022 with higher salt tolerance in germination, numbers of germinated seeds differed on the 3rd and the 4th day, with more germinated seeds for the ST variety (Figure 1; above dash lines). All three traits, GRG3, GRG4 and GIG, showed large variations (Figure 2), with the highest coefficient of variation observed for GRG4 (73.53%) under 0.3% NaCl condition, followed by GRG4 under 0.5% NaCl (57.31%), and GRG3 under 0.3% NaCl (53.43%) (Table 1). Phenotypic variations in subpopulations were also examined, and results showed that, under treatments of either 0.3% or 0.5% NaCl, *indica* varieties displayed lower GRG3 (Supplementary Figure S2A) and GRG4 (Supplementary Figure S2B) when compared with other 4 subpopulations that showed no significant differences, suggesting a higher salt tolerance of *indica* varieties. To be noted, no significant difference was observed for GIG among these subpopulations (Supplementary Figure S2C). In addition, on average, GRG3 was higher than GRG4 under both 0.3% and 0.5% NaCl (Table 1), suggesting that the germination of rice seeds on the 3rd day was more vulnerable to salt stress than that on the 4th day. Further analyses revealed that GRG3 and GRG4 had moderately positive correlations at these two NaCl concentrations (Supplementary Table S6).

3.2 QTLs associated with seed germination under salt stress

To dissect the genetic basis of rice seed germination under salt stress, GWAS was conducted based on the GLM model using 302,900 SNPs from public database and in-house re-sequencing project. These SNPs were evenly distributed across all 12 chromosomes, with a density of about 800 SNPs/Mb (Supplementary Table S7). The significance threshold for GWAS was set to 6.78 ($-\log_{10}(0.05/N)$, N = effective SNP number) after Bonferroni correction. Manhattan plots were generated, showing that 1,494 SNPs were significantly correlated with rice seed germination under salt stress, in particular, GRG3 (Figure 3A; Supplementary Table S8) and GRG4 (Figure 3B; Supplementary Table S8). These SNPs explained 4.54% to 10.06% of phenotypic variations. No SNP association was identified for GIG (Figure 3C).

To identify putative genomic regions associated with salt tolerance, we screened for co-located and clustered SNPs detected under both 0.3% and 0.5% NaCl treatments. Three QTLs, *qGRG3-1* (chr.3; 16,666,490 – 17,013,993) and *qGRG3-2* (chr.5; 27,858,716 – 28,081,822) associated with GRG3 (Figure 3A), and *qGRG4* (chr.4; 19,891,019 – 20,069,206) associated with GRG4 (Figure 3B), were

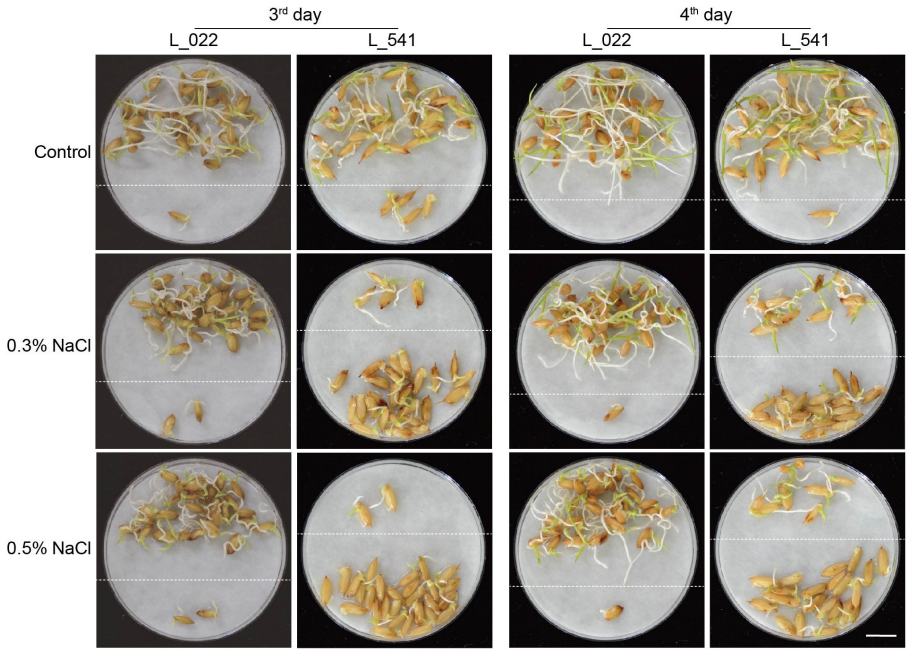

FIGURE 1
Differences in seed germination under salt stress in two representative rice varieties. Representative photos of rice seed germinations under salt stress, on the 3rd and 4th days for the salt-tolerant (ST) variety L_022 and the salt-sensitive (SS) variety L_541. Seeds were placed on filter paper soaked with deionized water (control), 0.3% or 0.5% NaCl for the indicated numbers of days. Germinated seeds, with root length longer than seed length and shoot length longer than half of the seed length, were repositioned above dashed lines. Scale bar, 1 cm.

10.3389/fpls.2024.1384246

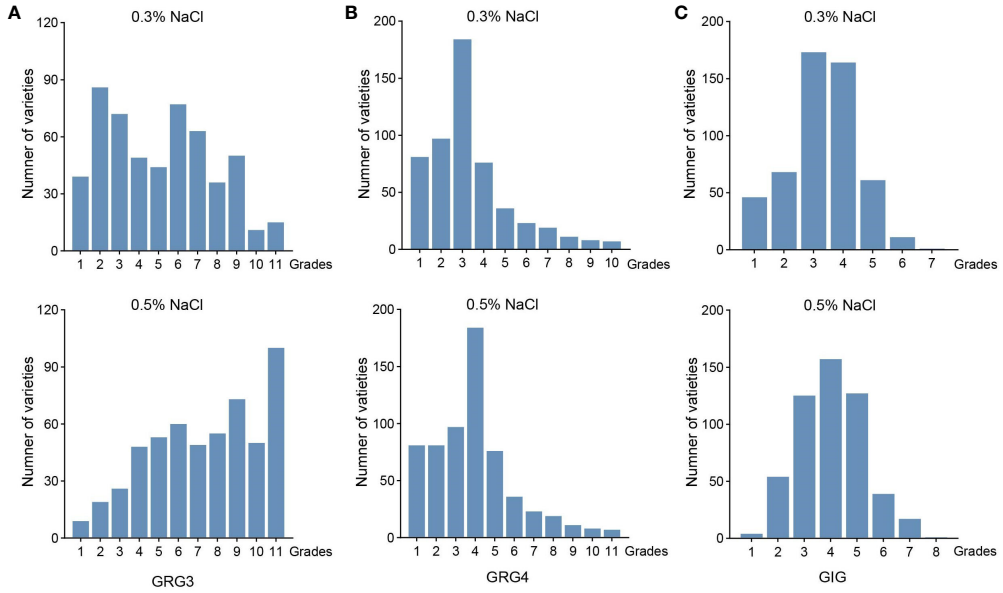

FIGURE 2
Phenotypic variations of 541 rice varieties in seed germinations under salt stress. **(A)** Germination rate grades on the 3rd day (GRG3) under the 0.3% (top) and 0.5% NaCl treatments (bottom). **(B)** Germination rate grades on the 4th day (GRG4) under the 0.3% (top) and 0.5% NaCl treatment (bottom). **(C)** Germination index grades (GIG) under the 0.3% (top) and 0.5% NaCl treatments (bottom).

identified. Notably, the *qGRG4* locus contained a high-affinity potassium transporter *OsHAK1*, harboring a significant SNP (S04_19891019, $-\log_{10}(p)$ = 7.19 under 0.3% and $-\log_{10}(p)$ = 7.58 under 0.5% NaCl). Since *OsHAK1* is known to regulate K^+/Na^+ homeostasis in rice seedlings under salt stress (Chen et al., 2015), our subsequent work was focused on two other loci, *qGRG3-1* and *qGRG3-2*.

3.3 Identification of candidate genes responsive to salt stress

To identify candidate genes that are responsive to salt stress in *qGRG3-1* and *qGRG3-2* loci, the roots and shoots of 7-day-old ZH11 seedlings grown under 0.3% or 0.5% NaCl treatments were collected, and expression analyses were performed using qRT-PCR to analyze expressions of genes located in these two loci. No consistent responses to salt stress were observed in any of the 19 genes in the *qGRG3-1* locus (Figure 4A). In contrast, 8 of 21 genes examined in the *qGRG3-2* locus showed responsive expressions under the salt stress (Figure 4B). In particular, LOC_Os05g48620, LOC_Os05g48730, and LOC_Os05g48900 were up-regulated in roots and shoots of seedlings exposed to either 0.3% or 0.5% NaCl, while expressions of LOC_Os05g48650 and LOC_Os05g48670 were only up-regulated under 0.5% NaCl treatment (Figure 4B). Three other genes, LOC_Os05g48600, LOC_Os05g48760 and LOC_Os05g48930, were down-regulated in roots upon exposure to 0.3% or 0.5% NaCl (Figure 4B, right). We selected these genes as candidates for further analysis.

We examined expressions of these eight candidate genes in three ST (L_363, L_417, and L_505) and three SS varieties (L_065,

TABLE 1 Results of seed germinations under salt stresses in 541 rice varieties.

Treatments	Traits	Germination grade ranges	Mean	Standard deviations	Coefficient of variations
0.3% NaCl	Germination rate grades on the 3rd day (GRG3)	1–11	5.0832	2.7160	53.43%
	Germination rate grades on the 4th day (GRG4)	1–10	2.7116	1.9940	73.53%
	Germination index grades (GIG)	1–7	3.3117	1.1779	35.57%
0.5% NaCl	Germination rate grades on the 3rd day (GRG3)	1–11	7.3401	2.8013	38.16%
	Germination rate grades on the 4th day (GRG4)	1–11	3.3346	1.9111	57.31%
	Germination index grades (GIG)	1–8	4.0286	1.2599	31.27%

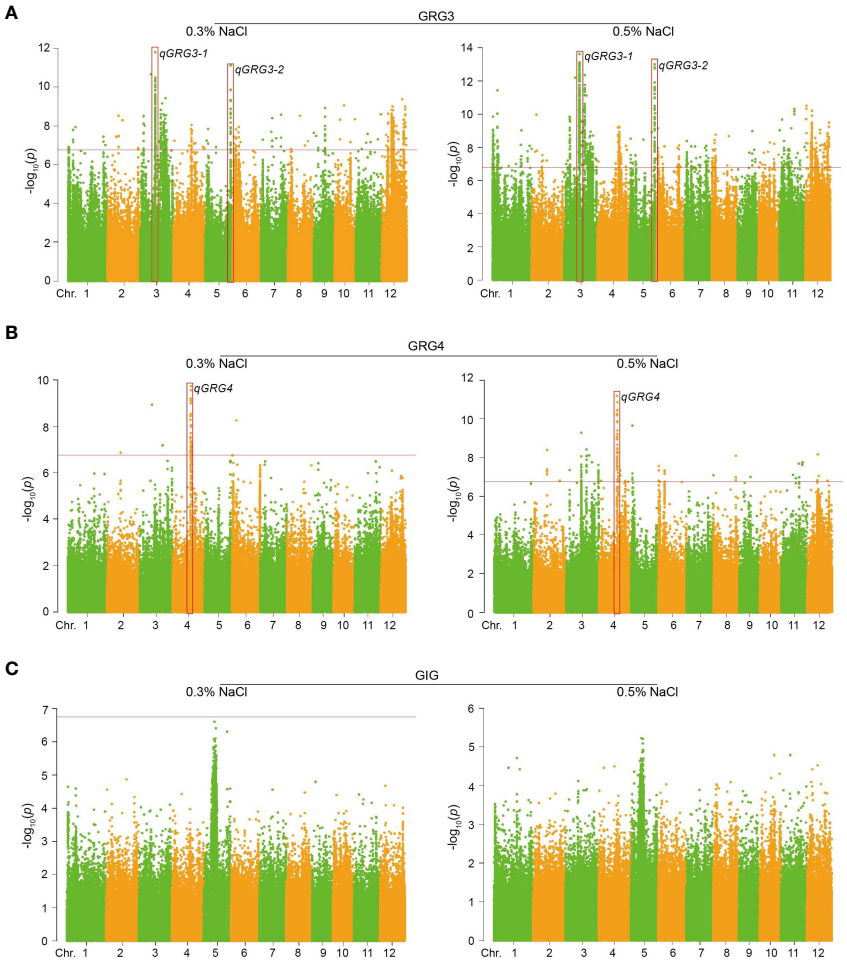

FIGURE 3
Manhattan plots for GWAS of rice seed germinations under salt stress. **(A)** Manhattan plots of GRG3 under 0.3% (left) or 0.5% NaCl treatments (right). **(B)** Manhattan plots of GRG4 under 0.3% (left) or 0.5% NaCl treatments (right). **(C)** Manhattan plots of GIG under 0.3% (left) or 0.5% NaCl treatments (right). Red boxes show genomic regions with clustered SNPs above the significance thresholds (–log10(*p*); indicated by horizontal red lines).

L_274, and L_352), selected as described in Materials and Methods. Results showed that LOC_Os05g48730 (Supplementary Figure S3A) and LOC_Os05g48930 (Supplementary Figure S3B) exhibited higher levels of expression in ST varieties than those in SS varieties, under both the control and salt stress conditions. Three other genes, LOC_Os05g48620 (Supplementary Figure S3C), LOC_Os05g48670 (Supplementary Figure S3D) and LOC_Os05g48760 (Supplementary Figure S3E), showed elevated expressions under salt stress in ST varieties, but not in SS varieties. For LOC_Os05g48600, elevated expressions were observed in L_363 (ST) and L_417 (ST) under salt stress, but no significantly changed expressions in L_505 (ST), and three SS varieties (L_065, L_274 and L_352; Supplementary Figure S3F). For LOC_Os05g48650 and LOC_Os05g48900, although no consistent pattern was observed between ST and SS varieties, elevated expressions were detected for LOC_Os05g48650 under salt stress in all varieties except L_065 (Supplementary Figure S3G), whereas no salt-induced expressions were observed for LOC_Os05g48900 in neither ST nor SS varieties (Supplementary Figure S3H).

3.4 Genetic characterization of genes underlying seed germination under salt stress

To further characterize the eight candidate genes in *qGRG3-2* locus, knockout mutants were generated using CRISPR/Cas9-mediated gene editing in ZH11. For each gene, at least two independent homozygous transgene-free lines with frameshifts in translation were identified in either T1 or T2 generations, confirmed by PCR amplifications and sequencing (Supplementary Table S5). We tested the germination rates of mature seeds from mutant lines under the control, 0.3% and 0.5% NaCl treatments. Among lines assayed, *ostmf-1* and *ostmf-2* (Figures 5A, B), carrying mutations in LOC_Os05g48620 that encodes OsTMF (a rice homolog of human TATA modulatory factor, TMF), exhibited delayed germination under 0.3% NaCl treatments when compared to ZH11 (Figures 5C, D). OsTMF was previously reported to attenuate cold tolerance in rice by modulating expressions of cell wall biosynthesis-related genes (Xu et al.,

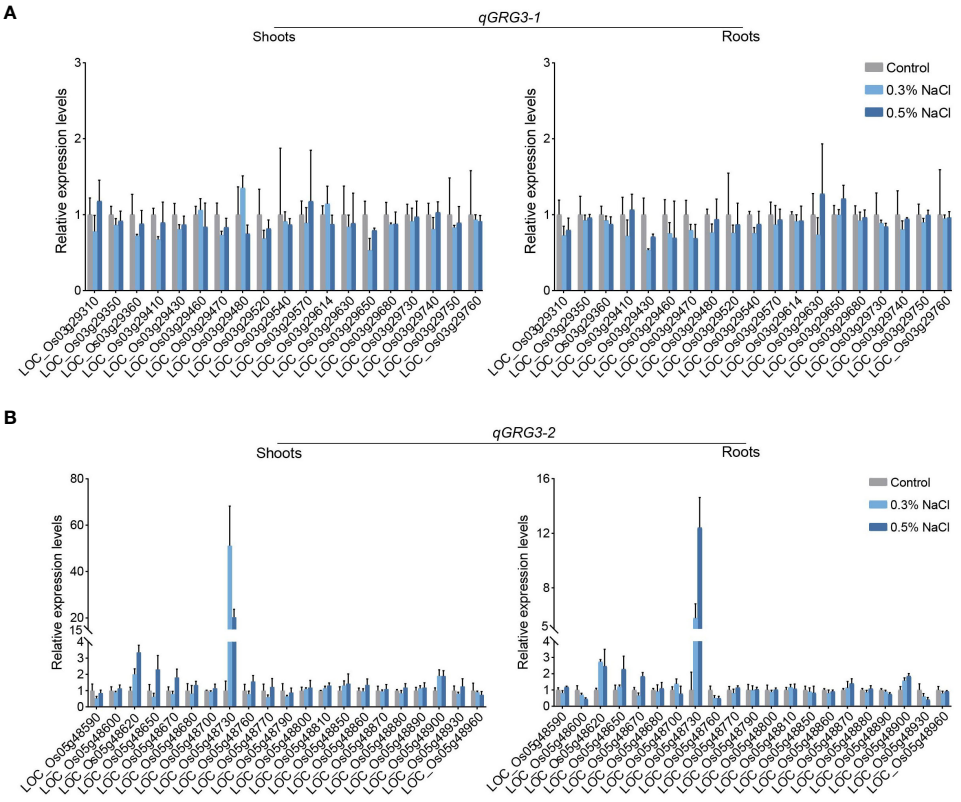

FIGURE 4
Relative expressions of genes in *qGRG3-1* and *qGRG3-2* loci under the salt stress. qRT-PCR analyses of genes in *qGRG3-1* **(A)** and *qGRG3-2* **(B)** loci in shoots (left) and roots (right) excised from 7-day-old ZH11 seedlings germinated under control (deionized water), 0.3% NaCl or 0.5% NaCl conditions. Data are shown as means ± SD from three biological replicates.

2020). With the increased NaCl concentration (0.5%), further delays of germination were observed (Figures 5C (below dashed lines), E).

To examine the germinations of *ostmf-1* and *ostmf-2* in saline soil, we sowed their seeds in pots, filled with soil, and soaked in deionized water or 0.5% NaCl. On the 10th day, no evident phenotypic difference was observed in *ostmf-1* and *ostmf-2* under the control conditions, when compared to ZH11 (Figure 5F). However, in soil soaked with 0.5% NaCl, both *ostmf-1* and *ostmf-2* showed lower germination rates (Figure 5G) and shorter shoot lengths (Figure 5H).

To investigate the expression of *OsTMF* in response to salt stress, we conducted qRT-PCR analyses in seeds and seedlings using RNAs collected at different days after growing in 0.5% NaCl and deionized water. Results showed that the *OsTMF* expression was increased in seeds after growing in 0.5% NaCl solution for 1 day, and then decreased gradually, whereas it maintained stable in those seeds grown in water (Figure 5I). In the shoots and roots of seedlings, salt stress enhanced *OsTMF* expressions from day 1 to 7, whereas in the control conditions, *OsTMF* expression remained at stable and low levels throughout the time course. These findings suggest that *OsTMF* may positively regulate seed germination under salt stress.

3.5 Haplotype analysis of *OsTMF*

To examine the relationship between *OsTMF* haplotypes and seed germination under salt stress, haplotype analysis was conducted in 541 rice varieties. In the coding region of *OsTMF*, six SNPs were detected (Figure 6A), with which we defined four major haplotypes, based on their presences in at least 20 varieties. We observed that Hap1, Hap2, and Hap4 are predominant present in the *indica* subpopulation, while Hap3 is predominant in the *japonica* subpopulation (Figures 6A, B). GRG3 of varieties harboring Hap2 were 3.710 and 5.794 under 0.3% and 0.5% NaCl treatments, respectively, which were lower than those varieties carrying Hap1, Hap3, or Hap4 (Figure 6C), indicating that Hap2 is more tolerant to salt stress. These results together suggest that Hap2 is a potential haplotype to be used for improving rice seed germination under salt stress.

4 Discussion

Efficient seed germination under salt stress is a crucial prerequisite for seedling establishment and subsequent crop production in saline land, and is a quantitative trait regulated by

10.3389/fpls.2024.1384246

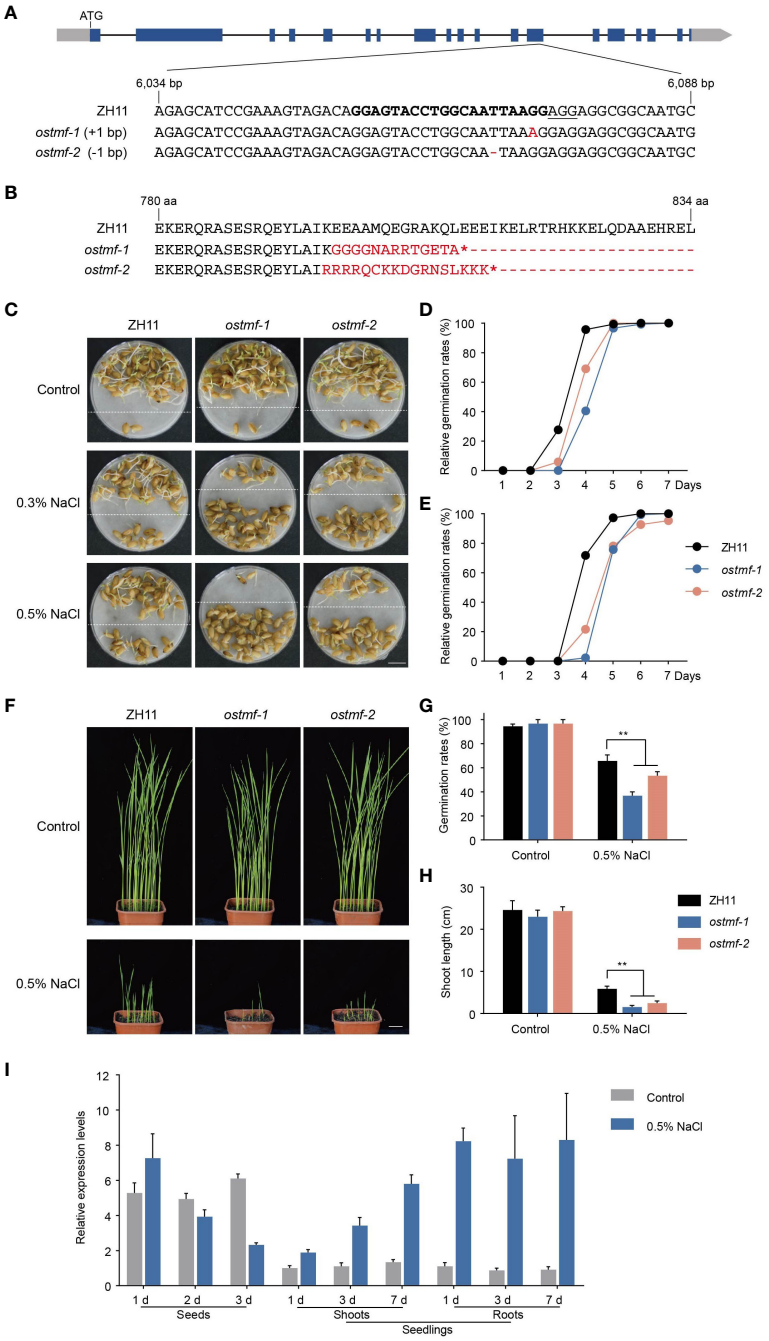

FIGURE 5
Mutations of *OsTMF* led to delayed seed germinations under salt stress. **(A)** A diagram of the *OsTMF* gene model (top), and partial sequence of *OsTMF* containing the target sites (in bold) for CRISPR/Cas9-based gene editing in ZH11, and the sequences of *ostmf-1* and *ostmf-2* mutants. Blue rectangles represent exons, black lines represent introns, and gray rectangles represent untranslated regions. The protospacer adjacent motif (PAM) is underlined, and mutations are in red. **(B)** Partial peptide sequences of OsTMF from ZH11, *ostmf-1* and *ostmf-2*. Red, altered sequences in *ostmf-1* and *ostmf-2*; asterisks, stop codon. **(C)** Representative photos for seed germinations of ZH11 and *ostmf* mutants under the control (deionized water), 0.3% or 0.5% NaCl treatments for 4 days. Germinated seeds were repositioned above the dashed lines. Scale bar, 1 cm. **(D, E)** Relative germination rates of ZH11 and *ostmf* mutants in different time points under 0.3% **(D)** and 0.5% **(E)** NaCl treatments. **(F)** Ten-day-old seedlings of ZH11 and *ostmf* mutants, germinated in soil-filled pots immersed in deionized water (the upper panel) or 0.5% NaCl (the lower panel). Scale bar, 2 cm. **(G)** Germination rates on the 10th day of ZH11 and *ostmf* mutants. germinated in soil-filled pots immersed in deionized water or 0.5% NaCl. **, $p < 0.05$. **(H)** Shoot length of seedlings of 10-day-old ZH11 and *ostmf* mutants germinated in soil-filled pots immersed in deionized water or 0.5% NaCl **, $p < 0.05$. **(I)** Expressions of *OsTMF* in seeds (treated with deionized water or 0.5% NaCl for 1, 2 or 3 days) and seedlings (treated with Hoagland solution or Hoagland solution containing 0.5% NaCl for 1, 3 or 7 days).

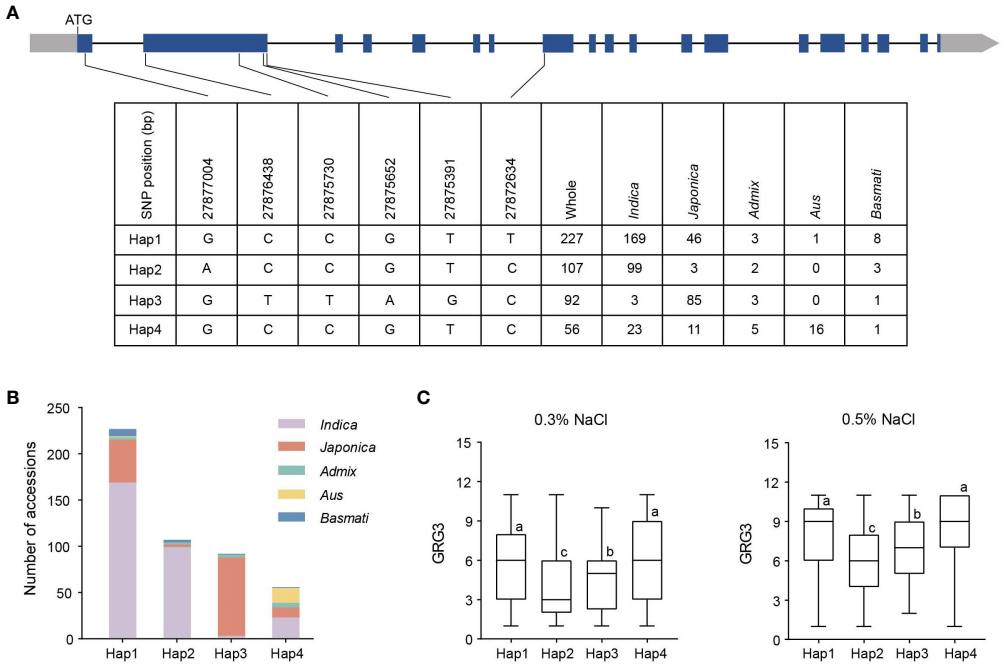

SNP position (bp)	27877004	27876438	27875730	27875652	27875391	27872634	Whole	*Indica*	*Japonica*	*Admix*	*Aus*	*Basmati*
Hap1	G	C	C	G	T	T	227	169	46	3	1	8
Hap2	A	C	C	G	T	C	107	99	3	2	0	3
Hap3	G	T	T	A	G	C	92	3	85	3	0	1
Hap4	G	C	C	G	T	C	56	23	11	5	16	1

FIGURE 6
Haplotype analyses in *OsTMF*. **(A)** Genomic variations in *OsTMF* coding region, showing the presence of 4 haplotypes (Hap) in 541 rice varieties. **(B)** Frequencies of 4 *OsTMF* haplotypes in different rice subpopulations. **(C)** Comparison of GRG3 under 0.3% (left) or 0.5% NaCl (right) in 4 *OsTMF* haplotypes. Lowercase letters indicate significant differences based on Duncan's multiple range post-hoc test ($p < 0.05$).

multiple genes (Shi et al., 2017; Li et al., 2022). In this study, we conducted GWAS to investigate the genetic basis of seed germination under salt stress utilizing a set of 541 rice varieties collected worldwide. We identified three QTLs, *qGRG3-1*, *qGRG3-2* and *qGRG4*, which are significantly associated with seed germination under salt stress, imposed by using 0.3% or 0.5% NaCl. Detailed analyses showed that the most likely candidate gene underlying *qGRG3-2* is *OsTMF*. Under salt stress, the expressions of *OsTMF* were up-regulated, and *ostmf* mutants exhibited delayed seed germinations when compared to the wild type.

In general, rice seed germination is defined visually by the emergence of the radicle penetrating through the hull, which has been used to study seed dormancy and germination (Jung et al., 2019; Prasad et al., 2022; Jin et al., 2023). However, under salt stress, rice seeds exhibit not only delayed germination, but also compromised growths of radicle and coleoptile, leading to lower seedling viability. Therefore, a more adequate criterion to define seed germination under salt stress is based on a combination of two measures: the root length longer than the seed length, and the shoot length longer than half of the seed length (Shi et al., 2017). To accurately measure seed germination in such a manner, we did the germination experiments on water- or NaCl solution-immersed filter paper in petri dishes (with a cover, but without seal), and refreshed the solutions in every two days. After counting germinated seeds, germination rate and germination index were calculated to evaluate seed germination status under salt stress (Shi et al., 2017; Ju et al., 2022; Li et al., 2022; Mei et al., 2022; Zhan et al., 2023). In this study, we established germination grades (1 to 11) using the GR3, GR4 and GI ratios of salt stress condition to the control condition. Under such a criterion, all varieties showed continuous and extensive phenotypic variations, suggesting that they are suitable for GWAS analysis.

Although GWASs have been performed in rice to decipher seed germination under salt stress (Shi et al., 2017; Yu et al., 2018; Islam et al., 2022; Ju et al., 2022; Li et al., 2022), no genes have been identified so far. In this study, three QTLs, two for GRG3 (*qGRG3-1* and *qGRG3-2*) and one for GRG4 (*qGRG4*), were consistently detected under 0.3% and 0.5% NaCl treatments. In the *qGRG4* locus, *OsHAK1*, a well-characterized high-affinity K^+ transporter that promotes rice seedling growth under salt stress, is present (Chen et al., 2015, 2018). The *OsHAK1* gene was also reported before in the *q4.8* locus (Zhang et al., 2023), and is associated with relative germination rate on the 3rd day under saline-alkali stress. In addition, other HAK genes such as *OsHAK12* (Zhang et al., 2021), *OsHAK16* (Feng et al., 2019) and *OsHAK21* (He et al., 2019; Song et al., 2021) are implicated in salt tolerance in rice. Among them, *OsHAK21* may play a role in seed germination under salt stress (He et al., 2019). Therefore, in experiments followed, we did not pay much attention to the genomic region of *qGRG4*. *qGRG3-1* overlaps with the reported 16.66–17.02 Mbp region on chromosome 3, which is associated with shoot fresh weight under salt stress (Yu et al., 2023). *qGRG3-2* overlaps with the reported *q5.11* locus that is associated with the relative germination rate under saline-alkali stress (Zhang et al., 2023). However, no salt tolerance-related gene has been reported in these regions.

Expression analysis is a powerful way to identify genes underlying salt tolerance, with either elevated (Chen et al., 2018;

Feng et al., 2019) or repressed expressions under salt stress (Wang et al., 2020), or differential expressions in ST and SS varieties (Zhang et al., 2018, 2019). We examined expressions of genes located in *qGRG3-1* and *qGRG3-2* loci, which allowed us to identify eight candidate genes in the *qGRG3-2* locus, which exhibited elevated or repressed expressions under salt stresses. Among them, five showed differential expressions between SS and ST varieties. To narrow down candidate genes in the *qGRG3-2* locus, we employed CRISPR/Cas9-based gene editing to generate mutants for all these eight genes. Seed germination analyses performed in these mutants under salt stress allowed us to establish that *OsTMF* is the most likely candidate gene, since *OsTMF* knockout mutants showed delayed seed germination under salt stress. We showed further that varieties with different *OsTMF* haplotypes showed differences in early seed germination under salt stress. However, as the germination progressed to the seventh day, the germination rates of *ostmf* mutants were comparable with ZH11, suggesting a major role of *OsTMF* in regulating early seed germination under salt stress, not so much in seedling establishment. *OsTMF* has previously been reported to be a negative regulator of cold tolerance in rice (Xu et al., 2020). In another report, it was shown that OsTMF interacted with Ski-Interacting Protein a (OsSKIPa), that regulates cell vitality, and overexpression of *OsSKIPa* led to enhanced vegetative growth under salt stress (Hou et al., 2009). Whether OsTMF acts through OsSKIPa in seed germination under salt stress warrants further investigation.

Data availability statement

The datasets presented in this study can be found in online repositories. The names of the repository/repositories and accession number(s) can be found in the article/Supplementary Material.

Author contributions

LL: Conceptualization, Data curation, Formal Analysis, Investigation, Methodology, Software, Writing – original draft, Writing – review & editing. YM: Data curation, Writing – review & editing. HZ: Writing – review & editing. LG: Investigation, Writing – review & editing. YG: Supervision, Validation, Writing – review & editing. C-ML: Formal Analysis, Funding acquisition, Project administration, Resources, Supervision, Validation, Visualization, Writing – original draft, Writing – review & editing.

Funding

The author(s) declare that financial support was received for the research, authorship, and/or publication of this article. This work was supported by grants from the National Key R&D Program of China (2020YFE0202300).

Conflict of interest

The authors declare that the research was conducted in the absence of any commercial or financial relationships that could be construed as a potential conflict of interest.

Publisher's note

Supplementary material

The Supplementary Material for this article can be found online at: https://www.frontiersin.org/articles/10.3389/fpls.2024.1384246/full#supplementary-material

SUPPLEMENTARY FIGURE 1
Phenotypic variations of 50 randomly selected rice varieties for seed germination in NaCl concentrations from 0.3% to 1%. Germination rate grades on the 3rd (GRG3; **A**) and the 4th day (GRG4; **B**), and germination index grades (GIG; **C**) under the treatments if indicated NaCl concentrations.

SUPPLEMENTARY FIGURE 2
Phenotypic variations for seed germinations under salt stresses among varieties in different subpopulations. **(A)** Germination rate grades on the 3rd day (GRG3) under 0.3% (top) and 0.5% NaCl (bottom) treatments in different subpopulations. **(B)** Germination rate grades on the 4th day (GRG4) under 0.3% (top) and 0.5% NaCl (bottom) conditions in different subpopulations. **(C)** Germination index grades (GIG) under the treatment of 0.3% (top) and 0.5% NaCl (bottom) in different subpopulations. Lowercase letters indicate significant differences based on Duncan's multiple range post-hoc test ($p < 0.05$).

SUPPLEMENTARY FIGURE 3
Expressions of candidate genes in the *qGRG3-2* locus in representative salt-tolerant and salt-sensitive varieties. ST, representative salt-tolerant varieties; SS, representative salt-sensitive varieties.

References

Bradbury, P. J., Zhang, Z. W., Kroon, D. E., Casstevens, T. M., Ramdoss, Y., and Buckler, E. S. (2007). TASSEL: software for association mapping of complex traits in diverse samples. *Bioinformatics* 23, 2633–2635. doi: 10.1093/bioinformatics/btm308

Chen, G., Hu, Q. D., Luo, L., Yang, T. Y., Zhang, S., Hu, Y. B., et al. (2015). Rice potassium transporter *OsHAK1* is essential for maintaining potassium-mediated growth and functions in salt tolerance over low and high potassium concentration ranges. *Plant Cell Environ.* 38, 2747–2765. doi: 10.1111/pce.12585

Chen, G., Liu, C., Gao, Z., Zhang, Y., Zhang, A., Zhu, L., et al. (2018). Variation in the abundance of *OsHAK1* transcript underlies the differential salinity tolerance of an *indica* and a *japonica* rice cultivar. *Front. Plant Sci.* 8. doi: 10.3389/fpls.2017.02216

Cheng, Z. X., Sun, Y., Yang, S. H., Zhi, H., Yin, T., Ma, X. J., et al. (2021). Establishing in *planta* haploid inducer line by edited *SiMTL* in foxtail millet (*Setaria italica*). *Plant Biotechnol. J.* 19, 1089–1091. doi: 10.1111/pbi.13584

Du, L. Y., Ding, L., Huang, X. L., Tang, D. L., Chen, B., Tian, H., et al. (2024). Natural variation in a K^+-preferring HKT transporter contributes to wheat shoot K^+ accumulation and salt tolerance. *Plant Cell Environ.* 47, 540–556. doi: 10.1111/pce.14746

Farooq, M., Siddique, K., Rehman, H., Aziz, T., Lee, D., and Wahid, A. (2011). Rice direct seeding: experiences, challenges and opportunities. *Soil Tillage. Res.* 111, 87–98. doi: 10.1016/j.still.2010.10.008

Feng, H. M., Tang, Q., Cai, J., Xu, B. C., Xu, G. H., and Yu, L. (2019). Rice OsHAK16 functions in potassium uptake and translocation in shoot, maintaining potassium homeostasis and salt tolerance. *Planta* 250, 549–561. doi: 10.1007/s00425-019-03194-3

Hasseb, N. M., Sallam, A., Karam, M. A., Gao, L., Wang, R. R. C., and Moursi, Y. S. (2022). High-LD SNP markers exhibiting pleiotropic effects on salt tolerance at germination and seedlings stages in spring wheat. *Plant Mol. Biol.* 108, 585–603. doi: 10.1007/s11103-022-01248-x

He, L. R., and Luo, Y. H. (2021). Effects of long-term sand mixing ameliorating measures on soil salinity characteristics of saline-alkali land in northern shaanxi. *IOP. Conf. Series.: Earth Environ. Sci.* 781, 1–5. doi: 10.1088/1755-1315/781/2/022084

He, Y. Q., Yang, B., He, Y., Zhan, C. F., Cheng, Y. H., Zhang, J. H., et al. (2019). A quantitative trait locus, *qSE3*, promotes seed germination and seedling establishment under salinity stress in rice. *Plant J.* 97, 1089–1104. doi: 10.1111/tpj.14181

Hou, X., Xie, K. B., Yao, J. L., Qi, Z., and Xiong, L. Z. (2009). A homolog of human ski-interacting protein in rice positively regulates cell viability and stress tolerance. *Proc. Natl. Acad. Sci. U. S. A.* 106, 6410–6415. doi: 10.1073/pnas.0901940106

Hu, S. K., Tao, H. J., Qian, Q., and Guo, L. B. (2012). Genetics and molecular breeding for salt tolerance in rice. *Rice Genom. Genet.* 3, 39–49. doi: 10.5376/rgg.2012.03.0007

Huang, X. Y., Chao, D. Y., Gao, J. P., Zhu, M. Z., Shi, M., and Lin, H. X. (2009). A previously unknown zinc finger protein, DST, regulates drought and salt tolerance in rice via stomatal aperture control. *Gene. Dev.* 23, 1805–1817. doi: 10.1101/gad.1812409

Islam, M. R., Naveed, S. A., Zhang, Y., Li, Z. K., Zhao, X. Q., Fiaz, S., et al. (2022). Identification of candidate genes for salinity and anaerobic tolerance at the germination stage in rice by genome wide association analyses. *Front. Genet.* 13. doi: 10.3389/fgene.2022.822516

Jin, X. K., Li, X. X., Xie, Z. Z., Sun, Y., Jin, L., Hu, T. Z., et al. (2023). Nuclear factor OsNF-YC5 modulates rice seed germination by regulating synergistic hormone signaling. *Plant Physiol.* 193, 2825–2847. doi: 10.1093/plphys/kiad499

Ju, C. Y., Ma, X. D., Han, B., Zhang, W., Zhao, Z. W., Geng, L. Y., et al. (2022). Candidate gene discovery for salt tolerance in rice (*Oryza sativa* L.) at the germination stage based on genome-wide association study. *Front. Plant Sci.* 13. doi: 10.3389/fpls.2022.1010654

Julkowska, M. M., Koevoets, I. T., Mol, S., Hoefsloot, H., Feron, R., Tester, M. A., et al. (2017). Genetic components of root architecture remodeling in response to salt stress. *Plant Cell* 29, 3198–3213. doi: 10.1105/tpc.16.00680

Jung, Y. J., Lee, H. J., Bae, S., Kim, J. H., Kim, D. H., Kim, H. K., et al. (2019). Acquisition of seed dormancy breaking in rice (*Oryza sativa* L.) via CRISPR/Cas9-targeted mutagenesis of *OsVP1* gene. *Plant Biotechnol. Rep.* 13, 511–520. doi: 10.1007/s11816-019-00580-x

Kawahara, Y., Bastide, M., Hamilton, J. P., Kanamori, H., McCombie, W. R., Ouyang, S., et al. (2013). Improvement of the *Oryza sativa* Nipponbare reference genome using next generation sequence and optical map data. *Rice (N. Y).* 6, 4. doi: 10.1186/1939-8433-6-4

Li, C. J., Lu, C. S., Zou, B. L., Yang, M. M., Wu, G. L., Wang, P., et al. (2022). Genome-wide association study reveals a genetic mechanism of salt tolerance germinability in rice (*Oryza sativa* L.). *Front. Plant Sci.* 13. doi: 10.3389/fpls.2022.934515

Lin, H. X., Zhu, M. Z., Yano, M., Gao, J. P., Liang, Z. W., Su, W. A., et al. (2004). QTLs for Na^+ and K^+ uptake of shoot and root controlling rice salt tolerance. *Theor. Appl. Genet.* 108, 253–260. doi: 10.1007/s00122-003-1421-y

Mansueto, L., Fuentes, R. R., Borja, F. N., Detras, J., Abriol-Santos, J. M., Chebotarov, D., et al. (2016). Rice SNP-seek database update: new SNPs, indels, and queries. *Nucleic Acids Res.* 45, 1075–1081. doi: 10.1093/nar/gkw1135

Mei, S., Zhang, G. G., Jiang, J., Lu, J. B., and Zhang, F. (2022). Combining genome-wide association study and gene-based haplotype analysis to identify candidate genes for alkali tolerance at the germination stage in rice. *Front. Plant Sci.* 13. doi: 10.3389/fpls.2022.887239

Munns, R., and Tester, M. (2008). Mechanisms of salinity tolerance. *Annu. Rev. Plant Biol.* 59, 651–681. doi: 10.1146/annurev.arplant.59.032607.092911

Nishimura, A., Aichi, I., and Matsuoka, M. (2007). A protocol for *Agrobacterium*-mediated transformation in rice. *Nat. Protoc.* 1, 2796–2802. doi: 10.1038/nprot.2006.469

Prasad, C. T. M., Kodde, J., Angenent, G. C., de Vos, R. C. H., Diez-Simon, C., Mumm, R., et al. (2022). Experimental rice seed aging under elevated oxygen pressure: Methodology and mechanism. *Front. Plant Sci.* 13. doi: 10.3389/fpls.2022.1050411

Ren, Z. H., Gao, J. P., Li, L. G., Cai, X. L., Huang, W., Chao, D. Y., et al. (2005). A rice quantitative trait locus for salt tolerance encodes a sodium transporter. *Nat. Genet.* 37, 1141–1146. doi: 10.1038/ng1643

Shi, Y. Y., Gao, L. L., Wu, Z. C., Zhang, X. J., Wang, M. M., Zhang, C. S., et al. (2017). Genome-wide association study of salt tolerance at the seed germination stage in rice. *BMC Plant Biol.* 17, 92. doi: 10.1186/s12870-017-1044-0

Song, T. Z., Shi, Y. Y., Shen, L. K., Cao, C. J., Shen, Y., Jing, W., et al. (2021). An endoplasmic reticulum-localized cytochrome *b5* regulates high-affinity K^+ transport in response to salt stress in rice. *Proc. Natl. Acad. Sci. U.S.A.* 118, e2114347118. doi: 10.1073/pnas.2114347118

Takagi, H., Tamiru, M., Abe, A., Yoshida, K., Uemura, A., Yaegashi, H., et al. (2015). MutMap accelerates breeding of a salt-tolerant rice cultivar. *Nat. Biotechnol.* 33, 445–449. doi: 10.1038/nbt.3188

Takehisa, H., Shimodate, T., Fukuta, Y., Ueda, T., Yano, M., Yamaya, T., et al. (2004). Identification of quantitative trait loci for plant growth of rice in paddy field flooded with salt water. *Field Crops Res.* 89, 85–95. doi: 10.1016/j.fcr.2004.01.026

Turner, S. D. (2014). qqman: an R package for visualizing GWAS results using Q-Q and manhattan plots. *J. Open Source Software* 3, 1731. doi: 10.21105/joss.00731

Wang, W. Y., Barratt, B. J., Clayton, D. J., and Todd, J. A. (2005). Genome-wide association studies: theoretical and practical concerns. *Nat. Rev. Genet.* 6, 109–118. doi: 10.1038/nrg1522

Wang, W. S., Mauleon, R., Hu, Z. Q., Chebotarov, D., Tai, S. S., Wu, Z. C., et al. (2018). Genomic variation in 3,010 diverse accessions of Asian cultivated rice. *Nature* 557, 43–49. doi: 10.1038/s41586-018-0063-9

Wang, J., Qin, H., Zhou, S. R., Wei, P. C., Zhang, H. W., Zhou, Y., et al. (2020). The ubiquitin-binding protein OsDSK2a mediates seedling growth and salt responses by regulating gibberellin metabolism in rice. *Plant Cell* 32, 414–428. doi: 10.1105/tpc.19.00593

Xie, X. R., Ma, X. L., Zhu, Q. L., Zeng, D. C., Li, G. S., and Liu, Y. G. (2017). CRISPR-GE: a convenient software toolkit for CRISPR-based genome editing. *Mol. Plant* 10, 1246–1249. doi: 10.1016/j.molp.2017.06.004

Xiong, M., Xu, J., Zhou, Z., Peng, B., Shen, Y., Shen, H., et al. (2024). Salinity inhibits seed germination and embryo growth by reducing starch mobilization efficiency in barley. *Plant Direct.* 8, e564. doi: 10.1002/pld3.564

Xu, E. S., Chen, M. M., He, H., Zhan, C. F., Cheng, Y. H., Zhang, H. S., et al. (2017). Proteomic analysis reveals proteins involved in seed imbibition under salt stress in rice. *Front. Plant Sci.* 7. doi: 10.3389/fpls.2016.02006

Xu, Y., Hu, D., Hou, X., Shen, J. Q., Liu, J. H., Cen, X., et al. (2020). *OsTMF* attenuates cold tolerance by affecting cell wall properties in rice. *New Phytol.* 227, 498–512. doi: 10.1111/nph.16549

Yan, H., Nie, Y., Cui, K., and Sun, J. (2022). Integrative transcriptome and metabolome profiles reveal common and unique pathways involved in seed initial imbibition under artificial and natural salt stresses during germination of halophyte quinoa. *Front. Plant Sci.* 13. doi: 10.3389/fpls.2022.853326

Yang, Y. Q., and Guo, Y. (2018). Unraveling salt stress signaling in plants. *J. Integr. Plant Biol.* 60, 796–804. doi: 10.1111/jipb.12689

Yang, W., Liu, X., Yu, S. W., Liu, J. S., Jiang, L. J., Lu, X. D., et al. (2023). The maize ATP-binding cassette (ABC) transporter ZmMRPA6 confers cold and salt stress tolerance in plants. *Plant Cell Rep.* 43, 13. doi: 10.1007/s00299-023-03094-7

Yu, J., Zhao, W. G., Tong, W., He, Q., Yoon, M. Y., Li, F. P., et al. (2018). A genome-wide association study reveals candidate genes related to salt tolerance in rice (*Oryza sativa*) at the germination stage. *Int. J. Mol. Sci.* 19, 3145. doi: 10.3390/ijms19103145

Yu, J., Zhu, C. S., Xuan, W., An, H. Z., Tian, Y. L., Wang, B. X., et al. (2023). Genome-wide association studies identify OsWRKY53 as a key regulator of salt tolerance in rice. *Nat. Commun.* 14, 3550. doi: 10.1038/s41467-023-39167-0

Zhan, C. F., Zhu, P. W., Chen, Y. J., Chen, X. Y., Liu, K. X., Chen, S. S., et al. (2023). Identification of a key locus, *qNL3.1*, associated with seed germination under salt stress via a genome-wide association study in rice. *Theor. Appl. Genet.* 136, 58. doi: 10.1007/s00122-023-04252-x

Zhang, G. G., Bi, Z. Y., Jiang, J., Lu, J. B., Li, K. Y., Bai, D., et al. (2023). Genome-wide association and epistasis studies reveal the genetic basis of saline-alkali tolerance at the germination stage in rice. *Front. Plant Sci.* 14. doi: 10.3389/fpls.2023.1170641

Zhang, M., Cao, Y. B., Wang, Z. P., Wang, Z. Q., Shi, J. P., Liang, X. Y., et al. (2018). A retrotransposon in an HKT1 family sodium transporter causes variation of leaf Na^+ exclusion and salt tolerance in maize. *New Phytol.* 217, 1161–1176. doi: 10.1111/nph.14882

Zhang, M., Liang, X. Y., Wang, L. M., Cao, Y. B., Song, W. B., Shi, J. P., et al. (2019). A HAK family Na^+ transporter confers natural variation of salt tolerance in maize. *Nat. Plants* 5, 1297–1308. doi: 10.1038/s41477-019-0565-y

Zhang, L. N., Sun, X. Y., Li, Y. F., Luo, X., Song, S. W., Chen, Y., et al. (2021). Rice Na^+-permeable transporter OsHAK12 mediates shoots Na^+ exclusion in response to salt stress. *Front. Plant Sci.* 12. doi: 10.3389/fpls.2021.771746

frontiers | Frontiers in Plant Science

TYPE Original Research
PUBLISHED 10 April 2024
DOI 10.3389/fpls.2024.1378738

OPEN ACCESS

EDITED BY
Guowei Li,
Shandong Academy of Agricultural Sciences, China

REVIEWED BY
Zhonglin Shang,
Hebei Normal University, China
Xinhua Zhao,
Shenyang Agricultural University, China

*CORRESPONDENCE
Haobao Liu
liuhaobao@caas.cn
Qian Wang
wangqian01@caas.cn

RECEIVED 30 January 2024
ACCEPTED 26 March 2024
PUBLISHED 10 April 2024

CITATION
Yuan G, Nong T, Hunpatin OS, Shi C, Su X, Xu F, Wang Y, Zhang Z, Ning Y, Liu H and Wang Q (2024) Genome-wide identification of Shaker K^+ channel family in *Nicotiana tabacum* and functional analysis of *NtSKOR1B* in response to salt stress.
Front. Plant Sci. 15:1378738.
doi: 10.3389/fpls.2024.1378738

Genome-wide identification of Shaker K^+ channel family in *Nicotiana tabacum* and functional analysis of *NtSKOR1B* in response to salt stress

Guang Yuan[1,2], Tongjia Nong[1,2], Oluwaseyi Setonji Hunpatin[1,2], Chuhan Shi[1,2], Xiaoqing Su[1,3], Fangzheng Xu[1], Yihui Wang[4], Zhaoting Zhang[5], Yang Ning[1], Haobao Liu[1]* and Qian Wang[1]*

[1]Tobacco Research Institute, Chinese Academy of Agricultural Sciences, Qingdao, China, [2]Graduate School of Chinese Academy of Agricultural Sciences, Beijing, China, [3]College of Agriculture, Qingdao Agricultural University, Qingdao, China, [4]China Tobacco Shandong Industrial Co., LTD Cigar Operation Center, Jinan, China, [5]Xuancheng City Xuanzhou District Tobacco Industry Development Center, Xuancheng, China

Soil salinization poses a mounting global ecological and environmental threat. The identification of genes responsible for negative regulation of salt tolerance and their utilization in crop improvement through gene editing technologies emerges as a swift strategy for the effective utilization of saline-alkali lands. One efficient mechanism of plant salt tolerance is maintaining the proper intracellular K^+/Na^+ ratio. The Shaker K^+ channels play a crucial role in potassium absorption, transport, and intracellular potassium homeostasis in plant cells. Here, the study presents the first genome-wide identification of Shaker K^+ channels in *Nicotiana tabacum* L., along with a detailed bioinformatic analysis of the 20 identified members. Transcriptome analysis revealed a significant up-regulation of *NtSKOR1B*, an outwardly-rectifying member predominantly expressed in the root tissue of tobacco seedlings, in response to salt stress. This finding was then confirmed by GUS staining of *ProNtSKOR1B::GUS* transgenic lines and RT-qPCR analysis. Subsequently, *NtSKOR1B* knockout mutants (*ntskor1*) were then generated and subjected to salt conditions. It was found that *ntskor1* mutants exhibit enhanced salt tolerance, characterized by increased biomass, higher K^+ content and elevated K^+/Na^+ ratios in both leaf and root tissues, compared to wild-type plants. These results indicate that *NtSKOR1B* knockout inhibits K^+ efflux in root and leaf tissues of tobacco seedlings under salt stress, thereby maintaining higher K^+/Na^+ ratios within the cells. Thus, our study identifies *NtSKOR1B* as a negative regulator of salt tolerance in tobacco seedlings.

KEYWORDS

tobacco, Shaker K+ channel, SKOR1B, salt stress, K+/Na+ ratio

1 Introduction

Saline soils are widespread globally, with excessive exchangeable Na^+ being the main factor that impairs crop growth and development. Salinization is typically measured by electrical conductivity (dS/m), with levels above 8 dS/m classified as moderately saline (Zaman et al., 2018). The escalating severity of soil salinization contributes to substantial losses in global agricultural production. An estimated 20% of arable land and about 33% of irrigated land globally are affected by salt stress (Meena et al., 2021). According to the Food and Agriculture Organization (FAO), under moderate salinization conditions, with soil salinity ranging from 8 to 10 dS/m, yields of maize, wheat, and cotton are reduced by 55%, 28%, and 15%, respectively (Zaman et al., 2018). Developing crop varieties adapted to saline soil conditions is a key strategy in combating soil salinization (Zörb et al., 2018).

In soils with high salinity levels, crops simultaneously experience osmotic and ionic stress (Pantha and Dassanayake, 2020; Zhao et al., 2020). Initially, higher salinity levels increase soil osmotic pressure, hindering water uptake by plant roots (Kaur and Nayyar, 2015). Additionally, excessive Na^+ cause ionic toxicity, disrupting cellular metabolism. This disruption triggers reactive oxygen species production, leading to lipid peroxidation in cell membranes or membrane proteins. Such damage impairs the structural and functional integrity of the cell membrane, ultimately restricting plant growth and, in severe cases, resulting in plant death (Miller et al., 2010). Additionally, the excessive presence of Na^+ and Cl^- inhibits the plant's ability to absorb essential nutrients such as K^+, Ca^{2+}, Mg^{2+}, and HPO_4^{2-}, leading to nutrient deficiencies in crops (Isayenkov and Maathuis, 2019).

Throughout evolution, plants have developed various mechanisms to adapt to increased salt stress. Plants can reduce Na^+ uptake through selective root absorption or sequester excess Na^+ in central vacuoles of cells in roots, stem bases, nodes, leaf sheaths, and older leaves (Hossain et al., 2017; Shi, 2023). Furthermore, plants maintain intracellular ionic balance by actively absorbing ions such as K^+ from their surroundings or synthesizing organic osmolytes for osmotic regulation. (Hasegawa, 2013). Additionally, plants achieve cellular ionic homeostasis by exchanging Na^+, K^+ and H^+, a process facilitated by specialized transport proteins, including High Affinity K^+ Transporters (HKTs) and Sodium/Proton Antiporters (NHXs) (Hauser and Horie, 2010; Han et al., 2018); Keeping a stable K^+/Na^+ ratio in cells is a crucial strategy for plant salt tolerance (Cuin et al., 2008; Zörb et al., 2018). Studies have shown that salt-tolerant barley and alfalfa cultivars consistently maintain a higher K^+/Na^+ ratio in their root systems (Chen et al., 2007; Smethurst et al., 2008). Additionally, salt-tolerant barley and wheat cultivars show reduced K^+ efflux under saline conditions, resulting in a higher K^+/Na^+ ratio (Wu et al., 2013, 2014). Therefore, a stable K^+/Na^+ ratio is a significant indicator of plant salt tolerance.

Identifying negative regulatory genes associated with salt tolerance is crucial for deciphering the mechanisms of plant responses to salt stress, and has emerged as a focal point of recent research. Transcription factors serve as central regulators and molecular switches within the intricate networks of salt stress signal transduction. The overexpression of the zinc finger transcription factor *MtZPT2-2* diminishes salt tolerance in Medicago truncatula. This factor can directly bind to the promoters of high-affinity potassium transporters *MtHKT1;1* and *MtHKT1;2*, inhibiting their expression, leading to Na^+ imbalance and reduced activity of antioxidant enzymes (Huang et al., 2024). *CONSTANS* (CO), a pivotal transcription factor in the flowering pathway, adversely affects salt tolerance in Arabidopsis. Mutants with a loss of CO function exhibit enhanced salt tolerance compared to wild-type plants (Du et al., 2023). Protein phosphorylation, mediated by kinases, is crucial in the signal transduction pathways responding to salt stress. In rice, the transcription factor *OsWRKY53* acts as a negative regulator, controlling the expression of the *OsMKK10.2* kinase, impacting root Na^+ balance, and inhibiting the sodium transporter *OsHKT1;5*, thereby orchestrating the defense mechanisms against ion stress (Yu et al., 2023). Silencing the calmodulin gene *HvCAM1* in barley through RNAi enhances the plant's salt tolerance. Overexpressing *TaCIPK25* (Cbl Interacting Protein Kinases) in wheat increases Na^+ sensitivity, disrupts root cell Na^+/H^+ exchange, and results in excessive Na^+ accumulation. Additionally, certain proteins directly exert negative regulatory functions in relation to salt stress. Transgenic apple calli overexpressing *MdGRF6* displayed heightened sensitivity to salt stress, whereas *MdGRF6*-RNAi transgenic calli demonstrated increased salt tolerance (Jin et al., 2016). These investigations uncover the intricate mechanisms of plant response to salt stress, highlighting the critical role of negative regulators in modulating salt tolerance.

Shaker K^+ channels play a crucial role in K^+ absorption, transport, and the regulation of intracellular K^+ balance in plants (Véry et al., 2014). Numerous studies have demonstrated that Shaker potassium channels regulate plant salt tolerance through the modulation of the K^+/Na^+ ratio. Recent research indicates that the soybean Shaker inward rectifier potassium channel gene *GmAKT1* is significantly upregulated under salt stress conditions. Overexpressing *GmAKT1* in yeast and Arabidopsis akt1 mutants compensates for their low K^+ condition deficits. Under salt stress, transgenic Arabidopsis and soybean plants overexpressing *GmAKT1* exhibit improved growth, increased K^+ concentration, decreased Na^+ concentration, and a reduced Na^+/K^+ ratio. Further analysis revealed that *GmAKT1* overexpression significantly boosts the expression of genes involved in plasma membrane absorption and transport such as *GmsSOS1*, *GmHKT1*, and *GmNHX1*, enhancing K^+ uptake, facilitating Na^+ exclusion, maintaining intracellular ion equilibrium, and augmenting salt tolerance (Wang et al., 2021). The rice Shaker outward rectifier potassium channel homolog gene *OsK5.2* regulates stomatal closure in leaf guard cells, reducing water transpiration and Na^+ transport to leaves, and enhances K^+ secretion into the xylem sap in roots, thus maintaining and enhancing K^+ transport under salt stress conditions. The *OsK5.2* knockout mutant exhibited increased sensitivity to salt stress, further affirming *OsK5.2*'s critical role in regulating rice salt tolerance (Zhou et al., 2022). Previous research has indicated that Shaker potassium channels are involved in salt stress response through their impact on K^+/Na^+ balance. However, specific members that act as negative regulators of salt tolerance have yet to be identified.

Tobacco, a classic model crop, has had its genome fully sequenced (Sierro et al., 2014). However, studies focusing on the functionality of the Shaker K^+ channel family in tobacco, particularly in relation to resistance to salt stress, are limited. This

study delineates the genome-wide identification of the Shaker K^+ channels in tobacco, examining its members, conserved domains, and promoter elements to establish a groundwork for subsequent investigations into the gene family's potential biological functions within tobacco. Transcriptome data revealed a gene upregulated by salt stress, and gene editing technology confirmed its role in negatively regulating tobacco's salt tolerance. This enhances our comprehension of plants' response mechanisms to salt stress through the regulation of K^+/Na^+. By elucidating this protein's role in K^+ and Na^+ regulation, this research not only identifies a potential target for enhancing crop salt tolerance but also offers a viable approach for the holistic use of saline soils.

2 Materials and methods

2.1 Identification of Shaker K^+ channel family genes in tobacco

Protein sequences for the nine *Arabidopsis thaliana* Shaker family members were obtained from the TAIR database (https://www.arabidopsis.org/).These sequences were then used as queries for a subsequent BLAST search in the NCBI database (https://www.ncbi.nlm.nih.gov/) to identify Shaker K^+ channel family in tobacco (*N. tabacum*), using an E-value threshold of $1e^{-5}$. Redundant sequences were manually removed. The redundant entries caused by alternative splicing were removed manually, and the identified sequences were then used as new queries to do a second BLASTP search. The sequences without Shaker K^+ channel family-specific motifs were removed after sequence alignment and SMART analysis (http://smart.embl-heidelberg.de/). The molecular weight, isoelectric point, and amino acid number of proteins were calculated with the ExPASy tool (https://web.expasy.org/protparam/).

2.2 Analysis of protein sequences and promoter elements of tobacco Shaker K^+ channel family

A phylogenetic tree of Shaker K^+ channel family members from *N. tabacum*, *Arabidopsis thaliana* and *Oryza sativa* was constructed using the Neighbor-Joining method in MEGA6, under the default parameters (bootstrap replicates=1000) (Tamura et al., 2013). Multi-sequence alignment was performed using Clustal Omega (https://www.ebi.ac.uk/Tools/msa/clustalo/) and the result was presented by GeneDoc (Nicholas, 1997). InterPro (https://www.ebi.ac.uk/) was utilized for conserved domain analysis, with findings visualized in Microsoft PowerPoint. To find cis-acting elements localized in the promoter region of Shaker K^+ channel family genes, 3000 bp of promoter regions upstream of the 5'-UTR of Shaker K^+ channel family genes were queried. The cis-acting elements were predicted by PlantCARE (http://bioinformatics.psb.ugent.be/webtools/plantcare/html/) (Rombauts et al., 1999) and presented with a heatmap by Tbtools (Chen et al., 2020).

2.3 Tobacco plant cultivation, salt stress treatment, and sampling

This study used the tobacco variety Zhongyan 100 (*N. tabacum*), grown in a greenhouse under controlled conditions: 16 hours of light and 8 hours of darkness, at temperatures of 23-25°C and 70% relative humidity. Initially, tobacco seeds were sown in soil. After 20 days of germination, seedlings were transplanted onto floating rafts for hydroponic cultivation in a 1/2 Hoagland nutrient solution. Following a 6-day acclimatization period, salt treatment was administered (1/2 Hoagland solution with 100 mM NaCl), while controls received the 1/2 Hoagland solution alone. Nutrient solutions were refreshed every three days.

For the *NtSKOR1B* RT-qPCR analysis, root, stem, and leaf samples were collected at specific intervals: immediately (0 h), 6 h, 12 h, 30 h, 60 h, and 6 days following a 6-day hydroponic culture period with salt treatment (100 mM NaCl). The samples were immediately flash-frozen in liquid nitrogen and then stored at -80°C.

GUS staining experiments began with the sowing of *NtSKOR1B* promoter plants (*ProNtSKOR1B::GUS*). Following 20 days of germination and a 6-day hydroponic culture period, samples of roots, stems, and leaves were collected at designated intervals: immediately (0 h), 12 h, and 30 h after salt treatment exposure. GUS staining was then conducted using β-Galactosidase Reporter Gene Staining Ki (Beijing Leagene Biotech. Co., Ltd., Cat No./ID: DP0013, Beijing, China), with observations made post-staining.

Sampling to measure physiological indicators: Following a 6-day adaptation to hydroculture, tobacco seedlings are subjected to salt stress (1/2 Hoagland nutrient solution with 100 mM NaCl), while the control group receives only 1/2 Hoagland nutrient solution. Young tobacco plants were harvested on the 11th day post-salt stress treatment for the measurement of the following indicators. Plants from various strains and treatments were selected, focusing on the fourth leaf position (the first mature leaf post-salt treatment) to assess leaf length and width, followed by curing the entire plant at 105°C for 30 minutes and drying at 80°C until a constant weight was achieved. Biomass was weighed, n=6. Measurement of ion content: Leaves and roots were separated. Root samples were initially rinsed with ddH2O and subsequently dried with absorbent paper to eliminate external ions. Fresh samples were dried at 105°C until reaching a stable weight, followed by grinding the dried tissue into powder. Approximately 0.01 g of dry sample was placed into a test tube, to which 8 mL of 0.5 M HCl was added, and the mixture was extracted at 20°C and 150 rpm for 30 minutes. Subsequently, the mixture was filtered and adjusted to the extraction volume for testing. A standard K^+ solution was prepared using 0.5 M HCl, and a flame spectrophotometer (6400A) was employed to quantify the ion content, n=3. Formula for calculating potassium content:

$$K^+(\mu g/mg\ DW) = ((A/M)\text{Dilution factor} * 0.001)/m$$

A: Concentration calculated from readings based on standard curve; M: Relative molecular mass of K^+; V: Reading volume; m: Dry weight of sample.

2.4 RT-qPCR

Total RNA was isolated from tissues of young tobacco plants and purified with the RNeasy Plus Mini Kit (Qiagen, Cat No./ID: 74134) following the manufacturer's protocol. The RT-qPCR program was described in (Mao et al., 2021). RNA was reverse transcribed into cDNA using Evo M-MLV Mix Kit with gDNA Clean for qPCR (Accurate Biotechnology (Hunan) Co., Ltd, Cat No./ID: AG11728, Changsha, China) and the cDNA was amplified using SYBR Green Pro Taq HS qPCR Premix (Accurate Biotechnology (Hunan) Co., Ltd, Cat No./ID: AG11701, Changsha, China) on the LightCycler® 96 Instrument (F. Hoffmann-La Roche Ltd, Switzerland). All the primers used for RT-qPCR are listed in Supplementary Table 1. The amplification reactions were performed in a total volume of 10 µl, containing 5 µl 2×SYBR Green Pro Taq HS qPCR Premix, 0.6 µl forward and reverse primers (10 µM), 1 µl cDNA (10 times diluted), and 3.4 µl ddH2O. The RT-qPCR amplification program was as follows: 95oC for 10 min; 95oC for 10 s, 60oC for 30 s and amplification for 40 cycles. Analysis of the relative gene expression data was conducted using the $2^{-\Delta C't}$ method (Mao et al., 2021).

2.5 Construction and identification of *NtSKOR1B* knockout mutants

Specific primers, *NtSKOR1B*-1F and *NtSKOR1B*-1R, were designed from the LOC104103384 gene sequence for PCR amplification, using *N. tabacum* L. cDNA to obtain the *NtSKOR1B* sequence. The knockout site within the *NtSKOR1B* sequence was identified, leading to the design of knockout primers *NtSKOR1B*-Crispr-58F and *NtSKOR1B*-Crispr-58R for constructing the pORE-Cas9/gRNA-*NTSKOR1B* gene knockout vector. The pORE-Cas9/gRNA-*NtSKOR1B* construct was introduced into Zhongyan 100 using the Agrobacterium-mediated leaf disk method, generating T0 transgenic mutants. Plants were initially screened for various editing outcomes using primers *NTSKOR1B*-Crispr-9734F and *NtSKOR1B*-Crispr-10293R. Nine C1 generation lines were cultivated, and DNA from homozygous mutants was extracted for PCR amplification and sequencing with specific primers *NtSKOR1B*-Crispr-9734F and *NtSKOR1B*-Crispr-10293R. This led to the identification of two homozygous knockout lines, characterized by distinct edits: C2 with a T insertion at position 911, and C6 with an 11-base deletion starting at position 989, causing translational termination (Supplementary Figure 1).

2.6 Construction and identification of *ProNtSKOR1B::GUS* transgenic lines

Genomic DNA from plants was extracted using the CTAB method, and the *NtSKOR1B* promoter sequence upstream of the ATG start codon for LOC104103384 was obtained through PCR amplification with primers *NtSKOR1B*pro-1F and *NtSKOR1B*pro-1R. This yielded a 2439 bp *NtSKOR1B* promoter sequence, which was then cloned into the plasmid pMD19-T-*NtSKOR1B*pro and confirmed by sequencing. Using the plasmid pMD19-T-*NtSKOR1B*pro as a template and primers *NtSKOR1B*pro-2F and *NtSKOR1B*pro-2R for amplification, the binary vector pBI101-*NtSKOR1B*pro was obtained, which drives the GUS gene under the *NtSKOR1B* promoter's control. The Agrobacterium-mediated leaf disk method was employed for transforming this vector into tobacco plants, generating T0 transgenic lines. The T0 generation lines was confirmed positive (Supplementary Figure 2), using the identification primers *NtSKOR1B*pro-3F and *NtSKOR1B*pro-1R. Harvest T0 generation seeds from positive plants and sow them on 1/2 MS plates with 50 mg/L kanamycin sulfate. Following resistance screening, strictly self-cross lines displaying a 3:1 resistance ratio, selecting for resistant lines. Staining was performed on T1 generation homozygous plants.

2.7 Statistical analysis

Statistical analysis was done using IBM SPSS Statistics 23 software. Significant differences were examined by one-way ANOVA using the LSD test at $p<0.05$ and $p<0.01$. The figures were drawn by GraphPad Prism 6.0.

3 Result analysis

3.1 Genome-wide identification and phylogenetic analysis of Shaker K^+ channel family in *N. tabacum*

Genomic screening identified 20 members of the *N. tabacum* L. Shaker K^+ channel family using NCBI and SMART tools. Members were systematically numbered according to their similarity to *Arabidopsis thaliana* Shaker K^+ channel family counterparts (Figure 1, Table 1). Ten Shaker K^+ family members were attributed to the maternal ancestor, *Nicotiana sylvestris*, and labeled with the suffix "A", while the remaining ten were derived from the paternal ancestor, *Nicotiana tomentosiformis*, and marked with "B". The K^+ channel proteins varied in length from 598 to 892 amino acids, with molecular weights ranging from 69.5 to 100.5 kDa.

To construct a phylogenetic tree (Figure 1A), members were selected from the Shaker K^+ channel families in *Arabidopsis thaliana*, *Oryza sativa*, and *N. tabacum*. The results showed that, like the other two species, *N. tabacum* Shaker K^+ channel family were categorized into five groups.

In 2007, at a time when tobacco genome data were not yet available, Toshio Sano's team utilized Degenerate PCR and RACE technology to clone four members of the Shaker K^+ channels from the BY-2 cell line. These channels were designated as *NKT1*, *NKT2*, *NtKC1*, and *NTORK1*, respectively (Sano et al., 2007). To avoid potential confusion and align with Arabidopsis nomenclature conventions, this study renamed these four genes *NKT2B*, *NKT6B*, *NKC1B*, and *NtGORKA*. All members of the tobacco Shaker K^+ channel families possess the signature sequence TXXTXGYG, characteristic of selective K^+ channels. (Figure 1B).

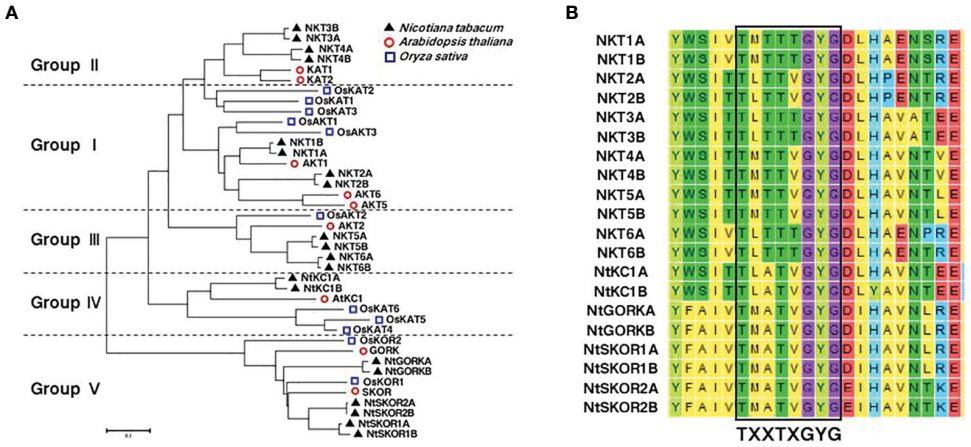

FIGURE 1
Evolutionary tree analysis and signature sequence alignment of Shaker family members in *Arabidopsis thaliana*, *Oryza sativa*, and *N. tabacum*. **(A)** Phylogenetic Analysis of *N. tabacum*, *Arabidopsis thaliana* and *Oryza sativa* Shaker K^+ channels: Amino acid sequences for *Arabidopsis thaliana* and *Oryza sativa* were sourced from TAIR (https://www.arabidopsis.org/), NCBI (https://www.ncbi.nlm.nih.gov/), and Sol Genomics Network (https://solgenomics.net/) respectively. The phylogenetic tree was generated using MEGA6 through the Neighbor-Joining method. **(B)** The black box highlights the characteristic signature sequence TXXTXGYG, a hallmark of selective K^+ channels.

3.2 Analysis of the conserved domains in the members of *N. tabacum* Shaker K^+ channel family

InterPro analysis predicted six conserved domains in *N. tabacum*. Shaker K^+ channel family members: K^+ channel KAT/AKT domain, Ion transport domain, Cyclic nucleotide-binding domain, KHA domain, Ankyrin repeat domain, and voltage-dependent K^+ channel EAG/ELK/ERG domain (Figure 2). The K^+ channel KAT/AKT domain, present in all *N. tabacum* L. Shaker proteins, is the most fundamental conserved domain. The Ion transport domain plays a crucial role in regulating K^+ transmembrane transport. The Cyclic nucleotide-binding and KHA domains are essential for channel function regulation, whereas the Ankyrin repeat domain primarily mediates protein-protein interactions. The voltage-dependent K^+ channel EAG/ELK/ERG domain senses voltage changes across the cell membrane.

TABLE 1 Fundamental characteristics of Shaker K^+ channel family in *N. tabacum*.

New Name	Diploid Progenitors	Classification	The Name/ID of Arabidopsis based on NCBI	Representative Protein Accession or Previous Name	Gene ID in NCBI	AA	*pI*	MW (Da)
NKT1A	*N. sylvestris*	Group I	AKT1/817206	XP_009772048.1	LOC104222515	893	6.54	100508.19
NKT1B	*N. tomentosiformis*	Group I		XP_009619489.1	LOC104111487	892	7.06	100290.93
NKT2A	*N. sylvestris*	Group I	AKT6/817099	XP_009799565.1	LOC104245633	881	6.56	99362.20
NKT2B	*N. tomentosiformis*	Group I		XP_009621376.1 (NKT1)	LOC104113012	879	6.64	98765.52
NKT3A	*N. sylvestris*	Group II	KAT1/834666	XP_009804747.1	LOC104249919	682	6.77	78146.90
NKT3B	*N. tomentosiformis*	Group II		XP_009602722.1	LOC104097809	681	7.19	77910.82
NKT4A	*N. sylvestris*	Group II	KAT2/827555	XP_009760491.1	LOC104212831	713	5.96	82266.82
NKT4B	*N. tomentosiformis*	Group II		XP_009616640.1	LOC104212831	709	5.96	81884.84
NKT5A	*N. sylvestris*	Group III	AKT2/828311	XP_009795716.1	LOC104242371	864	6.71	99138.50
NKT5B	*N. tomentosiformis*	Group III		XP_009616703.1	LOC104109179	847	6.71	97218.22
NKT6A	*N. sylvestris*	Group III		XP_009791067.1	LOC104238419	837	7.33	95932.75

(Continued)

10.3389/fpls.2024.1378738

TABLE 1 Continued

New Name	Diploid Progenitors	Classification	The Name/ID of Arabidopsis based on NCBI	Representative Protein Accession or Previous Name	Gene ID in NCBI	AA	*pI*	MW (Da)
NKT6B	*N. tomentosiformis*	Group III		XP_009614130.1 (NKT2)	LOC104107110	824	6.71	94602.29
NtKC1A	*N. sylvestris*	Group IV	AtKC1/829400	XP_009801140.1	LOC104246930	641	7.29	73061.33
NtKC1B	*N. tomentosiformis*	Group IV		XP_018628621.1 (NtKC1)	LOC104103008	642	6.99	73381.65
NtGORKA	*N. sylvestris*	Group V	GORK/833728	XP_009771768.1 (TORK1)	LOC104222255	834	6.56	95114.16
NtGORKB	*N. tomentosiformis*	Group V		XP_009597240.1	LOC104093217	598	7.53	69487.16
NtSKOR1A	*N. sylvestris*	Group V	SKOR/821052	XP_009762658.1	LOC104214657	827	6.52	94792.21
NtSKOR1B	*N. tomentosiformis*	Group V		XP_009609577.1	LOC104103384	827	6.64	94970.55
NtSKOR2A	*N. sylvestris*	Group V		XP_009802068.1	LOC104247691	821	6.45	94205.60
NtSKOR2B	*N. tomentosiformis*	Group V		XP_009626879.1	LOC104117520	810	6.55	92899.10

In Groups I, III, and V, 13 out of 14 members possess all six conserved domains mentioned, whereas Groups II and IV lack the Ankyrin repeat domain. The count of voltage-dependent K^+ channel EAG/ELK/ERG domains varies among subgroups, with six in Group I, five in Groups II, III, and V, and six in Group IV. Variations in types, lengths, and numbers of conserved domains likely affect the proteins' response functions.

3.3 Analysis of promoter elements in *N. tabacum* Shaker K^+ channel family members

To elucidate the potential functions and regulatory mechanisms of Shaker K^+ channels in *N. tabacum*, we analyzed the cis-acting elements in promoter sequences (3000 bp upstream of the ATG

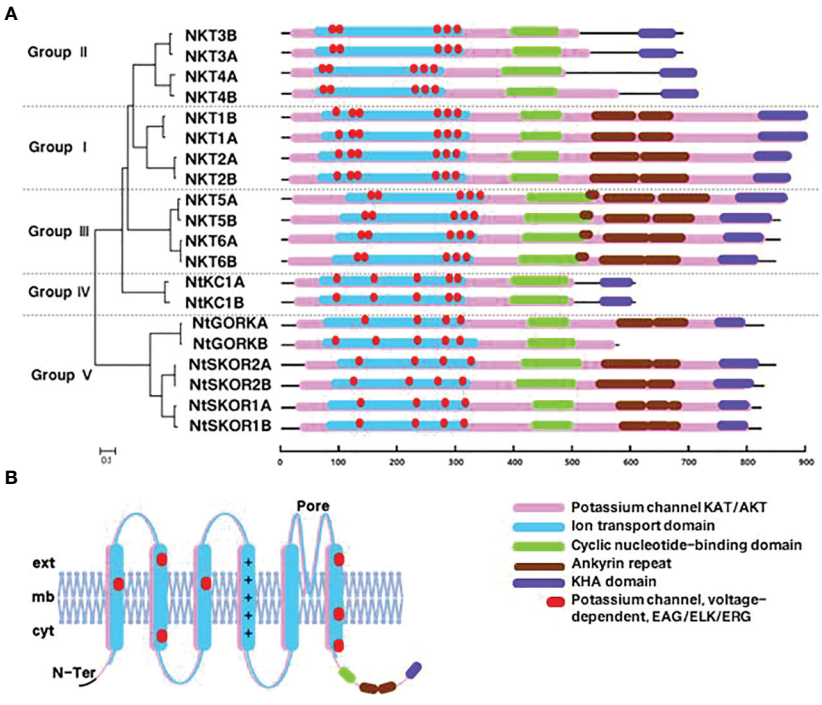

FIGURE 2
Analysis of the conserved domains in the members of *N. tabacum* Shaker K^+ channel family. **(A)** Conserved domains analysis. **(B)** Using *NKT1B* as an example, this panel presents a schematic of the simulated transmembrane structure of a Shaker family protein. Here, "ext" represents the extracellular region, "mb" the cell membrane, "cyt" the intracellular region, and "N-ter" the N-terminal beginning of the protein.

start codon) of 20 Shaker K^+ channel family using PlantCARE software. Analysis revealed that Shaker K^+ channel promoters predominantly contain cis-acting elements associated with three major biological processes: abiotic stress response, plant hormone response, and growth and development. Specifically, there are 10 types of elements each for abiotic stress and plant hormones, and 6 for growth and development. (Figure 3) This indicates that the Shaker K^+ channel family significantly influences tobacco's response to abiotic stress, hormone regulation, and growth and development processes.

Abiotic stress response elements are the most abundant in the promoter regions of *N. tabacum* Shaker K^+ channel genes, comprising 31.58%-71.93% of all identified elements. MYB and MYC elements represent 40% and 19% of stress response elements, respectively. The antioxidant response element (ARE) was found in 19 Shaker members, making up 9% of stress elements. The drought response element (MBS) was present in 17 members (5%), and the W-box, linked to K^+ uptake and signal transduction, was found in 16 members (6%). Phytohormone response elements constituted 10.53%-38.60% of elements. The ABA response element (ABRE) was identified in 19 Shaker members, comprising 27% of stress elements. Elements related to growth and development accounted for 5.26%-21.05% of the total, with all members containing the light-responsive element (Box 4), comprising 64% of these elements.

3.4 Transcriptomic analysis of *N. tabacum* Shaker K^+ channel family members under salt treatment in roots

In a prior study, we performed transcriptomic analysis on the roots of N. tabacum variety Zhongyan 100 under 100 mM NaCl salt treatment (Mao et al., 2021). Leveraging this dataset, the current study explores the gene expression variations across the tobacco Shaker family members. The findings indicate elevated expression levels of Group I members *NKT1A* and *NKT1B* in the roots of tobacco seedlings, in contrast to the lower expression levels of *NKT2A* and *NKT2B*. Similarly, Group II members *NKT3A*, *NKT3B*, *NKT4A*, and *NKT4B* displayed low expression levels. Group III analysis showed low expression levels for *NKT5A* and *NKT5B*, with slightly higher levels for *NKT6A* and *NKT6B*. Notably, Group IV members *NtKC1A* and *NtKC1B*, along with Group V members *NtSKOR1A*, *NtSKOR1B*, *NtSKOR2A*, *NtSKOR2B* and *NtGORKA*, exhibited higher expression levels, while *NtGORKB* was comparatively lower. Post-salt stress treatment comparison revealed that the expression levels of Group V outward rectifying potassium channel members *NtSKOR1A* and *NtSKOR1B* were significantly increased due to salt stress. This suggests a potential involvement of these two genes in the ion transport process under salt treatment conditions. Specifically, *NtSKOR1A* and *NtSKOR1B* were up-regulated by 1.31 and 3.18 times, respectively, compared to

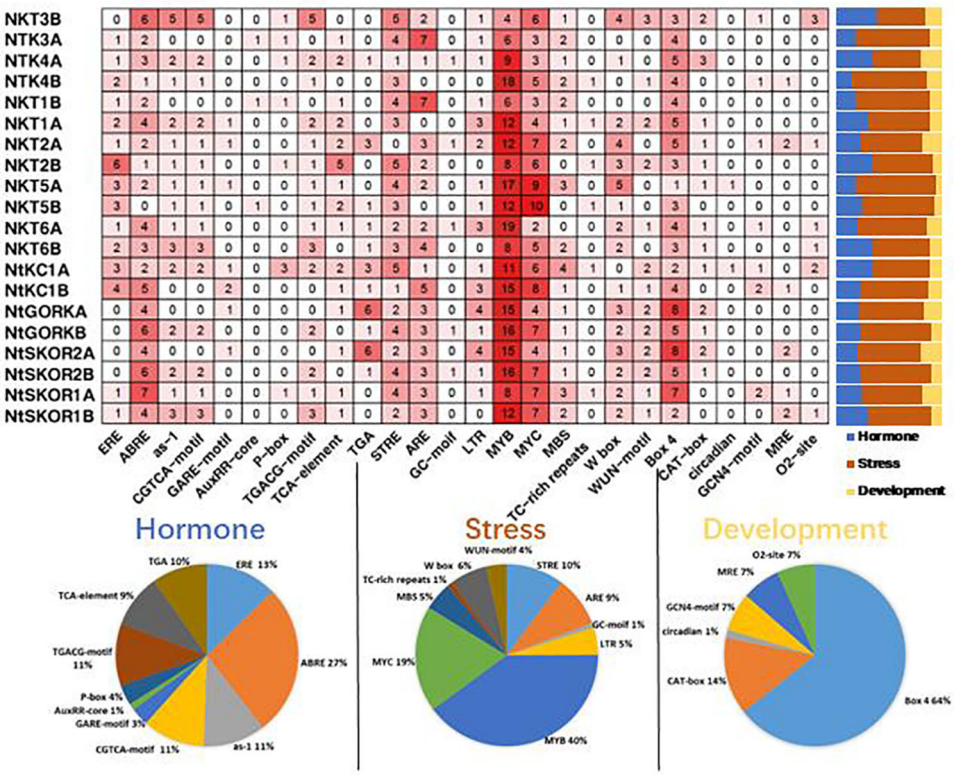

FIGURE 3
Analysis of promoter elements in *N. tabacum* Shaker K^+ channel family members. The bar graph shows the proportion of elements related to hormone response (blue), stress response (orange), and growth and development (yellow) in the total number of elements in the promoter region of each member; the pie chart shows the proportion of a specific element in the total number of elements related to hormone response (blue), stress response (orange), and growth and development (yellow).

pre-treatment levels. Given the higher expression increase of *NtSKOR1B* compared to *NtSKOR1A*, it is posited that *NtSKOR1B* may play a more significant role in this process (Figure 4).

3.5 Expression pattern analysis of *NtSKOR1B* in *N. tabacum* under salt treatment

To further investigate *NtSKOR1B* expression changes under salt stress, RT-qPCR was conducted. Results indicated a significant upregulation of *NtSKOR1B* expression in roots with prolonged salt exposure, reaching 9.98-fold after 30 hours compared to the initial level. While *NtSKOR1B* expression in stems and leaves was lower than in roots, it also exhibited a gradual increase over the duration of salt treatment (Figure 5A).

A homozygous Zhongyan 100 transgenic line, with the *NtSKOR1B* promoter fused to the GUS reporter gene, was then developed. GUS histochemical staining for the *NtSKOR1B* promoter was consistent with the RT-qPCR findings. GUS staining revealed negligible activity in tobacco seedlings without salt treatment (Figures 5B–D). However, GUS activity emerged in the roots, stems, and leaf veins, becoming pronounced after 12 hours and intensifying after 30 hours of salt treatment. This indicates that under standard cultivation conditions, *NtSKOR1B* expression in tobacco seedlings is minimal. Following salt exposure, expression markedly rises in the root cortex, stems, and leaf veins' vascular tissues, escalating with prolonged treatment (Figures 5E–H).

3.6 Phenotypic analysis of *NtSKOR1B* knockout mutants under salt treatment

To elucidate *NtSKOR1B*'s function under salt stress, two distinct homozygous knockout lines with varied editing methods were exposed to salt treatment (see Materials and Methods for construction and editing details). Under salt stress, *NtSKOR1B* knockout lines demonstrated higher biomass, increased leaf length, and greater leaf width than wild types, with enhancements of 34.06%-39.24%, 15.87%-21.63%, and 14.89%-17.02%, respectively (Figures 6A–D). Knockout of *NTSKOR1B* led to increased K^+ levels in both leaf and root tissues of tobacco seedlings over wild type, showing increases of 22.64%-25.47% and 18.06%-21.02%, with significant differences in aerial tissues (Figures 6E, H). Furthermore, *NTSKOR1B* knockout reduced Na^+ levels in both leaf and root tissues compared to wild types, with reductions of 9.83%-11.48% and 7.52%-7.95%, notably in aerial tissues (Figures 6F, I). The *NtSKOR1B* knockout mutants markedly increased the plant's K^+/Na^+ ratio (Figures 6G, J). Under control conditions, no significant differences were observed in these physiological indicators or ion levels (Figures 6A–J).

4 Discussion

Initially, genetic research concentrated on leveraging positive regulatory genes and transgenic technology to elucidate gene-mediated biological process control and its applications in agriculture and related sectors. The advent of CRISPR gene editing technology has redirected research emphasis towards more precise and efficient gene modification techniques, particularly for enhancing crop stress resistance. Recently, negative regulatory genes, or genes exerting inhibitory effects, have emerged as focal points in research aimed at bolstering crop resistance to stress. Investigating these genes is pivotal for pinpointing critical factors that enhance crop survival in harsh conditions, underpinning sustainable agricultural development. Using tobacco as a case study, this research initially pinpointed a negative regulatory gene impacting salt stress resistance. Under salt stress conditions, this gene's expression can lower the potassium-to-sodium ratio, diminish plant biomass, and weaken salt stress resistance. This suggests that CRISPR-mediated gene editing could markedly enhance crop salt stress tolerance, offering fresh strategies and targets for agricultural enhancement. This discovery not only enriches our comprehension of plant responses to salt stress mechanisms but also underscores the potential of gene editing technology in advancing agricultural science.

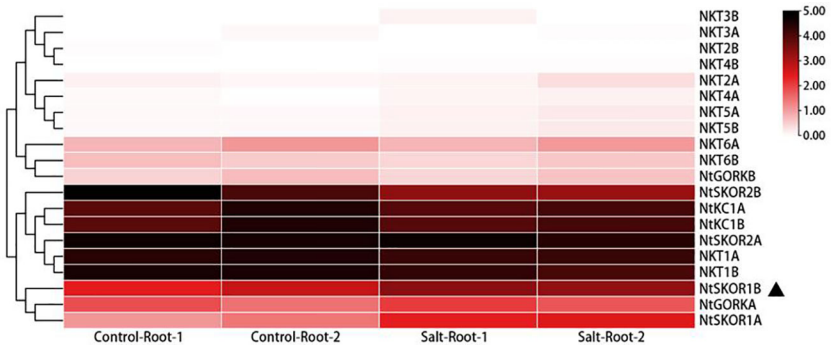

FIGURE 4
Differential expression of *N. tabacum* Shaker K^+ channel family members in roots subjected to salt stress. "1" signifies Experiment 1, "2" denotes Experiment 2. "Control" refers to the normal treatment condition, wherein tobacco seedlings were irrigated with 1/2 Hoagland nutrient solution. "Salt" describes the salt stress treatment condition, which involves supplementing the 1/2 Hoagland nutrient solution with 100 mM NaCl. "Root" indicates that the sampling site for these experiments was the root of the tobacco seedlings.

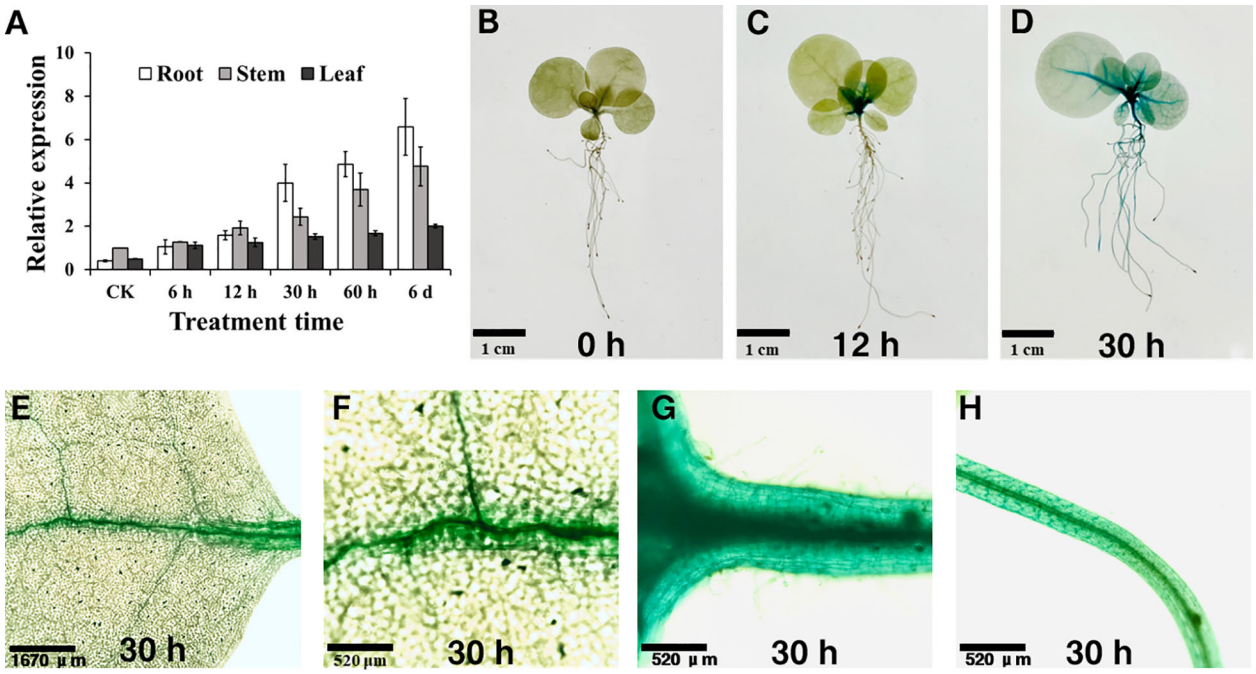

FIGURE 5
NtSKOR1B expression analysis in *N. tabacum* under salt treatment. **(A)** RT-qPCR Analysis of *NtSKOR1B* Gene Expression in Tobacco Seedlings Under Salt Stress. **(B–D)** Time-course GUS Staining in Leaves, Veins, Stems, and Roots at 0h, 12h, and 30h Post-Salt Treatment. **(E–H)** GUS Staining of Leaves, Veins, Stems, and Roots 30h Post-Salt Treatment.

4.1 The *NtSKOR1B* gene displays diverse expression patterns and functions in different species, suggesting varied roles depending on its expression sites

Gene expression varies across species and tissues, reflecting gene regulation complexity and biological adaptive evolution (Hill et al., 2021). Current studies demonstrate that the outward rectifying K^+ channel SKOR is pivotal in regulating intracellular K^+ balance through mediating cytoplasmic K^+ efflux, significantly influencing plant responses to salt, drought, and nutritional stresses. The SKOR analogue, OsK5.2, part of the rice Shaker family, resides within the root vascular bundle. During salt stress, OsK5.2 expression boosts K^+ efflux from the root vascular bundle to the xylem, elevating plant K^+ levels and thus enhancing salt tolerance through an increased K^+/Na^+ ratio. Furthermore, OsK5.2's presence in guard cells amplifies K^+ efflux under salt stress, leading to stomatal closure, diminished water loss, and reduced salt buildup, which in turn decreases Na^+ transport to leaves(Nguyen et al., 2017). In summary, this potassium channel positively influences plant salt tolerance by ensuring a superior K^+/Na^+ balance(Zhou et al., 2022). The *NtSKOR1B* outward potassium channel, part of the tobacco Shaker family, is located in the root cortex and leaf vascular bundles. Under salt stress, plants activate K^+ channels in root cortex cells, leading to K^+ loss. Outward K^+ channels play a crucial role in this process (Wakeel, 2013; Demidchik, 2014). *NtSKOR1B* expression speeds up K^+ efflux, hindering K^+ level maintenance. K^+ primarily move from leaves to other plant parts via the phloem. *NtSKOR1B* is found in leaf vascular bundles, not in guard cells. Under salt stress, leaf vascular bundles accelerate K^+ loss. Analysis revealed that tobacco with *NtSKOR1B* knockout exhibited a higher K^+/Na^+ ratio and increased salt tolerance under salt stress (Figure 6). Analysis of expression sites (Figures 5E–H) shows *NtSKOR1B*'s abundant expression in the root cortex. Knocking out *NtSKOR1B* reduces K^+ efflux under salt stress. *NtSKOR1B*, also expressed in leaf veins and stem vascular bundles, reduces K^+ loss in leaves when knocked out. This collectively boosts the plant's K^+/Na^+ ratio and the salt tolerance of tobacco seedlings (Figure 7). This study revealed that NtSKOR1B is involved in the negative regulation of salt tolerance in tobacco seedlings, which lays the foundation for further investigation of the function of this gene in intracellular K^+ and Na^+ transport in plant wounding fluid and different leaf positions.

4.2 The Shaker K^+ channel member *NtSKOR1B* may be involved in a complex regulatory network

The complexity of gene product interactions and tissue-specific expression patterns, adapted to environmental and physiological demands, are crucial for biological evolution and functional diversity. Shaker K^+ channels, prevalent in plants, regulate the transmembrane transport of K^+, playing critical roles in stress response, growth, development, and electrical signal transmission. Arabidopsis *AKT1*, a classic example of a phosphorylation-regulated Shaker K^+ channel, is activated by CBL1/9-CIPK23 phosphorylation (Wang et al., 2016). Recent studies have elucidated this regulatory pathway further, revealing how plants modulate the plasma membrane CBL1/9-CIPK9/23-*AKT1* in response to external K^+ levels (Li et al., 2023). Gene expression involves intricate regulatory processes. This study

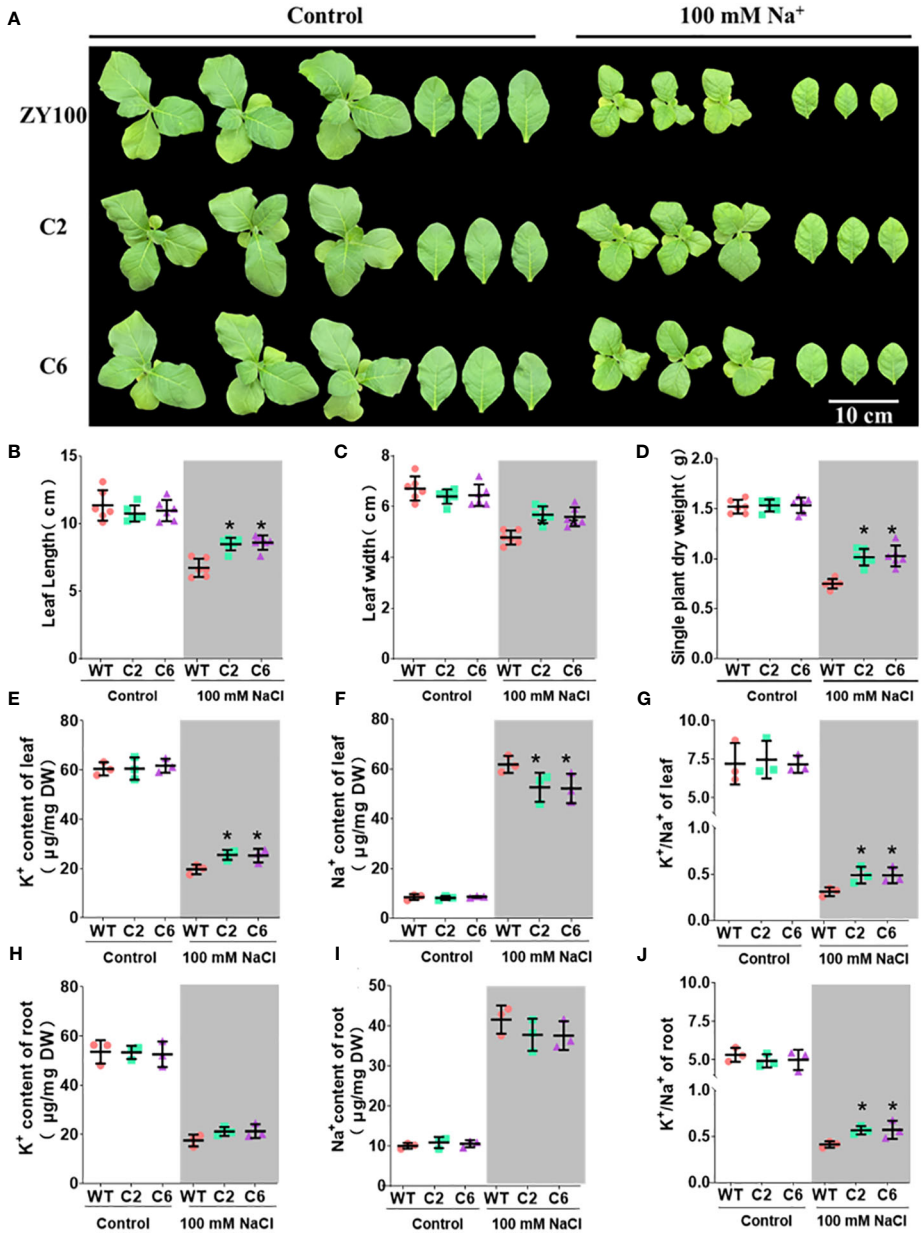

FIGURE 6
Phenotypic analysis of *NtSKOR1B* knockout mutants under Salt Stress. **(A)** Comparison of Wild-Type and *NtSKOR1B* Knockout mutants Phenotypes Under Control and Salt-Stress Conditions. **(B–J)** Changes in Leaf Length, Leaf Width, Biomass, Leaf and Root K^+ and Na^+ Contents, and K^+/Na^+ Ratios in Wild-Type and *NtSKOR1B* Knockout mutants Under Control and Salt Stress. "*" represents significant difference compared with wild type, ($p<0.05$).

revealed that *NTSKOR1B* negatively influences the salt tolerance of tobacco seedlings. Bioinformatics analysis identified conserved domains within this gene family related to voltage sensing, K^+ absorption, and the Ankyrin repeat domain for protein-protein interactions. Specifically, the Ankyrin repeat domain in Arabidopsis thaliana can interact with CIPK family proteins to regulate gene expression and respond to environmental stress (Sedgwick and Smerdon, 1999; Wei and Li, 2009). Furthermore, the promoter region is rich in elements tied to stress response, hormonal signals, and growth, such as MYB for drought, cold, and salt stress responses (Yang et al., 2012; Li et al., 2019; Wang et al., 2022), and the hormone response element ABRE (Gomez-Porras et al., 2007). These findings suggest that *NtSKOR1B* is regulated by a complex gene network, offering insights for further detailed exploration of its regulatory mechanisms through techniques such as transcriptome analysis and yeast two-hybrid assays.

4.3 *NtSKOR1B* may influence Na^+ absorption and transport in plants under salt stress by altering K^+ transport mechanisms

Under salt stress, excessive Na^+ competes with K^+ for plasma membrane uptake sites, inhibiting K^+ absorption and disrupting

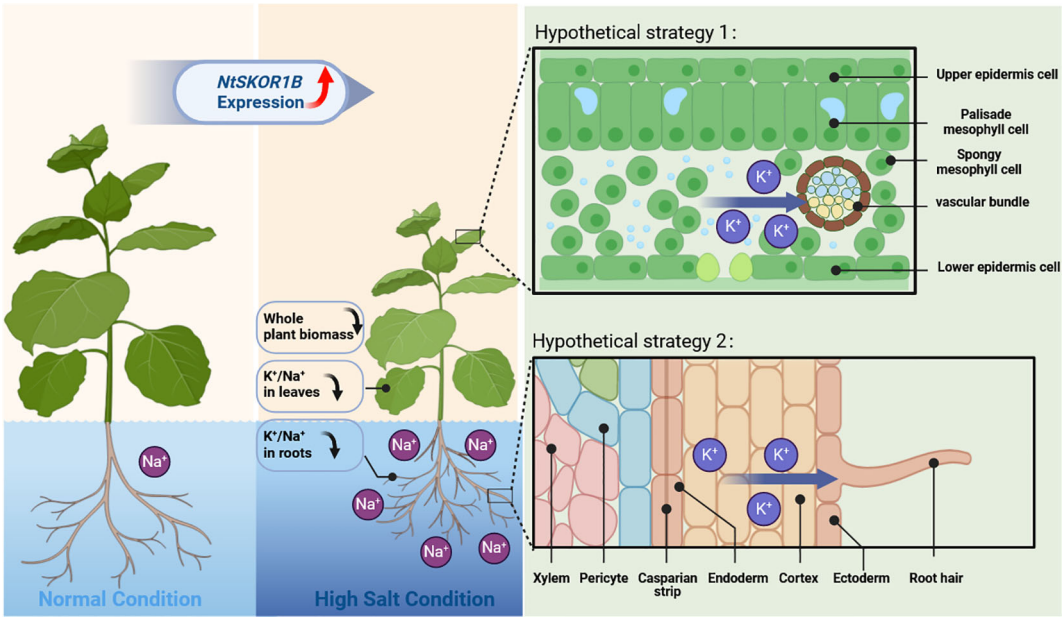

FIGURE 7
Schematic Representation of *NtSKOR1B* Gene Function in Response to Salt Treatment. The dark blue arrow indicates a decrease in value, while the red arrow shows the direction of K^+ movement.

plant tissue metabolism (Mulet et al., 2023). Excessive Na^+ influx leads to cell membrane depolarization, reducing the driving force for K^+ uptake. Consequently, plants in high salinity environments inevitably suffer from chronic K^+ deficiency. A stable K^+/Na^+ ratio is critical for salt tolerance (Horie et al., 2009; Ordonez et al., 2014). Thus, the regulation and distribution of K^+ are essential for balancing the ionic imbalance caused by Na^+. K^+ activates plasma membrane H^+-ATPase, crucial for cell functioning (Weng et al., 2020). Plasma membrane H^+-ATPase creates an electrochemical gradient, powering the Na^+/H^+ antiporter to exchange H^+ for Na^+, reducing Na^+'s toxic effects (Xie et al., 2022). This study revealed that *NtSKOR1B* knockout in *N. tabacum* L. seedlings under salt stress leads to increased K^+ and decreased Na^+ levels, solely at the ionic content level. Further research into Na^+ transporters, proton pump activities, and expression levels will enhance understanding of *NtSKOR1B*'s role in regulating the K^+- Na^+ relationship under salt stress.

4.4 Perspectives on the study of negatively regulated genes for salt tolerance

A comprehensive exploration of plant adaptation to salt stress, particularly via analyzing genes that negatively regulate salt tolerance, illuminates the molecular responses of plants to environmental stresses. In response to salt stress, these genes modulate gene expression, preserve ion equilibrium, boost osmoregulator synthesis, fortify antioxidant defenses, and activate distinct signaling pathways. These mechanisms enable plants to regulate ion uptake and distribution, synthesize protective molecules for osmotic balance, and augment antioxidant systems for cellular protection against oxidative stress. Furthermore, the activation of signal transduction pathways triggers a cascade of adaptive and defensive responses in plants. Such research not only enhances our comprehension of plant adaptation mechanisms to environmental stress but also lays the scientific groundwork for developing salt-tolerant crops, pivotal for agricultural productivity and ecological restoration.

Data availability statement

The original contributions presented in the study are included in the article/Supplementary Material, further inquiries can be directed to the corresponding author/s.

Author contributions

GY: Conceptualization, Data curation, Formal analysis, Investigation, Methodology, Software, Validation, Visualization, Writing – original draft, Writing – review & editing. TN: Conceptualization, Data curation, Formal analysis, Investigation, Methodology, Software, Validation, Visualization, Writing – original draft, Writing – review & editing. OH: Writing – review & editing. CS: Investigation, Writing – review & editing. XS: Investigation, Methodology, Writing – review & editing. FX: Investigation, Methodology, Writing – review & editing. YW: Methodology, Resources, Writing – review & editing. ZZ: Methodology, Resources, Writing – review & editing. YN: Methodology, Resources, Writing – review & editing. HL: Conceptualization, Funding acquisition, Methodology, Project administration, Resources, Supervision,

Writing – original draft, Writing – review & editing. QW: Conceptualization, Funding acquisition, Methodology, Project administration, Resources, Supervision, Writing – original draft, Writing – review & editing.

Funding

The author(s) declare financial support was received for the research, authorship, and/or publication of this article. This work was funded by the National Natural Science Foundation of China (32170387); the Agricultural Science and Technology Innovation Program (ASTIP-TRIC02); the Key Funding of CNTC (No. 110202101035(JY-12)), SDTI (No.202201020) and XZ-CTID.

Conflict of interest

Author YW is employed by China Tobacco Shandong Industrial.

The remaining authors declare that the research was conducted in the absence of any commercial or financial relationships that could be construed as a potential conflict of interest.

Publisher's note

Supplementary material

The Supplementary Material for this article can be found online at: https://www.frontiersin.org/articles/10.3389/fpls.2024.1378738/full#supplementary-material

References

Chen, C., Chen, H., Zhang, Y., Thomas, H. R., Frank, M. H., He, Y., et al. (2020). TBtools: an integrative toolkit developed for interactive analyses of big biological data. *Mol. Plant* 13, 1194–1202. doi: 10.1016/j.molp.2020.06.009

Chen, Z., Pottosin, I. I., Cuin, T. A., Fuglsang, A. T., Tester, M., Jha, D., et al. (2007). Root plasma membrane transporters controlling K^+/Na^+ homeostasis in salt-stressed barley. *Plant Physiol.* 145, 1714–1725. doi: 10.1104/pp.107.110262

Cuin, T. A., Betts, S. A., Chalmandrier, R., and Shabala, S. (2008). A root's ability to retain K^+ correlates with salt tolerance in wheat. *J. Exp. Bot.* 59, 2697–2706. doi: 10.1093/jxb/ern128

Demidchik, V. (2014). Mechanisms and physiological roles of K^+ efflux from root cells. *J. Plant Physiol.* 171, 696–707. doi: 10.1016/j.jplph.2014.01.015

Du, J., Zhu, X., He, K., Kui, M., Zhang, J., Han, X., et al. (2023). CONSTANS interacts with and antagonizes ABF transcription factors during salt stress under long-day conditions. *Plant Physiol.* 193, 1675–1694. doi: 10.1093/plphys/kiad370

Gomez-Porras, J. L., Riano-Pachon, D. M., Dreyer, I., Mayer, J. E., and Mueller-Roeber, B. (2007). Genome-wide analysis of ABA-responsive elements ABRE and CE3 reveals divergent patterns in Arabidopsis and rice. *BMC Genomics* 8, 260. doi: 10.1186/1471-2164-8-260

Han, Y., Yin, S., Huang, L., Wu, X., Zeng, J., Liu, X., et al. (2018). A Sodium transporter HvHKT1;1 confers salt tolerance in barley via regulating tissue and cell ion homeostasis. *Plant Cell Physiol.* 59, 1976–1989. doi: 10.1093/pcp/pcy116

Hasegawa, P. M. (2013). Sodium (Na^+) homeostasis and salt tolerance of plants. *Environ. Exp. Botany.* 92, 19–31. doi: 10.1016/j.envexpbot.2013.03.001

Hauser, F., and Horie, T. (2010). A conserved primary salt tolerance mechanism mediated by HKT transporters: a mechanism for sodium exclusion and maintenance of high $K(^+)/Na(^+)$ ratio in leaves during salinity stress. *Plant Cell Environ.* 33, 552–565. doi: 10.1111/j.1365-3040.2009.02056.x

Hill, M. S., Vande Zande, P., and Wittkopp, P. J. (2021). Molecular and evolutionary processes generating variation in gene expression. *Nat. Rev. Genet.* 22, 203–215. doi: 10.1038/s41576-020-00304-w

Horie, T., Hauser, F., and Schroeder, J. I. (2009). HKT transporter-mediated salinity resistance mechanisms in Arabidopsis and monocot crop plants. *Trends Plant Sci.* 14, 660–668. doi: 10.1016/j.tplants.2009.08.009

Hossain, M. M., Imran, S., Islam, M. A., Kader, M. A., and Uddin, M. I. (2017). Uptake of Na^+ into roots and its transport into the shoot and leaf of salt tolerant cultivar (FR13A) and salt sensitive rice cultivar (BRRI dhan29). *Biotechnol. Biochem.* 3, 16–21. doi: 10.9790/264X-03051621

Huang, R., Jiang, S., Dai, M., Shi, H., Zhu, H., and Guo, Z. (2024). Zinc finger transcription factor MtZPT2-2 negatively regulates salt tolerance in Medicago truncatula. *Plant Physiol.* 194, 564–577. doi: 10.1093/plphys/kiad527

Isayenkov, S. V., and Maathuis, F. J. M. (2019). Plant salinity stress: many unanswered questions remain. *Front. Plant Science.* 10. doi: 10.3389/fpls.2019.00080

Jin, X., Sun, T., Wang, X., Su, P., Ma, J., He, G., et al. (2016). Wheat CBL-interacting protein kinase 25 negatively regulates salt tolerance in transgenic wheat. *Sci. Rep.* 6, 28884. doi: 10.1038/srep28884

Kaur, S., and Nayyar, H. (2015). Selenium fertilization to salt-stressed mungbean (Vigna radiata L. Wilczek) plants reduces sodium uptake, improves reproductive function, pod set and seed yield. *Scientia Horticulturae.* 197, 304–317. doi: 10.1016/j.scienta.2015.09.048

Li, J., Han, G., Sun, C., and Sui, N. (2019). Research advances of MYB transcription factors in plant stress resistance and breeding. *Plant Signaling Behavior.* 14, 1613131. doi: 10.1080/15592324.2019.1613131

Li, S., Wang, Y., Wang, C., Zhang, Y., Sun, D., Zhou, P., et al. (2023). Cryo-EM structure reveals a symmetry reduction of the plant outward-rectifier potassium channel SKOR. *Cell Discovery.* 9, 67. doi: 10.1038/s41421-023-00572-w

Mao, J., Yuan, J., Mo, Z., An, L., Shi, S., Visser, R. G. F., et al. (2021). Overexpression of NtCBL5A leads to necrotic lesions by enhancing Na^+ sensitivity of tobacco leaves under salt stress. *Front. Plant Science.* 12. doi: 10.3389/fpls.2021.740976

Meena, R., Singh, U. P., Singh, A. B., and Dadarwal, B. K. (2021). Effect of soil salinity stress on crops and their management. (New Delhi, India: AkiNik Publications) 8, 154. doi: 10.22271/ed.book.929

Miller, G., Suzuki, N., Ciftci-Yilmaz, S., and Mittler, R. (2010). Reactive oxygen species homeostasis and signalling during drought and salinity stresses. *Plant Cell And Environment.* 33, 453–467. doi: 10.1111/j.1365-3040.2009.02041.x

Mulet, J. M., Porcel, R., Yenush, L., and García, I. (2023). Modulation of potassium transport to increase abiotic stress tolerance in plants. *J. Exp. Botany.* 74, 5989–6005. doi: 10.1093/jxb/erad333

Nicholas, K B. (1997). Genedoc: a tool for editing and annoting multiple sequence alignments. Available at: http://wwwpscedu/biomed/genedoc.

Nguyen, T. H., Huang, S., Meynard, D., Chaine, C., Michel, R., Roelfsema, M. R. G., et al. (2017). A dual role for the OsK5.2 ion channel in stomatal movements and K^+ loading into xylem sap. *Plant Physiol.* 174, 2409–2418. doi: 10.1104/pp.17.00691

Ordonez, N. M., Marondedze, C., Thomas, L., Pasqualini, S., Shabala, L., Shabala, S., et al. (2014). Cyclic mononucleotides modulate potassium and calcium flux responses to H_2O_2 in Arabidopsis roots. *FEBS Lett.* 588, 1008–1015. doi: 10.1016/j.febslet.2014.01.062

Pantha, P, and Dassanayake, M. (2020). Living with Salt. *Innovation (Camb)* 1, 100050. doi: 10.1016/j.xinn.2020.100050

Rombauts, S., Déhais, P., Montagu, M. V., and Rouzé, P.. (1999). PlantCARE, a plant cis-acting regulatory element database. *Nucleic Acids Res.* 27, 295–296. doi: 10.1093/nar/27.1.295

Sano, T., Becker, D., Ivashikina, N., Wegner, L. H., Zimmermann, U., Roelfsema, M. R., et al. (2007). Plant cells must pass a K^+ threshold to re-enter the cell cycle. *Plant J.* 50, 401–413. doi: 10.1111/j.1365-313X.2007.03071.x

Sedgwick, S., and Smerdon, S. (1999). The ankyrin repeat a diversity of interactions on a common structural framework. *Trends In Biochem. Sci.* 24, 311–316. doi: 10.1016/S0968-0004(99)01426-7

Shi, D. (2023). Morning twilight of crop breeding for sodic land. *The Innovation Life* 1. doi: 10.59717/j.xinn-life.2023.100020

Sierro, N., Battey, J. N., Ouadi, S., Bakaher, N., Bovet, L., Willig, A., et al. (2014). The tobacco genome sequence and its comparison with those of tomato and potato. *Nat. Commun.* 5, 3833. doi: 10.1038/ncomms4833

Smethurst, C. F., Rix, K., Garnett, T., Auricht, G., Bayart, A., Lane, P., et al. (2008). Multiple traits associated with salt tolerance in lucerne: revealing the underlying cellular mechanisms. *Funct. Plant Biol.* 35, 640–650. doi: 10.1071/FP08030

Tamura, K., Stecher, G., Peterson, D., Filipski, A., and Kumar, S. (2013). MEGA6: molecular evolutionary genetics analysis version 6.0. *Mol. Biol. Evol.* 30, 2725–2729. doi: 10.1093/molbev/mst197

Véry, A.-A., Nieves-Cordones, M., Daly, M., Khan, I., Fizames, C., and Sentenac, H. (2014). Molecular biology of K^+ transport across the plant cell membrane: what do we learn from comparison between plant species? *J. Plant Physiol.* 171, 748–769. doi: 10.1016/j.jplph.2014.01.011

Wakeel, A. (2013). Potassium-sodium interactions in soil and plant under saline-sodic conditions. *J. Plant Nutr. Soil Science.* 176, 344–354. doi: 10.1002/jpln.201200417

Wang, X.-P., Chen, L.-M., Liu, W.-X., Shen, L.-K., Wang, F.-L., Zhou, Y., et al. (2016). AtKC1 and CIPK23 synergistically modulate AKT1-mediated low-potassium stress responses in Arabidopsis. *Plant Physiol.* 170, 2264–2277. doi: 10.1104/pp.15.01493

Wang, C., Wang, L., Lei, J., Chai, S., Jin, X., Zou, Y., et al. (2022). IbMYB308, a sweet potato R2R3-MYB gene,improves salt stress tolerance in transgenic tobacco. *Genes (Basel).* 13. doi: 10.3390/genes13081476

Wang, X., Zhao, J., Fang, Q., Chang, X., Sun, M., Li, W., et al. (2021). GmAKT1 is involved in K^+ uptake and Na^+/K^+ homeostasis in Arabidopsis and soybean plants. *Plant Science.* 304. doi: 10.1016/j.plantsci.2020.110736

Wei, L., and Li, Y. (2009). Distribution of an ankyrin-repeat protein on the endoplasmic reticulum in Arabidopsis. *J. Integr. Plant Biol.* 51, 140–146. doi: 10.1111/j.1744-7909.2008.00791.x

Weng, L., Zhang, M., Wang, K., Chen, G., Ding, M., Yuan, W., et al. (2020). Potassium alleviates ammonium toxicity in rice by reducing its uptake through activation of plasma membrane H^+-ATPase to enhance proton extrusion. *Plant Physiol. Biochem.* 151, 429–437. doi: 10.1016/j.plaphy.2020.03.040

Wu, H., Shabala, L., Barry, K., Zhou, M., and Shabala, S. (2013). Ability of leaf mesophyll to retain potassium correlates with salinity tolerance in wheat and barley. *Physiologia Plantarum.* 149, 515–527. doi: 10.1111/ppl.12056

Wu, H., Zhu, M., Shabala, L., Zhou, M., and Shabala, S. (2014). K^+ retention in leaf mesophyll, an overlooked component of salinity tolerance mechanism: A case study for barley. *J. Integr. Plant Biol.* 57, 171–185. doi: 10.1111/jipb.12238

Xie, Q., Zhou, Y., and Jiang, X. (2022). Structure, function, and regulation of the plasma membrane Na^+/H^+ antiporter salt overly sensitive 1 in plants. *Front. Plant Science.* 13. doi: 10.3389/fpls.2022.866265

Yang, A., Dai, X., and Zhang, W.-H. (2012). A R2R3-type MYB gene, OsMYB2, is involved in salt, cold, and dehydration tolerance in rice. *J. Exp. Botany.* 63, 2541–2556. doi: 10.1093/jxb/err431

Yu, J., Zhu, C., Xuan, W., An, H., Tian, Y., Wang, B., et al. (2023). Genome-wide association studies identify OsWRKY53 as a key regulator of salt tolerance in rice. *Nat. Commun.* 14, 3550. doi: 10.1038/s41467-023-39167-0

Zaman, M., Shahid, S. A., and Heng, L. (2018). Soil salinity: Historical perspectives and a world overview of the problem. *Guideline for salinity assessment, mitigation and adaptation using nuclear and related techniques.* 43–53.

Zhao, C., Zhang, H., Song, C., Zhu, J.-K., and Shabala, S. (2020). Mechanisms of plant responses and adaptation to soil salinity. *Innovation.* 1. doi: 10.1016/j.xinn.2020.100017

Zhou, J., Nguyen, T. H., Hmidi, D., Luu, D. T., Sentenac, H., and Véry, A. A. (2022). The outward Shaker channel OsK5.2 improves plant salt tolerance by contributing to control of both leaf transpiration and K^+ secretion into xylem sap. *Plant Cell And Environment.* 45, 1734–1748. doi: 10.1111/pce.14311

Zörb, C., Geilfus, C.-M., and Dietz., K.-J. (2018). Salinity and crop yield. *Plant Biol.* 21, 31–38. doi: 10.1111/plb.12884

frontiers | Frontiers in Plant Science

TYPE Original Research
PUBLISHED 15 April 2024
DOI 10.3389/fpls.2024.1382397

OPEN ACCESS

EDITED BY
Hui Song,
Qingdao Agricultural University, China

REVIEWED BY
Aziz Akkak,
University of Foggia, Italy
Linhai Wang,
Chinese Academy of Agricultural Sciences, China
Pravin Jadhav,
Dr. Panjabrao Deshmukh Krishi Vidyapeeth, India

*CORRESPONDENCE
İlker Sönmez
ilkersonmez@akdeniz.edu.tr

RECEIVED 05 February 2024
ACCEPTED 28 March 2024
PUBLISHED 15 April 2024

CITATION
Han Ş, Sönmez İ, Qureshi M, Güden B, Gangurde SS and Yol E (2024) The effects of foliar amino acid and Zn applications on agronomic traits and Zn biofortification in soybean (*Glycine max* L.). *Front. Plant Sci.* 15:1382397. doi: 10.3389/fpls.2024.1382397

The effects of foliar amino acid and Zn applications on agronomic traits and Zn biofortification in soybean (*Glycine max* L.)

Şule Han[1], İlker Sönmez[1]*, Moin Qureshi[2], Birgül Güden[2], Sunil S. Gangurde[3] and Engin Yol[2]

[1]Department of Soil Science and Plant Nutrition, Faculty of Agriculture, University of Akdeniz, Antalya, Türkiye, [2]Department of Field Crops, Faculty of Agriculture, University of Akdeniz, Antalya, Türkiye, [3]International Crops Research Institute for the Semi-Arid Tropics, Hyderabad, India

The production and consumption of soybeans are widespread due to their nutritional and industrial value. Nutrient enrichment is vital for improving the nutritional quality of soybeans. This study aimed to evaluate the effect of foliar application of amino acids (AA) and zinc (Zn) on agronomic traits and the accumulation of grain Zn in soybeans. The experimental design comprised 16 treatment combinations involving four levels of amino acid application (0, 50, 100, and 150 ml 100 L^{-1}) and Zn (0, 2, 4, and 6 mg L^{-1}) following a randomized complete block design with three replications in field conditions. The results demonstrated that the application of foliar Zn and AA did not affect the yield, whereas that of AA_{50}*Zn_2 and AA_{150}*Zn_2 affected the number of pods and branches. The effects of AA application on N and the protein content in grains were determined to be significant. The application of AA_{100}*Zn_6 emerged as the most effective treatment for the enhancement of Zn biofortification in soybean grains. The combined foliar application of AA and Zn contributed to enhanced Zn accumulation in the grains.

KEYWORDS

amino acid, biofortification, mineral nutrition, soybean, zinc

Introduction

Increasing the nutrient density and bioavailability in crops is important for combating hidden hunger and ensuring food security in growing populations. There has been an increase in the number of applications aiming to optimize the utilization of the consumption of goods by living organisms and address shortages of essential nutrients. Organizations such as the World Health Organization (WHO) and the Consultative Group on International Agricultural Research (CGIAR) emphasize the importance of

biofortification and prioritize the enrichment of the consumed parts of plant products with amino acids, proteins, vitamin A, and elements such as calcium, magnesium, iron, zinc, copper, selenium, and iodine (Orman and Ok, 2016). Nutrient enrichment studies in plants using agronomic biofortification have gained significant importance in recent years, with the demand for items with elevated nutritional value in the food industry notably increasing. Fundamental nutrition philosophy emphasizes the use of high-quality, nutrient-dense items over quantity in terms of the preservation of living health. Researchers have attempted to address micronutrient deficiencies with different interventions, which may be categorized into four main groups—pharmaceutical supplementation, industrial fortification, dietary diversification, and biofortification (Meenakshi et al., 2010).

The most appropriate method to reduce microelement deficiency is biofortification, which involves the biological enrichment of staple food crops with essential micronutrients. The biofortification process prioritizes the strategies of breeding new cereal genotypes rich in microelements or expanding the use of fertilizers containing microelements (Cakmak, 2008). Agronomic biofortification through fertilization (soil, foliar fertilization, and grain coating) aims to increase the nutrient content of plants without changing their genetic structure (Storksdieck and Hurrell, 2009). The foliar application of mineral fertilizers to plants is an environmentally friendly and cost-effective agronomic strategy for biofortification in an easily phyto-available form (White and Broadley, 2011; Rawat et al., 2013). The efficacy of agronomic biofortification in enhancing zinc (Zn) levels however, a combination of soil and foliar treatment for Zn yields the most favorable results. Zinc plays an important role in the synthesis of tryptophan, the basic component of some important proteins, and with its deficit, plants experience a drop in tryptophan concentration, cessation of protein synthesis, and accumulation of free amino acids (Turan and Horuz, 2012; Acık and Oncan Sumer, 2023). This condition inherently results in reduced yield up to 40% and quality (Noulas et al., 2018). Zn deficiency also causes physiological stress, which results in the development of abnormalities such as stunted growth, chlorosis in leaves, small leaves, and spikelet sterility (Alloway, 2009). Plants become more susceptible to damage from high light intensity and temperature, as well as to infection by certain fungal diseases (Marschner, 1995; Cakmak, 2000).

The use of Zn sulfate is the optimum form for meeting zinc requirements. The timing of foliar Zn application is important; it is generally known to be more effective during the middle phase of root development or in the early milk stage (Lyons and Cakmak, 2012). It is an effective way to improve the concentration of Zn in cereals. The application of 0.5% (w/v) Zn foliar fertilizer at later growth stages of the crop resulted in a greater Zn increase in edible parts, such as grains, indicating that this technique can maximize Zn accumulation (Cakmak et al., 2010). Zinc, a cofactor with structural and catalytic activities in 10% of human proteins (Acık and Oncan Sumer, 2023), plays a crucial role in human health and immune systems (Brown et al., 2004; Sánchez-Palacios et al., 2023). 17% of the global population has insufficient zinc intake (Kumssa et al., 2015), and many individuals do not get enough zinc in their diets (Bouis and Welch, 2010). Prior studies have established that the zinc needed for nutrition can be supplied by using zinc fertilizer in grains (Joy et al., 2015; Wang et al., 2016). Agronomic biofortification through the application of fertilizers that promote the fortification of food crops (especially Zn-containing crops) may be an important strategy in countries with high nutrient deficiency (Joy et al., 2015).

Amino acids (AA) are crucial due to their extensive use in the production of a broad range of chemical molecules, increasing yields and quality, and reducing the productive cycle while improving dry material content (Wahba et al., 2015). They may be used as adjuvants to improve the efficiency of foliar fertilization by increasing the permeability of the leaf cuticle and enhancing nutrient uptake efficiency (Moreira et al., 2015; Moreira and Moraes, 2017).

Soybeans (*Glycine max* L.) are a valuable high-protein source that can help meet human nutrient requirements (Zhan et al., 2019). It has a significant position as a crucial seed legume, accounting for 25% of world vegetable oil output and two-thirds of its protein concentrate used for animal feed (Agarwal et al., 2013). Soybean is well-suited for biofortification because of its elevated protein and oil levels, flexibility as a food and feed component, and adaptability in various conditions. Fertilizer containing zinc (Zn) have been widely accepted as prompt and convenient treatments to address Zn deficiency issues in cereal crops. Although several studies have been conducted on the addition of Zn to different crops focusing on correcting Zn deficiency and increasing grain yield, the majority of the research has focused on yield parameters in cereals. With the HarvestPlus Biofortification Challenge Programme, there is an increasing focus on the biofortification of food crops with Zn using plant breeding (genetic) and agronomic approaches (Lyons and Cakmak, 2012). This study, therefore, aimed to improve the effectiveness of Zn biofortification in soybeans by the combined application of Zn and AA via foliar spraying.

Materials and methods

Plant material

The Victoria soybean cultivar was used as the genetic material in this study. This variety has a protein content ranging from 39% to 41%, and an oil content ranging from 18% to 20%. It is additionally characterized by a brown pod color, high potential for yield in secondary crop production, and notable adaptation and tolerance to various diseases, lodging, whitefly infestations, and shedding.

Site description

The experiment was carried out in a field condition (36° 53'54.4"N 30°38'28.9" E) at Akdeniz University, Turkey between June and September 2022. The physical and chemical parameters of

the soil samples were analyzed in detail and were obtained at a depth of 0–20 cm in each plot within the experimental area. The total $CaCO_3$ (Evliya, 1964), organic matter (Black, 1965), pH (Jackson, 1967), EC (Thomas, 1982), texture (Bouyoucos, 1955), total N (Black, 1957), available P (Olsen and E.L., 1982), extractable K, Ca, and Mg (Kacar, 1972), and available Zn, Mn, and Cu (Lindsay and Norvell, 1978) were determined. Some soil properties (0–20 cm) assessed as follows: loamy in texture, organic matter (1.23%), $CaCO_3$ (20.9%), pH = 7.7, EC (0.045%), 0.089% total (N), 4.03 mg kg^{-1} available (P), 96.8 g kg^{-1} extractable potassium (K), 2425.5 g kg^{-1} extractable calcium (Ca) and 146 g kg^{-1} extractable magnesium (Mg), 0.82 mg kg^{-1} available zinc (Zn), 5.51 mg kg^{-1} available manganese (Mn) and 0.88 mg kg^{-1} available copper (Cu) (Supplementary Table S1). The mean monthly rainfall, air temperature, and humidity are presented in Supplementary Figure S1.

Experimental parameters: dosages and chemicals

Zinc treatments were applied to the plants as zinc sulfate ($ZnSO_4.7H_2O$). The amino acid liquid products comprised total amino acids of 46.70%, total organic matter, organic N, and organic carbon concentrations of 51.35%, 5.42%, and 24.38%, respectively. Amino acids and $ZnSO_4$ were applied twice during the BBCH (Biologische Bundesanstalt, Bundessortenamt and Chemical industry) 13 (3 leaf) and BBCH 60-62 stages (beginning of flowering) of soybean plant growth. All amino acids were diluted 100 times with water and sprayed onto the plant leaves each time. The control plants (AA_1 and Zn_1) were sprayed with tap water. The chemical composition of the commercial amino acid preparation included glycine (1.45 g 100 g^{-1}), alanine (0.25 g 100 g^{-1}), valine (0.56 g 100 g^{-1}), isoleucine (0.34 g 100 g^{-1}), threonine (0.06 g 100 g^{-1}), serine (0.14 g 100 g^{-1}), lysine (0.28 g 100 g^{-1}), phenylalanine (0.23 g 100 g^{-1}), glutamate (0.42 g 100 g^{-1}), aspartate (0.12 g 100 g^{-1}), arginine (0.72 g 100 g^{-1}), proline (1.65 g 100 g^{-1}), leucine (0.37 g 100 g^{-1}), histidine (0.11 g 100 g^{-1}), asparagine (0.09 g 100 g^{-1}), cystine (0.04 g 100 g^{-1}), hydroxyproline (0.78 g 100 g^{-1}), methionine (0.45 g 100 g^{-1}), tryptophan (0.04 g 100 g^{-1}) and tyrosine (0.13 g 100 g^{-1}).

Experimental design

The experiment was performed with 16 treatment combinations involving four levels of amino acids (0, 50, 100, and 150 ml 100 L^{-1} as AA_1, AA_2, AA_3, and AA_4, respectively) and Zn (0, 2, 4, and 6 mg L^{-1} as Zn_1, Zn_2, Zn_3 and Zn_4, respectively), followed by a randomized complete block design with three replicates. The field was plowed twice followed by planking. In terms of basic fertilization, 12 kg da^{-1} NPK (15:15:15) fertilizer was applied to the soil, but the use of zinc was limited to foliar application. Sowing was performed in the second week of June using the Viapora method with a 4–5 cm plant spacing, and row-to-row spacing was maintained at 70 cm. A total of ten soybean grains were planted on each parcel.

Sample collection

The plant height (cm), number of branches, number of pods, first pod length (cm), and grain yield (g per plant) were also measured in selected plants. The concentrations of nitrogen and zinc were also analyzed in soybean leaves and grains. Leaf samples were taken together with the petiole at the R2 growth stage (Fehr et al., 1971) after 2-week foliar treatments.

Recommended agronomic practices were applied as per crop and climatic parameters. Harvesting was performed manually from the experimental plots after grain hardening (leaf yellowing). In terms of agronomic measurements, five healthy plants were randomly selected from each plot and labeled to determine their developmental characteristics.

For the mineral analysis of the leaf and grain samples, each dried plant and grain sample (0.5 g) was digested with an acid mixture of 10 mL $HNO_3/HClO_4$ (4:1) on a hot plate. The samples were then heated until a clear solution was obtained. This procedure was repeated several times. The concentrations of zinc (Zn) in the digests were determined using inductively coupled plasma (Perkin Elmer Optima DV7000-ICP OES) (Kacar and Inal, 2008). The total nitrogen (N) was determined using the modified Kjeldahl method (Bremmer, 1965).

Statistical analysis

The data were analyzed using analysis of variance (ANOVA) using SAS statistical software (SAS Institute, 2011). The least significant difference (LSD) test was used at a significance level of $p<0.05$.

Results

Foliar doses of AA and Zn significantly increased the average number of pods in soybeans ($p<0.001$). As shown in Table 1, While the highest average number of pods of soybean was obtained from treatment A_3 (155.6 $plant^{-1}$) in AA treatment dose, the same was observed Zn_2 (158 $plant^{-1}$) in the Zn treatment dose. The results demonstrated that foliar doses of AA and Zn increased the number of pods in the plants, with the AA × Zn interaction being statistically significant ($p<0.001$). The highest number of pods was recorded in the AA_2*Zn_2 treatment (191 $plant^{-1}$), with no linear relationship between the number of pods and dose increase (Figure 1). The effects of foliar AA and Zn treatments on the number of soybean branches are presented in Table 1 and Figure 2. The results indicated that foliar doses of AA and Zn increased the number of branches and that the AA × Zn interaction was statistically significant ($p<0.001$). The highest number of branches was recorded in the AA_4*Zn_2 treatment (8.3 $plant^{-1}$), and foliar treatment doses of AA and Zn significantly increased the average number of branches in soybeans ($p<0.001$). The highest average value was observed in A_4 (6.3 $plant^{-1}$) under the AA treatment, and in Zn_2 (6.3 $plant^{-1}$) under the Zn treatment. Statistical analysis revealed that there was no significant effect on the plant height or

10.3389/fpls.2024.1382397

TABLE 1 Effect of foliar AA and Zn treatments on average number of pods (NOP), number of branch (NOB), grain yield (GY), plant height (PH) and first capsule lenght (FCL) of soybeans.

Treatments	NOP	NOB	GY	PH	FCL
	(plant^{-1})	(plant^{-1})	(g plant^{-1})	(cm)	(cm)
AA_1	132.5 C	5.1 B	1.19	117.2	16.0
AA_2	143.2 B	5.3 B	1.18	115.5	18.8
AA_3	155.6 A	5.7 B	1.27	110.9	15.9
AA_4	133.3 C	6.3 A	1.30	114.3	17.8
Zn_1	134.8 B	5.4 BC	1.17	113.8	18.4
Zn_2	158.0 A	6.3 A	1.25	114.5	15.4
Zn_3	120.3 C	5.9 AB	1.31	116.3	18.6
Zn_4	151.5 A	4.8 C	1.23	113.2	16.1
AA	16.517***	5.828**	1.230ns	1.619ns	0.761ns
Zn	41.034***	7.575***	1.055ns	0.430ns	0.984ns
AA*Zn	17.22***	6.962***	0.992ns	1.223ns	0.402ns

The values followed by uppercase letters indicate the difference between the mean values of amino acid treatments. Values followed by uppercase letters in brackets indicate the difference between Zn treatments. ** p<0.01 *** p<0.001 ns, non-significant.

first pod length of soybean when treated with AA and Zn. The recorded values for soybean plant height ranged from 110.9 cm to 117.2 cm, whereas the first pod length varied between 15.4 cm and 18.8 cm. The effects of foliar AA and Zn treatments on the grain yield of soybean plants are presented in Figure 3. The effects of AA and Zn treatments on grain yield were not found to be statistically significant. The soybean seed yield varied between 1.03 and 1.48 g plant^{-1}. There was no significant correlation observed between foliar AA and Zn treatments or grain yields.

The effects of foliar AA and Zn treatments on the nitrogen content of soybean plants and grains are presented in Table 2 and Figure 4. The findings of this study indicate that foliar spraying with AA and Zn resulted in increased nitrogen levels in soybean plants and their corresponding grains. Foliar treatment with AA and Zn significantly increased the average nitrogen content of soybeans (p<0.001). The highest average nitrogen content was obtained in the A_4 treatment in soybean leaves (3.45%) and grains (7.16%) with AA treatment doses. Statistical analysis did not reveal any significant interactions between AA and Zn treatments in either the leaves or grains. Furthermore, the application of different Zn dosages did not significantly affect the nitrogen content in the leaves and grains.

The effects of foliar AA and Zn treatments on the protein content of soybean grains are presented in Table 2 and Figure 5. This indicated that higher doses of AA resulted in increased grain protein content in soybean grains, a plant known for its high protein content. The highest protein content of grain was observed in A_4 (44.8%), and a linear relationship was observed between increasing AA doses and grain protein content. The application of Zn, however, did not result in any significant alterations in the protein composition of soybean grains. The effects of foliar AA and Zn treatments on the Zn content of soybean leaves and grains are presented in Table 2 and Figure 6.

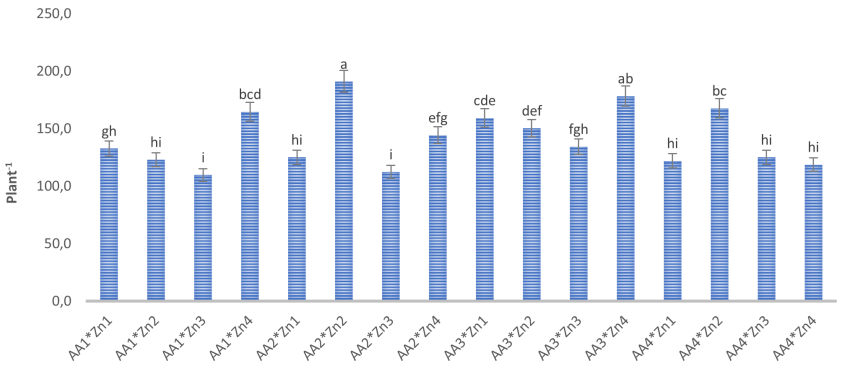

FIGURE 1
Effect of foliar AA and Zn treatments on number of pods (plant^{-1}) of soybeans. The letters on the bars indicate the difference between the mean values.

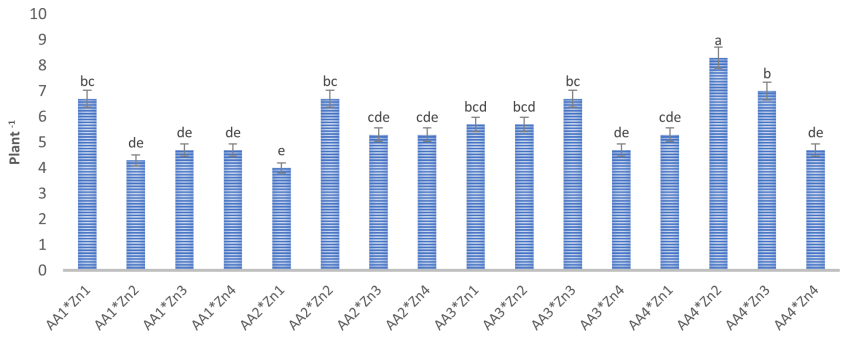

FIGURE 2
Effect of foliar AA and Zn treatments on number of branch (plant^{-1}) of pods of soybeans. The letters on the bars indicate the difference between the mean values.

The findings of this study indicate that foliar treatment with AA and Zn led to a notable increase in the Zn levels of both soybean leaves and grains. These results were found to be statistically significant ($p<0.001$). The application of AA and Zn increased the zinc (Zn) content in soybean leaves, as well as the average concentration of Zn. The greatest values of Zn concentration 35.2 and 33.6 mg kg^{-1} were notably observed in the maximal dosages of AA_4 and Zn_4, respectively.

The interactions between AA and Zn treatments were found to be statistically significant in grains ($p<0.05$), and the effective AA*Zn dose was determined from the AA_3*Zn_4 treatment (61.2 mg kg^{-1}). In terms of the combined effect of AA and Zn treatments, it was determined that both AA and Zn treatments increased the Zn concentration in soybean grains and contributed to Zn biofortification. In terms of the average Zn concentration of grain, it was observed that the maximal dosages (AA_4 and Zn_4) provided the highest values (51.3 and 59.5 mg kg^{-1}). The changes in Zn concentrations in the leaves and grains of the AA and Zn treatments are presented in Figure 6. This study revealed a positive correlation between Zn dose of zinc (Zn) and grain accumulation, indicating a linear increase in grain accumulation with higher dose application of Zn. The application of increasing doses of AA additionally promoted an increase in grain accumulation. A considerable increase in the biofortification effect was observed after the application of maximal dosages of AA and Zn.

Discussion

The objective of this study was to enhance the nutritional quality of soybean crops using improved fertilization programs, focusing specifically on the foliar application of AA and Zn. The combination of Zn treatment and AA was effective for soybean growth, especially in terms of the number of pods and branches. Correlative results were obtained by Abd El-Aal and Eid (2018), highlighting the favorable impact of foliar amino acid spraying on soybean growth and yield. The results of this study are similarly consistent with the research conducted by Zewail (2014), which indicated that the application of amino acids by foliar approaches enhances the growth attributes of bean plants, including increased plant height and an increased number of branches and leaves per plant. The requirement of amino acid nitrogen is one way to increase the growth and yield of all crops. Nitrogen and/or amino acids are essential components of protein synthesis; they are important due to their widespread use in the biosynthesis of a wide variety of non-protein nitrogenous substances, such as pigments, vitamins, coenzymes, purines, and pyrimidine bases. Several studies have reported that foliar application of amino acids results in increased plant growth, yield, and composition (Kamar and Omar, 1987; El-Shabasi et al., 2005). Zinc is another trace element that is essential to all living organisms. In this study, we identified that zinc application increases the number of branches

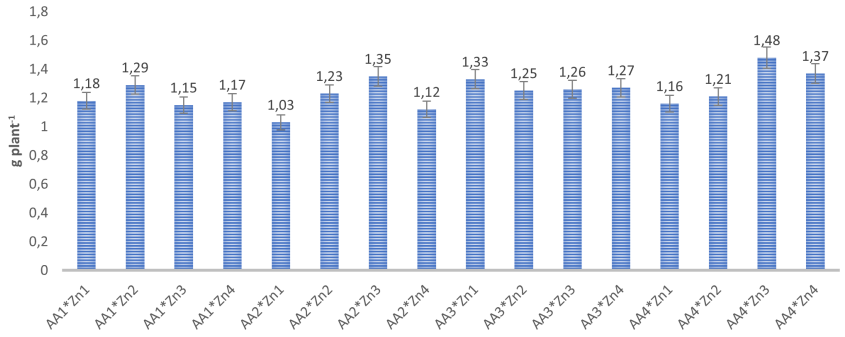

FIGURE 3
Effect of foliar AA and Zn treatments on grain yield of soybeans.

10.3389/fpls.2024.1382397

TABLE 2 Effect of foliar AA and Zn treatments on average N concentration, Zn concentration and proetin content of soybeans.

Treatments	N concentration		Protein	Zn concentration	
	%		%	mg kg^{-1}	
	Leave	Grain	Grain	Leave	Grain
AA_1	2.43 D	6.24 C	39.0 C	26.3 D	48.3 B
AA_2	2.74 C	6.57 B	41.0 B	29.3 C	48.6 B
AA_3	3.27 B	6.73 B	42.1 B	32.2 B	50.5 A
AA_4	3.45 A	7.16 A	44.8 A	35.2 A	51.3 A
Zn_1	3.02	6.60	41.2	27.7 D	40.4 D
Zn_2	2.92	6.69	41.8	30.1 C	47.8 C
Zn_3	2.90	6.75	42.2	31.7 B	51.0 B
Zn_4	3.04	6,66	41.6	33.6 A	59.5 A
AA	59.487***	15.886***	15.850***	41.363***	13.667***
Zn	1.405ns	0.462ns	0.448ns	98.138***	415.813***
AA*Zn	1.592ns	1.845ns	0.840ns	1.367ns	3.354*

The values followed by uppercase letters indicate the difference between the mean values of amino acid treatments. Values followed by uppercase letters in brackets indicate the difference between Zn treatments. * p<0.05 *** p<0.001 ns, non-significant.

and pods. The finding was also in partial conformity with the works of Choudhary et al. (2014) and Kanase et al. (2008), who outlined that zinc application increases the number of branches and pods. Similar to our findings, Imsong et al. (2023) outlined that the number of pods was highest at the highest level of zinc and lowest in the control group. Also, the authors noted that elevated zinc fertilization resulted in a more pronounced plant response with enhanced branch numbers. This change in growth parameters may be linked to the involvement of zinc in tryptophan synthesis, nitrogen metabolism, and the production of growth hormones like indole acetic acid (Imsong et al., 2023). The above findings align with the research conducted by Raghuwanshi et al. (2017) and Singh et al. (2017), which stated the enhanced growth characteristics of soybean with the application of zinc.

The foliar application of AA and Zn demonstrated no significant effect on soybean grain yield (Table 1). These findings are consistent with those of Enderson et al. (2015), indicating that the foliar applications of B, Cu, Mn, Zn, and their mixture did not result in an increase in soybean grain yield across all 42 sites. Similar findings have been reported in other studies for soybean. For example, Souza et al. (2019) identified no significant effect of Zn and AA foliar fertilization on yield components, and Mallarino et al. (2001) reported that foliar fertilization with various nutrient mixtures, including Zn, resulted in very small and infrequent yield increases. Similar results have also been identified for different crops; Teixeira et al. (2008) found no effect of Zn foliar application on the grain weight of beans grown in soil with a sufficient Zn concentration. Cakmak et al. (2010) reported that foliar Zn treatments did not affect wheat grain yield. These studies support the claim that soybeans are less sensitive to Zn fertilizer than other crops (Sutradhar et al., 2017). The findings contrast with those reported by Vahedi (2011); Tousi et al. (2014), and Teixeira et al. (2018), indicating that foliar application of amino acids improves the yield components of soybean plants.

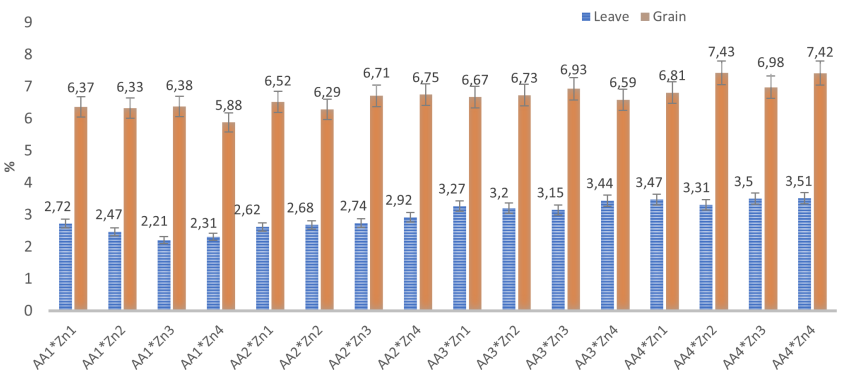

FIGURE 4
Effect of foliar AA and Zn treatments on N contents (%) of soybeans leaves and grains.

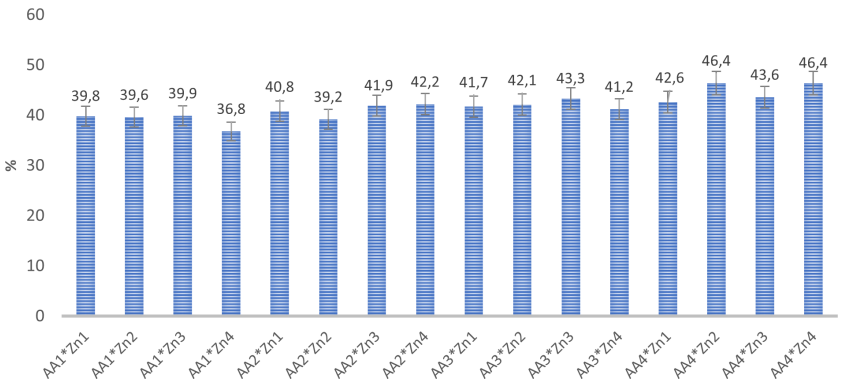

FIGURE 5
Effect of foliar AA and Zn treatments on protein contents (%) of soybeans grains.

Foliar AA treatment was found to increase the nitrogen concentration in soybean leaves and grains. Zn treatments were not as effective as increasing the nitrogen concentration in the leaves and grains of soybeans (Table 2). Amino acids help increase nitrogen and some nutrients in plants (Liu et al., 2008; Abo Sedera et al., 2010). This might be because amino acids demonstrate chelation properties with nutrients, thereby enhancing the uptake and translocation of these vital elements inside the plant. This phenomenon may be related to the effects on cell membrane permeability, which enhances the efficiency of nutrient absorption (Marschner, 1995). The use of amino acids as nitrogen (N) and carbon (C) sources by plants has been widely documented in studies (Thornton and Robinson, 2005). Furthermore, the application of lithovit at a rate of 500 mg and amino acids at a rate of 4 ml l^{-1} provided the highest values of leaf chemical composition (N, P, K, Ca, Mg %, and Fe ppm) in soybean plants (Abd El-Aal and Eid, 2018). Similarly, the application of amino acids by foliar spraying resulted in an enhancement of nitrogen content in plants compared to that in the control group in another study (Shehata et al., 2011). Several studies have demonstrated the efficiency of amino acid uptake by plants, with the foliar application of amino acids demonstrating promising results (Abdel-Mawgoud et al., 2011; Sadak et al., 2014).

The results of this study indicated that higher doses of AA led to an increase in the protein content of soybean grains. Varying the dosages of Zn, however, did not have a significant impact on the protein content of the soybean grains. The use of amino acids may have favorable effects, which may be attributed to their internal roles as osmoregulatory agents (Treichel, 1975). This is due to their high solubility in water, which leads to an increase in the concentration of osmotic components inside the cells (Abdel-Mawgoud et al., 2011). Suciu et al. (2022) reported that the application of biofertilizers containing amino acids contributed to the protein content of soybeans. Research on the positive effect of biostimulants on the protein content in legume seeds is available in terms of common beans; the treatment of *Fabaceae* plants with biostimulants containing amino acids has resulted in an increase in protein content in the seeds of common beans (Zewail, 2014; Kocira et al., 2017).

Foliar treatments of AA and Zn increased the average Zn concentration of soybean leaves and grains. The most effective dose was obtained from the AA_3*Zn_4 treatment in the AA*Zn interaction in grain Zn concentration. Increasing the treatment rates of AA and Zn increased the Zn accumulation in both leaves and grains, and the AA*Zn combination contributed to Zn biofortification, especially in

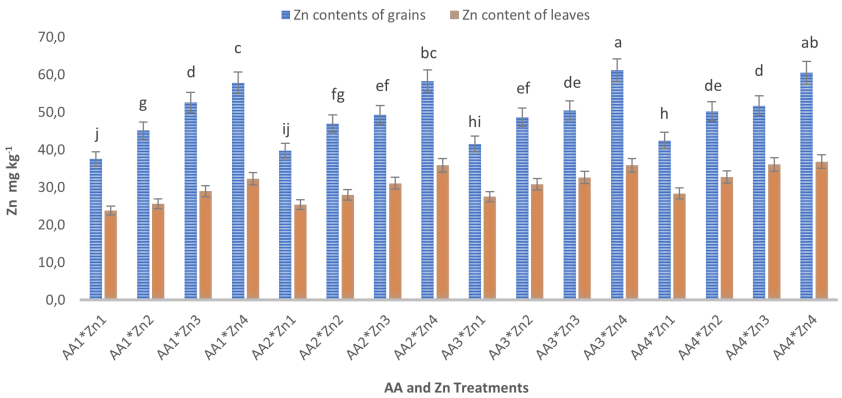

FIGURE 6
Effect of foliar AA and Zn treatments on Zn contents (mg kg^{-1}) of soybeans leaves and grain. The letters on the bars indicate the difference between the mean values.

the grains. The application of foliar zinc sulfate was effective in biofortifying winter wheat by increasing the grain Zn from 20 to 30 mg kg^{-1} (Mao et al., 2014). Choudhary et al. (2014) stated that by increasing the Zn doses, the Zn content increased in soybean grain, with the highest Zn content of soybean grain being measured at 57.4 mg kg^{-1}. Foliar fertilization with Zn at a ratio of 4 (0, 0.91, 1.82, 2.73, and 6.37 mg kg^{-1}) increased plant height, grain mass, and protein content in soybean grains (Oliveira et al., 2018). In addition, Zn is crucial for the function of dehydrogenase, proteinase, RNA enzymes, and chlorophyll synthesis (Hansch and Mendel, 2009). These results can be considered preliminary in establishing the optimal dosage of AA*Zn for future studies aimed at gaining information into these mechanisms.

Foliar application, which contributes to the rapid uptake of nutrients from leaves and minimizes environmental pollution and groundwater contamination (Dehnavard et al., 2017), may be a viable agronomic biofortification practice for zinc at the advanced stages of soybean development. A greenhouse study on soybeans reported that foliar Zn applied at the full-pod stage at low soil Zn concentrations was more effective than other treatments in improving seed Zn concentration (Oliveira et al., 2018). Moreover, considering the low canopy height of soybeans, it allows the use of a ground sprayer (Cuesta et al., 2023).

Conclusion

In this study, foliar Zn and amino acids, an organic compound and biostimulant, were applied together to soybean to determine plant development and Zn biofortification performance, particularly in the grain. Positive effects of the co-use were observed in some foliar applications. While no effect of foliar treatments was observed on the yield values, the combined treatments demonstrated significant effects on the pod number (AA_2*Zn_2) and branch number (AA_4*Zn_2). There was a significant combined effect of AA and Zn, where the application of AA_3*Zn_4 provided the maximum value for Zn biofortification. In addition to foliar Zn application at later stages of cultivation, the application of materials with organic components (AA, seaweed, etc.) may have increased the availability of Zn by supporting the uptake in leaves and grains.

Data availability statement

The raw data supporting the conclusions of this article will be made available by the authors, without undue reservation.

Author contributions

ŞH: Methodology, Writing – original draft. İS: Conceptualization, Formal analysis, Methodology, Writing – original draft. MQ: Writing – review & editing. BG: Methodology, Writing – original draft. SG: Writing – original draft. EY: Formal analysis, Writing – review & editing.

Funding

The author(s) declare that no financial support was received for the research, authorship, and/or publication of this article.

Acknowledgments

We appreciate the Scientific Research Projects Coordination Unit of Akdeniz University for continuous support.

Conflict of interest

The authors declare that the research was conducted in the absence of any commercial or financial relationships that could be construed as a potential conflict of interest.

Publisher's note

Supplementary material

The Supplementary Material for this article can be found online at: https://www.frontiersin.org/articles/10.3389/fpls.2024.1382397/full#supplementary-material

SUPPLEMENTARY FIGURE S1
The mean monthly rainfall, air temperature, and humidity during the growing period.

References

Abd El-Aal, M. M. M., and Eid, R. S. M. (2018). Effect of foliar spray with lithovit and amino acids on growth, bioconstituents, anatomical and yield features of soybean plant. *Plant Biotechnol.* 56, 187–202. doi: 10.21608/assjm.2018.65137

Abdel-Mawgoud, A. M. R., El-Bassiouny, A. M., Ghoname, A., and Abou-Hussein, S. D. (2011). Foliar application of amino acids and micronutrients enhance performance of green bean crop under newly reclaimed land conditions. *Aust. J. Basic Appl. Sci.* 5, 51–55.

Abo Sedera, F. A., El-Latif., A. A. A., Bader, L. A. A., and Rezk, S. M. (2010). Effect of NPK mineral fertilizer levels and foliar application with humic and amino acids on yield and quality of strawberry. *EgypJ Appl. Sci.* 25, 154–169.

Acık, A., and Oncan Sumer, F. (2023). Foliar Application of Zinc Improves Agronomical and Quality Parameters and Biofortification of Cowpea (*Vigna sinensis*) under Deficit Irrigation. *Agronomy* 13, 1021. doi: 10.3390/agronomy13041021

Agarwal, D. K., Billore, S. D., Sharma, A. N., Dupare, B. U., and Srivastava, S. K. (2013). Soybean: Introduction, improvement, and utilization in India—Problems and prospects. *Agric. Res.* 2, 293–300. doi: 10.1007/s40003-013-0088-0

Alloway, B. J. (2009). Soil factors associated with zinc deficiency in crops and humans. *Environ. Geochem Health* 31, 537–548. doi: 10.1007/s10653-009-9255-4

Black, C. A. (1957). *Soil-plant relationships* (New York: John Wiley and Sons, Inc).

Black, C. A. (1965). Methods of soil analysis. *American Society of Agronomy*. Madison, Wisconsin, part I. 1965, 1–770.

Bouis, H. E., and Welch, R. M. (2010). Biofortification—A sustainable agricultural strategy for reducing micronutrient malnutrition in the global south. *Crop Sci.* 50, S-20–S-32. doi: 10.2135/cropsci2009.09.0531

Bouyoucos, G. J. (1955). A recalibration of the hydrometer method for making mechanical analysis of the soils. *Agron. J.* 4, 434.

Bremmer, J. M. (1965). ""Total nitrogen,"," in *Methods of soil analysis: Part 2. Chemical and Microbiological Properties*. Ed. C. A. Black (American Society of Agronomy, Madison), 1149–1176.

Brown, K. H., Rivera, J. A., Bhutta, Z., Gibson, R. S., King, J. C., and Lönnerdal, B. (2004). International Zinc Nutrition Consultative Group (IZiNCG) technical document# 1. Assessment of the risk of zinc deficiency in populations and options for its control. *Food Nutr. Bull.* 25, S99–S203.

Cakmak, I. (2000). Role of zinc in protecting plant cells from reactive oxygen species. *New Phytol.* 146, 185–205. doi: 10.1046/j.1469-8137.2000.00630.x

Cakmak, I. (2008). Enrichment of cereal grains with zinc: Agronomic or genetic biofortification? *Plant Soil* 302, 1–17. doi: 10.1007/s11104-007-9466-3

Cakmak, I., Kalayci, M., Kaya, Y., Torun, A. A., Aydin, N., Wang, Y., et al. (2010). Biofortification and localization of zinc in wheat grain. *J. Agric. Food Chem.* 58)16, 9092–9102. doi: 10.1021/jf101197h

Choudhary, P., Jhajharia, A., and Kumar, R. (2014). Influence of sulphur and zinc fertilization on yield, yield components and quality traits of soybean (Glycine max L. *Bioscan* 9, 137–142.

Cuesta, N. N., Carciochi, W., Wyngaard, N., Rozas, H. S., Silva, S., Salvagiotti, F., et al. (2023). Zinc fertilization strategies in soybean: plant uptake, yield, and seed concentration. *J. Plant Nutr.* 46, 1134–1144. doi: 10.1080/01904167.2022.2067059

Dehnavard, S., Souri, M. K., and Mardanlu, S. (2017). Tomato growth responses to foliar application of ammonium sulfate in hydroponic culture. *J. Plant Nutr.* 40, 315–323. doi: 10.1080/01904167.2016.1240191

El-Shabasi, M. S., Mohamed, S. M., and Mahfouz, S. A. (2005). Effect of foliar spray with amino acids on growth, yield and chemical composition of garlic plants. *6th Arabian Conf. Hort.*

Enderson, J., Mallarino, A. P., and Haq, M. U. (2015). Soybean yield response to foliar-applied micronutrients and relationships among soil and tissue tests. *Agron. J.* 107, 2143–2161. doi: 10.2134/agronj14.0536

Evliya, H. (1964). *Kültür bitkilerinin beslenmesi* Vol. 10 (Sayı: Ankara Üniversitesi Ziraat Fakültesi Yayınları).

Fehr, W. R., Caviness, C. E., Burmood, D. T., and Pennington, J. S. (1971). Stage of development descriptions for soybeans, Glycine max (L.) Merril. *Crop Sci.* 11, 929–931. doi: 10.2135/cropsci1971.0011183X001100060051x

Hansch, R., and Mendel, R. R. (2009). Physiological functions of mineral micronutrients (Cu, Zn, Mn, Fe, Ni, Mo, B, Cl). *Curr. Opin. Plant Biol.* 12, 259–266. doi: 10.1016/j.pbi.2009.05.006

Imsong, W., Tzudir, L., Longkumer, L. T., Gohain, T., and Kawikhonliu, Z. (2023). Effect of Sulphur and Zinc Fertilization on Growth and Yield of Soybean [*Glycine max* (L.) Merrill] under Nagaland Condition. *Agric. Sci. Digest.* 43, 637–642. doi: 10.18805/ag.D-5758

Jackson, M. L. (1967). *Soil chemical analysis* (New Delhi: Prentice Hall of India Private'Limited).

Joy, E. J. M., Alexander, J. S., Young, S. D., Ander, E. L., Watts, M. J., and Broadley, M. R. (2015). Zinc-enriched fertilisers as a potential public health intervention in Africa. *Plant Soil* 389, 1–24. doi: 10.1007/s11104-015-2430-8

Kacar, B. (1972). *Chemical Analyses of Plant and Soil*. Ankara: Ankara University, Faculty of Agriculture.

Kacar, B., and Inal, A. (2008). Plant analysis. Ankara University, Faculty of Agriculture, Ankara: Nobel Publications, 1241.

Kamar, M. E., and Omar, A. (1987). Effect of nitrogen levels and spraying with animal-forte (amino acids salvation) on yield of cucumber and potatoes. *J. Agric. Sci. Mansoura Univ* 12, 900–907.

Kanase, N., Jadhao, S. M., Konde, N. M., and Patil, J. D. (2008). Response of soybean to application of zinc. *Agric. Sci. Dig.* 28, 63–64.

Kocira, S., Kocira, A., Kornas, R., Koszel, M., Szmigielski, M., and Krajewska, M. (2017). Effects of seaweed extract on yield and protein content of two common bean (Phaseolus vulgaris L.) cultivars. *Legume Res.* 41, 589–593. doi: 10.18805/LR-383

Kumssa, D. B., Joy, E. J., Ander, E. L., Watts, M. J., Young, S. D., Walker, S., et al. (2015). Dietary calcium and zinc deficiency risks are decreasing but remain prevalent. *Sci. Rep.* 5, 10974. doi: 10.1038/srep10974

Lindsay, W. L., and Norvell, W. A. (1978). Development of a DTPA soil test for Zinc, Iron, Manganese and Copper. *Soil Sci. Soc Am. J.* 42, 421–428. doi: 10.2136/sssaj1978.03615995004200030009x

Liu, X., Chen, V., Qin-xue, N., and Seung, L. K. (2008). Evaluation of the Role of mixed amino acids in nitrate uptake and assimilation in leafy radish by using 15n-labeled nitrate. *Agric. Sci. In* 7, 1196–1202. doi: 10.1016/S1671-2927(08)60164-9

Lyons, G., and Cakmak, I. (2012). Agronomic Biofortification of Food Crops with Micronutrients. Fertilizing Crops to Improve Human Health: a Scientific Review. *Norcross* (GA, USA; IFA, Paris, France: Food and Nutrition Security IPNI), 97.

Mallarino, A. P., Haq, M. U., Wittry, D., and Bermudez, M. (2001). Variation in soybean response to early season foliar fertilization among and within fields. *Agron. J.* 93, 1220–1226. doi: 10.2134/agronj2001.1220

Mao, H., Wang, J., Wang, Z., Zan, Y., Lyons, G., and Zou, C. (2014). Using agronomic biofortification to boost zinc, selenium, and iodine concentrations of food crops grown on the loess plateau in China. *J. Soil Sci. Plant Nutr.* 14, 459–470. doi: 10.4067/S0718-95162014005000036

Marschner, H. (1995). *Mineral Nutrition of Higher Plants. 2nd ed* (New York, USA: Academic press).

Meenakshi, J. V., Johnson, N. L., Manyong, V. M., DeGroote, H., Javelosa, J., Yanggen, D. R., et al. (2010). How cost-effective is biofortification in combating micronutrient malnutrition? An ex ante assessment. *World Dev.* 38, 64–75. doi: 10.1016/j.worlddev.2009.03.014

Moreira, A., and Moraes, L. A. C. (2017). Yield nutritional status and soil fertility cultivated with common bean in response to amino-acids foliar application. *J. Plant Nutr.* 40, 344–351. doi: 10.1080/01904167.2016.1240194

Moreira, A., Moraes, L. A. C., and Fageria, N. K. (2015). Zinc and amino-acids on the yield and nutritional state of alfalfa grown in the tropical soil. *J. Plant Nutr.* 38, 780–794. doi: 10.1080/01904167.2014.944710

Noulas, C., Tziouvalekas, M., and Karyotis, T. (2018). Zinc in soils, water and food crops. *J. Trace Elem. Med. Biol.* 49, 252–260. doi: 10.1016/j.jtemb.2018.02.009

Oliveira, N. T., Rezende, P. M., Bruzi, A. T., and Melville, C. C. (2018). Effects on food-type soybean cultivars when biofortified with different rates of zinc. *Rev. Ciênc. Agrár.* 41, 647–654. doi: 10.19084/RCA17151

Olsen, S., and E.L., S. R. (1982). Phosphorus Availability Indices. Phosphorus soluble in sodium bicarbonate. *Methods Soil Anal. Part II Chem. Microbiol. Prop. ASA and SSSA*, 404–430.

Orman, Ş., and Ok, H. (2016). Biofortification in cultivation of crop plants. *Çukurova J. Agric. Food Sci.* 31, 221–227.

Raghuwanshi, N., Sharma, B., Uikey, I., and Prajapati, S. (2017). Residual and Cumulative effect of Zinc on Yield, Quality of Soybean (*Glycine max* L.) and Various pools of Zinc in a Vertisol of Madhya Pradesh, cv. JS 97-52. *Int. J. Bio-resource Stress Manage.* 8, 444–449. doi: 10.23910/IJBSM/2017.8.3.1800c

Rawat, N., Neelam, K., Tiwari, V. K., Malik, S., Tripathi, S. K., Randhawa, G. S., et al. (2013). Biofortification of cereals to overcome hidden hunger. *Plant Breed* 132, 437–445. doi: 10.1111/pbr.12040

Sadak, M. S. H., Abdelhamid, M. T., and Schmidhalter, U. (2014). Effect of foliar application of amino acids on plant yield and some physiological parameters in bean plants irrigated with seawater. *Acta Biol. Colomb* 20, 141–152. doi: 10.15446/abc.v20n1.42865

SAS Institute. (2011). *SAS/STAT Statistical Analysis SystemManual (v.9.3.)* (Cary, NC: SAS Institute).

Sánchez-Palacios, J. T., Henry, D., Penrose, B., and Bell, R. (2023). Formulation of zinc foliar sprays for wheat grain biofortification: a review of current applications and future perspectives. *Front. Plant Sci.* 2, 247600. doi: 10.3389/fpls.2023.1247600

Shehata, S. M., Abdel-Azem, H. S., Abou El-Yazied, A., and El-Gizawy, A. M. (2011). Effect of foliar spraying with amino acids and seaweed extract on growth chemical constitutes, yield and its quality of celeriac plant. *Eur. J. Sci. Res.* 58, 257–265.

Singh, S., Singh, V., and Layek, S. (2017). Influence of sulphur and zinc levels on growth, yield and quality of soybean (*Glycine max* L.). *Int. J. Plant Soil Science.* 18, 1–7. doi: 10.9734/IJPSS/2017/35590

Souza, J. A., Moraes, L. A. C., and Moreira, A. (2019). Zinc and amino acids on wheat-soybean intercropping under no-till management. *J. Plant Nutr.* 42, 1992–2002. doi: 10.1080/01904167.2019.1648665

Storksdieck, S., and Hurrell, R. F. (2009). "The impacts of trace elements from plants on human nutrition: A case for biofortification," in *Biofortified Agricultural Products*. (Boca Raton, FL, USA: CRC Press), 1–15.

Suciu, V., Rusu, T., Urdă, C., Muntean, E., Rezi, R., Negrea, A., et al. (2022). Effect of fertilizers on yield component attributes, yield and quality in soybean crop. *AgroLife Sci. J.* 11, 221–229. doi: 10.17930/AGL2022126

Sutradhar, A. K., Kaiser, D. E., and Behnken, L. M. (2017). Soybean response to broadcast application of boron, chlorine, manganese, and zinc. *Agron. J.* 109, 1048–1059. doi: 10.2134/agronj2016.07.0389

Thomas, G. W. (1982). Exchangeable Cations. Methods of Soil Analysis. Number 9, Part 2, *American Society of Agronomy, Soil Science Society of America, Madison*, Wisconsin, 159–165.

Teixeira, I. R., Borem, A., Silva, A. G., and Kikuti, H. (2008). Sources and doses of zinc in common bean cultivated in different sowing seasons. *Acta Sci. Agron.* 30, 255–259.

Teixeira, W. F., Fagan, E. B., Soares, L. H., Soares, J. N., Reichardt, K., and Neto, D. D. (2018). Seed and foliar application of amino acids improve variables of nitrogen metabolism and productivity in soybean crop. *Front. Plant Sci.* 9, 396. doi: 10.3389/fpls.2018.00396

Thornton, B., and Robinson, D. (2005). Uptake and assimilation of nitrogen from solutions containing multiple N sources. *Plant Cell Environ.* 28, 813–821. doi: 10.1111/j.1365-3040.2005.01332.x

Tousi, P., Tajbakhsh, M., and Esfahani, M. (2014). Effect of spray application of nano-Fe chelate, amino acid compounds and magnetic water on protein content and fatty acids composition of oil of soybean (*Glycine max*) in different harvest time. *Iran. J. Crop Sci.* 16, 125–136.

Treichel, S. (1975). The effect of NaCl on the concentration of proline in different halophytes. *Z Pflanzenphysiol* 76, 56–68. doi: 10.1016/S0044-328X(75)80046-8

Turan, M., and Horuz, A. (2012). *Bitki Beslemenin Temel Ilkeleri. Bitki Besleme* (Ankara: Gübretaş Rehber Kitaplar Dizisi).

Vahedi, A. (2011). The effects of micronutrient application on soybean seed yield and on seed oil and protein content. *J. Am. Sci.* 7, 672–677.

Wahba, H. E., Motawe, H. M., and Ibrahim, A. Y. (2015). Growth and chemical composition of Urtica pilulifera L. plant as influenced by foliar application of some amino acids. *J. Mater Environ. Sci.* 6, 499–506.

Wang, B., Abdalla, E., Atrio-Barandela, F., and Pavon, D. (2016). Dark matter and dark energy interactions: Theoretical challenges, cosmological implications and observational signatures. *Rep. Prog. Phys.* 79, 096901. doi: 10.1088/0034-4885/79/9/096901

White, P. J., and Broadley, M. R. (2011). Physiological limits to zinc biofortification of edible crops. *Front. Plant Sci.* 80, 1–11. doi: 10.3389/fpls.2011.00080

Zewail, R. M. Y. (2014). Effect of seaweed extract and amino acid on growth and productivity and some biocostituents of common bean *(Phaseolus vulgaris* L.) plants. *J. Plant Prod. Mansoura Univ* 5, 1441–1453. doi: 10.21608/jpp.2014.64669

Zhan, J., Twardowska, I., Wang, S. Q., Wei, S. H., Chen, Y. Q., and Ljupco, M. (2019). Prospective sustainable production of safe food for growing population based on the soybean (*Glycine max* L. Merr.) crops under Cd soil contamination stress. *J. Clean. Prod.* 212, 22–36. doi: 10.1016/j.jclepro.2018.11.287

frontiers | Frontiers in Plant Science

TYPE Original Research
PUBLISHED 29 April 2024
DOI 10.3389/fpls.2024.1378186

OPEN ACCESS

EDITED BY
Guowei Li,
Shandong Academy of Agricultural Sciences, China

REVIEWED BY
Xilong Liang,
Heilongjiang Bayi Agricultural University, China
Klára Kosová,
Crop Research Institute (CRI), Czechia

*CORRESPONDENCE
Faiçal Brini
faical.brini@cbs.rnrt.tn
Carla Ceoloni
ceoloni@unitus.it

†These authors have contributed equally to this work

RECEIVED 29 January 2024
ACCEPTED 09 April 2024
PUBLISHED 29 April 2024

CITATION
Tounsi S, Giorgi D, Kuzmanović L, Jrad O, Farina A, Capoccioni A, Ben Ayed R, Brini F and Ceoloni C (2024) Coping with salinity stress: segmental group 7 chromosome introgressions from halophytic *Thinopyrum* species greatly enhance tolerance of recipient durum wheat.
Front. Plant Sci. 15:1378186.
doi: 10.3389/fpls.2024.1378186

Coping with salinity stress: segmental group 7 chromosome introgressions from halophytic *Thinopyrum* species greatly enhance tolerance of recipient durum wheat

Sana Tounsi[1], Debora Giorgi[2†], Ljiljana Kuzmanović[3†], Olfa Jrad[1], Anna Farina[2], Alessandra Capoccioni[3], Rayda Ben Ayed[4,5], Faiçal Brini[1*] and Carla Ceoloni[3*]

[1]Biotechnology and Plant Improvement Laboratory, Centre of Biotechnology of Sfax (CBS), University of Sfax, Sfax, Tunisia, [2]ENEA Casaccia Research Center, Department for Sustainability, Biotechnology and Agroindustry Division, Rome, Italy, [3]Department of Agriculture and Forest Sciences (DAFNE), University of Tuscia, Viterbo, Italy, [4]Department of Agronomy and Plant Biotechnology, National Institute of Agronomy of Tunisia (INAT), University of Carthage, Tunis, Tunisia, [5]Laboratory of Extremophile Plants, Centre of Biotechnology of Borj-Cédria, Hammam-lif, Tunisia

Increased soil salinization, tightly related to global warming and drought and exacerbated by intensified irrigation supply, implies highly detrimental effects on staple food crops such as wheat. The situation is particularly alarming for durum wheat (DW), better adapted to arid/semi-arid environments yet more sensitive to salt stress than bread wheat (BW). To enhance DW salinity tolerance, we resorted to chromosomally engineered materials with introgressions from allied halophytic *Thinopyrum* species. "Primary" recombinant lines (RLs), having portions of their 7AL arms distally replaced by $7el_1L$ *Th. ponticum* segments, and "secondary" RLs, harboring *Th. elongatum* 7EL insertions "nested" into $7el_1L$ segments, in addition to near-isogenic lines lacking any alien segment (CLs), cv. Om Rabia (OR) as salt tolerant control, and BW introgression lines with either most of $7el_1$ or the complete 7E chromosome substitution as additional CLs, were subjected to moderate (100 mM) and intense (200 mM) salt (NaCl) stress at early growth stages. The applied stress altered cell cycle progression, determining a general increase of cells in G1 and a reduction in S phase. Assessment of morpho-physiological and biochemical traits overall showed that the presence of *Thinopyrum* spp. segments was associated with considerably increased salinity tolerance versus its absence. For relative water content, Na^+ accumulation and K^+ retention in roots and leaves, oxidative stress indicators (malondialdehyde and hydrogen peroxide) and antioxidant enzyme activities, the observed differences between stressed and unstressed RLs versus CLs was of similar magnitude in "primary" and "secondary" types, suggesting that tolerance factors might reside in defined $7el_1L$ shared portion(s). Nonetheless, the incremental contribution of 7EL segments emerged in various instances, greatly mitigating the effects of salt stress on root and leaf growth and on the quantity of photosynthetic pigments, boosting accumulation of compatible solutes and minimizing the decrease of a powerful antioxidant like ascorbate. The seemingly synergistic effect of $7el_1L$ + 7EL segments/genes made

"secondary" RLs able to often exceed cv. OR and equal or better perform than BW lines. Thus, transfer of a suite of genes from halophytic germplasm by use of fine chromosome engineering strategies may well be the way forward to enhance salinity tolerance of glycophytes, even the sensitive DW.

KEYWORDS

abiotic stress, alien gene transfer, chromosome engineering, wild wheat relatives, *Thinopyrum ponticum*, *Thinopyrum elongatum*, *Triticum*, sustainability

Introduction

Due to the many environmental components that soil salinization severely affects, it is considered an ecological disaster (Tedeschi, 2020). Whether induced by natural processes and/or anthropogenic activities (principally irrigation), it leads to degradation of soil quality and, in turn, to detrimental effects on all directly or indirectly soil-dependent organisms, including crop plants that represent major food source for mankind, such as wheat (Eynard et al., 2005; Cuevas et al., 2019; El Sabagh et al., 2021; Ullah et al., 2021). Increased salinization, mainly due to excess accumulation of sodium chloride (NaCl), is tightly related to other climate change–driven abiotic stresses. In fact, as a result of global warming and drought, an array of phenomena, from an increase in evaporation and a decrease in precipitation to sea level rise and seawater intrusion into freshwater ecosystems, up to prolonged irrigation supply, poor drainage conditions, and use of marginal water, are concurring to increase the percentage of saline-alkali soils, particularly in arid and semi-arid regions (Cuevas et al., 2019; Tedeschi, 2020; Hopmans et al., 2021; Mazhar et al., 2022; Pearce, 2022; Singh, 2022). Excess salinity currently affects nearly 7% of the world's total land area, but projections for 2050 indicate as much as 50% of arable land being salinized (Hu and Schmidhalter, 2023), a figure already approached in irrigated soils, providing nearly half of global food production (Bannari and Al-Ali, 2020; Hopmans et al., 2021; Ullah et al., 2021; Singh, 2022). Therefore, if cropping will take place more and more on salt-affected soils, substantial improvements in the salt tolerance of crops are needed. This concern is particularly alarming for wheat (*Triticum* spp.), ranking first in global grain production and representing the staple food for over 36% of world's population, yet with relatively limited tolerance to high soil salinity levels (Hasanuzzaman et al., 2017; El Sabagh et al., 2021).

Salinity stress significantly impairs all plant growth phases, from seed germination (SG) and seedling establishment to vegetative and reproductive development, ultimately impacting on yield. Excess salinity causes an early osmotic stress and a later ionic toxicity (Munns and Tester, 2008; Hu and Schmidhalter, 2023). Salt-induced osmotic changes in the rootzone lower plant ability to extract water from the soil and accelerate water loss from leaves, reducing turgor and overall disturbing plant water relations and, hence, plant growth. Over time, excess accumulation of Na^+ and/or Cl^- ions in plant tissues compromises ion homeostasis, leading to imbalance of other essential ions and nutrients, altogether hampering fundamental metabolic processes and physiological functions, such as photosynthesis (Hasanuzzaman et al., 2017; Guellim et al., 2019; Arif et al., 2020; El Sabagh et al., 2021; Hu and Schmidhalter, 2023). At the cellular level, in addition to impairing regular cell cycle progression (Qi and Zhang, 2020), excess salinity, as other stresses, triggers a burst in production of reactive oxygen species (ROS), responsible for oxidative stress, leading to lipid peroxidation (e.g., membrane damage), protein degradation (e.g. photosynthetic enzymes), and DNA mutation (Carillo et al., 2011; Hasanuzzaman et al., 2017).

Along with the ability to reduce the ionic stress by minimizing the Na^+ cytosolic amount, particularly in transpiring leaf tissue, and limiting the K^+ efflux (Wu et al., 2018b), ROS scavenging represents an essential mechanism of plant salt tolerance (Hasanuzzaman et al., 2020). ROS, which also work as important signal transduction molecules integrated in various stress response pathways, are normally kept at basal non-toxic levels by an array of antioxidative mechanisms (Mittler, 2017; Hasanuzzaman et al., 2020). As these mechanisms become less efficient under stress conditions, a complex system of enzymatic and non-enzymatic reactions and components is triggered to maintain the cellular redox homeostasis (Feki et al., 2017; Hasanuzzaman et al., 2020). Superoxide dismutase (SOD), catalase (CAT), peroxidase (POD), ascorbate peroxidase (APX), glutathione reductase, and glutathione

Abbreviations: APX, Ascorbate peroxidase; AsA, Ascorbic acid; BW, Bread wheat; CAR, Carotenoid content; CAT, Catalase; CHL, Chlorophyll content; CL, Control line; CS, Chinese Spring; CS7E(7D), CS substitution line of chromosome 7E in place of 7D; CSTr#12, CS transfer line No. 12; DAS , Days after sowing; DW, Durum wheat; EC, Electrical conductivity; K.L, K^+ content in leaves; K.R, K^+ content in roots; LDW, Leaf dry weight; LL, Leaf length; LSA, Leaf surface area; MDA, Malondialdehyde; Na.L, Na^+ content in leaves; Na.R, Na^+ content in roots; OR, Om Rabia; POD, Peroxidase; PRO, Proline; RDW, Root dry weight; RE, Root elongation; RL, Recombinant line; ROS, Reactive oxygen species; RWC, Relative water content; SG, Seed germination; SOD, Superoxide dismutase; TSS, Total soluble sugars; 7EL, Long arm (L) of *Thinopyrum elongatum* chromosome 7E; $7el_1L$, Long arm (L) of *Thinopyrum ponticum* chromosome $7el_1$.

peroxidase are among the most frequently activated ROS-detoxifying enzymes (e.g. Hasanuzzaman et al., 2017; Tounsi et al., 2023). As for non-enzymatic antioxidant molecules, ascorbic acid (AsA) and glutathione (GSH), belonging to the AsA–GSH pathway, play a vital and universal role, along with α-tocopherol (vitamin E), flavonoids, anthocyanins, phenolic compounds, and carotenoids (Foyer and Noctor, 2011; Suzuki et al., 2012; Venkatesh and Park, 2014; Hasanuzzaman et al., 2019, 2020; El Sabagh et al., 2021). Small organic molecules referred to as osmoprotectants or osmolytes are additional fundamental players in the plant response to salinity stress. Certain amino acids, particularly proline, ammonium compounds, sugars, and sugar alcohols, are effective protectants that act not only as compatible solutes in osmotic adjustment but also in maintenance of ion homeostasis, ROS scavenging, modulation of antioxidant enzyme activities, and stabilization of cell structures and of key metabolisms (Hasanuzzaman et al., 2017; El Sabagh et al., 2021).

Plant species vary widely in their response to salinity stress, with osmotic and ion effects being interconnected and often collectively impacting on the plant (Hopmans et al., 2021). Most crop plants, including cereals, are glycophytes. Among them, barley shows the highest ability to withstand salt stress, followed by wheat and then rice (Munns et al., 2006; Roy et al., 2014; Hopmans et al., 2021). Durum wheat (*Triticum durum* Desf., $2n = 4x = 28$, genome AB; DW) is one of the most important crops cultivated in countries surrounding the Mediterranean basin (Xynias et al., 2020). Geographical and environmental/climatic characteristics of the Mediterranean area make it particularly prone to salinization surge: a rapid decay of freshwater resources is registered here, along with temperatures rising faster than the global average and a 25%–30% decline in rainfall predicted by 2080 (Borghini et al., 2014; Cannon, 2022; Pearce, 2022). DW is more adapted to arid and semi-arid conditions compared with bread wheat (*Triticum aestivum* L., $2n = 6x = 42$, genome ABD; BW), yet more sensitive than the latter to excess soil salinity (Yousfi et al., 2010; Carillo et al., 2011; Annunziata et al., 2017). Distinctive traits between the two wheat species include a superior ability to maintain lower Na^+ accumulation and a higher K^+/Na^+ ratio in the root and leaf/shoot tissues manifested by BW (Colmer et al., 2006; Wu et al., 2014; Wu et al., 2018a, Wu et al., 2018b), along with an overall higher expression of salt-responsive homoeologous genes located on the D-subgenome (Yang et al., 2014; Zhang et al., 2016). To enhance DW salinity tolerance via transfer of BW homoeoloci, DW chromosome 4B was engineered with a BW chromosome 4D introgression containing the *Knal* gene for K^+/Na^+ discrimination (Dvořák et al., 1994; Luo et al., 1996).

Although with intra-specific variation, marked salinity tolerance characteristics are present in closely related wild Triticeae species, including diploid A genome species (*T. urartu*, *T. monococcum*; see, e.g., Munns et al., 2012; Tounsi et al., 2016) and various diploid or polyploid *Aegilops* species (e.g. Colmer et al., 2006; Farooq and Azam, 2007; Inbart-Pompan et al., 2013; Darko et al., 2020; Pour-Aboughadareh et al., 2021). However, it is within perennial wheatgrasses, belonging the wheat tertiary gene pool, that the greatest number of highly salt tolerant or even truly halophytic Triticeae species can be found, notably those belonging to the *Thinopyrum* genus (Colmer et al., 2006; Flowers and Colmer, 2008). Such species, carriers of many beneficial traits, rarely or not represented in cultivated wheat or closely allied gene pools (Ceoloni et al., 2015), were since long identified as among the few representatives of the Triticeae tribe occupying specialized ecological niches with high salinity features (Dewey, 1960; McGuire and Dvořák, 1981; Dvořák et al., 1988; Farooq, 2009; Ceoloni et al., 2015; Arzani and Ashraf, 2016; Mujeeb-Kazi et al., 2019). They are indigenous of southern Europe, western Asia, and northern Africa, where frequently occur on saline meadows and seashores (e.g., Monsen et al., 2004). Moreover, they were widely naturalized and exploited in disturbed wastelands throughout North America (Scheinost et al., 2008), as well as in Argentina, some European countries, and China (Li et al., 2023 and references therein). Remarkable adaptive abilities in critical environments, such as saline and sodic soils, are exhibited by the decaploid *Thinopyrum ponticum* ($2n = 10x = 70$). From BW-*Th. ponticum* hybrids and amphiploids, introgression of single (Yuan and Tomita, 2015) or multiple (Chen et al., 2004) chromosomal segments from the wild parent was obtained, which conferred several major salt tolerance traits to BW. In neither case, however, were the *Th. ponticum* segments assigned to corresponding chromosomes. This was, instead, the case for another salt tolerant *Thinopyrum* species, that is, the diploid *Th. elongatum* ($2n = 2x = 14$). From single chromosome addition and substitution lines into BW cv. Chinese Spring (CS), the enhanced salt tolerance exhibited by the CS/*Th. elongatum* amphiploid was found to be controlled by additively acting genes located on many *Th. elongatum* chromosomes, 3E and 7E containing the major determinants of the improved performance of the recipient BW (Dvořák et al., 1988; Omielan et al., 1991; Deal et al., 1999; Zeng et al., 2023). Several recombinant lines (RLs) carrying 3E introgressions on 3A or 3D were obtained (Mullan et al., 2009), and their effects upon salt stress application were analyzed (Deal et al., 1999; Mullan et al., 2009; Zeng et al., 2023). On the other hand, little knowledge is available on the contribution of 7E, of which both arms seem to contribute to the enhancement of the K^+/Na^+ ratio in BW, but with a more significant impact of the long arm, that is, 7EL (Deal et al., 1999).

The opportunity to analyze the effects upon salt stress exposure of introgression of group 7 long arms of *Thinopyrum* spp. chromosomes, specifically 7EL from *Th. elongatum* and $7el_1L$ (formerly 7AgL) from *Th. ponticum*, has been offered by DW-*Thinopyrum* spp. RLs, developed through chromosome engineering strategies and carrying small distal portions of either $7el_1L$ alone (Ceoloni et al., 2005) or with a "nested" 7EL insertion into the respective $7el_1L$ segment (Kuzmanović et al., 2019). The *Thinopyrum* spp. introgressions provide the RLs with several valuable attributes, from resistance to wheat diseases, quality- and yield-related traits (Kuzmanović et al., 2014; Ceoloni et al., 2015; Kuzmanović et al., 2016, 2018, 2019, Rossini et al., 2020; Kuzmanović et al., 2021; Fanelli et al., 2023), to enhanced tolerance to heat and combined heat and water deficit stress (Giovenali et al., 2023). However, they were not tested so far for their response to salt stress. Therefore, in view of exploiting such materials in DW sustainable and stress-responsive breeding, this

10.3389/fpls.2024.1378186

study aimed at assessing the behavior of primary and secondary DW-*Thinopyrum* spp. RLs, along with specific BW-*Thinopyrum* spp. introgression and other control lines (CLs), when exposed to salt (NaCl) stress under controlled conditions. Several morpho-physiological, cellular, and biochemical parameters were evaluated. The analysis revealed an overall highly positive impact of *Thinopyrum* spp. introgressions on DW performance toward salt stress and highlighted specific/major contributions to given tolerance traits of defined alien chromosome portions.

Materials and methods

Plant materials

Six DW-*Thinopyrum* spp. RLs represented the target materials for the salinity assays. They were developed at the University of Tuscia, Viterbo (Italy) and consist of near-isogenic RLs, obtained through chromosome engineering methodologies and repeated backcrosses ($BC_{4\text{-}5}$) of the original RLs with the recurrent Italian DW cv. Simeto, followed by several self-generations. RLs included three "primary" types (Ceoloni et al., 2005), carrying a distal *Th. ponticum* $7el_1L$ segment occupying a different percentage of the recipient DW 7AL arm, namely R5+ (23%), R112+ (28%), and R23 + (40%). Also employed were "secondary" RLs, harboring a small *Th. elongatum* 7EL insertion "nested" in the most telomeric portion of the *Th. ponticum* segment of R5+ and R112+; these were named R69-9/R5+, R69-9/R112+, and R74-10/R112+, with the R74-10 7EL fraction resulted genetically longer than the R69-9 one (Ceoloni et al., 2017; Kuzmanović et al., 2019), yet both segments being of undefined physical length (Figure 1). Together with the "+" RLs, which are homozygous carriers of the given *Thinopyrum* segment, corresponding sib lines, non-carrier of the given alien segment, and, hence, with a "–" symbol accompanying their designations, were also employed in the analyses as CLs. The Tunisian cv. OR was included as a salt-tolerant reference genotype (Brini et al., 2009). Seeds of OR were supplied by INRAT (Institut National de la Recherche Agronomique de Tunisie).

BW lines, all sharing the cv. CS background, were also part of the materials assayed (Figure 1). They were as follows: (1) CSTr#12, whose chromosome 7A is mostly replaced by *Th. ponticum* chromosome $7el_1$ (formerly 7Ag; Eizenga, 1987; Ceoloni et al., 1996), employed as donor line of the $7el_1L$ segments to the DW recombinants described above; (2) CS7E(7D), whose chromosome 7D is substituted by a complete *Th. elongatum* 7E, used in the chromosome engineering work to develop the "nested" recombinants (Ceoloni et al., 2017; Kuzmanović et al., 2019); (3) CS, working as control of the two previous lines. Seeds of CS and CSTr#12 were originally provided to C.C. by Prof. E.R. Sears, University of Missouri, Columbia, MO (USA), and those of the CS7E(7D) substitution line by Prof. Moshe Feldman, Weizmann Institute of Science, Rehovot (Israel).

Germination assays and morphological measurements at early stages

For a first assay, 30 seeds of each genotype were surface sterilized and placed in triplicates on Petri dishes on two sheets of wet filter paper with 0 mM NaCl, 100 mM NaCl, or 200 mM NaCl solution and then kept in a growth chamber for 3 days until germination. Germination ability was calculated at day 3 as percentage number of germinated seeds/total number of seeds.

For a second assay, which was repeated twice, a subset of DW RLs, namely, R112+ and R74-10/112+, together with their CLs, R112–, and R74-10/112–, were analyzed. Thirty seeds per genotype and salt concentration were grown in Petri dishes in 0 mM NaCl, 100 mM NaCl, or 200 mM NaCl. At 4 and 10 days after sowing (DAS) the following morphological traits were measured: root length 4 DAS (RL4, mm), root length 10 DAS (RL10, mm), leaf

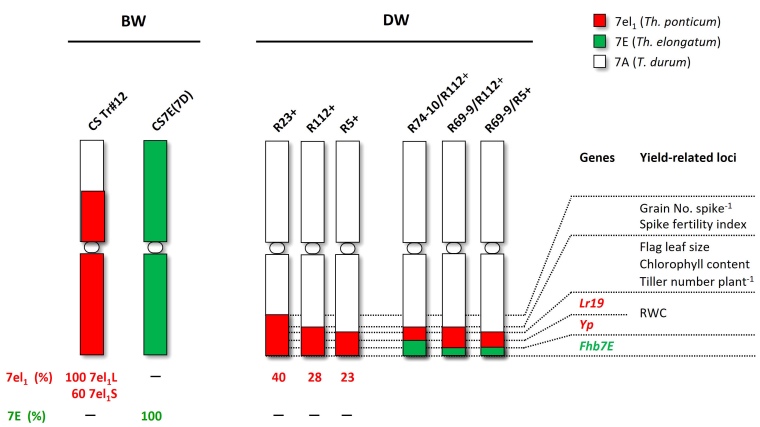

FIGURE 1
Wheat-*Thinopyrum* spp. lines tested for salt stress tolerance. Six are durum wheat (DW) recombinant lines (RLs), including R5+, R112+, and R23+ (*Th. ponticum* introgressions) and R69-9/R5+, R69-9/R112+, and R74-10/R112+ (*Th. ponticum* + *Th. elongatum* introgressions), and three bread wheat (BW) lines, namely cv. Chinese Spring (CS), the CSTr#12 RL, and the CS7E(7D) substitution line. Relative physical sizes of *Th. ponticum* segments are on scale in the respective 7A chromosomes, whereas for the 7E *Th. elongatum* introgressions, nested into the $7el_1$ *Th. ponticum* segments of the DW recombinants, their relative size versus the hosting segment is roughly deduced from genetic map data (see text).

length 4 DAS (LL4, cm), and leaf length 10 DAS (LL10, cm). At 10 DAS, leaf dry weight (LDW, g) and root dry weight (RDW, g) were also measured. RDW was determined on roots pooled from five plantlets, due to the very low root weight after drying. Root and leaf length were measured using ImageJ software (https://www.imagej.nih.gov/ij/download.html).

Growth conditions and salt treatment in the hydroponics assay

Seeds were surface sterilized with sodium hypochlorite for 15 min, rinsed 3 times with distilled water and then placed in Petri dishes containing Whatman filter paper. The dishes were transferred to a growth chamber at 23°C and 65% relative humidity, with a 16h light/8h dark photoperiod. Seven days after germination, seedlings were transferred to a hydroponic system. The boxes were filled with half-strength Hoagland nutrient solution, which was refreshed every week (Davenport et al., 2005). Each box was constantly aerated by two adjustable air diffusers. After 2 weeks, NaCl concentration was increased progressively for 3 days until reaching 100 mM and 200 mM (Figure 2). Control plants were kept in nutrient solution. Plant tissues (roots and leaves) were harvested after 3 days of salt treatment (i.e., on the 21st day after sowing, DAS; Figure 2) and used for morpho-physiological and biochemical analyses. For all traits, measurements were performed using at least three biological and three technical replicates. Whole, fully expanded leaves were used for measurements of relative water content (RWC) and leaf surface area (LSA). In the latter case, the third leaf of representative plants of each genotype was consistently employed. The remaining leaves were harvested and used for biochemical analyses. Root elongation (RE) was measured on the main seminal roots and the total biomass used for ion determination.

Morpho-physiological and biochemical analyses in the hydroponics assay

Measurement of root length and leaf surface area

Root elongation (RE, cm) was determined using ImageJ software (https://www.imagej.nih.gov/ij/download.html), while LSA (cm^2) was analyzed by UTHSCA (http://ddsdx.uthscsa.edu/dig/itdesc.html) image tool software.

Relative water content

RWC was calculated as described by Tounsi et al. (2017), using the formula: RWC (%) = (fresh weight – dry weight)/(saturated fresh weight – dry weight) ×100.

Chlorophyll and carotenoid contents

Fresh leaves were weighed, immersed in 80% acetone and kept at 4°C in the dark for 24h. Total chlorophyll and carotenoid contents were measured using a spectrophotometer at 646.6 nm, 663.6 nm, and 450 nm, respectively (de Carvalho et al., 2012; Tounsi et al., 2017).

Proline and total soluble sugar contents

Proline content was determined according to Bates et al. (1973). Briefly, fresh leaves (0.25 g) were mixed in 5 mL of 3% (w/v) sulfosalicylic acid and filtered. Then, 2 mL of filtrate were mixed with 2 mL of acidic ninhydrin reagent and 2 mL of glacial acetic acid. The mixture was incubated for 1h at 100°C. After incubation, 4

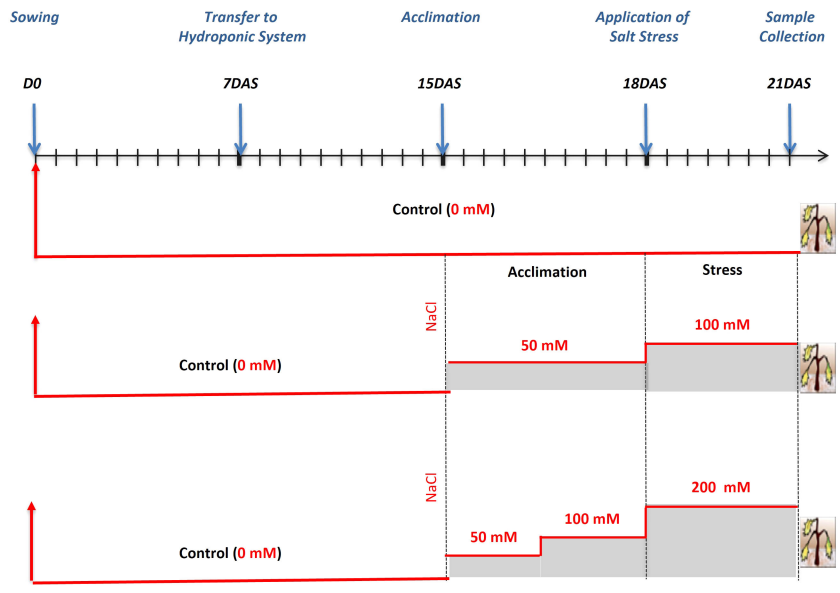

FIGURE 2
Schematic representation of salt stress application. DAS, days after sowing.

mL of toluene were added and vigorously mixed for 20 s. The chromophore was aspirated from the aqueous phase and the absorbance measured at 520 nm.

Total soluble sugar (TSS) content was measured in leaves as described by Bouteraa et al. (2022). Fresh leaves (0.2 g) were vigorously mixed in 80% ethanol solution and the mixture was centrifuged for 10 min at 10,000×g at 4°C. One milliliter of supernatant was added to 3 mL of anthrone reagent and the reaction mixture was heated for 10 min at 100°C. After cooling the reaction, optical density was measured at 620 nm.

Malondialdehyde and hydrogen peroxide contents

Malondialdehyde (MDA) content, content, a commonly used measure of the extent of lipid peroxidation, was determined according to Draper and Hadley (1990). Fresh leaves were homogenized in 0.1% TCA and centrifuged for 30 min at 12,000×g. One milliliter of supernatant was added to 1 mL of 0.5% TBA, incubated for 30 min at 95°C and then cooled for 10 min. After centrifugation at 12,000×g for 5 min, the absorbance of supernatant was measured at 532 nm and 600 nm.

Hydrogen peroxide (H_2O_2) content was measured as described by Velikova et al. (2000). Fresh leaves were homogenized in 0.1% TCA and centrifuged for 30 min at 12,000×g. Thereafter, 0.5 mL of supernatant was mixed with 0.5 mL potassium phosphate buffer (10 mM, pH 7.0) and 1 mL potassium iodide (1 M). The absorbance was determined at 390 nm.

Antioxidant activities

Fresh leaves (0.2 g) were homogenized with 2 mL of chilled extraction buffer (50 mM phosphate buffer pH 7.0, 2% PVP, and 1 mM PMSF). The homogenate was centrifuged at 10,000×g for 20 min at 4°C and the supernatant was collected and kept at 4°C to determine the antioxidant activities of the following enzymes: SOD, CAT, POD, and APX. Protein concentration in the different extracts was determined as described by Bradford (1976).

SOD activity was determined by quantifying the enzyme ability to inhibit the photochemical reduction of nitro-blue tetrazolium (NBT) (Djemal and Khoudi, 2016). Briefly, 20 µg of crude enzyme extract was added to the reaction mixture composed of 50 mM phosphate buffer (pH 7.8), 0.1 mM EDTA, 13 mM L-methionine, 2 mM riboflavin, and 75 mM NBT. The mixture was exposed to cool-white, fluorescent light for 15 min and absorbance was determined at 560 nm.

CAT activity was determined by measuring the reduction of H_2O_2 at 240 nm (Aebi, 1984). The reaction solution was composed of 50 mM potassium phosphate buffer (pH 7.0), 30 mM H_2O_2, and 20 µg of crude enzyme extract.

POD activity was measured as described by Bouteraa et al. (2022) via the guaiacol oxidation method. The reaction mixture was composed of 50 mM phosphate buffer (pH 7), 20 mM guaiacol, 40 mM H_2O_2, and 20 µg of crude enzyme extract. The absorbance was determined at 470 nm.

APX activity was determined as described by Nakano and Asada (1981). The reaction mixture contained 50 mM potassium phosphate (pH 7.0), 0.5 mM ascorbate, 0.1 mM H_2O_2, and 0.1 mM EDTA in a total volume of 1 ml. The absorbance was measured at 290 nm.

As for non-enzymatic antioxidant molecules, AsA content was determined following the method described by Feki et al. (2017). Briefly, plant material (0.5 g) was vigorously ground in 10 mL of 6% (w/v) TCA solution and then mixed with 2% dinitrophenylhydrazine, followed by addition of one drop of thio-urea. The mixture was boiled for 15 min and cooled for 10 min at room temperature. Thereafter, 5 mL of 80% (v/v) H_2SO_4 were added to the mixture at 0°C and the absorbance was measured at 530 nm.

Na^+ and K^+ contents

Na^+ and K^+ concentrations were measured in roots and leaves as previously described by Tounsi et al. (2017). Briefly, tissues were dried at 70°C and then solubilized in 0.1 N hydrochloric acid for 24h. Each sample was diluted to measure Na^+ and K^+ contents using flame spectrophotometry (SpectrAA 220 FS, Varian).

Cell cycle analysis

To evaluate the effect of salt stress on cell cycle progression, 3-day-old seedlings of 7 DW genotypes, namely, R112+, R112−, R69-9/R5+, R69-9/R5−, R74-10/R112+, R74-10/R112− and cv. OR, and 3 BW genotypes, that is, CS7E(7D), CSTr#12, and CS, were placed in aerated Hoagland solution (Doležel et al., 1999), supplemented with 200 mM NaCl or 0 mM NaCl (control condition), at 22 ± 1°C for 24h. After the salt treatment, roots from 3–6 plants/genotype/treatment were excised and fixed in 2% (v/v) formaldehyde in 1X Tris-HCl buffer pH 7.5 for 10 min at 5°C (Doležel et al., 1992). Root tip nuclei from each plant were isolated in LB01 buffer (Doležel and Lucretti, 1989) by homogenization with a Mini-Turrax T8 with a S10N-5G generator (IKA, Staufen, Germany) for 12 s at 9,500 rpm. After DNA staining with DAPI (4,6-diamidino-2-phenylindole), nuclei were run on a CytoFLEX S flow analyzer (Beckman Coulter Flow Cytometry, Milan, Italy), using as internal reference standard (IRS) 2.5 µm polystyrene microspheres (Alignflow Beads for UV lasers cod. A16502, Thermo Fisher Scientific, Milan, Italy) to monitor instrument stability and to ensure a reliable comparison among experiments. DNA fluorescence emission was evaluated on at least 3,000 DAPI stained nuclei/plant, excited by a violet laser (ext. 405 nm), and the main DAPI fluorescence emission was collected at 525/40 nm. The distribution of cells at each of G1, S and G2 cell cycle phases was investigated by processing data with the cell cycle modeling utility in Kaluza 1.2 software (Beckman Coulter Life Science, IN, USA). The Kaluza tool facilitates determination of the percentage distribution of nuclei in G1, S and G2 phases according to their fluorescence, which is proportional to nuclear DNA content.

Statistical analysis

For all experiments, datasets of DW and BW genotypes were analyzed separately. Two-way analysis of variance (ANOVA) was

10.3389/fpls.2024.1378186

performed using the statistical software SPSS V23 (IBM Corp, Armonk, NY, USA) or SYSTAT12 (Systat Software Incorporated, San Jose, CA, USA), where Genotype (G) and Treatment (T) were inserted as main factors. For the second germination assay, Replica (R) was inserted as a covariance, corresponding to the two assay repetitions in time. In all analyses, the second order interaction G × T was also analyzed. When significant F values were observed, a pairwise post-ANOVA analysis was carried out by the Tukey Honestly Significant Difference test (Tukey test) at $p < 0.05$. Principal component analysis (PCA) for each of the DW and BW datasets was performed in R Environment (R Project for Statistical Computing 4.3.3), using functions included in "FactoMineR," "ggplot2," and "factoextra" packages.

Results

The salt (NaCl) stress conditions applied in the present work had an overall major impact on the traits assayed, as shown by several indicators of morpho-physiological, biochemical, and cellular plant features and functions. To the stress, the tested genotypes responded differently, particularly in relation to presence/absence of given *Thinopyrum* introgressions. For the majority of traits described in the following, ANOVA (Tables 1, 2; Supplementary Table S1) revealed highly significant differences due to the treatment (T, stressed versus unstressed conditions), to the genotype (G, several introgression versus CLs of DW and BW) and to their interaction (G × T).

Seed germination

Salt stress application caused a significant reduction in SG ability of all genotypes (Figure 3), but with RLs showing, mainly at 200 mM NaCl, superior performance versus their control ("–" sib) lines (CLs). At the highest salt concentration, SG was increased in lines R23+, R112+, R69-9/R5+, R69-9/R112+, R74-10/R112+ versus their controls by 104%, 94%, 90%, 141%, and 94%,

TABLE 1 Mean values ± standard error and ANCOVA mean squares of morphological traits after exposure to salt stress of primary (R112+) and secondary (R74-10/R112+) DW recombinant lines (+) and their respective controls, lacking the alien segment (–).

Genotype	Trait					
	RL4 (mm)	LL4 (cm)	RL10 (mm)	LL10 (cm)	RDW (g)	LDW (g)
0 mM NaCl						
R112+	6.20 ± 0.27 a	2.53 ± 0.11 a	18.16 ± 0.39 ab	12.22 ± 0.24 a	0.05 ± 0.00 ab	0.02 ± 0.00
R112–	4.88 ± 0.17 b	2.58 ± 0.10 a	12.45 ± 0.58 c	11.61 ± 0.20 ab	0.04 ± 0.00 b	0.02 ± 0.00
R74-10/R112+	5.12 ± 0.18 b	2.17 ± 0.09 b	18.80 ± 0.31 a	10.91 ± 0.22 b	0.06 ± 0.00 a	0.02 ± 0.00
R74-10/R112–	5.51 ± 0.20 b	2.13 ± 0.07 b	16.95 ± 0.48 b	10.03 ± 0.20 b	0.05 ± 0.00 ab	0.02 ± 0.00
100 mM NaCl						
R112+	3.47 ± 0.13 c	1.62 ± 0.06 c	8.18 ± 0.20 de	8.70 ± 0.20 c	0.03 ± 0.00 c	0.01 ± 0.00
R112–	2.50 ± 0.12 d	1.24 ± 0.08 d	5.82 ± 0.24 f	6.69 ± 0.25 d	0.02 ± 0.00 ce	0.01 ± 0.00
R74-10/R112+	3.51 ± 0.11 c	1.27 ± 0.05 d	8.99 ± 0.22 d	7.25 ± 0.20 d	0.02 ± 0.00 cd	0.01 ± 0.00
R74-10/R112–	3.11 ± 0.13 cd	1.18 ± 0.04 d	7.66 ± 0.13 e	6.90 ± 0.16 d	0.02 ± 0.00 df	0.01 ± 0.00
200 mM NaCl						
R112+	0.98 ± 0.07 e	0.50 ± 0.02 e	2.39 ± 0.14 g	1.36 ± 0.13 e	0.01 ± 0.00 f	0.00 ± 0.00
R112–	1.16 ± 0.08 e	0.56 ± 0.03 e	2.91 ± 0.13 g	1.26 ± 0.13 e	0.01 ± 0.00 f	0.00 ± 0.00
R74-10/R112+	1.32 ± 0.08 e	0.54 ± 0.02 e	3.04 ± 0.13 g	1.17 ± 0.08 e	0.01 ± 0.00 ef	0.00 ± 0.00
R74-10/R112–	0.99 ± 0.09 e	0.51 ± 0.02 e	2.13 ± 0.20 g	1.31 ± 0.11 e	0.01 ± 0.00 f	0.00 ± 0.00
ANCOVA						
G	11.9***	1.8***	265.7***	44.7***	0.000**	0.000
T	907.0***	132.4***	9926.6***	4269.1***	0.020***	0.004***
G x T	7.4***	0.9**	95.9***	18.1***	0.000*	0.000
Rep	42.5***	2.9**	72.3***	90.1***	0.000	0.000**

RL4, root length 4 days after sowing (DAS); RL10, root length 10 DAS; LL4, leaf length 4 DAS; LL10, leaf length 10 DAS; LDW, leaf dry weight; RDW, root dry weight. LDW and RDW were measured 10 DAS. Letters in each column correspond to ranking of Tukey test at $p < 0.05$ level for significant Genotype (G) x Treatment (T) interactions; Rep, replica included as a covariant; *, **, and *** indicate significance at $p < 0.05$, $p < 0.01$, and $p < 0.001$, respectively.

10.3389/fpls.2024.1378186

TABLE 2 Mean values (%) ± standard error and ANOVA mean squares of nuclei in cell cycle phases G1, S, and G2 of DW (A) and BW (B) introgression and control lines subjected to salt stress versus control conditions.

(A)			
DW lines	G1	S	G2
0 mM NaCl			
R112+	49.11 ± 1.04	17.62 ± 0.47 ab	33.28 ± 1.08 bc
R112–	47.72 ± 0.87	17.82 ± 1.29 ab	33.46 ± 0.78 ac
R69-9/R5+	49.69 ± 0.97	19.10 ± 0.42 a	31.26 ± 1.26 c
R69-9/R5–	49.35 ± 1.62	19.24 ± 2.07 a	31.41 ± 0.56 bc
R74-10/R112+	52.57 ± 1.03	13.44 ± 1.52 ae	33.98 ± 0.83 ac
R74-10/R112–	51.84 ± 1.19	15.49 ± 1.09 ad	32.67 ± 0.44 bc
Om Rabia	47.37 ± 1.05	17.35 ± 0.77 ab	35.27 ± 0.60 ac
200 mM NaCl			
R112+	52.92 ± 1.12	9.65 ± 1.43 e	37.60 ± 2.06 ab
R112–	50.77 ± 1.54	16.63 ± 1.57 ac	32.83 ± 1.17 bc
R69-9/R5+	55.11 ± 0.43	9.97 ± 1.13 de	34.92 ± 1.10 ac
R69-9/R5–	54.86 ± 2.49	12.76 ± 1.15 ae	32.37 ± 1.57 bc
R74-10/R112+	58.28 ± 0.69	12.27 ± 0.68 be	29.46 ± 1.12 c
R74-10/R112–	57.67 ± 1.43	11.67 ± 1.08 ce	30.66 ± 0.96 c
Om Rabia	49.91 ± 2.06	10.53 ± 1.04 de	39.57 ± 1.74 a
ANOVA			
G	61.0***	19.3*	47.2***
T	303.2***	399.5***	11.0
G x T	4.3	21.9**	28.0**
(B)			
BW lines	G1	S	G2
0 mM NaCl			
CS7E(7D)	55.77 ± 0.68	15.51 ± 0.83	28.73 ± 0.83
CSTr#12	56.25 ± 0.86	15.21 ± 1.06	28.54 ± 0.55
CS	55.19 ± 1.33	16.31 ± 1.37	28.50 ± 1.00
200 mM NaCl			
CS7E(7D)	68.84 ± 1.23	5.19 ± 0.65	25.97 ± 0.72
CSTr#12	67.06 ± 0.89	6.79 ± 0.76	26.14 ± 1.19
CS	68.47 ± 1.23	7.99 ± 0.22	23.55 ± 1.23
ANOVA			
G	1.2	8.6	5.9
T	1184.0***	627.4***	87.9***
G x T	4.8	3.3	4.8

Letters in columns of S and G2 phases of nuclei of DW genotypes (A) correspond to ranking of Tukey test at $p < 0.05$ level for genotype (G) x treatment (T) interactions. *, **, and *** indicate significance at $p < 0.05$, $p < 0.01$, and $p < 0.001$, respectively.

10.3389/fpls.2024.1378186

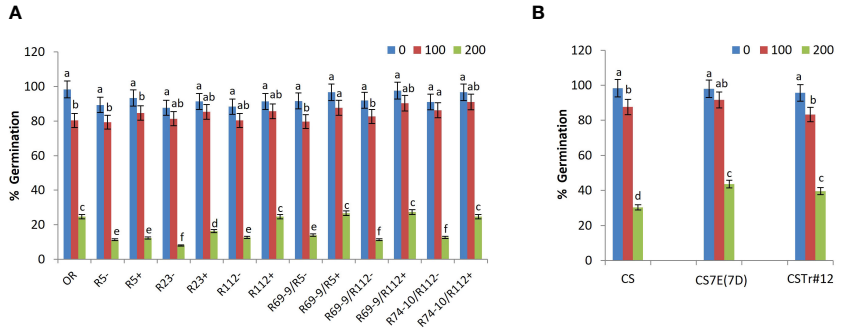

FIGURE 3
Effect of salt stress application on seed germination. Comparison between DW recombinant (+) versus control (–) lines and cv. OR **(A)** and between BW lines CSTr#12 and CS7E(7D) versus normal CS **(B)**. Values are expressed as means ± SE. Letters above histograms correspond to the ranking of Tukey test at $p < 0.05$ significance level. Color-coded legend: NaCl concentration (mM).

respectively (Figure 3A). Albeit not significant, at 200 mM NaCl recombinants R69-9/R5+ and R69-9/R112+ exhibited even higher SG (+8% and +10%, respectively) than the salt-tolerant Tunisian cv. OR. Similarly in the BW lines, although to a lesser extent than in DW, SG was significantly improved by the presence of the entire 7E chromosome in CS7E(7D) and most of the $7el_1$ in CSTr#12 (+43% and +30%, respectively) into the background of the recipient BW cv. CS (Figure 3B).

Plant growth and cell cycle progression

In the of hydroponic assay, already under control conditions significant differences for RE were displayed by primary RL R112+ and all secondary RLs (R69-9/R5+, R69-9/R112+, and R74-10/R112 +) versus their CLs. At 100 mM NaCl compared to 0 mM, the smallest decline of RE was observed in R5+ and in all the secondary RLs, among which R69-9/R5+ showed no significant stress effect on this trait. The remaining genotypes, including cv. OR, had conspicuous reductions of RE already at this salt concentration (Figure 4A). Then, at 200 mM NaCl, secondary RLs R69-9/R5+, R69-9/R112+, and R74-10/R112+ not only outperformed their "–" controls (+130%, +135%, +59%, respectively) and OR (+30%, +43%, +52%, respectively) but also their corresponding primary types, R5+ and R112+ (Figure 4A). Some incremental effect on RE was also observed at both NaCl concentrations in BW introgression lines, CS7E(7D) and CSTr#12, with respect to normal CS (Figure 4B), but neither one reached the high values of DW secondary RLs.

Likewise, under high salt stress, LSA was considerably larger in R69-9/R5+, R69-9/R112+, and R74-10/R112+ than in their CLs (+24%, +36%, and +40%, respectively) and in OR (+16%, +34%, and +42%, respectively, Figure 4C). Among primary RLs, R5+ did not differ from secondary types at 100 mM NaCl, but at 200 mM it did not maintain the same LSA values as those of secondary types. As for RE, also LSA values were higher in DW secondary RLs than in CS7E(7D) and CSTr#12, even at 200 mM NaCl (Figure 4D), supporting the hypothesis that presence of both alien segments ($7el_1L$ + 7EL) has an additive effect on both growth traits compared with their separate condition.

As for plants grown in Petri dishes and directly exposed to salt stress from germination up to 10 DAS, the statistical analysis showed significant differences for most of the measured parameters, namely, RL4, RL10, LL4, and LL10 and LDW and RDW at 0 mM and 100 mM NaCl (Table 1). The presence of the $7el_1$ *Th. ponticum* segment in R112+ was associated with a greater root length when compared to R112– at 0 mM NaCl (+27%) and at 100 mM NaCl (+39%), though not at higher salt concentration. On the other hand, at 200 mM NaCl, in the frame of a general major impairment of root growth, presence of the composite $7el_1$ + 7E segment in R74-10/R112+ led to increased RL4 by 33% and RL10 by 42% versus its absence (R74-10/R112–). Leaf growth was enhanced in R112+ versus R112– (+30% for LL4 and LL10), but only under the milder salt stress condition (100 mM), and a similar result was observed also for root biomass (+50% for RDW). No significant difference was observed in R74-10/R112+ versus R74-10/R112– for LL4, LL10, LDW, and RDW, at all salt concentrations (Table 1).

Since at cellular level plant growth depends on cell proliferation through the mitotic cycle and subsequent cell expansion, we investigated whether salt treatment differentially affected cell cycle progression in a subset of DW RLs (R112+, R69-9/R5+, and R74-10/R112+), their CLs and cv. OR, as well as in BW lines CS7E(7D), CSTr#12, and the CS control. DAPI-stained nuclei isolated from root tips of young seedlings exposed to 0 or 200 mM NaCl were analyzed by flow cytometry. Based on fluorescence emission, the percentage distribution of nuclei in G1, S and G2 phases was determined (Table 2). As for DW lines, in all of them salt stress versus the unstressed condition caused an increase of nuclei in G1, ranging from 5.4% in cv. OR to around 11% in R69-9/R5 and R74-10/R112, with no major difference between each RL and its CL. A similar variation was also detected for nuclei in G2 of stressed versus unstressed RLs R112+ and R69-9/R5+ and cv. OR (+13%, +11.7%, and +12.2%, respectively), which was not exhibited by R112– and R69-9/R5–. Conversely, R74-10/R112+ and, to a minor extent, its R74-10/R112– CL, showed a reduction of cell population in G2 (–13.3% and –6.1%, respectively) in stressed versus unstressed plants. On the other hand, a more prominent and unidirectional genotype effect upon salt treatment was displayed by S phase data, with all genotypes exhibiting a reduction of nuclei in this phase at the 200 mM versus 0 mM NaCl

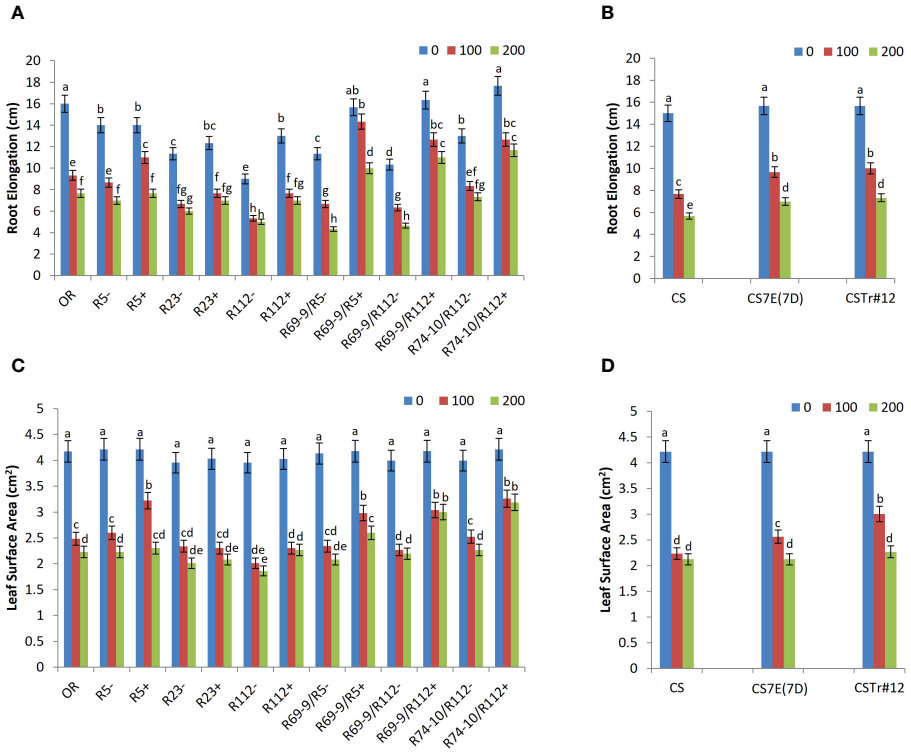

FIGURE 4
Effect of salt stress application on root elongation **(A, B)** and leaf surface area **(C, D)** of wheat lines. Comparison between DW recombinant (+) versus control (–) lines and cv. OR **(A, C)** and between BW lines CSTr#12 and CS7E(7D) versus normal CS **(B, D)**. Values are expressed as means ± SE. Letters above histograms correspond to the ranking of Tukey test at $p < 0.05$ significance level. Color-coded legend: NaCl concentration (mM).

(Table 2). The decrease was particularly strong in R112+ (–45%) compared with R112– (–12%) (Table 2A; Supplementary Figure S1), the difference between the two lines resulting in the only significant one among the RL versus CL pairs subjected to this analysis. As the two lines showed almost identical figures of nuclei in S phase under the unstressed condition (Table 2A; Supplementary Figure S1), the difference under stress is clearly ascribable to the *Th. ponticum* segment present in R112+. The same comparison showed a less dramatic difference between R69-9/R5+ and R69-9/R5– (–48% and –34% at 200 mM NaCl versus 0 mM NaCl, respectively), and between R74-10/R112+ versus its CL (–9% and –25%, respectively). The Tunisian cv. OR had a 40% reduction at 200 mM salt. Regarding the BW lines, ANOVA revealed no significant genotype effect for all cycle phases (Table 2B). Both introgression lines and their CS control showed a similar increment of percentage nuclei in G1 (from 19% to 24%), a decrease in G2 [by 9.6%, 8.4% and 17% in CS7E(7D), CSTr#12 and CS, respectively], and a pronounced reduction in S phase (by 55%, 66%, and 51% for the same genotypes as above). Thus, presence/absence of either *Thinopyrum* introgression did not seem to have in BW a significant impact on cell cycle modulation due to salt stress, at least under the experimental conditions applied here.

Relative water content

The ability to maintain high RWC is a critical strategy to mitigate the negative effect of salinity. All DW-*Thinopyrum* spp. RLs+ displayed a better water uptake ability compared with CLs at both 100 mM NaCl and 200 mM NaCl. At 100 mM NaCl, the RWC increment spanned from a minimum of 10% (R112+) to a maximum of 29% (R69-9/R112+), the difference being significant for R5+, R23+, R69-9/R112+, and R74-10/R112+. At 200 mM NaCl, the difference increased, being on average nearly 27% higher in RLs+ versus their "–" controls, with the greatest increments exhibited by the secondary recombinants R69-9/R5+ and R69-9/R112+ (+30% and +33%, respectively; Figure 5A). Notably, R69-9/R5+, R69-9/R112+, and R74-10/R112+ showed the highest RWC absolute values under both saline conditions, better than those of primary types and of the Tunisian cv. OR. For this trait, no significant difference was observed in BW introgression lines compared with normal CS at 100 mM salt, while a higher water content was retained in leaves of CS7E(7D) substitution line and CSTr#12 at 200 mM, although absolute values were inferior to those of DW RLs, particularly secondary types with "nested" *Th. ponticum* + *Th. elongatum* introgressions (Figures 5B versus 5A).

Photosynthetic pigments

All DW-*Thinopyrum* spp. recombinant genotypes showed significantly higher total chlorophyll and total carotenoid content in comparison with their CLs under salt stress conditions (Figures 5C, D). With respect to the untreated condition, the genotypes that best maintained their photosynthetic pigments were R69-9/R112+ and R74-10/R112+, showing similar values under both NaCl

10.3389/fpls.2024.1378186

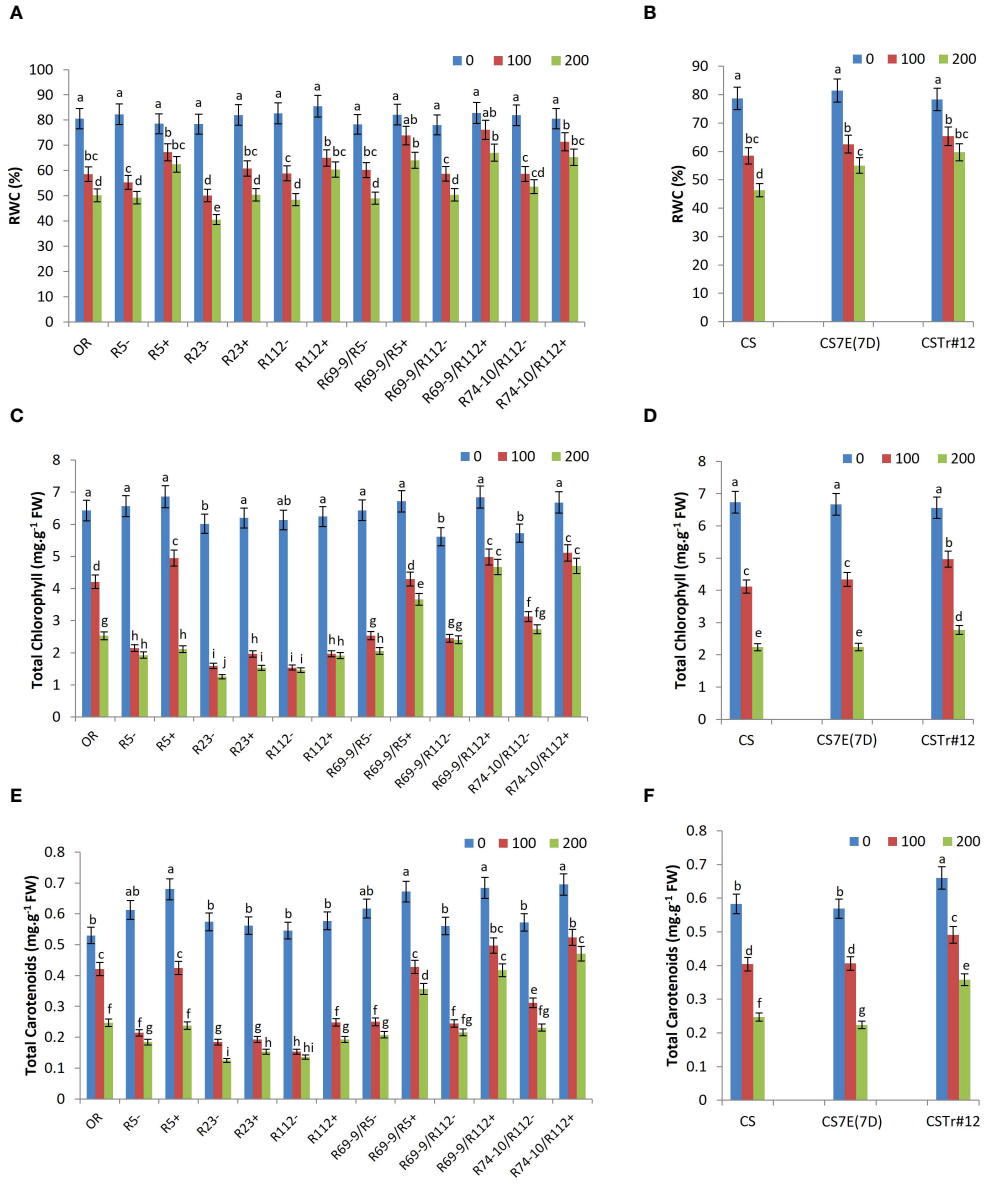

FIGURE 5
Relative water content (RWC, **A, B**), total chlorophyll **(C, D)**, and carotenoids **(E, F)** of wheat lines subjected to salt stress application. Comparison between DW recombinant (+) versus control (–) lines and cv. OR **(A, C, E)** and between BW lines CSTr#12 and CS7E(7D) versus normal CS **(B, D, F)**. Values are expressed as means ± SE. Letters above histograms correspond to the ranking of Tukey test at $p < 0.05$ significance level. Color-coded legend: NaCl concentration (mM).

concentrations, slightly higher than those of R69-9/R5+, but remarkably higher than those of primary recombinants (R5+, R112+, and R23+) and cv. OR, particularly at 200 mM NaCl. At this concentration, total chlorophyll of R69-9/R5+, R69-9/R112+, and R74-10/R112+ exceeded that of CLs by 78%, 94%, and 72%, respectively, and that of cv. OR by 44%, 84%, and +86%, respectively. Moreover, comparing secondary recombinants versus corresponding primary types, the better performance of the former ones clearly emerged: R69-9/R5+ exceeded R5+ by 73% and so was for R69-9/R112+ and R74-10/R112+ versus R112+ (+143% and +145%, respectively, Figure 5C).

A similar picture was true for total carotenoid content, considerably higher in the three secondary DW RLs versus their controls (+71%, +93%, and +103%, respectively) and cv. OR (+44%, +68%, and +90%, respectively, Figures 5E, F). Under 200 mM NaCl, a significant difference was also observed in R69-9/R5+ versus R5+ (+50%) and in R69-9/R112+ and R74-10/R112+ versus R112+ (+116% and +144%, respectively), which confirmed the more relevant contribution of the "nested" introgression than the sole *Th. ponticum* introgression to these parameters. On the other hand, at the hexaploid level, presence of the entire 7E chromosome from *Th. elongatum*, as in the CS7E(7D) substitution line, was not apparently beneficial for all photosynthetic pigment content, whereas some advantage versus normal CS seemed to be associated with the *Th. ponticum* introgression of CSTr#12 (Figures 5D, F).

10.3389/fpls.2024.1378186

Osmolyte accumulation

A significant accumulation of proline and TSS was observed in all wheat genotypes under salt stress versus control conditions, significantly increasing from the mild stress of 100 mM to 200 mM NaCl (Figure 6). Among DW RLs, secondary RLs R69-9/R5+, R69-9/R112+, and R74-10/R112+ reached the highest values, which were significantly higher than those of their CLs under both salt concentrations (Figure 6A). Compared to secondary RLs, lower proline amounts were displayed by cv. OR and the R5+ RL (−30% to 40% at 100 mM and −25% at 200 mM). Rather unexpectedly, primary RLs R112+ and R23+, and so their respective CLs, produced the lowest proline levels, with small incremental effects of their *Th. ponticum* segments, albeit significant at 100 mM (Figure 6A). As to the BW lines, proline content was not affected by *Th. elongatum* chromosome 7E substitution in place of wheat 7D, whereas presence of the *Th. ponticum* introgression (CSTr#12) onto chromosome 7A caused a 20% increase in comparison with normal CS at both salt concentrations (Figure 6B).

An analogous trend was observed for TSS levels, which were slightly higher in both BW introgression lines versus CS at 100 mM salt but accumulated in significantly higher amount in CSTr#12 only at 200 mM (Figure 6D). Also, for the DW lines the tendency for TSS accumulation was comparable to that of proline, with a clearer discrimination between primary and secondary RLs. The latter, particularly under the most stressful treatment (200 mM NaCl), had the highest values in absolute terms, in most cases significantly differing from their CLs and in all cases significantly exceeding the primary RLs and cv. OR (Figure 6C). For TSS, the behavior of primary RLs was more uniform across lines, with slightly lower values of R23+ versus R112+ and R5+.

Biochemical analyses of oxidative stress

At the cellular level, excessive salt induces oxidative stress, due to overproduction and accumulation of harmful ROS, as well as membrane damage. To further elucidate the response of DW RLs to salt application, the MDA and hydrogen peroxide (H_2O_2) content as well as the activities of SOD, CAT, POD, and APX enzymes were determined.

MDA and H_2O_2 content

Under control conditions, MDA and H_2O_2 contents were similar in all wheat genotypes (Figure 7). However, under salt stress conditions, the accumulation of MDA and H_2O_2, both indicative of higher stress impact, was significantly lower in DW and BW lines carrying *Thinopyrum* spp. introgressions with respect to their CLs lacking any alien transfer and in cv. OR. Under 200 mM NaCl, the MDA content of R5+, R23+, R112+, R69-9/R5+, R69-9/R112+, and R74-10/R112+ was

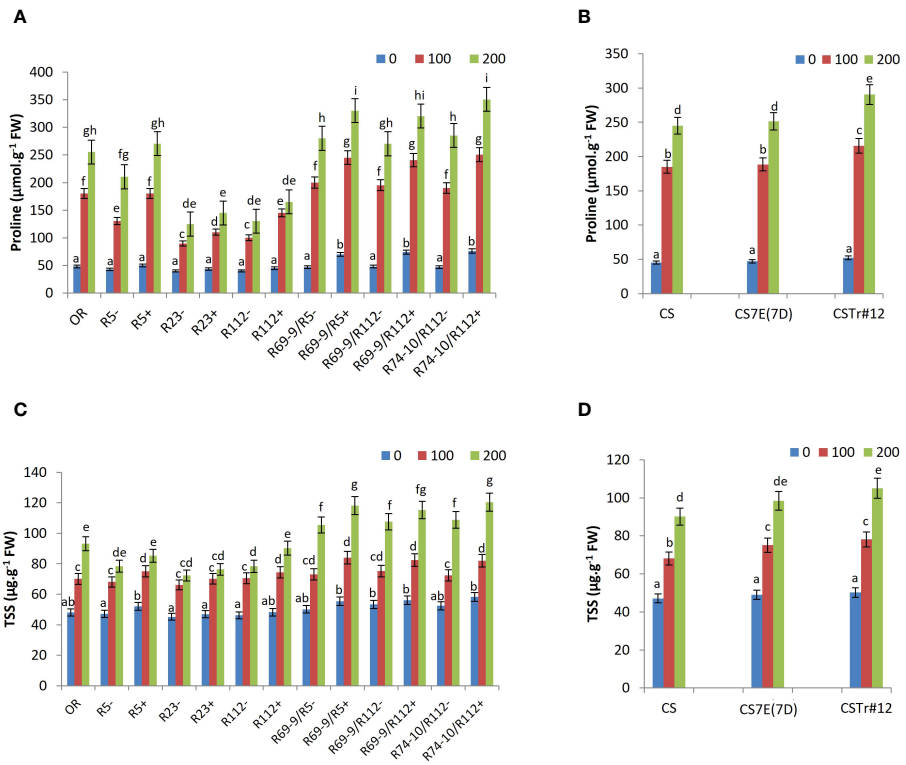

FIGURE 6
Effect of salt stress application on proline **(A, B)** and total soluble sugars (TSS; **C, D**). Comparison between DW recombinant (+) versus control (–) lines and cv. OR **(A, C)** and between BW lines CSTr#12 and CS7E(7D) versus normal CS **(B, D)**. Values are expressed as means ± SE. Letters above histograms correspond to the ranking of Tukey test at $p < 0.05$ significance level. Color-coded legend: NaCl concentration (mM).

10.3389/fpls.2024.1378186

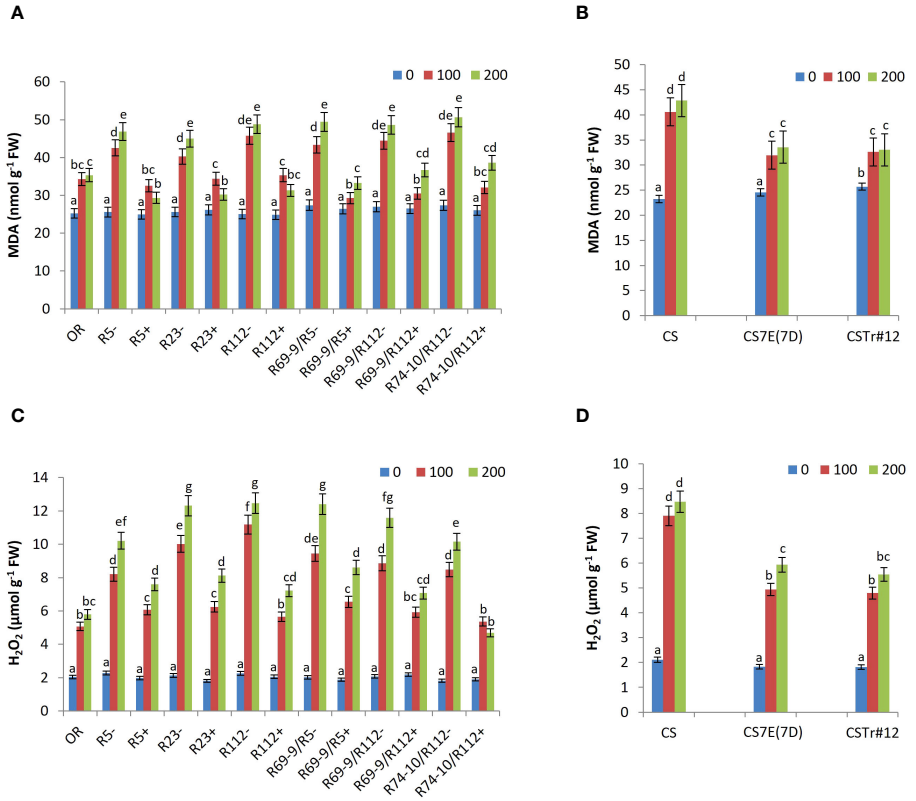

FIGURE 7
Malondialdehyde (MDA; **A, B**) and hydrogen peroxide (H_2O_2) content **(C, D)** in leaf tissues of wheat lines following salt stress exposure. Comparison between DW recombinant (+) versus control (–) lines and cv. OR **(A, C)** and between BW lines CSTr#12 and CS7E(7D) versus normal CS **(B, D)**. Values are expressed as means ± SE. Letters above histograms correspond to the ranking of Tukey test at $p < 0.05$ significance level. Color-coded legend: NaCl concentration (mM).

significantly reduced by 37%, 32%, 35%, 32%, 24%, and 23% compared with their CLs, respectively (Figure 7A). Likewise, these six lines showed a significant reduction in H_2O_2 accumulation (−25%, −34%, −42%, −30%, −38%, and −53% versus their respective CLs; Figure 7C). For both MDA and H_2O_2, primary and secondary recombinants had a largely similar behavior, which suggests a common genetic control, possibly at the level of the shared *Th. ponticum* segment (see Figure 1). However, it is worth noting that R74-10/R112+ exhibited the lowest H_2O_2 levels, particularly at 200 mM NaCl, even compared to OR, which showed lower amounts of H_2O_2 than the other DW RLs (Figure 7C). Regarding the BW lines, the effect of their *Th. ponticum* or *Th. elongatum* introgressions had a comparable effect on reducing both MDA and H_2O_2 accumulation as compared with the CS performance (Figures 7B, D).

Antioxidant activities

The ability of plants to neutralize ROS and limit their harmful effects is due to the presence of efficient scavenging systems, involving enzymatic and non-enzymatic antioxidants, including SOD, CAT, POD, and APX enzymes, as well as ascorbate.

SOD, which catalyzes the conversion of superoxide radical (O_2^-) to hydrogen peroxide (H_2O_2), is the first enzyme to be involved in ROS removal. Whereas under control (0 mM salt) condition its activity was similar among DW lines, it significantly increased in all RLs compared to CLs lacking the alien segments, in addition that in OR (Figure 8). Maximum values were reached under the high salt stress condition of 200 mM, when SOD activity of R5+, R23+, R112+, R69-9/R5+, R69-9/R112+, and R74-10/R112 + exceeded that of respective controls by 62%, 48%, 62%, 55%, 35%, and 38%, respectively. In recombinant genotypes R112+, R69-9/R5 +, R69-9/R112+, and R74-10/R112+ SOD activity reached the highest values, resulting significantly higher than those of the Tunisian salt tolerant cv. OR (Figure 8A). BW introgression lines also showed a significantly augmented SOD activity versus normal CS in both NaCl concentrations, with no statistical difference between introgression types (Figure 8B).

Likewise, salt stress caused in all wheat RLs a significant increase in CAT activity, reaching the highest values in plants treated with 200 mM NaCl. Under this condition, the maximum increase was observed in R5+, R112+, R69-9/R5+, R69-9/R112+, and R74-10/R112+ (+66%, +65%, +41%, +50%, +52%, respectively versus their respective controls), with enzyme peaks exhibited by secondary RLs (Figure 8C). Notably, in the latter recombinant types, CAT activity was significantly enhanced by about 20% versus cv. OR (Figure 8C). BW introgressions behaved similarly as described for SOD (Figure 8D). Similarly, POD activity was significantly higher in DW RLs versus CLs

10.3389/fpls.2024.1378186

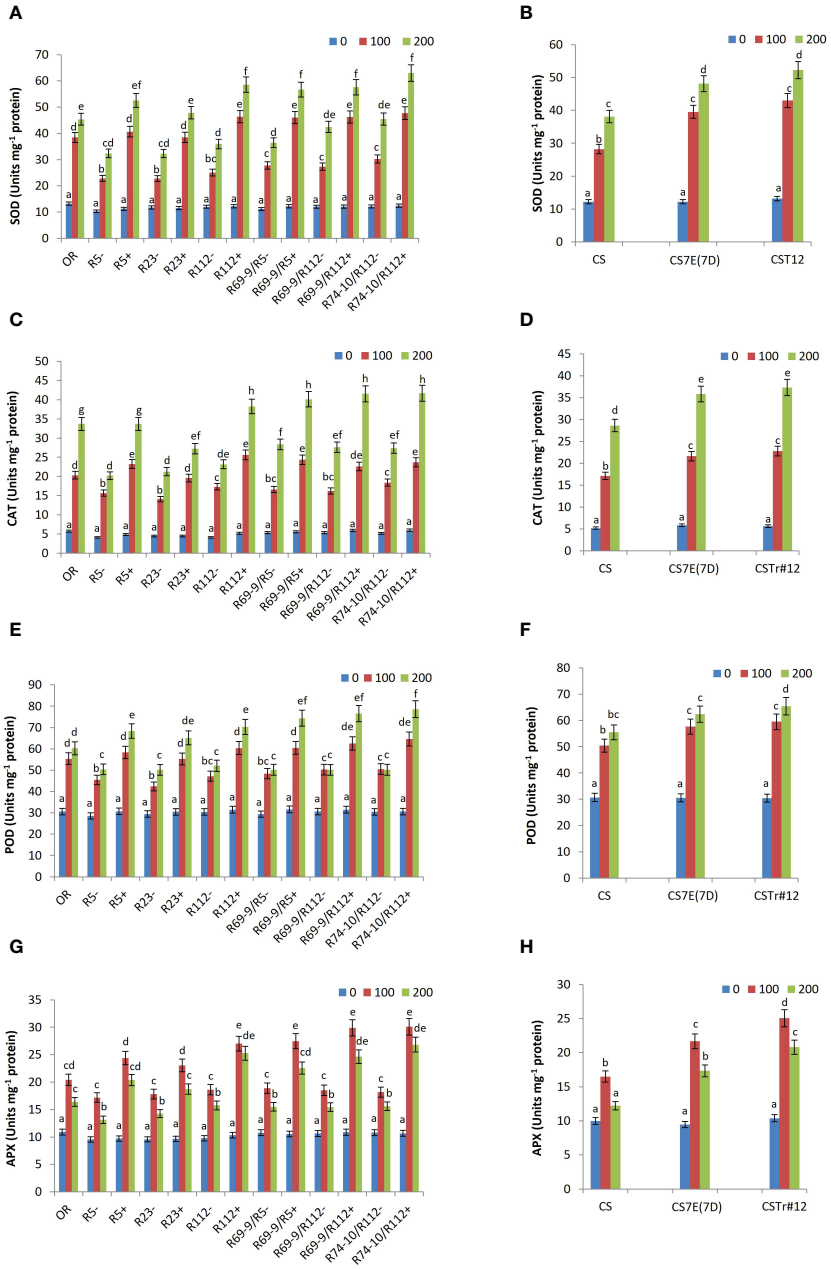

FIGURE 8
Effect of salt stress application on the activity of the following antioxidant enzymes: superoxide dismutase, SOD **(A, B)**, catalase, CAT **(C, D)**, peroxidase, POD **(E, F)** and ascorbate peroxidase, APX **(G, H)**. For each enzyme, DW recombinant lines (+) are compared to the respective control lines (–) and cv. OR **(A, C, E, G)** and BW lines CSTr#12 and CS7E(7D) to normal CS **(B, D, F, H)**. Values are expressed as means ± SE. Letters above histograms correspond to the ranking of Tukey test at $p < 0.05$ significance level. Color-coded legend: NaCl concentration (mM).

at both NaCl concentrations, the increment varying from 30% to 56% under high salt stress (200 mM NaCl) (Figure 8E). As for the previous enzymes, at this concentration secondary RLs displayed the highest values of POD activity with respect to the primary types and to cv. OR. On the other hand, at the hexaploid level, both introgression lines also increased POD activity under salt stress compared with normal CS, with no major difference at the two NaCl concentrations, except for CSTr#12 (*Th. ponticum* introgression), which had a more intense activity at 200 mM compared with the *Th. elongatum* substitution line CS7E(7D) (Figure 8F).

As for activity of APX, a highly effective enzyme in H_2O_2 scavenging, a considerable increase was recorded in all wheat-*Thinopyrum* spp. lines under salt stress treatments compared with control (untreated) conditions, with presence of any *Thinopyrum* introgression (at both ploidy levels) corresponding to a significantly higher activity than that exerted by the respective CLs (Figures 8G, H). Interestingly, however, after exposure to the 100 mM salt treatment, all lines reached their peak APX activity, which then somewhat declined at 200 mM salt, although to a variable extent, sometimes significantly, in others not so (Figures 8G, H). This trend

10.3389/fpls.2024.1378186

matches with that of ascorbate (see ahead, Figure 9), the specific electron donor used by APX to reduce H_2O_2 to H_2O (e.g., Caverzan et al., 2012; Pandey et al., 2017), whose availability may thus represent the limiting factor of this reaction of the AsA-GSH cycle. In all cases, among DW lines those that exhibited the highest values (not significantly different at 100 and 200 mM NaCl) were RLs R112+ and its derivatives R69-9/R112+ and R74-10/R112+, while lower APX activity was detected in the remaining RLs and in OR (Figure 8G). Similarly to the DW evidence, indicating a promoting activity within the R112 segment shared by the mentioned three lines, the BW $7el_1$ CSTr#12 introgression line to be able to induce a higher APX activity than CS7E(7D) substitution line versus the CS control (Figure 8H).

Given the many direct and indirect protective functions against oxidative stress brought about by ascorbate (e.g., Akram et al., 2017; Hasanuzzaman et al., 2019), its content is expected to undergo some decline after exposure to stress (see, e.g., Feki et al., 2017). However, the reduction versus the untreated condition was significantly lower in all DW and BW lines possessing *Thinopyrum* spp. introgressions at both 100 and 200 mM NaCl (Figure 9). After the more extreme treatment, ascorbate content of DW RLs R5+, R23+, R112+, R69-9/R5+, R69-9/R112+, and R74-10/R112+ reached similar values to each other and to cv. OR, exceeding that of respective CLs by 67%, 84%, 35%, 54%, 44%, and 47%, respectively (Figure 9A). However, RLs with *Th. ponticum* + *Th. elongatum* segments, namely, R69-9/R5+, R69-9/R112+, and R74-10/R112+, not only displayed the highest values in controlled conditions but also a non-significant reduction at 100 mM NaCl (Figure 9A). In BW introgression lines, presence of either chromosome 7E or $7el_1$ (the latter in CSTr#12) conferred higher ascorbate amount to recipient CS in control condition and a minor and comparable reduction after salt exposure, irrespective of salt concentration (Figure 9B).

Na^+ and K^+ contents in roots and leaves

Controlling sodium homeostasis is considered as a key determinant of salt stress tolerance. Thus, Na^+ and K^+ ion concentration was measured in roots and leaves under control and salt stress conditions. Irrespective of genotype, the dynamics of Na^+ accumulation differed in the two organs. In roots, directly exposed to the saline solution, Na^+ reached in most lines the highest values already after 100 mM salt exposure, with minor increments at 200 mM, while in leaves the increment in salt concentration in the medium determined a considerable Na^+ surge, particularly in the more sensitive lines (Figure 10). However, in both organs of all wheat-*Thinopyrum* spp. lines, a substantial reduction in Na^+ content versus CLs was observed both under control conditions (constitutive) and after salt exposure (Figures 10A–D). All stress-induced differences were significant at 100 mM, and still were at 200 mM NaCl in roots of DW RLs R112+, R69-9/R5+, R69-9/R112+, and R74-10/R112+ (–16%, –30%, –26%, and –25% versus. CLs, Figure 10A). The trend was largely similar in both BW introgression lines versus CS (Figure 10B). The difference between genotypes carrying or lacking *Thinopyrum* spp. introgressions became even more evident when leaves were considered, with around 70% lower Na^+ values in DW RLs (and so cv. OR) versus CLs (Figure 10C), suggesting that the presence of alien segments efficiently contributes to controlling the amount of sodium delivered from roots to leaves. Likewise, CS7E(7D) and CSTr#12 had much lower Na^+ concentration in their leaves, both in untreated condition and under salt stress compared with CS (Figure 10D).

On the other hand, no significant difference was observed in K^+ content between DW and BW lines, with or without *Thinopyrum* introgressions, under unstressed conditions (Figures 10E–H). However, under 100 mM NaCl, a higher K^+ ion concentration was observed in roots and leaves of all wheat-*Thinopyrum* spp. lines compared with "wheat-only" controls. Under this condition, the increase of K^+ content in roots ranged from 26-38% in R5+, R23+, R112+ and R69-9/R5+, to 50%–60% in R69-9/R112+ and R74-10/R112+ (Figure 10E), and from 23 to about 40% in their leaves (Figure 10G). In cv. OR, K^+ content was lower than that of DW-*Thinopyrum* spp. RLs, remaining more similar to that of CLs, especially in leaves (Figures 10E, G). Exposure to 100 mM NaCl similarly led to a significantly increased K^+ concentration in roots and leaves of CS7E(7D) and CSTr#12 in comparison with cv. CS (Figures 10F, H), although the increase was of minor extent with respect to that observed at the DW level. Under 200 mM NaCl, root

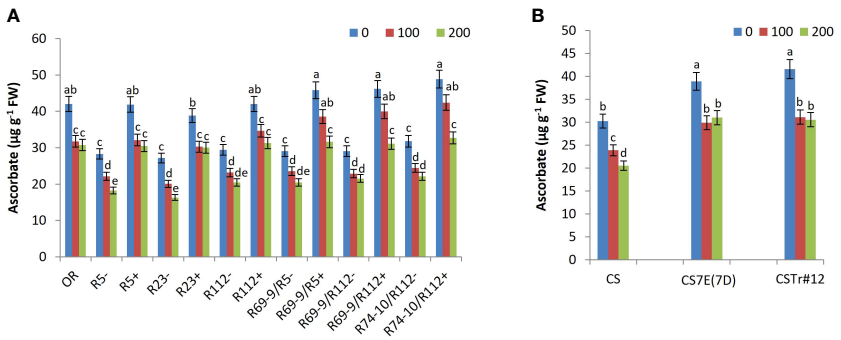

FIGURE 9
Ascorbate content in DW recombinant lines (+), the respective control lines (–) and in cv. OR **(A)** as well as in BW lines CSTr#12 and CS7E(7D) lines and normal CS **(B)**. Values are expressed as means ± SE. Letters above histograms correspond to the ranking of Tukey test at $p < 0.05$ significance level. Color-coded legend: NaCl concentration (mM).

10.3389/fpls.2024.1378186

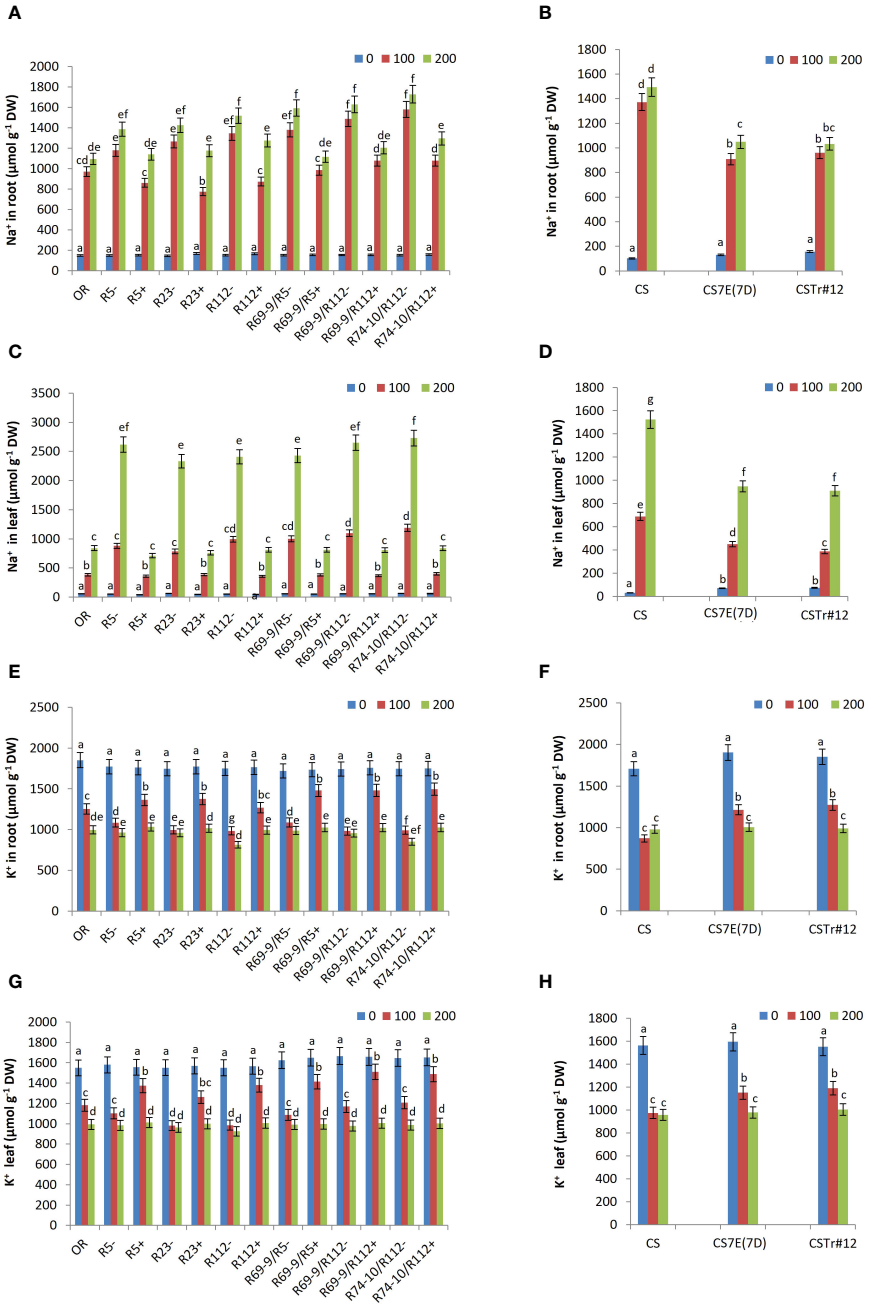

FIGURE 10
Effect of salt stress treatment on Na^+ and K^+ content in roots and leaves of DW-*Thinopyrum* spp. recombinant (+) and corresponding control (–) lines and in cv. OR **(A, C, E, G)**, as well as in BW introgression lines CSTr#12 and CS7E(7D) and in normal CS **(B, D, F, H)**. Values are expressed as means ± SE. Letters above histograms correspond to the ranking of Tukey test at $p < 0.05$ significance level. Color-coded legend: NaCl concentration (mM).

and leaf K^+ content decreased in all lines (except for CS) with respect to the 100 mM condition, more markedly in DW lines, reaching comparable levels across genotypes (Figures 10E–H).

Principal component analysis

To identify traits that are majorly responsible for the difference between genotypes in the response to salt stress, PCAs were performed on the 19 traits measured in both DW and BW groups of materials grown in hydroponics (Figure 11). The first two principal components (PCs) explained 87.7% and 92.3% of the variation for DW and BW genotypes, respectively. The impact of the analyzed traits on the observed variability was stronger for DW than BW genotypes, as shown by the bigger distance of the trait vectors form the origin of biplots in the former group. Overall, for both genotype groups the traits clustered in a similar way, indicating the existence of a similar response mechanism in the two species, determined by the donor introgressions in BW lines and their chromosomally engineered smaller fractions in DW lines. PC1 clearly separated the

10.3389/fpls.2024.1378186

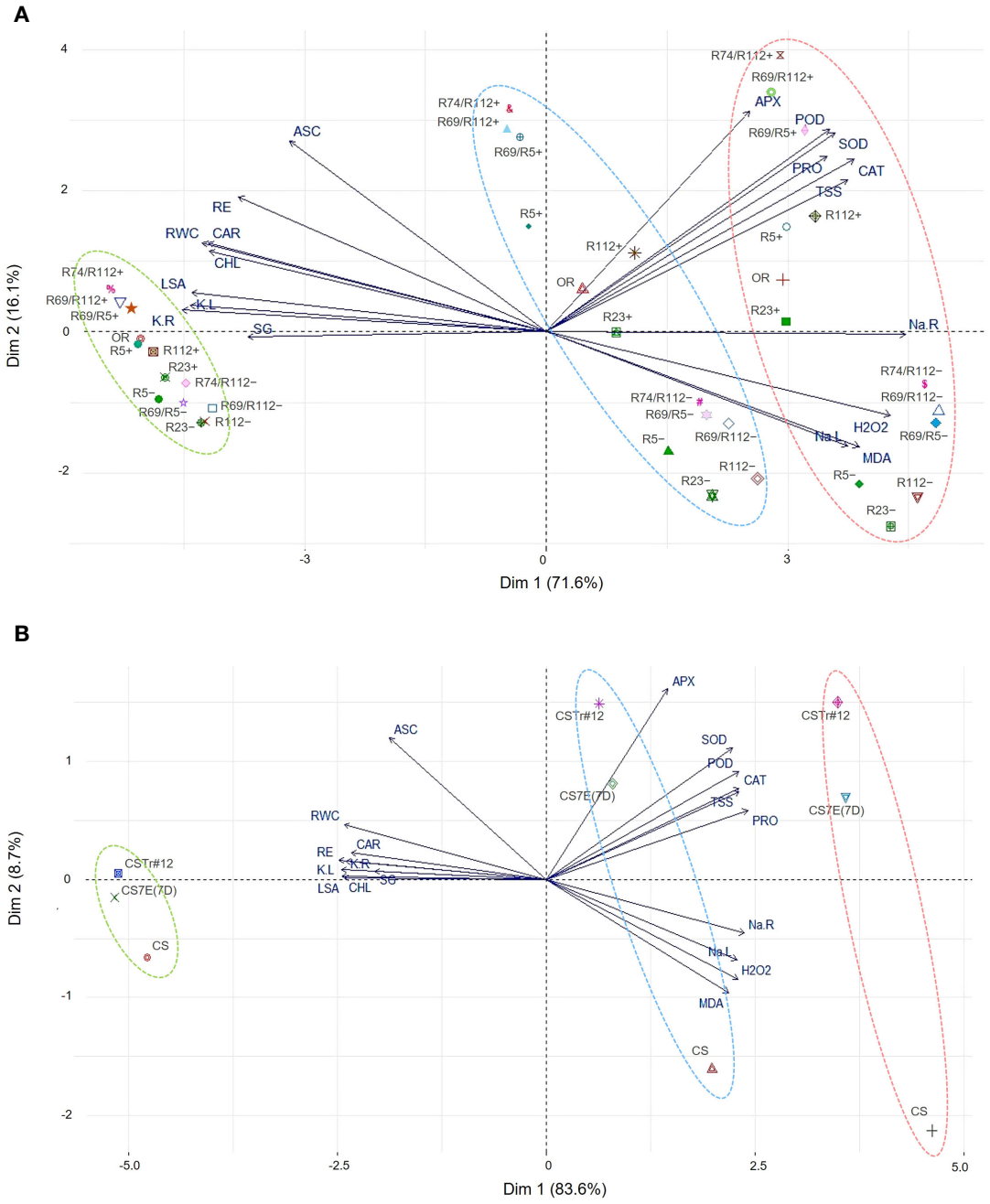

FIGURE 11
Principal component analysis (PCA) for morpho-physiological and biochemical traits assessed on DW **(A)** and BW **(B)** genotypes grown in hydroponics under salt stress (100 mM NaCl and 200 mM NaCl) and control (0 mM NaCl) conditions. Some DW recombinant (+) and control (–) lines were indicated by shortened names, with R69/R5, R69/R112, and R74/R112 standing for R69-9/R5, R69-9/R112, and R74-10/R112, respectively. For vector-associated trait acronyms/abbreviations, see the list of abbreviations. Color-coded ellipses identify different NaCl treatments: 0 mM, green; 100 mM, blue; 200 mM, red.

genotype behavior under the control condition (0 mM) from that under salt stress (100 mM and 200 mM). Two trait clusters largely contributed to this separation and were positively correlated with PC1 (Figures 11A, B): the first included the traits associated with the observed burst in antioxidant enzymatic activity (APX, POD, SOD, and CAT) and accumulation of osmoprotectants (PRO and TSS), while the other included traits associated with Na^+ content in leaves and roots (Na.L and Na.R), membrane stability (MDA) and oxidative stress (H_2O_2). PC2 separation clearly discriminated introgression carrier (+) and non-carrier (–) lines under stress, being positively correlated with the group of APX, POD, SOD, CAT, PRO, TSS, and ASC traits. In the case of DW lines, PC2 was also positively correlated with root growth (RE) and leaf physiological traits (RWC, CHL and CAR, Figure 11A). The PC2 showed limited contribution to the variation of K^+ content (K.R, K.L), leaf size (LSA) and germination rate (SG) for both DW and BW lines. This was also true for Na^+ content in roots (Na.R) for DWs, indicating its lower impact on the response to salt stress by these genotypes.

Discussion

Besides their direct use in saline environments for the many beneficial impacts they can provide to land and users (Flowers and Colmer, 2015; Sheikh-Mohamadi et al., 2022; Tong et al., 2022; Li et al., 2023), wheatgrasses (*Thinopyrum* spp.) have been the target of several attempts to transfer into cultivated *Triticum* spp. at least the major genetic determinants of their halophytic behavior. In fact, many hybrids, partial or complete amphiploids, and even some segmental introgressions have been obtained, but very few of them, if any, have been advanced to the variety status, ready to reach the farmers field (e.g., Colmer et al., 2006; Farooq, 2009; Mullan et al., 2009; Yuan and Tomita, 2015; Mujeeb-Kazi et al., 2019). In the face of rampant global salinity, one reason for this can be identified in the inherently complex nature of plant salinity tolerance, which, as with other abiotic stresses, has a typically polygenic control, where both dominance and additive effects are important for inheritance of the many contributing traits. This was shown to be the case also for the diploid *Th. elongatum*, whose genome partitioning into individual chromosomal components added to or substituted into BW cv. CS confirmed interactive effects to underlie the tolerant phenotype conferred by the entire genome (as in the CS-*Th. elongatum* amphiploid), but also highlighted the existence of major, dominant contributions independently associated to certain chromosomes, including 7E (see Introduction).

These early observations represented an important prerequisite knowledge and support to the research described here, based on a finely tuned chromosome engineering strategy which, while targeting short-sized transfers to optimize interspecific compensation and minimize linkage drag, also aimed at alien gene pyramiding by "nesting" via homoeologous recombination small chromosomal segments from closely related *Thinopyrum* species (Ceoloni et al., 2017; Kuzmanović et al., 2019). As a result, within the group 7 chromosome portions that were transferred from *Th. ponticum* ($7el_1L$ arm) and *Th. elongatum* (7EL arm) into the primary ($7el_1L$) and secondary (7EL nested into $7el_1L$) wheat RLs, several disease resistance genes, quality and yield-contributing traits could be allocated, thanks to the various chromatin breakpoints characterizing each recombinant chromosome (see Figure 1 and Kuzmanović et al., 2014, 2021). Thus, stimulated by consolidated literature information and by our previous extensive work on the same durum (DW) wheat near-isogenic RLs employed here (see, e.g., Ceoloni et al., 2015; Kuzmanović et al., 2018, 2019, 2021; Fanelli et al., 2023; Giovenali et al., 2023), we have exposed such RLs, along with the original BW-*Thinopyrum* spp. donor lines, to moderate (100 mM) and high (200 mM) salt (NaCl) stress, to verify whether their $7el_1L$ and 7EL specific portions could also contribute to salinity tolerance.

The impact of salt treatment on morpho-physiological, cellular, and biochemical features

A highly positive stress response by all wheat-*Thinopyrum* spp. introgressions when compared with their CLs lacking any alien portion was evident from the early experimental phases, starting with SG. At 200 mM NaCl concentration, when SG ability was significantly affected in all genotypes, no difference was observed between DW RL R5+ and its R5– control, whereas a differential behavior was exhibited by primary RLs with larger $7el_1L$ segments (R112+ and R23+, Figure 1) and by all secondary RLs versus their respective CLs. Thus, not only an SG promoting factor is likely to reside within the $7el_1L$ chromatin proximal to the R5+ breakpoint (Figure 1), but given the positive performance of R69-9/R5+ (in which this $7el_1L$ stretch is absent, see Figure 1), one can also hypothesize that another incremental factor might be located within the most distal 7EL segment, apparently working in a non-additive manner. This reasoning seems to be supported by the results of BW lines, in which both the presence of the complete 7E and of most of $7el_1$ led to a similar increment (Figure 3). In all cases, enhancement of SG is a highly positive attribute, as this is the most critical period in the life cycle of salt-affected plants, a period that is extremely sensitive to high salinity and crucial for seedling survival and growth (Yang et al., 2014). Whether caused by osmotic stress that hinders water uptake and/or by ionic toxicity, salinity inhibits cell division and expansion (see ahead), and so the activity of some key enzymes, ultimately reducing utilization of seed reserves (El-Hendawy et al., 2019). In this view, the use of *Thinopyrum* introgression lines appears as a valuable strategy to respond to the need of boosting cereal SG in saline environments (El Sabagh et al., 2021; Rossini et al., 2024).

Traits indicating seedling growth ability under salt stress, i.e. RE and LSA, clearly showed the superior performance of DW secondary RLs not only versus their CLs but also versus primary types and the Tunisian salt tolerant cv. OR (Figure 4). Values of DW secondary RLs largely exceeded those of BW introgression lines, again supporting the hypothesis of a positive $7el_1L$ + 7EL interaction in promoting root and leaf growth even under highly stressful conditions. On the other hand, when two RLs (R112+ and R74-10/R112+) and their CLs were exposed to a few days salt "shock" starting from germination, R112+ had a significant advantage over its CL for both root and leaf length, and over R74-10/R112+ for LL at 100 mM NaCl, before both root and leaf length sharply declined to similar values in all lines (Table 1).

At cellular level plant growth depends on cell proliferation through the mitotic cycle and subsequent cell expansion. Progression through the cycle, especially at the level of the G1/S and G2/M checkpoints, is controlled by a wide array of regulatory mechanisms, including the activity of cyclins and cyclin-dependent kinases (CDKs), as well as epigenetic changes-driven chromatin remodeling, and shows a variety of even conspicuous alterations in response to abiotic stresses (Zhao et al., 2014; Qi and Zhang, 2020; Kamal et al., 2021). In Arabidopsis, salt stress caused a severe disruption of mitotic activity, attributed to a block at the G2/M transition (West et al., 2004). In maize, heat and cold treatments induced a pronounced cell accumulation at the G2/M transition, NaCl treatment resulted in extensive inhibition of both S and G2/M phases, while drought stress caused most of the cells to be blocked in G1 (Zhao et al., 2014). In a later study (Kamal et al., 2021), both salt and drought stresses were found to arrest cell cycle in S phase. In wheat, knowledge of the effect of abiotic stress on cell cycle progression is very scarce. In seedlings subjected to mild water

stress, leaf elongation rate and mitotic activity were reduced in mesophyll cells, due to a slowed progress from the G1 to the G2 phase and decreased activity of CDKA, required for entry into mitosis (Schuppler et al., 1998). Overall, a similar situation was observed in the present study, where, compared to the unstressed condition, exposure to salt stress led to higher percentage of nuclei in G1, of higher degree in BW than in DW lines, but in all instances independent of the genotype (similar values in introgression and in wheat-only lines, see Table 2). In this frame, the stress impact on the subsequent S phase, corresponding to a lower proportion of cells than in the unstressed condition, can be considered an expected consequence. Among the present materials, BW lines had a higher reduction (>50%), with no apparent effect of presence/absence of any *Thinopyrum* introgression (Table 2B). Instead, the behavior of DW lines was less homogeneous: RLs R112+ and R69-9/R5+, with similar percent reduction to cv. OR, had a more conspicuous decrease than their CLs (particularly evident in R112+ versus. R112–), suggestive of a specific influence of the alien introgression(s) on the stress response (Table 2A). However, an opposite trend was detected in R74-10/R112, exhibiting a lower decrease of S-phase nuclei in the RL (+) than in its CL (–) in the comparison between stressed and unstressed condition. Furthermore, the stress-induced alteration involving the G2 phase consisted of an increment (12%–13%) in RLs R112+ and R69-9/R5+ (and so in cv. OR), while a similar variation but in opposite direction was exhibited by R74-10/R112+ and by all BW lines. At present, no sufficiently substantiated explanation can be provided to account for the observed differences among genotypes in relation to their performance toward salinity stress. However, the overall behavior of materials analyzed here is in line with the early considerations by West et al. (2004), based on their work in Arabidopsis, and those of subsequent literature on various stresses and species (see above), suggesting that a block in cell cycle progression is rapidly induced by stress exposure. This would prevent entry into stages where cells are more vulnerable to damage (e.g. S or M-phase) and allow the cellular defense system to be activated, before progressing again at default rates once the plant has adapted to the stress.

Among the early adaptive mechanisms is the control of water uptake, disrupted by the early occurring osmotic stress due to salt increase around the roots. This, through immediate reduction of stomatal conductance, represents the initial and most profound cause of decline in CO_2 assimilation rate and hence photosynthesis (Munns, 1993, 2002; James et al., 2008; Carillo et al., 2011; Hu and Schmidhalter, 2023). In all DW RLs, a better plant growth under salt stress was accompanied by a less compromised water status (higher RWC) than in CLs, with secondary RLs and corresponding primary types (R5+ and R112+) showing significantly higher values than cv. OR at the highest NaCl concentration. Indeed, in two of the secondary RLs (R69-9/R5+ and R69-9/R112+), no water stress was evident at 100 mM salt, and the same lines maintained the highest RWC absolute values at 200 mM. Co-presence of $7el_1L$ and 7EL, particularly in R69-9/R112+ and R74-10/R112+, also contributed to limit the stress-induced decrease of photosynthetic pigments (both total chlorophylls and carotenoids, see Figure 5), with no major difference between the two salt stress conditions applied. Maintenance or, more, increase of carotenoids, acting as auxiliary light-collecting pigments and protectors of photosynthetic apparatus, seems to be a distinctive feature of halophytes compared with glycophytes (Bose et al., 2014). Here, the complete 7E chromosome from *Th. elongatum*, as in the CS7E(7D) substitution line, was not apparently contributing to maintenance of photosynthetic pigment content under stress, while a more positive effect was exerted by *Th. ponticum* $7el_1$ in CSTr#12. A similar $7el_1$ effect was not expressed by DW primary RLs (except for somewhat better values in R5+ at 100 mM salt), although R112+, among them, had shown high photosynthetic efficiency under normal field conditions (Kuzmanović et al., 2016) and induced heat stress (Giovenali et al., 2023).

Na^+ and K^+ ion accumulation and compatible solutes

In addition to buffering the changes in water relations (osmotic tolerance), common to plants subjected to a water stress (e.g. Munns, 2002), a specific and essential salt tolerance mechanism takes place in a later phase and consists in the ability to minimize ion accumulation, mainly of Na^+, particularly in transpiring leaves. In its absence, ions build up rapidly in cell walls, leading to cell dehydration, and in the cytoplasm, impairing physiological functions such as photosynthesis as well as protein synthesis and enzyme activity, while boosting ROS generation (e.g., Munns, 2002; Munns et al., 2006; Carillo et al., 2011). For many such cell functions, of both basic metabolism and salt stress-defense related, not only low Na^+ content, but also adequate levels of K^+ are essential (Wu et al., 2018b). In all mechanisms underlying control of ion concentration in the various tissues (from Na^+ extrusion in the RE zone and vacuolar Na^+ sequestration ability in the mature root zone and hence its limited transfer to shoot and leaves, up to K^+/Na^+ selectivity and K^+ retention ability in the root and leaf mesophyll, thus maintaining functional K^+/Na^+ ratios), DW proved to be less efficient than BW (Wu et al., 2014; Yang et al., 2014; Wu et al., 2018a; Wu et al., 2018b). In fact, all CLs of DW RLs, lacking any *Thinopyrum* introgression, showed much higher (almost doubled) Na^+ accumulation in their leaves than BW cv. CS, particularly at 200 mM salt (Figure 10C). However, in the presence of either $7el_1$ or $7el_1$+7E segments, in all DW RLs, and so in the tolerant cv. OR, Na^+ sharply decreased (by around 70% at 200 mM NaCl), reaching approximately equivalent amounts to those of the BW introgression lines at both salt concentrations. A similar trend was observed in roots, although in this case presence of any *Thinopyrum* introgression seemed somewhat more effective at the BW level and did not represent a major discriminating factor between RLs and CLs, as shown by the PCA analysis (Figure 11). An accompanying effect of *Thinopyrum* transfers concerned K^+ concentrations in root and leaf tissues. Of this critical ion for several functions associated with tolerance to salinity and other stresses, including a signaling role in various adaptive responses, regulation

of cell cycle progression and accumulation of water-soluble carbohydrates (Wu et al., 2018b), DW RLs retained over 20% higher amounts than BW introgression lines, both in roots and leaves (Figures 10E, H), and exceeded as well the DW cv. OR, at least under moderate salinity stress.

Whereas beneficial factors were provided by the segmental introgressions of halophytic origin which minimized entry and cytosolic concentration of salt into juvenile plants of DW-*Thinopyrum* spp. RLs, not less effective was their impact on tolerance mechanisms (collectively referred to as "tissue tolerance"; Munns et al., 2006; Munns and Tester, 2008), usually activated to contrast the effects of salt that inevitably gets in. Among these, is the increased production of compatible solutes, which have a fundamental role in balancing the altered cell osmotic pressure following early water stress (see above) and, together with K^+, also intracellular toxic ion compartmentalization. The amounts of both proline and TSS accumulated in the leaf tissue of DW secondary RLs largely exceeded those of primary types (and of respective CLs), besides that of cv. OR, especially at 200 mM NaCl. No major contribution to proline accumulation appeared to be due to the *Th. ponticum* $7el_1L$ segments, as, indeed, previously observed in response to heat stress (Giovenali et al., 2023). Thus, the observed higher production seems to be entirely due to the 7EL effect. The trend was similar for TSS, more abundantly built up in leaves of $7el_1$ +7E "nested" recombinants compared with $7el_1$ types and cv. OR subjected to the highest salt concentration. Particularly for TSS, the more severe stress condition was apparently the one specifically inducing this protection mechanism, not significantly differentiating the DW and BW genotypes' response under a less intense stress (Figure 7). One reason for this may reside in the high metabolic cost associated with synthesis of organic solutes (Munns, 2002; Munns et al., 2006; Munns and Tester, 2008).

Oxidative stress effects and antioxidant response

That cell structures of both DW and BW lines benefited for their integrity and functioning from presence of the alien introgressions, was proven by the lower membrane damage (as from lower MDA content) of all wheat-*Thinopyrum* spp. lines, showing similar or lower values than cv. OR, and significantly lower than their "wheat-only" CLs (Figures 7A, B). In BW, the effect of $7el_1$ (CSTr#12) and 7E in reducing MDA content versus CS was of comparable magnitude, and so it was, overall, among DW RLs. This indicates the absence of a clear-cut additivity between factors of either *Thinopyrum* derivation, if not some more prominent effect of $7el_1L$ segments (R5+, R112+, and R23+ RLs) at 200 mM salt (Figure 7A). Limited membrane lipid peroxidation is one important indicator of an efficient antioxidant system, able to contrast the deleterious effects of excessive ROS production. Additional evidence of a stronger antioxidant defense of the wheat-*Thinopyrum* materials than their controls came from lower amount of hydrogen peroxide (H_2O_2), the most stable of ROS, thus the only one that can diffuse to adjacent subcellular compartments and cross neighboring cells (e.g., Pandey et al., 2017). At 200 mM salt, H_2O_2 was reduced by 25% in BW introgressions versus normal CS, and in most DW RLs showed a 40% (R112+, R69-9/R112+) or even higher (R74-10/R112+) decrease versus their controls (Figures 7C, D).

To bring about effective scavenging of excessive ROS accumulation, the activity of enzymatic and non-enzymatic molecules with antioxidant properties was enhanced by the presence of *Thinopyrum* spp. introgressions (Figures 8, 9). A large body of evidence demonstrates a higher activity, either constitutive and/or salt-stress induced, of antioxidant enzymes in halophytic versus glycophytic species of the same or closely related plant genera (Bose et al., 2014). In *Th. ponticum* (Tong et al., 2022) and *Th. elongatum* (Sheikh-Mohamadi et al., 2022) lines/ecotypes, screened for potential cultivation in saline zones of Iran and China, respectively, and so in a *Tritipyrum* (BW-*Th. elongatum*) amphiploid (Peng et al., 2022), the best morpho-physiological and agronomic performance was always associated with the highest increase of enzymatic and non-enzymatic antioxidant activities. In the present materials, salt stress induced the most prominent activity of SOD, CAT, POD, and APX enzymes in R112+ among the DW primary RLs and in the three secondary RLs, particularly the R112+ derivatives (R69-9/R112+ and R74-10/R112+), all of them exceeding their CLs and the tolerant cv. OR, as confirmed by the PCA as well (Figure 11). This evidence suggests that main promoting factors might reside in the $7el_1L$ portion common to the mentioned RLs (R112-specific), and the somewhat better performance of CSTr#12 than CS7E(7D) versus normal CS (at least for POD and APX at 200 mM NaCl) seems to confirm this hypothesis. Nonetheless, a further contribution from presence of 7EL segments, which would explain the highly positive enzymes values of R69-9/R5+ and the highest activity peaks often displayed by R69-9/R112+ and R74-10/R112+ (Figure 8), cannot be excluded.

For a strong antioxidant activity, the concomitant increase of CAT and APX is certainly relevant, in view of their functional cooperation in H_2O_2 detoxification, although the most crucial role of APX is indisputable (see, e.g., Mizuno et al., 1998; Caverzan et al., 2012; Sofo et al., 2015; Pandey et al., 2017; Haider et al., 2021). In fact, APX (various isoforms) is a key enzyme for maintenance of the cell redox balance in all living organisms, functioning, among other things, as a linking molecule in the AsA–GSH cycle. In the latter, APX uses ascorbate, the physiologically active form of AsA, as specific electron donor to convert H_2O_2 into H_2O, while AsA and GSH pools are maintained in different cell compartments (Sofo et al., 2015; Pandey et al., 2017; Hasanuzzaman et al., 2019). Together with GSH, AsA is one of the universal non-enzymatic antioxidants involved not only in ROS scavenging, with high AsA levels being essential to keep the labile APX isoenzymes in full operation (Caverzan et al., 2012), but also in modulating several fundamental functions in plants, both under stress and non-stress conditions (Akram et al., 2017). Salt stress was found to decrease ascorbate content in wheat at the vegetative and reproductive stage, although to a minor extent in tolerant versus susceptible genotypes (Sairam et al., 2005; Athar et al., 2008; Feki et al., 2017). This was also the case for the present materials, all wheat-*Thinopyrum* spp. lines exhibiting a significantly lower reduction than lines devoid of

alien introgressions (Figure 9). In this frame, it is particularly noteworthy the performance of the three DW secondary RLs: not only they had the highest absolute ascorbate content in control conditions (0 mM NaCl) but also they were the only tolerant lines (including BW introgressions and DW cv. OR) that maintained it almost unchanged at 100 mM, before it declined to comparable values in all introgression lines and in cv. OR at 200 mM NaCl.

To make DW secondary RLs top performers in several aspects of the antioxidant and overall tolerant response to salinity stress, one of the likely multiple promoting factors of both $7el_1L$ and 7EL origin could reside in the peculiar gene content of their *Th. elongatum* introgression. Within the distal end of the 7EL arm, a gene encoding a GST type, not present in plants, was detected, which some accessions of *Thinopyrum* and related perennial species (though not the *Th. ponticum* accession possessing $7el_1L$) acquired from an endophytic fungal species via horizontal transfer (Wang et al., 2020; Guo et al., 2022). This gene was considered a likely candidate for the Fusarium resistance phenotype of BW-*Thinopyrum* introgression lines and identified with the *Fhb7* locus (Wang et al., 2020; Konkin et al., 2022). GSTs, a multigene family of isozymes that catalyze the conjugation of GSH to a wide array of electrophilic and hydrophobic substrates, are known to be responsive to a multitude of biotic and abiotic stressors (Kumar and Trivedi, 2018; Estévez and Hernández, 2020). In addition to quenching reactive and harmful molecules with the addition of GSH, certain GST types take part in the AsA-GSH pathway by regenerating ascorbate at the expense of GSH (Dixon et al., 2002; Whitbread et al., 2005). A recent analysis of the metabolome of the *Fusarium* spp. resistant DW secondary RL R69-9/R5+, carrier of *Fhb7E* locus (*Fhb7* specific to *Th. elongatum* 7E, Kuzmanović et al., 2019) and of its near-isogenic CL (no *Thinopyrum* introgression) clearly highlighted the former to constitutively express and more efficiently activate upon pathogen exposure a significantly more complex matrix of defense pathways and specific metabolites than its CL, including GSH (Fanelli et al., 2023). While a possible enhancing contribution of the GST of fungal origin to the antioxidant response of R69-9/R5+ was taken into consideration, a compound nature was hypothesized for the *Fhb7E* locus, with additional 7EL genes flanking the fungal *GST* and supporting the overall resistance function (Fanelli et al., 2023). This view, which would account for the wide array of metabolites and pathways differentiating the *Fhb7E*+ from the *Fhb7E*– response (Fanelli et al., 2023), might also apply to the present investigation, where several of the identified response mechanisms against a different stressor (NaCl), notably those contrasting the oxidative burst caused by ROS, are known to be similarly activated (e.g., Pandey et al., 2017; Ramegowda et al., 2020).

Besides the 7EL contribution, the important aid of $7el_1L$-derived factors, particularly associated with part of the R112-specific segment, emerged for several parameters expressed by the DW secondary RLs analyzed here (see above). This confirms the view that transfer of a suite of genes, rather than single genes, as in the finely engineered lines employed in this work, may well be the way forward to effectively impact on salinity tolerance of glycophytes by use of halophytic germplasm (Flowers and Yeo, 1995; Flowers and Colmer, 2015; Rawat et al., 2022). Remarkably, the $7el_1L$+7EL "nested" introgressions can be easily transferred into BW by recombination in the shared homologous 7A regions in DW × BW crosses.

Considering the common ancestry and cytogenetic affinity relating *Triticum* and *Thinopyrum* species, largely demonstrated for group 7 chromosomes (e.g., Ceoloni et al., 2014), one can assume that in this, as in similar comparisons between halophytes and allied glycophytes, differences in tolerance are predominantly due to the greater robustness of the employed mechanisms in the former, rather than to qualitative differences (Flowers and Colmer, 2008, 2015; Volkov, 2015; Isayenkov and Maathuis, 2019). Plausibly, apart from the exceptional case of the *GST* gene of exotic origin described above, different thresholds toward salinity-induced injuries are associated with different *Triticum* versus *Thinopyrum* homoeoalleles, which made our chromosomally engineered products much better responding to the imposed stress. While comparative genomic and transcriptomic investigations are currently underway on the DW-*Thinopyrum* spp. near-isogenic RLs to elucidate these aspects, an important result of practical value is the excellent performance of several of them in field trials recently carried out in an extremely stressful Algerian environment. In the experimental site of Biskra (South of Saharan Atlas), characterized by very arid and saline soil conditions (EC 11-15 ds/m; see, e.g., Singh, 2022), further exacerbated by indispensable irrigation (EC 16-20 ds/m in irrigated plots), top yielder for three consecutive seasons (2019–2022) turned out to be the R69-9/R5+ RL, followed by R69-9/R112+ and then R5+ (Kuzmanović et al., 2022).

In conclusion, the promising outcomes of the work described here, help pave the way to sustainably achieving the ambitious goal of growing wheat, even the less tolerant DW, on saline soils that the crop will have to increasingly cope with (Shahzad et al., 2013; Miransari and Smith, 2019; Rawat et al., 2022).

Data availability statement

The original contributions presented in the study are included in the article/Supplementary Material. Further inquiries can be directed to the corresponding authors.

Author contributions

ST: Writing – review & editing, Writing – original draft, Visualization, Investigation, Formal Analysis, Data curation. DG: Writing – review & editing, Writing – original draft, Visualization, Methodology, Investigation, Data curation, Conceptualization. LK: Visualization, Validation, Formal Analysis, Data curation, Writing – review & editing, Resources, Conceptualization. OJ: Validation, Investigation, Writing – review & editing. AF: Visualization, Investigation, Writing – review & editing. AC: Visualization, Data curation, Writing – review & editing. RBA: Validation, Formal Analysis, Writing – review & editing. FB: Methodology, Writing – review & editing, Writing – original draft, Resources, Project administration, Funding acquisition, Conceptualization. CC: Writing

– review & editing, Writing – original draft, Supervision, Resources, Project administration, Funding acquisition, Conceptualization.

Funding

The author(s) declare that financial support was received for the research, authorship, and/or publication of this article. This work was carried out under the frame of the Partnership for Research and Innovation in the Mediterranean Area (PRIMA) program supported by the European Union, Call 2018 - Project "IMPRESA" (IMProving RESilience to Abiotic stresses in durum wheat: enhancing knowledge by genetic, physiological and "omics" approaches and increasing Mediterranean germplasm biodiversity by crop wild relatives-based introgressiomics), ID 1496 (Coordinator C.C.). Part of the work was carried out within the Agritech National Research Center and received funding from the European Union Next-GenerationEU (PIANO NAZIONALE DI RIPRESA E RESILIENZA (PNRR) – MISSIONE 4 COMPONENTE 2, INVESTIMENTO 1.4 – D.D. 1032 17/06/2022, CN00000022). This manuscript reflects only the authors' views and opinions, neither the European Union nor the European Commission can be considered responsible for them.

Conflict of interest

The authors declare that the research was conducted in the absence of any commercial or financial relationships that could be construed as a potential conflict of interest.

Publisher's note

Supplementary material

The Supplementary Material for this article can be found online at: https://www.frontiersin.org/articles/10.3389/fpls.2024.1378186/full#supplementary-material

References

Aebi, H. (1984). Catalase in *vitro*. *Methods Enzymol.* 105, 121–126. doi: 10.1016/s0076-6879(84)05016-3

Akram, N. A., Shafiq, F., and Ashraf, M. (2017). Ascorbic acid-a potential oxidant scavenger and its role in plant development and abiotic stress tolerance. *Front. Plant Sci.* 8. doi: 10.3389/fpls.2017.00613

Annunziata, M. G., Ciarmiello, L. F., Woodrow, P., Maximova, E., Fuggi, A., and Carillo, P. (2017). Durum wheat roots adapt to salinity remodeling the cellular content of nitrogen metabolites and sucrose. *Front. Plant Sci.* 7, 2035. doi: 10.3389/fpls.2016.02035

Arif, Y., Singh, P., Siddiqui, H., Bajguz, A., and Hayat, S. (2020). Salinity induced physiological and biochemical changes in plants: an omic approach towards salt stress tolerance. *Plant Physiol. Biochem.* 156, 64–77. doi: 10.1016/j.plaphy.2020.08.042

Arzani, A., and Ashraf, M. (2016). Smart engineering of genetic resources for enhanced salinity tolerance in crop plants. *CRC Crit. Rev. Plant Sci.* 35, 146–189. doi: 10.1080/07352689.2016.1245056

Athar, H. U. R., Khan, A., and Ashraf, M. (2008). Exogenously applied ascorbic acid alleviates salt-induced oxidative stress in wheat. *Environ. Exp. Bot.* 63, 224–231. doi: 10.1016/j.envexpbot.2007.10.018

Bannari, A., and Al-Ali, Z. (2020). Assessing climate change impact on soil salinity dynamics between 1987–2017 in arid landscape using landsat TM, ETM+ and OLI data. *Remote Sens.* 12, 2794. doi: 10.3390/rs12172794

Bates, L. S., Waldren, R. P., and Teare, I. (1973). Rapid determination of free proline for water-stress studies. *Plant Soil* 39, 205–207. doi: 10.1007/BF00018060

Borghini, M., Bryden, H., Schroeder, K., Sparnocchia, S., and Vetrano, A. (2014). The Mediterranean is becoming saltier. *Ocean Sci.* 10, 693–700. doi: 10.5194/os-10-693-2014

Bose, J., Rodrigo-Moreno, A., and Shabala, S. (2014). ROS homeostasis in halophytes in the context of salinity stress tolerance. *J. Exp. Bot.* 65, 1241–1257. doi: 10.1093/jxb/ert430

Bouteraa, M. T., Mishra, A., Ben Romdhane, W., Ben Hsouna, A., Siddique, K. H., and Ben Saad, R. (2022). Bio-stimulating effect of natural polysaccharides from *Lobularia maritima* on durum wheat seedlings: improved plant growth, salt stress tolerance by modulating biochemical responses and ion homeostasis. *Plants* 11, 1991. doi: 10.3390/plants11151991

Bradford, M. M. (1976). A rapid and sensitive method for the quantitation of microgram quantities of protein utilizing the principle of protein-dye binding. *Anal. Biochem.* 72, 248–254. doi: 10.1006/abio.1976.9999

Brini, F., Imen, A., Kaouther, F., Hanin, M., Khoudi, H., and Masmoudi, K. (2009). Physiological and molecular analyses of seedlings of two Tunisian durum wheat (*Triticum turgidum* L. subsp. durum [Desf.]) varieties showing contrasting tolerance to salt stress. *Acta Physiol. Plant* 31, 145–154. doi: 10.1007/s11738-008-0215-x

Cannon, J. (2022). *Cradle of transformation: The Mediterranean and climate change* (Mongabay - News & Inspiration from nature frontline). Available at: https://news.mongabay.com/2022/04/cradle-of-transformation-the-mediterranean-and-climate-change/.

Carillo, P., Annunziata, M. G., Pontecorvo, G., Fuggi, A., and Woodrow, P. (2011). "Salinity stress and salt tolerance," in *Abiotic Stress in Plants - Mechanisms and Adaptations*. Eds. A. Shanker and B. Venkateswarlu (InTech) 2011. doi: 10.5772/22331

Caverzan, A., Passaia, G., Rosa, S. B., Ribeiro, C. W., Lazzarotto, F., and Margis-Pinheiro, M. (2012). Plant responses to stresses: Role of ascorbate peroxidase in the antioxidant protection. *Genet. Mol. Biol.* 35, 1011–1019. doi: 10.1590/S1415-47572012000600016

Ceoloni, C., Biagetti, M., Ciaffi, M., Forte, P., and Pasquini, M. (1996). Wheat chromosome engineering at the 4x level: the potential of different alien gene transfers into durum wheat. *Euphytica* 89, 87–97. doi: 10.1007/BF00015724

Ceoloni, C., Forte, P., Gennaro, A., Micali, S., Carozza, R., and Bitti, A. (2005). Recent developments in durum wheat chromosome engineering. *Cytogenet. Genome Res.* 109, 328–334. doi: 10.1159/000082416

Ceoloni, C., Forte, P., Kuzmanović, L., Tundo, S., Moscetti, I., De Vita, P., et al. (2017). Cytogenetic mapping of a major locus for resistance to Fusarium head blight and crown rot of wheat on *Thinopyrum elongatum* 7EL and its pyramiding with valuable genes from a *Th. ponticum* homoeologous arm onto bread wheat 7DL. *Theor. Appl. Genet.* 130, 2005–2024. doi: 10.1007/s00122-017-2939-8

Ceoloni, C., Kuzmanović, L., Forte, P., Virili, M. E., and Bitti, A. (2015). "Wheat-perennial Triticeae introgressions: major achievements and prospects," in Alien Introgression in Wheat -Cytogenetics, Molecular Biology, and Genomics. Eds. M. Molnár-Láng, C. Ceoloni and J. Doležel (Springer International Publishing, Switzerland), 273–313, ISBN: . doi: 10.1007/978-3-319-23494-6_11

Ceoloni, C., Kuzmanović, L., Gennaro, A., Forte, P., Giorgi, D., Grossi, M. R., et al. (2014). "Genomes, chromosomes and genes of perennial Triticeae of the genus *Thinopyrum*: the value of their transfer into wheat for gains in cytogenomic knowledge and 'precision' breeding"," in *Advances in Genomics of Plant Genetic Resources*. Eds. R. Tuberosa, A. Graner and E. Frison (Springer, Dordrecht, The Netherlands), 333–358. doi: 10.1007/978-94-007-7575-6_14

Chen, S. Y., Xia, G. M., Quan, T. Y., Xiang, F. N., Jin, Y., and Chen, H. M. (2004). Introgression of salt-tolerance from somatic hybrids between common wheat and *Thinopyrum ponticum*. *Plant Sci.* 167, 773–779. doi: 10.1016/j.plantsci.2004.05.010

Colmer, T. D., Flowers, T. J., and Munns, R. (2006). Use of wild relatives to improve salt tolerance in wheat. *J. Exp. Bot.* 57, 1059–1078. doi: 10.1093/jxb/erj124

Cuevas, J., Daliakopoulos, I. N., del Moral, F., Hueso, J. J., and Tsanis, I. K. (2019). A review of soil-improving cropping systems for soil salinization. *Agronomy* 9, 295. doi: 10.3390/agronomy9060295

Darko, E., Khalil, R., Dobi, Z., Kovacs, V., Szalai, G., Janda, T., et al. (2020). Addition of *Aegilops biuncialis* chromosomes 2M or 3M improves the salt tolerance of wheat in different way. *Sci. Rep.* 10, 22327–22336. doi: 10.1038/s41598-020-79372-1

Davenport, R., James, R. A., Zakrisson-Plogander, A., Tester, M., and Munns, R. (2005). Control of sodium transport in durum wheat. *Plant Physiol.* 137, 807–818. doi: 10.1104/pp.104.057307

Deal, K. R., Goyal, S., and Dvořák, J. (1999). Arm location of *Lophopyrum elongatum* genes affecting K^+/Na^+ selectivity under salt stress. *Euphytica* 108, 193–198. doi: 10.1023/A:1003685032674

de Carvalho, L. M. J., Gomes, P. B., de Oliveira Godoy, R. L., Pacheco, S., do Monte, P. H. F., de Carvalho, J. L. V., et al. (2012). Total carotenoid content, α-carotene and β-carotene, of landrace pumpkins (*Cucurbita moschata* Duch): A preliminary study. *Food Res. Int.* 47, 337–340. doi: 10.1016/j.foodres.2011.07.040

Dewey, D. R. (1960). Salt tolerance of twenty-five strains of *Agropyron*. *Agron. J.* 52, 631–635. doi: 10.2134/agronj1960.00021962005200110006x

Dixon, D. P., Davis, B. G., and Edwards, R. (2002). Functional divergence in the glutathione transferase superfamily in plants: identification of two classes with putative functions in redox homeostasis in *Arabidopsis thaliana*. *J. Biol. Chem.* 277, 30859–30869. doi: 10.1074/jbc.M202919200

Djemal, R., and Khoudi, H. (2016). *TdSHN1*, a WIN1/SHN1-type transcription factor, imparts multiple abiotic stress tolerance in transgenic tobacco. *Environ. Exp. Bot.* 131, 89–100. doi: 10.1016/j.envexpbot.2016.07.005

Doležel, J., Číhalíková, J., and Lucretti, S. (1992). A high-yield procedure for isolation of metaphase chromosomes from root tips of *Vicia faba* L. *Planta* 188, 93–98. doi: 10.1007/BF00198944

Doležel, J., Číhalíková, J., Weiserová, J., and Lucretti, S. (1999). Cell cycle synchronization in plant root meristems. *Methods Cell Sci.* 21, 95–107. doi: 10.1023/A:1009876621187

Doležel, J., and Lucretti, S. (1989). Analysis of nuclear-DNA content in plant-cells by flow cytometry. *Biol. Plant* 31, 113–120. doi: 10.1007/BF02907241

Draper, H. H., and Hadley, M. (1990). Malondialdehyde determination as index of lipid peroxidation. *Methods Enzymol.* 186, 421–431. doi: 10.1016/0076-6879(90)86135-i

Dvořák, J., Edge, M., and Ross, K. (1988). On the evolution of the adaptation of *Lophopyrum elongatum* to growth in saline environments. *Proc. Natl. Acad. Sci. U.S.A.* 85, 3805–3809. doi: 10.1073/pnas.85.11.3805

Dvořák, J., Noaman, M. M., Goyal, S., and Gorham, J. (1994). Enhancement of the salt tolerance of *Triticum turgidum* L. by the *Kna1* locus transferred from *Triticum aestivum* L. chromosome 4D by homoeologous recombination. *Theor. Appl. Genet.* 87, 872–877. doi: 10.1007/BF00221141

Eizenga, G. C. (1987). Locating the *Agropyron* segment in wheat-*Agropyron* 'transfer No. 12'. *Genome* 29, 365–366. doi: 10.1139/g87-061

El-Hendawy, S., Elshafei, A., Al-Suhaibani, N., Alotabi, M., Hassan, W., Dewir, Y. H., et al. (2019). Assessment of the salt tolerance of wheat genotypes during the germination stage based on germination ability parameters and associated SSR markers. *J. Plant Interact.* 14, 151–163. doi: 10.1080/17429145.2019.1603406

El Sabagh, A., Islam, M. S., Skalicky, M., Ali Raza, M., Singh, K., Anwar Hossain, M., et al. (2021). Salinity stress in wheat (*Triticum aestivum* L.) in the changing climate: Adaptation and management strategies. *Front. Agron.* 3. doi: 10.3389/fagro.2021.661932

Estévez, I. H., and Hernández, M. R. (2020). Plant glutathione S-transferases: an overview. *Plant Gene* 23, 100233. doi: 10.1016/j.plgene.2020.100233

Eynard, A., Lal, R., and Wiebe, K. (2005). Crop response in salt-affected soils. *J. Sustain. Agric.* 27, 5–50. doi: 10.1300/J064v27n01_03

Fanelli, G., Kuzmanović, L., Giovenali, G., Tundo, S., Mandalà, G., Rinalducci, S., et al. (2023). Untargeted metabolomics reveals a multi-faceted resistance response to Fusarium head blight mediated by the *Thinopyrum elongatum Fhb7E* locus transferred *via* chromosome engineering into wheat. *Cells* 12, 1113. doi: 10.3390/cells12081113

Farooq, S. (2009). "Triticeae: the ultimate source of abiotic stress tolerance improvement in wheat," in *Salinity and Water Stress*. Eds. M. Ashraf, M. Ozturk and H.R. Athar (Springer, New York), 65–71, ISBN: . doi: 10.1007/978-1-4020-9065-3_7

Farooq, S., and Azam, F. (2007). Differences in behavior of salt tolerant and salt and water deficiency tolerant wheat genotypes when subjected to various salinity levels. *Cereal Res. Commun.* 35, 63–70. doi: 10.1556/CRC.35.2007.1.8

Feki, K., Tounsi, S., and Brini, F. (2017). Comparison of an antioxidant system in tolerant and susceptible wheat seedlings in response to salt stress. *Span. J. Agric. Res.* 15, e0805. doi: 10.5424/sjar/2017154-11507

Flowers, T. J., and Colmer, T. D. (2008). Salinity tolerance in halophytes. *New Phytol.* 179, 945–963. doi: 10.1111/j.1469-8137.2008.02531.x

Flowers, T. J., and Colmer, T. D. (2015). Plant salt tolerance: adaptations in halophytes. *Ann. Bot.* 115, 327–331. doi: 10.1093/aob/mcu267

Flowers, T. J., and Yeo, A. R. (1995). Breeding for salinity resistance in crop plants: where next? *Aust. J. Plant Physiol.* 22, 875–884. doi: 10.1071/PP9950875

Foyer, C. H., and Noctor, G. (2011). Ascorbate and glutathione: the heart of the redox hub. *Plant Physiol.* 155, 2–18. doi: 10.1104/pp.110.167569

Giovenali, G., Kuzmanović, L., Capoccioni, A., and Ceoloni, C. (2023). The response of chromosomally engineered durum wheat-*Thinopyrum ponticum* recombinant lines to the application of heat and water-deficit stresses: effects on physiological, biochemical and yield-related traits. *Plants* 12, 704. doi: 10.3390/plants12040704

Guellim, A., Catterou, M., Chabreri, O., Tetu, T., Hirel, B., Dubois, F., et al. (2019). Identification of phenotypic and physiological markers of salt stress tolerance in durum wheat (*Triticum durum* Desf.) through integrated analyses. *Agronomy* 9, 844. doi: 10.3390/agronomy9120844

Guo, X., Wang, M., Kang, H., Zhou, Y., and Han, F. (2022). Distribution, polymorphism and function characteristics of the GST-encoding *Fhb7* in *Triticeae*. *Plants* 11, 2074. doi: 10.3390/plants11162074

Haider, M. S., Jaskani, M. J., and Fang, J. (2021). "Overproduction of ROS: underlying molecular mechanism of scavenging and redox signaling," in *Biocontrol Agents and Secondary Metabolites*. Ed. S. Jogaiah (Elsevier-Woodhead Publishing, UK), 347–382. doi: 10.1016/B978-0-12-822919-4.00014-4

Hasanuzzaman, M., Bhuyan, M. H. M. B., Anee, T. I., Parvin, K., Nahar, K., Al Mahmud, J., et al. (2019). Regulation of ascorbate-glutathione pathway in mitigating oxidative damage in plants under abiotic stress. *Antioxidants* 8, 384. doi: 10.3390/antiox8090384

Hasanuzzaman, M., Bhuyan, M. H. M. B., Zulfiqar, F., Raza, A., Sayed, M. M., Al Mahmud, J., et al. (2020). Reactive oxygen species and antioxidant defense in plants under abiotic stress: revisiting the crucial role of a universal defense regulator. *Antioxidants* 9, 681. doi: 10.3390/antiox9080681

Hasanuzzaman, M., Nahar, K., Rahman, A., Anee, T. I., Alam, M. U., Bhuiyan, T. F., et al. (2017). "Approaches to enhance salt stress tolerance in wheat," in *Wheat Improvement, Management and Utilization*. Eds. R. Wanyera and J. Owuoche (InTech), 2017. doi: 10.5772/672472017

Hopmans, J. W., Qureshi, A. S., Kisekka, I., Munns, R., Grattan, S. R., Rengasamy, P., et al. (2021). Critical knowledge gaps and research priorities in global soil salinity. *Adv. Agron.* 169, 1–191. doi: 10.1016/bs.agron.2021.03.001

Hu, Y., and Schmidhalter, U. (2023). Opportunity and challenges of phenotyping plant salt tolerance. *Trends Plant Sci.* 28, 552–566. doi: 10.1016/j.tplants.2022.12.010

Inbart-Pompan, H., Eilam, T., and Eshel, A. (2013). Searching for salt tolerance among wild relatives of wheat: what should we look for? *Aust. J. Crop Sci.* 7, 2116–2127.

Isayenkov, S. V., and Maathuis, F. J. M. (2019). Plant salinity stress: many unanswered questions remain. *Front. Plant Sci.* 10. doi: 10.3389/fpls.2019.00080

James, R. A., von Caemmerer, S., Condon, A. G., Zwart, A. B., and Munns, R. (2008). Genetic variation in tolerance to the osmotic stress component of salinity stress in durum wheat. *Funct. Plant Biol.* 35, 111–123. doi: 10.1071/FP07234

Kamal, K. Y., Khodaeiaminjan, M., Yahya, G., El-Tantawy, A. A., Abdel El-Moneim, D., El-Esawi, M. A., et al. (2021). Modulation of cell cycle progression and chromatin dynamic as tolerance mechanisms to salinity and drought stress in maize. *Physiol. Plant* 172, 684–695. doi: 10.1111/ppl.13260

Konkin, D., Hsueh, Y.-C., Kirzinger, M., Kubaláková, M., Haldar, A., Balcerzak, M., et al. (2022). Genomic sequencing of *Thinopyrum elongatum* chromosome arm 7EL, carrying fusarium head blight resistance, and characterization of its impact on the transcriptome of the introgressed line CS-7EL. *BMC Genomics* 23, 228. doi: 10.1186/s12864-022-08433-8

Kumar, S., and Trivedi, P. K. (2018). Glutathione S-transferases: role in combating abiotic stresses including arsenic detoxification in plants. *Front. Plant Sci.* 9. doi: 10.3389/fpls.2018.00751

Kuzmanović, L., Gennaro, A., Benedettelli, S., Dodd, I. C., Quarrie, S. A., and Ceoloni, C. (2014). Structural-functional dissection and characterization of yield-contributing traits originating from a group 7 chromosome of the wheatgrass species *Thinopyrum ponticum* after transfer into durum wheat. *J. Exp. Bot.* 65, 509–525. doi: 10.1093/jxb/ert393

Kuzmanović, L., Giovenali, G., Ruggeri, R., Rossini, F., and Ceoloni, C. (2021). Small "nested" introgressions from wild *Thinopyrum* species, conferring effective resistance to Fusarium diseases, positively impact durum wheat yield potential. *Plants* 10, 579. doi: 10.3390/plants10030579

Kuzmanović, L., Mandalà, G., Tundo, S., Ciorba, R., Frangella, M., Ruggeri, R., et al. (2019). Equipping durum wheat–*Thinopyrum ponticum* recombinant lines with a *Thinopyrum elongatum* major QTL for resistance to Fusarium diseases through a cytogenetic strategy. *Front. Plant Sci.* 10. doi: 10.3389/fpls.2019.01324

Kuzmanović, L., Menasria, H., Rouabhi, A., Giovenali, G., Capoccioni, A., Saveriano, M., et al. (2022). "Performance of locally adapted durum wheat germplasm in the Mediterranean basin and recombinant lines with *Thinopyrum* spp. introgressions across Algerian and Italian environments with different water availability," in *From Seed To Pasta IV Intern. Conf*, Bologna, Italy, 26–29 October 2022. Available at: https://www.fromseedtopasta.com/wp-content/uploads/2022/10/45_Ceoloni.pdf.

Kuzmanović, L., Ruggeri, R., Able, J. A., Bassi, F. M., Maccaferri, M., Tuberosa, R., et al. (2018). Yield of chromosomally engineered durum wheat-*Thinopyrum ponticum* recombinant lines in a range of contrasting rain-fed environments. *Field Crop Res.* 228, 147–157. doi: 10.1016/j.fcr.2018.08.014

Kuzmanović, L., Ruggeri, R., Virili, M. E., Rossini, F., and Ceoloni, C. (2016). Effects of *Thinopyrum ponticum* chromosome segments transferred into durum wheat on yield

components and related morpho-physiological traits in Mediterranean rain-fed conditions. *Field Crop Res.* 186, 86–98. doi: 10.1016/j.fcr.2015.11.007

Li, H., Li, W., Zheng, Q., Zhao, M., Wang, J., Li, B., et al. (2023). Salinity threshold of tall wheatgrass for cultivation in coastal saline and alkaline land. *Agriculture* 13, 337. doi: 10.3390/agriculture13020337

Luo, M. C., Dubcovsky, J., Goyal, S., and Dvořák, J. (1996). Engineering of interstitial foreign chromosome segments containing the K^+/Na^+ selectivity gene *Kna1* by sequential homoeologous recombination in durum wheat. *Theor. App. Genet.* 93, 1180–1184. doi: 10.1007/BF00230144

Mazhar, S., Pellegrini, E., Contin, M., Bravo, C., and De Nobili, M. (2022). Impacts of salinization caused by sea level rise on the biological processes of coastal soils - a review. *Front. Environ. Sci.* 10. doi: 10.3389/fenvs.2022.909415

McGuire, P. E., and Dvořák, J. (1981). High salt-tolerance potential in wheatgrasses. *Crop Sci.* 21, 702–705. doi: 10.2135/cropsci1981.0011183X002100050018x

Miransari, M., and Smith, D. (2019). Sustainable wheat (*Triticum aestivum* L.) production in saline fields: a review. *Crit. Rev. Biotechnol.* 39, 999–1014. doi: 10.1080/07388551.2019.1654973

Mittler, R. (2017). ROS are good. *Trends Plant Sci.* 22, 11–19. doi: 10.1016/j.tplants.2016.08.002

Mizuno, M., Kamei, M., and Tsuchida, H. (1998). Ascorbate peroxidase and catalase cooperate for protection against hydrogen peroxide generated in potato tubers during low-temperature storage. *IUBMB Life* 44, 717–726. doi: 10.1080/15216549800201762

Monsen, S. B., Stevens, R., and Shaw, N. L. (2004). "Grasses" in *Restoring Western Ranges and Wildlands*, vol. 2. (U.S. Department of Agriculture Forest Service, Rocky Mountain Research Station, Fort Collins, CO, USA), 295–424.

Mujeeb-Kazi, A., Munns, R., Rasheed, A., Ogbonnaya, F. C., Ali, N., Hollington, P., et al. (2019). Breeding strategies for structuring salinity tolerance in wheat. *Adv. Agron.* 155, 121–187. doi: 10.1016/bs.agron.2019.01.005

Mullan, D. J., Mirzaghaderi, G., Walker, E., Colmer, T. D., and Francki, M. G. (2009). Development of wheat-*Lophopyrum elongatum* recombinant lines for enhanced sodium 'exclusion' during salinity stress. *Theor. Appl. Genet.* 119, 1313–1323. doi: 10.1007/s00122-009-1136-9

Munns, R. (1993). Physiological processes limiting plant-growth in saline soils – some dogmas and hypotheses. *Plant Cell Environ.* 16, 15–24. doi: 10.1111/j.1365-3040.1993.tb00840.x

Munns, R. (2002). Comparative physiology of salt and water stress. *Plant Cell Environ.* 25, 239–250. doi: 10.1046/j.0016-8025.2001.00808.x

Munns, R., James, R. A., and Läuchli, A. (2006). Approaches to increasing the salt tolerance of wheat and other cereals. *J. Exp. Bot.* 57, 1025–1043. doi: 10.1093/jxb/erj100

Munns, R., James, R. A., Xu, B., Athman, A., Conn, S. J., Jordans, C., et al. (2012). Wheat grain yield on saline soils is improved by an ancestral Na^+ transporter gene. *Nat. Biotechnol.* 30, 360–366. doi: 10.1038/nbt.2120

Munns, R., and Tester, M. (2008). Mechanisms of salinity tolerance. *Annu. Rev. Plant Biol.* 59, 651–681. doi: 10.1146/annurev.arplant.59.032607.092911

Nakano, Y., and Asada, K. (1981). Hydrogen peroxide is scavenged by ascorbate-specific peroxidase in spinach chloroplasts. *Plant Cell Physiol.* 22, 867–888. doi: 10.1093/oxfordjournals.pcp.a076232

Omielan, J. A., Epstein, E., and Dvořák, J. (1991). Salt tolerance and ionic relations of wheat as affected by individual chromosomes of salt-tolerant *Lophopyrum elongatum*. *Genome* 34, 961–974. doi: 10.1139/g91-149

Pandey, S., Fartyal, D., Agarwal, A., Shukla, T., James, D., Kaul, T., et al. (2017). Abiotic stress tolerance in plants: myriad roles of ascorbate peroxidase. *Front. Plant Sci.* 8. doi: 10.3389/fpls.2017.0058

Pearce, F. (2022). Salt scourge: The dual threat of warming and rising salinity. Yale Environment 360. Available at: https://e360.yale.edu/features/salt-scourge-the-dual-threat-of-warming-and-rising-salinity [accessed July 14, 2023].

Peng, Z., Wang, Y., Geng, G., Yang, R., Yang, Z., Yang, C., et al. (2022). Comparative analysis of physiological, enzymatic, and transcriptomic responses revealed mechanisms of salt tolerance and recovery in *Tritipyrum*. *Front. Plant Sci.* 12. doi: 10.3389/fpls.2021.800081

Pour-Aboughadareh, A., Kianersi, F., Poczai, P., and Moradkhani, H. (2021). Potential of wild relatives of wheat: ideal genetic resources for future breeding programs. *Agronomy* 11, 1656. doi: 10.3390/agronomy11081656

Qi, F., and Zhang, F. (2020). Cell cycle regulation in the plant response to stress. *Front. Plant Sci.* 10. doi: 10.3389/fpls.2019.01765

Ramegowda, V., Da Costa, M. V. J., Harihar, S., Karaba, N. N., and Sreeman, S. M. (2020). "Abiotic and biotic stress interactions in plants: a cross-tolerance perspective," in *Priming-mediated stress and cross-stress tolerance in crop plants* (Academic Press, United States), 267–302. doi: 10.1016/B978-0-12-817892-8.00017-9

Rawat, N., Wungrampha, S., Singla-Pareek, S. L., Yu, M., Shabala, S., and Pareek, A. (2022). Rewilding staple crops for the lost halophytism: toward sustainability and profitability of agricultural production systems. *Mol. Plant* 15, 45–64. doi: 10.1016/j.molp.2021.12.003

Rossini, F., Provenzano, M. E., Kuzmanović, L., Ceoloni, C., and Ruggeri, R. (2020). Assessing the ability of durum wheat-*Thinopyrum ponticum* recombinant lines to suppress naturally occurring weeds under different sowing densities. *Agronomy* 10, 709. doi: 10.3390/agronomy10050709

Rossini, A., Ruggeri, R., Mzid, N., Rossini, F., and Di Miceli, G. (2024). *Codium fragile* (Suringar) Hariot as biostimulant agent to alleviate salt stress in durum wheat: preliminary results from germination trials. *Plants* 13, 283. doi: 10.3390/plants13020283

Roy, S. J., Negrão, S., and Tester, M. (2014). Salt resistant crop plants. *Curr. Opin. Biotech.* 26, 115–124. doi: 10.1016/j.copbio.2013.12.004

Sairam, R. K., Srivastava, G. C., Agarwal, S., and Meena, R. C. (2005). Differences in antioxidant activity in response to salinity stress in tolerant and susceptible wheat genotypes. *Biol. Plant* 49, 85–91. doi: 10.1007/s10535-005-5091-2

Scheinost, P., Tilley, D., Ogle, D., and Stannard, M. (2008). Tall wheatgrass - *Thinopyrum ponticum* (Podp.). Z.–W. Liu and R.–C. Wang. In USDA-NRCS PLANTS Database, Plant Guides. Available at: https://plants.usda.gov/DocumentLibrary/plantguide/pdf/pg_thpo7.pdf. [accessed June 29, 2023]

Schuppler, U., He., P. H., John., P. C., and Munns., R. (1998). Effect of water stress on cell division and Cdc2-like cell cycle kinase activity in wheat leaves. *Plant Physiol.* 117, 667–678. doi: 10.1104/pp.117.2.667

Shahzad, A., Iqbal, M., Asif, M., Hirani, A. H., and Goyal, A. (2013). Growing wheat on saline lands: can a dream come true? *Aust. J. Crop Sci.* 7, 515–524.

Sheikh-Mohamadi, M. H., Etemadi, N., Aalifar, M., and Pessarakli, M. (2022). Salt stress triggers augmented levels of Na^+, K^+ and ROS alters salt-related gene expression in leaves and roots of tall wheatgrass (*Agropyron elongatum*). *Plant Physiol. Biochem.* 183, 9–22. doi: 10.1016/j.plaphy.2022.04.022

Singh, A. (2022). Soil salinity: a global threat to sustainable development. *Soil Use Manage.* 38, 39–67. doi: 10.1111/sum.12772

Sofo, A., Scopa, A., Nuzzaci, M., and Vitti, A. (2015). Ascorbate peroxidase and catalase activities and their genetic regulation in plants subjected to drought and salinity stresses. *Int. J. Mol. Sci.* 16, 13561–13578. doi: 10.3390/ijms160613561

Suzuki, N., Koussevitzky, S., Mittler, R., and Miller, G. (2012). ROS and redox signalling in the response of plants to abiotic stress. *Plant Cell Environ.* 35, 259–270. doi: 10.1111/j.1365-3040.2011.02336.x

Tedeschi, A. (2020). Irrigated agriculture on saline soils: a perspective. *Agronomy* 10, 1630. doi: 10.3390/agronomy10111630

Tong, C., Yang, G., AoenBolige,, Terigen,, Li, H., Li, B., et al. (2022). Screening of salt-tolerant *Thinopyrum ponticum* under two coastal region salinity stress levels. *Front. Genet.* 13. doi: 10.3389/fgene.2022.832013

Tounsi, S., Ben Amar, S., Masmoudi, K., Sentenac, H., Brini, F., and Véry, A.-A. (2016). Characterization of two HKT1; 4 transporters from *Triticum monococcum* to elucidate the determinants of the wheat salt tolerance *Nax1* QTL. *Plant Cell Physiol.* 57, 2047–2057. doi: 10.1093/pcp/pcw123

Tounsi, S., Feki, K., Hmidi, D., Masmoudi, K., and Brini, F. (2017). Salt stress reveals differential physiological, biochemical and molecular responses in *T. monococcum* and *T. durum* wheat genotypes. *Physiol. Mol. Biol. Plants* 23, 517–528. doi: 10.1007/s12298-017-0457-4

Tounsi, S., Jemli, S., Feki, K., Brini, F., and Saïdi, M. N. (2023). Superoxide dismutase (SOD) family in durum wheat: promising candidates for improving crop resilience. *Protoplasma* 260, 145–158. doi: 10.1007/s00709-022-01767-w

Ullah, A., Bano, A., and Khan, N. (2021). Climate change and salinity effects on crops and chemical communication between plants and plant growth-promoting microorganisms under stress. *Front. Sustain. Food Syst.* 5. doi: 10.3389/fsufs.2021.618092

Velikova, V., Yordanov, I., and Edreva, A. (2000). Oxidative stress and some antioxidant systems in acid rain-treated bean plants: protective role of exogenous polyamines. *Plant Sci.* 151, 59–66. doi: 10.1016/S0168-9452(99)00197-1

Venkatesh, J., and Park, S. W. (2014). Role of L-ascorbate in alleviating abiotic stresses in crop plants. *Bot. Stud.* 55, 38. doi: 10.1186/1999-3110-55-38

Volkov, V. (2015). Salinity tolerance in plants. Quantitative approach to ion transport starting from halophytes and stepping to genetic and protein engineering for manipulating ion fluxes. *Front. Plant Sci.* 6. doi: 10.3389/fpls.2015.00873

Wang, H., Sun, S., Ge, W., Zhao, L., Hou, B., Wang, K., et al. (2020). Horizontal gene transfer of *Fhb7* from fungus underlies *Fusarium* head blight resistance in wheat. *Science* 368, 6493. doi: 10.1126/science.aba5435

West, G., Inze, D., and Beemster, G. T. (2004). Cell cycle modulation in the response of the primary root of Arabidopsis to salt stress. *Plant Physiol.* 135, 1050–1058. doi: 10.1104/pp.104.040022

Whitbread, A. K., Masoumi, A., Tetlow, N., Schmuck, E., Coggan, M., and Board, P. G. (2005). Characterization of the omega class of glutathione transferases. *Method. Enzymol.* 401, 78–99. doi: 10.1016/S0076-6879(05)01005-0

Wu, H., Shabala, L., Azzarello, E., Huang, Y., Pandolfi, C., Su, N., et al. (2018a). Na^+ extrusion from the cytosol and tissue-specific Na^+ sequestration in roots confer differential salt stress tolerance between durum and bread wheat. *J. Exp. Bot.* 69, 3987–4001. doi: 10.1093/jxb/ery194

Wu, H., Shabala, L., Zhou, M., and Shabala, S. (2014). Durum and bread wheat differ in their ability to retain potassium in leaf mesophyll: implications for salinity stress tolerance. *Plant Cell Physiol.* 55, 1749–1762. doi: 10.1093/pcp/pcu10

Wu, H., Zhang, X., Giraldo, J. P., and Shabala, S. (2018b). It is not all about sodium: revealing tissue specificity and signalling roles of potassium in plant responses to salt stress. *Plant Soil* 431, 1–17. doi: 10.1007/s11104-018-3770-y

Xynias, I. N., Mylonas, I., Korpetis, E. G., Ninou, E., Tsaballa, A., Avdikos, I. D., et al. (2020). Durum wheat breeding in the Mediterranean region: current status and future prospects. *Agronomy* 10, 432. doi: 10.3390/agronomy10030432

Yang, C., Zhao, L., Zhang, H., Yang, Z., Wang, H., Wen, S., et al. (2014). Evolution of physiological responses to salt stress in hexaploid wheat. *Proc. Natl. Acad. Sci. U. S. A.* 111, 11882–11887. doi: 10.1073/pnas.1412839111

Yousfi, S., Serret, M. D., Voltas, J., and Araus, J. L. (2010). Effect of salinity and water stress during the reproductive stage on growth, ion concentrations, $\Delta^{13}C$, and $\delta^{15}N$ of durum wheat and related amphiploids. *J. Exp. Bot.* 61, 3529–3542. doi: 10.1093/jxb/erq184

Yuan, W.-Y., and Tomita, M. (2015). *Thinopyrum ponticum* chromatin-integrated wheat genome shows salt-tolerance at germination stage. *Int. J. Mol. Sci.* 16, 4512–4517. doi: 10.3390/ijms16034512

Zeng, J., Zhou, C., He, Z., Wang, Y., Xu, L., Chen, G., et al. (2023). Disomic substitution of 3D chromosome with its homoeologue 3E in tetraploid *Thinopyrum elongatum* enhances wheat seedlings tolerance to salt stress. *Int. J. Mol. Sci.* 24, 1609. doi: 10.3390/ijms24021609

Zhang, Y., Liu, Z., Khan, A. A., Lin, Q., Han, Y., Mu, P., et al. (2016). Expression partitioning of homeologs and tandem duplications contribute to salt tolerance in wheat (*Triticum aestivum* L.). *Sci. Rep.* 6, 21476. doi: 10.1038/srep21476

Zhao, L., Wang, P., Hou, H., Zhang, H., Wang, Y., Yan, S., et al. (2014). Transcriptional regulation of cell cycle genes in response to abiotic stresses correlates with dynamic changes in histone modifications in maize. *PloS One* 9, e106070. doi: 10.1371/journal.pone.0106070

frontiers | Frontiers in Plant Science

TYPE Original Research
PUBLISHED 27 March 2025
DOI 10.3389/fpls.2024.1407574

OPEN ACCESS

EDITED BY
Dayong Cui,
Qilu Normal University, China

REVIEWED BY
Jing Liu,
Qilu Normal University, China
Zilong Tan,
Qilu Normal University, China

*CORRESPONDENCE
Haydee Laza
haydee.laza@ttu.edu

†PRESENT ADDRESS
Aarti Gupta,
Department of Botany, Dr. Harisingh Gour Vishwavidyalaya (A Central University), Sagar, Madhya Pradesh, India

RECEIVED 26 March 2024
ACCEPTED 27 September 2024
PUBLISHED 27 March 2025

CITATION
Laza H, Bhattarai B, Mendu V, Burow MD, Emendack Y, Sanchez J, Gupta A, Abdelrahman M, Tran L-SP, Tissue DT and Payton P (2025) Peanut leaf transcriptomic dynamics reveals insights into the acclimation response to elevated carbon dioxide under semiarid conditions.
Front. Plant Sci. 15:1407574.
doi: 10.3389/fpls.2024.1407574

Peanut leaf transcriptomic dynamics reveals insights into the acclimation response to elevated carbon dioxide under semiarid conditions

Haydee Laza[1]*, Bishwoyog Bhattarai[1,2], Venugopal Mendu[3], Mark D. Burow[1,4], Yves Emendack[5], Jacobo Sanchez[5], Aarti Gupta[1†], Mostafa Abdelrahman[1], Lam-Son Phan Tran[1], David T. Tissue[6] and Paxton Payton[7]

[1]Department of Plant and Soil Science, Texas Tech University, Lubbock, TX, United States, [2]Division of Plant Science and Technology, University of Missouri-Columbia, Columbia, MO, United States, [3]Department of Agriculture, Agribusiness, and Environmental Sciences, Texas Agricultural and Mechanical (A&M) University-Kingsville, Kingsville, TX, United States, [4]Texas Agricultural and Mechanical (A&M) AgriLife Research, Texas Agricultural and Mechanical (A&M) University, Lubbock, TX, United States, [5]Cropping Systems Research Laboratory, United States Department of Agriculturertment, Agricultural Research Services (USDA-ARS), Lubbock, TX, United States, [6]Hawkesbury Institute for the Environment, Western Sydney University, Penrith, NSW, Australia, [7]Goanna Ag, Lubbock, TX, United States

Introduction: Elevated atmospheric carbon dioxide [CO_2] increases peanut carbon assimilation and productivity. However, the molecular basis of such responses is not well understood. We tested the hypothesis that maintaining high photosynthesis under long-term elevated [CO_2] is associated with the shift in C metabolism gene expression regulation.

Methods: We used a field CO_2 enrichment system to examine the effects of elevated [CO_2] (ambient + 250 ppm) across different soil water availability and plant developmental stages on the molecular responses in a peanut runner-type genotype. Plants under both [CO_2] treatments were grown in semiarid conditions. We evaluated a comparative leaf transcriptomic profile across three periodic water deficit/re-hydration (well-watered/recovery) cycles throughout the growing season using RNAseq analysis.

Results: Our results showed that the transcriptome responses were influenced by [CO_2], water availability, and developmental stages. The traditional Mercator annotation analysis based on percentage total revealed that lipid metabolism, hormone biosynthesis, secondary metabolism, amino acid biosynthesis, and transport were the most regulated biological processes. However, our new approach based on the comparative relative percentage change per individual category across stages revealed new insights into the gene expression patterns of biological functional groups, highlighting the relevance of the C-related pathways regulated by elevated [CO_2].

Discussion: The photosynthesis analysis showed that 1) The light reaction was the most upregulated pathway by elevated [CO_2] during water stress, 2) Photorespiration was downregulated across all stages, 3) Sucrose synthesis

genes were upregulated by elevated [CO_2] before stress, 4) Starch synthesis genes were upregulated by elevated [CO_2] under drought periods, and 5) CO_2 regulation of sucrose and starch degradation was critical under drought periods. Our findings provide valuable insights into the molecular basis underlying the photosynthetic acclimation response to elevated [CO_2] in peanuts.

KEYWORDS

drought, water stress, gene expression, photorespiration, acclimation

Highlights

- The transcriptome responses were influenced by [CO_2], water, and growth stages.
- The light reaction was the most up-regulated pathway by [CO_2] during water stress.
- Sucrose synthesis genes were upregulated by [CO_2] before stress.
- Starch synthesis genes were upregulated by [CO_2] under drought periods.
- CO_2 regulation of sucrose and starch degradation was critical under drought periods.
- Elevated [CO_2] downregulated photorespiration across all stages.

Introduction

Peanuts are primarily cultivated in semiarid regions and represent a significant source of protein and lipids for populations across the globe (Gangurde et al., 2019). Like most C3 plants, it is expected to benefit from rising atmospheric carbon dioxide concentration by enhanced photosynthesis and yield productivity under limited soil water availability Laza et al., 2021) and increasing the phytochemical shoot content, including total phenolics compounds (Novello et al., 2023). However, the positive CO_2 effects may be diminished under extreme weather events, including high temperatures (Prasad et al., 2003). Wild and cultivated peanuts are unusual legumes because they have pod and seed development below ground, which may enhance carbon capture capability in future climates (Laza et al., 2021) (Gangurde et al., 2019).

Wild-type peanuts usually harbor a single genome (A or B). Thus, diploids (AA, BB) (Bertioli et al., 2011) and, rarely, tetraploids (AAAA, BBBB) can be found in wild natural populations. However, the peanut type suitable for production and human consumption, known as cultivated peanut (*Arachis hypogaea* L.), is an allotetraploid (AABB; 2n=40) (Lu and Pickersgill, 1993; Seijo et al., 2007; Bertioli et al., 2016), whose origin is from two diploid wild types (*Arachis ipaensis* and *Arachis japensis*) has been recently described (Bertioli et al., 2016). Although the increase in ploidy level can result in genetic gain, this ploidy event did not translate into significantly enhanced genetic diversity for peanut (Halward et al., 1991; Burow et al., 2001). Hence, efforts to increase peanut genetic background diversity, especially for seed productivity and disease-related traits, are among the main targets in peanut research. Peanut is an arid crop, and most likely impacted by projected stochastic environmental events such as intensified drought, heat waves, and rising atmospheric [CO_2]. Hence, identifying key traits and their molecular basis will facilitate the development of climate-smart peanut varieties (Gangurde et al., 2019).

The impact of future climates on peanut productivity and leaf physiology has been previously studied (Vara Prasad et al., 1999; Prasad et al., 2003; Kottapalli et al., 2009; Laza et al., 2021). Like many plants, peanuts maintain homeostasis under different climatic scenarios through a coordinated pathways network. Thereby, carbon metabolism, including the coupling of establishes photosynthesis and respiration supplies a wide range of pathways with C-skeletons (Croteau et al., 2000). Three major photosynthesis-related pathways include light reactions, the Calvin cycle, and photorespiration. Photorespiration is a carbon C2 cycle that occurs when oxygen instead of CO_2, binds to the Rubisco enzyme (Walker et al., 2016). Sucrose and starch are major components of carbohydrate (CHO) metabolism. The coordinated sugar dynamic is maintained by regulating of the hexose phosphate and triose phosphate pools. In general, we can get an idea of the sugar status by looking at the expression of "famine" and "feast" genes, which represent sugar depletion or abundance, respectively (Parrott et al., 2005) and play a pivotal role in transcriptomic reprogramming (Yokoyama et al., 2006). Although the transcriptomic analysis of peanuts grown under drought conditions has been previously studied (Jain et al., 2001; Dramé et al., 2007; Qin et al., 2011; Chen et al., 2013; Pruthvi et al., 2013; Chopra et al., 2014; Furlan et al., 2014), the interactive effect of elevated [CO_2], high temperature and water deficit on peanut gene expression dynamics has not been addressed yet.

To gain a better understanding of the molecular mechanisms underlying the physiological, biochemical, and structural changes associated with elevated [CO_2], we investigated the molecular basis of

the photosynthetic acclimation response to elevated [CO_2] throughout the life cycle as a function of plant growth stage and soil water availability. The present investigation was undertaken to answer the following questions: 1) Which biological processes are more responsive to elevated [CO_2]? 2) Could the lack of leaf photosynthetic acclimation in peanuts be explained by the shift in gene expression caused by CO_2 fertilization? and 3) Do peanut plants use different genes or expression levels to cope with subsequent water stress over time? Is this response altered by elevated CO_2?

The acclimation response is usually explained by looking at the sink strength. In peanuts, developing new leaves and the symbiotic association with mycorrhizae and rhizobia might increase the sink strength, preventing the acclimation response from happening. The main objectives of this study were to 1) Identify relevant molecular mechanisms involved in the sustained enhanced photosynthetic rate induced by elevated [CO_2], which prevent the acclimation response from happening, and 2) Examine if elevated [CO_2] modifies. the capacity of peanut plants to acclimate to drought through transcriptomic reprogramming. We hypothesized that: 1) Enhanced photosynthetic rate at elevated [CO_2] might be explained by the sustained-up regulation of genes involved in carbon metabolism; and 2) The photosynthetic acclimation response to elevated [CO_2] might be altered in limited water conditions, due to differentially expressed genes induced by the interaction of these two factors compared to elevated CO_2 alone.

Materials and methods

Plant material, growth conditions, and [CO_2] treatments

This study (2015 and 2016) was conducted under semiarid conditions (water stress was not a studied treatment) in the research fields of the cropping system research laboratory at USDA-ARS Lubbock, Texas. *Arachis hypogaea* cv. C76-16; runner market type was planted at 2.5 cm depth at a planting density of 6 plants/m2 (60 x 103 plants ha^{-1}) in 15 m row plots with 1.0 m row spacing. The experiment included two long-term [CO_2] treatments (ambient; 400 ppm) and elevated; 650 ppm) under Canopy Evapotranspiration and Assimilation (CETA) chambers (Baker et al., 2014; Laza et al., 2021). Each treatment consisted of three replications. The chambers were placed on the plants in the field 10-15 days after sowing to ensure good stand establishment of selected areas. Peanut plants from both CO_2 treatments were subjected to three water deficit stress and recovery cycles, and each water stress episode was evaluated by comparing three stages: well-watered stage before any stress, pre-water deficit (pwd), water deficit (wd), and well-watered recovery (ww rec). Details about experimental settings and chamber operations are described elsewhere (Laza et al., 2021, 2023).

Transcriptome data collection

Although genomic analysis of peanuts has been previously conducted using a reference transcriptome, the completion of the peanut genome and the availability of the peanut reference genome (Bertioli et al., 2016), provide new opportunities to associate physiological responses to changes in transcription. In this study, we used a peanut reference transcriptome obtained from our sample profiling from leaves. We collected leaf samples at different growth stages from flowering to physiological maturity (R2-R8) through the growing season to develop the transcriptomic profile associated with the elevated [CO_2] response. All samples were placed in liquid nitrogen immediately after collection and stored at -80°C for further analysis. Forty-two samples (42 leaves) were used for RNA extraction. For the acclimation response study, we used leaf samples collected at the three stages of the drought episode, including, pre-water deficit, water deficit, and recovery, 3 days following irrigation pre-water deficit (pwd), water deficit (wd) well-watered/recovery (ww-rec), 3 days following irrigation.

RNA extraction, library preparation and sequencing

Frozen plant material (leaf) was ground using pre-cooled mortar and pestle with liquid nitrogen. Around 0.3 g (leaf) of the resulting fine powder was used to extract the total RNA using the RNeasy Sigma kit following the manufacturer's protocol. Final elution was done with preheated (64°C) RNAse-free water. RNA quality and quantity were first monitored using the NanoDrop 2200 Spectrophotometer (Thermo-Scientific, Waltham, MA). Only samples with A260/230 > 1.9 and a concentration higher than 100 ng/μl were selected for further analysis. We checked the integrity of these samples using the tape station, looking for 28S and 18S bands. We conducted serial dilutions of the total RNA samples (using RNAse-free water as a solvent) based on the concentrations obtained from the Qubit™ 2.0 fluorometer (Invitrogen, Life Technologies, Grand Island, NY). We diluted to 100, 25, 15, and 7.5 ng/μl for cDNA library construction and quantification using the NeoPrep following the manufacturer protocol. The 42 cDNA constructed libraries were validated by checking the insert size using the Agilent tape station 2200. The final concentration was confirmed using the Qubit™ 2.0 fluorometer. The libraries were kept at -80°C, ready for sequencing. Samples were prepared according to Illumina's RNA sequencing protocol and manufacturer's instructions. The 42 cDNA libraries were divided into two groups of 24 and proceeded with two Rapid mode sequencing runs on the HiSeq 2500 instrument at the Center for Biotechnology and Genomics, Texas Tech University.

Data analysis, functional annotation, and qRT-PCR analysis

Sequenced reads were obtained from bcl files using bcl2fastq software, and the quality of the Fastaq files was checked using FastQC software. The reads were then assembled into contigs to create a reference transcriptome using Trinity software. Reads were mapped to the reference transcriptome to determine differential expression using QSeq software. The list of DEGs

was mapped onto biological pathways using MapMan software (Lohse et al., 2014).

The concentration of total RNA in each sample was determined with the MULTISKAN SkyHigh microplate spectrophotometer (Thermo Fisher Scientific Inc., USA). The concentration of total RNA for all samples was normalized to 1 µg µL-1 using RNase-free water. Subsequently, following the instructions provided, first-strand cDNA synthesis was performed using the QuantiTect reverse transcription kit (Qiagen, Hilden, Germany). All real-time qPCR (RT-qPCR) assays were performed on 96-well plates CFX96 Real-Time system (BIO-RAD, CA, USA). The reaction volumes were 10 µL and contained 5 µL Sso Advanced Universal SYBR Green Supermix (BIO-RAD, CA, USA), three µL cDNA templates, and two µL primer pair mix (10 pmol each primer). In each run, triplicates of no-template control (NTC) comprising DEPC-treated water were incorporated. The thermal cycling conditions consisted of 40 cycles, starting with an initial denaturation at 96°C for 10 seconds, then annealing at 60°C for 30 seconds, and an extension phase at 72°C for 30 seconds. Melting curves were obtained using a thermal melting profile performed after the last PCR cycle: 65°C for 10 seconds, followed by a constant increase in the temperature between 65°C and 95°C. All the specific primer pairs employed in this study are given in Supplementary Table S1. Amplicon-based fluorescence thresholds were used to obtain the CT values. The eukaryotic elongation factor 1 beta (ELF1B) gene was used as a reference gene in the RT-qPCR analysis of RNA samples from three biological replicates (n = 3 × 2 technical replicates).

Statistical analysis

We performed the leaf transcriptomic analysis to elucidate the mechanistic basis of our physiological findings (Laza et al., 2021). To better understand the underlying mechanisms of the acclimation response, we conducted eight vertical pair comparisons between the [CO_2] treatments and three horizontal pair comparisons between growth stages (C8-R2/R3, C9-R3/R4, and C10-R2/R4) and soil water availability periods (pwd, wd, ww-rec) for each [CO_2] treatment (ambient, 400 ppm and elevated, 650 ppm) independently (Table 1). Data was expressed for each time point as the percentage of total DEGs and as the percentage change (i.e the change in DEGs as the percentage of the baseline between growth stages). Here, we focused our analysis on the effect of elevated [CO_2] on 1) the expression genes per functional of group across growth stages to examine if the lack of leaf photosynthetic acclimation in peanuts (Laza et al., 2021) could be explained by the shift in gene expression caused by CO_2 fertilization in one or more pathways and 2) plant ability to cope with subsequent water stress over time. The qualitative gene expression (up/down) was analyzed for each functional group (encoding gene transcripts) by examining the regulation type across stages for each DEG. This analysis provided new insights regarding the expression dynamics. DEGs were defined as genes with at least |log2 fold-change (FC)|>1 and adjusted P-value ≤ 0.05. T test (at $P<0.05$) was conducted to determine differences between the number of DEG between stages.

Results

Summary of the transcriptomic analysis

Overall, the number of DEGs increased over time, with a significant peak from pre-water deficit (R2; 1182) to first recovery (R4; 3044) (Table 2). The leaf transcriptomic analysis across different growth stages revealed a similar gene expression pattern in response to water deficit and recovery. Thus, 34 out of 35 biological processes (identified by Mercator software) were induced in peanut leaves, regardless of the atmospheric [CO_2] (Figure 1). Furthermore, for the seven data points considered, the differential expression was more pronounced for protein, RNA, and signaling categories, with maximum values up to 9.4%, 6.3%, and 5.3%, respectively. Conversely, an increased number of group functions were less responsive to CO_2. These functional groups include minor carbohydrate (CHO) metabolism, polyamine metabolism, biodegradation of xenobiotics, redox, co-factor/vitamin metabolism, and TCA (tricarboxylic acid) pathways, showing less than 0.2% percent of the total differentially regulated responses. Moreover, gluconeogenesis, oxidative pentose phosphate (OPP), C1-metabolism, tetrapyrrole synthesis, S assimilation, and N metabolism were not induced by elevated [CO_2] at the early plant reproductive stage before any water deficit event.

Expression of biological processes and patterns under elevated [CO_2]

The number of categories per functional group varied with growth stage/soil water availability and exhibited different patterns while transitioning from one stage to the other (Table 3). Although a higher number of functional groups (3044) was found during the first re-hydration event (Rec-1), the dynamic of quantified expression (number of functional groups) was different for each

TABLE 1 Summary of the 8-time points sample collection. Leaf samples of peanut plants grown under ambient atmospheric [CO_2] (400 ppm) and elevated [CO_2] treatments were collected to perform the comparison (C) analysis across different reproductive developmental stages (R) and soil water availability. C1 (beginning peg development-R2 at well-watered/pre-water deficit-pwd), C2 (beginning pod-development-R3 at the first water deficit-wd1), C3 (full pod-R4 at the first well-watered/recovery-rec1), C4 (beginning seed-R5 at the second water deficit-wd2), C5 (full seed-R6 at the second well-watered/recovery-rec2), C6-C7 (beginning maturity-R7 at third water deficit-wd3, followed by the third well-watered/recovery-rec3), and C8 (harvest maturity-R8, well-watered).

Comparisons	C1	C2	C3	C4	C5	C6	C7	C8
Soil water content	pwd	wd1	rec1	wd2	rec2	wd3	rec3	Harvest
Plant growth stage	R2	R3	R4	R5	R6	R7	R7	R8
	C9		C10					
	C11							

Each plot represents three biological replications.

10.3389/fpls.2024.1407574

TABLE 2 Summary of differentially expressed genes (DEGs) induced by elevated [CO_2] in peanut leaves.

	Pre-water deficit (R2)	First water deficit (R3)	First recovery (R4)
No. DEGs	1182	2979	3044
No. Assigned	678	1469	1845
Unknown	628	1331	1729
No. Ontology	50	138	116
Function groups	504	1510	1199
Down-regulated	655	1197	1151
Up-regulated	527	1782	1893
% Down-regulated	45	40	38
% Up-regulated	55	60	62

Changes across different developmental stages (R2, R3, and R4) and soil water availability (pre-water deficit, water deficit, and well-watered recovery) are presented.

biological process. To better understand the effect of elevated [CO_2] on gene expression dynamics, we looked at 1) each time point (ambient control *vs.* elevated [CO_2]) and 2) between time points (each [CO_2] treatment individually at different stages (well-watered [ww] *vs* water deficit [wd] periods). The quantitative gene expression pattern (number of functional groups differentially expressed between the treatments) for each time point was classified as 1a) modified (when the number of functional groups between treatments was different), or 1b) unchanged (same number of categories). This response also changed across growth stages. Thus, four major quantitative gene expression patterns were identified: 2a) up-pattern (the number of categories increases from one stage to the other); 2b) down-pattern (the number of categories is reduced from one stage to the other); 2c) unchanged-pattern (the number of categories remains the same), and 2d) mixed-pattern (were the response from the first transition between stages changed in the next transition).

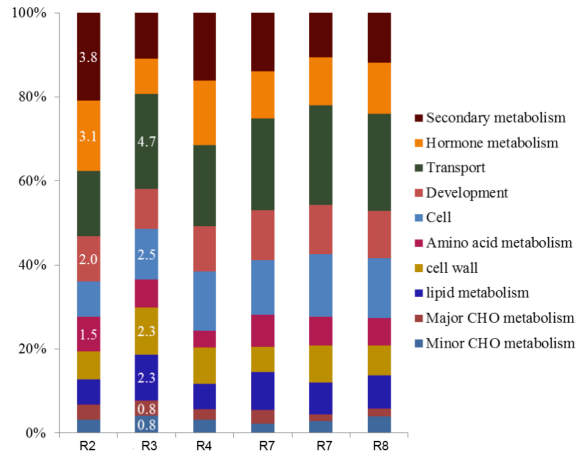

FIGURE 1
Effect of elevated CO_2 on the percentage of total (%) differentially expressed genes (DEGs) per functional group resulted from the peanut leaf transcriptomic. Differential gene expressions as a percentage of the total DGEs in six selected data points, representing different plant growth stages with different soil water availability: pre-water deficit (R2), first water deficit (R3), first recovery (R4), third water deficit (R7), third recovery (R7), and physiological maturity-harvest (R8). Carbohydrate-CHO.

The mixed pattern includes a variety of combinations resulting from the induction, inhibition, or unchanged expressions, such as up/down (increased number of DEGs from pre-water deficit (R2) to 1st water deficit (R3), followed by a reduction from 1st water deficit (R3) to 1st recovery (R4), down/up (the opposite effect described for up/down), unchanged/up, unchanged/down, etc. Understanding the gene expression dynamics is important to characterizing the molecular basis accurately and determining which factors (environmental, developmental, or a combination of both) drive the transcriptomic reprogramming over time. It also helps elucidate whether the responses are associated with current stress/signal or memory stress (prior stress within the organism's life span or even transgenerational background).

In our study, we used two approaches for the gene expression analysis. Our results showed different expression patterns for the two approaches. The first approach, "Percentage of total" (based on the percentage of the total DEGs per function), showed that the expression trend and dynamic were very similar in all the data points, regardless of the growth stage and water availability (Figure 2). This type of analysis, usually presented as a pie graph of functions (software generated), is perhaps one of the most popular approaches currently used for RNA data interpretation. However, because this functional analysis is based on the number of different types of transcripts per biological function, it doesn't represent normalized values; therefore, functions requiring the greater number of genes are more likely to have greater percentage of total than functions requiring a low number of genes. Hence, the % of Total analysis doesn't represent an actual expression pattern since functions and pathways differ on the number of genes/Transcription Factors (TF) required.

The second approach, "Percentage Change," revealed different gene expression patterns than the percentage of the total approach. Here, we demonstrated that using the percentage change (defined as the change in DEGs as a percentage of the baseline for a given function between two stages) while transitioning across stages provides a better representation of expression dynamics, with more accurate identification of relevant functions which have been altered between treatments. Thus, this analysis revealed distinct expression patterns for each transition (Figure 3), with the highest percentage change (mean of 307% averaged across all functions) during the first transition from high to low soil water content. This %mean of differential expression was reduced to almost zero (6%) when plants transitioned from severe water deficit to the following recovery period, and the change in the % mean between the two well-watered periods (pwd and recovery)

10.3389/fpls.2024.1407574

was also high (191%). In contrast with the "Percentage of total" approach, we were also able to identify the most relevant biological functions associated with elevated [CO_2] and water deficit using the "Percentage change" approach. The results showed that C metabolism-related functions were among those with the highest percentage change, suggesting that although the percentage of the total was low for these functions, the relative abundance of transcripts was significantly altered from the baseline stage. Therefore, we selected these functions for further analysis.

Photosynthesis pathways regulation under elevated [CO_2]

We examined the gene expression of the C-related pathways, including photosynthesis (PS), carbohydrate (CHO) metabolisms, and respiration. First, we pooled all the PS-DEG, further subdivided into pathways: 1) light reactions/photosynthetic electron transport chain, 2) C3-Calvin cycle, and 3) C2 cycle- photorespiration. Across the first stress cycle (pre-water deficit (R2), 1st water deficit (R3),

TABLE 3 Percentage change of functional groups differentially expressed across growth stages (R2-R4) with different soil water availability (pre-water deficit [pwd] at R2, water deficit[wd] at R3, and well-watered recovery [ww/rec] at R4).

Functional group	pwd R2	wd R3	ww R4	% change pwd/wd	Pattern Type	% change wd/ww	Pattern Type	% change pwd/ww	Pattern Type
photosynthesis	3	19	16	533	up	-16	down	433	up
major CHO	6	26	8	333	up	-69	down	33	up
minor CHO	2	24	11	1100	up	-54	down	450	up
glycolysis	2	5	6	150	up	20	up	200	up
fermentation	3	4	1	33	up	-75	down	-67	down
gluconeogenesis	0	1	1	na	up	0	nc	na	up
OPP	0	1	2	na	up	100	up	na	up
tricarboxylic acid	1	6	1	500	up	-83	down	0	nc
mitochondrial electron transport	2	4	7	100	up	75	up	250	up
cell wall	11	74	39	573	up	-47	down	255	up
lipid metabolism	9	63	17	600	up	-73	down	89	up
N-metabolism	0	2	3	na	up	50	up	na	up
amino acid metabolism	15	28	17	87	up	-39	down	13	up
S-assimilation	0	0	1	na	up	na	up	na	up
metal handling	6	9	3	50	up	-67	down	-50	down
secondary metabolism	33	57	50	73	up	-12	down	52	up
hormone metabolism	26	39	41	50	up	5	up	58	up
Co-factor, vitamin	6	7	9	17	up	29	up	50	up
tetrapyrrole synthesis	2	1	8	-50	down	700	up	300	up
stress biotic	32	95	102	197	up	7	up	219	up
redox	1	22	17	2100	up	-23	down	1600	up
polyamine metabolism	4	3	3	-25	down	0	nc	-25	down
nucleotide metabolism	5	15	8	200	up	-47	down	60	up
biodegradation of xenobiotics	3	7	3	133	up	-57	down	0	nc
C1-metabolism	0	1	1	na	up	0	nc	na	up
miscellaneous	56	169	82	202	up	-51	down	46	up

(Continued)

TABLE 3 Continued

Functional group	pwd R2	wd R3	ww R4	% change pwd/wd	Pattern Type	% change wd/ww	Pattern Type	% change pwd/ww	Pattern Type
RNA	58	165	155	184	up	-6	down	167	up
DNA	7	49	41	600	up	-16	down	486	up
protein	84	205	218	144	up	6	up	160	up
signaling	49	139	151	184	up	9	up	208	up
cell	20	70	52	250	up	-26	down	160	up
development	24	61	39	154	up	-36	down	63	up
transport	34	140	86	312	up	-39	down	153	up
Not assigned	678	1469	1845	117	up	26	up	172	up
Total	1182	2980	3044						nc
% mean				307		6		191	

Data for the percentage change between the pwd and wd (R2 to R3), wd and ww/Rec (R3 to R4), pwd and rec (R2-R4) are presented. Each data point represents an average between three biological replications. "nc" represents no change, and "na", no available/calculated. Carbohydrate-CHO, Oxidase Pentose Phosphate-OPP.

recovery (R4), and the following recovery, the greater number of unique DEGs (18) were associated with the light reaction. In contrast, the C3 and C2 cycles were less impacted, with only 6 and 4 unique DEG, respectively (Figure 4). We observed that elevated [CO_2] upregulated one of the photosystem II genes (mutarase; chlorophyll-binding to D1) in the light reactions (8.7 log2FC), coupling with a downregulation of the photorespiratory pathway. (-7.6 log2FC) (Supplementary Table S2). During the first recovery, a significant downregulation of two genes encoding a reduction phase enzyme, Glyceraldehyde-3-phosphate dehydrogenase (GAPDH), and a regeneration phase enzyme, Fructose 1,6-bisphosphatase (FBAse), with a greater reduction (-11.8 log2FC).

Carbohydrate metabolism pathways regulation under elevated [CO_2]

We further investigated three relevant carbohydrate (CHO) metabolism pathways, including the major-CHO and minor-CHO. The major-CHO metabolism includes synthesis and degradation of sucrose and starch. The major-CHO metabolism was controlled by 20 DEGs across three stages (pwd-R2, wd1-R3, and ww1-R4), from which 19 were unique and stage-specific (Figure 5). Like photosynthesis, the number of DEGs significantly increased from pre-water deficit (3) to first water deficit (16). The results showed that elevated [CO_2]: 1) upregulated the starch degradation genes including the starch cleavage alpha-amylase (AMY1, 3.2 log2FC) before the water stress (pwd) (Supplementary Table S3), 2) upregulate the sucrose synthesis (FBPase, 1.78 Log_2FC), starch synthesis, (ADP-glucose pyrophosphorylase-(AGPase, 1.00 log2FC, and starch synthase 1.61 log2FC) and starch branching (6.84 log2FC) during the water deficit stress (wd) period, and 3) induced both upregulation of starch synthesis(AGPase, 5.6 log2FC) and starch degradation (AMY1, 2.2 log2FC), as well as enhanced sucrose degradation (vacuolar invertase, 1.3 log2FC) during the well-watered recovery phase (Rec).

Respiratory pathways regulation under elevated [CO_2]

Our results showed that, in general, transcripts related to glycolysis, TCA, and Electron Transport Chain (ETC) were upregulated, indicating that C use was enhanced by elevated CO_2 in peanuts. Similarly, to PS and major CHO, the trend for respiratory pathways was the lower number of functional groups before any water deficit compared to the first water deficit and the first recovery periods. During the pre-water deficit, the TCA pathway was not significantly affected, with aconitase as the only TCA enzyme differentially regulated. This enzyme was significantly inhibited (-7.8 log2FC) (Supplementary Table S4) by elevated [CO_2] before the water deficit period. Furthermore, most of the mitochondrial genes were not altered, but ATP synthesis was significantly reduced (-1.3 log2FC). Similarly, metabolite transport function declined (-1.7 log2FC) in the mitochondrial. Although during pre-water deficit, glycolysis-related transcripts were upregulated, the major respiratory pathways, such as TCA, and ETC, were inhibited. A mix of up/down functions might be used for smaller adjustments to keep the C metabolism balanced. Conversely, when plants were exposed to severe water deficit conditions, the number of functional groups with DEGs significantly increased. Moreover, pathways not induced by elevated [CO_2] during well-watered conditions, including gluconeogenesis and oxidative pentose phosphate, were induced during severe water stress periods. Likewise, most of the glycolysis, TCA, and ETC-related transcripts were upregulated, suggesting that when the peanut plants experienced low soil water content, respiration was enhanced.

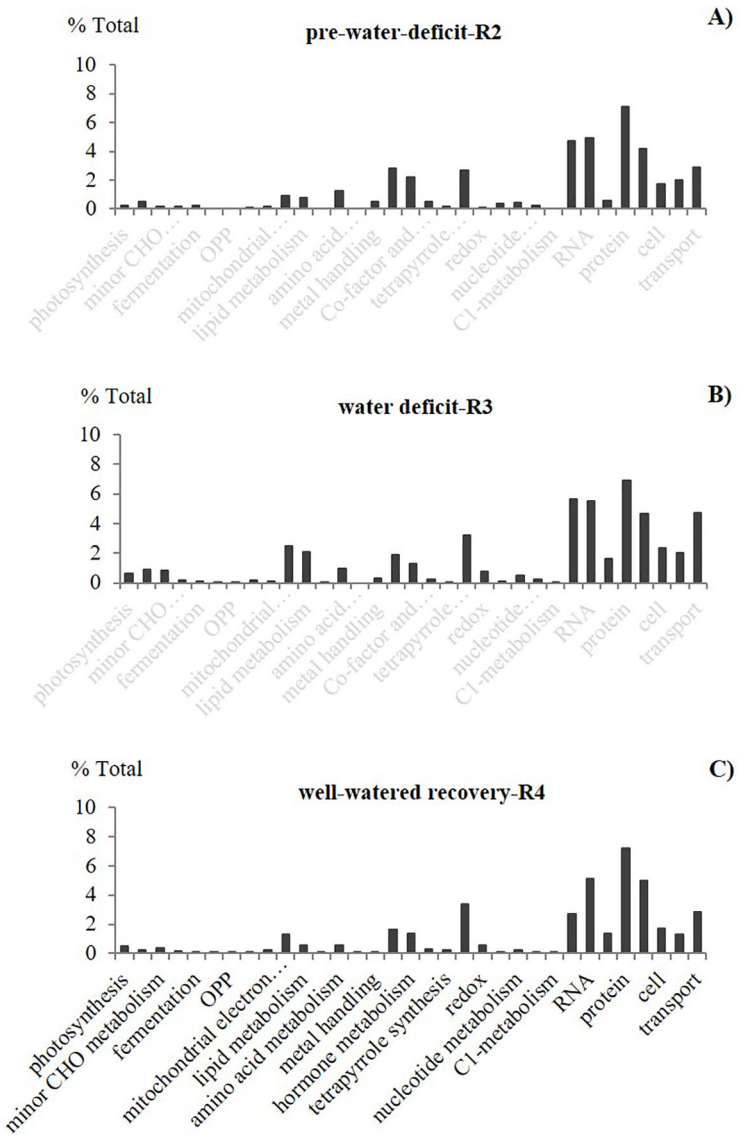

FIGURE 2
Effect of elevated CO_2 on the percentage of total differentially expressed genes (DEGs) for different functional groups. Leaf transcriptomic profile from pair vertical comparisons between the two CO_2 treatments (control, ambient 400 ppm and elevated 60 ppm) at selected growth stages with different soil water availability: **(A)** pre-water deficit (R2), **(B)** first water deficit (R3), and **(C)** well-watered/first recovery (R4)], using the "percentage of total" approach (% indicates the effect of elevated CO_2 over ambient treatment). Carbohydrate-CHO, the oxidative pentose phosphate-OPP. Stats criteria for differentially expressed genes. Genes with |log2 fold-change|>1and adjusted *P-value uc1≤ .05* (FDR (false discovery rate).

Discussion

Enhanced light reactions and Calvin cycle by elevated [CO_2] during water stress

Reductions in photosynthesis at elevated [CO_2] have been associated with lower leaf N, protein, and Rubisco content (Moore et al., 1999) and reduced ETC or Rubisco activase (RCA) content/activity (Sage et al., 2008), among other factors. Previous studies confirmed that peanut (runner type) protein and Rubisco content were significantly reduced when grown in enriched CO_2 (720 ppm, daytime) (Vu and Allen, 2009). High temperature has been found to reduce the light activation of Rubisco by RCA in several C3 plant species, including cotton and wheat, when the atmospheric temperature reaches values higher than 35°C and 30°C, respectively (Feller et al., 1998). In our gene expression study, we found that the Rubisco active form was downregulated. Our results suggest that high photosynthesis at elevated [CO_2] was mostly driven by the upregulation of the photosynthetic ETC and Calvin cycle and, to a lesser extent, the inhibition of RCA. In this context, previous studies found that the reduction in RCA content must be significant (-55%) to impact Rubisco activation (Yamori and von Caemmerer, 2009). It is well documented that Rubisco activation requires the incorporation of CO_2 and Mg^{+2} (Buchanan et al., 2015), but the mechanism of light activation by RCA is yet unknown. Hence, we could not identify the causative

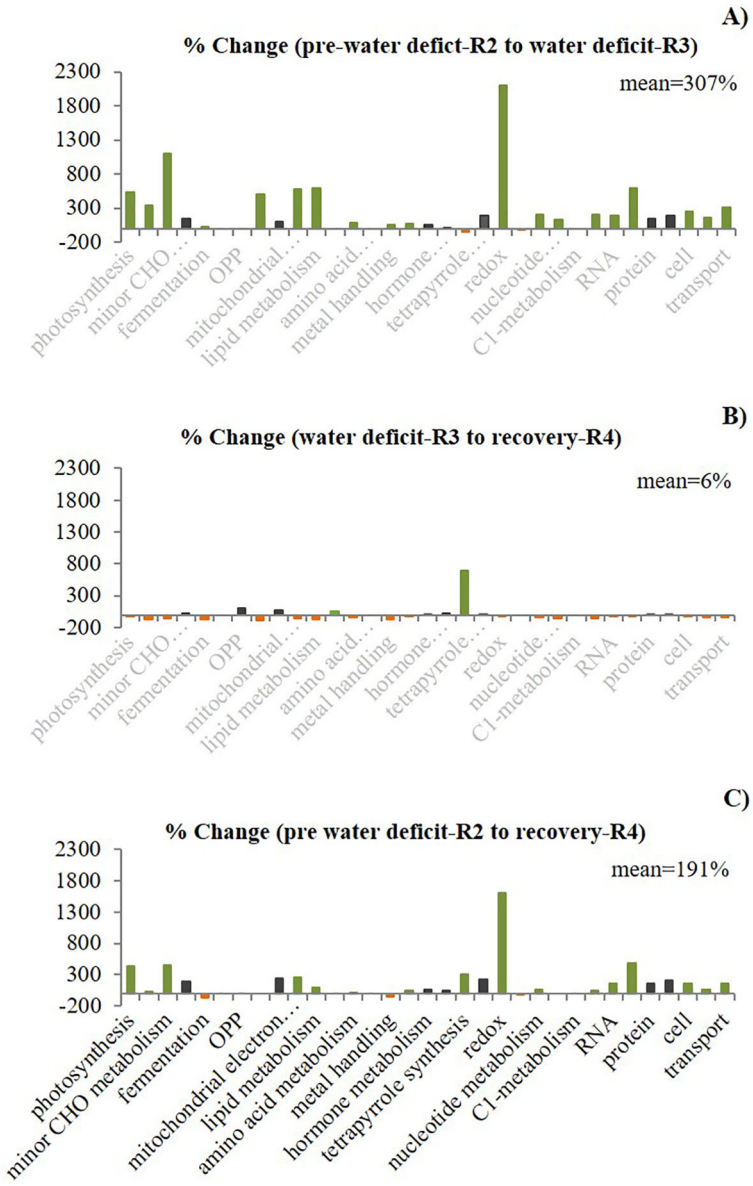

FIGURE 3
Effect of elevated CO_2 on the percentage change of differentially expressed genes (DEGs) per functional group and between stages (first stage as a baseline) in field-grown peanuts. The gene expression regulation exhibited conserved and altered patterns represented by three colors. Black indicates similar pattern ("no change pattern") for the three comparisons between stages **(A)** R2/R3, **(B)** R3/R4 and **(C)** R2/R4). for the three comparisons), green color indicates an increase ("up pattern") in the percentage change. Orange indicates a decrease in the percentage change. The % change mean across all the functional groups for each comparison between stages showed distinct expression patterns.

factors of RCA downregulation in this study, which needs further investigation.

We can assume that enhanced related photosynthetic pathways, such as light reactions and the Calvin cycle, could lead to enhanced sugar production. Depending on the coupling between C fixation and utilization, this response could result in carbohydrate accumulation or enhanced growth. In this context, sugar accumulation has been identified as a negative feedback mechanism of photosynthetic acclimation to elevated [CO_2] (Sims et al., 1998). Other studies showed that the magnitude and type of carbohydrate accumulation might also vary with N availability (Aranjuelo et al., 2013; Noguchi et al., 2015). Thus, studies integrating C and N metabolism will increase our understanding of the underlying basis of the acclimation response under elevated [CO_2].

Data from the first recovery showed significant downregulation of two genes encoding a reduction phase enzyme, Glyceraldehyde-3-phosphate dehydrogenase (GAPDH) and a regeneration phase enzyme, Fructose 1,6-bisphosphatase (FBAse), GAPDH catalyzes the interconversion between 1, 3-Bisphospho-glycerate and Glyceraldehyde 3-phosphate (GAP). At the same time, FBAse converts Fructose 1, 6-biphosphate into Fructose 6 phosphate by inorganic P removal. The greater inhibition of FBAse may be due to its involvement in several related pathways (Noguchi et al., 2015). The downregulation of these enzymes might suppress the Calvin

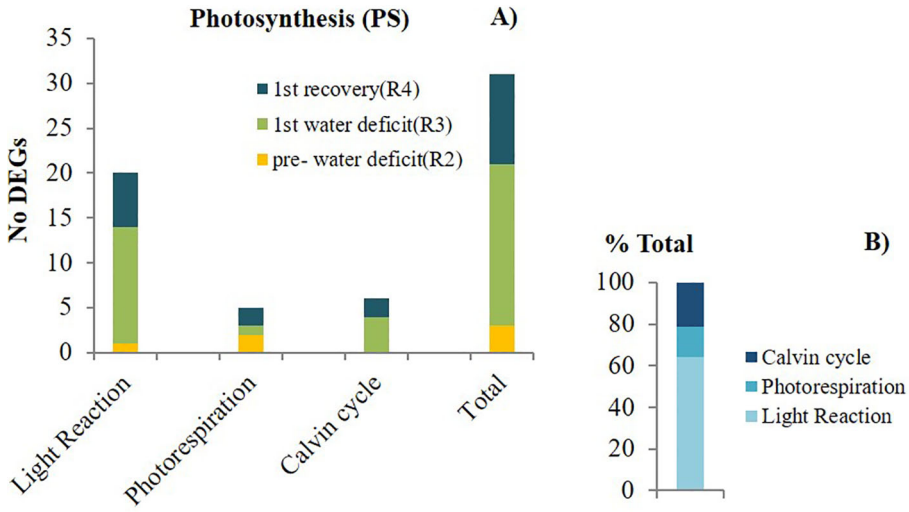

C)

PS	No DEG Total	pwd	wd	ww	% Total pwd	wd	ww
Light Reaction	18	1	13*	6*	33	72	60
Photorespiration	4	2	1	2	67	6	20
Calvin cycle	6	0	4*	2	0	22	20
Total DEG	28	3	18*	10*	11	64	36
% Unique DEG	22	3	15	4	100	83	40

FIGURE 4
Photosynthetic (PS)-related pathways modulation by elevated [CO_2]. **(A)** the number (No) of differentially expressed genes (DEGs) per pathway during pre-water deficit (at the R2 developmental stage), first water deficit (R3), and first recovery (R4); **(B)** the percentage of total for each pathway, averaging across stages; and **(C)** the summary of total and unique DEGs per stage and pathway. Stats criteria for determining the DEGs was *P-value uc1≤ .05* and |log2 fold-change|>1. The * indicates significant difference at $P<0.05$, T test (pwd as control).

cycle and, thereby generate less sugar production. If so, this inhibition does not reflect the enhanced photosynthetic rate observed at this stage and cannot be used as a proposed molecular basis of this physiological trait.

Enhanced sucrose synthesis by elevated [CO_2] during water stress

Our results showed that the major CHO metabolism-related genes followed a similar pattern as the PS-related genes, with the number of DEGs significantly increased in the transition from pre-water deficit to first water deficit stress, suggesting that drought enhanced the CHO gene expression under elevated [CO_2]. Moreover, sucrose metabolism-related transcripts were not affected during optimal soil water conditions. Before any water stress, C metabolism was exclusively controlled by starch metabolism, with 67% and 33% of the total DEGs involved with synthesis and degradation, respectively. In contrast, when plants experienced severe soil water deficit, C metabolism was controlled by both sucrose and starch metabolism. The significantly reduced number of DEGs during the first recovery event suggests that CHO metabolism-related pathways are more responsive to the interactive effect of water deficit and drought than to elevated [CO_2] alone. Enhanced sucrose synthesis was only found during the water deficit period. Sucrose can be synthesized via sucrose synthase and sucrose-phosphatase synthase (Baschetti, 1997). Its synthesis is usually activated with the accumulation of hexose phosphate (Guy et al., 1992). Thus, the increased sucrose synthesis in the enriched CO_2 environment might be associated with sugar accumulation and subsequent activation of the sucrose-phosphate enzyme.

Conversely, our results showed that the regulation of starch metabolism seems to take place during both low and high soil water availability. Across different stages (pre-water deficit; R2, first water deficit; R3, and first recovery; R4), the starch metabolism was similarly controlled by the upregulation of two common enzymes: 1) ADP-glucose pyrophoshorylase for starch synthesis, and 2) Alpha-amylase for starch degradation. Starch synthesis related-transcripts were enhanced at elevated [CO_2] and regulated via ADP-glucose pyrophosphorylase or Granule-bound starch synthase. In contrast, other unique transcripts, which were stage-specific, were used to generate distinct molecular strategies to cope with different scenarios. Here, during high soil water content periods, elevated [CO_2] increased

10.3389/fpls.2024.1407574

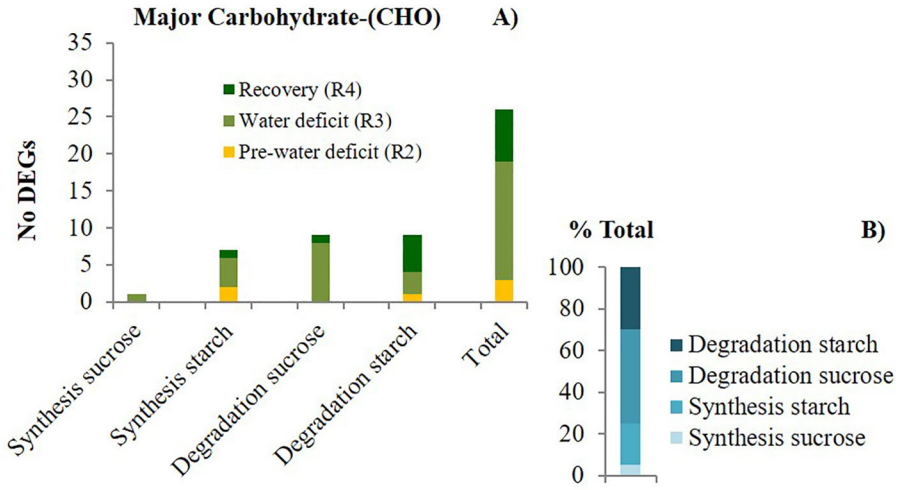

C)

Major CHO	No DEG				% Total		
	Total	pwd)	wd	ww	pwd	wd	ww
Synthesis sucrose	1	0	1	0	0	6	0
Synthesis starch	4	2	4*	1	67	25	14
Degradation sucrose	9	0	8*	1	0	50	14
Degradation starch	6	1	3	5	33	19	71
Total	20	3	16*	7*	15	80	35
Unique DEG	19	1	14	4	33	88	57

FIGURE 5
Major carbohydrate (CHO) metabolism-related pathways modulation by elevated [CO_2]. **(A)** the number of differentially expressed genes (DEGs) per pathway during pre-water deficit (at the R2 developmental stage), first water deficit (R3), and the first recovery (R4); **(B)** the percentage of total for each pathway, averaging across stages; and **(C)** summary of total and unique DEGs per stage and pathway. Stats criteria for determining the DEGs was P-value uc1≤ .05 and |log2 fold-change|>1. The * indicates significant difference at $P<0.05$, T test (pwd as control).

starch synthesis by the upregulation of genes encoding ADP-glucose pryrophoshorylase enzyme only, which is further regulated by the ratio of inorganic P and the photosynthetic intermediate, 3-phosphogycerate (3-PGA) (Ballicora et al., 2004).

We found that induced differential gene expression by elevated [CO_2] was more pronounced for protein, RNA, and signaling categories. This suggests that many genes associated with these processes are responsive to atmospheric [CO_2] changes and remain differentially regulated throughout the entire plant life cycle. Similarly, the transcriptomic analysis showed that stress, RNA, miscellaneous, protein, and signaling were among the functional categories with the most responsive genes to drought and high temperature in poplar species (Jia et al., 2017).

Most of the carbohydrate metabolism-related transcripts were upregulated, suggesting that the enhanced C assimilation rate at elevated [CO_2] in peanuts can be explained by an increased sugar metabolism. Furthermore, our gene expression analysis confirmed increased leaf photosynthesis (A_{net}) at elevated [CO_2] in peanuts, previously documented in (Laza et al., 2021).

Increased A_{net} could be the result of 1) upregulation of photosynthetic-related pathways such as the light reactions and Calvin cycle pathway or as an indirect inhibition of respiration and photorespiration processes, leading to an overall increased A_{net}, with similar gross photosynthetic rate. As expected, higher atmospheric [CO_2] reduced photorespiration, which might explain the enhanced A_{net} at the early reproductive stage (R2) and optimal soil water availability in enriched CO_2 peanut agroecosystems. In agreement with our results, photorespiration inhibition with increasing atmospheric [CO_2] has been reported in many plant species (Long et al., 2004).

Interestingly, transcripts related to the Calvin cycle were not affected by elevated [CO_2] (zero DEG) until plants experienced severe water deficit conditions. These results indicate that the previously reported enhanced leaf A_{net} during pre-water deficit (Laza et al., 2021) cannot be directly explained by changes in the Calvin cycle pathway. Instead, regulating other C-related processes could be responsible for this response. We also found that elevated [CO_2] upregulated one of the photosystem II genes (mutarase; chlorophyll-binding to D1) in the light reactions and downregulated the photorespiratory pathway. Walker et al. (2016) found that in the absence of stress (abiotic or biotic), photosynthesis is most likely to

increase by blocking the C2 cycle/photorespiratory pathway. In agreement with our findings, photorespiration was also significantly inhibited in *Arabidopsis* plants grown at high atmospheric [CO_2] (Zinta et al., 2014). Although photorespiration has been considered an inefficient process attached to photosynthesis, part of the C lost through this mechanism can be recovered and has been quantified (24-38%) for other C3 crops like rice and soybean (Busch et al., 2013).

High C assimilation under CO_2 is regulated by a different set of genes across stages

To understand the molecular basis of the photosynthetic acclimation response to elevated [CO_2] in peanuts under semiarid conditions, we examined the gene expression of relevant C-related pathways. Our gene expression analysis showed that very few common DEGs were found across stages. This suggests that different regulatory checkpoints delivered the same physiological outcome (the enhanced photosynthetic rate at elevated [CO_2]). In this context, we identified two molecular strategies used by peanuts under elevated [CO_2] before and during water deficit stress.

Strategy-1: Before the water stress, the downregulation of photorespiration was the major regulatory mechanism, but elevated [CO_2] did not induce the Calvin cycle-related transcripts. However, elevated [CO_2] down-regulated photorespiratory genes and upregulated the 3-PGA during the pre-water deficit period. This relative abundance of 3-PGA at elevated [CO_2] compared to ambient could have triggered the observed ADP-glucose pyrophosphorylase activation. The enhanced photosynthetic rate was not associated with changes in the C3 reductive photosynthetic carbon cycle (Calvin cycle; zero DEG). Similarly, in Arabidopsis, an increased C assimilation was not explained by changes in Calvin cycle metabolites (Noguchi et al., 2015).

Strategy-2: During water stress, at a later reproductive stage, the molecular mechanism responsible for the enhanced photosynthetic rate had more genes involved in the photosynthetic electron transport chain. This regulation might be related to an increased light absorption capacity, reflected in the greater number of DEG related to light harvesting complex (LHC). An increased light absorption capacity might help speed up the electron transport and C fixation. Similarly, an increased abundance of transcripts related to the Calvin cycle and upregulation of sucrose synthesis suggests the most likely molecular strategy responsible for the enhanced net C assimilation in enriched [CO_2] systems during severe water deficit periods.

Concluding remarks

This study reveals the complex dynamics of the peanut leaf transcriptome in response to the combined effect of plant development, soil water availability, and atmospheric [CO_2]. Based on quantitative and qualitative gene expression analysis, the molecular differential responses were more pronounced during water deficit periods than during periods of sufficient water. Our research suggests that high C assimilation under elevated CO_2 is associated with the significantly altered expression of transcripts that regulate C metabolism pathways, including the downregulation of transcripts controlling photorespiration. Our findings provide valuable insights into the molecular basis underlying the photosynthetic acclimation response to elevated [CO_2] in peanuts.

Data availability statement

The original contributions presented in the study are publicly available. This data can be found here: https://www.ebi.ac.uk/biostudies/arrayexpress, accession number E-MTAB-14869 and https://dx.doi.org/10.3389/fpls.2024.1407574.

Author contributions

HL: Writing – review & editing, Writing – original draft, Visualization, Validation, Supervision, Software, Resources, Project administration, Methodology, Investigation, Funding acquisition, Formal analysis, Data curation, Conceptualization. BB: Methodology, Writing – review & editing, Formal analysis. VM: Resources, Formal analysis, Writing – review & editing. MB: Visualization, Writing – review & editing, Methodology. YE: Funding acquisition, Writing – review & editing, Resources, Methodology. JS: Resources, Writing – review & editing, Methodology. AG: Writing – review & editing, Validation, Methodology, Data curation. MA: Writing – review & editing, Validation, Methodology, Data curation. LT: Validation, Methodology, Data curation, Writing – review & editing. DT: Writing – review & editing, Visualization. PP: Visualization, Supervision, Software, Resources, Project administration, Investigation, Funding acquisition, Data curation, Conceptualization, Writing – review & editing, Methodology, Formal analysis.

Funding

The author(s) declare that financial support was received for the research and/or publication of this article. The authors are grateful for the funding support of this project provided by Ogallala Aquifer Program grant number 3090-13000-015-11S, the National Institute of Food and Agriculture grant number 2013-67013-21108, USDA-ARS CRIS Projects 3096-21000-022-00-D and 3096-13000-009-00-D, and USDA-ARS 21A158-B51541-200.

Acknowledgments

The authors gratefully acknowledge Dr. Corley Holbrook for the peanut seed donation. The authors are grateful for the assistance

of Dr. Kottapalli with the RNAseq analysis at the Texas Tech University Center for Biotechnology and Genomics.

Conflict of interest

Author PP was employed by the company Goanna Ag. Goanna Ag had no role in the design, analysis, or interpretation of this study nor did they provide any funding for this project.

The remaining authors declare that the research was conducted in the absence of any commercial or financial relationships that could be construed as a potential conflict of interest.

The author(s) declared that they were an editorial board member of Frontiers, at the time of submission. This had no impact on the peer review process and the final decision.

Publisher's note

All claims expressed in this article are solely those of the authors and do not necessarily represent those of their affiliated organizations, or those of the publisher, the editors and the reviewers. Any product that may be evaluated in this article, or claim that may be made by its manufacturer, is not guaranteed or endorsed by the publisher.

Supplementary material

The Supplementary Material for this article can be found online at: https://www.frontiersin.org/articles/10.3389/fpls.2024.1407574/full#supplementary-material

SUPPLEMENTARY TABLE 1
List of genes and primers used for Real Time-Polymerase Chain Reaction (RT-PCR) gene expression validation of RNAseq transcriptomic in peanuts under elevated [CO_2] and water stress.

SUPPLEMENTARY TABLE 2
Leaf RNAseq analysis summary-Photosynthesis.

SUPPLEMENTARY TABLE 3
Leaf RNAseq analysis summary-CHO.

SUPPLEMENTARY TABLE 4
Leaf RNAseq analysis summary-Respiration.

References

Aranjuelo, I., Sanz-Sáez, Á., Jauregui, I., Irigoyen, J. J., Araus, J. L., Sánchez-Díaz, M., et al. (2013). Harvest index, a parameter conditioning responsiveness of wheat plants to elevated CO2. *J. Exp. Bot.* 64, 1879–1892. doi: 10.1093/jxb/ert081

Baker, J. T., Gitz, D. C., Payton, P., Broughton, K. J., Bange, M. P., and Lascano, R. J. (2014). Carbon dioxide control in an open system that measures canopy gas exchanges. *Agron. J.* 106, 789–792. doi: 10.2134/agronj13.0450

Ballicora, M. A., Iglesias, A. A., and Preiss, J. (2004). ADP-glucose pyrophosphorylase: A regulatory enzyme for plant starch synthesis. *Photosynth. Res* 79, 1–24. doi: 10.1023/B:PRES.0000011916.67519.58

Baschetti, R. (1997). Sucrose metabolism. *N. Z. Med. J* 110, 43. doi: 10.1002/9780470015902.a0021259

Bertioli, D. J., Cannon, S. B., Froenicke, L., Huang, G., Farmer, A. D., Cannon, E. K. S., et al. (2016). The genome sequences of Arachis duranensis and Arachis ipaensis, the diploid ancestors of cultivated peanut. *Nat. Genet.* 48, 438–446. doi: 10.1038/ng.3517

Bertioli, D. J., Seijo, G., Freitas, F. O., Valls, J. F. M., Leal-Bertioli, S. C. M., and Moretzsohn, M. C. (2011). An overview of peanut and its wild relatives. *Plant Genet. Resour.* 9, 134–149. doi: 10.1017/S1479262110000444

Buchanan, B. B., Gruissem, W., and Jones, R. L. (2015). Biochemistry & Molecular biology of plants. Biochem. *Mol. Biol. Plants* 1264.

Burow, M. D., Simpson, C. E., Starr, J. L., and Paterson, A. H. (2001). Transmission genetics of chromatin from a synthetic amphidiploid to cultivated peanut (Arachis hypogaea L.): Broadening the gene pool of a monophyletic polyploid species. *Genetics* 159, 823–837. doi: 10.1093/genetics/159.2.823

Busch, F. A., Sage, T. L., Cousins, A. B., and Sage, R. F. (2013). C3 plants enhance rates of photosynthesis by reassimilating photorespired and respired CO2. *Plant Cell Environ.* 36, 200–212. doi: 10.1111/j.1365-3040.2012.02567.x

Chen, X., Zhu, W., Azam, S., Li, H., Zhu, F., Li, H., et al. (2013). Deep sequencing analysis of the transcriptomes of peanut aerial and subterranean young pods identifies candidate genes related to early embryo abortion. *Plant Biotechnol. J.* 11, 115–127. doi: 10.1111/pbi.12018

Chopra, R., Burow, G., Farmer, A., Mudge, J., Simpson, C. E., and Burow, M. D. (2014). Comparisons of *de novo* transcriptome assemblers in diploid and polyploid species using peanut (Arachis spp.) RNA-Seq data. *PloS One* 9. doi: 10.1371/journal.pone.0115055

Croteau, R., Kutchan, T. M., Lewis, N. G., Buchanan, B., Wilhelm, G., and Jones, R. (2000). Biochemistry & Molecular biology of plants. *Physiol. Mol. Biol. plants*1250–1318.

Dramé, K., Clavel, D., and Repellin, A. (2007). Water deficit induces variation in expression of stress-responsive genes in two peanut (Arachis hypogaea L.) cultivars with different tolerance to drought. *Plant Physiol. Biochem.* 45, 236–243. doi: 10.1016/j.plaphy.2007.02.002

Feller, U., Crafts-Brandner, S. J., and Salvucci, M. E. (1998). Moderately high temperatures inhibit ribulose-1,5-bisphosphate carboxylase/oxygenase (Rubisco) activase-mediated activation of rubisco. *Plant Physiol.* 116, 539–546. doi: 10.1104/pp.116.2.539

Furlan, A. L., Bianucci, E., Tordable, M., del, C., Castro, S., and Dietz, K.-J. (2014). Antioxidant enzyme activities and gene expression patterns in peanut nodules during a drought and rehydration cycle. *Funct. Plant Biol.* 41, 704. doi: 10.1071/FP13311

Gangurde, S. S., Kumar, R., Pandey, A. K., Burow, M., Laza, H. E., Nayak, S. N., et al. (2019). "Climate-smart groundnuts for achieving high productivity and improved quality: Current status, challenges, and opportunities," in *Genomic Designing of Climate-Smart Oilseed Crops* (Cham, Switzerland: Springer International Publishing), 133–172. doi: 10.1007/978-3-319-93536-2_3

Guy, C. L., Huber, J. L., and Huber, S. C. (1992). Sucrose phosphate synthase and sucrose accumulation at low temperature. *Plant Physiol.* 100, 502–508. doi: 10.1104/pp.100.1.502

Halward, T., Stalker, H., Larue, E., and Kochert, G. (1991). Genetic variation detectable with molecular markers among unadapted germ-plasm resources of cultivated peanut and related wild species. *Genome* 34, 1013–1020. doi: 10.1139/g91-156

Jain, A. K., Basha, S. M., and Holbrook, C. C. (2001). Identification of drought-responsive transcripts in peanut (Arachis hypogaea L.). *Electron. J. Biotechnol.* 4, 59–67. doi: 10.2225/vol4-issue2-fulltext-2

Jia, J., Zhou, J., Shi, W., Cao, X., Luo, J., Polle, A., et al. (2017). Comparative transcriptomic analysis reveals the roles of overlapping heat-/drought-responsive genes in poplars exposed to high temperature and drought. *Sci. Rep.* 7, 43215. doi: 10.1038/srep43215

Kottapalli, K. R., Rakwal, R., Shibato, J., Burow, G., Tissue, D., Burke, J., et al. (2009). Physiology and proteomics of the water-deficit stress response in three contrasting peanut genotypes. *Plant Cell Environ.* 32, 380–407. doi: 10.1111/j.1365-3040.2009.01933.x

Laza, H. E., Acosta-Martinez, V., Cano, A., Baker, J., Mahan, J., Gitz, D., et al. (2023). Elevated [CO 2] enhances soil respiration and AMF abundance in a semiarid peanut agroecosystem. *Agriculture, Ecosystems & Environment* 355, 108592. doi: 10.1016/j.agee.2023.108592

Laza, H., Baker, J. T., Yates, C., Mahan, J. R., Burow, M. D., Puppala, N., et al. (2021). Effect of elevated CO2 on peanut performance in a semi-arid production region. *Agric. For. Meteorol.* 308–309, 108599. doi: 10.1016/J.AGRFORMET.2021.108599

Lohse, M., Nagel, A., Herter, T., May, P., Schroda, M., Zrenner, R., et al. (2014). Mercator: A fast and simple web server for genome scale functional annotation of plant sequence data. *Plant Cell Environ.* 37, 1250–1258. doi: 10.1111/pce.12231

Long, S. P., Ainsworth, E. A., Rogers, A., and Ort, D. R. (2004). Rising Atmospheric Carbondioxide: plants FACE the future. *Annu. Rev. Plant Biol.* 55, 591–628. doi: 10.1146/annurev.arplant.55.031903.141610

Lu, J., and Pickersgill, B. (1993). Isozyme variation and species relationships in peanut and its wild relatives (Arachis L. - Leguminosae). *Theor. Appl. Genet.* 85, 550–560. doi: 10.1007/BF00220913

Moore, B. D., Cheng, S. H., Sims, D., and Seemann, J. R. (1999). The biochemical and molecular basis for photosynthetic acclimation to elevated atmospheric CO 2. *Plant Cell Environ.* 22, 567–582. doi: 10.1046/j.1365-3040.1999.00432.x

Noguchi, K., Watanabe, C. K., and Terashima, I. (2015). Effects of elevated atmospheric CO 2 on primary metabolite levels in arabidopsis thaliana col-0 leaves: an examination of metabolome data. *Plant Cell Physiol.* 56, 2069–2078. doi: 10.1093/pcp/pcv125

Novello, N., Johnson, J. B., Walsh, K. B., Laza, H., and Naiker, M. (2023). Potential Implications of Elevated CO2 on Physiochemical Parameters in Peanut (Arachis hypogaea L.) Genotypes, in: Foods 2023. *MDPI Basel Switzerland*, 26(1), 11. doi: 10.3390/Foods2023-15115

Parrott, D., Yang, L., Shama, L., and Fischer, A. M. (2005). Senescence is accelerated, and several proteases are induced by carbon "feast" conditions in barley (Hordeum vulgare L.) leaves. *Planta* 222, 989–1000. doi: 10.1007/s00425-005-0042-x

Prasad, P. V. V., Boote, K., Allen, L., and Thomas, J. (2003). Super-optimal temperatures are detrimental to peanut (Arachis hypogaea L.) reproductive processes and yield at both ambient and elevated carbon dioxide. *Glob. Change Biol.* 9, 1775–1787. doi: 10.1046/j.1529-8817.2003.00708.x

Pruthvi, V., Rama, N., Govind, G., and Nataraja, K. N. (2013). Expression analysis of drought stress specific genes in Peanut (Arachis hypogaea, L.). *Physiol. Mol. Biol. Plants* 19, 277–281. doi: 10.1007/s12298-012-0156-0

Qin, H., Gu, Q., Zhang, J., Sun, L., Kuppu, S., Zhang, Y., et al. (2011). Regulated expression of an isopentenyltransferase gene (IPT) in peanut significantly improves drought tolerance and increases yield under field conditions. *Plant Cell Physiol.* 52, 1904–1914. doi: 10.1093/pcp/pcr125

Sage, R. F., Way, D. A., and Kubien, D. S. (2008). Rubisco, Rubisco activase, and global climate change. *J. Exp. Bot.*, 1581–1595. doi: 10.1093/jxb/ern053

Seijo, G., Lavia, G. I., Fernández, A., Krapovickas, A., Ducasse, D. A., Bertioli, D. J., et al. (2007). Genomic relationships between the cultivated peanut (Arachis hypogaea, Leguminosae) and its close relatives revealed by double GISH. *Am. J. Bot.* 94, 1963–1971. doi: 10.3732/ajb.94.12.1963

Sims, D. A., Luo, Y., and Seemann, J. R. (1998). Importance of leaf versus whole plant CO 2 environment for photosynthetic acclimation. *Plant Cell Environ.* 21, 1189–1196. doi: 10.1046/j.1365-3040.1998.00377.x

Vara Prasad, P. V., Craufurd, P. Q., and Summerfield, R. J. (1999). Fruit number in relation to pollen production and viability in groundnut exposed to short episodes of heat stress. *Ann. Bot.* 84, 381–386. doi: 10.1006/anbo.1999.0926

Vu, J. C. V., and Allen, L. H. (2009). Growth at elevated CO2 delays the adverse effects of drought stress on leaf photosynthesis of the C4 sugarcane. *J. Plant Physiol.* 166, 107–116. doi: 10.1016/j.jplph.2008.02.009

Walker, B. J., VanLoocke, A., Bernacchi, C. J., and Ort, D. R. (2016). The costs of photorespiration to food production now and in the future. *Annu. Rev. Plant Biol.* 67, 107–129. doi: 10.1146/annurev-arplant-043015-111709

Yamori, W., and von Caemmerer, S. (2009). Effect of rubisco activase deficiency on the temperature response of CO2 assimilation rate and rubisco activation state: insights from transgenic tobacco with reduced amounts of rubisco activase. *Plant Physiol.* 151, 2073–2082. doi: 10.1104/pp.109.146514

Yokoyama, K., Ishijima, S. A., Clowney, L., Koike, H., Aramaki, H., Tanaka, C., et al. (2006). Feast/famine regulatory proteins (FFRPs): Escherichia coli Lrp, AsnC and related archaeal transcription factors. *FEMS Microbiol. Rev* 30, 89–108. doi: 10.1111/j.1574-6976.2005.00005.x

Zinta, G., AbdElgawad, H., Domagalska, M. A., Vergauwen, L., Knapen, D., Nijs, I., et al. (2014). Physiological, biochemical, and genome-wide transcriptional analysis reveals that elevated CO_2 mitigates the impact of combined heat wave and drought stress in *Arabidopsis thaliana* at multiple organizational levels. *Glob. Change Biol.* 20, 3670–3685. doi: 10.1111/gcb.12626

Frontiers in
Plant Science

Cultivates the science of plant biology and its applications

The most cited plant science journal, which advances our understanding of plant biology for sustainable food security, functional ecosystems and human health.

Discover the latest Research Topics

See more →

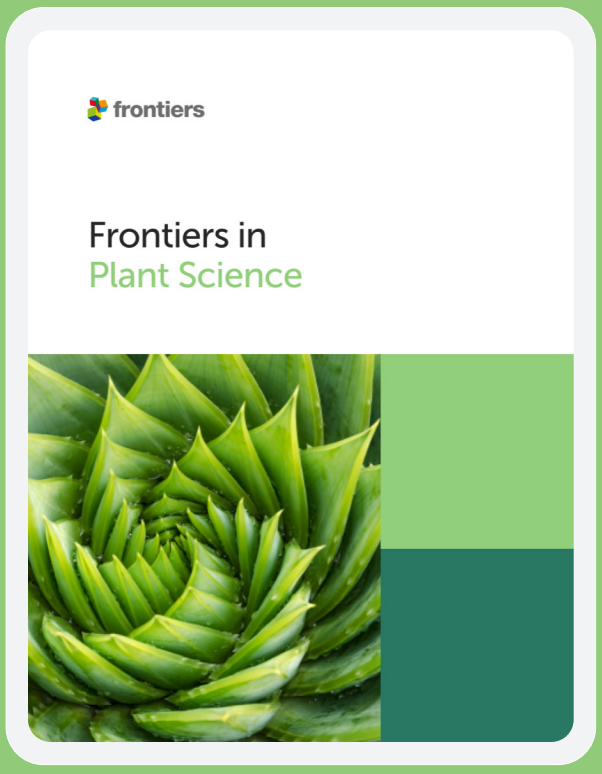

Frontiers

Avenue du Tribunal-Fédéral 34
1005 Lausanne, Switzerland
frontiersin.org

Contact us

+41 (0)21 510 17 00
frontiersin.org/about/contact